RANDOM SEAS AND DESIGN OF MARITIME STRUCTURES

Y. Goda

World Scientific

RANDOM SEAS AND DESIGN
OF MARITIME STRUCTURES

ADVANCED SERIES ON OCEAN ENGINEERING

Series Editor-in-Chief
Philip L- F Liu *(Cornell University)*

RANDOM SEAS AND DESIGN OF MARITIME STRUCTURES

Y. Goda
University of Tokyo

British Library Cataloguing-in-Publication Data
A catalogue record for this book is available from the British Library.

RANDOM SEAS AND DESIGN OF MARITIME STRUCTURES (2nd Edition)

This book is printed on acid-free paper.

Contents

PART II. STATISTICAL THEORIES OF RANDOM SEA WAVES

PART III. STATISTICAL ANALYSIS OF EXTREME WAVES

Chapter 11 Statistical Analysis of Extreme Waves

Preface

This is the second edition of the book first published in 1985 by University of Tokyo Press, which was an enlarged English edition of my book in Japanese published in 1977 by the Kajima Institute Publishing Company. The Japanese edition was revised in 1990 with the addition of new material, especially of a new chapter on the statistical analysis of extreme waves. In the present edition, further revisions have been made to update the book's content.

Additions to the first English edition are the new sections on the relationships between wave statistics and spectrum, the longshore currents induced by random waves, the motions of ships at mooring, the tests with multidirectional random waves, the advanced theories of directional spectral estimates, and the new chapter on extreme wave statistics. Several sections have been thoroughly rewritten, such as those on wave grouping, sampling variability of wave parameters, and numerical simulation of random wave profiles.

The objective of this book is twofold: to provide practicing engineers with design tools to deal with random seas (Part I), and to serve as a textbook of random wave theory for graduate students (Part II). The very warm response by many readers to the first English edition seems to reflect the success in achieving the objective. Because of the limited number of printed copies of the first edition, there was quite a large demand for the publication of the second edition. With the recommendation of Professor Philip L-F Liu of Cornell University, World Scientific Publishing Company succeeded in getting the transfer of the publishing copyright from the University of Tokyo Press in 1996. The present edition has been newly typeset from old text and additional new manuscript, the work of which took some time.

The major portion of the book is based on my research work at the Port and Harbour Research Institute, Ministry of Transport, Japan, where I worked from 1957 to 1988. Many staff members of my research group there assisted me in carrying out a number of laboratory experiments and field data analysis. I am very grateful for their dedicated efforts. Many research topics were brought to me by many government engineers in charge of port construction and coastal protection. They taught me what problems in the field were in need of rational engineering solutions.

The publication of the first English edition was suggested by Dr Nicholas C Kraus, presented at the Waterways Experimental Station, US Army Corps of Engineers. He critically reviewed the first manuscript, clearing up ambiguities

and correcting many idiomatic expressions. The success of the first edition owed much to him. My wife, Toshiko, patiently allowed me to spend many off-duty hours at home for study and writing of the first and second editions of this book. I would like to conclude this preface with gratitude to her.

Yokosuka, Japan
November 1999

Yoshima GODA

Preface to the First Edition

Our understanding of sea waves has grown considerably since the appearance of Minikin's celebrated book *Winds, Waves and Maritime Structures* in 1950. In particular, the random nature of sea waves has become much clearer, and sea waves are now described and analyzed by means of statistical theories. The ocean wave spectrum, for example, is presently a working tool of oceanographers and researchers in coastal and offshore engineering. However, engineering application of the random wave concept is as yet limited to a rather small number of researchers and engineers. This book appears to be the first attempt to present a systematic treatment and applications of the concept of random sea waves from the perspective of the engineer.

The original edition of this book was published in Japanese in October 1977 by Kajima Institute Publishing Company. I am pleased to say that the Japanese version was greeted with enthusiasm by a large number of coastal and harbor engineers in Japan. The present edition is a revision and translation of the Japanese edition.

The book is separated into two parts. Part I is mainly addressed to practicing engineers who are looking for immediate answers to their daily problems. This part consists of Chapters 1 to 7. Part II, consisting of Chapters 8 to 10, is directed toward researchers, engineers and graduate students who wish to learn the fundamental theory of random sea waves in order to carry out further developments in coastal and offshore engineering. It is hoped that the readership of Part II will not be limited to those who are civil engineers by training, but will also include naval architects, physical oceanographers and scientists in other disciplines who are interested in the complexity of random sea waves. It is assumed that the reader has a basic understanding of small amplitude wave theory, a description of which can be found in most textbooks on coastal engineering and physical oceanography.

For practicing engineers, Part II may be somewhat difficult, but perseverance will be rewarded by a glimpse of the theoretical foundation upon which the engineering application of the random wave concept is constructed. However, an understanding of Part II is not necessary, because Part I is self-contained. For those who are pursuing subjects at the forefront of knowledge, in contrast, the discussions and recommendations presented in Part I may sound subjective, or even dogmatic. It should be remembered, however, that engineers often face situations in which they must design structures and produce drawings for construction with minimal background information on the site and limited

reliable theoretical machinery for calculation. I have tried to provide guidelines for engineers — guidelines I believe to be the best available at present — in the hope of helping those who are tackling various problems related to sea waves. With advances in knowledge, some of the solutions and recommendations in this book will become obsolete and be replaced by new ones. But so long as this book serves for today's needs, its purpose will be judged to be fulfilled.

Major revisions made for the English edition are the rewriting of Chapter 4 on breakwaters and the addition of new material in Chapters 9 and 10, based on recent studies. Chapter 4 introduces Japan's vertical breakwaters and the procedures for their design, which are probably not well known to engineers outside Japan. The new material in Chapter 9 concerns the theory of wave grouping and the analysis of wave nonlinearity. In Chapter 10, discussions of the directional wave spectrum calculated by means of the maximum-likelihood method and a simulation technique for two-dimensional waves were added.

The material presented in this book mainly derives from research work conducted by the members of the Wave Laboratory of the Port and Harbour Research Institute, Ministry of Transport, Japan, which I headed from 1967 to 1978. I sincerely wish to acknowledge the efforts of the dedicated staff members of the Wave Laboratory in the successful accomplishment of many research projects. I am also indebted to many fellow government engineers who brought to my attention various stimulating problems of a difficult and urgent nature. Often they supported the research projects financially.

The publication of this English edition was suggested and initial arrangements were made by Dr N. C. Kraus of the Nearshore Environment Research Center, Tokyo. I am very grateful to him for the above and for his critical review of the manuscript. As the first reader of the English edition, he helped to clarify ambiguities and to correct many idiomatic expressions. The staff members of the International Publications Department, University of Tokyo Press, were helpful and supportive throughout the publication process. Kajima Institute Publishing Company, publishers of the Japanese-language book, generously lent the illustration plates for use in this edition. I am also grateful to my wife, who patiently allowed me to spend many off-duty hours at home for study and writing of this book. Finally, I wish to acknowledge the financial support of the Ministry of Education, Science and Culture, Japan, for translation of the text.

Yokosuka, Japan
May 1984

Yoshima GODA

Part I

Random Sea Waves
and Engineering Applications

Chapter 1

Introduction

1.1 Waves in the Sea

Engineers build various types of maritime structures. Breakwaters and quay-walls for ports and harbors, seawalls and jetties for shore protection, and platforms and rigs for the exploitation of oil beneath the seabed are some examples. These structures must perform their functions in the natural environment, being subjected to the hostile effects of winds, waves, tidal currents, earthquakes, etc. To ensure their designated performance, we must carry out comprehensive investigations in order to understand the environmental conditions. The investigations must be as accurate as possible so that we can rationally assess the effects of the environment on our structures.

Waves are the most important phenomenon to be considered among the environmental conditions affecting maritime structures, because they exercise the greatest influence. The presence of waves makes the design procedure for maritime structures quite different from that of structures on land. Since waves are one of the most complex and changeable phenomena in nature, it is not easy to achieve a full understanding of their fundamental character and behavior.

Waves have many aspects. They appear as the wind starts to blow, grow into mountainous waves amid storms and completely disappear after the wind ceases blowing. Such changeability is one aspect of the waves. An observer on a boat in the offshore region easily recognizes the pattern of wave forms as being made up of large and small waves moving in many directions. The irregularity of wave form is an important feature of waves in the sea. However,

upon reaching the shore, an undulating swell breaks as individual waves, giving the impression of a regular repetition. Yuzo Yamamoto, in his novel *Waves*, sees an analogy between successive waves and a son's succession to the father.

The generation of waves on a water surface by wind and their resultant propagation has been observed throughout history. However, the mathematical formulation of the motion of water waves was only introduced in the 19th century.[a] In 1802, Gerstner, a mathematician in Prague, published the trochoidal wave theory for waves in deep water, and in 1844, Airy in England developed a small amplitude wave theory covering the full range of water depth from deep to shallow water. Thereafter, in 1847, Stokes gave a theory of finite amplitude waves in deep water, which was later extended to waves in intermediate-depth water. This solution is now known as the Stokes wave theory. The existence of a solitary wave which has a single crest and propagates without change of form in shallow water was reported by Russell in 1844. Its theoretical description was given by Boussinesq in 1871 and Rayleigh in 1876. Later, in 1895, Koreteweg and de Vries derived a theory of permanent periodic waves of finite amplitude in shallow water. This is now known as the cnoidal wave theory.

Thus, the fundamental theories of water waves were established by the end of the 19th century. Nevertheless, several decades had passed before civil engineers were able to make full use of these theories in engineering applications. An exception is the theory of standing wave pressure derived in 1928 by Sainflou,[2] an engineer at Marseille Port. Sainflou's work attracted the attention of harbor engineers soon after publication; his pressure formula was adopted in many countries for the design of vertical breakwaters. It should be mentioned, however, that it was during the Second World War when the mathematical theory and engineering practice was successfully combined together. This led to the formation of the discipline of coastal engineering, which can be said to have begun with the wave forecasting method introduced by Sverdrup and Munk[3]; this later evolved into the more sophisticated S-M-B method, the calculation of wave diffraction by a breakwater developed by Penney and Price,[4] and other milestone developments.

In proposing the foundation for the present S-M-B method, Sverdrup and Munk clearly understood that sea waves are composed of large and small waves. They introduced the concept of the *significant wave*, the height of which is

---

[a]The following historical overview of the study of water waves is based on the literature listed by Lamb.[1]

equal to the mean of the heights of the highest one-third waves in a wave group, as representative of a particular sea state. Therefore, the significant wave concept was based upon the understanding of sea waves as a random process. However, the significant wave, expressed in terms of a single wave height and wave period, is sometimes misunderstood by engineers to represent waves of constant height and period. The theory of monochromatic waves and experimental results obtained from a train of regular waves have been directly applied to prototype problems in the real sea on the belief that the regular waves correspond exactly to the significant wave.

As early as in 1952, a group of American oceanographers, headed by Pierson,[5] took the first step in recognizing the irregularity of ocean waves as a fundamental property and incorporating this fact in the design process. The so-called P-N-J method[6] of wave forecasting, often compared with the S-M-B method, introduced the concept of wave spectrum as the basic tool for describing wave irregularity. The generation and development of wind waves, the propagation of swell and wave transformation near the shore were all explained in detail via the concept of wave spectrum. Although the spectral concept became widespread among oceanographers at an early stage, coastal and harbor engineers with the exception of a few researchers considered it too complicated. Hence, the introduction of spectral computation techniques into the design process for coastal structures was much delayed.

With advances in wave studies, however, engineers have gradually become aware of the importance of wave irregularity and its relevance in engineering applications. It has been demonstrated many times that the use of regular waves with height and period equal to those of significant wave can give inconsistent or erroneous results in the analysis of wave transformation and action of waves. Therefore, in this book, the concept of randomness in waves is taken as fundamental in the design procedures concerning waves in the sea. A total system of procedures for designing maritime structures against random sea waves is presented.

1.2 Outline of Design Procedures against Random Sea Waves

1.2.1 *Wave Transformation*

A prerequisite for the reliable estimation of waves on maritime structures is a detailed understanding of how waves transform during their propagation

① Generation of Wind Waves in Deep Water
A, E

② Attenuation of Swell by Dispersion
A, E

Deep Water

③ Wind Waves and/or Swell

④ Wave Diffraction by Islands and Headlands
E

⑤ Waves in the Offshore

Analysis Method

A. Significant Wave Representation

B. Highest Wave Representation

C. Probability Calculation

D. Irregular Wave Experiments

E. Spectral Calculation

⑥ Wave Refraction
E, A

⑦ Wave Diffraction by Breakwaters
E

Shallow Water

⑧ Equivalent Deepwater Waves

⑨ Wave Shoaling
A, D, E

⑩ Wave Deformation by Random Breaking
C, D

⑪ Influence of Reflected Waves
D, E

⑫ Waves at the Design Site

⑬ Wave Transmission over or through Breakwaters
D

⑭ Wave Diffraction by Breakwaters
E

⑱ Generation of Littoral Currents
C, E

⑮ Wave Agitations in Harbors

⑲ Accretion and/or Erosion of Beaches
D, C, E

⑯ Wave Runup and Overtopping of Seawalls
C, D

⑰ Wave Pressures and Forces upon Structures
B, D, E

Fig. 1.1. Flow of the transformations and actions of sea waves with suggested methods for their calculation.[7]

toward the shore, after they have been generated and developed by the wind in the offshore region. The various types of wave transformations are schematically shown in Fig. 1.1.[7]

First, wind waves become swell when they move out of the generating area. The height of the swell gradually decreases with distance as it propagates (② in Fig. 1.1). When wind waves and swell encounter an island or a headland during their propagation in deep water, they diffract and penetrate the obstacle (④ in Fig. 1.1).

When waves enter an area of depth less than about one-half of their wavelength, they are influenced by the sea bottom's topography. These waves are called intermediate-depth water waves. Where the water is shallower than about one-twentieth of a wavelength, the waves are called long waves. For the sake of simplicity, both intermediate-depth water waves and long waves may be classified together and called shallow water waves; this terminology is employed in the present chapter. Waves in an area having a depth greater than about one-half of a wavelength are called deepwater waves (⑤ in Fig. 1.1). In a shallow bay or estuary, wind-generated waves may become shallow water waves during their process of development. In such a case, wave forecasting or hindcasting needs to take into account the effect of water depth on the wave development.

Having propagated into a shallow region, waves undergo refraction by which the direction of wave propagation, as well as the wave height, varies according to the sea bottom's topography (⑥ in Fig. 1.1). Concerning waves inside a harbor, the phenomenon of diffraction by breakwaters is the governing process (⑦ in Fig. 1.1). Although not shown in Fig. 1.1, wave attenuation due to bottom friction and other factors may not be neglected in an area of relatively shallow water which extends over a great distance with a very gentle inclination in the sea bottom. For convenience, the change in wave height due to wave refraction, diffraction and attenuation is often incorporated into the concept of *equivalent deepwater waves* (⑧ in Fig. 1.1). Equivalent deepwater waves are assigned the same wave period as deepwater waves, but the wave height is adjusted to account for the change due to wave refraction, diffraction and attenuation.

Waves propagating in a shallow region gradually change in height as a result of the change in the rate of energy flux due to the reduction in water depth, even if no refraction takes place. This is the phenomenon of wave shoaling (⑨ in Fig. 1.1). When waves reach an area of depth less than a few times the significant wave height, waves of greater height in a group begin to break one by one and the overall wave height decreases as the wave energy dissipates. This is wave deformation caused by breaking (⑩ in Fig. 1.1).

Waves arriving at the site of a proposed structure (⑫ in Fig. 1.1) will experience the above transformations and deformations of wave refraction, diffraction, shoaling, breaking, etc. If a long extension of vertical breakwater is already located in the adjacent water area, or if the design site is within a harbor, the influence of waves reflected from neighboring structures must be added to that of the waves arriving directly from offshore (⑪ in Fig. 1.1). These wave transformations and deformations will be discussed in detail in Chapter 3. Once the characteristics of the waves at the site have been estimated, design calculations can be made according to the nature of the problem. For example, the problem of harbor tranquility requires the analysis of waves transmitted over or through breakwaters (⑬ in Fig. 1.1), waves diffracted through harbor entrances (⑭ in Fig. 1.1) and waves reflected within a harbor. These will be discussed in Chapter 6.

The planning of seawalls and revetments to stand against storm waves requires the estimation of wave run-up and wave overtopping rate. Technical information for such problems is usually provided by conducting a scale model test in the laboratory or a set of design diagrams based on laboratory data. In such cases, the flow of calculation takes a jump from ⑧ to ⑯ in Fig. 1.1, because these data are prepared using the parameter of equivalent deepwater waves by directly incorporating the effects of transformations ⑨ and ⑩ into the data. Problems related to wave overtopping are discussed in Chapter 5.

In the design of breakwaters, the magnitude of the wave pressure is the focal point that requires an appropriate selection of calculation formulas. Chapter 4 discusses the formulas for wave pressure and their applications. It is remarked here that littoral drift, which is associated with beach erosion and accretion, is closely related to wave deformation by breaking and is induced by the resultant longshore current (⑱ in Fig. 1.1).

In the process of calculating the wave transformations and deformations described above, the significant wave height and period are used as indices of the magnitude of random sea waves. These parameters are converted to those of the highest waves or other descriptive waves whenever necessary, as in the case of a wave pressure calculation. Thus, at first sight, this procedure may look the same as the conventional design procedure, for which the significant wave is regarded as a train of regular waves. In the present treatise, however, the effects of wave irregularity are accounted for the estimation of the respective wave transformations, and the resultant height of the significant wave after such

transformation often takes a value considerably different from that obtained with the regular wave approach.

1.2.2 *Methods of Dealing with Random Sea Waves*

At present, the following five methods are available to deal with the transformation and action of random sea waves:

    A. significant wave representation method
    B. highest wave representation method
    C. probability calculation method
    D. irregular wave test method
    E. spectral calculation method

The significant wave representation method takes a train of regular waves with height and period equal to those of the significant wave as representative of random sea waves. Transformations of sea waves are estimated with the data of regular waves on the basis of theoretical calculation and laboratory experiments. The method has widely been employed in the field of coastal engineering since the introduction of the significant waves as the basis of the S-M-B method for wave forecasting. It has the merits of easy understanding and simple application, but it also has the demerit of containing a possibly large estimation error, depending on the type of wave phenomenon being analyzed. Diffraction, to be discussed in Sec. 3.2, is an example: the wave height behind a single breakwater may be estimated to be less than a third of the actual height if the diffraction diagram of regular waves is directly applied. The design of a steel structure for the sea is another example in which the maximum force exerted by individual waves is the governing factor. If the structure is designed against a regular wave equal to the significant wave, the structure will most probably fail under the attack of waves higher than the significant wave height when the design storm hits the site.

The danger of underestimating wave forces through the use of significant waves was well understood at the early stages of construction of offshore structures such as oil drilling rigs. It is an established practice to use a train of regular waves of height and period equal to those of the highest wave, and to design structures against this train of regular waves. This is called the highest wave representation method herein. The method is mainly used for structural designs.

In contrast to the above examples, the phenomenon of diffraction is quite sensitive to the characteristics of the wave spectra, especially to the directional spreading of wave energy. In the analysis of diffraction, refraction and wave forces upon a large isolated structure such as oil storage tank in the sea, calculation is made for individual components of the directional spectrum. The resultant total effect is estimated by summing the contributions from all components. This is called the spectral calculation method.

The rate of wave overtopping of a seawall and the sliding of a concrete caisson of a vertical breakwater differ from the previous examples in the sense that the cumulative effect of the action of individual waves of random nature is important. The probability distribution of individual wave heights and periods is the governing factor in this type of problems. The phenomena of irregular wave run-up and wave deformation by random breaking belong to the same category. The calculation of these cumulative wave effects may be called the probability calculation method.

If a large wind-wave flume of a wave flume with a random wave generator is available, wave transformations and wave action on structures can be directly investigated by using simulated random water waves. This is the irregular wave test method. At the time of publication of the first edition of this book, the reproduction of directional random waves in model basins was possible only at a limited number of hydraulic laboratories in the world. Since then, many laboratories have been equipped with multidirectional random wave generators and become capable of carrying out model tests of various problems, including random wave refraction and diffraction. It may be said that the majority of hydraulic model tests related to sea waves are now carried out with random waves, and wave tests with regular waves are mostly reserved for fundamental research purposes.

In Fig. 1.1, the symbols A to E indicate the analysis method appropriate to the respective phenomenon. As can be seen, the problems related to random sea waves must be solved by selecting the appropriate calculation method among the five, A to E, to obtain a safe and rational design. None of the five methods can be used alone to treat all problems concerning sea waves. This stems from the complicated nature of waves in the real sea. In the following chapters, the above methods of analyzing the various wave phenomena are presented and discussed.

References

1. H. Lamb, *Hydrodynamics* (6th Ed.), Chap. IX, (Cambridge Univ. Press, 1932).
2. G. Sainflou, "Essai sur les digues maritimes verticales," *Annales de Ponts et Chaussées* **98** (4), (1928).
3. H. U. Sverdrup and W. H. Munk, *Wind, Sea, and Swell; Theory of Relations for Forecasting*, U.S. Navy Hydrographic Office, H. O. Publ. No. 601 (1947).
4. W. G. Penney and A. T. Price, "Diffraction of sea waves by breakwaters," *Directorate of Miscellaneous Weapons Development, Tech. History* No. 26, Artificial Harbours, Sec. 3-D (1944).
5. W. J. Pierson, Jr., J. J. Tuttell and J. A. Woolley, "The theory of the refraction of a short-crested Gaussian sea surface with application to the Northern New Jersey Coast," *Proc. 3rd Conf. Coastal Engrg.* (Cambridge, Mass., 1952), pp. 86–108.
6. W. J. Pierson, Jr., G. Neumann and R. W. James, *Practical Methods for Observing and Forecasting Ocean Waves by Means of Wave Spectra and Statistics*, U.S. Navy Hydrographic Office, H. O. Pub. No. 603 (1955).
7. Y. Goda, "Irregular sea waves for the design of harbour structures (integrated title)," *Trans. Japan Soc. Civil Engrs.* **8** (1976), pp. 267–271.

Chapter 2

Statistical Properties and Spectra of Sea Waves

2.1 Random Wave Profiles and Definitions of Representative Waves

2.1.1 *Spatial Surface Forms of Sea Waves*

Photograph 2.1 exemplifies the random nature of sea waves. It is a picture of the sea surface taken at a slanted angle, when a breeze is generating these wind waves. Sunbeams, which are reflected everywhere, produce patches of glitter. These reflected beams clearly show that there are many small and large wavelets moving in various directions. However, the waves as a whole are moving from right to left, following the direction of the wind. Photograph 2.2 is another example, showing laboratory waves generated by the wind blowing
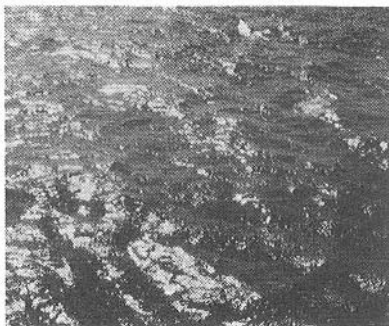
Photo 2.1. Glittering on the sea surface caused by wind waves.

(a) $s_{max} = 10$

$0 \leq \eta/H_{1/3} < 0.2$
$0.2 \leq \eta/H_{1/3} < 0.4$
$0.4 \leq \eta/H_{1/3}$

(b) $s_{max} = 75$

Wave Direction
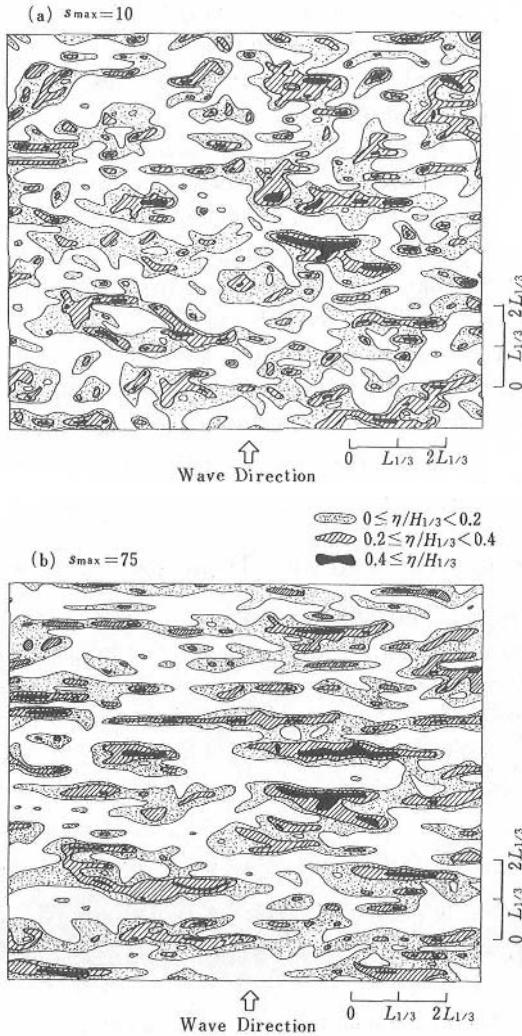
Fig. 2.1. Computer simulation of surface elevation contours of random waves.[1]

over the water surface. This photograph shows the profiles of the waves through a glass pane of the wind-wave flume, as well as a view of the surface.

Such surface forms of sea waves, as discussed above, can be depicted by means of a contour map of the surface elevation. The result will be similar to that shown in Fig. 2.1, though it is not the topography of a real sea surface

but the output of a computer simulation using the directional wave spectrum[1] which is to be discussed in Sec. 2.3. Figures 2.1 (a) and (b) may be taken as representative examples of wind waves and swell, respectively. In the legend, the symbol η denotes the water surface elevation above the mean water level. Dots, hatching and shadowing indicate the magnitude of the elevation while the blank areas designate the water surface below the mean water level. The actual surface topography of sea waves, given by an analysis using aerial stereo-photogrametry, closely resembles the example in Fig. 2.1. The wave pattern in Fig. 2.1 also indicates that wave crests do not have a long extent, but instead consist of short segments. Because of this feature, waves in the sea, especially wind waves, are termed as "short-crested waves."

In the theoretical treatment of water waves, their surface forms are often represented by sinusoidal functions. But such sinusoidal wave forms are observable only in the laboratory; sinusoidal waves are never found in the natural environment as single wave forms.

2.1.2 *Definition of Representative Wave Parameters*

In the profile shown in Photo 2.2, four waves are visible through the glass pane. If we were to trace such a wave profile over a much longer distance, we would get a wave profile undulating in an irregular manner. A longitudinal cross section of the water surface depicted in Fig. 2.1 will also yield a similar wave profile of irregular shape. Both profiles could be plotted against the horizontal distance.

Photo 2.2. Wind waves in a wind water tunnel.

On the other hand, a strip chart record from a wave gauge in the sea yields a wave form as shown in Fig. 2.2. In this example, the horizontal axis gives the elapsed time from the start of the recording. It is rather difficult to define individual waves appearing in such irregular wave records; in fact, there is no absolute method of definition. However, the customary practice
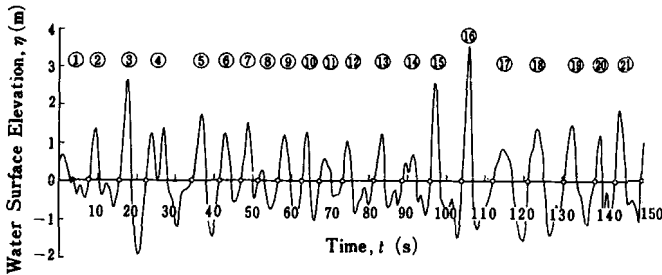
Fig. 2.2. Example of a wave record.

in wave analysis is to utilize either the zero-upcrossing method or the zero-downcrossing method as the standard techniques for defining waves.

We will now briefly describe these methods. First, the mean level of the water surface is deduced from the surface record and defined as the zero line. Next, a search is made for the point where the surface profile crosses the zero line upward. That point is taken as the start of one individual wave. Following the ups and downs of the irregular surface profile, a search is continued to find the next zero-upcrossing point after the surface profile has once gone below the zero line. When the next zero-upcrossing point is found, it defines the end of the first wave and the start of the second wave. The distance between the two adjacent zero-upcrossing points defines the wave period if the abscissa is the time, whereas an apparent wavelength[a] is defined if the abscissa is the horizontal distance. The vertical distance between the highest and lowest points between the adjacent zero-upcrossing points is defined as the wave height, disregarding small humps which do not cross the zero line. In the case of zero-downcrossing method, the points where the surface profile crosses the zero line downward are taken as the starting and ending points of individual waves. The difference between the two definitions is mainly conceptual; that is, whether the wave height is defined using a crest and the following trough or using a crest and the preceding trough. Statistically, they are equivalent except in the surf zone where the conspicuous forward tilting of surface profiles tends to yield the zero-downcrossing wave period slightly shorter than the zero-upcrossing wave period. However, no difference appears between the zero-upcrossing and zero-downcrossing wave height[3] (refer to Sec. 9.5 for further discussion).

---

[a]The wavelength defined in this way is an apparent one, being shorter than the wavelength derived from the wave period and water depth based on the small amplitude wave theory.[2]

Application of the zero-upcrossing method to the sample record of Fig. 2.2 yields 21 individual waves. Their heights and periods as read from the record are listed in Table 2.1 in the order of their appearance. The fourth column indicates the order beginning with the highest wave. In field wave observations, a standard procedure is to take records of about 100 consecutive waves, and thus a long list for the first to one-hundredth wave heights and periods similar to that in Table 2.1 must be made by reading off the values from a strip chart record. Nowadays, almost all the data are recorded in digital form, and the above process is executed by a computer.

Table 2.1. Wave heights and periods read from Fig. 2.2.

Wave number	Wave height H (m)	Wave period T (s)	Order number m	Wave number	Wave height H (m)	Wave period T (s)	Order number m
1	0.54	4.2	21	12	1.95	8.0	15
2	2.05	8.0	12	13	1.97	7.6	14
3	4.52	6.9	2	14	1.62	7.0	18
4	2.58	11.9	8	15	4.08	8.2	3
5	3.20	7.3	4	16	4.89	8.0	1
6	1.87	5.4	17	17	2.43	9.0	9
7	1.90	4.4	16	18	2.83	9.2	7
8	1.00	5.2	20	19	2.94	7.9	6
9	2.05	6.3	13	20	2.23	5.3	11
10	2.37	4.3	10	21	2.98	6.9	5
11	1.03	6.1	19				

Based on such a long list of height and period data, the following four types of representative waves are defined:

(a) *Highest wave:* $H_{\max}$, $T_{\max}$. This refers to the wave having the height and period of the highest individual wave in a record. The quantities are denoted as $H_{\max}$ and $T_{\max}$, respectively. In the case of the data in Table 2.1, the 16th wave is the highest wave, with $H_{\max} = 4.9$ m and $T_{\max} = 8.0$ s.

(b) *Highest one-tenth wave:* $H_{1/10}$, $T_{1/10}$. The waves in the record are counted and selected in descending order of wave height from the highest wave, until

one-tenth of the total number of waves is reached. The means of their heights
and periods are calculated and denoted as $H_{1/10}$ and $T_{1/10}$, respectively. In the
example of Table 2.1, the 16th and 3rd waves are selected for this definition,
yielding the values of $H_{1/10} = 4.7$ m and $T_{1/10} = 7.5$ s. An imaginary wave
train having height and period of $H_{1/10}$ and $T_{1/10}$ is defined as the highest
one-tenth wave.

(c) *Significant wave, or highest one-third wave:* $H_{1/3}$, $T_{1/3}$. For this represen-
tative wave, the waves in the record are counted and selected in descending
order of wave height from the highest wave, until one-third of the total num-
ber of waves is reached. The means of their heights and periods are calculated
and denoted as $H_{1/3}$ and $T_{1/3}$, respectively. In the example of Table 2.1, the
16th, 3rd, 15th, 5th, 21st, 19th and 18th waves are selected for this definition,
yielding the values of $H_{1/3} = 3.6$ m and $T_{1/3} = 7.8$ s. An imaginary wave
train having height and period equal to $H_{1/3}$ and $T_{1/3}$ is defined as the sig-
nificant wave or the highest one-third wave. The height $H_{1/3}$ is often called
the significant wave height, and the period $T_{1/3}$ is called the significant wave
period.

(d) *Mean wave:* $\overline{H}$, $\overline{T}$. The means of the heights and periods of all waves in a
record are calculated and denoted as $\overline{H}$ and $\overline{T}$, respectively. The example in
Table 2.1 has mean values of $\overline{H} = 2.4$ m and $\overline{T} = 7.0$ s. An imaginary wave
having height and period equal to $\overline{H}$ and $\overline{T}$ is defined as the mean wave.

Among the above definitions of representative waves, the significant wave
is most frequently used. The height and the period of wind waves and swell,
including the results of wave hindcasting, usually refer to the significant waves
unless otherwise specified.

2.2 Distributions of Individual Wave Heights and Periods

2.2.1 *Wave Height Distribution*

Among the various statistical properties of random waves in the sea, the dis-
tribution of individual wave heights will be examined first. Figure 2.3 is an
example of the histogram of wave heights obtained from a long wave record
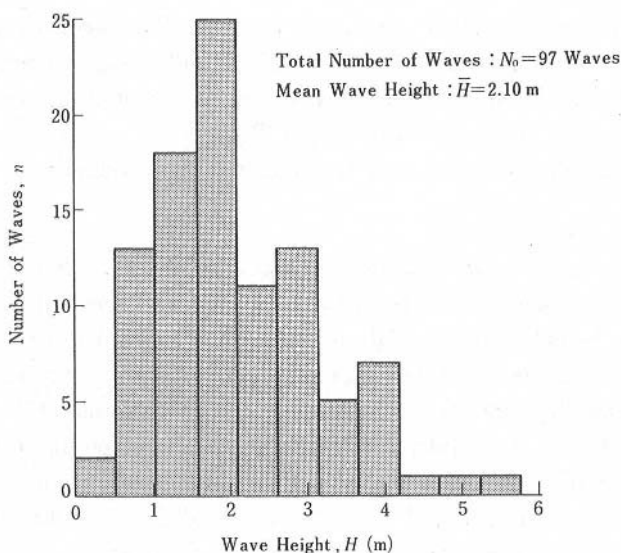
Fig. 2.3. Example of a histogram of wave heights.

which contained the wave profile as shown in Fig. 2.1. The ordinate n is the number of waves in the respective class of wave height H. The wave heights in this example are distributed in a wide range from 0.1 to 5.5 m, with the mode in the class $H = 1.57$ to 2.10 m (a uniform class interval of $\overline{H}/4 = 0.525$ m is used).

The histogram of wave heights of a wave record containing about 100 waves usually exhibits a rather jagged shape because of the relatively small sample size. However, we can obtain a smoother distribution of wave heights by assembling many wave records with the wave heights normalized by the mean heights of the respective records, and by counting the relative frequencies of the normalized wave heights in their respective classes. Figure 2.4 presents a typical result of such a manipulation,[4] in which the ordinate is the relative frequency, n/N_0 (N_0 is the total number of waves), divided by the class interval of the normalized wave height, $\Delta(H/\overline{H})$, so that the area under the histogram is equal to unity.

The smoothed histogram of normalized wave heights shown in Fig. 2.4 suggests the existence of some theoretical distribution function. The Rayleigh

52 Records
5111 Waves
$(H_{1/3}/h = 0 \sim 0.39)$
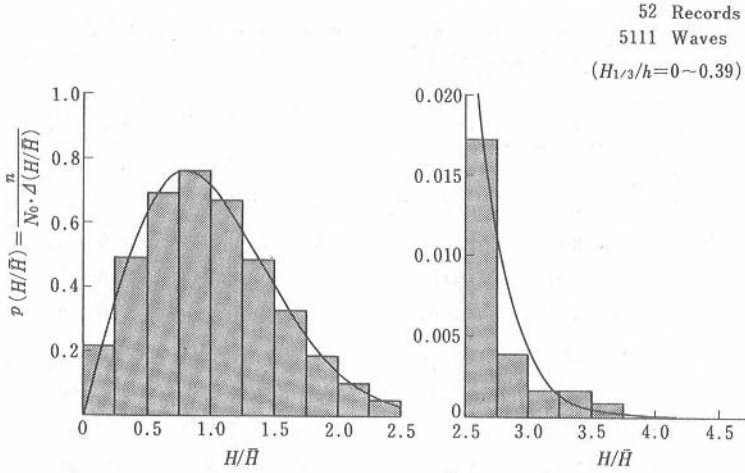
Fig. 2.4. Normalized histogram of wave heights.[4]

distribution given by Eq. (2.1) and drawn with the solid line in Fig. 2.4 has been proposed for the distribution of individual wave heights:

$$p(x) = \frac{\pi}{2} x \exp\left[-\frac{\pi}{4} x^2\right] \quad : x = \frac{H}{\bar{H}} . \qquad (2.1)$$

The function $p(x)$ represents the probability density; that is, the probability of a normalized wave height taking an arbitrary value between x and $x + dx$ is given by the product $p(x)\,dx$. The Rayleigh distribution commonly appears in the field of statistics. The ordinate of the plot in Fig. 2.4, $n/(N_0 \cdot \Delta x)$, is an approximation to $p(x)$. The integral of $p(x)$ over the range $x = 0$ to $x = \infty$ represents the probability of x taking a value between 0 and ∞. By the definition of probability, the integral over the full range should give unity and thus $p(x)$ is normalized.

Table 2.2 lists the values of $p(x)$ calculated for selected values of x. The function $P(x)$ listed in the third and sixth columns gives the probability of a particular wave height exceeding a prescribed value. It is given by

$$P(x) = \int_x^\infty p(\xi)\,d\xi = \exp\left[-\frac{\pi}{4} x^2\right] . \qquad (2.2)$$

The Rayleigh distribution was originally derived by Lord Rayleigh in the late 19th century to describe the distribution of the intensity of sounds emitted from an infinite number of sources. In 1952, Longuet-Higgins[5] demonstrated

Table 2.2. Probability density and exceedance probability of the
Rayleigh distribution.

$H/\overline{H}$	$p(H/\overline{H})$	$P(H/\overline{H})$	$H/\overline{H}$	$p(H/\overline{H})$	$P(H/\overline{H})$
0	0	1.0000	2.0	0.1358	0.0432
0.1	0.1559	0.9222	2.1	0.1033	0.0313
0.2	0.3044	0.9691	2.2	0.0772	0.0223
0.3	0.4391	0.9318	2.3	0.0567	0.0157
0.4	0.5541	0.8819	2.4	0.0409	0.0108
0.5	0.6454	0.8217	2.5	0.0290	0.00738
0.6	0.7104	0.7537	2.6	0.0202	0.00495
0.7	0.7483	0.6806	2.7	0.0138	0.00326
0.8	0.7602	0.6049	2.8	0.0093	0.00212
0.9	0.7483	0.5293	2.9	0.0062	0.00135
1.0	0.7162	0.4559	3.0	0.0040	0.00085
1.1	0.6680	0.3866	3.1	0.0026	0.00053
1.2	0.6083	0.3227	3.2	0.0016	0.00032
1.3	0.5415	0.2652	3.3	0.0010	0.00019
1.4	0.4717	0.2145	3.4	0.0006	0.00011
1.5	0.4025	0.1708	3.5	0.0004	0.000066
1.6	0.3365	0.1339	3.6	0.0002	0.000038
1.7	0.2759	0.1033	3.7	0.0001	0.000021
1.8	0.2219	0.0785	3.8	0.0001	0.000012
1.9	0.1752	0.0587	3.9	0.0000	0.000065
2.0	0.1358	0.0432	4.0	0.0000	0.000035

that this distribution is also applicable to the heights of waves in the sea. Since
then, the Rayleigh distribution has been universally employed to describe wave
heights. Strictly speaking, Longuet-Higgins only verified the applicability of
the Rayleigh distribution for irregular waves which have very small fluctuations
in the individual wave periods and whose heights exhibit a beat-like fluctua-
tion. However, real sea waves usually exhibit fairly wide fluctuations in the
individual wave periods. As of yet, no exact theory, which is applicable to real
waves in the sea characterized by certain fluctuations in wave periods, has been

proposed. Close examinations of wave records have already indicated a slight departure of the actually occurring wave height distribution from the Rayleigh distribution; the degree of departure depends on the frequency spectrum of sea waves (refer to Sec. 2.4 for a detailed discussion). Nevertheless the Rayleigh distribution provides a good approximation to the distribution of individual wave heights which are defined by the zero-upcrossing and zero-downcrossing methods. This is true not only for wind waves and swell individually, but also for the combined sea state of wind waves and swell propagating simultaneously. This seems to be one of the virtues of the zero-upcrossing and zero-downcrossing wave definitions.

2.2.2 *Relations between Representative Wave Heights*

If we adopt the Rayleigh distribution as an approximation to the distribution of individual wave heights, representative wave heights such as $H_{1/10}$ and $H_{1/3}$ can be evaluated by the manipulation of the probability density function. Thus, we have

$$H_{1/10} = 1.27 H_{1/3} = 2.03 \overline{H}, \quad H_{1/3} = 1.60 \overline{H}. \tag{2.3}$$

These results represent the mean values of a number of wave records ensembled together. Individual wave records containing only 100 waves or so may give noticeable departures from these mean relations. Figures 2.5 and 2.6 show the relative frequencies of the wave height ratio $H_{1/10}/H_{1/3}$ and $H_{1/3}/\overline{H}$, respectively, based on an examination of 171 observed wave records.[4] The ratio of $H_{1/10}/H_{1/3}$ is found to lie in the range from 1.15 to 1.45, while the ratio $H_{1/3}/\overline{H}$ is distributed from 1.40 to 1.75. The overall means are 1.27 for $H_{1/10}/H_{1/3}$ and 1.59 for $H_{1/3}/\overline{H}$, which are quite close to the theoretical predictions of Eq. (2.3).

The relation between H_{max} and $H_{1/3}$ can also be derived from the Rayleigh distribution (refer to Sec. 9.1.3 for a detailed discussion). However, the basic nature of H_{max} is such that individual wave records having the same value of $H_{1/3}$ contain different values of H_{max}, because H_{max} refers to the height of one wave which happens to have the greatest wave height in a particular wave train. For example, the relative frequency of the ratio $H_{max}/H_{1/3}$ for 171 wave records is shown in Fig. 2.7 [4]; the ratio is broadly spread in the range between 1.1 to 2.4. The ratio of $H_{max}/H_{1/3}$ is affected by the number of waves in a record. This will be discussed in connection with Eqs. (2.4) to (2.6). The solid and dashed-dot lines indicate the theoretical probability density function of
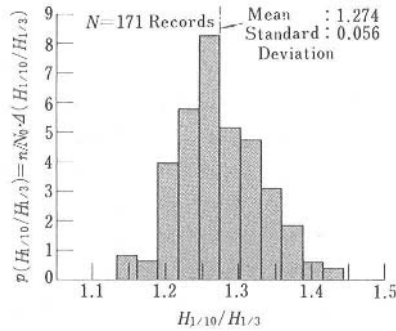
Fig. 2.5. Histogram of the wave height ratio $H_{1/10}/H_{1/3}$.[4]
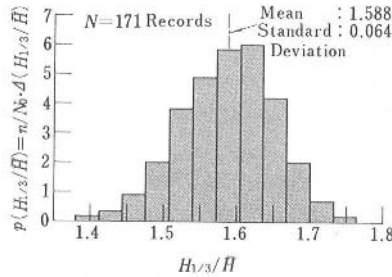
Fig. 2.6. Histogram of the wave height ratio $H_{1/10}\overline{H}$.[4]
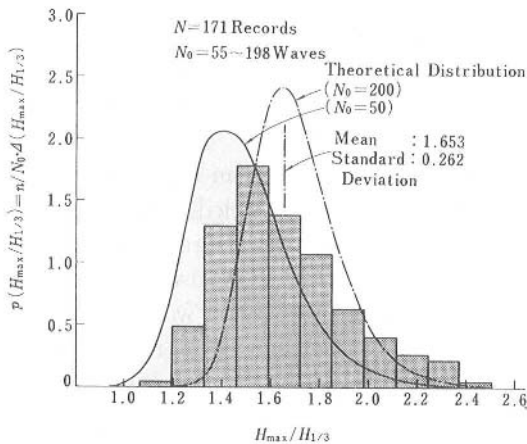
Fig. 2.7. Histogram of the wave height ratio $H_{max}/H_{1/3}$.[4]

$H_{max}/H_{1/3}$ for wave numbers of 50 and 200, respectively. The records, which contain from 55 to 198 waves per record exhibit a distribution of $H_{max}/H_{1/3}$ bounded by the two theoretical curves.

The deterministic prediction of particular values of H_{max} for individual wave trains is impossible. Although it has little meaning to attempt to derive a single value of H_{max} for one storm wave condition, based on the Rayleigh distribution, a probability density can be reasonably defined for the ratio of $H_{max}/H_{1/3}$. The most probable value, or the mode of distribution, is a function of the number of waves in a wave train or wave record. This is given by

$$(H_{max}/H_{1/3})_{mode} \simeq 0.706\sqrt{\ln N_0}\,, \qquad (2.4)$$

where N_0 refers to the number of waves.

The arithmetic mean of $H_{max}/H_{1/3}$ is greater than the most probable value, as seen from the skewed shape of the curves in Fig. 2.7. The mean is given approximately as

$$(H_{max}/H_{1/3})_{mean} \simeq 0.706\left[\sqrt{\ln N_0} + \gamma/(2\sqrt{\ln N_0})\right]\,, \qquad (2.5)$$

where γ is Euler's constant having the value of $0.5772\ldots$.

Furthermore, we can define a quantity $(H_{max})_\mu$ whose probability of exceeding is μ; that is, integration of a probability density of the largest wave height beyond $(H_{max})_\mu$ yields the probability of μ. The height $(H_{max})_\mu$ is given by

$$\frac{(H_{max})_\mu}{H_{1/3}} \simeq 0.706\sqrt{\ln\left[\frac{N_0}{\ln 1/(1-\mu)}\right]}\,. \qquad (2.6)$$

Example 2.1

A sea state with $H_{1/3} = 6.0$ m continues for the duration of 500 waves. Calculate the mode and arithmetic mean of H_{max} as well as the value of H_{max} with $\mu = 0.01$.

Solution

We have $\sqrt{\ln 500} = 2.493$ and $\sqrt{\ln[500/\ln(1/0.990)]} = 3.289$. Therefore,

$$(H_{max}/H_{1/3})_{mode} \simeq 0.706 \times 2.493 \times 6.0 = 10.6 \text{ m}\,,$$

$$(H_{max}/H_{1/3})_{mean} \simeq 0.706 \times [2.493 + 0.5772/(2 \times 2.493)] \times 6.0 = 11.1 \text{ m}\,,$$

$$(H_{max}/H_{1/3})_{0.01} \simeq 0.706 \times 3.289 \times 6.0 = 13.9 \text{ m}\,.$$

The nondeterministic property of the highest wave causes inconvenience as well as uncertainty in the design of maritime structures. It is an inevitable consequence, however, of the random nature of sea waves. The value of H_{max} should be estimated based upon consideration of the duration of storm waves and the number of waves, and by allowing some tolerance for a range of deviation. The prediction generally employed falls within the range

$$H_{max} = (1.6 \sim 2.0)H_{1/3}\,, \tag{2.7}$$

in which the particular final value is chosen by consideration of the reliability of the estimation of the design storm waves, the accuracy of the design formula, the importance of the structure, the type and nature of the possible structural failure, and other factors. In the design of offshore structures, $H_{max} = 2.0H_{1/3}$ or a higher value is often employed. For the design of vertical breakwaters, the author[6] has proposed the use of the relation $H_{max} = 1.8H_{1/3}$.

2.2.3 *Distribution of Wave Period*

The periods of individual waves in a wave train exhibit a distribution narrower than that of wave heights, and the spread lies mainly in the range of 0.5 to 2.0 times the mean wave period. However, when wind waves and swell coexist, the period distribution becomes broader. In some cases, the period distribution is bi-modal, with two peaks corresponding to the mean periods of the wind waves and swell. Thus the wave period does not exhibit a universal distribution law such as the Rayleigh distribution in the case of wave heights.

Nevertheless, it has been empirically found that the representative period parameters are interrelated. From the analysis of field wave data, the following results have been reported[4]:

$$\left.\begin{array}{l} T_{max} = (0.6 \sim 1.3)T_{1/3}\,, \\ T_{1/10} = (0.9 \sim 1.1)T_{1/3}\,, \\ T_{1/3} = (0.9 \sim 1.4)\overline{T}\,. \end{array}\right\} \tag{2.8}$$

The above indicates the range of variations. The average values for many wave records can be summarized as

$$T_{max} \simeq T_{1/10} \simeq T_{1/3} \simeq 1.2\overline{T}\,. \tag{2.9}$$

The ratio of $T_{1/3}$ to $\overline{T}$, indicated in Eq. (2.9), provides only a guideline because its value is affected by the functional shape of frequency spectrum analyzed from a wave record (refer to Sec. 2.4 for a detailed discussion).

Equations (2.8) and (2.9) reflect the characteristics of the joint distribution of wave heights and periods. Waves of smaller heights in a wave record often have shorter periods, whereas waves of heights greater than the mean height do not show a correlation with the wave period. Thus, the overall mean period is shorter than the mean periods of the higher waves (refer to Sec. 9.3 for a detailed discussion).

2.3 Spectra of Sea Waves

2.3.1 *Frequency Spectra*

The concept of spectrum can be attributed to Newton, who discovered that sunlight can be decomposed into a spectrum of colors (red to violet) with the aid of a prism.[7] The spectrum indicates how the intensity of light varies with respect to its wavelength. The concept is based on the principle that white light consists of numerous components of light of various colors (wavelengths). The technique of decomposing a complex physical phenomenon into individual components has been applied in many physical problems.

Sea waves, which at first sight appear very random, can be analyzed by assuming that they consist of an infinite number of wavelets with different frequencies and directions. The distribution of the energy of these wavelets when plotted against the frequency and direction is called the *wave spectrum*. More precisely, the wave energy distribution with respect to the frequency alone, irrespective of wave direction, is called the *frequency spectrum*, whereas the energy distribution expressed as a function of both frequency and direction is called the *directional wave spectrum*.

Figure 2.8 gives an example of an irregular wave profile which was constructed by adding five sinusoidal waves (component waves) of different heights and periods. Although the irregularity of the wave profile is not extreme in this example, we can obtain quite irregular profiles similar to those of real sea waves by increasing the number of component waves. The inverse process is also possible, and irregular wave profiles as shown in Fig. 2.2 can be broken into a number of component waves (refer to Sec. 10.2 for the actual computation procedure). The way in which the component waves are distributed is expressed by plotting the component wave energy, or the square of the component amplitude, against the frequency of component waves. The irregular
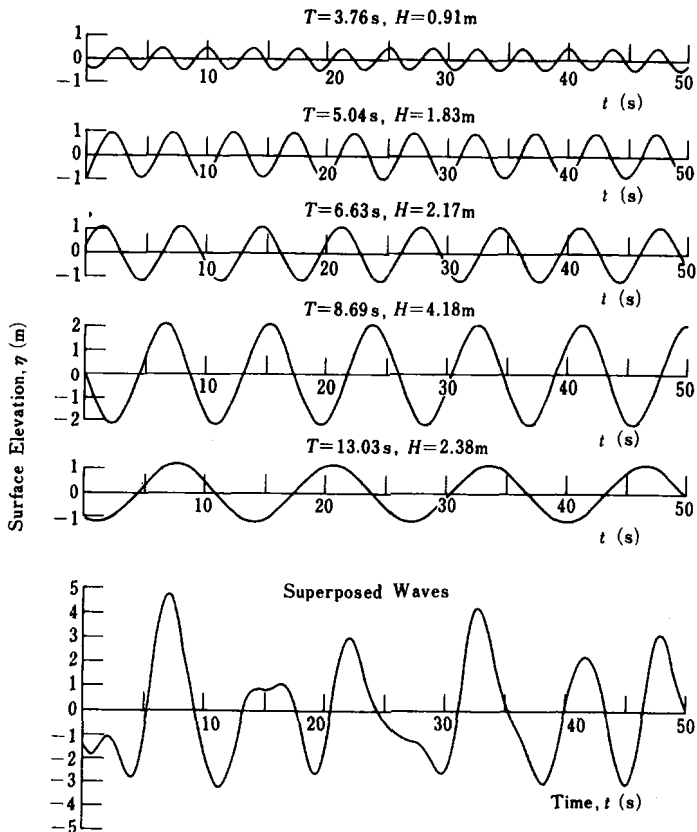
Fig. 2.8. Simulation of irregular waves by superposition of sinusoidal waves.

profile in Fig. 2.8, for example, is represented by the diagram with five bars shown in Fig. 2.9. In the case of sea waves, the energy distribution manifests itself as a continuous curve because there exists an infinite number of frequency components. The wave record which included the profile in Fig. 2.2 was used to calculate the frequency spectrum shown in Fig. 2.10. Such a continuous spectrum is called the *frequency spectral density function* in more precise language, and it has units of m²·s, or units of similar dimensions.

The wave spectrum in Fig. 2.10 indicates that the wave energy is spread in the range of about $f = 0.05 \sim 0.4$ Hz, or equivalently $T = 2.5 \sim 20$ s, even though the significant wave period is 8 s. The figure also indicates that the wave energy is concentrated around the frequency $f_p \simeq 0.11$ Hz, which is
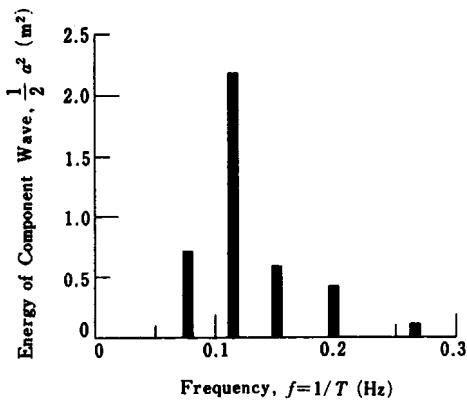
Fig. 2.9. Spectral representation of superposed waves.
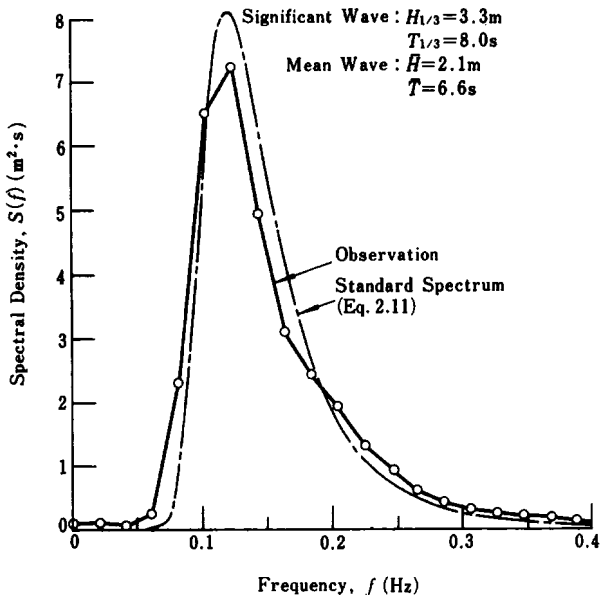
Fig. 2.10. Example of spectrum of sea waves.

slightly less than the frequency $f = 0.125$ Hz corresponding to the significant wave period.

The characteristics of the frequency spectra of sea waves have been fairly well established through analyses of a large number of wave records taken in various waters of the world. The spectra of fully developed wind waves, for example, can be approximated by the following standard formula:

$$S(f) = 0.257 H_{1/3}^2 T_{1/3}^{-4} f^{-5} \exp[-1.03(T_{1/3}f)^{-4}].$$ (2.10)

The dash-dot line in Fig. 2.10 is the result of fitting Eq. (2.10) with the values of the significant wave height and period of the record. Although some difference is observed between the actual and standard spectra, partly because of the shallow water effect in the wave record which was taken at the depth of 11 m, the standard spectrum describes the features of the actual spectrum quite well.

Equation (2.10) is based on the proposal by Bretschneider[8] with adjustment of the coefficients by Mitsuyasu.[9] There are several other expressions used as standard forms of the frequency spectrum, e.g., those of Pierson and Moskowitz,[10] Mitsuyasu,[11] Hasselmann *et al.*,[12] Ochi and Hubble,[13] etc. The formula of Pierson and Moskowitz includes the wind velocity as the principal parameter, because it was derived for the purpose of wave prediction in the ocean. But its expression can be converted into an equation equivalent to Eq. (2.10) by introducing the wave height and period, because the functional dependence with respect to frequency is the same. The coefficients in Eq. (2.10) have been so set by Mitsuyasu to yield the relation of $T_p \simeq 1.05 T_{1/3}$, which was derived by his field measurements (T_p denotes the wave period corresponding to the frequency f_p at the spectral peak, or $T_p = 1/f_p$). However, a number of later measurements suggests the relation of $T_p \simeq 1.1 T_{1/3}$ as more appropriate for wind waves. With further adjustment on the relation of the significant wave height and total wave energy, the following alternative formula has been proposed by the author[14] for the frequency spectrum of wind waves:

$$S(f) = 0.205 H_{1/3}^2 T_{1/3}^{-4} f^{-5} \exp[-0.75(T_{1/3}f)^{-4}].$$ (2.11)

Equations (2.10) and (2.11) are applied for the wind waves fully developed in the ocean. Wind waves rapidly developed in a relatively restricted water by very strong wind usually exhibit the spectral peak much sharper than that given by Eqs. (2.10) and (2.11). This feature has been taken up by Hasselmann *et al.*[12] in their proposal of wave spectrum, which was based on the results of

the joint wave observation program for the North Sea (referred to as JON-SWAP). The JONSWAP spectrum includes the wind speed as the parameter for the purpose of wave forecasting, but it can be rewritten in approximate form in terms of the parameters of wave height and period as follows[14]:[b]

$$S(f) = \beta_J H_{1/3}^2 T_p^{-4} f^{-5} \exp[-1.25(T_p f)^{-4}] \, \gamma^{\exp[-(T_p f - 1)^2/2\sigma^2]}, \qquad (2.12)$$

in which

$$\beta_J = \frac{0.0624}{0.230 + 0.0336\gamma - 0.185(1.9 + \gamma)^{-1}} \, [1.094 - 0.01915 \ln\gamma], \quad (2.13)$$

$$T_p \simeq T_{1/3}/[1 - 0.132(\gamma + 0.2)^{-0.559}], \qquad (2.14)$$

$$\sigma = \begin{cases} \sigma_a : f \leq f_p, \\ \sigma_b : f \geq f_p, \end{cases} \qquad (2.15)$$

$$\gamma = 1 \sim 7 \text{ (mean of 3.3)}, \ \sigma_a \simeq 0.07, \ \sigma_b \simeq 0.09.$$

The JONSWAP spectrum is characterized by a parameter γ which is called the peak enhancement factor; this controls the sharpness of the spectral peak. For $\gamma = 1$, Eq. (2.12) reduces to Eq. (2.11). For $\gamma = 3.3$, which is the mean value determined for the North Sea, the peak value of the spectral density function becomes 2.1 times higher than that of Eq. (2.11) for the same significant wave height and period.

In the shallow water area, the frequency spectrum tends to exhibit the attenuation of the spectral density at the high frequency region more gradual than that of the spectrum described by Eqs. (2.10) to (2.12). The TMA spectrum proposed by Bouws *et al.*[15] incorporates such a feature: some of its characteristics is discussed in Ref. 24. The flexibility in spectral shape can be realized by using the Wallops spectrum proposed by Huang *et al.*[16] The Wallops spectrum has been rewritten by the author[14] in terms of the parameters of wave height and period as follows:

$$S(f) = \beta_W H_{1/3}^2 T_p^{1-m} f^{-m} \exp\left[-\frac{m}{4}(T_p f)^{-4}\right], \qquad (2.16)$$

---

[b]The original spectral formula was integrated over the range $f = 0$ to $f = 6f_p$ for various values of γ. The integrated values were correlated to $H_{1/3}$ of simulated wave records together with Eq. (2.33) and Tables 2.3 and 2.4 to appear later, and the coefficient of proportionality was empirically determined as a function of γ.

in which

$$\beta_W = \frac{0.0624}{4^{(m-5)/4}\,\Gamma[(m-1)/4]}\left[1 + 0.7458(m+2)^{-1.057}\right], \qquad (2.17)$$

$$T_p \simeq T_{1/3}/\left[1 - 0.283(m - 1.5)^{-0.684}\right]. \qquad (2.18)$$

For $m = 5$, Eq. (2.16) reduces to Eq. (2.11). The symbol Γ in Eq. (2.17) denotes the gamma function.

The spectrum of swell is transformed from that of wind waves through its propagation over a long distance after it has left the wave generating area. The process of velocity dispersion (first discussed by Pierson, Neumann and James[17]) takes place during the swell propagation, because the low frequency wave components propagate faster than the high frequency components. The swell observed at a fixed station has a spectrum restricted to a narrow frequency range. Thus, the swell spectrum exhibits a peak much sharper than that of wind waves.

According to the analysis of swell which was generated off New Zealand, propagated over the distance of some 9000 km to the Pacific coast of Costa Rica and still maintained the significant wave height of about 3 m,[18] the swell spectral peaks were equivalent to the JONSWAP spectra of Eq. (2.12) with $\gamma = 8 \sim 9$, and to the Wallops spectra of Eq. (2.16) with $m = 8 \sim 10$, on the average. Thus, the swell spectrum for engineering applications may be approximated by the JONSWAP spectra of Eq. (2.12) with the peak enhancement factor being chosen between $\gamma = 3 \sim 10$, depending on the distance traveled.

Actual wave spectra usually exhibit some deviations from these standard forms. In particular, when swell coexists with wind waves, a secondary peak appears at the frequency corresponding to the representative period of swell or wind waves, depending on their relative magnitudes. In some cases, not only bi-modal but also tri-modal frequency spectra can be observed. The standard spectra proposed by Ochi and Hubble[13] can represent bi-modal spectra by means of 11 patterns which were developed from a data base of 800 ocean wave spectra. When the representative heights and periods of wind waves and swell are given *a priori*, the spectrum of the resultant sea state can be estimated by linearly superposing the standardized spectra of wind waves and swell.

2.3.2 Directional Wave Spectra

(A) General

Sea waves cannot be adequately described by using the frequency spectrum alone. Irregular waves specified solely by the frequency spectrum, if viewed from above in a manner similar to Fig. 2.1, would appear as so-called long-crested waves which have straight and parallel crestlines. The patterns of the wave crests, as shown in Fig. 2.1, imply the existence of many component waves propagating in various directions. The concept of directional spectrum is therefore introduced to describe the state of superimposed directional components. The directional spectrum represents the distribution of wave energy not only in the frequency domain but also in direction (angle θ). It is generally expressed as

$$S(f, \theta) = S(f) G(\theta|f), \tag{2.19}$$

where $S(f, \theta)$ is the directional wave spectral density function or simply the directional wave spectrum, and $G(\theta|f)$ is the directional spreading function, alternatively called the spreading function, the angular distribution function, or the directional distribution.

The function $G(\theta|f)$, which represents the directional distribution of wave energy in direction, has been found to vary with frequency. Therefore, the function $G(\theta|f)$ contains the frequency variable f. The directional spreading function carries no dimensions[c] and is normalized as

$$\int_{-\pi}^{\pi} G(\theta|f) \, d\theta = 1. \tag{2.20}$$

Thus the frequency spectrum $S(f)$ gives the absolute value of the wave energy density, while the function $G(\theta|f)$ represents the relative magnitude of directional spreading of wave energy.

(B) Directional spreading function of the Mitsuyasu-type

Knowledge of the directional distribution of the energy of sea waves is still limited because of the difficulty in making reliable field measurements. Techniques of field measurements and analyses will be discussed in Sec. 10.3. Only a few reports which give the results of measurements of directional spectra of

---

[c]However, the directional spreading function can be thought of as having the units of inverse angle, such as rad^{-1}.

ocean waves are available. Therefore, the establishment of a standard functional form for the directional wave spectrum has not been achieved yet, in contrast to the case of frequency spectrum. Nonetheless, Mitsuyasu et al.[20] have proposed the following function on the basis of their detailed field measurements with a special cloverleaf-type instrument buoy, as well as other available data:

$$G(\theta|f) = G_0 \cos^{2s}\left(\frac{\theta}{2}\right), \qquad (2.21)$$

where θ is the azimuth measured counterclockwise from the principal wave direction. In this expression, G_0 is a constant introduced to satisfy the condition of Eq. (2.16); i.e.,

$$G_0 = \left[\int_{\theta_{\min}}^{\theta_{\max}} \cos^{2s}\left(\frac{\theta}{2}\right)\right]^{-1}, \qquad (2.22)$$

and s is a parameter related to the frequency as further discussed below. If the range of the angle is $\theta_{\min} = -\pi$ and $\theta_{\max} = \pi$, the constant G_0 becomes

$$G_0 = \frac{1}{\pi} 2^{2s-1} \frac{\Gamma^2(s+1)}{\Gamma(2s+1)}, \qquad (2.23)$$

where Γ denotes the Gamma function. For example, by setting $s = 10$, G_0 becomes about 0.9033, and the directional spreading function is calculated as shown by the solid line in Fig. 2.11. The cumulative value of $G(\theta|f)$ from $\theta = -\pi$ is also shown in Fig. 2.11 as the dash-dot line. From this cumulative distribution of $G(\theta|f)$, it is observed that about 85% of the wave energy is contained in the angular range of $\pm 30°$.

The directional spreading function of Mitsuyasu et al.[19] has the features that the parameter s representing the degree of directional energy concentration takes a peak value around the frequency of the spectral peak, and that the value of s decreases as the value of the frequency moves away from that of the spectral peak toward both lower and higher frequencies. That is to say, the directional spreading of wave energy is narrowest around the spectral peak frequency. Although the original proposal of Mitsuyasu et al. relates the spreading parameter s to the wind speed U, Goda and Suzuki[20] have rewritten the original equation into the following form by introducing the peak value of s, denoted as $s_{\max}$, as the principal parameter for the purpose of engineering applications:

$$s = \begin{cases} (f/f_p)^5 s_{\max} & : f \leq f_p, \\ (f/f_p)^{-2.5} s_{\max} & : f \geq f_p. \end{cases} \qquad (2.24)$$
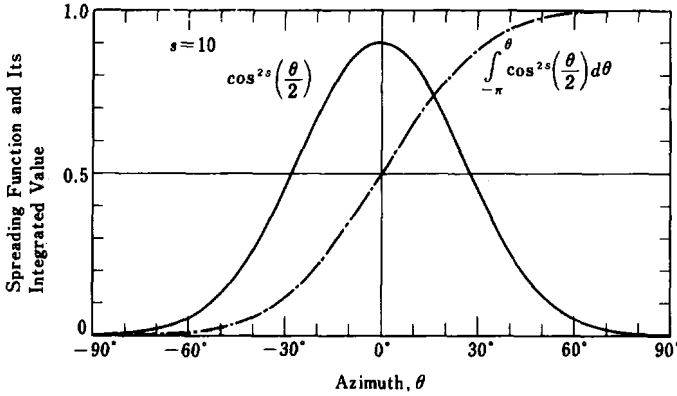
Fig. 2.11. Example of directional spreading function.

Here, f_p denotes the frequency at the spectral peak and is related to the significant wave period as $f_p = 1/(1.05T_{1/3})$ for the case of Bretschneider–Mitsuyasu frequency spectrum. The relation between f_p and $T_{1/3}$ for other frequency spectra can be obtained from Eqs. (2.14) and (2.18). Figure 2.12 illustrates the directional spreading function at various frequencies $f^* = f/f_p$ for $s_{max} = 20$. The range of the energy distribution is set as $-\pi/2 \leq \theta \leq \pi/2$ and the normalization constant G_0 is evaluated by numerical integration for each directional spreading function.
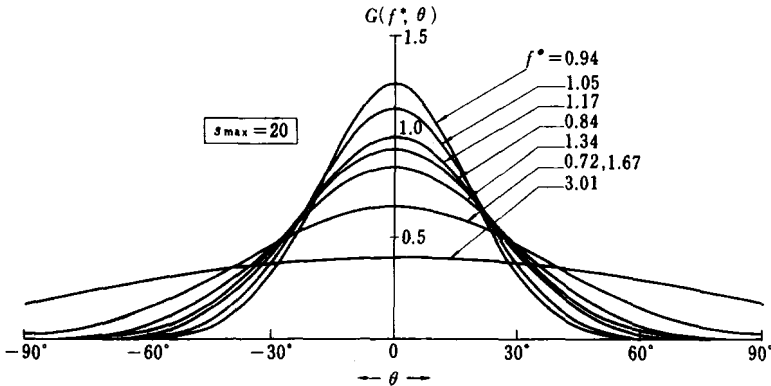
Fig 2.12. Example of Mitsuyasu-type spreading function for $s_{max} = 20$.

(C) *Estimation of the spreading parameter s_{max}*

The degree of directional spreading of wave energy greatly affects the extent of wave refraction and diffraction. This will be discussed in Chapter 3. Thus, the estimation of the value of the parameter s_{max} requires careful study of the nature of the waves at the design site. The observations by Mitsuyasu *et al.*[20] have shown that the peak value s_{max} increases as the parameter $2\pi f_p U/g$, which represents the state of wind wave growth, decreases or as the wind waves grow. They introduced the relation

$$s_{max} = 11.5 \left(2\pi f_p U/g\right)^{-2.5}, \tag{2.25}$$

where U denotes the wind speed.

On the other hand, Wilson's formula V[21] for the growth of wind waves suggests that the decrease of $2\pi f_p U/g$ can be related to the decrease of deepwater wave steepness H_0/L_0. By utilizing Wilson's formula, s_{max} can be related to H_0/L_0 by means of Eq. (2.25). Figure 2.13 shows the result of such a calculation.[20] The portion of the result in the range $H_0/L_0 < 0.026$, where Wilson's formula is not applicable, is an extrapolation using the slope of the curve drawn with the solid line. Qualitatively speaking, the inverse proportionality between s_{max} and H_0/L_0 in the range of swell is expected, as the pattern of wave crests should become long-crested as the swell propagates. The computer simulated crest patterns of Fig. 2.1 also demonstrates the tendency of long-crestedness with increase of s_{max}.

The curve in Fig. 2.13 is an estimation of the mean relationship between s_{max} and H_0/L_0. Actual wave data would show a wide scatter around the curve of Fig. 2.13, as Wilson's formula itself represents the mean relation of wind wave growth derived from data with a fairly large scatter. Consideration of such scatter in the data and other factors leads to the recommendation of the following values of s_{max} for engineering applications until the time when the nature of the directional wave spectrum becomes clear on the basis of detailed field observation[20]:

(i) Wind waves: $\qquad\qquad\qquad\qquad\quad s_{max} = 10,$

(ii) Swell with short decay distance: $\qquad s_{max} = 25,$

$\qquad$ (with relatively large wave steepness)

$$\left. \begin{array}{l} \\ \\ \\ \\ \\ \end{array} \right\} \qquad (2.26)$$

(iii) Swell with long decay distance: $\qquad s_{max} = 75.$

$\qquad$ (with relatively small wave steepness)
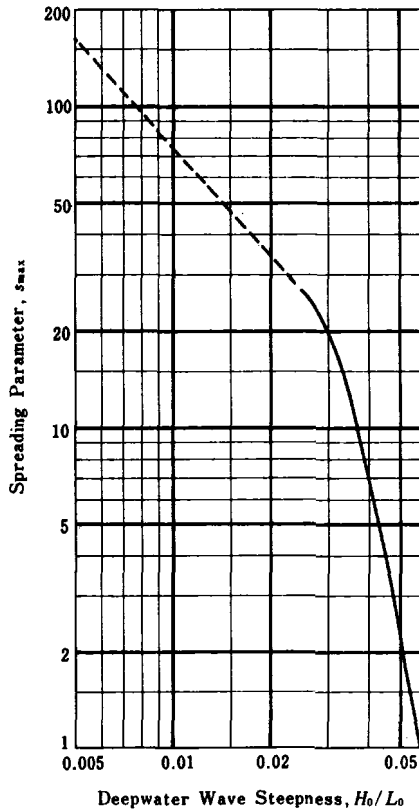
Fig. 2.13. Relationship between spreading parameter and deepwater wave steepness.[20]

Values in (2.26) as well as the relationship shown in Fig. 2.13 are to be applied to deepwater waves. In water of finite depth, where structures are to be built, waves have transformed under the effect of wave refraction which result in longer wave crests and reduced dispersion in wave directions. The directional wave spectrum also transforms accordingly. The degree of wave transformation by refraction depends on the bathymetry of the seabed. In an area where the seabed topography can be represented with straight, parallel depth-contours, the variation of the directional spreading function can be treated by means of an apparent increase in the value of s_{max}, as shown in Fig. 2.14.[20] In this figure, $(\alpha_p)_0$ denotes the angle of incidence of the deepwater waves and L_0 appearing in the abscissa is the length of the deepwater waves corresponding
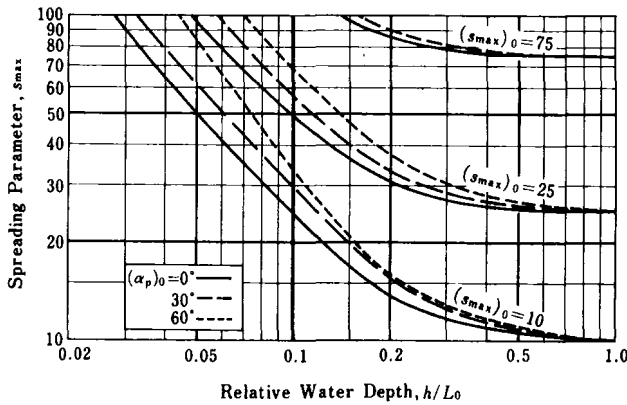
Fig. 2.14. Estimation of spreading parameter $s_{\max}$ in shallow water area.[20]

to the significant wave period; it is calculated as $L_0 = 1.56\,T_{1/3}^2$ in the units of meters and seconds. As the effect of the incident angle $(\alpha_p)_0$ on $s_{\max}$ is seen to be small in Fig. 2.14, this figure would appear to be applicable to a seabed of general topography as a reasonable approximation.

Example 2.2

Estimate the value of $s_{\max}$ when wind waves of $H_{1/3} = 6$ m and $T_{1/3} = 10$ s reach water of depth $h = 15$ m.

Solution

The deepwater wavelength corresponding to the significant wave period is $L_0 = 156$ m, and the deepwater wave steepness is fairly large, taking the value $H_0/L_0 \simeq 0.04$. The value of $s_{\max}$ in deepwater is thus estimated as $s_{\max} = 10$. Because $h/L_0 \simeq 0.096$ at the specified water depth, the spreading parameter $s_{\max}$ is estimated to increase to $25 \sim 35$ according to Fig. 2.14.

(D) *Cumulative distribution curve of wave energy*

The characteristics of the directional wave spectrum can also be expressed from the viewpoint of the directional distribution of total wave energy. The cumulative relative energy $P_E(\theta)$ is defined for this purpose as follows[20]:

$$P_E(\theta) = \frac{1}{m_0} \int_{-\pi/2}^{\theta} \int_0^{\infty} S(f,\theta)\,df\,d\theta\,, \tag{2.27}$$

where θ is the azimuth measured counterclockwise from the principal wave direction and m_0 denotes the representative value of the total wave energy and is given by

$$m_0 = \int_0^\infty \int_{-\pi/2}^{\pi/2} S(f,\theta)\, df\, d\theta. \tag{2.28}$$

The range of integration in the azimuth is set as $[-\pi/2, \pi/2]$ because the wave components moving in the direction opposite to the principal wave direction are discarded in most designs of maritime structures.
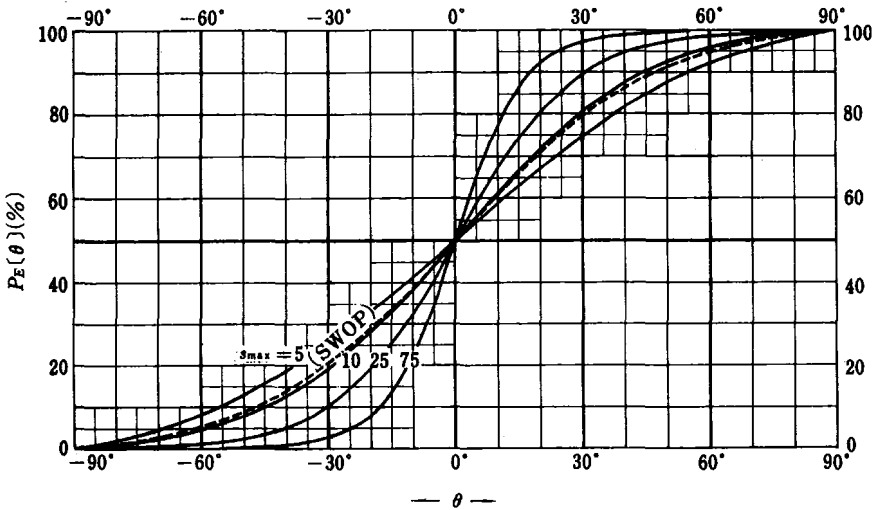
Fig. 2.15. Cumulative distribution of relative wave energy with respect to azimuth from principal wave direction.[20]

Figure 2.15 shows the calculated result for the cumulative distribution of relative wave energy with respect to direction.[20] The frequency spectrum of Eq. (2.10), the directional spreading function of Eq. (2.21) and the spreading parameter of Eq. (2.24) were employed to obtain Fig. 2.15. The cumulative distribution curves for $s_{\max} = 5, 10, 25$ and 75 are given, as well as the curve for the direction spreading function of SWOP, which will be discussed in the next subsection.

Example 2.3

Estimate the ratio of wave energy contained in the range of $\pm 15°$ from the principal wave direction for wind waves with $s_{\max} = 10$.

Solution

By reading off the values of the cumulative distribution curves of $s_{\max} = 10$ in Fig. 2.15 at $\theta = 15°$ and $\theta = -15°$, we obtain

$$\Delta E = P_E(15°) - P_E(-15°) = 0.67 - 0.33 = 0.34\,.$$

That is, 34% of the total energy is contained in the range between $\pm 15°$.

The above example may appear to be in disagreement with the cumulative distribution curve of Fig. 2.11. However, $s_{\max} = 10$ represents the peak value and the overall mean of s for the full frequency range remains low, while Fig. 2.11 represents the cumulative curve of $G(\theta|f)$ at a single frequency.

(E) *Other directional spreading functions*

The first practical formula for the directional spreading function was the cosine-squared-type of the following, which was used by Pierson *et al.*[22] for the analysis of directional wave refraction:

$$G(\theta|f) \equiv G(\theta) = \begin{cases} \dfrac{2}{\pi}\cos^2\theta & : |\theta| \le \dfrac{\pi}{2}\,, \\[2mm] 0 & : |\theta| > \dfrac{\pi}{2}\,. \end{cases} \tag{2.29}$$

The formula became well known as it was employed in the Pierson–Neumann–James method[17] for wave forecasting. It is still employed in many applications because of its simple functional form, although it does not seem to have been confirmed by field observation data of the directional wave spectrum.

On the other hand, the directional spectral analysis of sea surface contours obtained from a series of stereophographs has yielded the well-known directional spreading function of SWOP (Stereo Wave Observation Project)[23]:

$$G(\theta|\omega) = \frac{1}{\pi}\left\{ 1 + \left(0.50 + 0.82\exp\left[-\frac{1}{2}\left(\frac{\omega}{\omega_0}\right)^4 \right] \right)\cos 2\theta \right.$$

$$\left. + 0.32\exp\left[-\frac{1}{2}\left(\frac{\omega}{\omega_0}\right)^4 \right]\cos 4\theta \right\} \quad : |\theta| \le \frac{\pi}{2}\,, \tag{2.30}$$

in which $\omega = 2\pi f$, $\omega_0 = g/U_{5.0}$ and $U_{5.0}$ denotes the wind speed at an elevation of 5.0 m above the sea surface. This directional spreading function is similar to the Mitsuyasu-type in that the wave components in the high frequency region exhibit broad spreading of wave energy.

The directional spreading functions of Eqs. (2.29) and (2.30) produce almost the same distribution of the total energy as the Mitsuyasu-type function with $s_{\max} = 10$, though the energy spread with frequency is not the same. The agreement in the directional distribution of total wave energy is one of the reasons for the proposal of $s_{\max} = 10$ for wind waves.

There are several other proposals for the directional spreading function, all of which disregard the frequency-dependent characteristics of spreading function for the sake of simplicity (refer to Ref. 24 for an overview of these functions).

2.4 Relationship between Wave Spectra and Characteristic Wave Dimensions

2.4.1 *Relationship between Wave Spectra and Wave Heights*

The representation of sea waves with characteristic heights and period parameters and the spectral description of sea waves reflect two aspects of the same physical phenomenon, though they look quite different. It is possible to relate the two representations to each other. For example, spectral information for engineering applications can be obtained from the data of the significant wave by adopting one of the frequency spectra of Eqs. (2.10) to (2.16) and by combining the directional spreading function of Eq. (2.21) or other spreading functions.

It is also possible to estimate the heights and periods of representative waves from the wave spectrum. First, the representative value of the total wave energy m_0 is obtained by integrating the directional wave spectrum in the full frequency and directional ranges as given by Eq. (2.28). The integral, which has the units of m^2, cm^2, or similar dimensions, is by definition of the wave spectrum equal to the variance of the surface elevation. Thus,

$$m_0 = \overline{\eta^2} = \lim_{t_0 \to \infty} \frac{1}{t_0} \int_0^{t_0} \eta^2 dt. \tag{2.31}$$

The root-mean-square (rms) value of the surface elevation is then given by

$$\eta_{\text{rms}} = \sqrt{\overline{\eta^2}} = \sqrt{m_0} \,. \tag{2.32}$$

This rms value bears a certain relationship to the heights of representative waves when the wave height follows the Rayleigh distribution. In particular,

$$H_{1/3} = 4.004\eta_{\text{rms}} = 4.004\sqrt{m_0} \,. \tag{2.33}$$

The proportionality between the significant wave height and the rms surface elevation has been confirmed by many wave observation data taken throughout the world. The coefficient of proportionality is slightly different from that derived via the Rayleigh distribution. The significant wave height is better expressed by the mean relationship $H_{1/3} \simeq 3.8\sqrt{m_0}$ for deep water.[25] However, with decrease in water depth, the coefficient of proportionality tends to increase to a value of 4.0 or greater.[26]

To clarify the definition of the significant wave height, the IAHR Working Group on Wave Generation and Analysis[27] has proposed to use the notation of H_{m0} when estimated by m_0 or H_σ when estimated by η_{rms}: the significant wave height calculated from the zero-upcrossing or zero-downcrossing method is recommended to be denoted as $H_{1/3,\,u}$ or $H_{1/3,\,d}$.

The wave heights observed in the sea tend to indicate a distribution slightly narrower than the Rayleighan. Forristall,[28] for example, proposed the following function for the probability of exceedance:

$$P(\xi) = \exp[-\xi^{-2.126}/8.42] \quad : \xi = H/\eta_{\text{rms}} \,. \tag{2.34}$$

With the above equation, the statistical prediction of $H_{\max}$ becomes slightly smaller than those given by Eqs. (2.4) to (2.7). The coefficient of proportionality in Eq. (2.33) also becomes smaller than 4.0.

Such a departure of the wave heights from the Rayleigh distribution is due to the spread of wave spectra over a wide frequency range, contrary to the assumption of the narrow-banded spectrum in the derivation of the Rayleigh distribution. The effect of spectral shape on the wave height distribution has been examined by the author[14] by means of the Monte Carlo simulation technique. Table 2.3 lists the results of numerical simulations for the mean values of various wave height ratios for the JONSWAP-type spectrum of Eq. (2.12) and the Wallops-type spectrum of Eq. (2.16). In the case of the JONSWAP-type spectrum, the wave height ratios gradually increase toward those of the

Table 2.3. Mean values of wave height ratios for the JONSWAP-type and Wallops-type spectra.

Wave Height Ratio	Wallops-type Spectrum				JONSWAP-type Spectrum			Rayleigh Distribution
	$m = 3$	$m = 5$	$m = 10$	$m = 20$	$\gamma = 3.3$	$\gamma = 10$	$\gamma = 20$	
$[H_{\max}/\eta_{\mathrm{rms}}]^*$	0.89*	0.93*	0.96*	0.96*	0.93*	0.94*	0.93*	1.00*
$H_{1/10}/\eta_{\mathrm{rms}}$	4.66	4.78	4.91	5.01	4.85	4.92	4.96	5.090
$H_{1/3}/\eta_{\mathrm{rms}}$	3.74	3.83	3.90	3.95	3.87	3.91	3.93	4.004
$\overline{H}/\eta_{\mathrm{rms}}$	2.36	2.45	2.49	2.50	2.46	2.48	2.50	2.507
$[H_{\max}/H_{1/3}]^*$	0.96*	0.97*	0.98*	0.98*	0.97*	0.96*	0.95*	1.00*
$H_{1/10}/H_{1/3}$	1.247	1.248	1.263	1.268	1.253	1.259	1.261	1.271
$H_{1/3}/\overline{H}$	1.584	1.565	1.561	1.577	1.573	1.576	1.577	1.597

Note: 1) The values listed in this table are based on the results of numerical simulations of wave profiles with given wave spectra in the frequency range of $f = (0.5 \sim 6.0)f_p$.
2) Figures with the mark * refer to the ratio to the theoretical values based on the Rayleigh distribution.

Rayleigh distribution as the peak enhancement factor γ becomes large. In the case of the Wallops-type spectrum, approach to the wave height ratios of the Rayleigh distribution is realized with the increase of the exponent m. The ratio $H_{1/3}/\eta_{\mathrm{rms}}$ is about 3.8 when $\gamma = 1$ or $m = 5$, which is in good agreement with the result of field measurement data.

The frequency spectrum of Eq. (2.10) has been adjusted so as to yield the result $m_0 = 0.0624H_{1/3}^2$ when it is integrated in the range $f = 0$ to $f = \infty$. In the case of Eqs. (2.11), (2.12) and (2.16), adjustments have been made on the basis of the relationship between $H_{1/3}$ and η_{rms} listed in Table 2.3. Thus, the frequency spectra have been connected with the significant wave height on the basis of Eq. (2.33) or Table 2.3. Inversely, the estimation of significant wave height based on a given wave spectrum is always possible by evaluating the integral m_0 with Eq. (2.28). Such operations for the wave height estimation from spectral information become necessary in the analysis of wave refraction, diffraction, etc., in which the transformation of the directional wave spectrum is principally computed. A slight adjustment to the relationship of Eq. (2.33) using the result of Table 2.3 is possible, but will not be practical in the computation of wave transformations because the wave spectrum changes its shape through the transformations. The heights of representative waves other than the significant wave height can be derived by means of Eqs. (2.3) to (2.6).

2.4.2 *Relationship between Wave Spectra and Wave Periods*

According to the statistical theory of random waves (see Sec. 9.3), the mean wave period defined by the zero-upcrossing method is given by the zeroth and second moments of the frequency spectrum as follows:

$$\overline{T} = \sqrt{m_0/m_2} \quad : m_2 = \int_0^\infty f^2 \, S(f) \, df \, . \tag{2.35}$$

This relationship is often utilized when period information is sought from data of the wave spectrum. However, there have been reports that Eq. (2.35) produces a period shorter than the period directly counted on wave profiles (about 83%, on the average according to Ref. 4), though some other reports indicate quasi-equality between the two mean periods.[25] One reason is the different performances of wave recording instruments, and another is the effect of wave nonlinearity, in that actual sea waves are not simply composed of an infinite number of infinitesimal independent wavelets but are also accompanied by some phase-locked harmonic components (cf. Sec. 9.5).

Table 2.4. Mean values of wave period ratios for the JONSWAP-type and Wallops-type spectra.

Wave Period Ratio	Wallops-type Spectrum				JONSWAP-type Spectrum		
	$m = 3$	$m = 5$	$m = 10$	$m = 20$	$\gamma = 3.3$	$\gamma = 10$	$\gamma = 20$
$T_{1/10}/T_p$	0.82	0.89	0.93	0.96	0.93	0.96	0.97
$H_{1/3}/T_p$	0.78	0.88	0.93	0.96	0.93	0.97	0.98
$\overline{T}/T_p$	0.58	0.74	0.89	0.95	0.80	0.87	0.91
$T_{max}/T_{1/3}$	1.07	0.99	0.99	0.99	0.99	0.99	0.99
$T_{1/10}/T_{1/3}$	1.06	1.00	0.99	1.00	1.00	1.00	1.00
$T_{1/3}/\overline{T}$	1.35	1.19	1.06	1.02	1.16	1.11	1.09

Note: The values listed in this table are based on the results of numerical simulations of wave profiles with given wave spectra in the frequency range of $f = (0.5 \sim 6.0)f_p$.

The main period parameter obtainable from a wave spectrum is the peak period T_p defined as the inverse of the peak frequency f_p. The period parameters defined by the zero-upcrossing (or zero-downcrossing) method such as $T_{1/3}$ cannot be derived from a wave spectrum theoretically. Their relationship with T_p must be established on the basis of many field data or by means

of numerical simulations. Table 2.4 is the result of a Monte Carlo simulation study with various wave spectral shapes.[14] As the spectral peak becomes sharp, the differences between various wave period parameters become small and these periods approach the peak period T_p. In the wave transformation analysis for refraction, diffraction, etc., the information on the period parameters other than T_p is often sought for. For this purpose, the relationship between $\bar{T}$ computed by Eq. (2.35) and the input period parameter, such as $T_{1/3}$, is first investigated for the input wave spectrum. This relationship is utilized for correlating $\bar{T}$ computed from the spectrum after transformation to other period parameters of interest.

References

1. Y. Goda, "A proposal of systematic calculation procedures for the transformations and actions of irregular waves," *Proc. Japan Soc. Civil Engrs.* **253** (1976), pp. 59–68 (*in Japanese*).
2. W. J. Pierson, Jr., "An interpretation of the observable properties of sea waves in term of the energy spectrum of the Gaussian record," *Trans. American Geophys. Union* **35** (5) (1954), pp. 747–757.
3. Y. Goda, "Effect of wave tilting on zero-crossing wave heights and periods," *Coastal Engineering in Japan* **29** (1986), pp. 79–90.
4. Y. Goda and K. Nagai, "Investigation of the statistical properties of sea waves with field and simulation data," *Rept. Port and Harbour Res. Inst.* **13** (1) (1974), pp. 3-37 (*in Japanese*).
5. M. S. Longuet-Higgins, "On the statistical distributions of the heights of sea waves," *J. Marine Res.* **IX** (3) (1952), pp. 245–266.
6. Y. Goda, "New wave pressure formulae for composite breakwaters," *Proc. 14th Int. Conf. Coastal Engrg.*, (Copenhagen, 1974), pp. 1702–1720.
7. For example, "Light," *Encyclopaedia Britannica* **14** (1964), p. 59.
8. C. L. Bretschneider, "Significant waves and wave spectrum, *Ocean Industry* Feb. 1968, pp. 40–46.
9. H. Mitsuyasu, "On the growth of spectrum of wind-generated waves (2) – spectral shape of wind waves at finite fetch," *Proc. Japanese Conf. Coastal Engrg.* (1970), pp. 1–7 (*in Japanese*).
10. W. J. Pierson, Jr. and L. Moskowitz, "A proposed spectral form for fully developed wind seas based on the similarity law of S. A. Kitaigorodskii," *J. Geophys. Res.* **69** (24) (1964), pp. 5181–5190.
11. H. Mitsuyasu, "On the growth of the spectrum of wind-generated waves (1)," *Rept. Res. Inst. Applied Mech., Kyushu Univ.* **XVI** (55) (1968), pp. 459–482.
12. K. Hasselmann *et al.*, "Measurements of wind-wave growth and swell decay during the Joint North Sea Wave Project (JONSWAP)," *Deutsche Hydr. Zeit Reihe A* (8°) **12** (1973).

13. M. K. Ochi and E. N. Hubble, "On six-parameter wave spectra," *Proc. 15th Int. Conf. Coastal Engrg.* (Hawaii, 1976), pp. 301–328.

14. Y. Goda, "Statistical variability of sea state parameters as a function of a wave spectrum," *Coastal Engineering in Japan* **31** (1) (1988), pp. 39–52.

15. E. Bouws, H. Gunther, W. Rosenthal and C. Vincent, "Similarity of the wind wave spectrum in finite depth water," *J. Geophys. Res.* **90** (C1) pp. 975–986.

16. N. E. Huang *et al.*, "A unified two-parameter wave spectral model for a general sea state," *J. Fluid Mech.* **112** (1981), pp. 203–224.

17. W. J. Pierson, Jr., G. Neumann and R. W. James, *Practical Methods for Observing and Forecasting Ocean Waves by Means of Wave Spectra and Statistics*, U.S. Navy Hydrographic Office, H. O. Pub. 603 (1955).

18. Y. Goda, "Analysis of wave grouping and spectra of long-travelled swell," *Rept. Port and Harbour Res. Inst.* **22** (1) (1983), pp. 3–41.

19. H. Mitsuyasu *et al.*, "Observation of the directional spectrum of ocean waves using a cloverleaf buoy," *J. Physical Oceanogr.* **5** (4) (1975) pp. 750–760.

20. Y. Goda and Y. Suzuki, "Computation of refraction and diffraction of sea waves with Mitsuyasu's directional spectrum," *Tech. Note of Port and Harbour Res. Inst.* **230** (1975), 45p. (*in Japanese*).

21. B. W. Wilson, "Numerical prediction of ocean waves in the North Atlantic for December, 1959," *Deutche Hydr. Zeit* **18** (3) (1965), pp. 114–130.

22. W. J. Pierson, Jr., J. J. Tuttle and J. A. Wooley, "The theory of the refraction of a short-crested Gaussian sea surface with application to the northern New Jersey coast," *Proc. 3rd Conf. Coastal Engrg.* (Cambridge, Mass., 1952), pp. 86–108.

23. For example, B. Kinsman, *Wind Waves* (Prentice-Hall, Inc., 1965), p. 401 and pp. 460–471.

24. Y. Goda, "A comparative review on the functional forms of directional wave spectrum," *Coastal Engineering Journal* **41** (1) (1999), pp. 1-20.

25. For example, Y. Goda, "A review on statistical interpretation of wave data," *Rept. Port and Harbour Res. Inst.* **18** (1) (1979), pp. 5–32.

26. Y. Goda, "A unified nonlinearity parameter of water waves," *Rept. Port and Harbour Res. Inst.* **22** (3) (1983), pp. 3–30.

27. The IAHR Working Group on Wave Generation and Analysis. "List of sea-state parameters," *J. Wtrwy., Port, Coast., and Ocn. Engrg.*, ASCE **115** (6) (1989), pp. 793–808.

28. G. Z. Forristall, "On the statistical distribution of wave heights in a storm," *J. Geophys. Res.* **83** (C5) (1978), pp. 2353–2358.

Chapter 3

Transformation and Deformation of Random Sea Waves

3.1 Wave Refraction

3.1.1 *Introduction*

In an area where the water depth is greater than about one-half of the wavelength, i.e., a region of deep water, waves propagate without being affected by the sea bottom. When waves enter into a region of shallower water, however, the direction of wave propagation gradually shifts and the wave crestlines are bent into the pattern of the depth contours of the sea bottom. This process is the phenomenon of water wave refraction, which is analogous to that of light and sound waves, and is produced by the spatial variation of propagation speed.

Figure 3.1 exhibits a crest pattern of young swell approaching the shoreline of a planar coast with the uniform slope of 1 on 100 from the depth 20 m to 0.1 m. This has been obtained by numerical simulation of spatial wave profiles by assuming the directional spreading parameter of $s_{max} = 25$ and the deepwater incident angle of 30°.[1] As waves approach the shoreline, wavelengths are shortened and waves become long-crested, relative to the local wavelength.

The variation of the wave direction by refraction for the case of regular waves can be estimated graphically by hand or by numerical computation with a digital computer.[a] Figure 3.2 shows an example of the variation of wave direction analyzed by means of the graphical method for regular waves with a period of 12 s incident from SSE to a hypothetical water area. The solid

---

[a]See Refs. 2 to 5 for details of the techniques of refraction analysis.
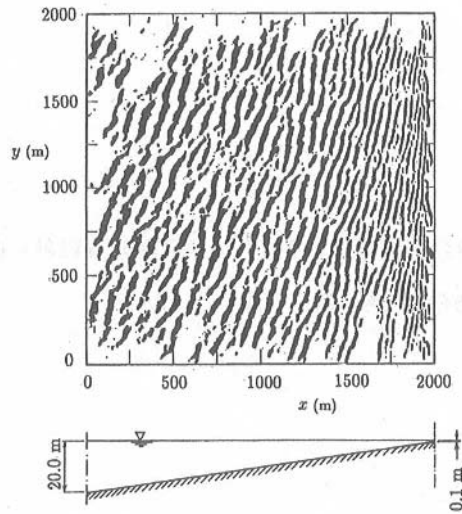
Fig 3.1.   Crest pattern of young swell being refracted in shoaling waters of planar beach
$(T_p = 8.01$ s).[1]
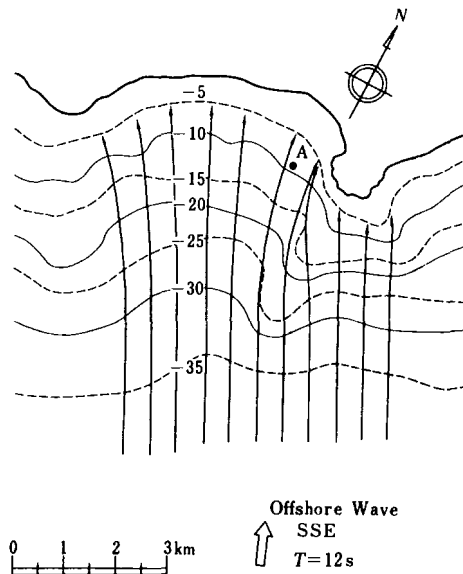
Fig. 3.2. Refraction diagram of regular waves.

lines with arrows are the wave rays, indicating the direction of wave prop-
agation. Such a diagram of wave rays is called a wave refraction diagram.
Although the distance between rays is constant in deep water (or in water of
uniform depth), the rays converge and diverge as they approach the shoreline,
depending on the local bottom features.

Since the flux of wave energy bounded by two rays is conserved if wave
energy dissipation is negligible, the variation in ray separation distance means
that the wave energy density varies inversely to the ray distance. Because the
wave energy is proportional to the square of the wave height, the variation in
wave height due to refraction is given by the following equation:

$$\frac{H}{H_o} = \sqrt{\frac{b_0}{b}} = K_r , \qquad (3.1)$$

where b denotes the distances between the two wave rays in the region of
interest and b_o is the distance between the same two rays in deep water. The
wave height ratio K_r is called the wave refraction coefficient. In the example
of Fig. 3.2, the refraction coefficient at Point A is estimated to be $K_r = 0.94$
for waves of $T = 12$ s incident from SSE.

3.1.2 *Refraction Coefficient of Random Sea Waves*

The above refraction coefficient corresponds to regular waves with constant
period and single direction of wave propagation. The variation in the heights
of real sea waves due to refraction is not necessarily well represented by a
refraction coefficient for regular waves. As discussed in Chapter 2, waves in
the real sea are composed of an infinite number of components having different
frequencies and directions. Therefore, the variation in the heights of sea waves
is determined by the contributions from all components, each component wave
undergoing the process of refraction individually. The fundamental equation
for the estimation of the refraction coefficient of random sea waves is given by

$$(K_r)_{\text{eff}} = \left[\frac{1}{m_{s0}} \int_0^\infty \int_{\theta\min}^{\theta\max} S(f,\theta)\, K_s^2(f)\, K_r^2(f,\theta)\, d\theta\, df \right]^{1/2} , \qquad (3.2)$$

in which

$$m_{s0} = \int_0^\infty \int_{\theta\min}^{\theta\max} S(f,\theta)\, K_s^2(f)\, d\theta\, df . \qquad (3.3)$$

The subscript "eff," standing for "effective," is used to denote quantities related to random waves, as opposed to regular waves. In the above, $S(f, \theta)$ denotes the directional wave spectrum, $K_s(f)$ is the wave shoaling coefficient to be introduced in Sec. 3.4, and $K_r(f, \theta)$ stands for the refraction coefficient of a component wave (i.e., a regular wave) with frequency f and direction θ. In actual calculations, the integration is replaced by a summation.

A simple way to make an approximate estimate of the refraction coefficient of random sea waves is to use the following equation:

$$(K_r)_{\text{eff}} = \left[\sum_{i=1}^{M} \sum_{j=1}^{N} (\Delta E)_{ij} \, (K_r)_{ij}^2\right]^{1/2} , \tag{3.4}$$

for which it is assumed that the effect of shoaling is negligible.

The term $(\Delta E)_{ij}$ in the above equation denotes the relative energy of component waves with ith frequency and jth direction, when the frequency range of the random sea waves is divided into segments running from $i = 1$ to M and the directional range is divided into segments running from $j = 1$ to N. That is,

$$(\Delta E)_{ij} = \frac{1}{m_0} \int_{f_i}^{fi+\Delta fi} \int_{\theta_j}^{\theta j + \Delta \theta j} S(f, \theta) d\theta \, df , \tag{3.5}$$

in which

$$m_0 = \int_0^\infty \int_{\theta \min}^{\theta \max} S(f, \theta) d\theta \, df . \tag{3.6}$$

In actual calculations, representative frequencies and directions of component waves must be selected. If the frequency spectrum of the Bretschneider–Mitsuyasu type as expressed by Eq. (2.10) in Sec. 2.3.1 is employed, the division of the frequency range can be made so as to equalize the wave energy in each frequency interval; note that Eq. (2.10) in Sec. 2.3.1 is integrable in closed form with respect to frequency. Such a division reduces the calculation time for the random refraction coefficient. The representative frequency in each interval is best determined as the mean of the second spectral moment of each interval so that the variation of wave period by refraction can be estimated with minimum error (because the mean wave period, Eq. (2.35), is given by the second moment of the frequency spectrum). The formula for the representative

frequency of the second spectral moment of each interval is[6]:

$$f_i = \frac{1}{0.9T_{1/3}} \left\{ 2.912M \left[\Phi \left(\sqrt{2 \ln \frac{M}{i-1}} \right) - \Phi \left(\sqrt{2 \ln \frac{M}{i}} \right) \right] \right\}^{1/2} , \quad (3.7)$$

in which $\Phi(t)$ is the error function defined by

$$\Phi(t) = \frac{1}{\sqrt{2\pi}} \int_0^t e^{-x^2/2} \, dx . \quad (3.8)$$

The representative frequencies by Eq. (3.7) have been converted to the wave periods listed in Table 3.1.

Table 3.1. Representative periods of component waves for refraction analysis.

Numbers of component waves	$T_i/T_{1/3}$						
	$i = 1$	$i = 2$	$i = 3$	$i = 4$	$i = 5$	$i = 6$	$i = 7$
3	1.16	0.90	0.54	–	–	–	–
4	1.20	0.98	0.81	0.50	–	–	–
5	1.23	1.04	0.90	0.76	0.47	–	–
7	1.28	1.11	1.00	0.90	0.81	0.69	0.43

For a rapid computation, the median frequency (the frequency which bisects the area of the wave spectrum in each interval) may be employed. It is given by

$$f_i = \frac{1}{0.9T_{1/3}} \left\{ \frac{0.675}{\ln[2M/(2i-1)]} \right\}^{1/4} = \frac{1.007}{T_{1/3}} \left\{ \ln[2M/(2i-1)] \right\}^{-1/4} . \quad (3.9)$$

When the representative frequencies are selected by either one of the above two methods, the relative energy of the component waves may be approximated with the following:

$$(\Delta E)_{ij} = \frac{1}{M} D_j . \quad (3.10)$$

The quantity D_j represents the ratio of the wave energy in each direction to the total energy. It is read off from the cumulative distribution curves of relative wave energy shown in Fig. 2.16 in Sec. 2.3. For a directional division with 16 or 8 point bearings, values of D_j have been prepared as listed in Table 3.2. If the directional range of component waves is limited to less than ± 90°, owing

to the topographic conditions at the site of interest, the values of D_j should be linearly increased so that the summation in the range of possible wave approaches will give unity. When the frequency division of the wave spectrum is different from that listed in Table 3.1, the energy ratio $(\Delta E)_{ij}$ must be computed by integrating the frequency spectrum and by evaluating the ratio of wave energy in each frequency interval.

Table 3.2. Ratio of wave energy in each direction to the total energy.

Direction of component waves	16-point bearing s_{max}			8-point bearing s_{max}		
	10	25	75	10	25	75
67.5°	0.05	0.02	0	—	—	—
45.0°	0.11	0.06	0.02	0.26	0.17	0.06
22.5°	0.21	0.23	0.18	—	—	—
0°	0.26	0.38	0.60	0.48	0.66	0.88
−22.5°	0.21	0.23	0.18	—	—	—
−45.0°	0.11	0.06	0.02	0.26	0.17	0.06
−67.5°	0.05	0.02	0	—	—	—
Total	1.00	1.00	1.00	1.00	1.00	1.00

The above assignment of relative wave energy by Eq. (3.10) and Table. 3.2 ignores the fundamental nature of the directional wave spectrum by neglecting the degree of directional spreading of wave energy with variation in the frequency. This technique should be reserved for situations when the weighted summation of Eq. (3.4) is done manually.

As an explanatory example, the refraction coefficient at the point A in Fig. 3.2 will be calculated for random sea waves. By employing three divisions in the frequency range, from Table. 3.1, the wave periods of the component waves are obtained as $T_1 = 14$ s, $T_2 = 11$ s, and $T_3 = 6.5$ s for $T_{1/3} = 12$ s. The directions of the component waves are chosen from a 16-point bearing within the range of $\pm 90°$ around the principal direction of SSE. The waves are assumed to be swell of relatively large wave steepness so that the spreading parameter s_{max} is set at the value of 25. The initial stage of the estimation process is to draw refraction diagrams and to estimate the refraction coefficient at the point A for all 21 component waves (three wave periods and seven

directions). The result is listed in the 2nd to 4th columns of Table 3.3. The second step is to calculate the sum $\sum_{i=1}^{M} K_r^2$ and to complete the 5th column of Table 3.3. Also, the wave energy ratio D_j is to be read from Table 3.2 for $s_{max} = 25$ and listed in the 6th column of Table 3.3. Then the products of the entries in the 5th and 6th columns divided by $M = 3$ are written in the 7th column. By summing the entries in the 7th column and by taking the square root, the refraction coefficient of random sea waves in this example is obtained as $(K_r)_{eff} = 0.94$. The refraction coefficient for the principal deepwater wave direction of SE or S can also be obtained by shifting the entry for D_j at the respective principal directions. The result becomes $(K_r)_{eff} = 0.94$ for SE and $(K_r)_{eff} = 0.89$ for S.

Table 3.3. Example of random wave refraction analysis.

Direction of component waves	K_r			$\sum K_r^2$	D_j	$\frac{D_j}{M} \sum K_r^2$
	14 s	11 s	6.5 s			
E	0.69	0.60	0.65	1.259	0.02	0.008
ESE	0.90	0.77	0.76	1.981	0.06	0.040
SE	1.07	1.11	0.95	3.280	0.23	0.251
SSE	1.11	0.86	0.95	2.874	0.38	0.364
S	0.64	0.78	0.99	1.998	0.23	0.153
SSW	0.84	0.95	1.02	2.649	0.06	0.053
SW	0.72	0.62	0.76	1.480	0.02	0.010

$$\sum \frac{D_j}{M} \sum K_r^2 = 0.879, \ (K_r)_{eff} = 0.938.$$

For comparison, the refraction coefficient corresponding to regular waves for the wave direction SSE is $K_r = 0.94$, which happens to be the same as the refraction coefficient found above for random sea waves from SSE. But the refraction coefficients of regular waves incident from SE and S are 1.10 and 0.70 respectively, which are seen to differ greatly from the value 0.94 found for the direction SSE. It is rather difficult, however, to believe that the wave conditions after refraction are so different for a change in the wave direction of only $\pm 22.5°$. The process of taking a weighted mean in Eq. (3.4) produces smoothing of the erratic values of the refraction coefficient as obtained for regular waves. Thus, by introducing the concept of directional wave spectrum, we obtain more realistic values for the refraction coefficient for random sea waves than those obtained for regular waves.

The prevailing direction of waves after undergoing refraction may be taken as that direction in the 7th column of Table 3.3 which has the maximum value. In the example of Table 3.3, the offshore wave direction which contains the greatest wave energy density after refraction is SSE. By referring to the refraction diagram of regular waves, the prevailing direction of the refracted waves at Point A is estimated to be N165°.

3.1.3 *Computation of Random Wave Refraction by Means of the Energy Flux Equation*

In addition to the above method of superposing refracted component waves, the refraction of random sea waves can be analyzed by numerically solving the equation for the flux of wave energy as described by the directional spectrum of waves in water of variable depth and topography (e.g., Refs. 7 to 9), which is due to Karlsson.[7] The fundamental equation takes the form

$$\frac{\partial}{\partial x}(Sv_x) + \frac{\partial}{\partial y}(Sv_y) + \frac{\partial}{\partial \theta}(Sv_\theta) = 0 \,, \tag{3.11}$$

where S denotes the directional wave spectral density and v_x, v_y and v_θ are given by

$$\left.\begin{array}{l} v_x = C_G \cos \theta \,, \\[2mm] v_y = C_G \sin \theta \,, \\[2mm] v_\theta = \dfrac{C_G}{C} \left(\dfrac{\partial C}{\partial x} \sin \theta - \dfrac{\partial C}{\partial y} \cos \theta \right) . \end{array}\right\} \tag{3.12}$$

The symbols C and C_G denote the phase and group velocities, respectively, and they are calculated with the following formulas for waves with period T and length L in water of depth h:

$$\left.\begin{array}{l} C = \dfrac{L}{T} = \dfrac{g}{2\pi} T \tanh \dfrac{2\pi h}{L} \,, \\[4mm] C_G = \dfrac{1}{2} \left[1 + \dfrac{4\pi h/L}{\sinh\left(4\pi h/L\right)} \right] C \,. \end{array}\right\} \tag{3.13}$$

The method has been applied to the case of wave refraction occurring at a spherical shoal as shown in Fig. 3.3, with a diameter of 40 m and water depth of 5 m at its top, set in water of uniform depth of 15 m.[9] The distributions of wave height and period by random wave refraction are shown in Fig. 3.4
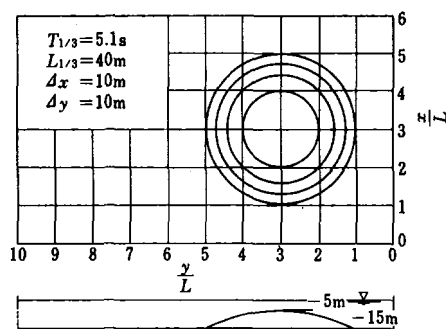
Fig. 3.3. Shape of spherical shoal.[9]
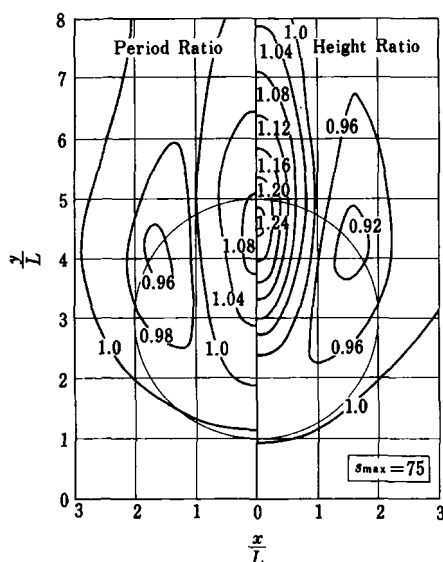
Fig. 3.4. Distributions of the ratios of heights and periods of random waves on a spherical shoal.[9]

for waves with $T_{1/3} = 5.1$ s. The directional wave spectrum was assumed to be the Bretschneider–Mitsuyasu frequency spectrum combined with the Mitsuyasu-type spreading function having $s_{max} = 75$. The right side of Fig. 3.4 gives the variation of refracted wave height, while the left side shows the variation of wave period. The transformation of random sea waves is generally

accompanied by some change in wave period because the directional spectrum varies through the wave transformation. Figure 3.4 is one such example.

The refraction of regular waves over this shoal has been solved by Ito *et al.*[10] with their numerical technique of wave propagation analysis. The result of the distribution of wave height is presented in Fig. 3.5. As seen in this figure, the refraction of regular waves often produces a significant spatial variation in the wave height. The computation of wave refraction using spectral components of various directions and frequencies brings forth the effect of smoothing such large spatial variations. Vincent and Briggs[11] have investigated the pattern of wave height behind an elliptical shoal in a laboratory for both regular and directional random waves. They reported that the most significant factor affecting the wave height distribution was the amount of directional spread.
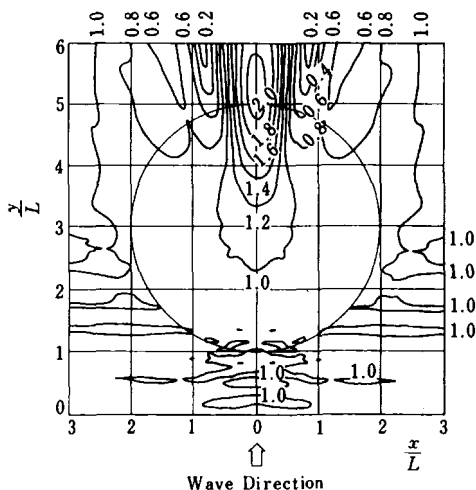
Fig. 3.5. Distribution of the height ratio of regular waves on a spherical shoal (after Ito *et al.*[10]).

Strictly speaking, waves over a shoal are affected not only by the refraction but also by the diffraction phenomenon, especially when wave caustics is formed by the crossing of wave rays over a shoal. A number of numerical schemes have been developed to solve such refraction-diffraction problems for regular waves (see Ref. 12). Even though the energy flux equation method of Eqs. (3.11) and (3.12) cannot take the diffraction effect into account, it provides a reasonable estimate of wave height for directional random waves

around a shoal, or over a sea bottom topography of such complexity that the conventional refraction analysis of regular waves will give the crossing of wave rays. It is especially so when the angular spread of incident spectrum is broad, as indicated by O'Reilly and Guza.[13]

3.1.4 *Wave Refraction on a Coast with Straight, Parallel Depth-Contours*

For the case of coastal water with straight, parallel depth-contours, the variation in the ray direction and the refraction coefficient of the component waves can be obtained analytically. Then, the computation of the refraction of random sea waves is rather easily made with the superposition method. The refraction coefficient of random sea waves and the variation in their predominant wave directions have been obtained as shown in Figs. 3.6 and 3.7, respectively.[9]
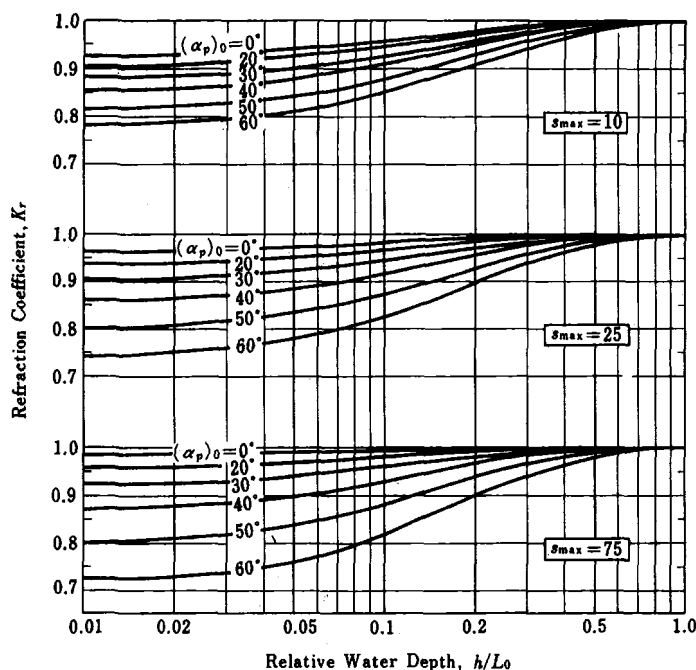
Fig. 3.6. Refraction coefficient of random sea waves on a coast with straight, parallel depth-contours.[9]
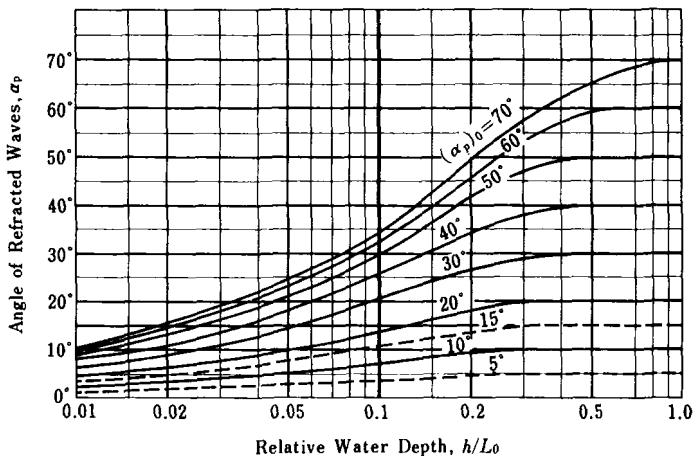
Fig. 3.7. Variation of predominant direction of random sea waves due to refraction on a coast with straight, parallel depth-contours.

The computation was made with the frequency and directional components of $M = N = 36$ for the directional spectrum, using the Bretschneider–Mitsuyasu frequency spectrum and the Mitsuyasu-type spreading function. The wavelength L_0 appearing in the abscissa of Figs. 3.6 and 3.7 is the deepwater wavelength corresponding to the significant wave period. The parameter $(\alpha_p)_0$ denotes the angle of incidence of the deepwater waves.

The refraction coefficient of random sea waves varies with the value of s_{max}, but the difference is less than several percent. The predominant direction of refracted waves, which was defined by Nagai[14] as the direction corresponding to the highest directional spectral density, is little affected by the value of s_{max}.

It should be noted in Fig. 3.6 that even normally incident waves experience a decrease in refraction coefficient as they propagate into shallow water. This is caused by refraction of the obliquely incident component waves on both sides of the principal direction of normal incidence, because waves described by means of a directional wave spectrum always contain component waves with directions different from the principal direction.

Example 3.1

Describe the condition of refracted waves at the water depths of 20 and 10 m, when swell with height of 2 m and period of 12 s is incident at an angle of 40° to a coast with straight, parallel depth-contours.

Solution

Referring to Eq. (2.26) in Sec. 2.3 with the information on swell condition, the spreading parameter s_{max} is set at 75. Since the deepwater wavelength corresponding to $T_{1/3} = 12$ s is $L_0 = 225$ m (refer to Table A.3 in the appendix), the relative water depth is $h/L_0 = 0.089$ at $h = 20$ m. The refraction coefficient is $K_r = 0.92$ by Fig. 3.6 and the predominant direction is $\alpha_p = 24°$ by Fig. 3.7. At the water depth of $h = 10$ m, $K_r = 0.90$ and $\alpha_p = 17°$ with $h/L_0 = 0.044$. The variation in predominant wave direction is illustrated in Fig. 3.8
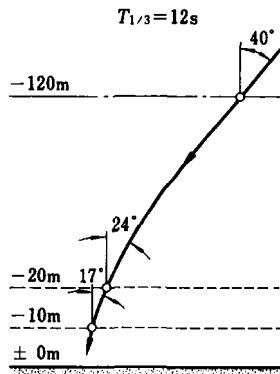
Fig. 3.8. Change in wave direction.

3.2 Wave Diffraction

3.2.1 *Principle of Random Wave Diffraction Analysis*

When water waves encounter an obstacle such as a breakwater, island, or headland during propagation, they pivot about the edge of the obstacle and move into shadow zone of the obstacle. This phenomenon is called the diffraction of water waves, and it is common with the other wave motions of sound, light, and electromagnetic waves. The spatial distribution of diffracted wave height of regular waves in uniform depth can be computed by means of the Sommerfeld solution based on velocity potential theory. The results are compiled as diagrams showing the distribution of the ratio of diffracted to incident wave heights, and are called diffraction diagrams. Conventional diagrams given in many references (e.g., Ref. 15) have been prepared for regular waves with constant period and single directional component. Direct application of such

conventional diagrams to real situations is not recommended, because they can lead to erroneous results.

The diffracted heights of real sea waves should be computed as follows by introducing the directional wave spectrum:

$$(K_d)_{\text{eff}} = \left[\frac{1}{m_0} \int_0^{\infty} \int_{\theta \min}^{\theta \max} S(f, \theta) \, K_d^2(f, \theta) \, d\theta \, df \right]^{1/2} , \qquad (3.14)$$

where $(K_d)_{\text{eff}}$ denotes the diffraction coefficient of random sea waves (i.e., the ratio of diffracted to incident heights of significant or other representative waves), $K_d(f, \theta)$ is the diffraction coefficient of component (regular) waves with frequency f and direction θ, and m_0 is the integral of the directional spectrum specified by Eq. (3.6).

The validity of the computation of random wave diffraction with Eq. (3.14) has been confirmed through simultaneous wave observations inside and outside the storm-surge breakwater at Nagoya Port.[15] Capacitance wave gauges were set at the point A outside and the point B inside the harbor as shown in Fig. 3.9. An example of the frequency spectra at both points is presented in Fig. 3.10. Because the breakwater is of the caisson type and reflects incident waves almost completely, the wave energy observed at the point A is considered to be the sum of incident and reflected wave energy. By taking one-half of the energy at the point A as that of the incident waves, the height and period of the incident waves were estimated as $H_{1/3} = 0.46$ m and $T_{1/3} = 2.8$ s. The wave direction was judged to be from SW on the basis of the observed wind direction. The spectrum of the diffracted waves was calculated for this wave condition, and the resultant spectrum was in good agreement with the observed spectrum at the point B. If the diffraction is calculated with the theory of regular waves,
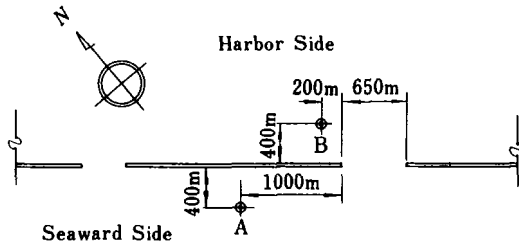
Fig. 3.9. Location of wave observation stations.
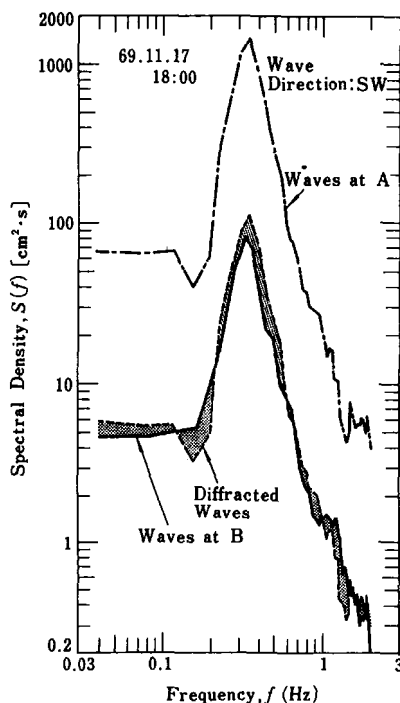
Fig. 3.10. Example of frequency spectrum of diffracted waves observed in the field.[16]

the diffraction coefficient becomes $K_d \simeq 0.07$ for the condition of $x/L \simeq 20$ and $y/L \simeq 31$ with the wavelength of $L \simeq 12$ m corresponding to the significant wave period. In terms of the spectral density, the theory of regular wave diffraction yields only 3% of the observed value.

3.2.2 *Diffraction Diagrams of Random Sea Waves*

Diffraction diagrams of random sea waves have been computed with Eq. (3.14), and they are shown in Figs. 3.11 to 3.15.[16] The directional wave spectrum employed is the combination of the Bretschneider–Mitsuyasu frequency spectrum and the Mitsuyasu-type spreading function. The integrations in Eq. (3.14) were replaced by summations over 10 frequency intervals by Eq. (3.7) and 20 to 36 directional intervals of equal spacing ($\Delta\theta = 9°$ to 5°). Figure 3.11 pertains to diffraction by a semi-infinite straight breakwater, whereas Figs. 3.12
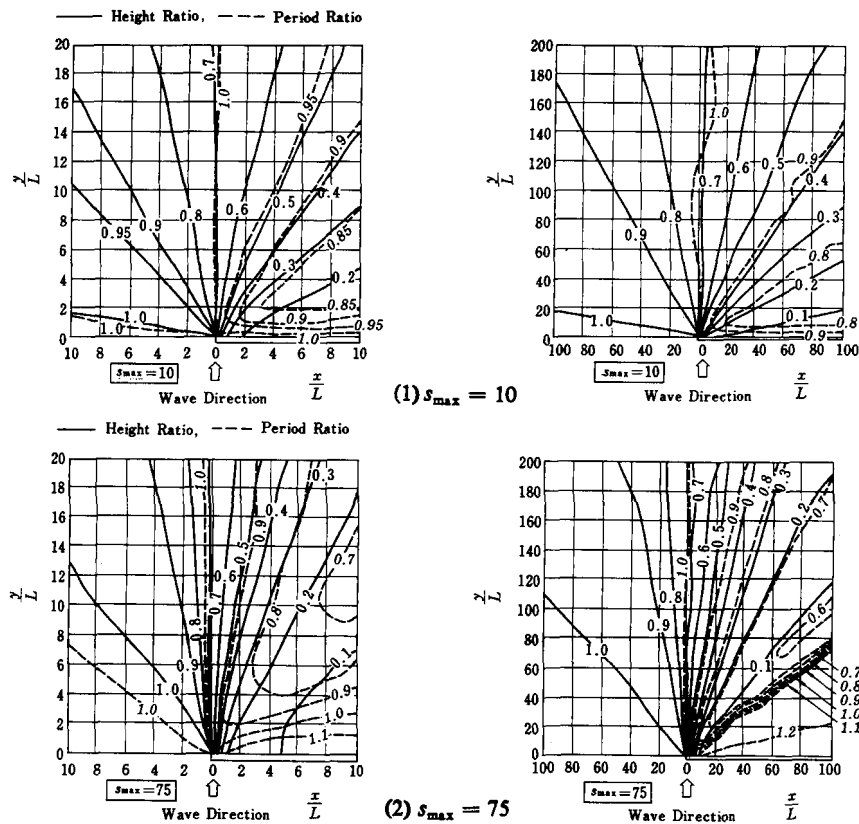
Fig. 3.11. Diffraction diagrams of a semi-infinite breakwater for random sea waves of normal incidence (solid lines for wave height ratio and dash lines for wave period ratio).[16]

(1) $s_{max} = 10$

(2) $s_{max} = 75$
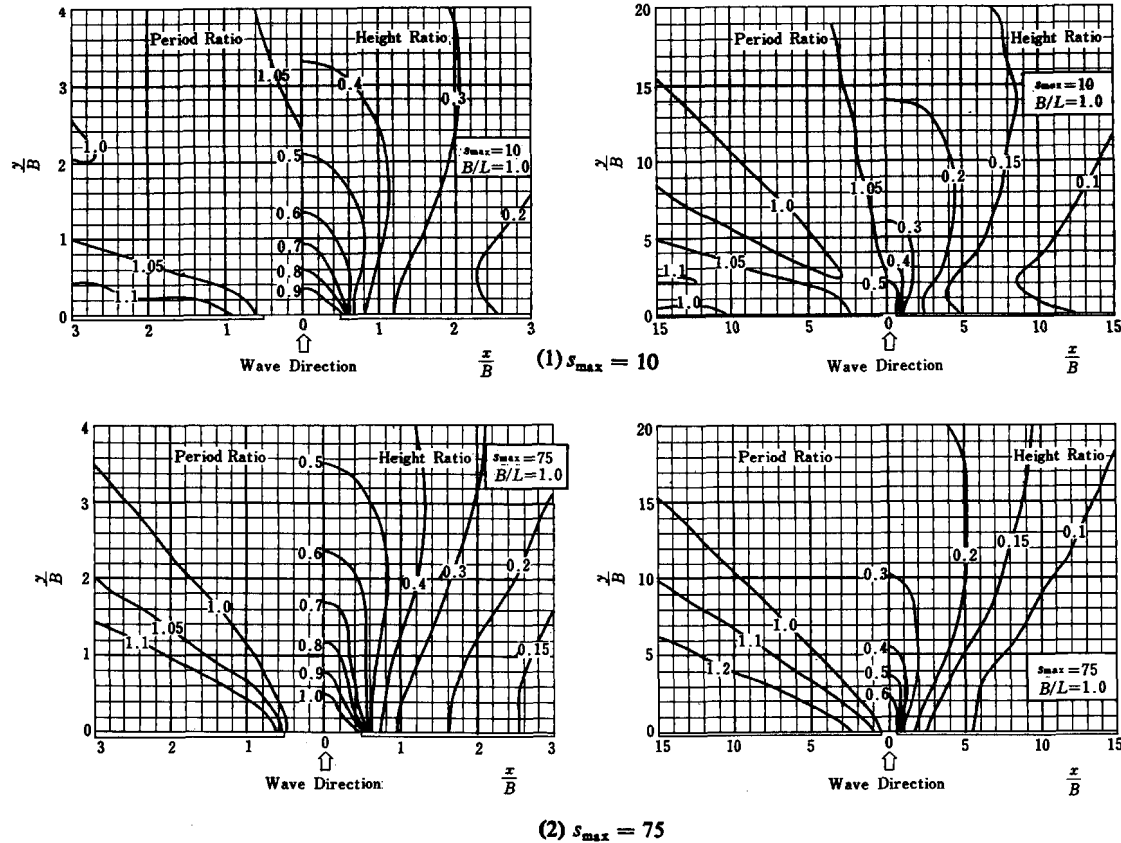
Fig. 3.12. Diffraction diagrams of a breakwater opening with $B/L = 1.0$ for random sea waves of normal incidence.[16]

(1) $s_{max} = 10$

(2) $s_{max} = 75$
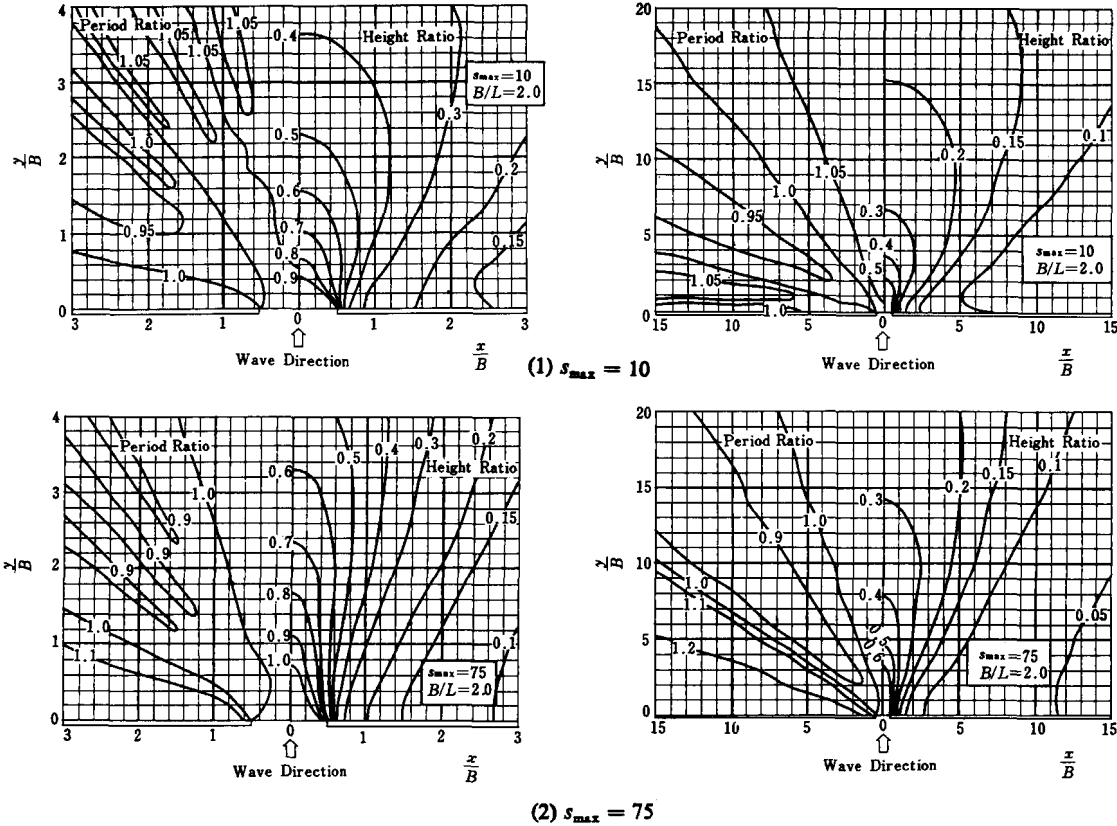
Fig. 3.13. Diffraction diagrams of a breakwater opening with $B/L = 2.0$ for random sea waves of normal incidence.[16]

(1) $s_{max} = 10$

(2) $s_{max} = 75$
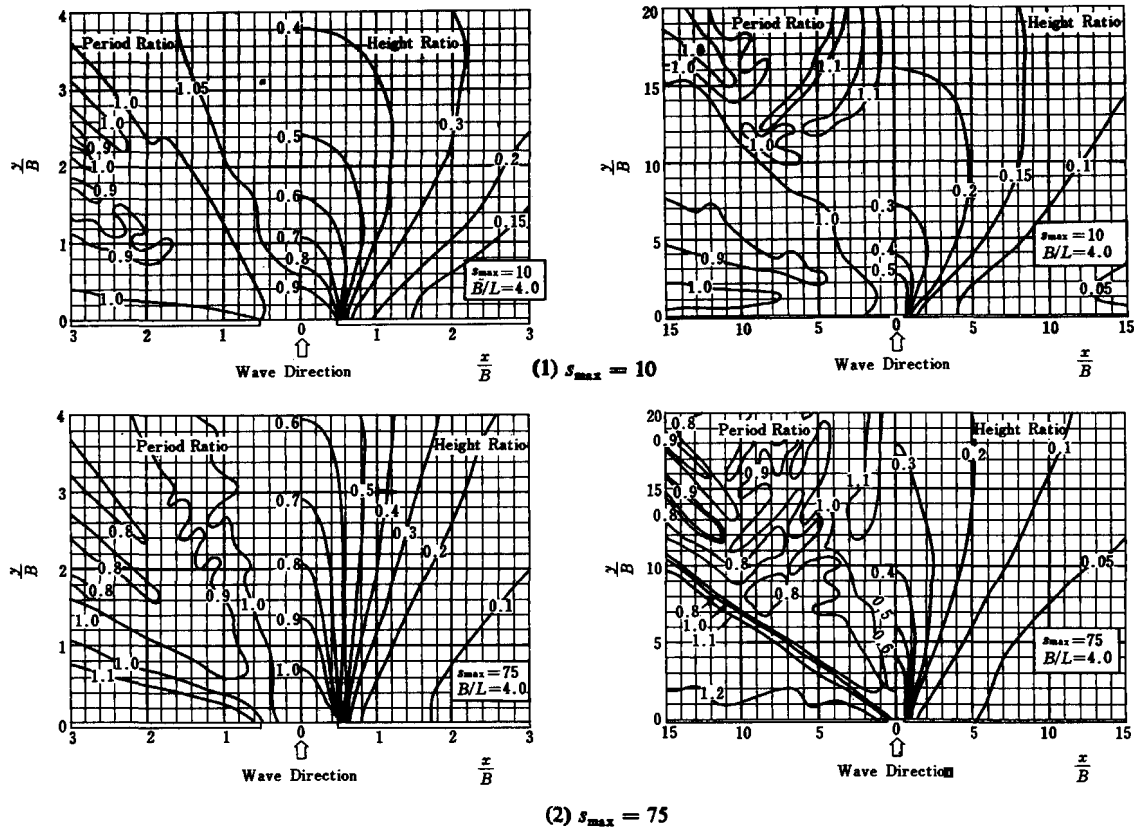
Fig. 3.14. Diffraction diagrams of a breakwater opening with $B/L = 4.0$ for random sea waves of normal incidence.[16]

(1) $s_{max} = 10$

(2) $s_{max} = 75$
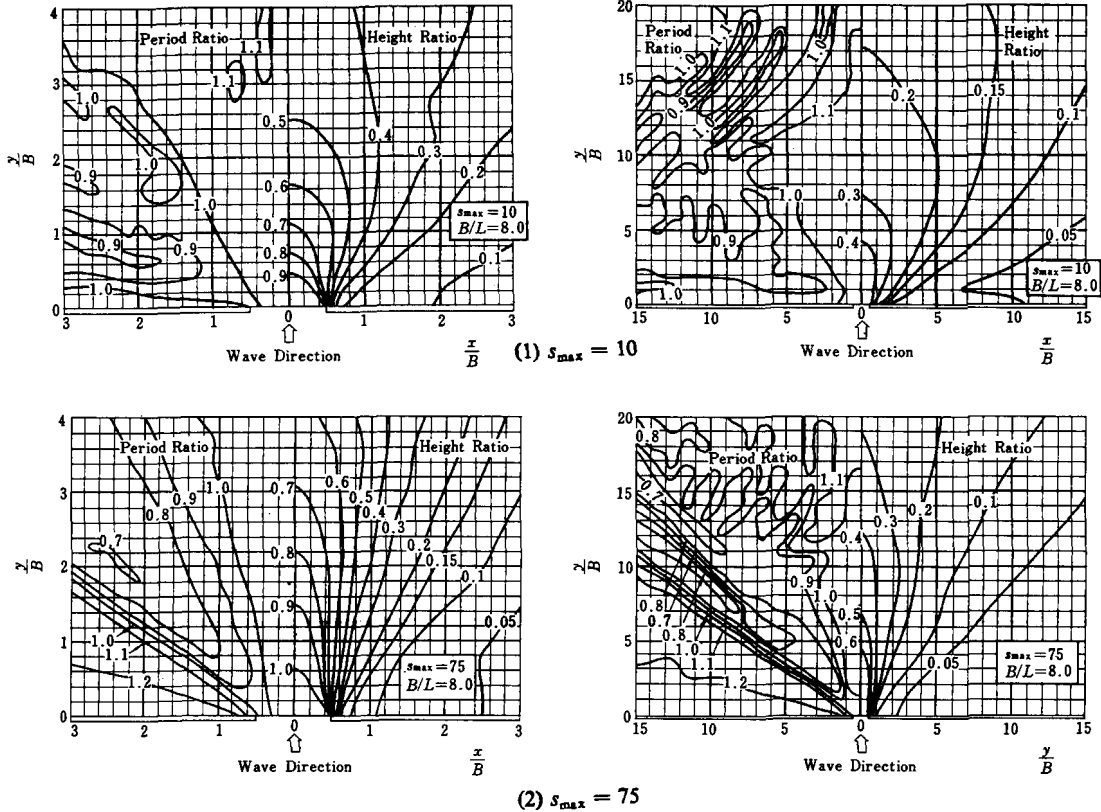
Fig. 3.15. Diffraction diagrams of a breakwater opening with $B/L = 8.0$ for random sea waves of normal incidence.[16]

to 3.15 are for diffraction from the opening between two semi-infinite straight breakwaters with the opening width being 1, 2, 4 and 8 times the wavelength corresponding to the significant wave periods. The wave direction is normal to the axis of the breakwaters. Each figure is composed of four diagrams for two values of s_{max} (10 and 75) in the near and distant areas.

This set of random wave diffraction diagrams shows not only variations in wave height but also variations in wave period. The variation in period is indicated with dash lines in Fig. 3.11 and on the left side of the diagrams of Figs. 3.12 to 3.15. The diffraction of random sea waves, especially those with a frequency-dependent directional spreading function, is characterized by changes in wave period in addition to wave height.

Another comment on Figs. 3.12 to 3.15 is that the horizontal coordinates are normalized by the opening with B instead of the wavelength L. By doing so, the difference in $(K_d)_{eff}$ for different values of the opening ration B/L appears much to be smaller than that given by plotting with the coordinates normalized by wavelengths.

The random diffraction coefficient values are quite different from those of regular waves. For example, the diffraction coefficient of random waves along the boundary of the geometric shadow (or the straight line from the tip of the breakwater parallel to the wave direction) takes the value of about 0.7, while regular wave diffraction theory gives a diffraction coefficient of about 0.5. The difference between the predictions increases in the sheltered area behind the breakwater, and would result in an underestimation of wave height there if diagrams for regular wave diffraction were employed. In the case of wave diffraction through an opening between breakwaters, the spatial variation of the diffraction coefficient is smoothed to some extent by the introduction of wave directionality. That is, the wave height ratio decreases in the area of direct wave penetration and increases in the sheltered area. As a result, the dependence of the diffracted wave height on the incident wave direction decreases.

As discussed above, there is considerable disparity between values of the diffraction coefficient computed for regular waves and for random sea waves. In addition to the example of Fig. 3.10, another example of wave diffraction from the field is shown in Fig. 3.16, illustrating the dissimilarity between regular and random wave. The data were taken by the Akita Port Construction Office, the First District Port Construction Bureau, Ministry of Transport, Japan.[17] Figure 3.16 compares the ratio of wave height inside to outside a single breakwater, measured with wave recorders of the inverted echo-sounder
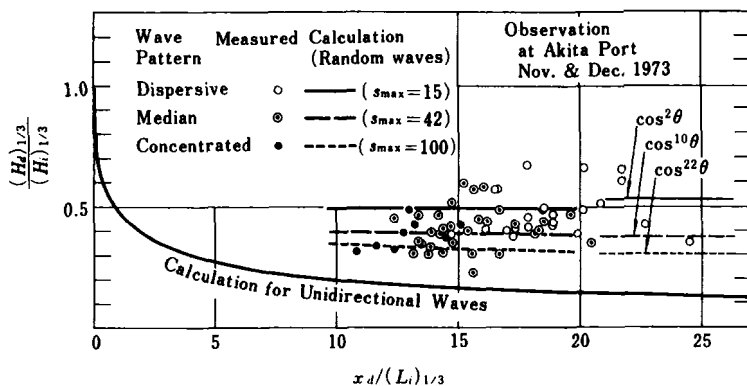
Fig. 3.16. Measured diffraction coefficients for single breakwater at Akita Port in comparison with calculation.[16]

type, with calculated values of the diffraction coefficient. The curves with the legends $s_{max} = 15$, 42 and 100 denote the results for random wave diffraction, while the continuous curve at the bottom represents the calculation for regular wave diffraction. It is clear from this figure that the calculation of random waves is in reasonable agreement with the (widely scattered) data, whereas the calculation for regular waves yields inadequately small values of the diffraction coefficient and does not describe the field data at all.

Recently, Briggs *et al.*[18] carried out laboratory tests of wave diffraction by a semi-infinite breakwater for both regular and directional random waves. Clear differences between traditional regular wave diffraction and irregular wave diffraction were observed in the test results. Briggs *et al.* concluded that directional spreading is very important and should be considered in diffraction analysis of engineering problems.

When using random diffraction diagrams, the effect of wave refraction upon the parameter s_{max} must be taken into account, because most breakwaters are built in relatively shallow water compared to the predominant wavelength, and the directional wave spectrum has transformed from that corresponding to deep water. The change in s_{max} can be estimated with the curves in Fig. 2.15 in Sec. 2.3.

3.2.3 *Random Wave Diffraction of Oblique Incidence*

Furthermore, waves will arrive at an oblique angle to a breakwater in most situations. In the case of wave diffraction by a semi-infinite breakwater, the
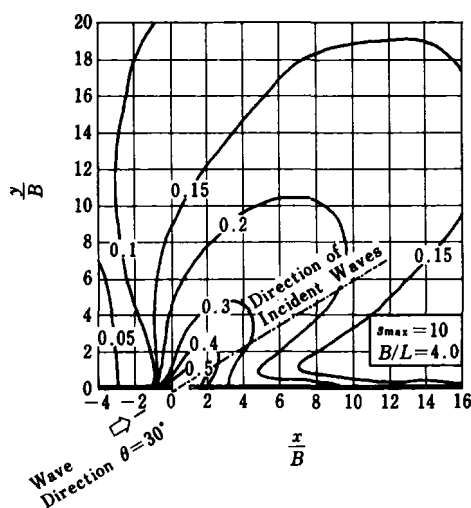
Fig. 3.17. Diffraction diagram of random sea waves of oblique incidence.

problem of oblique incidence can be treated by rotating the axis of the break-
water in the diffraction diagrams of Fig. 3.11 while keeping the wave direction
and the coordinate axes at their original positions. This technique produces
some error when the angle between the principal direction of wave approach
and the line normal to the breakwater exceeds $\pm 45°$. On the other hand, for
waves diffracted through an opening in a breakwater, the axis of the diffracted
waves or the line connecting the points of deepest penetration of contour lines
deviates slightly toward the line normal to the breakwaters as demonstrated
in Fig. 3.17. The angle of deviation varies depending on the angle between the
wave direction and the line parallel to the breakwaters, the relative opening
B/L, and the spreading parameter s_{max}. From the analysis of several diffrac-
tion diagrams for obliquely incident waves, the deviation angle of the axis of
the diffracted waves has been estimated as listed in Table 3.4. Unless the
diffraction diagrams of random sea waves are directly computed with the aid
of a computer, the diagrams in Figs. 3.12 to 3.15 for normal incidence must
be utilized to estimate wave heights behind breakwaters. When the waves are
obliquely incident, the direction of wave approach should be shifted by the
amount of the angle of deviation listed in Table. 3.4, and the apparent opening
width as viewed from the shifted wave direction should be employed instead
of the actual width of the opening.

Table 3.4. Deviation angle of diffracted waves through a breakwater opening for obliquely incident waves.

s_{max}	B/L	Deviation angle $\Delta\Theta$			
		$\Theta = 15°$	$\Theta = 30°$	$\Theta = 45°$	$\Theta = 60°$
	1.0	37°	28°	20°	11°
10	2.0	31°	23°	17°	10°
	4.0	26°	19°	15°	10°
	1.0	26°	15°	10°	6°
75	2.0	21°	11°	7°	4°
	4.0	15°	6°	4°	2°

Caution should be exercised whenever there are vertical quay walls or some reflective structure within the water area behind a breakwater. In such cases, the reflection of the diffracted waves needs to be included in the estimation of the wave height behind the breakwater (cf. Sec. 6.3).
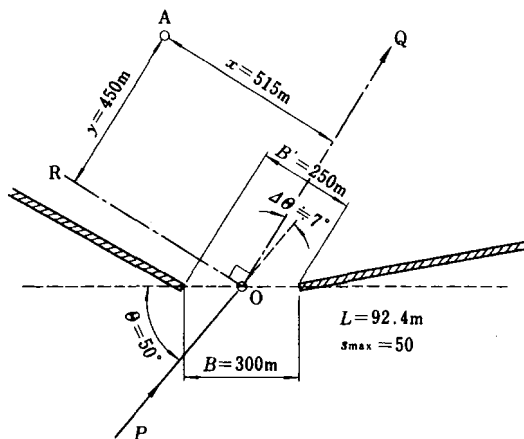
Fig. 3.18. Layout of breakwaters and calculation point.

Example 3.2

Estimate the diffraction coefficient at Point A for the layout of the breakwaters shown in Fig. 3.18 when wind waves with $T_{1/3} = 10$ s are incident from a direction which makes an angle of 50° with the line connecting the two breakwater heads. The water depth is $h = 10$ m.

Solution

The spreading parameter s_{max} is set at the value of 10 in deep water, from the condition of wind waves. However, as the site of the breakwaters is shallow, the parameter s_{max} must have increased there. By referring to Fig. 2.14 in Sec. 2.3.2, we estimate the parameter $s_{max} = 50$ for $h/L_0 = 0.064$. The wavelength corresponding to the significant wave period at the water depth of $h = 10$ m at the entrance is read as $L = 92.3$ m from Table A.2 in the Appendix. Next, the deviation angle of the axis of the diffracted waves needs to be estimated. For the opening ratio $B/L = 3.2$ and angle between the incident waves and breakwaters of $\Theta = 50°$, the deviation angel is interpolated as $\Delta\Theta \simeq 14°$ for $s_{max} = 10$ and $\Delta\Theta \simeq 4°$ for $s_{max} = 75$. Therefore, $\Delta\Theta \simeq 7°$ may be taken for $s_{max} = 50$.

When applying the diffraction diagram, the opening width is an apparent one as viewed from the direction $\overrightarrow{OQ}$ which is the predominant direction after diffraction. In this example, it is measured as $B' = 250$ m, giving $B'/L = 2.7$. By taking $\overrightarrow{OR}$ as the x-axis and $\overrightarrow{OQ}$ as the y-axis, the coordinates of the point A are read as $x = 515$ m and $y = 450$ m, or $x/B' = 2.1$ and $y/B' = 1.8$. By employing the diffraction diagrams with $B/L = 2.0$ as the ones with the opening ratio closest to the problem at hand, the diffraction coefficient is obtained as $(K_d)_{\text{eff}} = 0.26$ for $s_{max} = 10$ and $(K_d)_{\text{eff}} = 0.17$ for $s_{max} = 75$. Therefore, the interpolated diffraction coefficient for $s_{max} = 50$ is $(K_d)_{\text{eff}} \simeq 0.20$. The diffraction diagram for regular waves would yield the much smaller value of $K_d \simeq 0.14$ for this problem.

3.2.4 *Approximate Estimation of Diffracted Height by the Angular Spreading Method*

Diffraction diagrams of random sea waves for breakwaters are also applicable to the problem of wave diffraction by islands and headlands. Another method of estimating the effect of wave diffraction by large topographic barriers is to utilize the cumulative distribution curves of total wave energy discussed in Sec. 2.3.2, though this method should be considered as giving only an approximate estimate.

For this approximate method, in the fundamental equation, Eq. (3.14), it is assumed that $K_d = 0$ in the geometric shadow zone and $K_d = 1$ in the illuminated region. Then it will be understood that Eq. (3.14) takes a form similar to Eq. (2.24) for $P_E(\theta)$ by setting $K_d = 0$ or 1. In practice, the ratio of total wave energy penetrating directly to the point of interest is estimated by means of Fig. 2.15 in Sec. 2.3.2, and the wave height ratio is calculated by taking the

square root. The error introduced by setting the diffraction coefficient equal to either 0 or 1 is not large, as errors in the estimated diffraction coefficient around the boundary of the geometric shadow mostly cancel out among the many component waves from various directions. This method is based on the same principle as that of swell attenuation due to angular spreading as formulated in the Pierson–Neumann–James method for wave forecasting,[19] and it may be called the angular spreading method. In 1966, Hom-ma *et al.*[20] applied the same basic method to estimate the effect of wave sheltering by Sado Island on the Niigata Coast in Japan, though they employed the cosine square law for the directional spreading function.

A limitation on this method is that the dimensions of the barriers must be sufficiently large, on the order of several tens of wavelengths or greater: otherwise the error introduced by simplifying the diffraction coefficient may not be negligible.
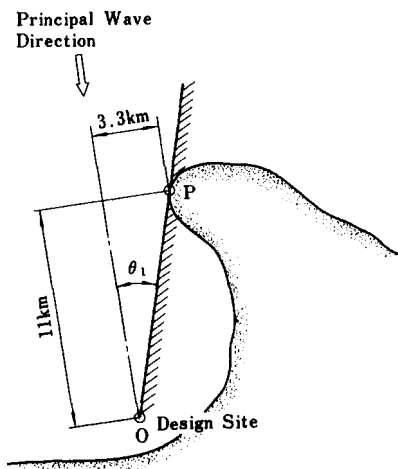
Fig. 3.19. Wave diffraction by a headland.

Example 3.3

Estimate the wave height ratio at Point O which is partly sheltered by the headland P sketched in Fig. 3.19.

Solution

The angle between the geometric shadow line $\overline{OP}$ and the principal direction of wave approach of wave approach is read on the sketch as $\theta_1 = 17°$. Among the component waves, those in the range of $\theta = 17°$ to $90°$ are assumed to be blocked by the headland so as not to reach Point O. If the waves are assumed to be wind waves with $s_{max} = 10$, the cumulative energy ratio at $\theta_1 = 17°$ is $P_E(17°) \simeq 0.685$ by Fig. 2.15. This means that 68.5% of the total wave energy will reach Point O and the wave height ratio is therefore estimated as

$$K_d \simeq 0.685 = 0.83 .$$

If the waves are assumed to be swell with $s_{max} = 75$, then $P_E(17°) \simeq 0.89$ and $K_d \simeq 0.94$.
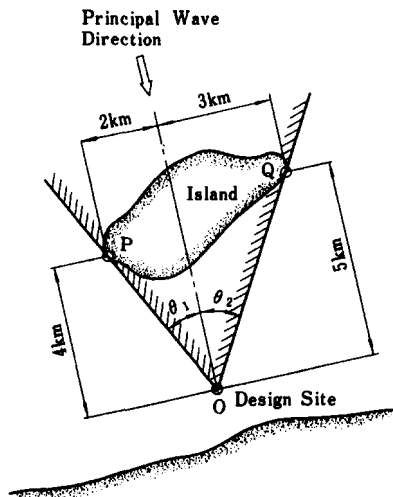
Fig. 3.20. Wave diffraction by an island.

Example 3.4

Estimate the wave height ratio at Point O which is sheltered by the island $\overrightarrow{PQ}$ shown in Fig. 3.20.

Solution

Referring to Fig. 3.20, the angles θ_1 and θ_2 are obtained as $-27°$ and $31°$, respectively. Thus, the ratio of wave energy blocked by the island to the total incident energy is estimated for the case of wind waves

(by assuming $s_{max} = 10$) as

$$\Delta E = P_E(31°) - P_E(-27°) = 0.82 - 0.22 = 0.60 \,.$$

Therefore the ratio of the wave height at Point O to the incident height is estimated to be

$$K_d = \sqrt{1 - \Delta E} = \sqrt{1 - 0.60} = 0.63 \,.$$

Although the above calculation gave a single wave height ratio, the actual situation is that waves are arriving at Point O from two different directions, from the left end and the right end of the island. The ratios of the respective wave heights to the incident height are estimated as follows:

Wave group from the left side

$$(K_d)_1 = \sqrt{P_E(-27°) - P_E(-90°)} = \sqrt{0.22} = 0.47 \,,$$

Wave group from the right side

$$(K_d)_2 = \sqrt{P_E(90°) - P_E(31°)} = \sqrt{1 - 0.82} = 0.42 \,.$$

When information on the wave direction as well as the wave height is important, such as in the case of harbor planning with the entrance at Point O, it is best to consider that there are two wave groups with height ratios of 0.47 and 0.42 incident from different directions instead of assuming a single wave group with a height ratio of 0.63.

In actual situations, waves will be refracted somewhat around the edges of islands and headlands, unless these are formed of cliffs which drop steeply into the sea. Because of such wave refraction effects, some energy from component waves incident from outside the geometric boundary will reach the design site. Therefore, from the viewpoint of the practicing engineer, the angle θ_1 in Fig. 3.19 should be set slightly larger than the geometric angle, while the angles θ_1 and θ_2 in Fig. 3.20 should be set slightly smaller. There is no guideline, however, for the amount of adjustment to be made. Refraction diagrams for the region of the tip of the island or headland may provide some clues. The analysis of random wave refraction described in Sec. 3.1 is an alternative approach to such a problem.

3.2.5 *Applicability of Regular Wave Diffraction Diagrams*

As explained so far, diffraction diagrams prepared for regular waves yield values of the diffraction coefficient differing considerably from those of actual wave

diffraction in the sea, and thus, they are not recommended for practical applications in general. The main cause of the discrepancy is the directional spreading of random sea waves. In other words, use of regular wave diffraction diagrams in real situations requires very narrow directional spreading of wave energy. Such a situation is realized at a harbor located at the inner end of a narrow bay when it is subject to swell penetration, and also for the case of secondary diffraction by inner breakwaters of waves which have already been diffracted by outer breakwaters. Another example is the diffraction of swell by a series of short breakwaters parallel to the shoreline to be build in order to promote formation of salients. As such breakwaters are usually built in water only several meters deep, the approaching swell has undergone the full effect of wave refraction; therefore its directional spread of energy has become very narrow. These are cases in which diffraction diagrams for regular waves are applicable.

3.3 Equivalent Deepwater Wave

The analysis of wave transformation is often facilitated by introducing the concept of the *equivalent deepwater wave*, which is listed as item ⑧ in Fig. 1.1 in Sec. 1.2. This wave is a hypothetical one devised for the purpose of adjusting the heights of waves which may have undergone refraction, diffraction and other transformations, so that the estimation of wave transformation and deformation can be more easily carried out when dealing with complex topographies. The height and period of the equivalent deepwater wave are defined by

$$H_0' = K_d K_r (H_{1/3})_0 , \quad T_{1/3} = (T_{1/3})_0 , \tag{3.15}$$

where

H_0' : equivalent deepwater wave height (corresponding to the significant wave),

$(H_{1/3})_0 = H_0$: deepwater significant wave height,

$(T_{1/3})_0$: significant wave period of deepwater waves,

and K_r and K_d denote the coefficients of random wave refraction and diffraction, respectively.

For example, if the deepwater waves have height $(H_{1/3})_0 = 5$ m and period $(T_{1/3})_0 = 12$ s, and the changes in wave height by refraction and diffraction at a particular point are given by $K_r = 0.92$ and $K_d = 0.83$, the equivalent deepwater wave is defined by $H_0' = 3.8$ m and $T_{1/3} = 12$ s, and subsequent calculations are done with these values.

In a water area where the average slope of the sea bottom is very gentle and in which the zone of shallow depth continues for a great distance, wave attenuation due to bottom friction may not be negligible. In such a case, the equivalent deepwater wave height is estimated by multiplying a coefficient of wave height attenuation K_f on the right side of Eq. (3.15). For details on the wave height attenuation coefficient K_f, reference is made to Bretschneider and Reid[21] and others (e.g., Ref. 22). The period of the equivalent deepwater wave is generally regarded as equal to the deepwater significant wave period, but in reality the significant wave period may vary during wave transformation, as in the sheltered area behind a breakwater.
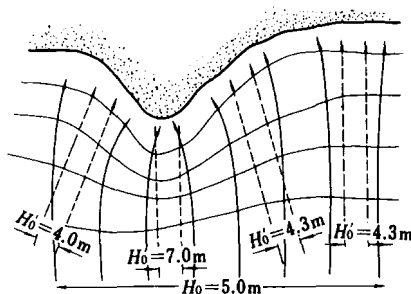
Fig. 3.21. Explanatory sketch of equivalent deepwater waves undergoing refraction.

The concept of equivalent deepwater wave was introduced in order to relate the phenomena of wave breaking, run-up, overtopping and other processes to the characteristics of the deepwater waves. Various processes of wave deformation and wave action are investigated through hydraulic tests in laboratory wave flumes, and data sets from many experiments are available. These investigations are usually carried out in flumes of uniform width. On the other hand, waves in the sea experience a variation in the distance between wave rays due to refraction, as shown in Fig. 3.21, and the wave height near the shore varies from place to place even though the deepwater wave height is constant.

It is possible to incorporate the effects of wave refraction and diffraction into hydraulic model tests of wave breaking, overtopping, etc., but it is not recommended in general because of the excessive cost and time required. Thus, a device is needed in order to utilize the laboratory data on wave breaking and other phenomena obtained in wave flumes of uniform width, and that device is the concept of the equivalent deepwater wave. In the example shown in Fig. 3.21, imaginary wave rays represented by dash lines are introduced, and a spatially varying deepwater wave height is specified at various locations instead of a uniform deepwater wave height.

The concept of equivalent wave height is restricted to use in connection with the significant wave as the representative wave of a wave group; it is not applied to other characteristic waves such as the highest wave or the mean wave.

3.4 Wave Shoaling

As waves propagate in a channel of gradually decreasing depth but of constant width, the wavelength and celerity decrease as approximately given by the theory of small amplitude waves. At the same time, the wave height also changes. The change in wave height due to varying depth is called wave shoaling.

The cause of the variation in wave height is the variation in the speed of energy propagation; i.e., the group velocity, with the water depth. For small amplitude waves with a single period, the variation in wave height due to the wave shoaling effect is calculated by the following equation:

$$K_s \equiv \frac{H}{H_0'} = \sqrt{\frac{(C_G)_0}{C_G}} = \frac{1}{\sqrt{\left[1 + \dfrac{4\pi h/L}{\sinh(4\pi h/L)}\right] \tanh \dfrac{2\pi h}{L}}}, \qquad (3.16)$$

where

K_s : shoaling coefficient,

C_G : group velocity given by Eq. (3.13),

$(C_G)_0$: group velocity in deep water $\simeq \dfrac{1}{2}C_0 = 0.78T(\text{m/s})$,

L : wavelength, and

h : water depth.

For random sea waves, some modifications to the shoaling coefficient given by Eq. (3.16) are necessary. One reason is the effect of the energy distribution in the frequency domain as expressed through the frequency spectra, and another is the effect of the finite amplitude of the individual waves. The former can be evaluated by computing the wave shoaling coefficient at various frequency intervals in the wave spectrum and by summing the results as in the calculation of random wave refraction and diffraction. This procedure produces a kind of smoothing of the variation of the shoaling coefficient with respect to the relative water depth. For example, the minimum value of the shoaling coefficient becomes $(K_s)_{min} = 0.937$ by introducing the frequency spectrum,[23] whereas it is $(K_s)_{min} = 0.913$ for regular waves. The difference is on the order of 2 to 3%, which may be neglected in practical design procedures.

The second effect, finite wave amplitude, can be calculated by making use of various theories of finite amplitude waves. Iwagaki and Sakai,[24] for example, have presented a design diagram for the estimation of the shoaling coefficient. Shuto,[25] on the other hand, has formulated the variation of wave height occurring in relatively shallow water with a set of fairly simple equations. In terms of the shoaling coefficient, these equations are rewritten as[23]:

$$\left.\begin{aligned}
K_s &= K_{si} & &: & h_{30} &\leq , \\
K_s &= (K_{si})_{30} \left(\frac{h_{30}}{h}\right)^{2/7} & &: & h_{50} &\leq h < h_{30} , \\
K_s(\sqrt{K_s} - B) - C &= 0 & &: & h &< h_{50} ,
\end{aligned}\right\} \tag{3.17}$$

in which K_{si} denotes the shoaling coefficient for a small amplitude wave as given by Eq. (3.16), h_{30} and $(K_{si})_{30}$ are the water depth satisfying Eq. (3.18) below and the shoaling coefficient for that depth, respectively, h_{50} is the water depth satisfying Eq. (3.19), and B and C are constants given by Eq. (3.20):

$$\left(\frac{h_{30}}{L_0}\right)^2 = \frac{2\pi}{30} \frac{H_0'}{L_0}(K_{si})_{30} , \tag{3.18}$$

$$\left(\frac{h_{50}}{L_0}\right)^2 = \frac{2\pi}{50} \frac{H_0'}{L_0}(K_s)_{50} , \tag{3.19}$$

$$B = \frac{2\sqrt{3}}{\sqrt{2\pi H_0'/L_0}} \frac{h}{L_0} , \quad C = \frac{C_{50}}{\sqrt{2\pi H_0'/L_0}} \left(\frac{L_0}{h}\right)^{3/2} , \tag{3.20}$$

where L_0 denotes the wavelength in deep water, $(K_s)_{50}$ is the shoaling coefficient at $h = h_{50}$ and C_{50} is a constant given by

$$C_{50} = (K_s)_{50}\left(\frac{h_{50}}{L_0}\right)^{3/2}\left[\sqrt{2\pi\frac{H_0'}{L_0}(K_s)_{50}} - 2\sqrt{3}\frac{h_{50}}{L_0}\right]. \tag{3.21}$$

In the computation of the shoaling coefficient, the water depths h_{30} and h_{50} satisfying Eq. (3.18) and (3.19) are first solved for by an iterative method, and then it can be determined in which range the water depth at the design site is located. If the water depth is less than h_{50}, Eq. (3.17) must be solved by a numerical method.

Figure 3.22 presents the shoaling coefficient including the finite amplitude effect based on Shuto's theory.[23] The shoaling coefficient in the upper right corner corresponds to water of relative depth h/L_0 greater than 0.09, where it is assigned the same value as that of small amplitude waves.
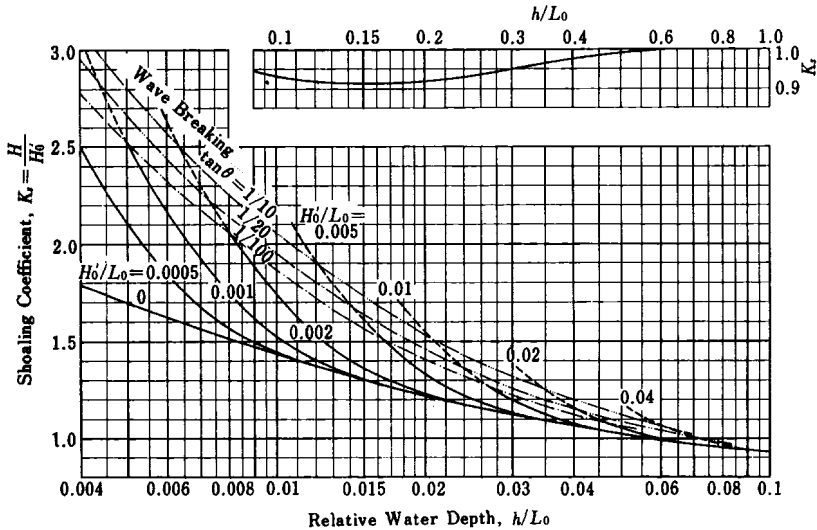
Fig. 3.22. Diagram of nonlinear wave shoaling.

Example 3.5

Estimate the wave height at water depth of 8 m for an equivalent deep-water wave of $H_0' = 4.5$ m and $T_{1/3} = 12$ s incident to a coast with a uniform slope of 1/10.

Solution

As the deepwater wavelength of this wave is $L_0 = 225$ m, we have

$$H_0'/L_0 = 4.5/225 = 0.0200 \quad \text{and} \quad h/L_0 = 8/225 = 0.036.$$

Therefore, by entering Fig. 3.22 and reading off the curve for $H_0'/L_0 = 0.02$ we obtain

$$K_s = 1.24, \quad \text{thus} \quad H_{1/3} = K_s H_0' = 1.24 \times 4.5 = 5.6 \text{ m}.$$

If the wave height is assumed to be very small in the above example, the shoaling coefficient becomes $K_s = 1.09$ by the curve for $H_0'/L_0 = 0$ in the figure, thus differing by about 12% from the previous result. If the bottom slope is much gentler, waves begin to break before they reach the depth of 8 m, and the wave height becomes smaller as a result of attenuation by breaking. The dash-dot curves with the legend "wave breaking" indicate the boundary beyond which the attenuation of $H_{1/3}$ exceeds 2%. In such shallow zones, the wave height should be estimated by taking into account the phenomenon of random wave breaking as described in the next section.

3.5 Wave Deformation Due to Random Breaking

3.5.1 *Limiting Wave Height of Regular Waves by Breaking*

We can easily observe that a train of regular waves in a laboratory flume undergoes shoaling over a sloping bottom and breaks at a certain depth. The location at which waves break is almost fixed for regular waves, and there is a distinct difference between the oscillatory wave motion before breaking and the turbulent wakes with air entrainment after breaking. The terminology *wave breaking point, depth* and *height* is employed to denote the location, water depth, and height of wave breaking, respectively. The expression "limiting breaker height" is sometimes also used, in the sense of the upper limit of progressive waves physically possible at a certain water depth for a given wave period. The ratio of limiting breaker height to water depth depends on the bottom slope and the relative water depth. Compilation of a number of laboratory results has yielded the design diagram of Fig. 3.23 as an average relation,[26] although a scatter in the data of more than 10% must be mentioned.

As an illustration, waves with a period of 10 s incident to a coast with a bottom slope of 1/30 are estimated to have a breaking wave height of $H_b = 7.6$ m at the water depth of $h_b = 10$ m according to Fig. 3.22, since the relative water depth is $h_b/L_0 = 10/156 = 0.064$ and $\tan \theta = 1/30$.
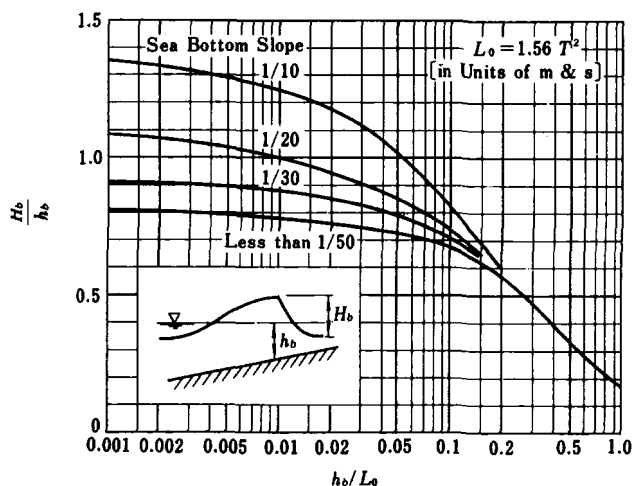
Fig. 3.23. Limiting breaker height of regular waves.[26]

3.5.2 *Computational Model of Random Wave Breaking*

As opposed to the breaking of a regular wave train, actual sea waves, in particular wind waves, exhibit a wide spatial spread in the region of breaking; some waves break far from shore, some at an intermediate distance, and others approach quite near to the shoreline before they break. In coastal waters, therefore, wave breaking takes place in a relatively wide zone of variable water depth, which is called the wave breaking zone or the surf zone. Only for the situation of swell incident to a coast with a single, well-developed longshore bar, we are able to define the unambiguous outer edge of the surf zone, at the off-shore side of the longshore bar.

The mechanism of wave attenuation within the surf zone is very difficult to understand because of the complicated nature of the wakes, turbulence, and air entrainment processes there. However, it is possible to analyze the macroscopic features of the change in the wave height distribution, and the apparent decrease in characteristic wave height, with the model of the wave height distribution sketched in Fig. 3.24 (Refs. 23 and 27). First, the distribution before wave breaking can be approximated as being Rayleighan, as described in Sec. 2.2. Thus, a group of random waves entering the surf zone is assumed to have a Rayleigh distribution as shown in Fig. 3.24(1). The abscissa x is a nondimensional wave height normalized with a reference height H^*.

(1) Wave height distribution before breaking

$p_0(x)$

$x = H/H_{\rm s}$

(2) Probability of wave breaking

x_2 x_1

(3) Distribution of unbroken waves

$p_r(x)$

x_2 x_1

(4) Redistribution of wave height

$p(x)$

x_2 x_1

Wave Height Ratio, x
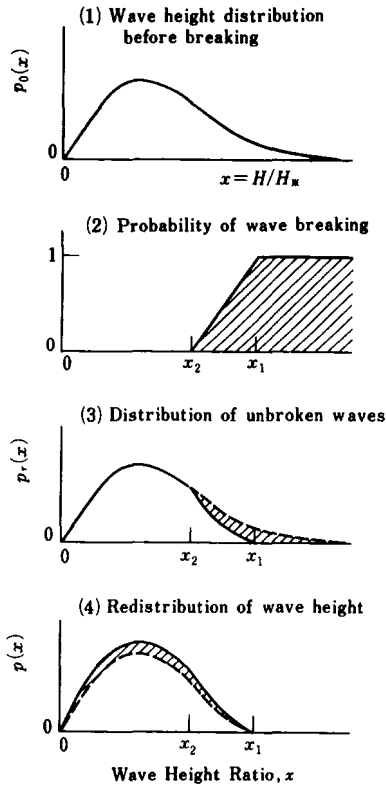
Fig. 3.24. Explanatory sketch of the model of random waves breaking.[23]

Among the waves obeying that distribution, those with height exceeding the breaking limit will break and cannot occupy their original position in the wave height distribution. The breaking limit for random sea waves should be allowed a range of variation because even a regular wave train exhibits some fluctuation in breaker height, and a train of random sea waves would show a greater fluctuation owing to the variation of individual wave periods and other characteristics. Therefore, wave breaking is assumed to take place in the range of relative wave height from x_2 to x_1 with a probability of occurrence which varies linearly between the two boundaries (Fig. 3.24(2)). With this assumption, the portion of waves which is removed from the original distribution due to the process of breaking is represented by the zone of slashed lines shown in Fig. 3.24(3). The broken waves do not lose all of their energy but retain some. Because no

information is available at present on the heights of individual random waves after breaking, they are assumed to be distributed in the range of nondimensional wave heights between 0 and x_1 with a probability proportional to the distribution of unbroken waves. With this model, the wave height distribution within the surf zone is expressed as shown in Fig. 3.24(4), where the area with slashed lines represents the heights of attenuated waves after breaking.

3.5.3 Computation of the Change in Wave Height Distribution Due to Random Wave Breaking

In order to compute the wave height distribution within the surf zone with the above model, we need to introduce some formulation of the limiting height of individual breaking waves. For this purpose the design diagram of Fig. 3.23, or its approximate representation given as follows,[28] can be employed:

$$\frac{H_b}{L_0} = A \left\{ 1 - \exp \left[-1.5 \frac{\pi h}{L_0} (1 + 15 \tan^{4/3} \theta) \right] \right\} , \qquad (3.22)$$

where θ denotes the angle between the sea bottom and the horizontal plane, and thus $\tan \theta$ represents the bottom slope. The coefficient A takes the value 0.17 for regular waves. In the present discussion of random wave breaking, A is set at 0.18 for the upper limit of random wave breaking at $x = x_1$, in consideration of the variability in random sea waves, and 0.12 for the lower breaking limit at $x = x_2$. In the process of doing this, the overall pattern of the wave height distribution within the surf zone is found to be well modeled.

It is also necessary to take into account the variation in the mean water level. One factor is the phenomenon of wave setup, which causes a quasi-linear rise in the mean water level toward the shoreline. This phenomenon is associated with the existence of a stress acting on the water due to the presence of wave motion, called the radiation stress. Its magnitude is related to the momentum flux accompanying wave propagation. When the wave height varies due to shoaling and breaking during wave propagation from offshore area toward the shoreline, the magnitude of the radiation stress also varies. This spatial variation in the radiation stress causes an inclination in the mean water level.[29] The change in mean water level is denoted by $\overline{\eta}$ and can be evaluated by numerically integrating the following differential equation from deep water toward the shoreline:

$$\frac{d\overline{\eta}}{dx} = -\frac{1}{(\overline{\eta} + h)} \frac{d}{dx} \left[\frac{1}{8} \overline{H^2} \left(\frac{1}{2} + \frac{4\pi h/L}{\sinh(4\pi h/L)} \right) \right] , \qquad (3.23)$$
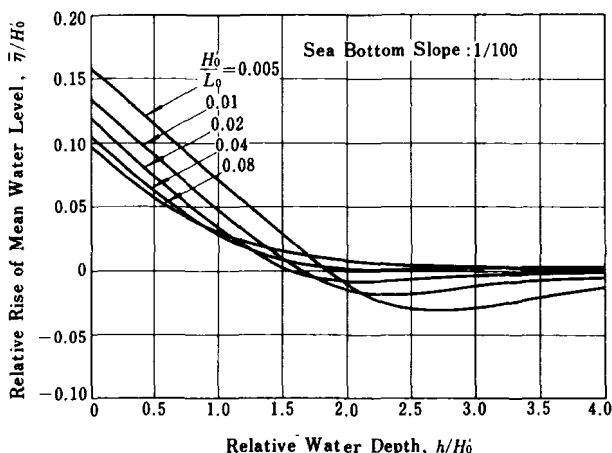
Fig. 3.25. Variation of mean water level due to shoaling and breaking of random sea waves.[23]

where $\overline{H^2}$ denotes the mean square of the heights of random water waves. The wave height itself is affected by the rise in mean water level through the wave breaking process, and thus the variations in the mean water level and the wave height distribution must be solved simultaneously. Figure. 3.25 presents the result of a computation of the wave setup on a bottom with a uniform slope of 1/100. Waves with low steepness produce a slight depression in the mean water level, which is called wave setdown, in the range $h/H_0' = 2$ to 4.

As indicated in Fig. 3.25, the amount of wave setup at the shoreline is on the order of $0.1H_0'$. Such wave setup can be detected in marigrams. The First District Port Construction Bureau of the Ministry of Transport of Japan[30] has verified the existence of wave setup of about $0.1H_0'$ by comparing the recorded tide curves with wave data. The coastal water on a steep slope may exhibit much higher wave setup (refer to Sec. 3.5.6 for further information).

Another source contributing to the variation in mean water level is the phenomenon of surf beat; i.e., the irregular fluctuation in mean water level with period of several to a few tens of times the period of the incoming surface waves. Although the amplitude of surf beat is on the order of 10% of the surface wave amplitude in water of 10 m depth or so, it may reach more than 30% of the deepwater wave amplitude near the shoreline, as reported in field observations.[27] An example of a surf beat profile is shown in Fig. 10.7 in
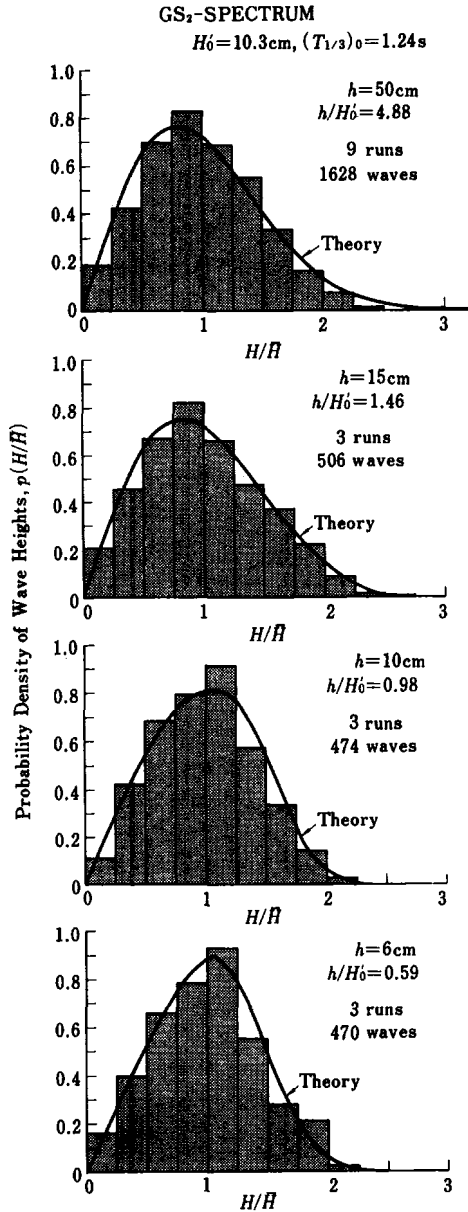
Fig. 3.26. Deformation of wave height distribution of irregular waves in a laboratory flume with the slope of 1 to 10.[23]

Sec. 10.5. The following is an empirical expression for estimating the amplitude of surf beat within the surf zone[27]:

$$\zeta_{\rm rms} = \frac{0.01 H_0'}{\sqrt{\dfrac{H_0'}{L_0}\left(1 + \dfrac{h}{H_0'}\right)}}, \qquad (3.24)$$

where $\zeta_{\rm rms}$ denotes the root-mean-square value of the profile of the surf beat.

The variation in the mean water level due to wave setup and surf beat acts to increase the upper limit of the distribution of the wave height toward higher values. Figure 3.26 presents the wave height distribution of laboratory random waves propagating in a flume with a bottom slope of 1/10 and undergoing the process of random wave breaking. The observed wave height distributions at several water depths are shown in the form of histograms expressed in the manner of a probability density, while the predicted distributions by the random wave breaking model sketched in Fig. 3.24 are drawn as smooth curves. The agreement between observation and prediction is quite good. The reference height employed in Fig. 3.26 is the mean wave height $\overline{H}$, which varies in this case from 6.1 cm at the depth of $h = 50$ cm at the offshore side to 6.9, 6.8 and 4.5 cm at the depth of 15, 10 and 6 cm, respectively.

The attenuation in the characteristic heights of irregular waves by breaking has been measured in a laboratory flume.[27] As shown in Fig. 3.27, the variations in the various wave heights are gradual. The experiments were done in a range of wave steepness with different wave spectral forms as indicated by the various symbols. Each data point represents the arithmetic mean of three runs with different input wave profiles about 200 waves long. The wave height variation predicted by the random breaking model is seen to describe the laboratory data well. Figure 3.28 presents a comparison of the computation to field data on the wave height variation near a coast. The data were taken at Sakata Port by the First District Port Construction Bureau of Japan[18]; three wave recorders were employed simultaneously at the depths 20, 14 and 10 m below the datum level. The equivalent deepwater wave height H_0' was estimated from the data taken with the deepest recorder by correcting for the effects of wave shoaling and refraction. Field wave measurements by their very nature exhibit large scatter due to the sampling variability originating from wave irregularity itself (refer to Sec. 9.6), and this is one such typical example. Although the wave attenuation seems to be slightly larger in the data than given by the
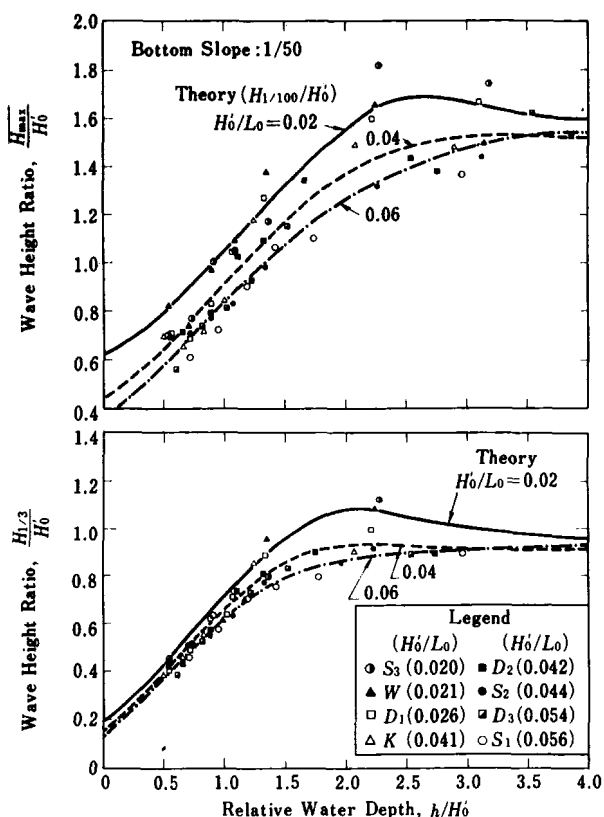
Fig. 3.27. Variations of the maximum and significant wave heights in a laboratory flume with the slope of 1 on 50.[23]

prediction as a whole, the pattern of the wave height variation in the field data is well predicted with the random wave breaking model.

3.5.4 *Diagrams for the Estimation of Wave Height in the Surf Zone*

The predictive formulas for the change in wave height shown in Figs. 3.27 and 3.28 and discussed previously have been given in terms of the parameter of equivalent deepwater wave steepness. This is because the effect of wave steepness enters quite strongly in the wave breaking process; waves of large steepness begin to break before they attain further appreciable increase in
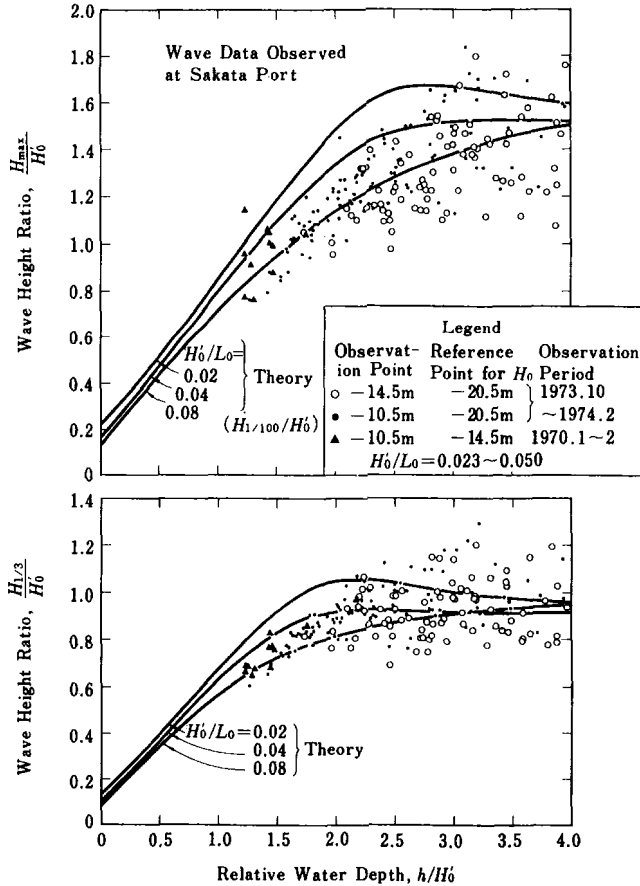
Fig. 3.28. Variations in the maximum and significant wave heights observed at Sakata Port.[23]

wave height by shoaling. Also, the slope of the bottom is important in regular or random wave breaking; waves approaching a coast of steep slope do not break until quite near to the shore.

By taking the wave steepness and the bottom slope as the principal parameters, changes in the largest and significant wave heights have been computed with the random wave breaking model discussed previously. The results are shown in Figs. 3.29 to 3.32 for bottom slopes of 1/10, 1/20, 1/30 and 1/100. The largest wave height H_{max} is set in the computation as that of the highest
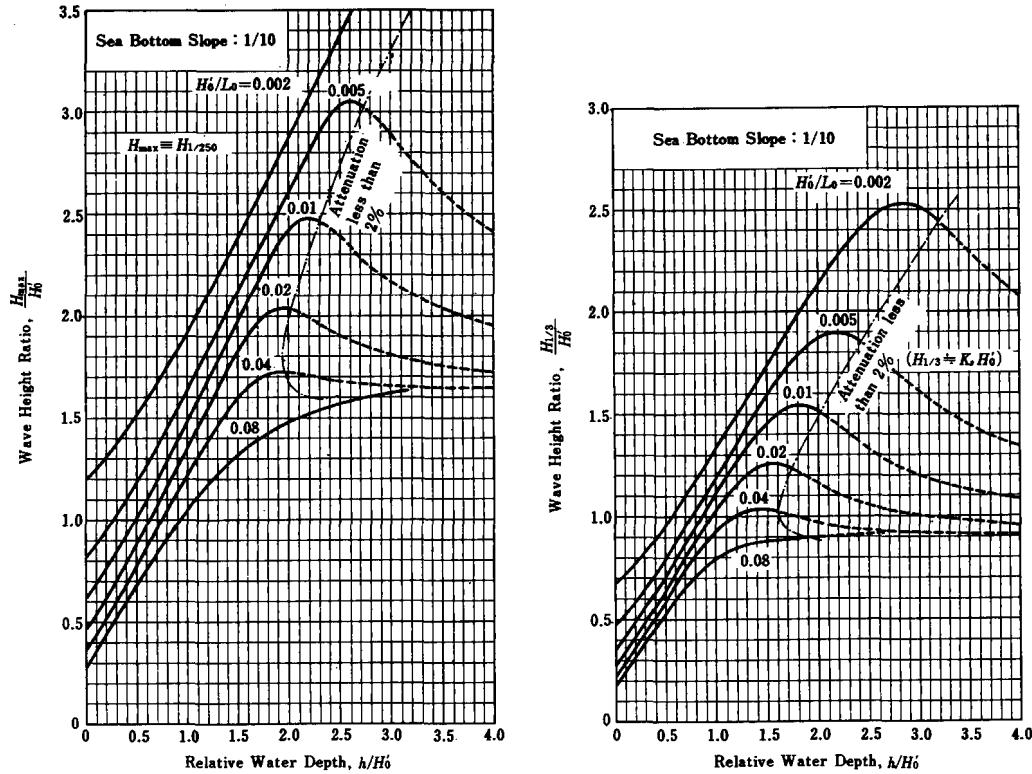
Fig. 3.29. Diagrams for the estimation of wave heights in the surf zone (sea bottom slope of 1/10).[23]
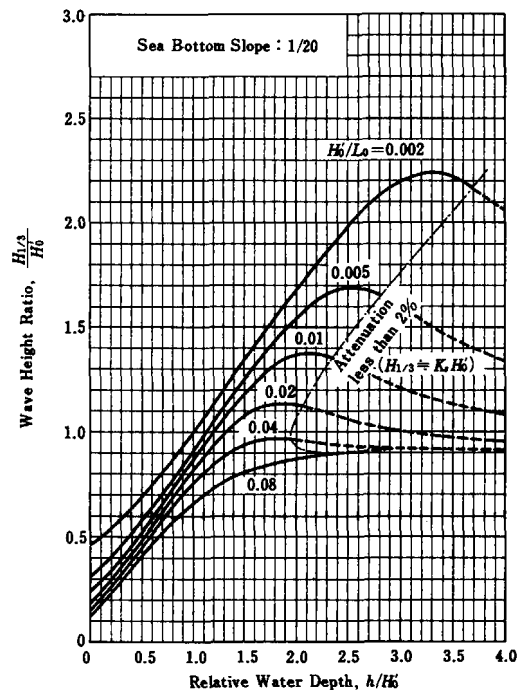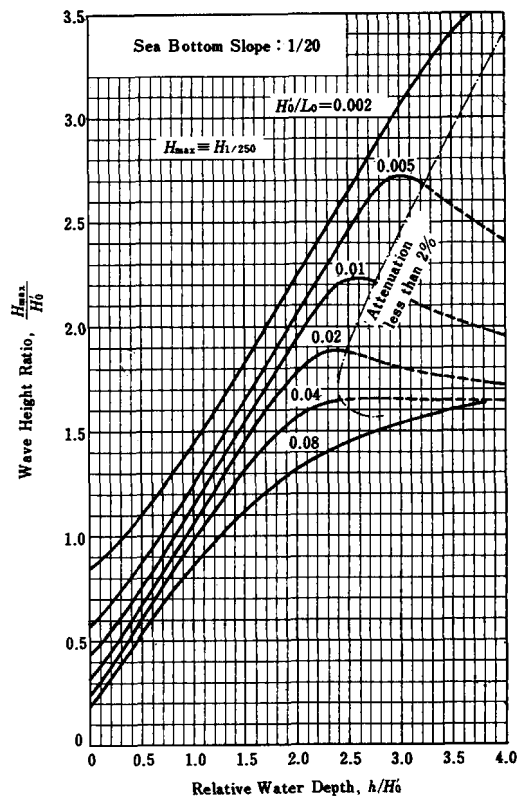
Fig. 3.30. Diagrams for the estimation of wave heights in the surf zone (sea bottom slope of 1/20).[23]
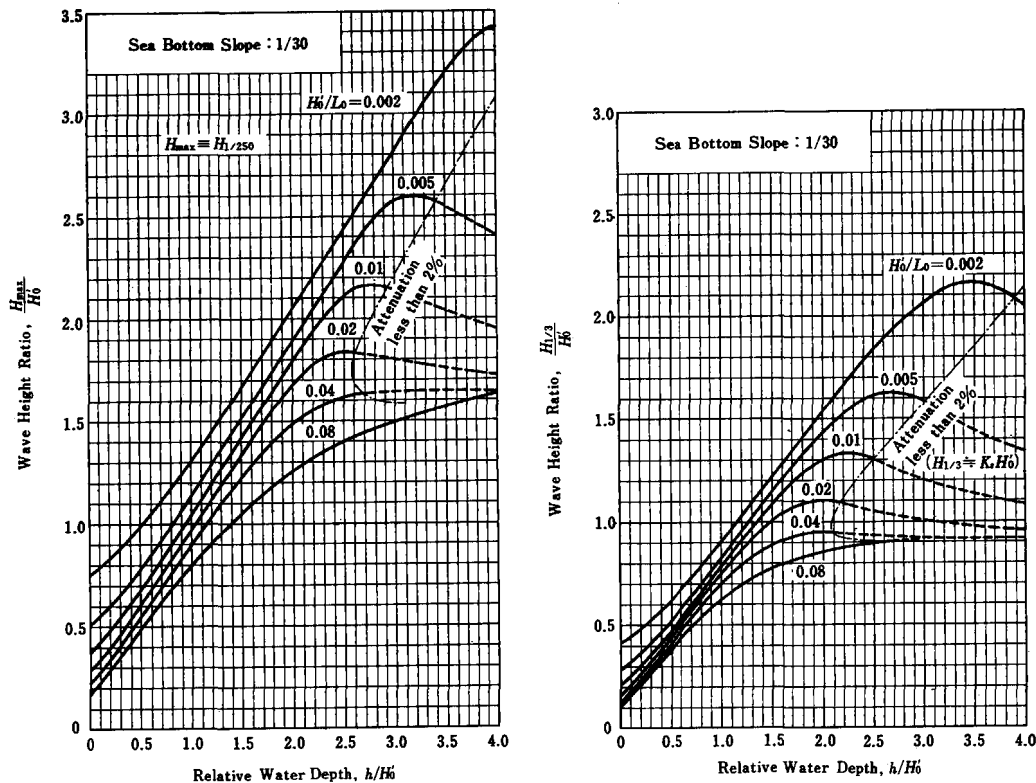
Fig. 3.31. Diagrams for the estimation of wave heights in the surf zone (sea bottom slope of 1/30).[23]
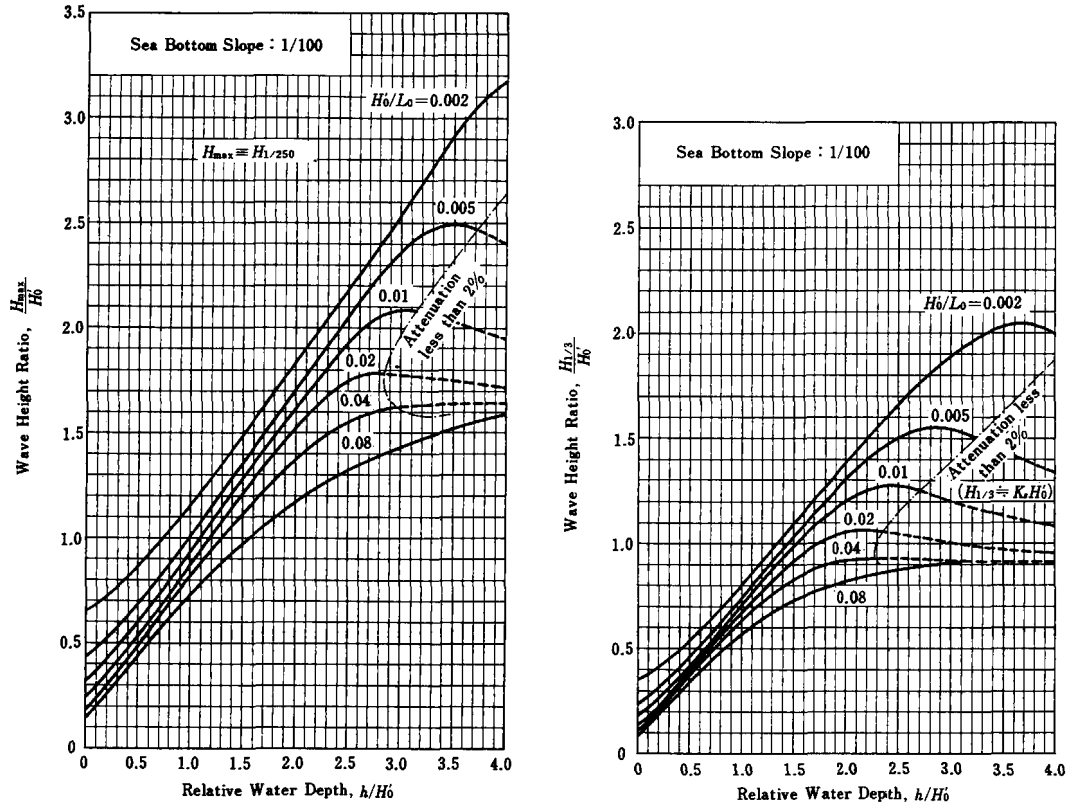
Fig. 3.32. Diagrams for the estimation of wave heights in the surf zone (sea bottom slope of 1/100).[23]

one-250th have $H_{1/250}$ (mean of the heights of the waves included in 1/250 of the total number of waves, counted in descending order of height from the highest wave). This definition yields the approximate relation of $H_{max} \simeq 1.8H_{1/3}$ outside the surf zone. Also, each figure contains a dash-dot curve denoted "attenuation less than 2%." In the zone to the right of this dash-dot curve, the attenuation in wave height due to wave breaking is less than 2% and the variation in wave height can be estimated by the shoaling coefficient presented in Fig. 3.22.

As an example of the usage of the diagrams, the variation in wave height from the offshore area to the shoreline has been estimated for swell with $H_0' = 4.5$ m and $T_{1/3} = 12$ s approaching a coast with uniform bottom slope of 1/10 or 1/100. By entering Figs. 3.22, 3.29 and 3.32, the wave heights at various water depths are estimated as listed in Table 3.5. Although H_0' is taken as constant in this example, it varies in actual situations because of wave refraction and other phenomena, and the values of H_0' and H_0'/L_0 must be evaluated at the respective water depths. According to Table 3.5, the significant wave height begins to decrease at a water depth between 10 to 8 m on a coast with a slope of 1/100, whereas H_{max} starts to decrease at a water depth between 20 and 10 m. Thus, the effect of random wave breaking appears earlier for H_{max} than

Table 3.5. Variation of wave height due to shoaling and random wave breaking.
— $H_0' = 4.5$ m, $T_{1/3} = 12$ sec —

Water depth h(m)	Sea bottom slope 1/10		Sea bottom slope 1/100	
	H_{max} (m)	$H_{1/3}$ (m)	H_{max} (m)	$H_{1/3}$ (m)
100	7.9	4.4	7.9	4.4
50	7.5	4.1	7.5	4.1
20	7.6	4.2	7.6	4.2
10	8.9	5.0	7.4	4.8
8	9.0	5.6	6.3	4.5
6	7.5	5.5	5.0	3.7
4	5.6	4.3	3.6	2.7
2	3.8	2.7	2.3	1.6
0	2.2	1.3	1.2	0.7

Note: $H_{max} \equiv H_{1/250}$

for $H_{1/3}$. As a result, the ratio of $H_{max}/H_{1/3}$, which is 1.8 in the offshore area, goes down to about 1.3 at some depth in the surf zone and then recovers to a higher value toward the shoreline. Table 3.5 also shows that the effect of the bottom slope is noticeable in water shallower than 10 m.

Concerning the breaking random sea waves, the breaking point as well as the breaking wave height cannot be defined clearly, in contrast to the case of regular waves. Although it may be possible to define a breaking point and height for individual waves within a train of random waves, there remains an ambiguity in the definition of the location at which waves as a group may be regarded to break. In practical applications, however, it is necessary to have an index for the breaking of a wave group in order to estimate the width of the surf zone and other design parameters. For such requirements, the peak value of significant wave height $(H_{1/3})_{peak}$ within the surf zone and the water depth $(h_{1/3})_{peak}$ at its appearance may be regarded as alternatives to the breaker height and depth, respectively. Figures 3.33 and 3.34 have been prepared for this purpose, obtained by reading off the diagrams of $H_{1/3}$ in Figs. 3.29 to 3.32.
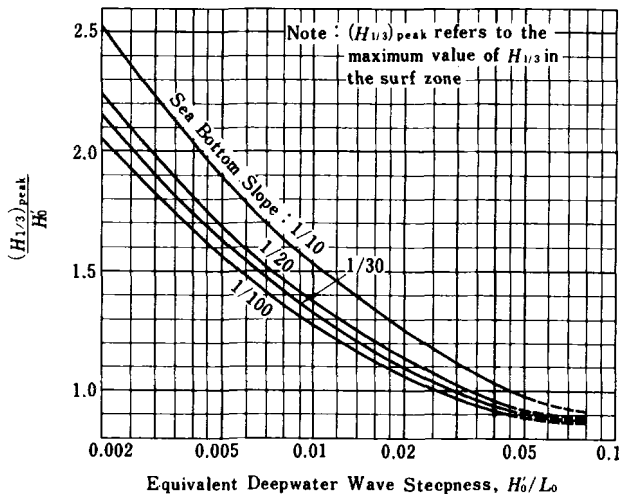
Fig. 3.33. Index curves for the maximum value of the significant wave height in the surf zone.[23]
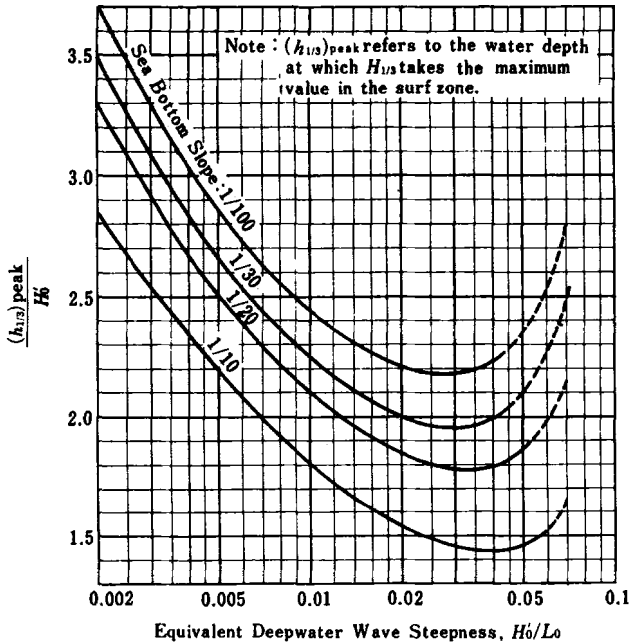
Fig. 3.34. Index curves for the water depth at which the significant wave height takes the maximum value in the surf zone.[23]

Example 3.6

Waves with the equivalent deepwater height of $H_0' = 2$ m and period of $T_{1/3} = 14$ s are incident to a coast with a uniform bottom slope of 1/50. Estimate the peak value of the significant wave height in the surf zone and the water depth at its appearance.

Solution

Since the deepwater wavelength is $L_0 = 306$ m and the wave steepness is $H_0'/L_0 = 2/306 = 0.0065$, the following can be obtained from Figs. 3.33 and 3.34:

$$(H_{1/3})_{\text{peak}}/H_0' = 1.46 \quad \therefore (H_{1/3})_{\text{peak}} = 2.9 \text{ m}$$

$$(h_{1/3})_{\text{peak}}/H_0' = 2.55 \quad \therefore (h_{1/3})_{\text{peak}} = 5.1 \text{ m}$$

3.5.5 *Formulas for Wave Height Estimation Within the Surf Zone*

The variation in wave height within the surf zone can be estimated without difficulty by means of Figs. 3.29 to 3.32 for most practical applications. However, the following approximation may be convenient to employ when a mathematical expression for the wave height is required:

$$H_{1/3} = \begin{cases} K_s H_0' & : h/L_0 \geq 0.2 \,, \\ \min\{(\beta_0 H_0' + \beta_1 h), \beta_{\max} H_0', K_s H_0'\} & : h/L_0 < 0.2 \,, \end{cases} \tag{3.25}$$

$$H_{\max} \equiv H_{1/250} = \begin{cases} 1.8 K_s H_0' & : h/L_0 \geq 0.2 \,, \\ \min\{(\beta_0^* H_0' + \beta_1^* h), \beta_{\max}^* H_0', 1.8 K_s H_0'\} & : h/L_0 < 0.2 \,. \end{cases} \tag{3.26}$$

The symbol $\min\{a, b, c\}$ stands for the minimum value among a, b and c. The coefficients $\beta_0, \beta_1, \ldots$ have been formulated as listed in Table 3.6.

Table 3.6. Coefficients for approximate estimation of wave heights within surf zone.[23]

Coefficients for $H_{1/3}$	Coefficients for $H_{\max}$
$\beta_0 = 0.028(H_0'/L_0)^{-0.38} \exp[20 \tan^{1.5}\theta]$	$\beta_0^* = 0.052(H_0'/L_0)^{-0.38} \exp[20 \tan^{1.5}\theta]$
$\beta_1 = 0.52 \exp[4.2 \tan\theta]$	$\beta_1^* = 0.63 \exp[3.8 \tan\theta]$
$\beta_{\max} = \max\{0.92, 0.32(H_0'/L_0)^{-0.29}$	$\beta_{\max}^* = \max\{1.65, 0.53(H_0'/L_0)^{-0.29}$
$\qquad \times \exp[2.4 \tan\theta]\}$	$\qquad \times \exp[2.4 \tan\theta]\}$

Note : max $[a, b]$ gives the larger of a or b.

Example 3.7

Estimate the significant wave height at the depth of $h = 8$ m by means of Eq. (3.25), when swell with $H_0' = 6$ m and $T_{1/3} = 15$ s is attacking a coast with a slope of 1/50.

Solution

Since the deepwater wavelength is $L_0 = 351$ m and the wave steepness is $H_0'/L_0 = 6/351 = 0.0171$, the β coefficients are calculated as follows:

$$\beta_0 = 0.028 \times (0.0171)^{-0.38} \times \exp[20 \times (0.02)^{1.5}] = 0.139 \,,$$

$$\beta_1 = 0.52 \times \exp[4.2 \times 0.02] = 0.566 \,,$$

$$\beta_{\max} = \max\{0.92, 0.32 \times (0.0171)^{-0.29} \times \exp[2.4 \times 0.02]\}$$

$$= \max\{0.92, 1.093\} = 1.093 \,.$$

As for the shoaling coefficient, in Fig. 3.22 the point corresponding to $h/L_0 = 0.023$ and $H_0'/L_0 = 0.0171$ is plotted above the dash-dot curve corresponding to $\tan \theta = 1/100$, indicating a large attenuation of wave height due to breaking. Nevertheless, by extrapolating the curves of K_s, the shoaling coefficient is estimated as $K_s \simeq 1.7$. Thus, the significant wave height is estimated as

$$H_{1/3} = \min\{(0.139 \times 6.0 + 0.566 \times 8.0), 1.093 \times 6.0, 1.7 \times 6.0\}$$

$$= \min\{5.36, 6.56, 10.2\} \simeq 5.4 \text{ m}.$$

Equations (3.25) and (3.26) may give a difference of several percent in the estimated heights compared to those read in Figs. 3.29 to 3.32. For waves of steepness greater than 0.04, the formulas yield a significant height in excess of 10% compared to that from the diagrams around the water depth at which the value of $H_{1/3} = \beta_0 H_0' + \beta_1 h$ becomes equal to the value of $H_{1/3} = \beta_{\max} H_0'$. A similar difference also appears for the case of $H_{\max}$. Waves of large steepness may have a discontinuity in the height $H_{\max}$ estimated with Eq. (3.26) at the boundary $h/L_0 = 0.2$. Caution should be exercised in applying Eqs. (3.25) and (3.26) in regard to such differences and discontinuity.

In the phenomenon of random wave breaking, there exist finite heights of $H_{1/3} = \beta_0 H_0'$ and $H_{\max} = \beta_0^* H_0'$ at the shoreline where the initial water depth is zero. This is due to the increase in actual water depth owing to the effects of wave setup and surf beat. The motion of water around the shoreline, however, is more intensive than that of ordinary wave motion corresponding to the height estimated above at the increased water depth, because of the uprushing and downrunshing surging motion of water there. Therefore, the estimated wave height at $h = 0$ should be regarded as an apparent one which does not adequately represent the magnitude of the wave action. Evaluation of the weight of armor stone at the shoreline with the above estimated wave height by means of Hudson's formula, for example, would be poor practice because it would underestimate the required weight of the stone. It may be safe to use the wave height at the depth of about $0.5H_0'$ for the area shallower than that depth for the estimation of wave force and action on structures.

3.5.6 *Wave Setup at Shoreline by Random Wave Breaking*

As exhibited in Fig. 3.25, the mean water level across the surf zone deviates from the still water level as the result of wave shoaling and breaking. The

lowering of mean water level is called the wave setdown and the rise is called the wave setup. The amount of wave setup at the shoreline of uniformly sloped beach has been computed with the random wave breaking model described in the present section, and the result is shown in Fig. 3.35.[23] The amount of the rise of mean water level increases as the beach becomes steep and the incident wave steepness becomes small.
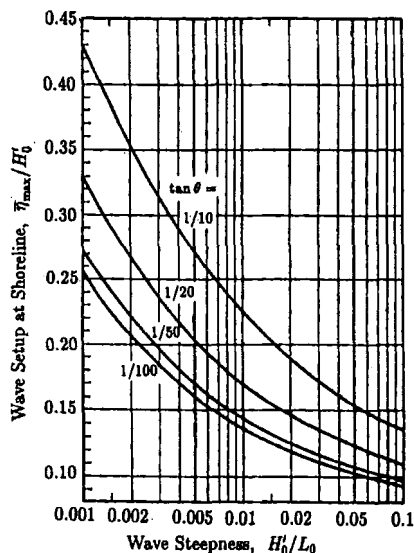
Fig. 3.35. Rise of mean water level at the shoreline of uniformly sloped beach.[23]

The validity of this diagram has been confirmed by field measurements of Yanagishima and Katoh.[31] They analyzed the one-year record of mean water level at an ocean observation pier located at the Hazaki Coast, Ibaraki, Japan. The astronomical tide level was subtracted from the observed mean water level and the effects of barometric pressure and wind setup were corrected. The remaining amount of mean water level rise was correlated with the significant wave height and period measured at an offshore station nearby. The average bottom slope around the observation pier was 1 on 60, and the equivalent deepwater wave steepness varied from 0.01 to 0.04. For this range of data, the normalized wave setup $\bar{\eta}/H_0'$ was approximately proportional to $(H_0'/L_0)^{-0.2}$, and the observed rise of mean water level was in good agreement with the value

read from Fig. 3.35. The rise of mean water level at times of storm waves was also observed at the tide station of Kashima Harbor, which is located about 15 km north of the Hazaki observation pier. However, the amount of mean water level rise was about one-half of the rise at Hazaki. The rise of mean water level in a harbor seems to be affected by the surrounding topography, breakwater layout, location of tide gage, and others.

3.5.7 *Other Models of Random Wave Breaking*

The random wave breaking model as previously described has been employed in many engineering applications. One shortcoming of this model is that the sea bottom should have a uniform slope. For coasts with nonuniform slopes, a compromise is made by defining a local slope and utilizing it in computation. However, it is difficult to apply this model to a seabed topography with bars and troughs.

In addition to the present model, a number of random wave breaking models have been proposed and are being utilized in numerical analysis of wave transformations: e.g., Battjes and Stive,[32] Dally,[33] Kweon and Goda,[34] Thornton and Guza,[35] among others. They are applicable for beaches of complicated profiles including those with longshore bars. They are mostly concerned with predictions of the root-mean-square wave height H_{rms}, whereas the deformation of wave height distribution in the surf zone is not computed except for the model by Dally.[33] The maximum wave height H_{max}, which is the important design parameter of vertical breakwaters and other structures, is not given by these models explicitly except for the model by Kweon and Goda.[34]

All the existing models of random wave breaking have the shortcoming that the phenomenon of surf beat is not duly taken into account. The model by the author employs an empirical estimate of the surf beat amplitude, as expressed by Eq. (3.24), to adjust the local water depth which controls the breaker height. A realistic estimate of wave heights at the shoreline has been obtained by the author's model through the incorporation of such surf beat amplitudes. However, Eq. (3.24) remains an engineering guess without true understanding of its physical processes. Many existing models do not even care for the surf beat phenomenon in the evaluation of wave heights in the surf zone.

The phenomenon of surf beat, or infragravity waves as being called now-adays, is being actively investigated in recent years in connection with the problems of ship mooring at berths, beach morphology in the swash zone, and others. The future model of random wave breaking is expected to include the surf beat model within it so that predictions of wave deformations in the surf and swash zones can be made more rationally and accurately.

3.6 Wave Reflection and Dissipation

3.6.1 *Coefficient of Wave Reflection*

When waves are reflected by a structure, the reflected waves cause increased agitation of the water in front of the structure, or they may propagate some distance to become a source of disturbance in an otherwise calm area of water. Thus, it is desirable to suppress the reflection of waves as much as possible. It is a problem of energy dissipation as well as estimation of the propagation of the reflected waves.

Concerning wave energy dissipation, the degree of wave reflection needs to be quantified. For this purpose, the coefficient of wave reflection K_R, which is the ratio of reflected wave height H_R to incident height H_I, is generally employed; i.e.,

$$K_R = H_R/H_I. \qquad (3.27)$$

Reflection coefficients for most structures are usually estimated by means of laboratory model tests, because a theoretical analysis is not feasible for wave reflection associated with partial wave breaking by structures. Approximate values of reflection coefficients as reported in various sources are listed in Table 3.7. The range in coefficients for a vertical wall depends on the degree of

Table 3.7. Approximate values of reflection coefficients.

Structural type	Reflection coefficient
Vertical wall with crown above water	$0.7 \sim 1.0$
Vertical wall with submerged crown	$0.5 \sim 0.7$
Slope of rubble stones (slope of 1 on 2 to 3)	$0.3 \sim 0.6$
Slope of energy dissipating concrete blocks	$0.3 \sim 0.5$
Vertical structure of energy dissipating type	$0.3 \sim 0.8$
Natural beach	$0.05 \sim 0.2$

wave overtopping, and it increases as the crown elevation increases. For sloped mounds and natural beaches, the reflection coefficient is inversely proportional to the steepness of the incident waves and the upper bounds correspond to swell of long period. Seeling and Ahrens[36] have given empirical formulas to estimate the reflection coefficient for beaches, revetments and rubble mound breakwaters, based on a large amount of laboratory data including that of irregular waves.

For a vertical wall of the energy dissipating type, such as a perforated wall, the reflection coefficient is governed by the shape of the structure, the width of the energy dissipating section of the structure relative to the incident wavelength, and other factors. Therefore, individual scale model tests are required to estimate the reflection coefficient for these types of structures for a given wave condition. Fig. 3.36 is a sample result of model tests performed by Tanimoto *et al.*[37] It gives the reflection coefficient for irregular waves incident on a concrete caisson with a front wall having circular perforations. The reflection
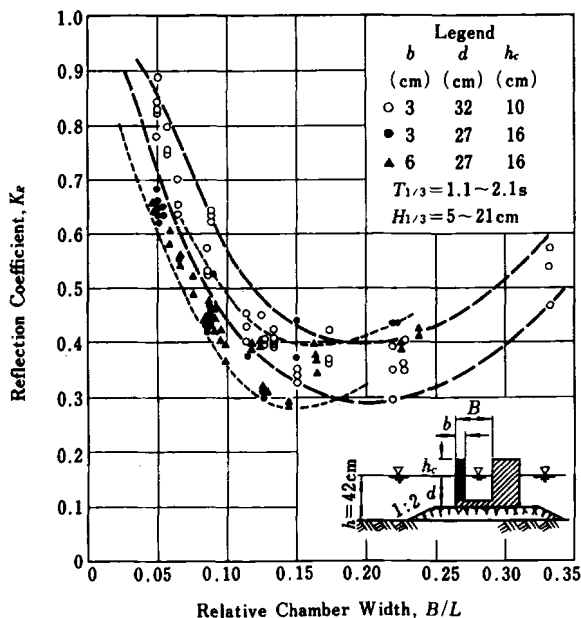
Fig. 3.36. Reflection coefficient for a perforated-wall caisson breakwater for irregular waves (after Tanimoto *et al.*[37]).

coefficient has a minimum value of $(K_R)_{\min} \simeq 0.3$ at the relative cell width of $B/L \simeq 0.15$ and it rises above 0.7 when the relative cell width becomes less than 0.05.

3.6.2 *Propagation of Reflected Waves*

Each component wave of a random sea is assumed to be reflected at an angle equal to the angle of incidence and to continue to propagate in that direction, as in the theory of geometrical optics. A possible departure from geometric wave reflection is the case of long-period waves of large amplitude incident at a large angle to a reflective structure in a shallow water area. In such a case, waves being incident nearly parallel to the structure may not produce clear reflected waves but instead form gradually swelling crests which run along the structure. This phenomenon is called Mach-stem reflection and has been observed on the occasion of tsunami attacks, as reported by Wiegel.[38]

Another aspect of reflected waves is that they have a finite length along their crest lines, because reflective structures such as caisson breakwaters or quay walls have limited extent. Therefore, reflected waves disperse during propagation away from the source of reflection in a manner similar to the phenomenon of wave diffraction. The dispersion of the reflected waves can be analyzed by means of the theoretical solution for wave reflection by an island barrier,[39,40] or by the numerical integration method for simulating wave propagation.[41]

As an engineering approximation, the spatial distribution of reflected wave height can be estimated by making use of diffraction diagrams for an opening between breakwaters. The idea is to treat the zone of wave reflection as the opening between fictitious breakwaters, as sketched in Fig. 3.38, and to apply a diffraction diagram accordingly. The direction of the imaginary incident
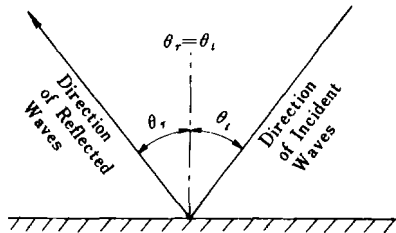
Fig. 3.37. Direction of reflected waves.

Fictious Diffraction Coefficient
= Wave Height Ratio of Reflected Waves
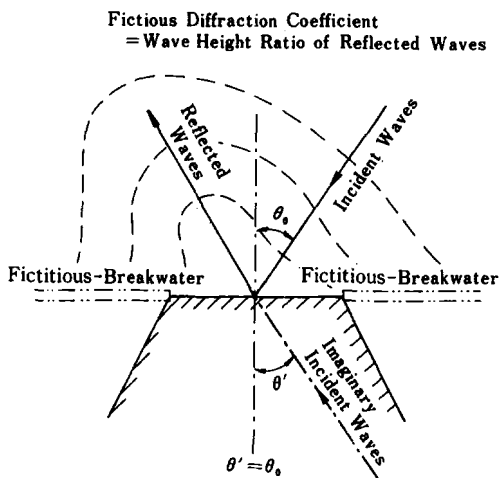
Fig. 3.38. Estimation of propagation of reflected waves by means of fictitious breakwaters.

waves is set at the mirror image of the actual waves at the reflective boundary. (In applying the diffraction diagram, a rotation of the axis of the diffracted waves specified in Table 3.4 in Sec. 3.2.3 must be made.) Then the amount of wave height attenuation of the reflected waves can be taken as equal to the diffraction coefficient obtained from the diagram thus applied.

The essential point in this method is to employ diffraction diagrams of random sea waves. This is because directional spectral characteristics must be taken into account in every problem involving two-dimensional propagation of sea waves. Likewise, if the problem is solved either analytically or numerically, the solution for a single direction of incidence with one wave period is not sufficient. The computation must be done for many wave components representative of the directional wave spectrum, and the results must be combined with the weight of the directional energy so as to yield a meaningful answer to the problem.

Sometimes a reflective structure extends over such a great distance as to make inapplicable the diffraction diagram for a breakwater opening. In that case, one can apply diffraction diagrams for a semi-infinite breakwater or use the angular spreading method with the cumulative distribution curve of total wave energy with respect to the azimuth from the principal wave direction.

Fig. 3.39. Estimation of the height of reflected waves by the angular spreading method.

Example 3.8

Wind waves are incident at an angle of 40° to vertical wall $\overline{\text{QR}}$ of length 2.5 km as shown in Fig. 3.39. Estimate the height of the reflected waves at Point P, assuming that the reflection coefficient of the vertical wall is 1.

Solution

First, the lines $\overline{\text{PQ}}$ and $\overline{\text{PR}}$ are drawn and the angles that the extensions of these lines make with the direction of the imaginary incident waves (mirror images of the actual waves) are measured. The angles are $\theta_1 = 12°$ and $\theta_2 = -49°$ in the example of Fig. 3.39. These angles are equal to the azimuths from the principal wave direction of the component waves which are reflected from the edges of Q and R and which propagate straight to Point P. Thus, the angle between θ_2 and θ_1 represents the azimuth of the component waves reflected from an arbitrary point between Q and R to reach Point P.

Next, the energy of the reflected waves reaching Point P is estimated as being equal to the energy of the component waves having an azimuth between θ_2 and θ_1. The ratio of this energy to the total energy is estimated with the cumulative distribution curve for $P_E(\theta)$ shown in Fig. 2.15 in Sec. 2.3.

By using the curve pertaining to $s_{\max} = 10$ for wind waves, we obtain $\Delta E = P_E(\theta_1) - P_E(\theta_2) = 0.63 - 0.08 = 0.55$. Therefore, the ratio of reflected to incident wave heights at Point P is obtained as the square root of the above energy ratio, or $\sqrt{0.55} = 0.74$.

If the structure has a reflection coefficient less than 1, the above estimate for the dispersion effect of reflected waves should be multiplied by the reflection coefficient of the structure to yield the final estimate of the reflected wave height reaching the point of interest. Another cause of the attenuation of reflected waves is energy dissipation by an adverse wind. We sometimes observe such a phenomenon when waves are reflected from a vertical wall; some of the wave crest are blown out by the opposing wind. The reflected waves lose additional energy through violent interaction with the incident waves. However, the rate of wave attenuation by adverse wind is not known quantitatively. It is only known empirically that wind waves of large steepness are quickly attenuated, whereas swell of low steepness continues to propagate over a long distance with only minor dissipation. In harbor planning and design, it will be on the safe side to disregard the attenuation of wave height by an adverse wind. If the water area in a harbor is quite broad and the harbor is to be designed against locally-generated wind waves, the effective value of the reflection coefficient of vertical walls within the harbor may be reduced by 80% or more as a measure of incorporating the effect of an adverse wind.

3.6.3 *Superposition of Incident and Reflected Waves*

The effect of reflected waves on harbor agitation and structural design is rather complicated, because not only the wave height but also the wave direction enters into the problem. When only the total wave height is of interest, however, it can be estimated by the principle of summation of energy components as in the following:

$$H_S = \sqrt{H_I^2 + (H_R)_1^2 + (H_R)_2^2 + \cdots}, \tag{3.28}$$

where H_S denotes the significant height of the superposed waves, and $(H_R)_1$, $(H_R)_2, \ldots$ represent the significant heights of the reflected waves originating from various reflective sources. Equation (3.28) is not applicable in the immediate vicinity of structures because of the fixed phase relation between incident and reflected waves. But the phase interference almost cancels out among the various components of random sea waves if the distance from the reflective structure is more than one wavelength or so, and Eq. (3.28) yields a reasonable estimate of the wave height.
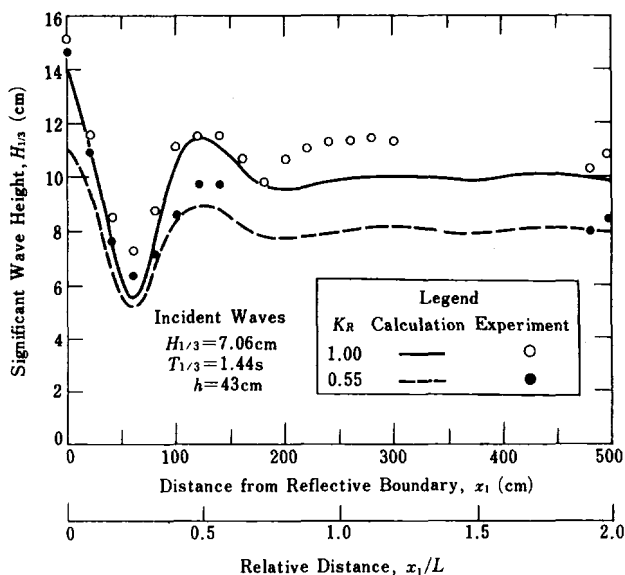
Fig. 3.40. Spatial variation of irregular standing wave height.[42]

The applicability of Eq. (3.28) is demonstrated in Fig. 3.40, which shows the spatial variations of significant wave height in front of model structures in a laboratory flume.[42] The incident waves are irregular trains with frequency spectra of the Bretschneider–Mitsuyasu type. Open circles represent the data for a fully reflective vertical wall, and filled circles represent the data for a model structure having a reflection coefficient of 0.55. The solid and dash lines indicate wave heights estimated from the frequency spectra of superposed wave systems, which were obtained by calculating the amplitudes of standing waves at each location for various frequency components of the incident wave spectrum. Although the significant height of the superposed waves exhibits a fluctuation corresponding to the nodes and antinodes of standing waves in the vicinity of the structures, as seen in Fig. 3.40, the fluctuations decrease rapidly with distance from the structure and the wave height approaches an asymptotic value. In fact, Eq. (3.28) predicts such an asymptotic value for points far from a reflective structure.

The theoretical basis of Eq. (3.28) is Eq. (2.33) in Sec. 2.4, which states that the significant wave height is proportional to the square root of the total wave energy, irrespective of the spectral shape.

3.7 Spatial Variation of Wave Height Along Reflective Structures

3.7.1 *Wave Height Variation near the Tip of a Semi-infinite Structure*

When waves are incident to a structure, a standing wave system is formed at its front. If the structure reflects the incident waves completely and the wave system is one-dimensional, the standing wave height at the front wall becomes twice the incident height. In actual situations, however, the standing wave height along the structure undulates, because there usually exists a two-dimensional effect owing to the finite extent of the structure. In addition, the plan shape of the structure may not be in straight lines.
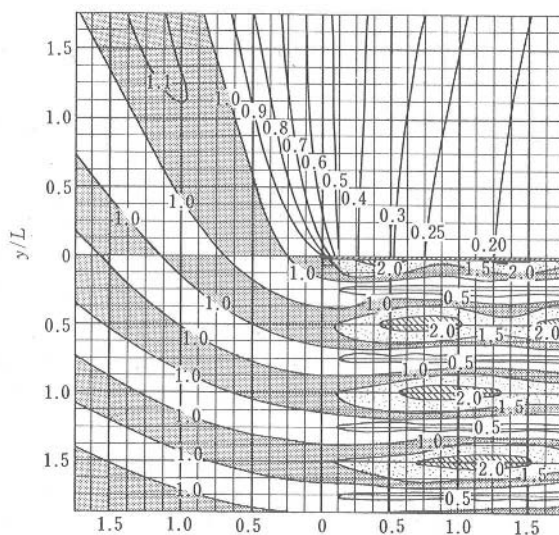
Fig. 3.41. Variation of the height of regular waves around a semi-infinite breakwater (after Morihira and Okuyama[43]).

First, the wave height around the tip of a structure is dominated by diffraction at the tip. Figure 3.41 exhibits such an example, which shows the spatial variation of wave height in the front as well as at the rear of a semi-infinite breakwater of perfect wave reflection when waves of a regular train are incident

normally.[43] Although a standing wave system is seen to be formed in front of the breakwater, the wave height along the anti-nodal line at $y/L = 0$, 0.5, 1.0, ... exceeds twice the incident wave height at some locations, whereas the wave height along the nodal lines remains at some finite value.

The ratio of the wave height along a breakwater to the incident height is generally calculated with the following formula, when waves approach the breakwater at an angle Θ between their direction of propagation and the face line of the breakwater[44]:

$$\frac{H_S}{H_I} = \sqrt{(C + S + 1)^2 + (C - S)^2}\,, \tag{3.29}$$

where C and S stand for the Fresnel integrals:

$$C = \int_0^u \cos\frac{\pi}{2}t^2 dt, \quad S = \int_0^u \sin\frac{\pi}{2}t^2 dt \quad : u = 2\sqrt{\frac{2x}{L}}\sin\frac{\Theta}{2}\,, \tag{3.30}$$

in which x denotes the distance from the breakwater tip and L is the wavelength.

Figure 3.42 shows the distribution of wave height along a breakwater as computed with Eq. (3.29) for the case of waves with period 10 s normally incident to a breakwater located in a water depth of 10 m. The solid line represents regular waves of period $T = 10$ s, and the dash line presents the result for long-crested random waves with $T_{1/3} = 10$ s. The random waves were assigned the Bretschneider–Mitsuyasu frequency spectrum of Eq. (2.10) in Sec. 2.3 without any directional spreading (all component waves normally incident to the
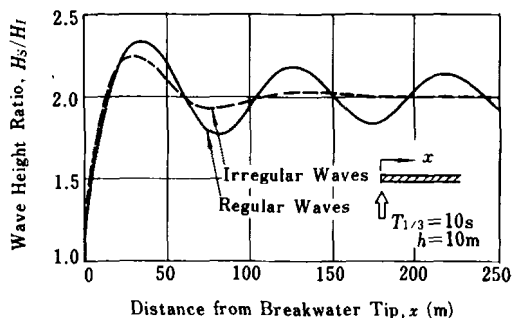
Fig. 3.42. Variation of wave height in front of a semi-infinite breakwater.

breakwater). The wave height ratio of random waves was computed with Eq. (3.14) in Sec. 3.2 by replacing the factor K_d with the ratio H_S/H_I given by Eq. (3.29). The computed wave height shows undulations around the line $H_S/H_I = 2.0$. The first peak takes a value of 2.34 for regular waves and 2.25 for random waves. A large undulation repeats several times for the regular waves, but it diminishes rapidly after the second peak for the random waves. If directional spreading is introduced, the undulation in the wave height will be further reduced.

The undulation in wave height along a breakwater produces a spatial variation in the wave pressure exerted on the breakwater. Because the waves diffracted into the back side of the breakwater are shifted in phase from the standing waves at the front of the breakwater, the variation in total wave force exerted on a unit length of breakwater is greater than the variation in the wave height itself. For example, the first peak of wave force shows an increase of more than 20% compared with the standing wave force on an infinitely long breakwater. Surveys of concrete caissons of vertical breakwaters which have slid due to wave action often reveal evidence of an undulation in the sliding distance. Ito and Tanimoto[44] have explained this phenomenon as the effect of the waves diffracted from the tip of the breakwater and called it "meandering damage" to breakwaters.

A similar undulation in wave height is predicted in the vicinity of the corner of reclaimed land protected by straight, reflective seawalls. The wave height distribution for such a configuration can be analyzed with the theory of Mitsui.[45]

3.7.2 *Wave Height Variation at an Inward Corner of Reflective Structures*

An inward corner of a reflective wall is sometimes formed when an extension of a vertical breakwater is made with an outward bend to the offshore, or when a short jetty is attached at the end of reclaimed land at an angle of bend toward the offshore. Waves incident to such a configuration are reflected toward the inward corner from the two reflective walls, and a pronounced increase in wave height can be observed at the corner. By denoting the angle between the two walls as β, as sketched in Fig. 3.43, the ratio of wave height at the corner to
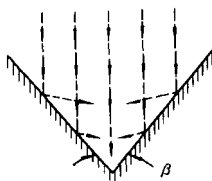
Fig. 3.43. Wave concentration at an inward corner.

the incident height is given by the following formula, provided the reflective walls at both sides are sufficiently long:

$$\frac{H_S}{H_I} = \frac{2\pi}{\beta} \,, \tag{3.31}$$

where β is expressed in radians. The formula is applicable to random sea waves described with directional wave spectra as well.

The distributions of the height of regular waves along both reflective walls usually exhibit large fluctuations, because of interference between the incident waves and the two reflected waves. Depending on the direction of wave incidence and the angle between the two walls, the wave height at some point along the walls may become greater than the height at the corner. In the case of random sea waves, the spatial fluctuation in wave height is mostly smoothed out because of the wide spread in the frequency and directional energy distributions. The wave height by Eq. (3.31) gives the maximum value along the two reflective walls for the case of random sea waves. Kobune and Osato[46] have made a series of computations for the distribution of the wave height along two reflective walls for several values of the angle between them for random sea waves having the Bretschneider–Mitsuyasu frequency spectrum and Mitsuyasu-type spreading function with a specific value of $s_{\max} = 75$. They proposed the following approximate method for estimating the wave height for such geometry:

(i) The wave height ratio at the inward corner is estimated with Eq. (3.31).

(ii) The distribution of the height of reflected waves along the wings of the reflective walls is estimated by the technique introduced in Sec. 3.6.2, as sketched in Fig. 3.44. Then the height of these waves reaching the line of the other wing is read from the estimated wave height distribution, and the overall wave height along the other wing is estimated with Eq. (3.28).
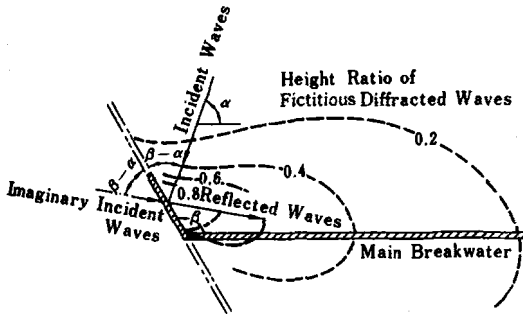
Fig. 3.44. Estimation of reflected wave height.

(iii) The distances at which the wave height ratio takes the minimum value of 2.0 are estimated for both wings by the following:

$$\frac{x_{\min}}{L} = 0.16 \exp\left[1.05 \tan\frac{\alpha}{2}\right], \tag{3.32}$$

where α denotes the angle between the direction of wave approach and the face line of the reflective wall along which $x_{\min}$ is to be determined.

(iv) The wave height distribution between the corner and the point $x = x_{\min}$ is assumed to vary linearly from the value obtained with Eq. (3.31) at $x = 0$ and the value 2.0 at $x = x_{\min}$.

(v) In the range $x > x_{\min}$, the mirror image of the line of wave height distribution estimated in Step (iv) is drawn about the axis of symmetry at $x = x_{\min}$. Then the resultant wave height ratio is compared with the value estimated in Step (ii), and the lesser of the two values is to be adopted as an estimation of the wave height ratio.

Figure 3.45 illustrates the above method of wave height estimation for an auxiliary reflective-type breakwater of length $L_{1/3}$ attached at an angle of $\beta = 120°$ to a main breakwater of the reflective-type with a length of 5 $L_{1/3}$. Random sea waves are incident to this structure with an angle of approach of $\alpha = 60°$ to the main breakwater. In Fig. 3.45, the result of the approximate estimation is denoted by the dash line, which can be compared with the result of a numerical computation with the directional wave spectrum, denoted by the solid line. Although some small differences are observed between the two estimations, the approximate method does represent the pattern of the wave height quite well.
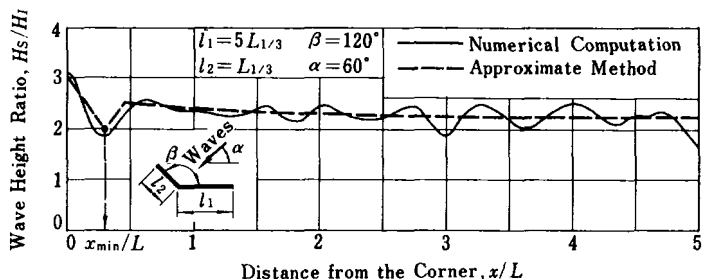
Fig. 3.45. Distribution of wave height along a main breakwater with an auxiliary breakwater (after Kobune and Osato).[46]

3.7.3 *Wave Height Variation along an Island Breakwater*

If the length of a single isolated breakwater in the offshore (hereafter called an island breakwater) is on the order of a few wavelengths of the incident waves or less, the distribution of the wave height along the breakwater will show considerable variation owing to the effects of the waves diffracted from both tips of the breakwater. Figure 3.46 presents the result of a computation of the height at the front and the rear of an island breakwater obtained with the solution of the velocity potential in problem.[39] The incident waves are regular trains with angles of approach of 30° (dash line) and 90° (solid line). When waves are obliquely incident, the wave height gradually increases toward the down-wave side from the up-wave side of the breakwater, probably because some distance is needed before the reflected waves can achieve full height.
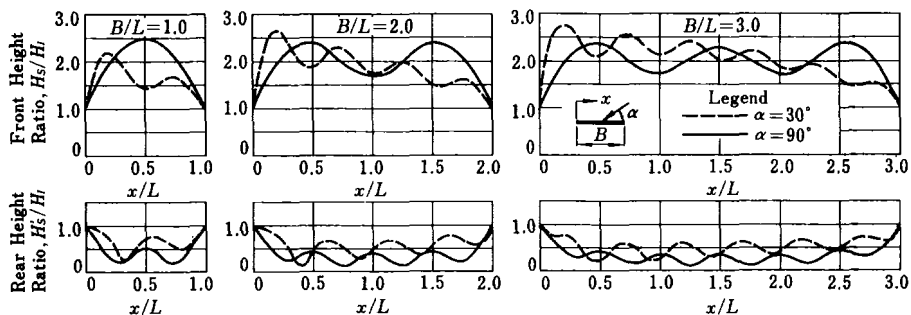
Fig. 3.46. Distributions of wave height along the front and rear of an island breakwater.[39]

Such a variation in the distribution of wave height modifies the wave force acting on the structure, as in the case of the tip of a semi-infinite breakwater. An island breakwater experiences a greater variation in wave force than a semi-infinite breakwater, because waves diffracted behind the island breakwater may be just opposite in phase to the waves in front of the breakwater while still maintaining appreciable height. If the waves arrive in regular trains, the total wave force per unit length of breakwater may reach 1.8 times that of an infinitely long vertical breakwater (one-dimensional standing wave system), though the spatial variation in total wave force along an island breakwater is reduced to some extent by the effect of the wave spectral characteristics for random sea waves.
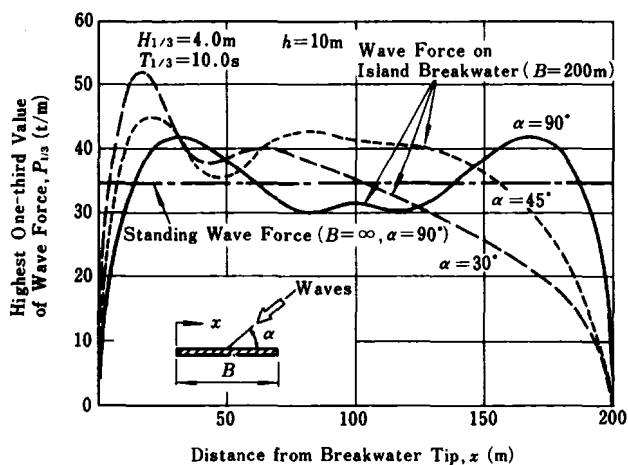
Fig. 3.47. Calculated distribution of wave force along an island breakwater due to irregular waves.[47]

Figure 3.47 is an example of the distribution of total force of irregular waves along an island breakwater when the frequency spectral characteristics are included in the computation, but with no directional spreading of wave energy considered.[47] The breakwater is of the upright type and 200 m in length, erected in water 10 m deep and subject to the attack of irregular waves with $H_{1/3} = 4$ m, $T_{1/3} = 10$ s, and $L_{1/3} = 92.3$ m from several directions. The total wave force is estimated from the force spectrum, computed at each frequency by using the theory of small amplitude standing wave force. The mean of the highest one-third wave force is calculated from the integral of the force

spectrum by means of Eq. (3.32) in Sec. 2.4; the coefficient of proportionality 4.0 has been changed to 2.0 for this case because the wave force refers to the height of the crest and not to the distance between crest and trough. In comparison with the standing wave force on an infinitely long breakwater, denoted by the horizontal line of heavy dash-dots in Fig. 3.47, the island breakwater is observed to experience an increase in total wave force by 20 to 50%, depending on the angle of wave approach.

3.8 Wave Transmission over Breakwaters

3.8.1 *Wave Transmission Coefficient*

The principal function of a breakwater is obviously to prevent the penetration of incident waves into a harbor. Therefore, waves passing through the gaps in a breakwater and waves generated on the leeside of a breakwater by wave overtopping must be reduced to a minimum. Complete stoppage of these permeating and overtopping waves may not be recommended, however, in consideration of excessive construction cost for doing so. Furthermore, for short detached breakwaters designed for beach protection, in practice some discharge through the breakwater is allowed to promote the formation of salients. Thus, hydraulic model tests have been performed to obtain information on the coefficient of wave transmission of various structural types of breakwaters. The following is a summary of these test results.

(A) *Wave transmission over a vertical breakwater*

Wave transmission in this case is mainly the result of waves generated in the lee of the breakwater by the impact of the fall of the overtopping water mass. Therefore, the ratio of the crest elevation of the breakwater to the incident wave height is the principal parameter governing the wave transmission coefficient. Figure 3.48 shows a compilation of the author's data from laboratory tests[48] with regular waves. The curves describing the transmission coefficient K_T, i.e., the ratio of transmitted to incident wave heights, have been drawn through data exhibiting a scatter amounting to $\pm$ 0.1 in the absolute value of K_T. The diagram is applicable to irregular waves also, as shown by the example of some tests with irregular waves[49] in Fig. 3.49. The curve drawn through the data points of K_T for irregular waves was taken from Fig. 3.48 for regular waves. Figure 3.49 also displays the data for the reflection coefficient.
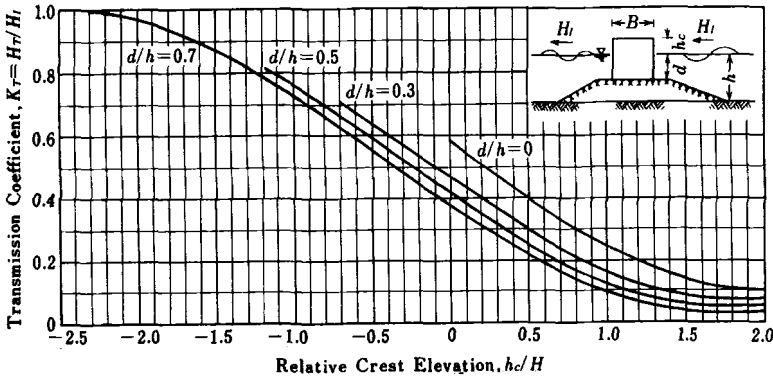
Fig. 3.48. Wave transmission coefficient for a vertical breakwater.[48]
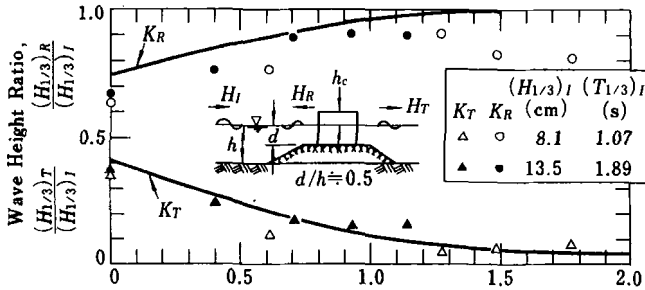
Fig. 3.49. Example from irregular wave tests on wave transmission and reflection coefficients for a vertical breakwater.[49]

Waves transmitted by overtopping tend to have shorter periods, because the impact of the falling water mass often generates harmonic waves with periods of one-half and one-third the incident wave period. Figure 3.50 shows the change in period of transmitted waves normalized by the period of the incident waves in the same irregular wave test shown in Fig. 3.49.

A simple expression for the wave transmission coefficient of a vertical breakwater has been given by Kondo and Sato[50]:

$$K_T = 0.3 \left(1.5 - \frac{h_c}{H_1} \right) \ : \ 0 \leq \frac{h_c}{H_1} \leq 1.25 , \tag{3.33}$$

in which h_c denotes the crest elevation of the breakwater above the still water level. They also proposed the following formula for a vertical breakwater
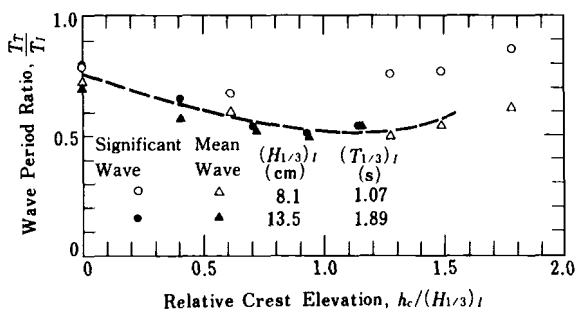
Fig. 3.50. Change in period of transmitted waves over a vertical breakwater in an irregular wave test.[49]

protected by a mound of wave-dissipating concrete blocks at its front:

$$K_T = 0.3 \left(1.1 - \frac{h_c}{H_1} \right) \; : \; 0 \le \frac{h_c}{H_1} < 0.75 . \tag{3.34}$$

Figure 3.48 as well as Eqs. (3.33) and (3.34) are approximately applicable to individual waves in an irregular train of waves. This implies that the wave height distribution of the waves transmitted over a protruding breakwater has a wider range than the Rayleigh distribution discussed in Sec. 2.2, because individual waves of large height have a low value of h_c/H and a large value of K_T compared to the mean wave.

(B) *Wave transmission through a breakwater consisting of energy-dissipating concrete blocks*

Many detached breakwaters in water of a few meters depth have been built solely with energy dissipating concrete blocks such as tetrapods in order to promote formation of salients on the beach behind them. The transmitted waves are produced mainly by penetration of some portion of the incident waves through the gaps between the concrete blocks. In general, the transmission coefficient is inversely proportional to the steepness of the incident waves. Figure 3.51 is due to Hattori,[51] who compared his laboratory test curves with some data from field observations.[52,53]

(C) *Wave transmission through a rubble mound breakwater*

A rubble mound breakwater has less void than a block mound breakwater, and the individual sizes of the gaps between rubble stones are much smaller than
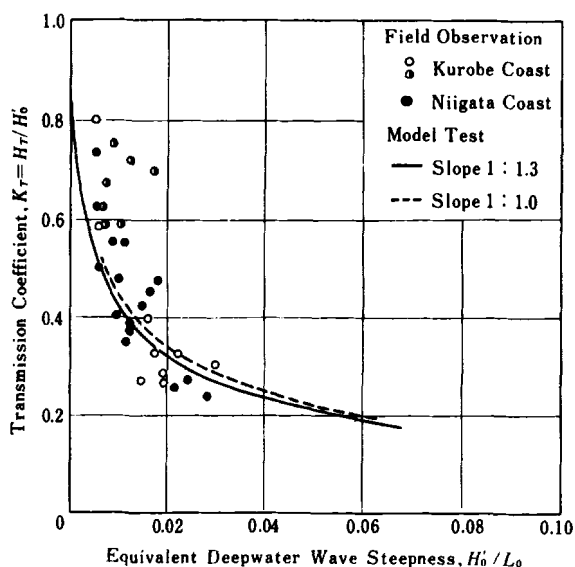
Fig. 3.51. Wave transmission coefficient of a mound breakwater constructed with tetrapods (after Hattori).[51]

those between blocks. As a result, wave permeation is considerably reduced compared with that for a block mound breakwater. Thornton and Calhoun[54] found a wave transmission coefficient of 10 to 30% for a prototype rubble mound breakwater in shallow water. Generally speaking, long-period waves with low steepness produce greater wave permeation than short-period waves with high steepness. However, no systematic hydraulic tests with irregular waves seem to have been made on the subject of wave permeation through a rubble mound breakwater. Such tests would required careful selection of the stone size in the model in consideration of scale effects, because the rate of energy dissipation of flow through gaps between stones is dependent on the Reynolds number.

3.8.2 *Propagation of Transmitted Waves in a Harbor*

Presently no reliable information is available on the subject of propagation and dispersion of waves transmitted to the lee of a breakwater. It is believed that for rubble and block mound breakwaters, the transmitted waves arising mainly from permeation would continue to propagate in a pattern similar to that of the

incident waves, but with much reduced wave heights. For vertical breakwaters, where wave transmission by overtopping is predominant, the generation of transmitted waves would take place intermittently at short distances here and there, because incident waves in the sea are random and their wave crests are discontinuous. Thus, the transmitted waves would take the pattern of dispersing crests of concentric circles, with the generating sources positioned at various points along the breakwater. There is the possibility that frequent wave overtopping may occur at a particular section of a breakwater, with frequent appearance of resultant transmitted waves, owing to the layout of the breakwater. Because a general description of such individual situations is not feasible, it is necessary to assume in the analysis of harbor agitation that the transmitted waves with heights described as above would propagate in a pattern similar to that of the incident waves.

There is a report[55] of two-dimensional laboratory tests on obliquely incident waves to a vertical breakwater that indicates a decrease in the wave transmission coefficient by several percent compared to the case of normal incidence. Also, the direction of propagation of the transmitted waves by overtopping was observed to be deflected slightly toward the line normal to the breakwater. This can be understood as the effect of generation by overtopping of short-period waves, which propagate with a celerity less than that of the incident waves, and a process similar to wave refraction over varying water depth must have taken place.

3.9 Longshore Currents by Random Waves on Planar Beach

3.9.1 *Longshore Currents by Unidirectional Irregular Waves*

Longshore currents induced by waves obliquely incident to the beach are one of the important driving forces of sediment transport and beach deformation. Several empirical and theoretical formulas were proposed after World War II. Then in 1970, Longuet-Higgins[56] clarified the mechanism of longshore currents generation by using the concept of the radiation stress, and gave the theoretical basis for their quantitative evaluation. He introduced the idea of lateral mixing to smooth out an abrupt drop of longshore current velocity just outside the breaking point, which was predicted by theory for regular waves but never observed in laboratory experiments.

The theoretical prediction of the abrupt change of longshore current velocity originates from the fact that all waves in a regular train break at a single, fixed location, thus producing a sudden rise of the gradient of radiation stress. In a train of irregular waves, individual waves break over a wide distance across the surf zone. The magnitude of radiation stress varies gradually, and the velocity of longshore currents is predicted to have a smooth variation across the surf zone. Battjes[57] was the first in computing the longshore current velocities across the surf zone induced by irregular waves. He obtained the cross-shore profile of longshore current velocity, which varies smoothly, without resorting to the artifice of lateral mixing.
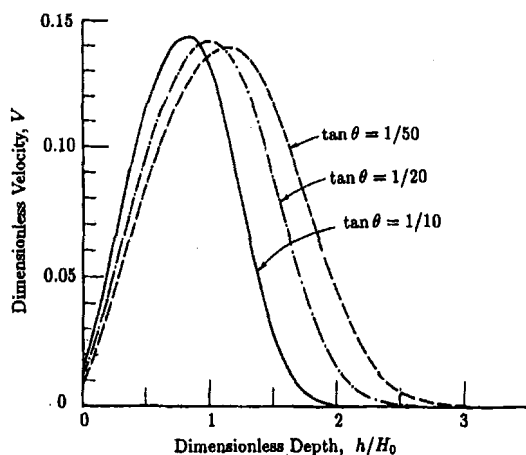
Fig. 3.52. Longshore current velocity profiles computed by Goda's random wave breaking model for deepwater wave steepness $H_0/L_0 = 0.02$ and incident angle $\alpha_0 = 30°$ for several bottom slopes.[58]

The predicted velocity of the longshore currents by irregular waves is dependent on the random breaking model being employed. Goda and Watanabe[58] utilized the model described in Sec. 3.5 to compute the longshore current velocity induced by unidirectional random waves. A planar beach with straight and parallel depth-contours is assumed. Figure 3.52 shows examples of the cross-shore profile of current velocity, exhibiting the effect of bottom slope. The ordinate is the dimensionless velocity defined by

$$V = \frac{C_f\, v}{\sqrt{gH_0}\, \tan\theta\, \sin\alpha_0}\,, \tag{3.35}$$

where v denotes the velocity of longshore currents, C_f denotes the coefficient of friction, g denotes the acceleration of gravity, H_0 and L_0 stand for the deepwater significant wave height and wavelength, respectively, $\tan\theta$ denotes the sea bottom slope, and α_0 denotes the deepwater incident wave angle.

Computation was carried out for a number of combinations of bottom slope, deepwater wave steepness and deepwater incident angle. For the set of many cross-shore velocity profiles thus obtained, the following empirical formula of the Weibull-type distribution has been fitted successfully:

$$v(z) = v_0 \left[\frac{z - B}{A}\right]^{k-1} \exp\left[\frac{z - B}{A}\right]^k \quad : z = \frac{h}{H_0}, \qquad (3.36)$$

in which the velocity term v_0 and the constants A, B and k are evaluated by the following equations:

$$v_0 = \frac{\sqrt{gH_0}\tan\theta}{C_f} \left\{0.195 + 0.26\exp\left[-\frac{0.008}{H_0/L_0}\right]\right\} \sin\alpha_0 \cos(0.7\alpha_0), \quad (3.37)$$

$$A = (1.51 - 3.9\tan\theta)\left\{1 + \exp\left[-46\left(\frac{H_0}{L_0}\right)^{0.7}\right]\right\}\cos\left(\frac{2}{3}\alpha_0\right), \qquad (3.38)$$

$$B = 0.0117\ln\frac{H_0}{L_0} + 0.010, \qquad (3.39)$$

$$k = 2.65\exp[-0.7\,(\tan\theta)^{0.75}] - 10.4\frac{H_0}{L_0} + \left[0.08 + 140\frac{H_0}{L_0}\tan\theta\right]$$

$$\times \sin^2\left(\frac{\alpha_0}{2}\right). \qquad (3.40)$$

The maximum velocity of longshore currents $v_{\max}$ and the water depth h_{mode} at which $v_{\max}$ appears are derived from the velocity profile of Eq. (3.34) as follows:

$$v_{\max} = v_0\left(1 - \frac{1}{k}\right)^{1-1/k}\exp\left[-\left(1 - \frac{1}{k}\right)\right] \quad \text{at}$$

$$\frac{h_{\text{mode}}}{H_0} = B + A\left(1 - \frac{1}{k}\right)^{1/k}. \qquad (3.41)$$

Example 3.9

Estimate the maximum longshore current velocity and the water depth of its appearance on a planar beach with the slope $\tan\theta = 1/50 = 0.02$ for incident deepwater significant wave of $H_0 = 3.0$ m and $T_0 = 9.0$ s, with the incident angle of $\alpha_0 = 30°$.

Solution

The deepwater wavelength is $L_0 = 126.4$ m and the wave steepness is $H_0/L_0 = 0.0237$. The friction coefficient is assumed to be $C_f = 0.01$. For the given conditions, the velocity term v_0 and constants, A, B and k, are calculated by Eqs. (3.35) to (3.38) as follows:

$$v_0 = \frac{\sqrt{9.8 \times 3.0} \times 0.02}{0.01} \times \left\{ 0.195 + 0.26 \exp\left[-\frac{0.008}{0.0237} \right] \right\}$$

$$\times \sin 30° \times \cos(0.7 \times 30°) = 1.93 \text{ m/s},$$

$$A = (1.51 - 3.9 \times 0.02) \times \{1 + \exp[-46 \times 0.0237^{0.7}]\}$$

$$\times \cos(\frac{2}{3} \times 30°) = 1.393,$$

$$B = 0.0117 \times \ln 0.0237 + 0.010 = -0.034,$$

$$k = 2.65 \exp[-0.7 \times 0.02^{0.75}] - 10.4 \times 0.0237$$

$$+ (0.08 + 140 \times 0.0237 \times 0.02) \times \sin^2(30°/2) = 2.316.$$

With the above result, the maximum velocity and the water depth of its appearance are calculated by Eq. (3.41) as

$$v_{max} = 1.93 \times (1 - 1/2.316)^{1 - 1/2.316} \times \exp[-(1 - 1/2.316)] = 0.81 \text{ m/s},$$

$$h_{mode} = 3.0 \times [-0.034 + 1.393 \times (1 - 1/2.316)^{1/2.316}] = 3.2 \text{ m}.$$

Though the set of empirical formulas of Eqs. (3.36) to (3.41) have rather complicated expressions, it has the merit such that the longshore current velocity can be predicted by the deepwater wave condition alone: no parameter based on field wave data is required. These empirical formulas have been applied on the field data of longshore current velocity profiles measured by Thornton and Guza.[59] The formulas yielded the prediction which agrees with the field data as good as the result obtained by Thornton and Guza, who calculated their prediction using the values of empirical coefficients, which were related to the breaker types and breaker height, and adjusted to their field data.

3.9.2 *Longshore Currents by Directional Random Waves*

Compared with unidirectional irregular waves, directional random waves generate longshore currents weaker than those by the former. In the directional random wave system, the wave energy is spread around the principal wave direction. This energy spread causes the decrease of the radiation stress component S_{xy} normal to the wave direction, the gradient of which is the driving force of longshore currents as explained by Longuet-Higgins.[56]
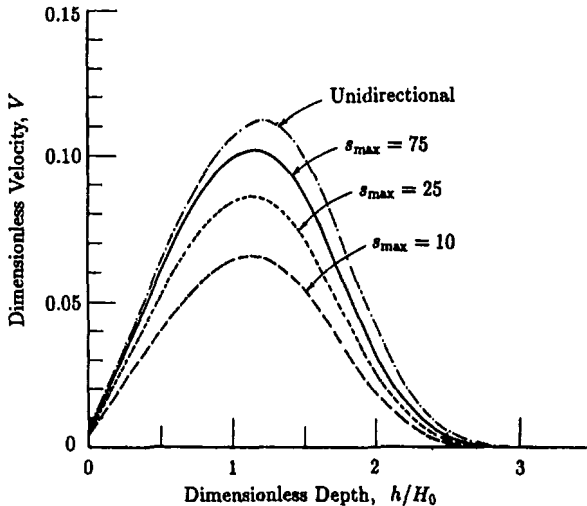
Fig. 3.53. Effect of directional spreading parameter on the longshore current velocity profiles on planar beach with the slope $\tan\theta = 1/50$ for incident waves with $H_0/L_0 = 0.01$ and $\alpha_0 = 40°$.[60]

Computation of longshore currents induced by directional random waves has been undertaken by Goda[60] for a limited number of cases. Figure 3.53 exhibits the effect of directional spreading parameter on the longshore current velocities. The ordinate is the dimensionless velocity V, defined by Eq. (3.35), and the abscissa is the dimensionless water depth h/H_0. The directional spectrum is given by the product of the Bretschneider–Mitsuyasu frequency spectrum and the Mitsuyasu-type directional spreading function. As the directional spread increases with the decrease in the s_{max} value, the magnitude of longshore current velocity decreases with little change in the cross-shore profiles.
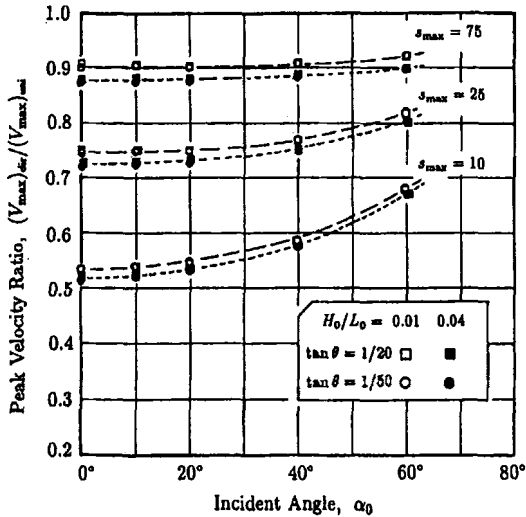
Fig. 3.54. The ratio of the maximum longshore current velocity by directional random waves to that by unidirectional irregular waves versus incident wave angle.[60]

The amount of decrease in the longshore current velocity due to directional spreading is affected by the incident wave angle. Figure 3.54 shows the extent of velocity reduction by directional spreading. The ordinate is the ratio of maximum velocity induced by directional random waves to that by unidirectional random waves and the abscissa is the deepwater incident angle. The velocity ratio $(V_{max})_{dir}/(V_{max})_{uni}$ is lowered as the angle of wave incidence becomes small and as the directional spreading parameter s_{max} decreases. The extent of velocity reduction is also affected slightly by the shape of frequency spectrum: the sharper the spectral peak is, the smaller is the current reduction by directional spreading.

References

1. Y. Goda, "Transformation of wave crest pattern in shoaling water," *Proc. 23rd Int. Conf. Coastal Engrg.* (Venice, 1992), pp. 199–211.
2. U.S. Army Coastal Engineering Research Center, *Shore Protection Manual*, U.S. Govt. Printing Office (1977), pp. 2–69 ∼ 2–75.
3. A. T. Ippen (ed.), *Estuary and Coastline Hydrodynamics*, (McGraw-Hill, Inc., 1966), pp. 260–263.
4. G. M. Griswold, "Numerical calculation of wave refraction," *J. Geophys. Res.* **68** (10) (1963), pp. 1715–1723.

5. W. S. Wilson, "A method for calculating and plotting surface wave rays," *U.S. Army Corps of Engrs., Coastal Engrg. Res. Center, Tech. Memo.* (17) (1966), 57p.

6. K. Nagai, "Diffraction of the irregular sea due to breakwaters," *Coastal Engineering in Japan* **15** (1972), pp. 59–69.

7. T. Karlsson, "Refraction of continuous ocean wave spectra," *Proc. ASCE* **95** (WW4) (1969), pp. 437-448.

8. K. Nagai, T. Horiguchi and T. Takai, "Computation of the propagation of sea waves having directional spectra from offshore to shallow water," *Proc. 21st Japanese Conf. Coastal Engrg.* (1974), pp. 349-253 (*in Japanese*).

9. Y. Goda and Y. Suzuki, "Computation of refraction and diffraction of sea waves with Mitsuyasu's directional spectrum," *Tech. Note of Port and Harbour Res. Inst.* **230** (1975), 45p (*in Japanese*).

10. Y. Ito, K. Tanimoto and S. Yamamoto, "Wave height distribution in the region of ray crossings–application of the numerical analysis method of wave propagation," *Rept. Port and Harbour Res. Inst.* **11** (3) (1972), pp. 87–109 (*in Japanese*).

11. C. L. Vincent and M. J. Briggs, "Refraction-diffraction of irregular waves over a mound," *J. Wtrwy., Port, Coast. and Ocn. Engrg.* **115** (2) (1989), pp. 269–284.

12. Y. Goda "Directional wave spectrum and its engineering applications," *Adv. Coast. and Ocn. Engrg.* (Ed. P. L.-F. Liu) **3** (World Scientific, 1997), pp. 67–102.

13. W. C. O'Reilly and R. T. Guza, "Comparison of spectral refraction and refraction-diffraction wave models," *J. Wtrwy., Port, Coast. and Ocn. Engrg.* ASCE **117** (3) (1991), pp. 195–215.

14. K. Nagai, "Computation of refraction and diffraction of irregular sea," *Rept. Port and Harbour Res. Inst.* **11** (2) (1972), pp. 47–119 (*in Japanese*).

15. U.S. Army Coastal Engineering Research Center, *loc. cit.* Ref. 2, pp. 2-83 ∼ 2-109.

16. Y. Goda, T. Takayama and Y. Suzuki, "Diffraction diagrams for directional random waves," *Proc. 16th Int. Cont. Coastal Engrg.* (Hamburg, 1978.) pp. 628–650.

17. I. Irie, "Examination of wave deformation with field observation data," *Coastal Engineering in Japan* **18** (1975), pp. 27–34.

18. M. J. Briggs, E. T. Thompson and C. L. Vincent, "Wave diffraction around breakwater," *J. Wtrwy., Port, Coast. and Ocn. Engrg.* **121** (1) (1995), pp. 23–35.

19. W. J. Pierson, Jr., G. Neumann and R. W. James, *Practical Methods for Observing and Forcasting Ocean Waves by Means of Wave Spectra and Statistics* (U.S. Navy Hydrographic Office, H.O. Pub. No. 603, 1955).

20. M. Hom-ma, K. Horikawa and Y. T. Chau, "Sheltering effects of Sado Island on wind waves off Niigata Coast," *Coastal Engineering in Japan* **9** (1966), pp. 27–44.

21. C. L. Bretschneider and R. O. Reid, "Modification of wave height due to bottom friction, percolation, and refraction," *U.S. Army Corps of Engrs., Beach Erosion Board, Tech. Memo.* (45) (1954).

22. O. H. Shemdin *et al.*, "Mechanisms of wave transformation in finite-depth water," *J. Geophys. Res.* **85** (C9) (1980), pp. 5012–5018.
23. Y. Goda, "Deformation of irregular waves due to depth-controlled wave breaking," *Rept. Port and Harbour Res. Inst.* **14** (3) (1975), pp. 59–106 (*in Japanese*).
24. Y. Iwagaki and T. Sakai, "On the shoaling of finite amplitude waves (2)," *Proc. 15th Japanese Conf. Coastal Engrg.* (1968), pp. 10–15 (*in Japanese*).
25. N. Shuto, "Nonlinear long waves in a channel of variable section," *Coastal Engineering in Japan* **17** (1974), pp. 1–12.
26. Y. Goda, "A synthesis of breaker indices," *Trans. Japan Soc. Civil Engrs.* **2** (2) (1970), pp. 227–230.
27. Y. Goda, "Irregular wave deformation in the surf zone," *Coastal Engineering in Japan* **18** (1975), pp. 13–26.
28. Y. Goda, "New wave pressure fromulae for composite breakwaters," *Proc. 14th Int. Conf. Coastal Engrg.* (Copenhagen, 1974), pp. 1702–1720.
29. M. S. Longuet-Higgins and R. W. Stewart, "Radiation stress and mass transport in gravity waves, with application to 'surf beats,'" *J. Fluid Mech.* **13** (1962), pp. 481–504.
30. Niigata Investigation and Design Office, First District Port Construction Bureau, Ministry of Transport, "On the winter storm waves of 1971," *NID Note* (45–6) (1971), pp. 93–107 (*in Japanese*).
31. S. Yanagishima and K. Katoh, "Field observation on wave set-up near the shoreline," *Proc. 22nd Int. Conf. Coastal Engrg.* (Delft, 1990), pp. 95–108.
32. J. A. Battjes and M. J. F. Stive, "Calibration and verification of a dissipation model for random breaking model," *J. Geophys. Res.* **90** (C5) (1985), pp. 9155–9167.
33. W. R. Dally, "Random breaking waves: Field verification of a wave-by-wave algorithms for engineering applications," *Coastal Engineering,* **16** (4) (1992), pp. 369–397.
34. H. M. Kweon and Y. Goda, "A parametric model for random wave deformation by breaking on arbitrary beach profiles," *Proc. 25th Int. Conf. Coastal Engrg.* (Orlando, Florida, 1996), pp. 281–274.
35. E. B. Thornton and R. T. Guza, "Transformation of wave height distribution," *J. Geophys. Res.* **88** (C10) (1983), pp. 5925–5938.
36. W. N. Seelig and J. P. Ahrens, "Estimation of wave reflection and energy dissipation coefficients for beaches, revetments, and breakwaters," *U.S. Army. Corps of Engrs., Coastal Engrg. Res. Center, Tech. Paper* (81–1), (1981), 40p.
37. T. Tanimoto *et al.*, "An experimental investigation of wave reflection, overtopping and wave forces for several types of breakwaters and seawalls," *Tech. Note of Port and Harbour Res. Inst.* **246** (1976), 38p (*in Japanese*).
38. R. L. Wiegel, *Oceanographical Engineering* (Prentice-Hall, Inc., 1964), pp. 72–75, p. 194.
39. Y. Goda, T. Yoshimura and M. Ito, "Reflection and diffraction of water waves by an insular breakwater," *Rept. Port and Harbour Res. Inst.* **10** (2) (1971), pp. 3–52 (*in Japanese*).

40. H. Mitsui, Y. Kawamura and K. Komatsu, "On the wave height distribution along coastal structures of uneven alignments (6th Report)," *Proc. 22nd Japanese Conf. Coastal Engrg.* (1975), pp. 103–107 (*in Japanese*).

41. K. Tanimoto, K. Kobune and K. Komatsu, "Numerical analysis of wave propagation in harbours of arbitrary shape," *Rept. Port and Harbour Res. Inst.* **14** (3) (1975), pp. 35–58 (*in Japanese*).

42. Y. Goda and Y. Suzuki, "Estimation of incident and reflected waves in random wave experiments," *Proc. 15th Int. Conf. Coastal Engrg.* (Hawaii, 1976), pp. 828–845.

43. M. Morihira and Y. Okuyama, "Presentation of wave diffraction diagrams obtained through a digital computer," *Tech. Note of Port and Harbour Res. Inst.* **21** (1965), 45p (*in Japanese*).

44. Y. Ito and K. Tanimoto, "Meandering damage of composite type breakwaters," *Tech. Note of Port and Harbour Res. Inst.* **112** (1971), 20p (*in Japanese*).

45. H. Mitsui and H. Murakami, "On the wave height distribution along coastal structures of uneven alignments (2nd Report)," *Proc. 14th Japanese Conf. Coastal Engrg.* (1967), pp. 53–59 (*in Japanese*).

46. K. Kobune and M. Osato, "A study of wave height distribution along a breakwater with a corner," *Rept. Port and Harbour Res. Inst.* **25** (2) (1976), pp. 55–88 (*in Japanese*).

47. Y. Goda and T. Yoshimura, "Wave force computation for structures of large diameter, isolated in the offshore," *Rept. Port and Harbour Res. Inst.* **10** (4) (1971), pp. 3–52 (*in Japanese*).

48. Y. Goda, "Re-analysis of laboratory data on wave transmission over breakwaters," *Rept. Port and Harbour Res. Inst.* **8** (3) (1969), pp. 3–18.

49. Y. Goda, Y. Suzuki and Y. Kishira, "Some experiences in laboratory experiments with irregular waves," *Proc. 21st Japanese Conf. Coastal Engrg.* (1974), pp. 237–242 (*in Japanese*).

50. H. Kondo and I. Sato, "A study on the required elevation of breakwater crown," *Hokkaido Development Bureau, Civil Engineering Institute, Monthly Report* **117** (1964), pp. 1–15 (*in Japanese*).

51. S. Hattori, "Coastal development and wave control," *Lecture Series on Hydraulic Engineering,* 75-B2, Hydraulics Committee, Japan Soc. Civil Engrs. (1975), pp. B2-1 ~ B2-24 (*in Japanese*).

52. M. Tominaga and T. Sakamoto, "Field measurements of wave attenuation by offshore breakwaters," *Proc. 18th Japanese Conf. Coastal Engrg.* (1971), pp. 149-154 (*in Japanese*).

53. T. Katayama, I. Irie and T. Kawakami, "Effects of Niigata Coast offshore breakwaters on beach protection and wave attenuation," *Proc. 20th Japanese Conf. Coastal Engrg.* (1973), pp. 519–524 (*in Japanese*).

54. E. B. Thornton and R. J. Calhoun, "Spectral resolution of breakwater reflected waves," *Proc. ASCE* **98** (WW4) (1972), pp. 443-460.

55. Niigata Investigate and Design Office, First District Port Construction Bureau, Ministry of Transport, "Several problems on breakwaters related to the safety of harbors (III)," *Proc. 14th District Symp. Port Construction Works* (1976) 76p (*in Japanese*).

56. M. S. Longuet-Higgins, "Longshore current generated by obliquely incident sea waves, 1 & 2," *J. Geophys. Res.* **75** (33) (1970), pp. 6778–6801.

57. J. A. Battjes, "Computation of set-up, longshore currents, run-up and over-topping due to wind-generated waves," *Dept. Civil Engrg., Delft Univ. of Tech., Report* No. 74-2 (1974), 244p.

58. Y. Goda and N. Watanabe, "A longshore current formula for random breaking waves," *Coastal Engineering in Japan* **34** (2) (1991), pp. 159–175.

59. E. B. Thornton and R. T. Guza, "Surf zone longshore currents and random waves: Field data and models," *J. Phys. Oceanogr.* **16** (1986), pp. 1165–1178.

60. Y. Goda, "Longshore current generation by directional random waves on a planar beach," *Proc. XXIV Congress, Int. Assoc. Hydraulic Res.* (Madrid, 1991), pp. B223–B230.

Chapter 4

Design of Vertical Breakwaters

4.1 Vertical Breakwaters in Japan

Breakwaters are generally classified as either mound breakwaters or vertical breakwaters. Sometimes a third category, the mixed or composite type, is also employed. Functionally, mound breakwaters dissipate the energy of incident waves by forcing them to break on a slope, and thus they do not produce appreciable reflection. Vertical breakwaters, on the other hand, reflect the incident waves without dissipating much wave energy. Composite breakwaters function as mound breakwaters when the tide level is low and as vertical breakwaters when the tide level is high.[1] According to this functional point of view, vertical breakwaters are not limited to those erected directly on the sea bottom, but they also include structures built on artificial foundations of rubble mounds. The present chapter adopts this definition of a vertical breakwater.

In Western countries, vertical breakwaters are usually built in water of sufficient depth where wave breaking is not a problem.[2] But in the modern history of harbor construction in Japan, vertical breakwaters have been built primarily to withstand breaking waves. The construction of mound breakwaters has been confined to quite shallow water where construction work by barges is difficult. The scarcity of mound breakwaters is partly attributed to the recent geological formation of the Japanese islands and to the humid climate, which made rock fragile. Therefore it is difficult to quarry sufficient amounts of large-sized rocks. This tendency to favor vertical breakwaters has been reinforced by many successful experiences in the construction of vertical breakwaters in Japan.

YOKOHAMA PORT East Breakwater (1890~1896)

[Units in m]

$H=3$m

(a)

OTARU PORT North Breakwater (1897~1907)

[Units in m]

$H=6$m

(b)

OTARU PORT Island Breakwater (1912~1917)

[Units in m]

$H=6$m

(c)
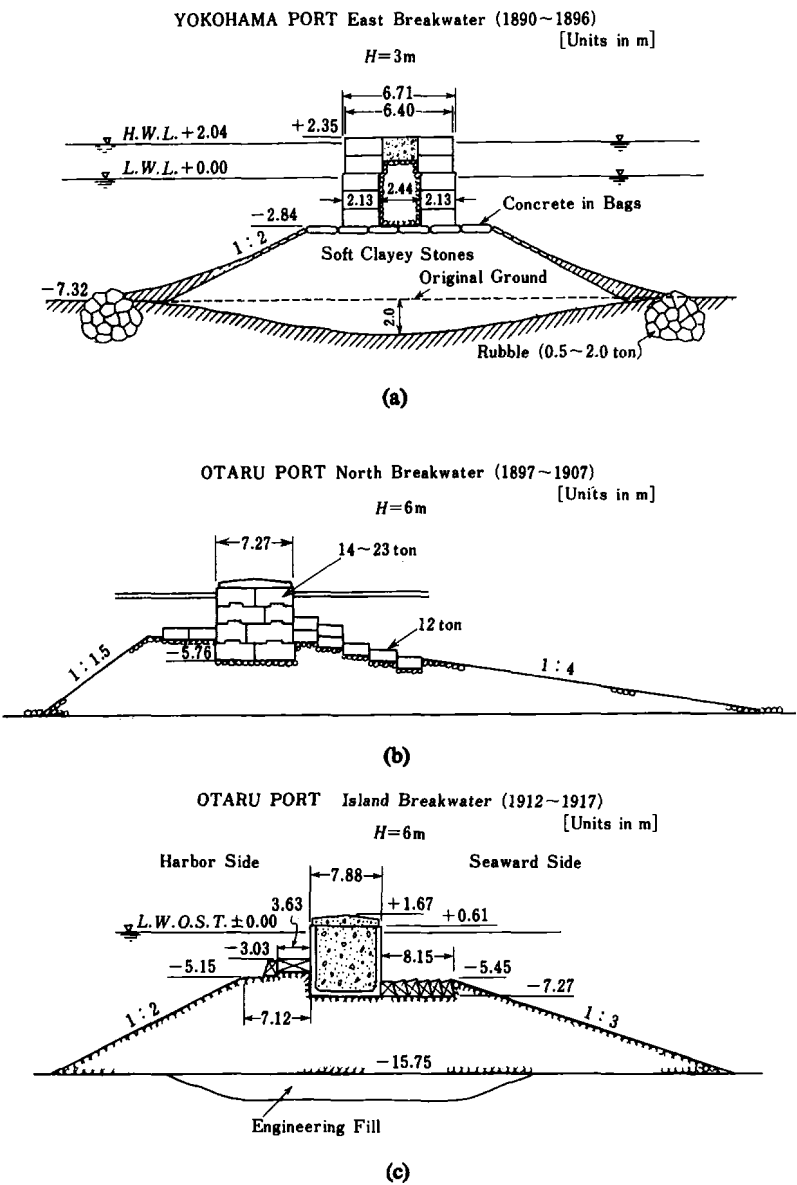
Fig. 4.1(a–c). Historical development of vertical breakwaters in Japan.

ONAHAMA PORT First Breakwater (1929~1938)

$H_{max} = 8.5$ m

[Units in m]

Seaward Side   Harbor Side

(d)

YOKOHAMA PORT Outer Breakwater (1928~1943)

$H = 3$ m

[Units in m]

(e)

WAKAYAMA North Harbor-West Breakwater (1957~1960)

$H_{1/3} = 6$ m   [Units in m]
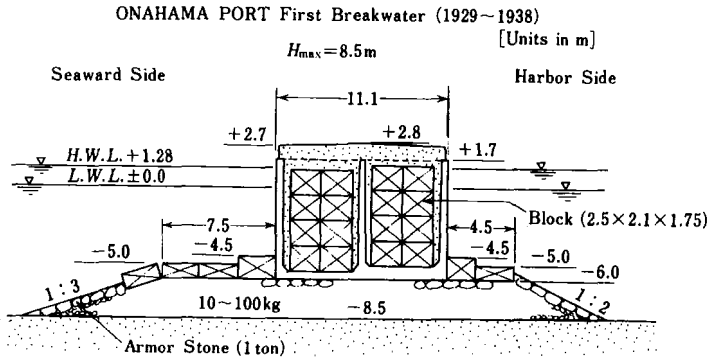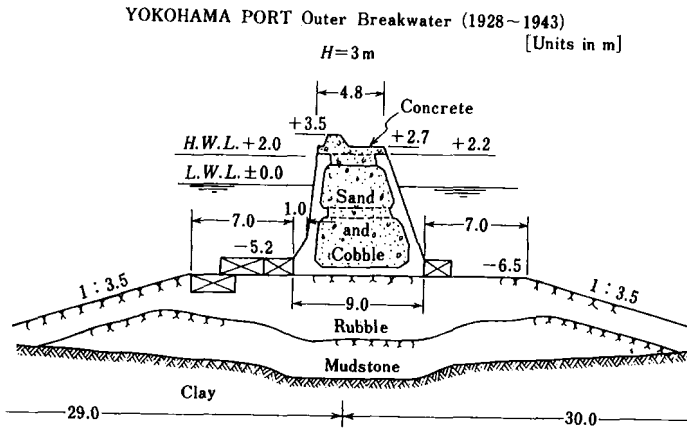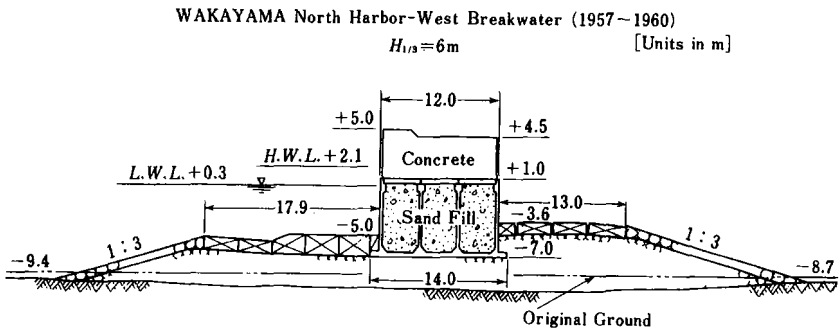
(f)

Fig. 4.1(d–f). Historical development of vertical breakwaters in Japan (continued).

OFUNATO PORT Tsunami Breakwater (1962~1968)

[Units in m]

Tsunami : H=6 m,　T=15~40 min
Wind Waves:$H_{1\,3}$=4 m, $T_{1\,3}$=9 s
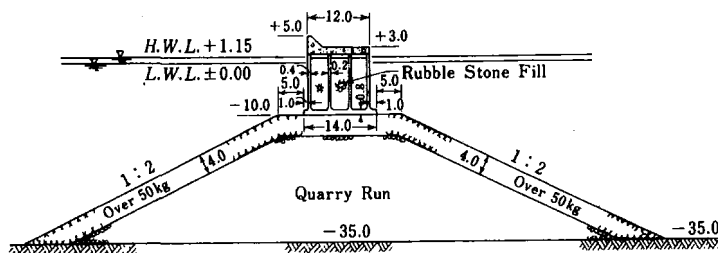
(g)

HOSOJIMA PORT Breakwater (1974~1985)

$H_{1/3}$=8.3 m, $T_{1/3}$=14.0 s
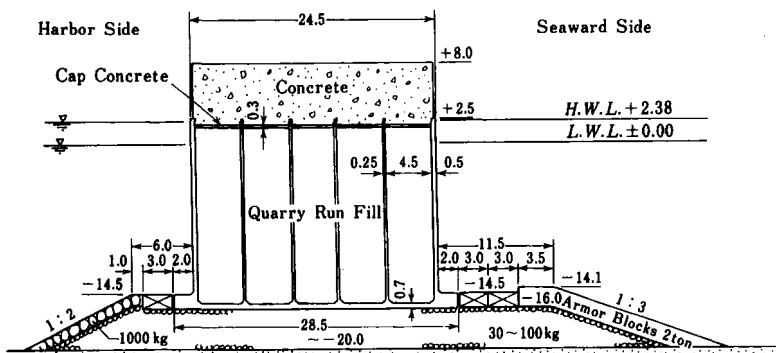
[Unit in m]

(h)

ONAHAMA PORT Offshore Breakwater (1980~)

$H_{1\,3}$=7.4 m, H_{max}=13.3 m, $T_{1\,3}$=13.0 s

[Unit in m]
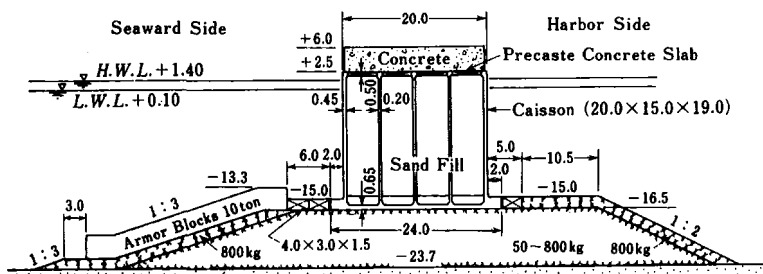
(i)

Fig. 4.1(g–i). Historical development of vertical breakwaters in Japan (continued).

The first vertical breakwaters in the modern age of Japan are those at Yokohama Port, which were designed by H. S. Palmer (a retired British Major-General) and built from 1890 to 1896. One of the sections is shown in Fig. 4.1(a). They were redesigned with solid concrete blocks for the whole upright section after damage by a storm in 1902. A vertical breakwater consisting of solid concrete blocks was first built at Otaru Port in Hokkaido by I. Hiroi (a professor of civil engineering at Hokkaido University and later at the University of Tokyo) from 1897 to 1907. Figure 4.1(b) shows its cross section. He took as examples the breakwaters at Karachi, Madras, and Colombo. After that, breakwaters with reinforced concrete caissons were introduced at Kobe Port for the first time in 1911, and then utilized for the island breakwater at Otaru Port in 1912. Because the wave conditions are much severer at Otaru than Kobe, the breakwater, as shown in Fig. 4.1(c), was quite sturdy. The caissons weighed 883 tons and were filled with poured concrete. Caisson breakwaters soon became the major structural type of breakwater for use in withstanding rough seas. Figure 4.1(d) shows the first breakwater of Onahama Port in Fukushima Prefecture. In this case, precast concrete blocks were placed in the caisson cells to save work time. Another noteworthy point is that the engineer-in-charge designed it against a maximum possible breaker height of about 8.5 m at a water depth of 9.7 m below the high water level. Many vertical breakwaters in Japan have been designed and built against breaking waves, such as the one in this example.

The filler material for the caisson cells has gradually evolved from concrete to gravel and then to sand. One of the early examples of a sand-filled breakwater is the outer breakwater at Yokohama Port, which was designed by S. Samejima (a distinguished government civil engineer at the time) and built from 1928 to 1943. As shown in Fig. 4.1(e), the caissons were very sturdy, with an outer wall 60 cm thick. The interiors of the caissons were filled with a mixture of sand and cobble to give the greatest possible density. Filling of caissons with sand was first done in water areas where the wave conditions were relatively mild, but sand filler soon became popular in areas of rough seas as well. This was particularly so in the period shortly after World War II, when cement was scarce because of damage to production facilities.

Figure 4.1(f) is one such breakwater built after World War II. Because of soft ground conditions, the breakwater was given a wide rubble foundation to counteract circular slip of the ground. Figure 4.1(g) is the tsunami breakwater

at Ofunato Port in Iwate Prefecture, built 35 m deep into the water. One of the largest breakwater caissons is found in the breakwater at Hosojima Port in Miyazaki Prefecture, shown in Fig. 4.1(h). It has a mass of nearly 5,000 Mg (ton), launched from a floating dock. Figure 4.1(i) presents a typical cross section of contemporary Japanese vertical breakwaters having been designed with the author's wave pressure formulas.

The largest breakwater in the world is the tsunami breakwater under construction at Kamaishi Port, Iwate Prefecture, Japan. The construction site has the maximum water depth of 63 m, and specially-shaped caissons with a mass of 16,000 Mg (ton), each are set on top of a rubble mound foundation at the elevation 25 m below the datum. Tanimoto and Goda[3] provide some details of this breakwater. In addition, Takahashi[4] describes various aspects of vertical breakwater designs in Japan.

Harbor engineers of many countries appear to be rather unfamiliar with the design of vertical breakwaters; therefore the present chapter is dedicated to the introduction of Japanese design formulas and some of the design principles. Figures 4.2 and 4.3 are provided to acquaint the reader with the terminology associated with vertical breakwaters. Figure 4.2 illustrates the various parts of a vertical breakwater which appear in the present chapter. Figure 4.3 shows the possible modes of major failures of vertical breakwaters by wave action. These are sliding and overturning of the upright section as well as failure of the rubble mound foundation or original seabed. In addition to the failures shown in Fig. 4.3, displacement of individual foot-protection blocks and armor stones may also occur under wave action. The subject of wave pressure and the design of vertical breakwaters is discussed in subsequent sections.
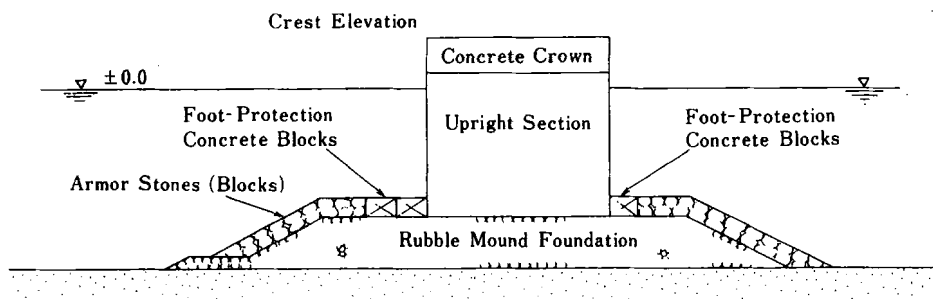
Fig. 4.2. Idealized typical section of a vertical breakwater.

(A) Sliding

(B) Overturning

(C) Failure of Foundation
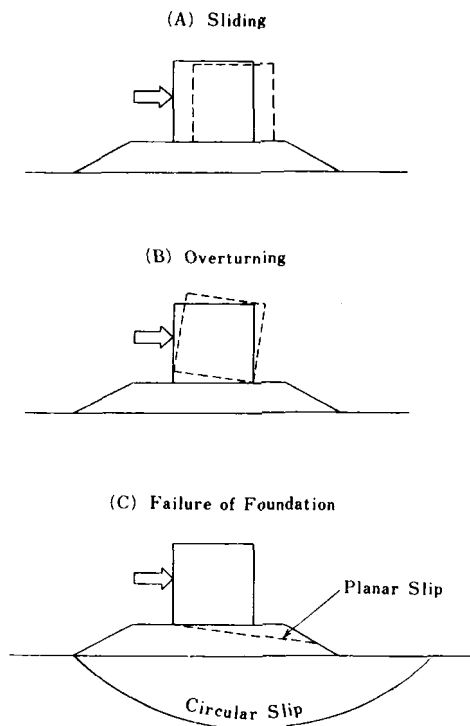
Fig. 4.3. Modes of major failure of vertical breakwaters.

4.2 Wave Pressure Formulas for Upright Sections

4.2.1 *Overview of Development of Wave Pressure Formulas*

In parallel with the history of the construction of vertical breakwaters themselves, the formulas for the wave pressure exerted on upright sections have a long history of their own.[a] As early as 1842, Stevenson[5] measured wave pressure with a special gauge which he invented. Then from 1890 to 1902, Gaillard[6] made several series of wave pressure measurements and proposed a formula for estimating wave pressure on the basis of water particle velocities. In Japan, Hiroi also measured wave pressures with a modified version of Stevenson's

---

[a]For the content of this paragraph, the author gratefully acknowledges the treatise by Ito.[2]

gauge. Although he obtained pressures as high as 350 kPa, he correctly regarded such a high pressure as a local phenomenon and did not relate it directly to the stability of upright sections. Instead, he considered wave pressure as similar to the pressure of a water jet and derived the following formula,[7] which was published in 1919:

$$p = 1.5\rho g H. \tag{4.1}$$

The wave pressure p is assumed to act uniformly over the full height of an upright section, or to an elevation of 1.25 times the wave height above the still water level, whichever is less. The symbol ρ in Eq. (4.1) denotes the density of sea water ($= 1030 \text{ kg/m}^3$), g is the acceleration of gravity, and H is the incident wave height. In situations where information on the design wave is unreliable, Hiroi recommended taking 0.9 times the water depth as the design wave height. Hiroi's formula was apparently intended for calculating the pressure caused by breaking waves, and it has been so used in breakwater design in Japan for more than 60 years.

A pressure formula for standing waves was introduced by Sainflou[8] in 1928, and it acquired immediate acceptance by harbor engineers throughout the world. Before 1979, Japanese harbor engineers have employed a dual system of wave pressure formulas, using both Hiroi's formula for breaking waves and Sainflou's formula for nonbreaking waves. Although Minikin[9] proposed a formula for breaking wave pressure in 1950, based partly on Bagnold's laboratory data,[10] Minikin's formula is rarely employed in actual breakwater design because of the excessive values which it predicts. Until the 1960s even Sainflou's formula was infrequently used in Japan, because design waves are relatively large and most vertical breakwaters built at the time did not reach to a water depth where design waves could be safely regarded as nonbreaking.

In the 1960s, extensive port development in Japan, keeping pace with national economic development, resulted in new circumstances in the application of wave pressure formulas. That is to say, many new breakwaters had to be built over long stretches from the shoreline to water deeper than 20 m to accommodate very large bulk carriers. At some point, the pressure formula for the design of these breakwaters had to be switched from that pertaining to breaking waves to nonbreaking waves. At that boundary point of the applicability of the two pressure formulas, the predicted wave pressure abruptly changes by more than 30%. A slight modification of the design wave height immediately moves the location of the cutoff between the two formulas, and

the design section of a vertical breakwater has, in principle, to be changed accordingly. Such a situation is considered too artificial, and it is hard to convince engineers of the appropriateness of the dual formula system for wave pressure on breakwaters.

Another problem with the formulas of Hiroi and Sainflou was the ambiguity of the wave height to be used in design works. With advances in instrumental wave recording, engineers came to realize the complexity of sea waves and began to question which height, $H_{1/3}$, $H_{1/10}$, or H_{max}, should be substituted into the wave pressure formulas.

To resolve the above predicament, based on hydraulic model experiments, in 1966 Ito[11] proposed a single formula covering both breaking and nonbreaking wave pressures, including the effect of the presence of a rubble mound foundation. At the same time, he specified H_{max} as the height to be employed in his formula. Later, in 1973, the author extended Ito's work through the use of much more laboratory data[12] as well as theoretical considerations.[13] He also examined many cases of sliding and nonsliding of vertical breakwaters, and proposed a new set of wave pressure formulas for upright sections of vertical breakwaters.[14] With a later modification by Tanimoto *et al.*[15] to account for the effect of oblique wave approach, these formulas have been employed as the standard formulas for the design of vertical breakwaters in Japan since 1979.

4.2.2 *Formulas of Wave Pressure under Wave Crests*

The wave pressure formulas proposed by the author for the design of vertical breakwaters assume the existence of a trapezoidal pressure distribution along a vertical wall, as shown in Fig. 4.4, regardless of whether the waves are breaking or nonbreaking. In this figure, h denotes the water depth in front of the breakwater, d the depth above the armor layer of the rubble foundation, h' the distance from the design water level to the bottom of the upright section, and h_c the crest elevation of the breakwater above the design water level. The wave height for the pressure calculation and other factors are specified below.

(A) *Design wave*

The highest wave in the design sea state is to be employed. Its height is taken as $H_{max} = 1.8H_{1/3}$ seaward of the surf zone, whereas within the surf zone the height is taken as the highest of random breaking waves H_{max} at the location at a distance $5H_{1/3}$ seaward of the breakwater. The latter height
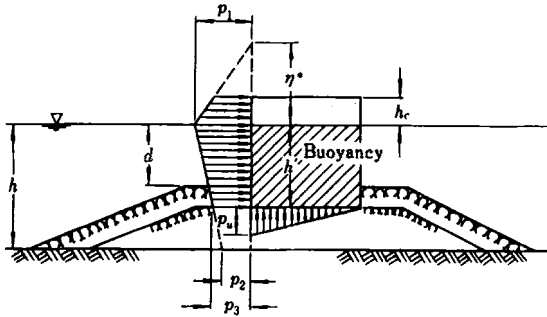
Fig. 4.4. Distribution of wave pressure on an upright section of a vertical breakwater.

$H_{1/3}$ is to be estimated with the random wave breaking model described in Sec. 3.5 at the depth of the location of the breakwater.

The period of the highest wave is taken as that of significant wave, as in Eq. (2.9) of Section 2.2.3; i.e., $T_{\max} = T_{1/3}$.

(B) *Elevation to which the wave pressure is exerted*

$$\eta^* = 0.75(1 + \cos\beta)H_{\max}, \tag{4.2}$$

in which β denotes the angle between the direction of wave approach and a line normal to the breakwater. The wave direction should be rotated by an amount of up to 15° toward the line normal to the breakwater from the principal wave direction. This directional adjustment is made in view of the uncertainty in the estimation of the design wave direction. The practice of adjusting the wave direction up to 15° has been employed in the design of Japanese breakwaters ever since Hiroi proposed his wave pressure formula.

(C) *Wave pressure on the front of a vertical wall*

$$p_1 = \frac{1}{2}(1 + \cos\beta)(\alpha_1 + \alpha_2 \cos^2\beta)\rho g H_{\max}, \tag{4.3}$$

$$p_2 = \frac{p_1}{\cosh(2\pi h/L)}, \tag{4.4}$$

$$p_3 = \alpha_3 p_1, \tag{4.5}$$

in which

$$\alpha_1 = 0.6 + \frac{1}{2} \left[\frac{4\pi h/L}{\sinh(4\pi h/L)} \right]^2 , \tag{4.6}$$

$$\alpha_2 = \min \left\{ \frac{h_b - d}{3h_b} \left(\frac{H_{\max}}{d} \right)^2 , \frac{2d}{H_{\max}} \right\} , \tag{4.7}$$

$$\alpha_3 = 1 - \frac{h'}{h} \left[1 - \frac{1}{\cosh(2\pi h/L)} \right] , \tag{4.8}$$

$\min\{a, b\}$: smaller of a and b,

h_b: water depth at the location at a distance $5H_{1/3}$ seaward of the breakwater.

The above pressure intensities are assumed not to change even if wave overtopping takes place. The value of the coefficient α_1 can be read off of Fig. 4.5, and the value of $1/\cosh(2\pi h/L)$ for α_3 is obtained from Fig. 4.6. The symbol L_0 in both figures denotes the wavelength corresponding to the significant wave period in deep water.

(D) *Buoyancy and uplift pressure*

The buoyancy is to be calculated for the displacement volume of the upright section in still water below the design water level, and the uplift pressure
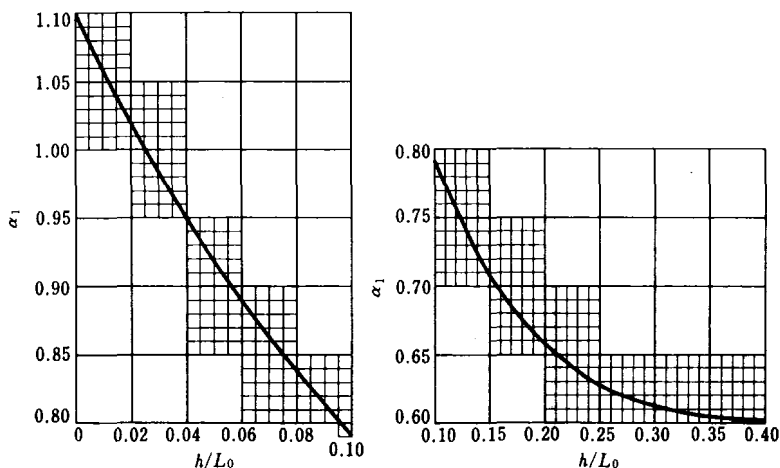
Fig. 4.5. Calculation diagrams for the parameter α_1.[12]
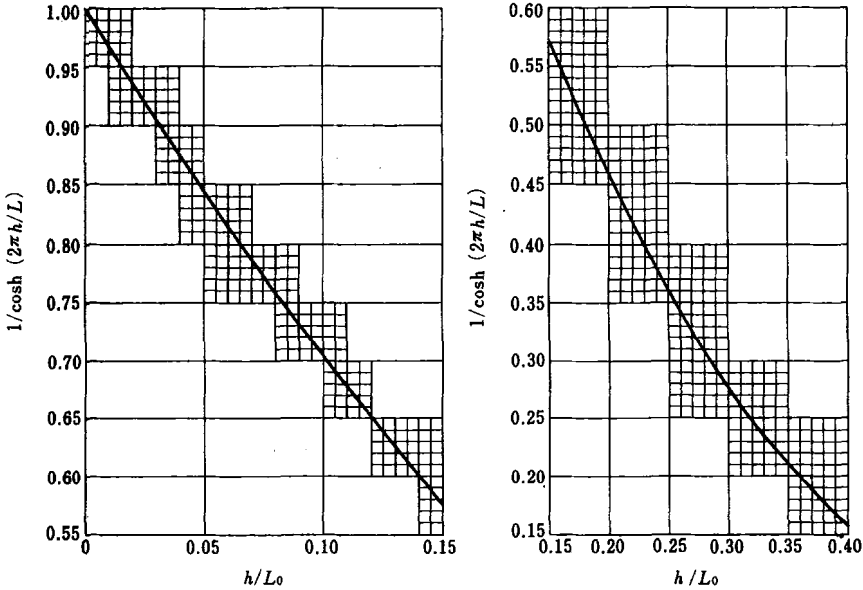
Fig. 4.6. Calculation diagrams for the factor of $1/\cosh(2\pi/L)$.[12]

acting on the bottom of the upright section is assumed to have a triangular distribution with toe pressure p_u given by Eq. (4.9) below, and with a heel pressure of zero. Both the buoyancy and uplift pressure are assumed to be unaffected by wave overtopping

$$p_u = \frac{1}{2}(1 + \cos\beta)\alpha_1\alpha_3\rho g H_{\max}. \qquad (4.9)$$

Adoption of the wave height $H_{\max}$ in the above pressure formulas is taken after the proposal by Ito.[11] It is based on the principle that a breakwater should be designed to be safe against the single wave with the largest pressure among storm waves. As discussed in Sec. 2.2.2, the height $H_{\max}$ is a probabilistic quantity. But to avoid possible confusion in design, a definite value of $H_{\max} = 1.8H_{1/3}$ is recommended in consideration of the performance of many prototype breakwaters as well as with regard to the accuracy of the wave pressure estimation. Certainly there remains the possibility that one or two waves exceeding $1.8H_{1/3}$ will hit the site of the breakwater when

storm waves equivalent to the design condition attack. But the distance of sliding of an upright section, if it were to slide, would be very small. It should be remarked, however, that the prescription $H_{max} = 1.8H_{1/3}$ is a recommendation and not a rule. The design engineer can use his judgment in choosing another value, such as $H_{max} = 1.6H_{1/3}$, $H_{max} = 2.0H_{1/3}$, or some other value.

The recommended design water depth as discussed above is based on recognition of the fact that the greatest wave pressure is exerted not by waves just breaking at the site, but by waves which have already begun to break at a short distance seaward of the breakwater, midway through the plunging distance. Although this distance depends on the wave conditions and other factors, a single criterion of $5H_{1/3}$ has been adopted in consideration of some laboratory data on breaking wave pressures, for the sake of convenience.

The value of the coefficient α_1 in the pressure intensity p_1 at the still water level has been empirically determined on the basis of laboratory data. The formula for the coefficient α_1 represents the mean tendency of wave pressure in that it increases with the wave period; its functional representation does not carry any theoretical significance. The simple functional form of the coefficient α_2 represents the tendency of the pressure to increase with the height of the rubble foundation. The increase of wave pressure due to the presence of a rubble foundation may be regarded as result of the change in behavior of waves from nonbreaking to breaking, although actual waves never exhibit such marked changes. With this consideration, the reduction factor $\cos^2\beta$ for the effect of oblique wave attack is multiplied to the coefficient α_2 in addition to the general reduction factor $0.5(1+\cos\beta)$. The coefficient α_3 was derived based on the simplifying assumption of a linear pressure variation between p_1 and p_2 along a vertical wall.

Theoretically, the intensity of uplift pressure p_u at the toe of an upright section should be the same as the front pressure p_3. It was judged, however, that the uplift pressure would be assigned too great a value if p_u were set equal to p_3, in view of the performance of prototype breakwaters and other considerations. Thus, p_u is set as given by Eq. (4.9). Although the uplift pressure is not appreciably affected by the occurrence of wave overtopping, as evidenced in the laboratory data reported by the author,[12] a very low crown elevation of breakwater is expected to result in some reduction in the uplift pressure.
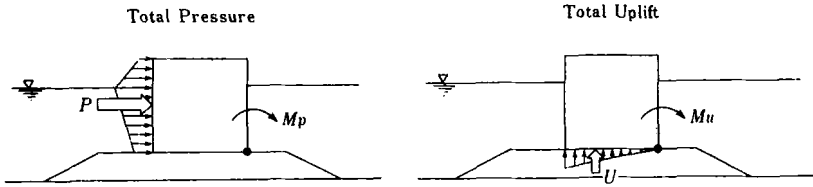
Fig. 4.7. Definition sketch of total pressure and uplift as well as their moments.

With the above formulas for the wave pressure, the total wave pressure and its moment around the bottom of an upright section (see Fig. 4.7) can be calculated with the following equations:

$$P = \frac{1}{2}(p_1 + p_3)h' + \frac{1}{2}(p_1 + p_4)h_c^* \,, \tag{4.10}$$

$$M_p = \frac{1}{6}(2p_1 + p_3)h'^2 + \frac{1}{2}(p_1 + p_4)h'h_c^* + \frac{1}{6}(p_1 + 2p_4)h_c^{*2} \,, \tag{4.11}$$

in which

$$p_4 = \begin{cases} p_1(1 - h_c/\eta^*) & : \ \eta^* > h_c \,, \\ 0 & : \ \eta^* \le h_c \,, \end{cases} \tag{4.12}$$

$$h_c^* = \min\{\eta^*, h_c\} \,. \tag{4.13}$$

The total uplift pressure and its moment around the heel of the upright section (see Fig. 4.7) are calculated with

$$U = \frac{1}{2}p_u B \,, \tag{4.14}$$

$$M_U = \frac{2}{3}UB \,, \tag{4.15}$$

where B denotes the width of the bottom of the upright section.

Example 4.1

Calculate the wave pressure, uplift pressure, and their moments produced by waves of the following characteristics incident on the upright section of the vertical breakwater shown in Fig. 4.8.
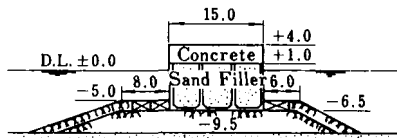
Fig. 4.8. Cross section of a vertical breakwater (units in meters).

$$\text{Waves} \ : \ H_0' = 6.3 \text{ m}, \ T_{1/3} = 11.4 \text{ s}, \ \beta = 15°,$$
$$\text{Tide level} \ : \ \text{W.L.} = +0.6 \text{ m},$$
$$\text{Sea bottom slope} \ : \ \tan\theta = 1/100.$$

Solution

i) Water depth and crest elevation

$$h = 10.1 \text{ m}, \quad h' = 7.1 \text{ m}, \quad d = 5.6 \text{ m}, \quad h_c = 3.4 \text{ m}.$$

ii) Wavelength and wave height

$L_0 = 202.7$ m (by Table A-3 in the appendix, or by $L_0 = 1.56 \ T^2$),

$H_0'/L_0 = 0.031, \quad h/L_0 = 0.050,$

$H_{1/3} = 5.8$ m (estimated with Eq. (3.25) in Sec. 3.5.5
using $h = 10.1$ m),

$$h_b = 10.1 + 5 \times 5.8 \times \frac{1}{100} = 10.4 \text{ m},$$

$H_{\max} = 8.0$ m (estimated by Eq. (3.26) in Sec. 3.5.5
with $h_b = 10.4$ m).

iii) Coefficients for the wave pressure

$\alpha_1 = 0.920$ (by Fig. 4.5),

$$\alpha_2 = \min \left\{ \frac{10.4 - 5.6}{3 \times 10.4} \times \left(\frac{8.0}{5.6}\right)^2, \frac{2 \times 5.6}{8.0} \right\} = \min \{0.314, 1.40\}$$

$$= 0.314,$$

$$1/\cosh(2\pi/L) = 0.847 \text{ (by Fig. 4.6)},$$

$$\alpha_3 = 1 - \frac{7.1}{10.1} \times (1 - 0.847) = 0.892.$$

iv) Maximum elevation of the wave pressure

$$\cos \beta = 0.966 \,, \quad 0.5 \times (1 + 0.966) = 0.983 \,,$$

$$\eta^* = 0.75 \times (1 + 0.966) \times 8.0 = 11.8 \text{ m} \,.$$

v) Pressure components

$$p_1 = 0.983 \times [0.920 + 0.314 \times (0.966)^2] \times 1030 \times 9.8 \times 8.0$$

$$= 96.3 \text{ kPa} \,,$$

$$p_3 = 0.892 \times 96.3 = 85.9 \text{ kPa} \,,$$

$$p_4 = 96.3 \times \left(1 - \frac{3.4}{11.8}\right) = 68.6 \text{ kPa} \,,$$

$$p_u = 0.983 \times 0.920 \times 0.892 \times 1030 \times 9.8 \times 8.0 = 65.1 \text{ kPa} \,.$$

vi) Total pressure and uplift

$$h_c^* = \min \{11.8, 3.4\} = 3.4 \text{ m} \,,$$

$$P = \frac{1}{2} \times (96.3 + 85.9) \times 7.1 + \frac{1}{2} \times (96.3 + 68.6) \times 3.4$$

$$= 927 \text{ kN/m} \,,$$

$$U = \frac{1}{2} \times 65.1 \times 15.0 = 488 \text{ kN/m} \,.$$

vii) Moment of wave pressure

$$M_p = \frac{1}{6} \times (2 \times 96.3 + 85.9) \times 7.1^2 + \frac{1}{2} \times (96.3 + 68.6) \times 7.1$$

$$\times 3.4 + \frac{1}{6} \times (96.3 + 2 \times 68.6) \times 3.4^2 = 4780 \text{ kN} \cdot \text{m/m} \,.$$

viii) Moment of uplift pressure

$$M_U = \frac{2}{3} \times 488 \times 15.0 = 4880 \text{ kN} \cdot \text{m/m} \,.$$

4.2.3 *Pressure under a Wave Trough*

When the trough of an incident wave makes contact with a vertical wall, the pressure exerted on the wall becomes less than the hydrostatic pressure under the still water level. As a result, the vertical wall experiences a net pressure

directed offshore. Such a pressure may govern the stability of an upright section against sliding seaward, the structural design of the front walls of concrete caissons, etc.

The problem of wave pressure under a wave trough, in particular that of breaking waves, has not been examined in detail. But as far as the pressure of standing waves is concerned, the author[13] has prepared a set of diagrams shown in Figs. 4.9 to 4.11. These diagrams are based on theoretical calculations using finite amplitude standing waves, with modifications introduced on the basis of laboratory data. Figure 4.9 gives the total offshore-directed pressure under a wave trough, Fig. 4.10 shows its lever arm length, and Fig. 4.11 gives the magnitude of the bottom pressure at the time of the greatest offshore-directed total pressure. Figure 4.11, for example, indicates that the negative pressure near the bottom can become quite large even under the condition of quasi-deepwater waves, if the wave height is sufficiently large. In comparison to the onshore-directed pressure under a wave crest, the pressure under a trough is seen to become larger than that under a crest if the ratio of the water depth to wavelength exceeds about 0.25. This is caused by the appearance of second harmonic pressure components of appreciable amplitude due to wave
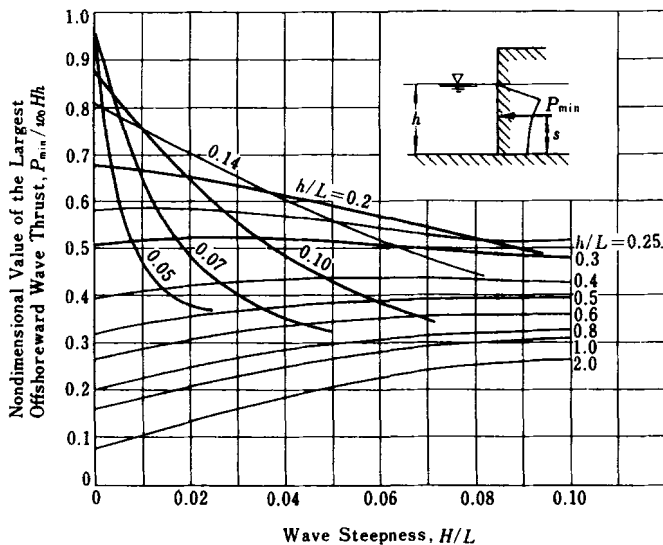
Fig. 4.9. Calculation diagram for the total pressure of standing waves under a wave trough.[13]
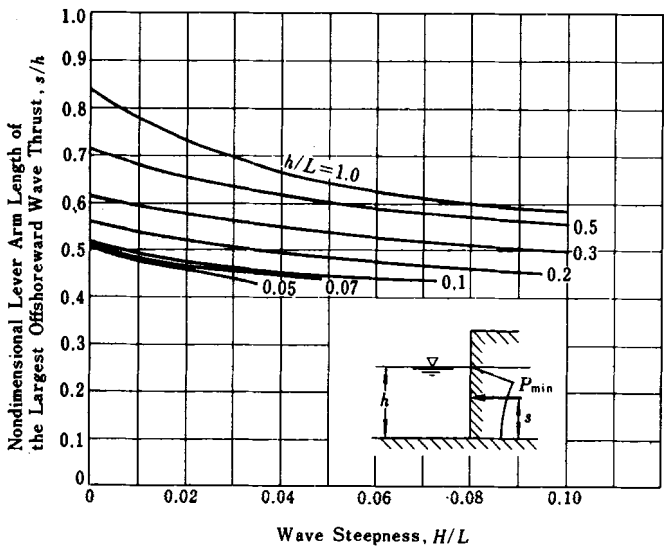
Fig. 4.10. Calculation diagram for the lever arm length of the total standing wave pressure under a wave trough.[13]
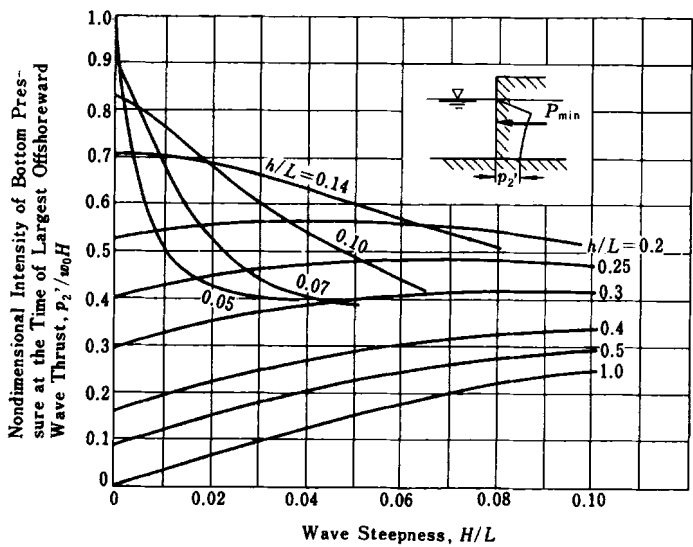
Fig. 4.11. Calculation diagram for the bottom pressure at the time of the largest offshoreward wave thrust during wave trough.[13]

nonlinearity. Under such a condition, an upright section may slide toward the offshore during heavy wave action.

4.2.4 *Accuracy of Wave Pressure Formulas*

The reliability of the calculation method for the wave pressure on a vertical breakwater is judged by the accuracy of the prediction of breakwater stability. The fundamental data for that judgement are the records of the sliding of breakwaters under storm waves as well as the records of breakwaters which withstood the attacks of high waves without experiencing any damage. The author[14] has made a survey of the performance of prototype breakwaters under waves with heights nearly equal to or greater than the heights of the design waves. With a collection of cases for 21 breakwaters which experienced sliding (with sliding distances of 0.1 m to several meters) and 13 nondamaged breakwaters, the stability of these breakwaters was examined by means of the conventional pressure formulas of Sainflou and Hiroi, the new pressure formulas, and Minikin's formula. The significant wave heights listed in the reports of the breakwater performance were assumed to refer to the estimated heights of the incident waves at the locations of the breakwaters without consideration of the random wave breaking effect. From these heights, the equivalent deepwater heights were calculated as $H'_0 = H_{1/3}/K_s$ and the wave heights were then corrected for the effect of random wave breaking.

The stability of prototype breakwaters was examined by using the safety factor against sliding of the upright section. This safety factor is defined as the ratio of the sliding resistance of an upright section against the wave force (see Eq. (4.16) in the next section). If the safety factor is less than 1, the upright section is thought to slide under wave action.

Figure 4.12 illustrates the safety factors against sliding for the examined breakwaters, calculated by means of the conventional pressure formulas and the new formulas.[b] Open circles denote cases of breakwaters which did not slide, filled circles represent cases of sliding, and half-filled circles denote a case judged to be at the threshold condition. The letters A to R next to the circles

---

[b]Results perviously presented by the author[14] did not properly incorporate the effect of random wave breaking. Also, the effect of oblique wave incidence was estimated in a slightly different manner. Thus, the results shown here, based on increased knowledge, differ to a certain extent from the previous results.
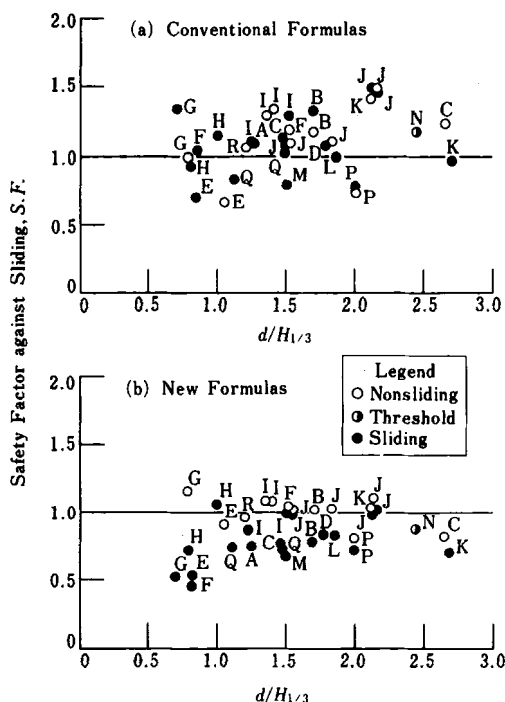
Fig. 4.12. Examination of the safety factor of prototype breakwaters against sliding.

refer to the associated harbors (the harbor names are given in Ref. 14). If the wave conditions were exactly known and the estimation of the wave pressure accurate, all the breakwaters which slid would have had safety factors less than 1.0, whereas those which did not slide would have had safety factors equal to or greater than 1.0. In other words, the filled circles would lie below the line S.F. = 1.0, whereas the open circles would lie above the line S.F. = 1.0, thus showing a clear distinction between the cases of sliding and nonsliding.

The actual trend of the calculated breakwater stability is not so clear. In particular, the analysis with the conventional pressure formulas as shown in Fig. 4.12(a) has yielded a rather ambiguous mixture of open and filled circles. For example, the breakwater at E Harbor did not slide though it had a safety factor of 0.67, whereas the breakwater at J Harbor slid even though the safety factor was 1.49. In the case of the new pressure formulas in Fig. 4.12(b), a separation between open and filled circles can be observed with a boundary

around S.F. $= 0.9 \sim 1.0$, though some mixing still remains. Application of Minikin's formula to this set of prototype breakwater performance data (the wave height for the calculation being taken as the significant height) yielded the poorest prediction of breakwater stability; some breakwaters remained in position with estimated safety factors of less than 0.4, while some others slid with safety factors of more than 2.0. Thus, Minikin's formula is found to be impractical, and the accuracy of the new wave pressure formulas is judged superior to that of the conventional pressure formulas.

4.3 Design of Upright Sections

4.3.1 *Stability Condition for an Upright Section*

The upright section of a vertical breakwater must be designed to be safe against sliding and overturning. At the same time, the bearing capacity of the rubble mound foundation and the seabed should be examined to ascertain that they remain below the allowable limit. The safety factors against sliding and overturning of an upright section under wave action are defined by the following:

$$\text{Against sliding:} \qquad \text{S.F.} = \frac{\mu(Mg - U)}{p}\,, \qquad (4.16)$$

$$\text{Against overturning:} \quad \text{S.F.} = \frac{Mgt - M_U}{M_p}\,, \qquad (4.17)$$

where M denotes the mass of the upright section per unit extension in still water, μ the coefficient of friction between the upright section and the rubble mound, and t the horizontal distance between the center of gravity and the heel of the upright section.

In the design of vertical breakwaters in Japan, the safety factors against sliding and overturning must not be less than 1.2. The coefficient of friction between concrete and rubble stones is usually taken as 0.6.

The bearing capacity of the foundation is to be analyzed by means of the methodology of foundation engineering for eccentric inclined loads. At sites where the seabed consists of a dense sand layer or soil of good bearing capacity, however, a simplified technique of examining the magnitude of the heel pressure is often employed. For this method, it is assumed that a trapezoidal or triangular distribution of bearing pressure exists beneath the bottom

of the upright section, and the largest bearing pressure at the heel p_e is calculated as

$$p_e = \begin{cases} \dfrac{2W_e}{3t_e} & : t_e \leq \dfrac{1}{3}B, \\[2ex] \dfrac{2W_e}{B}\left(2 - 3\dfrac{t_e}{B}\right) & : t_e > \dfrac{1}{3}B, \end{cases} \qquad (4.18)$$

in which

$$t_e = \frac{M_e}{W_e}, \quad M_e = Mgt - M_U - M_p, \quad W_e = Mg - U. \qquad (4.19)$$

The bearing pressure at the heel is to be kept below the value of 400 to 500 kPa, but recent breakwater designs are gradually increasing this limit to 600 kPa or greater, with advancement of breakwater construction sites into deeper water and with increases in the weight of upright sections.

Example 4.2

Examine the stability of the upright section of the breakwater shown in Example 4.1, assuming its mass is $M_a = 342.9$ Mg(ton)/m.

Solution

The weight of the upright section in still water is calculated as

$$W = Mg = (342.9 - 1.03 \times 15 \times 7.1) \times 9.8 = 2285 \text{ kN/m}.$$

Thus, the safety factors are

Against sliding: $\quad$ S.F. $= \dfrac{0.6 \times (2285 - 488)}{927} = 1.16$,

Against overturning: S.F. $= \dfrac{2285 \times 0.5 \times 15.0 - 4880}{4780} = 2.56$.

Therefore, the upright section has sufficient stability against overturning, but the safety factor for stability against sliding does not have a sufficient margin.

Next, the bearing pressure at the heel is examined as

$$W_e = 2285 - 488 = 1797 \text{ kN/m},$$
$$M_e = 2285 \times 0.5 \times 15.0 - 4880 - 4780 = 7478 \text{ kN·m/m},$$
$$t_e = \frac{7478}{1797} = 4.16 \text{ m} < \frac{1}{3}B = 5.0 \text{ m},$$
$$p_e = \frac{2 \times 1797}{3 \times 4.16} = 288 \text{ kPa}.$$

This value is far less than the allowable limit, and there would be no problem concerning the bearing capacity of the foundation.

4.3.2 *Width of Upright Section*

The wave pressure exerted on an upright section of a vertical breakwater is approximately proportional to the height of the waves incident to the break-water, but it is also controlled somewhat by the wave period, the sea bottom slope, the shape and dimensions of the rubble mound foundation, and other factors. The new wave pressure formulas described in the preceding sections are characterized by the incorporation of these factors. Tanimoto *et al.*[15] calculated the minimum width of the upright section of a breakwater required for various combinations of design conditions such as the wave height, wave period, water depth, mound thickness and bottom slope. They utilized a breakwater of the shape shown in Fig. 4.13, and searched for the minimum width satisfying the conditions of safety factors against sliding and overturning greater than 1.2. The density of the upright section was taken to be $\gamma' = 1.1$ Mg(ton)/m^3 (concrete caisson filled with sand) for the submerged portion, $\gamma = 2.1$ Mg(ton)/m^3 for the portion of the caisson above the still water level, and $\gamma = 2.3$ Mg(ton)/m^3 for the concrete crown. The crest elevation was set at a height of 0.6 times the significant wave height.[c] The coefficient of friction was taken as $\mu = 0.6$.

First, Fig. 4.14 shows the variation in the required design caisson width for a given water depth in the range of $h = 4.5 \sim 30.5$ m (the depth above the mound being $d = 0 \sim 26$ m) for several wave conditions, for a constant thickness of the rubble mound of $D = 3$ m. The bottom slope was taken to be 1/100. The wave period was selected so as to keep the steepness of the
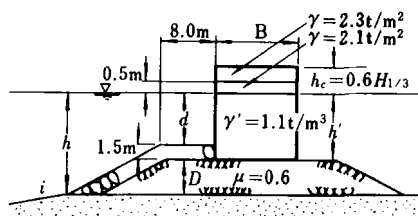
Fig. 4.13. Specification of vertical breakwater for trial calculation of the required caisson width (after Tanimoto *et al.*[15]).

---

[c]This criterion for specifying the crest elevation is used in breakwater design in Japan in situations where a small amount of wave overtopping and resultant wave transmission are tolerated. If very little wave overtopping is to be allowed, the crest elevation is set higher.
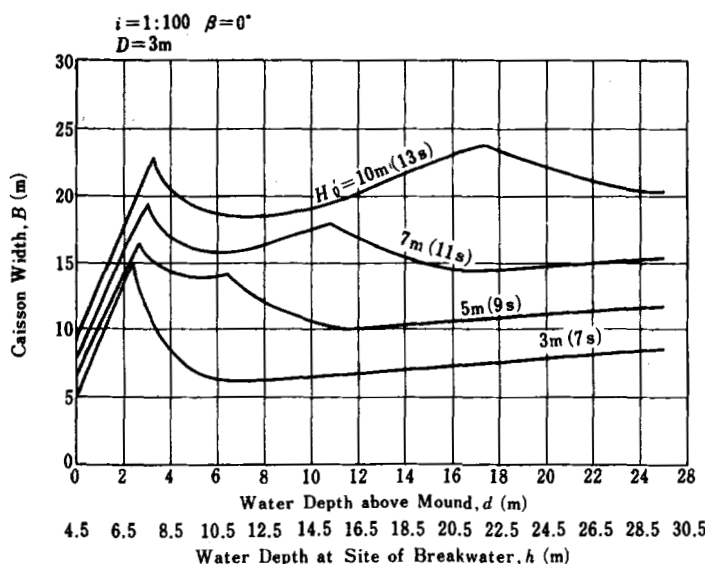
Fig. 4.14. Variation of the required caisson width for different incident wave heights.[15]

equivalent deepwater waves in the range of $H_0'/L_0 = 0.037 \sim 0.040$ for wave heights of $H_0' = 3 \sim 10$ m. The wave height $H_{\max}$ for breakwater design will vary with the water depth due to the effect of random wave breaking, but the effect of wave refraction was not taken into account. In the case of $H_0' = 10$ m, $H_{\max}$ as well as the caisson width take their greatest values at the water depth of $h = 21.8$ m. The appearance of a mildly sharp peak at this depth is an artifice of Eq. (3.26) in Sec. 3.5.5 for the estimation of $H_{\max}$, used for the sake of convenience in the calculation. The peak would be more rounded if $H_{\max}$ were estimated by means of Fig. 3.32. Another group of peaks appearing in the region of $d = 2.5 \sim 3.5$ m correspond to the water depth at which the coefficient α_2 takes the following maximum value:

$$(\alpha_2)_{\max} = \left[\frac{4}{3}\left(1 - \frac{d}{h_b}\right)\right]^{1/3} \quad \text{at} \quad \frac{d}{H_{\max}} = \left[\frac{1}{6}\left(1 - \frac{d}{h_b}\right)\right]^{1/3} . \quad (4.20)$$

The requirement that the quantities d, $H_{\max}$ and h_b satisfy Eq. (4.20) approximately corresponds to the occurrence condition of impulsive breaking wave pressure; i.e., incident waves just break on the rubble mound and strike the vertical wall with an impulsive pressure. The condition of impulsive breaking

wave pressure, however, is quite sensitive to small changes in several factors (cf. 4.3.3). Therefore, one should not overlook the possibility that a high breaking wave pressure may act on an upright section at a water depth somewhat different from that given by the peak condition of Eq. (4.20).
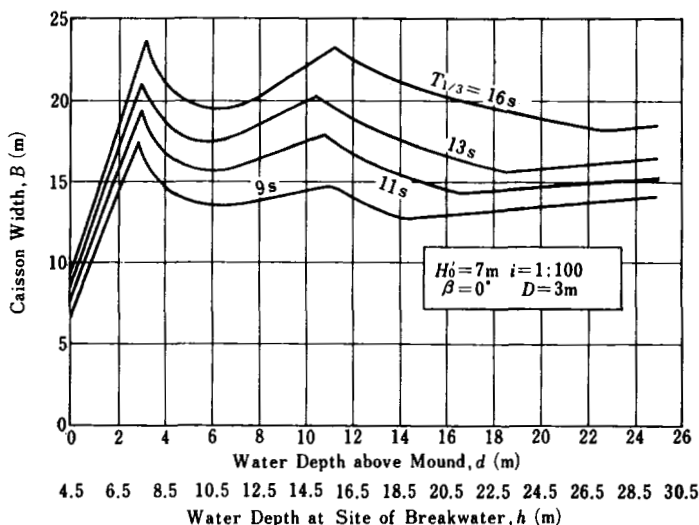
Fig. 4.15. Variation of the required caisson width for different incident wave periods.[15]

Next, Fig. 4.15 shows that the required caisson width depends on the wave period. In this figure the wave period varies from $T_{1/3} = 9$ s to 16 s, and the equivalent deepwater wave height is constant at $H'_0 = 7$ m. The required caisson width is seen to increase as the wave period increases. This is partly due to the increase in the coefficient α_1 with decrease in relative water depth h/L. The increase in required caisson width is also affected by the process of random wave breaking in that the attenuation of $H_{\max}$ is less for long-period waves than for short-period waves. Because of the effect of wave period on the wave pressure and the resultant required caisson width, careful examination of the design wave is required not only for the wave height but also for the wave period. In the past, insufficient attention has been paid to the wave period effect in the design of breakwaters.

Several laboratory tests specifically performed to determine the wave pressure on vertical walls have demonstrated that the breaking wave pressure
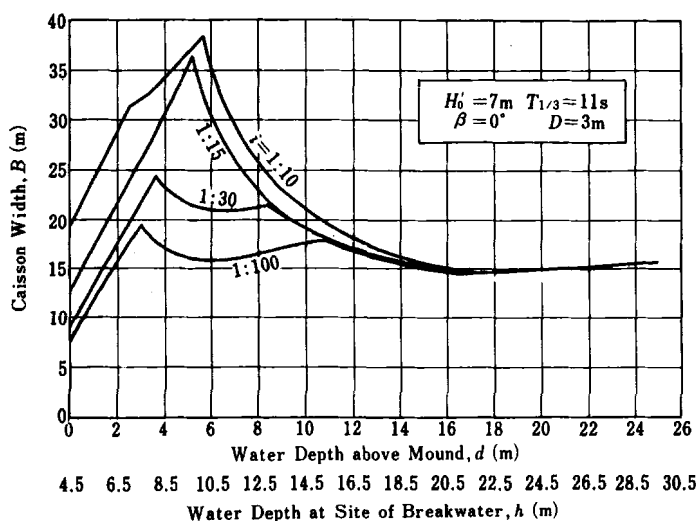
Fig. 4.16. Variation of the required caisson width for different sea bottom slopes.[15]

increases as the sea bottom slope becomes steeper. Figure 4.16 shows the effect of bottom slope on the required caisson width as calculated with the new wave pressure formulas. In the region of the breaker zone, an increase in required caisson width with steepening of the bottom slope is clearly evident. This effect is introduced through the pressure formulas, not directly in the pressure itself, but indirectly via the term for the design wave height H_{max}. This happens because, first, the limiting height of the breaking waves increases as the bottom slope becomes steeper; second, the proposed technique of estimating H_{max} to be the height at a distance $5H_{1/3}$ seaward from the breakwater enhances the effect of slope on the design value of H_{max} to be employed in the pressure calculation. In an area where the slope is steeper than 1/30, the design of a vertical breakwater should be done very carefully, as the increase in required caisson width is significant.

The height of the rubble mound foundation also affects the resultant wave pressure exerted on a structure. Figure 4.17 displays the effect of the thickness of a rubble mound on the required caisson width. Since the abscissa is the water depth d above the armor layer of the rubble mound, the original water depth h corresponding to a given value of d depends on the mound thickness D. Although it is difficult to draw a general conclusion, the increase in the
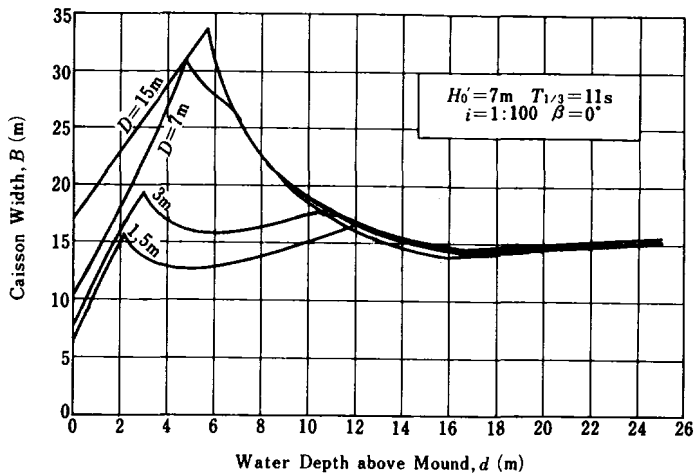
Fig. 4.17. Variation of the required caisson width for different thicknesses of the rubble mound.[15]
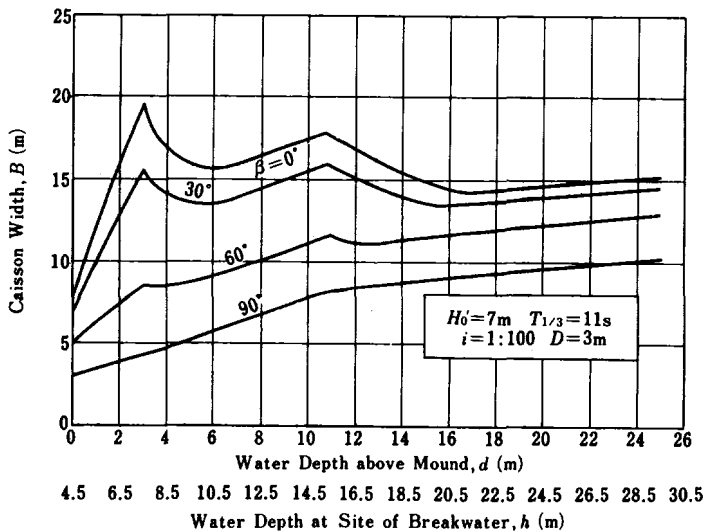
Fig. 4.18. Variation of the required caisson width for different angles of wave incidence.[15]

wave pressure is large if the depth d above the mound is less than half the original water depth.

Finally, Fig. 4.18 illustrates the dependence of the required caisson width on the angle of wave incidence to the breakwater. The adjustment of the wave

direction toward the line normal to the breakwater up to 15° is not made in this calculation. The wave pressure and the required width of the upright section of the breakwater gradually decrease as the incident angle increases. In particular, the increase in wave pressure due to the presence of a rubble mound is suppressed as the waves approach the breakwater obliquely.

4.3.3 *Precautions against Impulsive Breaking Wave Pressure*

As demonstrated in the laboratory experiments performed by Bagnold[10] and many other researchers, as well as by the results of field measurements, a gauge embedded in a vertical wall will record very high pressures due to breaking waves. This pressure may rise to more than ten times the hydrostatic pressure corresponding to the wave height, though its duration will be very short. Such an abnormally high breaking wave pressure is called an impulsive (breaking wave) pressure.

An impulsive pressure is exerted on a vertical wall when an incident wave begins to break in front of the wall and collides with it, having the wave front being almost vertical as shown in Fig. 4.19. The impinging wave loses its forward momentum in the short time during which the collision takes place. The forward momentum is converted into an impulse which is exerted on the
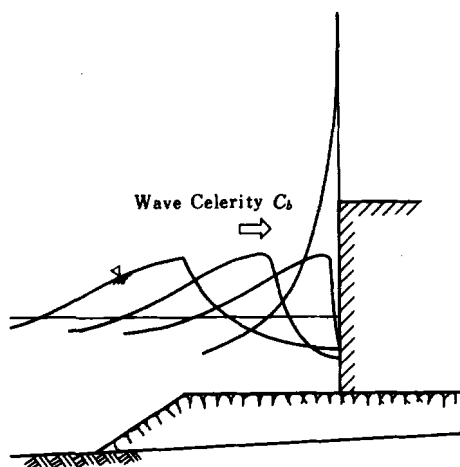
Fig. 4.19. Profiles of a breaking wave colliding with a vertical wall.

vertical wall. By denoting the forward momentum of the breaking wave per unit width as M_v, the total impulsive pressure on the wall as P_I, and its duration as τ, the momentum equation for the pressent situation becomes as follows:

$$\int_0^\tau P_I dt = M_v \,. \tag{4.21}$$

To estimate the magnitude of this momentum, let us consider the case of a water mass in the form of a semi-circular cylinder with a diameter of H_b advancing with the speed of the wave C_b. Thus, we have

$$M_v \simeq \frac{\pi \rho g}{8g} C_b H_b^2 \,, \tag{4.22}$$

where g denotes the acceleration of gravity $(= 9.8 \text{ m/s}^2)$.

If it is assumed that the impulsive pressure increases linearly at the start of the collision $(t = 0)$ to a maximum value at $t = \tau$, and then reduces to zero for $t > \tau$, the peak value of the impulsive pressure is obtained as

$$(P_I)_{\text{max}} \simeq \frac{\pi \rho g C_b H_b^2}{4g\tau} \,. \tag{4.23}$$

It is seen that for this model the impulsive pressure is inversely proportional to its duration. Thus, the impulsive pressure can attain a very large value when the front face of the breaking wave is in the form of a vertical flat plane and collides with the vertical wall over a very short time duration.

However, it is found in laboratory experiments that the front face of an impinging breaking wave is always curved and a small amount of air is entrapped at the instant of collision. As suggested by Bagnold[10] and formulated in a theoretical model by Takahashi and Tanimoto,[16] the entrapped air acts to dampen the impulsive pressure and prevents it from becoming abnormally high. Furthermore, the rubble mound foundation and the ground around a prototype breakwater will be elastically deformed under the application of an impulsive breaking wave pressure, and this softens the wave impact on the upright section. A computation of such elastic deformation of the foundation[17] indicates that the effective wave pressure in causing an upright section to slide is at most twice to thrice the hydrostatic pressure corresponding to the wave height, when the wave pressure is averaged over the exposed area of wall.

Nevertheless, the impulsive pressure caused by breaking waves is much greater than the pressure usually adopted in breakwater design. It would be rather foolish to design a vertical breakwater to be directly exposed to impulsive breaking wave pressure. A mound breakwater would be the natural choice in such a situation. If space is limited, or if little wave transmission is to be allowed, a vertical breakwater protected by a mound of concrete blocks of the energy-dissipating type might be an alternative design. From the engineering point of view, it is not the magnitude of the greatest pressure but, rather, the occurrence condition of the impulsive breaking wave pressure that is most important. Although it is difficult to describe the occurrence condition precisely, Tanimoto[18] has examined this problem using his own experimental data, in addition to other data. Table 4.1 is a guide for judging the possible danger of impulsive breaking wave pressure; it was prepared by referring to Tanimoto's examination.

The angle of incidence β to the breakwater is an important factor affecting the impulsive breaking wave pressure. With increase in the incident angle, the impulsive pressure decreases rapidly (Question A-1 in Table 4.1). This is due to the decrease in the normal component of the forward momentum of the impinging wave to the breakwater, which is proportional to $\cos^2 \beta$. The decrease in impulsive pressure is enhanced by the fact that the duration time of the pressure on a caisson increases in proportion to $\sin \beta$ due to oblique wave incidence. Tanimoto has suggested that the threshold angle is about 20°; for incident angles greater than 20°, the generation of impulsive breaking wave pressure will be slight. Thus, a breakwater cutting obliquely across the bottom contour lines has less probability of being exposed to dangerous impulsive breaking wave pressure than a breakwater constructed parallel to the contour lines.

The next important factor affecting the impulsive pressure is the size of the rubble mound foundation, but this needs to be judged on the basis of the sea bottom slope. Mitsuyasu[19] has demonstrated that an impulsive breaking wave pressure can be exerted on a vertical wall lacking a rubble mound if the bottom slope is equal to or steeper than about 1/30. Thus, a vertical breakwater with a rubble mound of negligible size or no mound at all is judged with the A series questions in Table 4.1, whereas if a rubble mound exists, the B series questions are to be used. The criteria behind questions A-3 to A-5 are mainly drawn from the experimental results of Mitsuyasu, and they are also consistent with other findings. Question A-6 owes to the experiment by Hamada *et al.*[20]

Table 4.1. Questionnaire for judging the danger of impulsive breaking wave pressure.

A-1   Is the angle between the wave direction and the line $\xrightarrow{\text{No}}$ Little Danger
       normal to the breakwater less than 20°?

                            ↓ Yes

A-2   Is the rubble mound sufficiently small to be considered $\xrightarrow{\text{No}}$ Go to B-1
       negligible?

                            ↓ Yes

A-3   Is the sea bottom slope steeper than 1/50? $\xrightarrow{\text{No}}$ Little Danger

                            ↓ Yes

A-4   Is the steepness of the equivalent deepwater wave less $\xrightarrow{\text{No}}$ Little Danger
       than about 0.03?

                            ↓ Yes

A-5   Is the breaking point of a progressive wave (in the absence $\xrightarrow{\text{No}}$ Little Danger
       of a structure) located only slightly in front of the
       breakwater?

                            ↓ Yes

A-6   Is the crest elevation so high as not to allow much $\xrightarrow{\text{No}}$ Little Danger
       overtopping

                            ↓ Yes

       | Danger of Impulsive Pressure Exists |

(Continued from Question A-2)
―――――――――――――――

B-1   Is the combined sloping section and top berm of the $\xrightarrow{\text{No}}$ Little Danger
       rubble mound broad enough (refer to Fig. 4.20)?

                            ↓ Yes

B-2   Is the mound so high that the wave height becomes nearly $\xrightarrow{\text{No}}$ Little Danger
       equal to or greater than the water depth above the mound
       (refer to Fig. 4.21)?

                            ↓ Yes

B-3   Is the crest elevation so high as not to cause much $\xrightarrow{\text{No}}$ Little Danger
       overtopping?

                            ↓ Yes

       | Danger of Impulsive Pressure Exists |

Fig. 4.20. Examples of the effect of berm width on the generation of impulsive breaking wave pressure (after Tanimoto[18]).

For vertical breakwaters built on rubble mounds of appreciable sizes, an impulsive pressure may be generated when the incident wave plunge on the slope or berm of the mound (Question B-1). Figure 4.20 is an example showing the effect of the berm width of a rubble mound on the average pressure on an upright section. The data were obtained by Tanimoto[18] for a rubble mound with a front slope of 1:2.5. The average pressure was estimated from the threshold weight of a model section against sliding. The result indicates that the average pressure attains a peak at a certain berm width, the value of which varies with the relative height of the rubble mound d/h.

Based on a systematic laboratory test of sliding of model upright sections by Tanimoto *et al.*,[21] Takahashi *et al.*[22] proposed a set of formulas to estimate the magnitude of impulsive pressure. The proposal is to rewrite Eq. (4.3) as in the following so as to include the term of impulsive pressure in the coefficient α_2:

$$p_1 = \frac{1}{2}(1 + \cos\beta)(\alpha_1 + \alpha^* \cos^2\beta)\rho g H_{\max} \; : \; \alpha^* = \max\{\alpha_2, \alpha_I\}, \quad (4.24)$$

where the coefficient α^* is taken as the maximum of α_2 of Eq. (4.7) or the following newly-defined coefficient α_I for impulsive breaking wave pressure:

$$\alpha_I = \alpha_{IH}\,\alpha_{IB}, \quad (4.25)$$

The coefficients α_{IH} and α_{IB} are evaluated with the following set of equations:

$$\alpha_{IH} = \min\{H/d, 2.0\}, \tag{4.26}$$

$$\alpha_{IB} = \begin{cases} \cos\delta_2/\cosh\delta_1 & : \delta_2 \le 0, \\ 1/(\cosh\delta_1 \cosh^{1/2}\delta_2) & : \delta_2 > 0, \end{cases} \tag{4.27}$$

$$\delta_1 = \begin{cases} 20\delta_{11} & : \delta_{11} \le 0, \\ 15\delta_{11} & : \delta_{11} > 0, \end{cases} \tag{4.28}$$

$$\delta_2 = \begin{cases} 4.9\delta_{22} & : \delta_{22} \le 0, \\ 3.0\delta_{22} & : \delta_{22} > 0, \end{cases} \tag{4.29}$$

$$\delta_{11} = 0.93\left(\frac{B_M}{L} - 0.12\right) + 0.36\left(0.4 - \frac{d}{h}\right), \tag{4.30}$$

$$\delta_{22} = -0.36\left(\frac{B_M}{L} - 0.12\right) + 0.93\left(0.4 - \frac{d}{h}\right). \tag{4.31}$$

The coefficient of impulsive pressure α_I has been so set that it will have the maximum value 2.0 at the conditions of $B/L = 0.12$, $d/h = 0.4$ and $H/h \ge 2.0$. Takahashi *et al.*[22] comment that the impulsive pressure coefficient α_I is always nearly zero and smaller than α_2 when $d/h \ge 0.7$.

Example 4.3

Check the possibility of the occurrence of impulsive breaking wave pressure for the upright section shown in Example 4.1.

Solution

The upright section has the values of $B = 8.0$ m, $d = 5.6$ m, and $h = 10.1$ m. The wavelength L for the period 11.4 s at the depth 10.1 m is 107.5 m. The impulsive pressure coefficient α_I is evaluated by Eqs. (4.25) to (4.30) as below.

$$\delta_{11} = 0.93 \times (8.0/107.5 - 0.12) + 0.36 \times (0.4 - 5.6/10.1) = -0.0980,$$
$$\delta_{22} = -0.36 \times (8.0/107.5 - 0.12) + 0.93 \times (0.4 - 5.6/10.1) = -0.127,$$
$$\delta_1 = 20 \times (-0.0980) = -1.960,$$
$$\delta_2 = 4.9 \times (-0.127) = -0.622,$$
$$\alpha_{IB} = \cos(-0.622)/\cosh(-1.960) = 0.813/3.62 = 0.225,$$
$$\alpha_{IH} = \min\{8.0/5.6, 2.0\} = \min\{1.43, 2.0\} = 1.43,$$
$$\alpha_I = 1.43 \times 0.225 = 0.320.$$

The pressure coefficient α_2, has been evaluated as 0.314 in Example 4.1. This value is slightly smaller than that of $\alpha_I = 0.320$ in the above, and thus the coefficient α^* is assigned the value 0.320. However, the pressure intensity calculated by Eq. (4.24) is much lower than that of impulsive pressure, and it can be judged that the upright section of Example 4.1 is not subject to the action of impulsive breaking wave pressure.

Finally, a vertical breakwater with a low crest elevation will not be in danger of impulsive pressure even though all other conditions may indicate such a possibility (B-3). The threshold elevation seems to be about 0.3 times the wave height for ordinary vertical breakwaters. However, an impulsive pressure may be exerted on a vertical breakwater with a low crest elevation if the rubble mound is quite large and if the incident waves break on its slope in the form of surging breakers.

The danger of the generation of impulsive breaking wave pressure can be judged to a certain extent with the criteria in Table 4.1. But it is admitted that the criteria are of a rather qualitative nature, and many cases may fall in the border zone. This uncertainty is inevitable because the phenomenon is affected by many factors in a complex and delicate manner. Therefore, it is advisable to resort to hydraulic model testing whenever there remains the suspicion of the generation of impulsive breaking wave pressure.

4.3.4 *Comments on Design of Concrete Caissons*

The upright section of a vertical breakwater can be composed of layers of solid concrete blocks, of layers of cellular concrete blocks with some filler, or of concrete caissons. Experience in Japanese breakwater construction has demonstrated the reliability of reinforced concrete caissons since the early days of their use.

As seen in the examples in Fig. 4.1, a concrete caisson is divided into rows and columns of inner cells with partition walls. The width of the caisson is determined by the stability condition against wave action. The length of the caisson is mostly determined by the maximum allowable size in the caisson manufacturing yard. As a precaution against uneven settling of the rubble mound and the ground, as well as possible scouring, the length is usually selected in the range of 0.5 to 2.0 times the width of the caisson. The height of the caisson is determined by considerations of the capacity of the caisson yard,

an analysis of the total cost, efficiency of divers' work in leveling the top of the rubble mound foundation, and other factors. Concrete caissons must have sufficient buoyant stability, unless they are to be carried and set in position with the aid of a huge floating crane.

The maximum dimension of the inner cells is usually designed to be less than 5 m. This determination is done in conjunction with selection of the thickness of the outer walls (between 40 to 50 cm) and the thickness of the partition walls (between 20 to 25 cm). The thickness of the bottom slab is usually 50 to 70 cm. The outer walls must be designed against the pressure exerted by the filler material and internal hydrostatic pressure. In addition, the front wall must be able to withstand the stress caused by wave pressure. If the dimensions of the inner cells are designed to be much greater than 5 m, the downward wave pressure by green water on the crown of the breakwater may need to be examined. Further details of caisson design can be found in *Technical Standards for Port and Harbour Facilities in Japan.*[23]

Few breakwater caissons in Japan have shown indications of deterioration due to corrosion. The standard design strength of the concrete for breakwater caissons in Japan is 24 MPa, and for many years the thickness of the covering for reinforcement has been specified to be not less than 7 cm on the seaward side and 5 cm on the landward side. It appears that continuous submergence of the major portion of a caisson acts to prevent deterioration of the reinforced concrete.

4.4 Design of Rubble Mound Foundation

4.4.1 *Dimensions of Rubble Mound*

It is best to set the height of the rubble mound as low as possible to prevent the generation of large wave pressure. But the function of a rubble mound — to spread the vertical load due to the weight of the upright section and the wave force over a wide area of the seabed — necessitates a minimum height, which is required to be not less than 1.5 m in Japan. Furthermore, the top of the rubble mound should not be too deep, in order to facilitate underwater operations of divers in leveling the surface of the mound for even setting of the upright section. A cost analysis on breakwater construction will yield the optimum height of the rubble mound under the above constraints.

The berm width is a factor to be selected empirically. If the seabed is soft, the dimensions of the rubble mound should be determined by safety considerations against circular slip of the ground. The berm in front of an upright section functions to provide protection against possible scouring of the seabed. A wide berm is desirable in this respect, but the cost and danger of inducing impulsive breaking wave pressure precludes the design of too great a berm width. The practice in Japan is for a minimum of 5 m under normal conditions and about 10 m in areas attacked by large storm waves. The berm to the rear of an upright section has the function of safely transmitting the vertical load to the seabed. It also provides an allowance of some distance if sliding of an upright section should occur. The gradient of the slope of the rubble mound is usually set at 1 : 2 to 1 : 3 for the seaward side and 1 : 1.5 to 1 : 2 for the harbor side.

4.4.2 *Foot-Protection Blocks and Armor Units*

In breakwater construction in Japan, it is customary to provide a few rows of foot-protection concrete blocks at the front and rear of the upright section, as seen in Fig. 4.2. The foot-protection usually consists of rectangular blocks weighing from 100 to 400 kN (10 to 40 tons), depending on the design wave height. Foot-protection blocks are indispensable, especially when storm waves attack a vertical breakwater at an oblique angle.

The remainder of the berm and slope of the rubble mound foundation must be protected with armor units of sufficient weight to withstand wave action. The question of the minimum mass of armor units baffled engineers for many years, forcing them to rely on experience. However, Tanimoto *et al.*[24,25] succeeded in formulating a calculation method for the weight required of armor units, based on irregular wave tests and theoretical analysis. According to their study, the minimum mass of armor units for a rubble mound foundation can be calculated by a formula of the Hudson type:

$$M = \frac{\rho_r}{N_s^3(S_r - 1)^3} H_{1/3}^3, \tag{4.32}$$

where M is the mass of the armor unit, ρ_r the density of the armor unit, S_r the ratio of ρ_r to the density of seawater, $H_{1/3}$ the design significant height, and N_s the stability number. The value of the stability number depends on the wave conditions and mound dimensions, as well as on the shape of the armor units.

For normally incident waves, irregular wave tests have shown that the most unstable location along a breakwater is the corner between the slope and the horizontal section of the berm. Through analysis of the fluid dynamic forces of drag and lift acting on a single armor unit, together with the results of laboratory experiments, Tanimoto *et al.* proposed the following function for the stability number N_s for armor stones:

$$N_s = \max\left\{1.8, \left(1.3\frac{1-\kappa}{\kappa^{1/3}}\frac{h'}{H_{1/3}} + 1.8\exp\left[-1.5\frac{(1-\kappa)^2}{\kappa^{1/3}}\frac{h'}{H_{1/3}}\right]\right)\right\}, \quad (4.33)$$

in which

$$\kappa = \frac{4\pi h'/L}{\sinh(4\pi/L)}\sin^2\left(\frac{2\pi B_M}{L'}\right), \qquad (4.34)$$

$$\max\{a,b\} : \text{larger of } a \text{ and } b,$$

and where h' denotes the water depth at which armor units are placed, L' the wavelength at the depth h', and B_M the berm width.

Example 4.4

Calculate the minimum mass of the rubble stone required to armor the rubble mound foundation of the breakwater presented in Fig. 4.8, assuming the waves are incident normal to the structure.

Solution

i) Wave and mound dimensions

$$H_{1/3} = 5.8 \text{ m}, \quad T_{1/3} = 11.4 \text{ s},$$
$$h' = 7.1 \text{ m}, \quad L' = 91.6 \text{ m}, \quad \text{and } B_M = 8.0 \text{ m}.$$

ii) Parameter κ and stability number N_s

$$\kappa = \frac{4\pi \times 7.1/91.6}{\sinh(4\pi \times 7.1/91.6)} \times \sin^2\left(\frac{2\pi \times 8.0}{91.6}\right) = 0.233,$$

$$N_s = \max\left\{1.8, \left(1.3 \times \frac{1-0.233}{0.233^{1/3}} \times \frac{7.1}{5.8} + 1.8\right.\right.$$

$$\left.\left. \times \exp\left[-1.5 \times \frac{(1-0.233)^2}{0.233^{1/3}}\frac{7.1}{5.8}\right]\right)\right\}$$

$$= \max\{1.8, 2.29\} = 2.29.$$

iii) Mass of armor stone

Assuming $\rho_r = 2650$ kg/m^3 and $S_r = 2.57$, we have

$$M = \frac{2650}{2.29^3 \times (2.57 - 1)^3} \times 5.8^3 = 11.1 \text{ Mg(ton)}.$$

In actual design, heavy concrete blocks may be required as the armor units of this breakwater.

For obliquely incident waves, Tanimoto *et al.*[25] suggested the following parameter, based on calculations of the orbital velocity of water particles in a three-dimensional standing wave system.

$$\kappa = \frac{4\pi h'/L'}{\sinh(4\pi h'/L')} \kappa_2 , \tag{4.35}$$

$$\kappa_2 = \max \left\{ \alpha_S \sin^2 \beta \cos^2 \left(\frac{2\pi x}{L'} \cos \beta \right) , \right.$$

$$\left. \cos^2 \beta \sin^2 \left(\frac{2\pi x}{L'} \cos \beta \right) \right\} : 0 \le x \le B_M , \tag{4.36}$$

in which the distance x from the foot of the upright section should be varied to give the maximum value of κ_2. For normal wave incidence ($\beta = 0$), Eqs. (4.35) and (4.36) reduce to Eq. (4.34) at $x = B_M$. The factor α_S has been introduced by Kimura *et al.*[26] to account for the effect of slope, and the value of $\alpha_S = 0.45$ is given based on measured data. According to irregular wave tests for oblique incidence by Kimura *et al.*, waves with the incidence angle $\beta = 60°$ caused greater damage than waves with $\beta = 0°$ and $45°$: damage occurred at $x = 0$ when $\beta = 60°$.

Around the corners of caisson at a breakwater head, strong oscillatory flow is generated at the sea bottom and on top of the rubble mound. The armor units around a breakwater head should be provided with the weight much greater than those along the trunk section. Kimura *et al.*[26] propose to calculate the κ value for Eq. (4.33) as follows:

$$\kappa = \frac{\pi h'/L'}{\sinh(4\pi h'/L')} \alpha_S \tau^2 , \tag{4.37}$$

where τ is the correction factor for local rapid flow around the corners. Kimura *et al.* recommend the following value for τ, based on their test result:

$$\tau = \begin{cases} 1.4 & : \ \beta = 0°, 45°, \\ 2.5 & : \ \beta = 60°. \end{cases} \tag{4.38}$$

In any case, the stability of the foot-protection blocks and armor units of a rubble mound foundation should be examined with a hydraulic scale model employing irregular trains of laboratory waves. The previously mentioned studies by Tanimoto *et al.*[24,25] indicated that trains of regular waves should have a height of 1.37 times the significant height of irregular waves in order to produce the same amount of damage on the armor units of a rubble mound foundation.

4.4.3 *Protection against Scouring of the Seabed in Front of a Breakwater*

A vertical breakwater reflects most of the wave energy incident on it, thus creating greater agitation at its front than that created by a mound breakwater. This agitation is thought to produce scouring of the bed in front of the breakwater. The disaster of the Mustapha breakwater in Alger Port in 1934 is a well-known example of seabed scouring, which is considered to have accelerated the collapse of the upright section.[27] It is interesting to note that in Japan there has been no case of the collapse of a breakwater due to seabed scouring, even though several hundred kilometers of vertical breakwaters have been built along the coast. Scouring takes place at the breakwaters in a number of ports and the tips of the rubble mounds are dislocated, but repairs are always made before the stability of the upright sections is threatened. The absence of breakwater collapse may also owe to the practice of providing a quite broad berm and gentle slope for the rubble mound in front of the upright section.

Nonetheless, dislocation of the rubble mound foundation due to scouring of the seabed is a phenomenon against which precautions must be taken. For this purpose, various materials such as plastic filters and asphalt mats are spread beneath the area of the tip of the rubble mound and extended beyond it. However, no effective method has yet been found to stop scouring of the bed and dislocation of the tip of a rubble mound. Present practice is toward the revival of gravel matting, i.e., a thin layer of quarry run extended beyond the tip of the armor layer. Gravel may be dispersed by strong wave agitation,

but a mixture of gravel and original bed material will withstand wave action for a longer duration than an unprotected seabed.

References

1. J. Larras, *Cours d'Hydraulique Maritime et de Travaux Maritimes* (Dunod, Paris, 1961), pp. 244–245.
2. Y. Ito, "A treatise on historical development of breakwater design," *Tech. Note of Port and Harbour Res. Inst.* (69) (1969), 78p (*in Japanese*).
3. K. Tanimoto and Y. Goda, "Stability of deep water caisson breakwater against random waves," *Coastal Structures and Breakwaters* (The Inst. Civil Engrs., Thomas Telford, 1992), pp. 221–206.
4. S. Takahashi, "Design of vertical breakwaters," *Reference Document* (34) (Port and Harbour Res. Inst., 1996), 85p.
5. Th. Stevenson, *The Design and Construction of Harbours* (3rd Ed.) (Adam & Charles Blacks, 1886).
6. B. Gaillard, "Wave action in engineering structure," *Engineering News* 23 Feb. 1905.
7. I. Hiroi, "On a method of estimating the force of waves," *Memoirs of Engrg. Faculty, Imperial Univ. Tokyo*, X (1) (1919), p. 19.
8. G. Sainflou, "Essai sur les digues maritimes, verticales," *Annales Ponts et Chaussées* **98** (4) (1928).
9. R. R. Minikin, *Winds, Waves and Maritime Structures* (Griffin, London, 1950), pp. 38–39.
10. R. A. Bagnold, "Interim report on wave-pressure research," *J. Inst. Civil Engrs.* **12** (1939), pp. 202–226.
11. Y. Ito, M. Fujishima, and T. Kitatani, "On the stability of breakwaters," *Rept. Port and Harbour Res. Inst.* **5** (14) (1966), 134p. (*in Japanese*) or *Coastal Engineering in Japan* 14 (1971), pp. 53–61.
12. Y. Goda and T. Fukumori, "Laboratory investigation of wave pressures exerted upon vertical and composite walls," *Rept. Port and Harbour Res. Inst.* **11** (2) (1972), pp. 3–45 (*in Japanese*) or *Coastal Engineering in Japan* **15** (1972), pp. 81–90.
13. Y. Goda and S. Kakizaki, "Study on finite amplitude standing waves and their pressures upon a vertical wall," *Rept. Port and Harbour Res. Inst.* **5** (10) (1966), 57p. (*in Japanese*) or *Coastal Engineering in Japan* 10 (1967), pp. 1–11.
14. Y. Goda, "A new method of wave pressure calculation for the design of composite breakwater," *Rept. Port and Harbour Res. Inst.* **12** (3) (1973), pp. 31–70 (*in Japanese*) or *Proc. 14th Int. Conf. Coastal Engrg.* (Copenhagen, 1974), pp. 1702–1720.
15. K. Tanimoto, K. Moto, S. Ishizuka, and Y. Goda, "An investigation on design wave force formulae of composite-type breakwaters," *Proc. 23rd Japanese Conf. Coastal Engrg.* (1976), pp. 11–16 (*Japanese*).

16. S. Takahashi and K. Tanimoto, "Generation mechanism of impulsive pressure by breaking wave on a vertical wall," *Rept. Port and Harbour Res. Inst.* **22** (4) (1983), pp. 3–31 (*in Japanese*).

17. Y. Goda, Dynamic response of upright breakwaters to impulsive breaking wave forces," *Coastal Engineering* **22** (1 & 2) (1994), pp. 135–158.

18. K. Tanimoto, "Wave forces on a composite-type breakwater," *Proc. 1976 Annual Res. Present. of Port and Harbour Res. Inst.* (1976), pp. 1–26 (*in Japanese*).

19. H. Mitsuyasu, "Experimental study on wave force against a wall," *Rept. Transportation Tech. Res. Inst., Ministry of Transport, Japan* (47) (1962), 39p.

20. T. Hamada, H. Mitsuyasu, and N. Hasegawa, "Wave forces exerted upon structures," *Proc. 3rd Japanese Conf. Coastal Engrg.* (1956), pp. 67–83 (*in Japanese*).

21. K. Tanimoto, S. Takahashi, and T. Kitatani, "Experimental study of impact breaking wave forces on a vertical-wall caisson of composite breakwater," *Rept. Port and Harbor Res. Inst.* **20** (2) (1981), pp. 3–39 (*in Japanese*).

22. S. Takahashi, K. Tanimoto, and K. Shimosako, "A proposal of impulsive pressure coefficient for the design of composite breakwaters," *Proc. Int. Conf. Hydro-Technical Engrg. for Port and Harbor Constr. (Hydro-Port '94)* (Yokosuka, Japan 1994), pp. 489–504.

23. Bureau of Ports and Harbours, and Port and Harbour Res. Inst., Ministry of Transport, *Technical Standards for Port and Harbour Facilities in Japan* (1980), pp. 92–104.

24. K. Tanimoto *et al.*, "Stability of armour units for foundation mounds of composite breakwaters by irregular wave tests," *Rept. Port and Harbour Res. Inst.* **21** (3) (1982), pp. 3–42 (*in Japanese*).

25. K. Tanimoto, T. Yagyu, and Y. Goda, "Irregular wave tests for composite breakwater foundations," *Proc. 18th Int. Conf. Coastal Engrg.* (Cape Town, 1982), pp. 2144–2163.

26. K. Kimura, S. Takahashi, and K. Tanimoto, "Stability of rubble mound foundations of composite breakwaters under oblique wave attack," *Proc. 24th Int. Conf. Coastal Engrg.* (Kobe, 1994), pp. 1227–1240.

27. R. Pierre, "La jetée de Mustapha au Port d Alger," *Annales des Ponts et Chaussées* Avr.-Mai, 1935.

Chapter 5

Design of Seawalls

5.1 Wave Overtopping Rate of Seawalls

5.1.1 *Overtopping Rate by Random Sea Waves*

Seawalls and revetments are built along existing beaches and waterlines of reclaimed land in order to protect the land area from high waves during storm tide. The main body of the seawall must be strong enough to withstand the attack of storm waves, and the crest must be high enough to prevent the intrusion of sea water onto the land by overtopping. Wave overtopping is primarily governed by the absolute heights of individual waves relative to the crest elevation of the seawall. Overtopping is not a continuous process but an intermittent occurrence at times of attack of individual high waves among the storm waves. The degree of wave overtopping is measured by the amount of overtopped water onto the land area, either as the amount (volume) per wave per unit length of seawall or as the mean rate of overtopping volume per unit length during the occurrence of storm waves.

The rate of overtopping averaged over the duration of the storm waves is hereby denoted as q. The overtopping rate is calculated by means of the amount of overtopping by individual waves $Q(H_i, T_i)$ as

$$q = \frac{1}{t_0} \sum_{i=1}^{N_0} Q(H_i, T_i), \qquad (5.1)$$

where

$$t_0 = \sum_{i=1}^{N_0} T_i \quad : \text{ duration of storm waves}, \qquad (5.2)$$

N_0 : total number of waves,

H_i, T_i : height and period of the ith individual
wave attacking the seawall.

The mean rate of wave overtopping must be obtained through laboratory tests with irregular waves or through field measurements at seawalls with appropriate installations. But when a set of laboratory data on the rate of overtopping q_0 by regular waves with various combination of heights and periods is available, an approximate value of the mean rate of random wave overtopping can be estimated with the following formula:

$$q = \frac{1}{t_0} \sum_{t=1}^{N_0} T_i q_0(H_i, T_i) \,. \tag{5.3}$$

The above estimate is not expected to be too accurate, because the estimation neglects the random process of wave breaking, the presence of surf beat inherent to random waves, and the effects of interference by the preceding waves. Nevertheless, Eq. (5.3) provides engineers with a practical method of obtaining an estimate of random wave overtopping. A further simplification of Eq. (5.3) can be made by assuming that all wave periods are equal to some representative wave period, such as the significant period $T_{1/3}$. Thus,

$$q \simeq q_{\text{EXP}} = \int_0^\infty q_0(H|T_{1/3}) p(H) dH \,, \tag{5.4}$$

where

$q_0(H|T_{1/3})$: overtopping rate by regular waves with height H
and period $T_{1/3}$,

$p(H)$: probability density function of wave height.

Although Eq. (5.4) does not include the correlation between individual wave heights and periods, the correlation exists only among waves of smaller heights, being nil among waves with larger heights (refer to Sec. 9.3.2). Therefore the assumption is acceptable for the design of seawalls, because seawalls are designed to allow only occasional overtopping by a small number of high waves in a wave group. As for the probability density function $p(H)$, the Rayleigh

distribution described in Sec. 2.2.1 can be employed if the laboratory data have been given in terms of the equivalent deepwater wave height.

The estimate of the mean overtopping rate, q_{EXP} of Eq. (5.4), has been termed the expected rate of wave overtopping by the author.[1,2] A comparison was made between the estimated overtopping rate by Eq. (5.4), based on regular wave data, and the results of direct measurements with irregular waves in the laboratory for vertical walls and block mounds backed up by upright revetments. It was found that Eq. (5.4) gave reasonably good approximations to the measured values, except for seawalls close to the shoreline, where surf beat dominates.

An important feature of wave overtopping of prototype seawalls is its random nature. The analysis of wave overtopping requires incoporation of the probability distribution of individual wave heights and periods, especially of the former. If regular wave data for overtopping are directly applied to the design of a seawall by interpreting the regular wave height as equivalent to the significant height, the error introduced in the estimate of the overtopping rate may be quite large. For a seawall with a relatively high crest elevation, the overtopping rate will be underestimated in regular wave data, because the estimation ignores the existence of individual waves higher than the significant wave. Such an estimate of overtopping rate will lead to an unsafe design of the seawall.

5.1.2 *Wave Overtopping Rate of Vertical Revetments and Block Mound Seawalls*

One of the typical shapes of a seawall is that of a revetment in the form of a vertical wall jutting directly from the seabed. There are several laboratory data sets available on wave overtopping of such revetments. Figures 5.1 and 5.2 are design diagrams compiled by the author[3] for the estimation of wave overtopping rate of vertical revetments. They were prepared on the basis of irregular wave tests and calculation of wave deformation in the surf zone. Figure 5.1 is for a sea bottom slope of 1/10, and Fig. 5.2 is for a slope of 1/30. The symbol H_0' in the figures denotes the equivalent deepwater wave height, h the water depth, h_c the crest elevation of the seawall above the still water level, and g the acceleration of gravity (= 9.8 m/s^2). As seen in the insets of the figures, a simple wall with no recurved parapet and no foot-protection rubble mound is being considered.
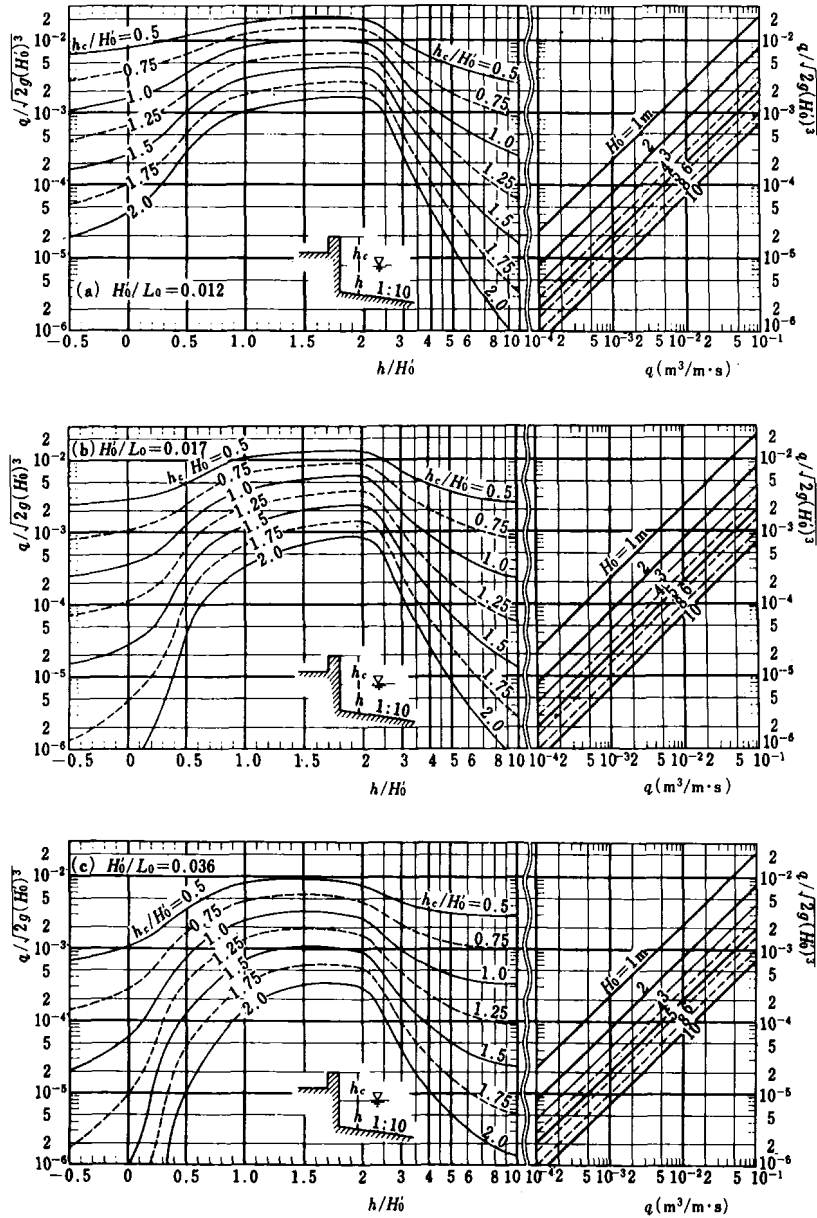
Fig. 5.1. Design diagrams of wave overtopping rate of vertical revetments on a sea bottom slope of 1/10.[3]
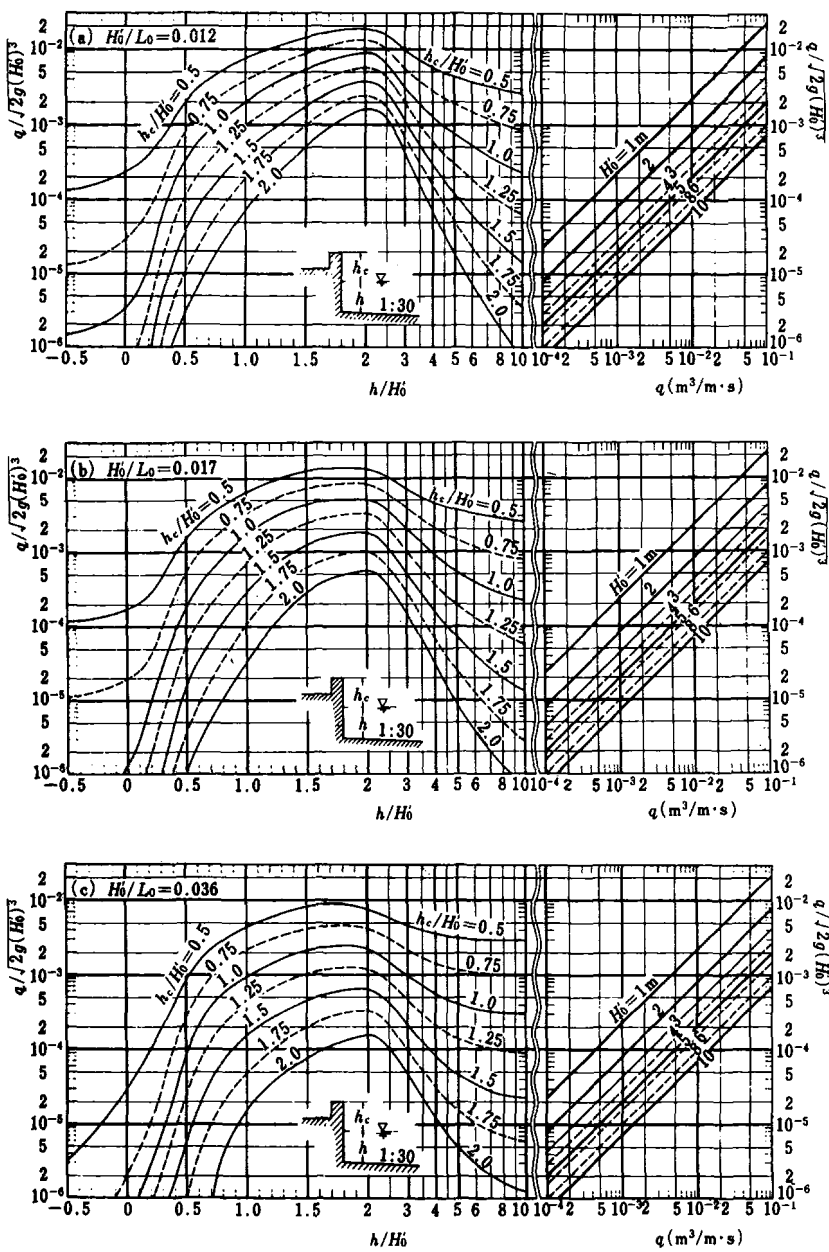
Fig. 5.2. Design diagrams of wave overtopping rate of vertical revetments on a sea bottom slope of 1/30.[3]

Example 5.1

A vertical revetment with a crest elevation + 6.0 m above the datum level is built in water of depth − 5.0 m on a bottom with slope 1/30. Estimate the mean rate of wave overtopping when waves with the equivalent deepwater height of $H_0' = 4.1$ m and $T_{1/3} = 8.5$ s attack the revetment at the tide level of + 1.5 m.

Solution

Since the deepwater wavelength is $L_0 = 113$ m and the wave steepness is $H_0'/L_0 = 0.040$, the relative water depth and crest elevation become

$$h/H_0' = (5.0 + 1.5)/4.5 = 1.44\,,$$

$$h_c/H_0' = (6.0 - 1.5)/4.5 = 1.0\,.$$

By referring to Fig. 5.2(c) we obtain

$$q/\sqrt{2g(H_0')^3} = 2 \times 10^{-3}\,. \quad \text{Thus} \quad q \simeq 0.08 \ \text{m}^3/\text{m} \cdot \text{s}\,.$$

If either the wave steepness or the bottom slope differs from those in Figs. 5.1 and 5.2, interpolation or extrapolation becomes necessary. If the bottom slope is milder than 1/30, the wave overtopping rate in water shallower than $2H_0'$ becomes less than that given by Fig. 5.2 in general. The rate of reduction in overtopping rate increases as the relative crest elevation h_c/H_0' increases.

Seawalls made of sloping mounds of rubble stones and concrete blocks of the energy-dissipating type are more popular than vertical revetments. In Japan, block mound seawalls of relatively steep slope backed by a vertical retaining wall are quite common, especially along coasts facing rough seas. Figure 5.3 is a sketch of such a seawall. The wave overtopping rate of block mound seawalls
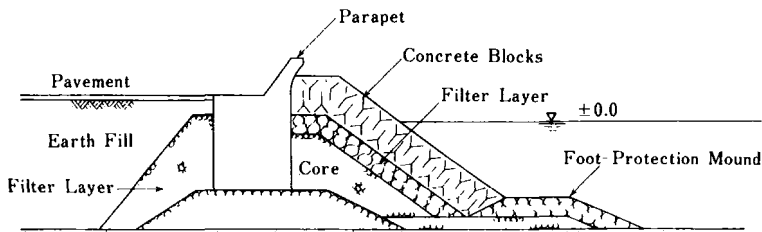
Fig. 5.3. Idealized typical section of a seawall built with concrete block mound of the energy-dissipating type.
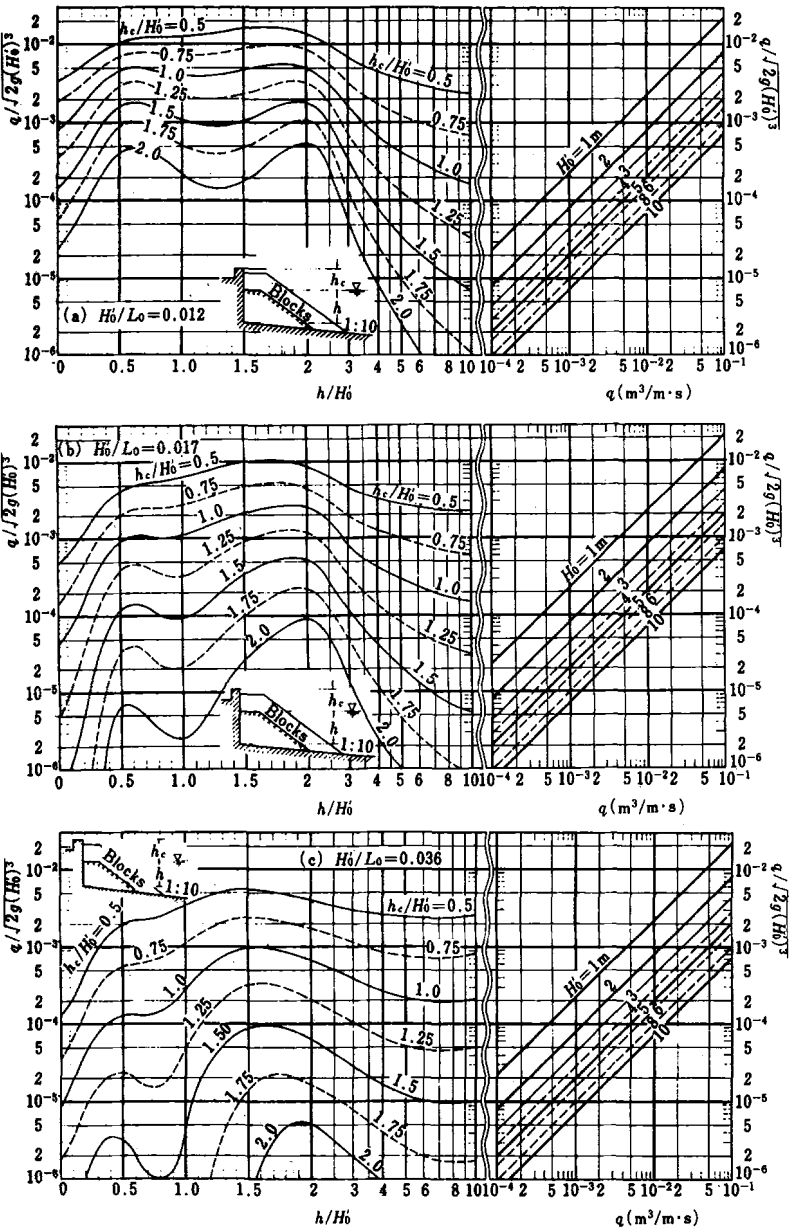
Fig. 5.4. Design diagrams of wave overtopping rate of block mound seawalls on a sea bottom slope of 1/10.[3]
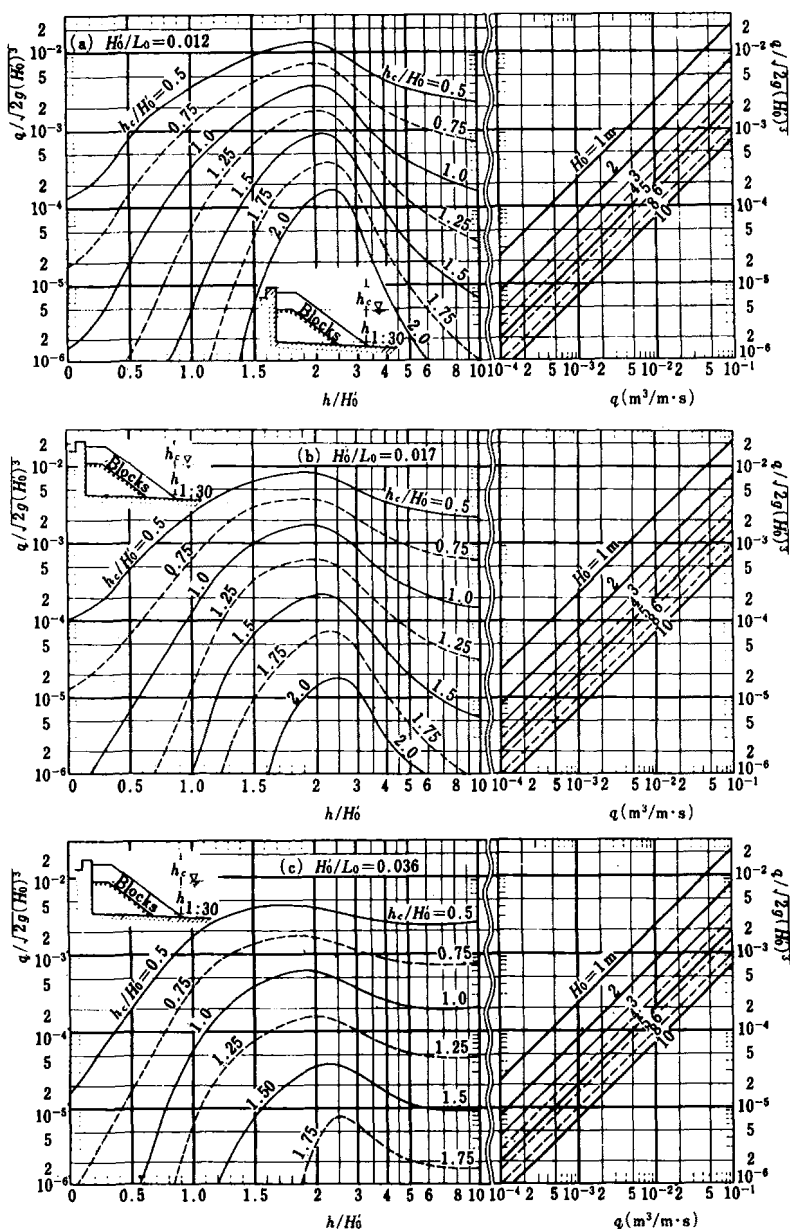
Fig. 5.5.   Design diagrams of waves overtopping rate of block mound seawalls on a sea bottom slope of 1/30.[3]

is governed not only by the characteristics of the incident waves, water depth and crest elevation, but also by the size and shape of the mound. Therefore, the compilation of generalized design diagrams for the overtopping rate of block mound seawalls is more difficult than for the case of vertical revetments. Nevertheless, the author[3] has proposed the diagrams shown in Figs. 5.4 and 5.5. The symbol h_c in the figures refers to the crest elevation of the vertical parapet. The seawalls under consideration have two layers of tetrapods resting on mounds of crushed stones placed in front of the vertical wall. The lower layer of tetrapods at the crest of the block mound consists of two rows of tetrapods. The top of the vertical parapet is set at a height of about 0.1 H_0' above the crest of the block mound, and no recurvature is given to the parapet. Furthermore, no foot-protection mound beneath the block mound is provided. The slope of the mound has a gradient of 1:1.5. As in the case of Figs. 5.1 and 5.2, laboratory tests were made with irregular trains of waves.

Example 5.2

How much of a reduction in wave overtopping rate can be expected by changing the seawall from the vertical revetment to the block mound type for the same conditions as in Example 5.1?

Solution

By reading the value of the ordinate corresponding to the input data of $h/H_0' = 1.44$ and $h_c/H_0' = 1.0$ in Fig. 5.5(c), we obtain

$$q/\sqrt{2g(H_0')^3} = 3 \times 10^{-4} . \quad \text{Thus} \quad q \simeq 0.013 \text{m}^3/\text{m} \cdot \text{s} .$$

Thus, the overtopping rate is reduced to 1/6 that of the vertical revetment.

In studies of wave overtopping, scatter in the (laboratory) data is inevitable. The scatter becomes greatest when the crest of the seawall is high and the amount of wave overtopping is small. The diagrams presented as Figs. 5.1, 5.2, 5.4 and 5.5 contain a certain range of variation due to this scatter in the original data. Comparing the limited available data of field measurements, the range of variation in the estimation of wave overtopping rate is obtained as listed in Table 5.1. The range of variation is greater for block mound seawalls than for vertical revetments. Although the range of variation is relatively large for the estimation of the overtopping rate of a seawall with specific dimensions,

Table 5.1. Probable range of variation of estimated rate
of wave overtopping to the true value.

$q/\sqrt{2g(H_0')^3}$	Vertical revetment	Block mound seawall
10^{-2}	$0.7 \sim 1.5$ times	$0.5 \sim 2$ times
10^{-3}	$0.4 \sim 2$ times	$0.2 \sim 3$ times
10^{-4}	$0.2 \sim 3$ times	$0.1 \sim 5$ times
10^{-5}	$0.1 \sim 5$ times	$0.05 \sim 10$ times

the variation is small when the crest elevation is sought for a given rate of overtopping; the range of the variation of estimated crest elevation is thought to be less than $\pm$ 20%. The difference in the ranges of variation stems from the nature of the equicontour lines of the overtopping rate in Figs. 5.1, 5.2, 5.4 and 5.5. Because the slope of the equicontour lines is quite steep in the zone of small values of nondimensional overtopping rate, a slight change in wave conditions and other factors produces a significant change in the rate of overtopping.

5.1.3 *Influence of Various Factors upon the Rate of Wave Overtopping*

Wave overtopping is affected by many factors. Even a small modification of the geometry of a seawall may change the amount of wave overtopping. For example, wave overtopping can be reduced to zero by redesigning the parapet into a curved shape, if the seabed conditions and the frontal shape of the seawall are suitable, and if no wind is blowing from the sea. The wave overtopping rate of a block mound seawall can be reduced to some extent by replacing the entire volume of rubble stones in the underlayer and the core of the mound with concrete energy-dissipating blocks. The crown width of the block mound also affects the wave overtopping rate. The shape of the foot-protection mound is another factor, but its influence is too complex to enable one to draw general conclusions. In comparison to a vertical revetment, a sloped seawalll with a smooth surface, which is one of the typical coastal dikes, usually has a greater rate of wave overtopping.

Thus, the wave overtopping rate of a seawall to be designed for a specific situation is best determined through hydraulic model tests. Figures 5.1, 5.2, 5.4 and 5.5 can be utilized to estimate the order of magnitude of the overtopping

rate for the planning of the hydraulic tests. Irregular wave tests are most desirable, but regular wave tests may suffice for the purpose if an irregular wave generator is not available, provided that the expected rate of overtopping is estimated from the test results by means of Eq. (5.4).

Wind is an important factor in wave overtopping. However, no reliable conclusion has yet been obtained on the wind effect because of the lack of a reliable modeling law. Generally speaking, it is believed that the increase of wave overtopping by an onshore wind is large when the quantity of overtopping is small and that the wind effect decreases gradually as the overtopping rate increases. However, Takada[4] has reported that the wind effect is not negligible even when wave overtopping is intensive, and thus this problem requires further investigation.

5.2 Crest Elevation

5.2.1 *Design Principles for the Determination of Crest Elevation*

The planning of a seawall requires comparative designs of several structural types of seawalls. For each design, the crest elevation must be determined according to the wave run-up or overtopping characteristics. The crest elevation should be specified in order to give a height above the design storm tide sufficient to prevent wave overtopping during the attack of design storm waves. The determination of the design storm tide and design waves is a difficult and intricate problem in itself. The statistical method to derive design values for a given return period is discussed in Chapter 11.

The crest elevation of a seawall is determined by one of the following two principles. One is to take the wave run-up height as the reference and to set the crest of the seawall higher than the run-up height so that no wave overtopping will occur. The other is to take the wave overtopping amount as the reference and to set the crest of the seawall at such a height as to keep the overtopping below some maximum tolerable quantity.

An unknown factor entering into the first methods is the problem of wave irregularity; that is, which characteristic wave height, e.g., $H_{1/3}$, $H_{1/10}$, or H_{max}, should be used in estimating the run-up height? In recent years, several laboratory reports have become available on the irregular wave run-up on seawalls e.g., Ref. 5. Still, the same question is asked: which characteristic run-up

height, $\bar{R}$, $R_{1/3}$, or $R_{2\%'}$, for example, should be considered in seawall design? For a seawall to be built on land with a ground elevation higher than the design storm tide, its crest elevation may be set higher than the maximum run-up height of random waves without much difficulty, because the maximum run-up is not too large. For a seawall to be built in the sea, however, the same procedure cannot be adopted because the maximum run-up height is very large. Even for the planning of a seawall to be built on land, the same problem may be encountered if the beach slope is very steep.

As an example, 13 people lost their lives on the Yoshihara Coast along the Bay of Suruga in Japan on the occasion of the attack of Typhoon No. 6626 in 1966. Although the coast was protected by a dike with an elevation of 13 m above the mean sea level, storm waves overran the dike and flooded the area behind it. The situation was later examined through a hydraulic model test,[6] and the waves which had caused such damage were estimated to have had $H_{1/3} \simeq 11$ m, $H_{max} \simeq 20$ m, and $T_{1/3} \simeq 20$ s. The maximum run-up height for this wave condition would have been greater than 20 m above the mean sea level, though this was not confirmed in the test.

Another problem inherent to the principle of runup-based seawall design is the possible danger of incurring excessive damage in the hinterland upon the attack of the design storm. People may become overconfident because the zero wave overtopping occurs under normal conditions, and utilize the land directly behind the seawall without providing a drainage system capable of dealing with possible overtopping water. However, the magnitudes of natural phenomena such as storm surge and storm waves are most difficult to assess as they occur very infrequently. There always remains some probability that an abnormal storm may hit the design site with a magnitude in excess of the design level. Therefore, the concept that a seawall can completely stop the overtopping of storm waves at any time may lead to a coastal disaster in the event of the attack of an extraordinary storm.

The problem with applying the principle of overtopping-based seawall design is how to determine the tolerance limit of wave overtopping amount. Nevertheless, at least in this method the designer is aware of the existence of an overtopped water mass behind the seawall and is prepared to deal with it. Thus, the extent of damage even in the event of an extraordinary storm will be much less than in the case of the runup-based seawall design. Until the early 1970s, the estimation method for the overtopping rate of random sea waves had not been acknowledged by design engineers in general, in part due

to insufficient design data. Thus, the number of overtopping-based seawall designs seems to have remained low in comparison to runup-based seawalls designs. However, it is expected that the principle of overtopping-based design will become popular in the determination of crest elevations of seawalls, by making use of hydraulic model tests with irregular waves.

5.2.2 *Tolerable Rate of Wave Overtopping*

The amount of wave overtopping tolerable with regard to the structural integrity of a seawall is greater than the tolerable amount for the protection of the land behind the seawall. Even a seawall constructed with utmost care cannot escape the danger of structural failure if it is exposed to heavy wave overtopping for many hours. The mode of failure may be loss of earth-fill from the core of the seawall by leakage, cracks and breakage of the armoring surfaces of the crown and back slope, or total collapse. The structurally tolerable limit of wave overtopping depends on the type of seawall structure.

The author analyzed about 30 cases of coastal dikes and revetments damaged in the aftermath of typhoons, estimating the wave overtopping rate for each seawall.[1,2] This yielded an estimate of the maximum tolerable limit of wave overtopping rate as listed in Table 5.2.

From the viewpoint of structural safety, the limits given in Table 5.2 are applicable to seawalls built along embayments and exposed to storm waves

Table 5.2. Tolerable limit of wave overtopping rate from the viewpoint of structural safety.

Type	Surface armoring	Overtopping rate $(m^3/m \cdot s)$
Coastal dyke	Concrete on front slope, with soil on crown and back slope	less than 0.005
	Concrete on front slope and crown, with soil on back slope	0.02
	Concrete on front slope, crown and back slope	0.05
Revetment	No pavement on ground	0.05
	Pavement on ground	0.2

a few meters high which continue for a few hours only, since most of the sea-walls examined belong to this category. It is believed that the tolerable limit should be lowered for seawalls facing the ocean and exposed to the attack of large waves, or for seawalls subject to many hours of storm wave action. For example, the First District Port Construction Bureau of the Ministry of Trans-port, Japan, reported that a coastal dike of the sloping type with concrete surfacing at the front slope, crown, and back slope at Himekawa Port col-lapsed at the estimated overtopping rate of $q_{\text{EXP}} = 0.015$ m^3/m·s. The dike was struck by storm waves of $H_0' = 6$ m generated in the Sea of Japan by a slowly moving extratropical cyclone.[7] The Bureau also reported another ex-ample of a coastal dike on the Niigata Coast which lost part of its sand fill due to wave suction, and some of the paving concrete blocks at the crown slumped. The wave overtopping was estimated as having the rate of only $q_{\text{EXP}} = 0.002$ m^3/m·s.

The amount of damage to a coastal dike of the earth-filled sloping type by wave overtopping is largely dependent on the size of gaps existing between the earth fill and the armor surfaces of the sloping face and crown. The setting of tolerance limits according to structural type may be too crude without consideration of the particular construction conditions, but it is hoped that Table 5.2 will serve as a guideline for design engineers. The user is encouraged to consider some lowering of the values, taking into account the magnitude of the wave height and the duration of the storm waves.

Another tolerance limit of the wave overtopping rate must be set from the standpoint of utilization of the land behind a seawall. For the protec-tion of a relatively densely populated coastal area, the overtopping rate of $q = 0.01$ m^3/m·s is currently adopted as a guideline in port areas in Japan. This guideline evolved from the previous coastal protection policy based on run-up height. If the safe passage of vehicles is to be secured at all times along a coastal highway protected by a continuous seawall, the tolerable limit seems to be on the order of 10^{-4} m^3/m·s or less.[7,8] The reliable measurement of such a small wave overtopping rate is rather difficult in laboratory tests due to limitations in the accuracy of the measurement as well as due to the inherent variability of the wave overtopping phenomenon. If a seawall is designed to have such a small overtopping amount, the crest elevation should be raised higher than the value inferred from hydraulic model tests, and a larger section of concrete block mound should be used, if it is not a vertical revetment.

In any case, the acceptable limit for the wave overtopping rate needs to be set by consideration of not only technical aspects but also many other factors. It is regarded as a constraint attached to the design of seawalls.

5.2.3 *Determination of Crest Elevation of a Seawall*

Examples will be given of the decision process for the crest elevation as determined by the criterion of tolerable overtopping rate. By arbitrarily setting the tolerable limit at $q = 0.01$ m^3/m·s, the required crest elevation for a vertical revetment is estimated from Figs. 5.1 and 5.2, as shown in Fig. 5.6 for wind waves with steepness of $H_0'/L_0 \simeq 0.036$. The crest elevation of a block mound seawall is shown in Fig. 5.7. The crest elevation is displayed as a ratio formed with the equivalent deepwater wave height. The solid lines are for a sea bottom slope of 1/30 and the dash lines for a slope of 1/10. It will be observed in these figures that the relative crest elevation must be increased for larger waves in order to maintain the overtopping rate below a fixed value. Furthermore, it is seen that the required crest elevation for wind waves is highest in an area where the effective water depth is 1.5 to 2.5 times the equivalent deepwater wave height and that the effect of bottom slope is greatest in an area of shallow water. Similar diagrams for the required crest elevation for different values of the tolerable wave overtopping rate or for incident waves of lesser steepness such as swell can be prepared from Figs. 5.1, 5.2, 5.4 and 5.5.
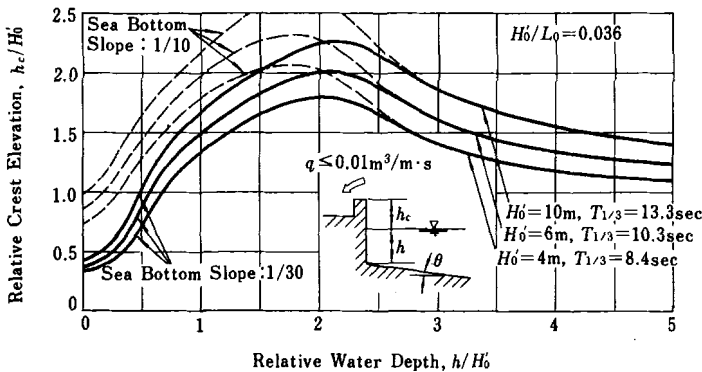
Fig. 5.6. Crest elevation of vertical revetment for the condition of overtopping rate not greater that 0.01 m^3/m·s.[3]

Fig. 5.7. Crest elevation of block mound seawall for the condition of overtopping rate not greater than 0.01 m³/m·s.[3]

By comparing the curves in Figs. 5.6 and 5.7, it can be concluded that the required crest elevation of a seawall protected by a concrete block mound of the energy-dissipating type is about 60 to 70% of that of a vertical revetment for wind waves. Similar comparisons have been made for other wave steepnesses, and the results are shown in Figs. 5.8 and 5.9. Although the tolerable overtopping rate (dimensionless) varies in the range of $q/\sqrt{2g(H_0')^3} = 5 \times 10^{-5} \sim 2 \times 10^{-3}$, no appreciable difference is observed in the ratio of the required crest elevation of a block mound seawall to that of a vertical revetment. It should be noted in Fig. 5.8 that the placement of a concrete energy-dissipating block mound in front of a vertical revetment causes a rise in the required crest elevation when the seawall is designed against swell of low steepness incident to a coast with a bottom slope of 1/10. This may be understood as follows: the effect of the rough, porous surface of the block mound in reducing wave run-up height has been superseded by the effect of the slope in enhancing wave run-up in this particular situation, especially because the block mound is small compared to the wavelength of the incident waves. As previously discussed, the amount of wave overtopping is quite sensitive to the geometry and material making up the seawall, and the above result cannot be considered as general. But it will be necessary to check the design section of a seawall through the aid of hydraulic model tests with irregular waves, when the seawall is to be located at a water depth of about 0.4 times the equivalent deepwater wave height on a coast of steep slope.

The effect of the crown width of a block mound seawall upon the overtopping rate has been tested with irregular model waves for a few cases.
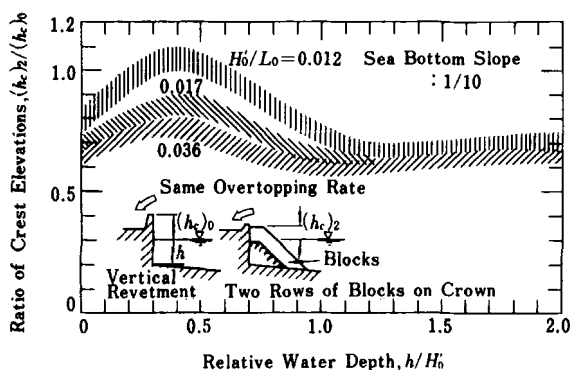
Fig. 5.8. Ratio of crest elevations of block mounds to vertical revetments for the same over-topping rate (sea bottom slope of 1/10).[3]
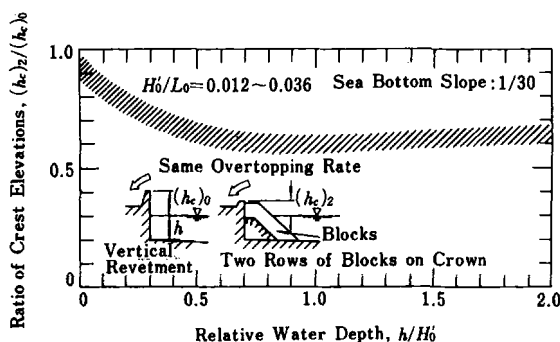
Fig. 5.9. Ratio of crest elevations of block mounds to vertical revetments for the same over-topping rate (sea bottom slope of 1/30).[3]

Figure 5.10 illustrates the results of such tests, conducted at a relative water depth of $h/H_0' = 0.98$ on a slope of 1/30, and at $h/H_0' = 0.37$ and 1.00 on a slope of 1/10. The crown width of a block mound seawall was varied by using one to four rows of blocks in the lower layer of a two-layer arrangement. The upper figure shows the ratio of required elevations of the block mound to the vertical revetment. The lower figure shows the ratio of the required crest elevations of the block mound seawall to that of a seawall having two rows of concrete blocks in the lower layer. The range of wave overtopping rate (dimensionless) considered is $q/\sqrt{2g(H_0')^3} = 2 \times 10^{-4} \sim 2 \times 10^{-3}$. As seen in Fig. 5.10, the required crest elevation decreases with widening of the crown of the block mound.
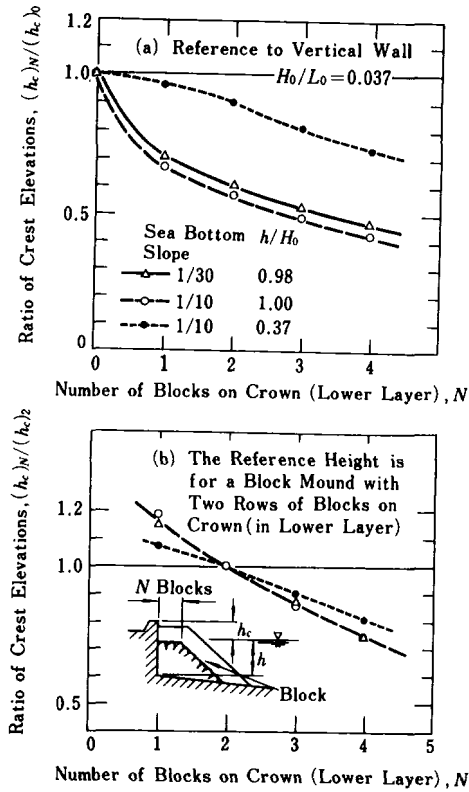
Fig. 5.10. Effect of crown width of block mound on design crest elevation.[9]
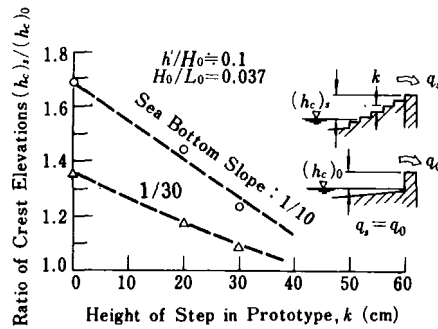
Fig. 5.11. Ratio of crest elevations of sloped seawall to vertical revetment.[9]

Figure 5.11 compares seawalls having a front slope of 1 : 2 with vertical revetments.[9] The model seawalls were set near the shoreline and the wave overtopping rate was measured for several crest elevations. From the resultant data on the overtopping rate, the design crest elevations of both types of seawall for a given tolerable overtopping rate were estimated and compared. Although Saville[10] has reported no effect of the front slope of a seawall upon the run-up height when the seawall is located at the shoreline or on land, the effect of the front slope appears in the amount of overtopping of seawalls which have crests lower than the maximum run-up height. As seen in Fig. 5.11, a sloped seawall requires a higher crest elevation than a vertical revetment for a given tolerable overtopping rate. The replacement of a smooth slope with a stepped one can reduce the required crest elevation to the extent that the crest elevation will be only 10 to 20% greater than that of a vertical revetment, if the height of each step is about 30 cm for an incident significant wave height of about 5 m.

In the practical design of a seawall, the crest elevation as calculated from the above considerations of wave run-up and overtopping is usually given a small amount of additional rise to allow for unknown factors. If some ground settlement or subsidence is expected owing to the foundation characteristics, the estimated amount of settlement must be taken into account in the determination of the final crest elevation.

5.3 Additional Design Problems Related to Seawalls

Structural details of seawall designs may be found elsewhere, e.g., Ref. 11. In Japan, the technical standards for design and construction of coastal protection facilities were offically established in 1958 and have undergone subsequent revisions. From the perspective of vulnerability to wave attack, precautions should be taken against scouring of the seabed in front of a seawall and leakage of filling material in the core of a sloped wall or in the rear of a vertical revetment. Unfortunately, both factors are difficult to control, especially on a sandy coast. Nevertheless, frequent inspections and repairs should be made if necessary, so as to maintain the structural strength of a seawall at a good level after construction. The design of the seawall itself should provide maximum possible protection against both scouring and leakage.

When a vertical seawall is constructed of concrete caissons or L-shaped concrete blocks, gaps between the caissons or L-shaped blocks create a zone of strong oscillatory water flow. The filler material in the rear of the revetment may be washed away by the water flow through such gaps. Plastic sheets and plates are sometimes applied to the rear of the caissons or L-shaped blocks in order to shield the gap, but they easily tear off or become dislocated by strong wave action in coastal areas subject to high waves, before they perform their intended function. In such cases, two or three layers of rubble and gravel filters with varying grain diameters should be provided just behind the revetment, so that the strength of the oscillatory flow is weakened gradually and no appreciable washing of filler material takes place.

In the design of seawalls, the drainage system for the overtopped water should be well planned, because the overtopping amount by storm waves is quite large. In the preceding section, the tolerable rate of wave overtopping was arbitarily set at $q = 0.01$ m^3/m·s for an example of the determination of the crest elevation. This amount is equivalent to a discharge of 10 m^3/s or 36,000 m^3 for every 1000 m of seawall extension. The best way to handle such a large volume of overtopped water is to provide an outlet of sufficient width and strong paving to withstand the impact of the falling water mass immediately behind the seawall; the overtopped water should then be allowed to flow down the channel to the sea at appropriate outlets. The channel width may be a few tens of meters if the overtopping rate is on the order of 0.01 m^3/m·s. If the ground elevation behind the seawall is lower than the storm tide level or if the hinter area is too extensively utilized to allow provision of a wide outlet, then the rate of wave overtopping should be reduced to the order of 10^{-3} m^3/m·s or less.

Another problem connected with the handling of overtopped water is the time variation of the amount of wave overtopping. The data on the overtopping rate presented in Figs. 5.1, 5.2, 5.4 and 5.5 pertain to an average over several hundred waves; i.e., an average over a duration of 30 minutes to one hour. In a shorter time interval, a much larger amount of wave overtopping than estimated by Figs. 5.1, 5.2, 5.4 and 5.5 might occur, because irregular trains of sea waves contain many short groups of high waves appearing in succession. Although it is possible to calculate the probability of the appearance of high wave groups (refer to Sec. 9.2) and the fluctuation in the short-term average of overtopping amount,[12] the selection of the averaging time and the level of probability to be taken are left to the judgment of the design engineer.

References

1. S. Tsuruta and Y. Goda, "Expected discharge of irregular wave overtopping," *Proc. 11th Int. Conf. Coastal Engrg.* (London, 1968), pp. 833–852.
2. Y. Goda, "Estimation of the rate of irregular wave overtopping of seawalls," *Rept. Port and Harbour Res. Inst.* **9** (4) (1970), pp. 3–41 (*in Japanese*).
3. Y. Goda, Y. Kishira, and Y. Kamiyama, "Laboratory investigation on the overtopping rate of seawalls by irregular waves," *Rept. Port and Harbour Res. Inst.* **14** (4) (1975), pp. 3-44 (*in Japanese*).
4. A. Takada, "Wind effect on regular wave overtopping," *Proc. 23rd Japanese Conf. Coastal Engrg.* (1976), pp. 170–175 (*in Japanese*).
5. J. P. Ahrens, "Irregular wave run-up on smooth slopes," *U.S. Army, Corps of Engrg. Coastal Engrg. Res. Center, Coastal Engrg. Tech. Aid.* (81–17) (1981), 26p.
6. Y. Tominaga, H. Hashimoto, and T. Nakamura, "On the disaster at Yoshihara Coast caused by Typhoon No. 6626," *Proc. 14th Japanese Conf. Coastal Engrg.* (1967), pp. 206–213 (*in Japanese*).
7. N. Fukuda, T. Uno, and I. Irie, "Field measurements of wave overtopping of seawalls (2nd Report)," *Proc. 20th Japanese Conf. Coastal Engrg.* (1973), pp. 113–118 (*in Japanese*).
8. T. Hamada, H. Mitsuyasu, Y. Goda, and H. Hashimoto, "Discussions of various problems on waves and maritime structures," *Jour. Japan Soc. Civil Engrg.* **58** (4) (1973), pp. 57–64 (*in Japanese*).
9. Y. Goda and Y. Kishira, "Experiments on irregular wave overtopping characteristics of seawalls of low crest types," *Tech. Note of Port and Harbour Res. Inst.* (242) (1976), 28p. (*in Japanese*).
10. T. Saville, Jr., "Wave run-up on shore structures," *Proc. ASCE* **82** (WW2), Paper No. 925 (1956), 14p.
11. U.S. Army Coastal Engineering Research Center, *Shore Protection Manual* (1977), pp. 6–1 ∼ 6–15.
12. A. Kimura, A. Seyama, and T. Yamada, "Statistical properties of the short-term overtopping discharge," *Proc. 28th Japanese Conf. Coastal Engrg.* (1981), pp. 335–338 (*in Japanese*).

Chapter 6

Harbor Tranquility

6.1 Parameters Governing Harbor Tranquility

The fundamental functions of a harbor are to provide safe anchorage for vessels and to facilitate smooth and unhindered transfer of passengers and cargo between vessels and land. Guaranteed harbor tranquility is not only essential for safe anchorage, but it is also important for efficient port operation. The problem of harbor tranquility essentially reduces to the questions of the motions of ships moored at anchorage or along a wharf and of the mooring forces. Many hydraulic laboratories in Europe have been testing harbor tranquility by measuring the motions of model ships moored at strategic places in a harbor and thus judging the goodness of harbor planning by the degree of ship motions, e.g., Ref. 1.

Generally speaking, however, most hydraulic model tests of harbor tranquility are still made by measuring the distribution of wave height in a given harbor layout and comparing various harbor layouts by means of either the absolute magnitude of wave height or its ratio to the incident wave height. But it should be kept in mind that the effect of wave action on ships is different for wind waves with a period of 5 s and for swell with a period of 15 s, even if the wave height is the same. Also, a large ship may not feel wave agitation whereas a small boat may be violently swung by the same waves. Thus, harbor tranquility needs to be judged from the viewpoint of ship motions. The motions of ships, especially of ships moored in water of finite depth, is a very complex hydrodynamic problem. The layout of the mooring lines, their elastic characteristics, and the response of fenders further complicate the problem. Although much progress has been made quite recently in the numerical analysis of the

problem, it will still require some time before engineers can have detailed information on the characteristic of ship motions. From the viewpoint of port operation, the relationship between ship motion and cargo handling works also enters into the judgment of harbor tranquility. For example, loading and unloading by means of mast cranes of a ship will not be hindered much by movements of a ship by a meter or so. But the handling of containers stacked inside the deep hull of a container ship will have to be halted if the ship moves to and fro more than half a meter. Wind is an additional factor affecting the safety of ships and the efficiency of cargo handling in a harbor, and thus the wind also enters into the problem of harbor tranquility.

In addition to physical factors, there are several other factors connected with the evaluation of harbor tranquility, such as the ease of ship navigation at the harbor entrance, the question of whether ship will remain within the harbor during severe storm conditions, and the limiting conditions of maritime operations. Also important are economic factors, such as the efficiency of cargo handling works, the cost of demurrage during the suspension of ship operation, and the cost of breakwaters and other protective facilities. Figure 6.1 is an example of a flow chart which illustrates the complicated and diverse factors connected with the problem of harbor tranquility and the way to deal with them. The solution should begin with an understanding of the offshore waves and storm winds, and then proceed to the estimation of the waves and winds in the harbor by taking into account the sheltering effects of the breakwaters and other protective facilities. The data on the waves and winds in a harbor should be combined with the motions of the ships and cargo handling equipment to yield the limit for workable conditions in the harbor. Then the questions of ship navigation at the entrance and ship refuge at the times of heavy storms must be taken into account in the judgment of safety. Finally, the tranquility of a harbor under planning should be judged with due consideration to various economic factors. Planning and design of harbor facilities should proceed by such steps to guarantee the desired degree of harbor tranquility.

The above or a similar procedure for the analysis of harbor tranquility is rather difficult to carry out if all the factors are to be evaluated quantitatively (because of the lack of various necessary data). Nevertheless, efforts are being directed at clarifying the roles of these factors, and it is hoped that a systematic and comprehensive procedure such as shown in Fig. 6.1 will be followed in the near future. For the time being, a practical approach to the problem of harbor tranquility may still be the evaluation of the wave height in the harbor under

```
┌─────────────────────────────────────┐
│ 1. Data of Wind and Waves outside    │
│    Harbor                            │
├─────────────────────────────────────┤
│ a. Statistics of wave climate        │
│ b. Spectral wave characteristics     │
│ c. Statistics of long-period waves   │
│ d. Statistics of wind                │
└─────────────────────────────────────┘
```

```
┌─────────────────────────────────────┐
│ 2. Change of Wind and Waves by Har-  │
│    bor Facilities                    │
├─────────────────────────────────────┤
│ a. Layout and crest elevation of break-│
│    waters                            │
│ b. Effect of wave absorbing structures│
│ c. Effect of wind screens            │
└─────────────────────────────────────┘
```

```
┌─────────────────────────────────────┐
│ 3. Estimating the Wind and Wave Con- │
│    ditions inside the Harbor         │
├─────────────────────────────────────┤
│ a. Establishment of the method to esti-│
│    mate wave conditions in the harbor│
│    (diffraction, reflection & transmis-│
│    sion)                             │
│ b. Estimation of wave statistics in the│
│    harbor                            │
│ c. Observation of waves within the   │
│    harbor for data for the tranquility│
│    analysis                          │
│ d. Comparison of estimated and actual│
│    wave statistics in the harbor     │
└─────────────────────────────────────┘
```

```
┌─────────────────────────────────────┐
│ 7. Planning and Construction of Harbor│
│    Facilities to Improve Harbor Tran-│
│    quility                           │
├─────────────────────────────────────┤
│ a. Breakwaters                       │
│ b. Wave absorbing structures         │
│ c. Wind screens                      │
│ d. others                            │
└─────────────────────────────────────┘
```

```
┌─────────────────────────────────────┐
│ 5. Estimating the Workable Limits of │
│    Pilotage and Cargo Handling Opera-│
│    tions                             │
├─────────────────────────────────────┤
│ a. Field study of working conditions │
│ b. Survey of workable limits         │
└─────────────────────────────────────┘
```

```
┌─────────────────────────────────────┐
│ 4. Clarification of the Motions of Ships│
│    and Cargo Handling Equipment      │
├─────────────────────────────────────┤
│ a. Establishment of numerical model for│
│    ship motions in harbors and its verifi-│
│    cation                            │
│ b. Field observation of ship motions │
│ c. Analysis of wind effect on cargo  │
│    handling equipment                │
└─────────────────────────────────────┘
```

```
┌─────────────────────────────────────┐
│ 6. Evaluation of Harbor Tranquility  │
│    from Viewpoints of Safety and Eco-│
│    nomical Feasibility               │
├─────────────────────────────────────┤
│ a. Ship navigation at entrance       │
│ b. Ship refuge in storm              │
│ c. Efficiency of cargo handling and ship│
│    demurrage                         │
│ d. Construction cost of harbor facilities│
│ e. Cost-benefit analysis             │
└─────────────────────────────────────┘
```

Fig. 6.1. Elements of harbor tranquility and a flow chart for tranquility analysis.

planning, especially because engineering practice prefers continuity of design method based on conventional techniques of hydraulic model tests, as well as on numerical analysis of harbor tranquility. But the description of the wave height in a harbor either as an absolute value or as its ratio to the offshore height under certain storm conditions alone represents only one part of the complex problem of harbor tranquility. It is necessary to reanalyze the wave height data in the form of the days of exceedance of the significant wave height above certain levels during a year at several strategic points in the harbor. By doing so, the safety and economic feasibility of a planned harbor can be evaluated somewhat quantitatively.

6.2 Estimation of the Probability of Wave Height Exceedance Within a Harbor

6.2.1 *Estimation Procedure*

When harbor tranquility is to be evaluated by means of the number of days of a certain wave height exceedance, the following calculation steps are recommended:

(i) Preparation of the joint distribution of significant wave height, period and direction outside the harbor.

(ii) Selection of strategic points within the harbor at which the wave height is to be estimated.

(iii) Estimation of the ratio of wave height inside to outside the harbor.

(iv) Calculation of the absolute height of waves in the harbor at various levels of the offshore wave height.

(v) Calculation of the probability of exceedance of the wave height at selected points in the harbor.

The procedure may be compiled in a flow chart as shown in Fig. 6.2. The flow chart combines various sources of information and synthesizes them for the estimation of the exceedance probability of the wave height. The procedure shown here assumes that the effect of wave period is negligible for the sake of simplifying the calculation. But it has become apparent that ship motion is strongly dependent on the wave period. Thus, it is recommended that in practice the analysis of the exceedance of the probability of wave height be carried out separately for a few classes of wave period.

Joint Distribution of
Wave Height and Direc-
tion outside Harbor

Plans of the Layout of
Harbor Facilities

Cross-Section of Break-
water

Joint Distribution of
Wave Height and Period
in All Directions

Observation and Hind-
casting of Locally-Gen-
erated Waves within
Harbor

Selection of locations
for wave height analysis

Exceedance probability
of local wave height for
several directions

· Hydraulic tests
· Numerical analysis
· Graphical solution

Empirical formula
or diagram

Data for Estimation of Wave
Direction
· Directional distribution of
  strong wind
· Prevailing direction of swell
· Visual wave observation
· Other

Estimation of diffract-
ed and reflected wave
height ratio

Estimation of propaga-
tion of transmitted
waves

Estimation of wave trans-
mission coefficient over
breakwater

Correlation of local
wave height with in-
cident wave height

Absolute height of dif-
fracted and reflected
waves for several classes
of incident wave height

Absolute height of trans-
mitted waves for several
classes of incident wave
height

Exceedance probability of wave
height outside harbor for in-
dividual wave directions

Estimation of absolute height of
waves within harbor for several
classes of incident wave height

Exceedance probability of wave
height inside harbor for individ-
ual wave directions

Exceedance Probability of Wave
Height inside Harbor in All
Directions

Fig. 6.2. Flow chart for the exceedance probability of wave height within a harbor.

Random Seas and Design in Maritime Structures

6.2.2 *Joint Distribution of Significant Wave Height, Period and Direction Outside a Harbor*

The statistics of the wave climate outside a harbor under planning, obtained either by instrumental wave measurements (backed up by visual observations) or by wave hindcasting, are best analyzed in the form of exceedance probabilities of significant wave height for several directions of wave approach, and separately for a few classes of wave period. In the following, however, an explanation is given for an example without separation by wave period for simplicity.

The probability of exceedance is to be expressed as a percentage over the total number of wave data points inclusive of calm days. It is a standard technique to analyze wave climate statistics on the basis of wave data covering a period of more than five years, but it might be necessary to be content with the data for only three years if a reliable record of sufficient length is not available, or if a wave hindcasting project must be undertaken for a site where no field measurement data exist. Wave hindcasting for climatic information should yield an estimate of wind waves and swell several times a day for the duration of the given period. It is advisable to select, not a continuous three-year period, but a total period of three years comprising a year of rough seas, a year of normal seas and a year of moderate seas. This can be accomplished by referring to meteorological information and any wave statistics available at neighboring harbors.

The wave direction is usually described by using a system of 16-point bearings. This system should also be employed in the analysis of the wave height exceedance probability. If the available wave data are scant, a compromise by using an 8-point bearing system may become necessary. Although many stations are now measuring the wave height and period with automatic recording instruments, only a limited number of stations are making an effort to simultaneously measure the wave direction. Therefore, it is quite a fortunate circumstance if the required statistics of wave height and direction can be obtained from the records of field measurements. In many instances, the wave direction must be estimated subjectively by the person in charge of the analysis, by referring to the frequency diagrams of strong wind direction, the characteristics of the swell persisting at the site, the available data of visual observations of the wave direction, etc.

Table 6.1 is an example of the directionwise exceedance probability of significant wave height at Akita Port, based on the instrumental wave records

Table 6.1. Example of exceedance probability of wave height in different directions.
-Akita Port (1974)-

Wave	Percentage	Significant wave height $H_{1/3}$						
direction	(%)	Over 0 m	Over 1 m	Over 2 m	Over 3 m	Over 4 m	Over 5 m	Over 6 m
SW	1.4	1.4	0.4	0.1	0	0	0	0
WSW	29.0	29.0	9.2	2.5	1.2	0.5	0.3	0.1
W	68.2	68.2	21.6	6.2	2.8	1.2	0.7	0.2
WNW	1.4	1.4	0.4	0.1	0	0	0	0
Total	100.0	100.0	31.6	8.9	4.0	1.7	1.0	0.3
Prevailing period $T_{1/3}$		7.0 s			9.0 s		11.0 s	

from January through December, 1974. It was prepared by the First District Port Construction Bureau of the Ministry of Transport, Japan. The daily wave direction was analyzed off the screen of a special imaging radar. Although the wave observation itself has continued for many years, the exceedance probability was analyzed for only one year for the purpose of comparing the result of the estimation of the wave height within the harbor to the observed wave height inside the harbor for the same period.

The example shown here employs the class interval of 1 m for the wave height. A narrower class interval of 0.5 m or less would be more suitable for a coast with a mild wave climate, such as a site located within a bay or in another relatively confined body of water. The present example will not involve making a periodwise analysis, as discussed earlier. Even without the distinction of wave period, it is necessary to determine the predominant wave period with respect to wave direction, or to the respective class of wave height, by referring to the joint distribution of significant wave height, period and direction. The predominant wave period associated with certain directions or heights should be employed in the estimation of the wave height ratio in a harbor.

In a harbor of large dimensions, wind waves generated within the harbor may become a source of disturbance for small craft, such as coastal vessels and lighters.[a] In this situation, a statistical analysis of the local wind waves must

---

[a]In a harbor, accommodating large ocean-going vessels along piers and wharves, local wind waves do not in any way hinder a ship's mooring and cargo handling operations, because the sizes of such vessels are very large compared to the wavelength.

be performed mainly on the basis of hindcast data inferred from the annual wind statistical data. If possible, the data of the local wind waves should be related to information of the offshore waves so that a certain class of offshore wave heights is associated with a certain height of the local wind waves.

6.2.3 *Selection of the Points for the Wave Height Estimation*

The estimation of wave height within a harbor is made at a limited number of points taken to be representative of the situation for port operation. When harbor tranquility is investigated through hydraulic scale models, the harbor is divided into areas; in each area several points are selected for measurement of the wave height. The exceedance probability of the wave height in a harbor is usually calculated with the wave height ratio averaged over individual areas. When the ratio of wave height inside to outside the harbor is estimated by numerical computations, to be described below, the wave height ratio is obtained at a number of points. In such cases, too, an area average of the wave height ratio facilitates the overall analysis of harbor tranquility. If the graphical solution method to be described in Sec. 6.3 is used, the number of estimation points is best limited to a dozen or so in consideration of the amount of manual labor involved and the inherent low level of accuracy of the graphical solution itself. The points to be used for the wave height analysis should not be in the proximity of quaywalls and recessed corners of structures, where interference by reflected waves is intense; they should be at the centers of channels, basins and other such locations.

6.2.4 *Estimation of Wave Height in a Harbor Incident Through an Entrance*

The major portion of the waves in a harbor are those incident through the harbor entrance. Their height is estimated through hydraulic model tests, numerical computations and/or graphical solution methods. The discussion on hydraulic model tests will be made in Sec. 7.3. As for numerical computations, several techniques have been proposed, based on different principles. For example, Barailler and Gaillard[2] solved the problem by means of Green functions, Tanimoto *et al.*[3] calculated the propagation of individual waves by solving the wave equation, and Abbott *et al.*[4] used the Bernoulli equation for an efficient solution of wave propagation. All these methods require the harbor

area to be represented on a grid with a mesh spacing of an eighth of the wavelength or so, thus limiting their applicability to a harbor of several wavelengths or less in size. On the other hand, Takayama[5] has extended the solution of wave diffraction, so as to include the effects of wave reflection from various boundaries within a harbor as well as the effects of secondary diffraction by auxiliary breakwaters and groins. It may be classified as a computer implementation of the graphical solution method to be described in Sec. 6.3. Although at present the technique of Takayama is limited to water of constant depth, there are no limitations concerning the size of the harbor, and in addition it has the capability of dealing with random sea waves specified with directional spectra. Further progress is expected in refining and upgrading the techniques of numerical computations of the wave height distribution within a harbor.

The wave height in a harbor is in essence estimated as a ratio formed with the height of the incident waves at the entrance or in the offshore. The estimation must be done with due consideration of the random nature of sea waves, especially of the directional spreading of wave energy. With installation of multidirectional wave generators in many hydraulic laboratories in the 1990s, it has become possible to carry out harbor model tests using directional random waves. If model tests are made with unidirectional irregular waves owing to the unavailability of multidirectional wave generators, the tests must be done for several wave directions so as to take into account the effect of directional spreading of wave energy. The test results are synthesized by the following formula:

$$K_{\text{eff}} = \left[\frac{\sum K_j^2 D_j}{\sum D_j} \right]^{1/2} , \qquad (6.1)$$

where K_j denotes the ratio of wave height at a point or of an area within the harbor to the incident height for the jth direction of wave approach, D_j represents the relative wave energy in the respective directions listed in Table 3.2 in Sec. 3.1, and K_{eff} is the effective wave height ratio accounting for the directional wave characteristics. The operation expressed by Eq. (6.1) is simply to take a weighted mean of the wave energy for several directional components, on the basis of unidirectionally estimated ratios of wave height.

When hydraulic model tests are carried out with regular waves or when numerical solutions are only capable of providing an answer for regular waves, the resultant wave height ratio must be modified so as to yield the response of the harbor to random directional incident waves. Wave height ratios are to be

obtained for several representative values of the wave period and direction, just as in the case of the estimation of random wave refraction discussed in Sec. 3.1. The results of hydraulic tests or numerical computations for a constant train of regular waves cannot be said to truly represent the conditions of wave agitation in a harbor even if the period and direction of test waves exactly correspond to those of significant waves in the prototype. The situation is the same as the application of diffraction diagrams for regular and random waves to prototype breakwaters, which was discussed in conjunction with Figs. 3.10 and 3.16 in Sec. 3.2.

When the graphical solution of the wave height ratio is obtained with the aid of diffraction diagrams for random sea waves, no correction is necessary.

In the example of Akita Port, for which the wave statistics are listed in Table 6.1, the wave measurements[b] continued for one year at a location 800 m inward from the tip of the south breakwater (with its axis approximately in the direction of NW) and with an offset of 620 m to the breakwater. The ratio of the wave height at that location to the incident wave height was obtained in calculation of the diffraction of random sea waves by a semi-infinite breakwater. The results are listed in Table 6.2. In this example, the differences in diffraction coefficients between the three wave periods are rather small, indicating relatively little effect of the incident wave period in this case.

Table 6.2. Diffraction coefficient of random sea waves at the location under study.

Wave direction	Diffraction coefficient		
	$T = 7$ s	$T = 9$ s	$T = 11$ s
SW	0.101	0.116	0.130
WSW	0.277	0.290	0.303
W	0.508	0.587	0.595
WNW	0.849	0.852	0.855

6.2.5 *Estimation of Waves Transmitted over a Breakwater*

If some wave energy is transmitted to the interior of a harbor by wave overtopping or passing through breakwaters, the wave transmission coefficient is to be estimated by means of Fig. 3.48 in Sec. 3.8, or by other laboratory data.

---

[b]A portion of these results was presented in Fig. 3.16 as the verification data for the random wave diffraction diagrams.

Table 6.3. Estimated height of transmitted waves.

Incident height H_I (m)	1.0	2.0	3.0	4.0	5.0	6.0
Transmitted height H_T (m)	0.03	0.06	0.09	0.24	0.45	0.81

Then the absolute height of the transmitted waves is calculated for several classes of the incident wave height. In the example of Akita Port, the south breakwater had values of the pertinent parameters of $h_c = 5.0$ m, $d = 8.5$ m and $h = 12.0$ m. Thus, the transmitted wave height in terms of the incident height was estimated as listed in Table 6.3.

As discussed in Sec. 3.8.2, little is known about the pattern of propagation of waves transmitted over a breakwater. Nevertheless, some estimate of wave propagation may be necessary in the analysis of harbor tranquility. Therefore, unless a hydraulic model test is done with a scale large enough to be capable of simulating wave transmission by overtopping (which is not the case in most harbor tranquility tests), a practical method is to treat the extent of the length of overtopped breakwater as an imaginary opening in a breakwater and to estimate the propagation of transmitted waves as waves diffracted from the opening. A further simplification which may be used, depending on the harbor layout, is the assumption of nondispersive propagation of transmitted waves to the points of interest for a certain range of wave direction and no propagation from outside that range, that is, to assume a coefficient of propagation of unity for the former and zero for the latter.

6.2.6 *Estimation of the Exceedance Probability of Wave Height Within a Harbor*

The first step is to calculate the absolute height of waves at respective locations within a harbor for various classes of incident wave height, separately for several directions. The absolute height of the waves incident through the entrance is calculated with the wave height ratio data obtained as discussed in Sec. 6.2.4, and the absolute height is combined with the information on transmitted wave height over the breakwater. The combined height of waves is estimated as the square root of the sum of the squares of both heights on the basis of the addition of wave energy as expressed by Eq. (3.28) in Sec. 3.6.3. The calculation for the data of Akita Port is listed in Table 6.4. In a case where the locally generated wind waves within the harbor may present some hindrance to port operation,

their contribution must be added in the above calculation at the respective class of incident height using the same principle.

Table 6.4. Superposition of diffracted and transmitted wave height.

Wave direction		H_I (m)					
		1.0	2.0	3.0	4.0	5.0	6.0
SW	H_d	0.10	0.20	0.35	0.46	0.65	0.78
	H_T	0.03	0.06	0.09	0.24	0.45	0.81
	H_S	0.10	0.21	0.36	0.52	0.80	1.12
WSW	H_d	0.28	0.55	0.87	1.16	1.52	1.82
	H_T	0.03	0.06	0.09	0.24	0.45	0.81
	H_S	0.28	0.55	0.87	1.18	1.59	1.99
W	H_d	0.51	1.02	1.76	2.35	2.98	3.57
	H_T	0.03	0.06	0.09	0.24	0.45	0.81
	H_S	0.51	1.02	1.76	2.36	3.01	3.66
WNW	H_d	0.85	1.70	2.56	3.41	4.28	5.13
	H_T	0	0	0	0	0	0
	H_S	0.85	1.70	2.56	3.41	4.28	5.13

Note: Transmitted waves were assumed to arrive at the site without dissipation for the direction of SW to W, but not to arrive for the direction of WNW.
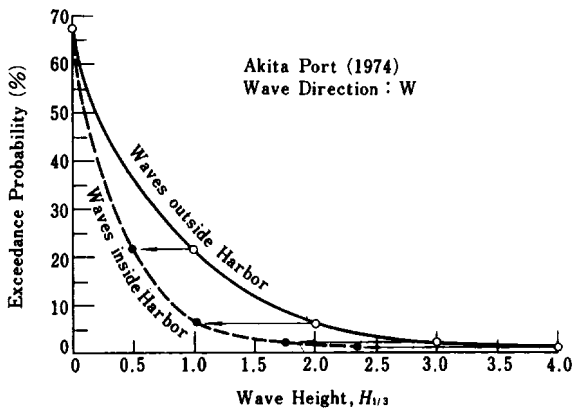
Fig. 6.3. Preparation of exceedance probability curve of wave height inside a harbor.

From the results of the estimated wave height within the harbor for the relevant wave directions, the exceedance probability curves of wave height within the harbor are drawn by combining the exceedance probability of the offshore wave height. This can be done as shown in Fig. 6.3. First, the exceedance curve for the offshore waves is drawn for one wave direction, then the abscissas of the respective wave height classes are shifted toward the left according to the values of the wave height such as listed in Table 6.4, and finally the ordinates at shifted locations are connected with a smooth curve.

The probability of exceedance at predetermined values of the wave height such as 0.25 m, 0.5 m and 1.0 m is then read from the exceedance curves obtained for each wave direction. The probabilities in percentages are listed in a form such as shown in Table 6.5. By repeating this procedure for every wave direction and then taking the sum of probabilities of exceedance at each class of wave height, the overall exceedance probability of wave height within the harbor can be obtained as listed in the bottom row of Table 6.5. Figure 6.4 plots this result, with the open circles denoting results for offshore waves and filled circles denoting results of estimation of wave height inside the harbor. The diagonal crosses give the results of a wave observation of one year's duration with a rate of return of 84%. Although the calculation of the wave height in the harbor yielded an estimate of exceedance probability slightly higher than the observation in the range of wave height in excess of 1.5 m, the reliability of the wave height estimation seems to be rather satisfactory considering the accuracy of each step involved.

By following the procedure described above, the exceedance probability of wave height within a harbor under planning can be evaluated quantitatively. The exceedance probability is best converted to the number of days of wave height exceedance per year by multiplying the probability by 365 days so that the results are more easily understood. The interpretation of the exceedance probability data available for a harbor for the evaluation of harbor tranquility is a task which will be improved and refined through further applications. There are no established criteria for the allowable exceedance probability of wave height in a harbor, for example, how many days can be tolerated with the wave height exceeding 0.5 m in a mooring basin or along a wharf, because judgment can only be made with various other operational and economic factors taken into consideration. Nevertheless, the description of the degree of wave agitation in a harbor with the exceedance probability such as shown in Table 6.5

Table 6.5. Result of estimation of the exceedance probability of wave height inside the harbor (percent).

Direction of offshore waves	Interior wave height H_s					
	Over 0 m	Over 0.5 m	Over 1.0 m	Over 1.5 m	Over 2.0 m	Over 2.5 m
SW	1.4	0	0	0	0	0
WSW	29.0	3.0	0.8	0.4	0.1	0
W	68.2	21.5	6.5	3.0	2.0	1.2
WNW	1.4	0.4	0.1	0	0	0
Total (all directions)	100.0	24.9	7.4	3.4	2.1	1.2
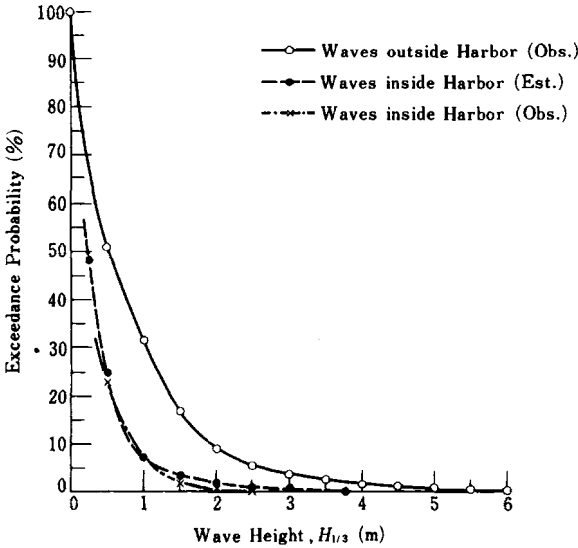
Fig. 6.4. Exceedance probability of wave height within Akita Port.

and Fig. 6.4 provides a common basis for the quantitative evaluation of the workability of port facilities.

Many more investigations need to be done on the wave height in a harbor, the motions of a ship at berth, the working limits of port operation, etc., in order to make a more quantitative and rational assessment of the serviceability of a particular harbor.

6.2.7 *Examination of Storm Wave Height in a Harbor*

The discussion of the wave height exceedance probability in a harbor up to now was mainly concerned with the workability of port operation. The waves in question were mostly waves of medium height, which comprise the major portion of wave climate statistics. As stated in the beginning of the present chapter, harbors also have the important function of providing safe anchorage for vessels in times of storms. The breakwaters must be capable of providing sufficient shelter for vessels from attacking storm waves and for preventing large waves from reaching port facilities. Thus, the waves of concern are those rare ones that occur only once in several years or once in several tens of years. The wave conditions in a harbor thus need to be investigated for rare storms too. The data for the statistics of such storm waves usually come from a source different from that of the wave climate statistics, which are based on wave measurements over several years at most. Wave hindcasting for major storms which occurred over a few score of years is the major source of data. Preferably the hindcasting technique should be calibrated with some instrumentally recorded storm wave data. The hindcast wave data are from the same data source used to determine the design wave for breakwaters and other structures. But the waves of extreme height must be chosen corresponding to several separate directions of wave approach for the examination of harbor tranquility at times of storm attacks.

The method of utilization of the estimated storm wave height information is not well established, as no definite criteria exist for the maximum allowable height of storm waves in a harbor. Generally speaking, if the significant wave height in a mooring basin can be kept below 1 m even for the design storm, the harbor may be considered calm. In any case, the description of the storm wave condition in a harbor in terms of the absolute value of the significant wave height will facilitate the judgment of the safety of the harbor in a quantitative manner.

6.3 Graphical Solution of the Distribution of Wave Height in a Harbor

Diffraction diagrams provide an indispensable means for the estimation of the wave height behind breakwaters and other barriers. If all the waterfronts of a harbor are composed of natural beaches and/or wave-absorbing structures,

direct application of diffraction diagrams to the harbor can yield a good esti-
mate of the wave height distribution. In most cases, however, there exist some
sort of reflective structures, such as vertical quaywalls within a harbor, which
cause additional wave agitation. Some modification in the usage of diffraction
diagrams is necessary for a harbor with reflective waterfront lines. For this
purpose the author devised a so-called mirror-image method,[6] inspired by the
suggestion of Carr quoted in the textbook edited by Ippen.[7] The method is a
graphical technique of applying diffraction diagrams (for random sea waves)
to a harbor, by transferring the geometry of the harbor layout in the plane
of a mirror image along the boundary of wave reflection, and by treating the
reflected waves as waves progressing in the mirror-image plane. Since the
technique enables the estimation of the effects of reflected waves in a harbor
in a relatively simple manner, an explanation will be given with an illustrative
example.

Let us consider a harbor sketched in Fig. 6.5. Wharves G and H are built
with vertical walls, and the seawalls indicated with diagonal crosses are pro-
vided with wave-absorbing structures. Points A, B and C are the locations
at which the wave height is to be estimated. The first step in the graphical
solution is to draw the diffraction diagram corresponding to the geometry of
the harbor entrance and the conditions of incident waves. In this example,
swell with $H'_0 = 4.3$ m and $T_{1/3} = 12$ s will be assumed to be incident to the
harbor. The opening of the entrance is measured as $B = 310$ m along the line
between the tips of the two breakwaters, and this line makes an angle of 41°
with the direction of the approaching swell.
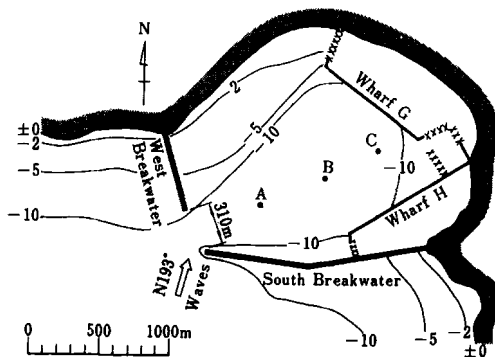
Fig. 6.5. Harbor geometry for application of graphical solution of wave height distribution.

By assuming the tide level of $+1.0$ m above the datum, the water depth at the entrance becomes $h = 11$ m, and the wavelength at this depth is read from Table A.3 in the Appendix as $L = 118$ m. Thus, the relative opening width becomes $B/L = 2.63$. The value of the directional spreading parameter is given as $(s_{max})_0 = 25$, because the swell is considered to have a short decay distance with $H_0'/L_0 = 0.019$. At the harbor entrance, the parameter is thought to have increased to the value of $s_{max} = 100$ due to the effect of wave refraction corresponding to the relative water depth of $h/L_0 = 0.049$ there, according to Fig. 2.14 in Sec. 2.3.2. Then the deviation angle of the axis of the diffracted waves is estimated as $\Theta \simeq 8°$ with the data listed in Table 3.4 in Sec. 3.2.3. The apparent direction of the diffracted waves thus makes an angle of $49°$ with the line connecting the tips of the two breakwaters. The apparent opening width of the entrance from this direction is $B' = 234$ m, and therefore $B'/L = 1.98$. The random wave diffraction diagram which has the conditions closest to the present situation is Fig. 3.13 (2) in Sec. 3.2.2. By transferring this diagram to the plan shape of the harbor under consideration, we obtain the contour lines of the wave height as sketched in Fig. 6.6. The diffraction diagram should be extended to an area larger than the harbor area (Zone I) itself.

If there were no wave reflection from the wharves, the wave height ratios at Points A, B and C could be read immediately from Fig. 6.6 with the aid of contour lines. But it is necessary to estimate the effect of wave reflection from Wharves G and H. In order to analyze the wave reflection from Wharf G, the plan shape of the harbor is transferred in the plane of the mirror image (Zone II) with the wharf line $\overline{g_1 h_1}$ as the reflective boundary. This operation can be performed easily, first by tracing the platform of the harbor on transparent paper, then by turning it over with the line $\overline{g_1 h_1}$ fixed in place and finally by tracing the outline of the harbor in Zone II on the other side of the transparent paper. On the mirror image of harbor in Zone II, Points A_2, B_2 and C_2, which are the mirror images of A, B and C, are plotted. In the same manner the mirror image of the harbor for the wave reflection from Wharf H is drawn in Zone III. Among the mirror images of the harbor in Zones II and III, the shaded portions represent areas to which reflected waves will not reach directly as they are in shadow zones as viewed from the harbor entrance. For example, Point B_3 in Zone III does not receive waves reflected from Wharf H.

In addition to primary reflection, there is secondary wave reflection from the back face of the south breakwater (if it is of vertical type) in the area $\overline{b_2 c_2 d_2}$
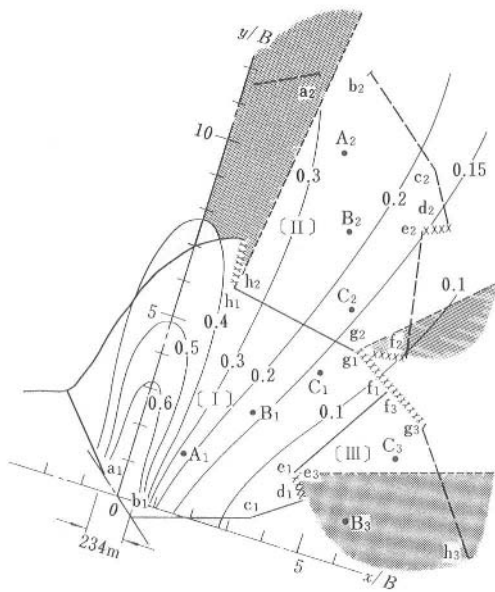
Fig. 6.6. Mirror-imaged diffraction diagram applied to a particular harbor geometry.

in Zone II and from Wharf H in the area $\overline{e_2 f_2}$ in Zone II. The graphical solution of the wave height distribution must included such secondary wave reflections, obtained by drawing the mirror images of the harbor with secondary reflective mirror images taken separately along lines $\overline{b_2 c_2}$, $\overline{c_2 d_2}$ and $\overline{e_2 f_2}$. However, these secondary wave reflections are omitted in the present explanation for the sake of brevity.

Next the values of the diffraction coefficient at the selected points in the respective zones are read and compiled as shown in Table 6.6. The resultant wave height at each point is estimated as the square root of the sum of the squares of the incident and all reflected wave heights, based on the principle of the summation of wave energy. If Wharf G does not have a vertical wall but consists of some sort of energy-dissipating structure, the wave height ratio entered in the column for Zone II should be reduced by the ratio of the reflection coefficient. Furthermore, in a harbor of large dimensions principally planned against wind waves, the reflection coefficient of a vertical quaywall may be reduced to 80% or so in consideration of the wave decay suffered during propagation in the harbor, as discussed in Sec. 3.6.2.

Table 6.6. Superposition of diffracted and reflected wave heights.

Point	Diffraction coefficient			Ratio of superposed to offshore wave height
	Zone I	Zone II	Zone III	
A	0.27	0.27	–	0.38
B	0.17	0.22	–	0.28
C	0.14	0.16	0.07	0.22

A reminder should be given that the application of diffraction diagrams for regular waves produces a wave height ratio quite different from actual situations. In the present example, regular wave diffraction would produce wave height ratios on the order of one half of those listed in Table 6.6, thus resulting in an underestimation of wave agitation in the harbor.

This mirror-image method of graphical solution cannot be applied to a harbor of complicated shape, as might be understood from the above illustrative example. Thus, the shape of a harbor needs to be approximated by a simpler form before the application of the graphical method. There is also the need of a somewhat subjective modification of the diffraction coefficient around the vicinity of the boundaries of geometric shadows viewed from the harbor entrance, such as the areas along the dashed lines extending from the points e_1, g_1 and h_1 in Fig. 6.6, because reflected waves penetrate into these shadow zones just as in the case of the diffraction of waves in the sheltered area behind a semi-infinite breakwater. It would not be appropriate to have an abrupt change in wave height across the boundary of a geometric shadow of reflected waves. There should be a smooth variation in wave height similar to that of the diffraction coefficient for a semi-infinite breakwater.

If a reflective structure in a harbor has an extent equivalent to only a few wavelengths or less, waves reflected by it will disperse in the harbor in a manner similar to the diffraction of waves through a narrow opening. In such a case, the propagation of the reflected waves is best estimated with the technique of fictitious wave diffraction, which treats the reflective boundary as an imaginary opening of a breakwater, as discussed in Sec. 3.6.2. A diffraction diagram corresponding to regular waves would be more suitable for this situation, because the waves incident to the reflected boundary have a narrow range of directional spreading, limited by the opening width of the entrance viewed from the location of the reflective boundary.

In summary, the graphical solution of the mirror-image method requires sound judgment of the analyst with appropriate modifications of the technique, depending on the harbor geometry and wave conditions.

6.4 Some Principles for Improvement of Harbor Tranquility

Although the tranquility of a harbor cannot be completely characterized by means of the wave height alone, as discussed at the beginning of the present chapter, in harbor planning, tranquility can only be achieved by suppressing the heights of waves within the harbor. This is the essence of harbor planning, which many experienced engineers have endeavored to realize. There are many good discussions in the textbooks of harbor engineering, but the author would also like to contribute to the subject by listing several principles for the improvement of harbor tranquility.

(i) *The harbor should have a broad interior.* Some harbors have only a long narrow water area, probably due to the local topographic conditions or by reason of historical development. Such harbors surely suffer the problem of too little dispersion of the intruding waves and of multireflection of the waves inside. The initial planning of a harbor should provide for a broad water area with sufficient room for future expansion.

(ii) *The portion of the waterfront from where the outer sea can be viewed through the harbor entrance should be left as a natural beach or be provided with wave-absorbing revetments.* The essential measures for reducing the wave height in a harbor are to minimize the intrusion of waves from the entrance and to dissipate the energy of the intruding waves at the place where they first reach the waterfront. That is to say, ones should try to control wave agitation at the first encounter of the waves with the harbor facilities. If a wharf or the revetment of a vertical bulkhead is built at a location where the intruding waves arrive directly from the entrance, this implies the worst kind of harbor layout because waves reflected from the bulkhead will cause considerable agitation within the harbor.

Figure 6.7 is a sketch of the layout of a harbour discussed by Ozaki.[8] It was reported that the water surface at Quay AB could not be maintained calm because of the waves reflected by the newly-built Wharf DC, and engineers had difficulty in finding effective countermeasures.
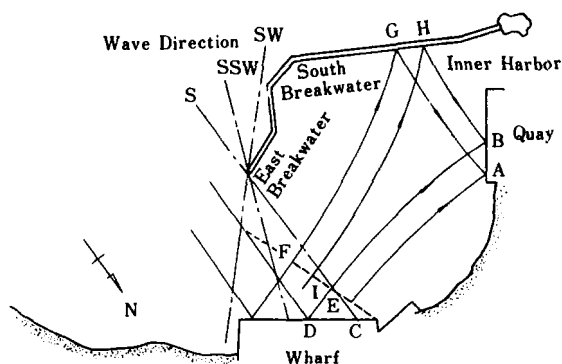
Fig. 6.7. Example of harbor agitation by reflected waves (after Ozaki[8]).
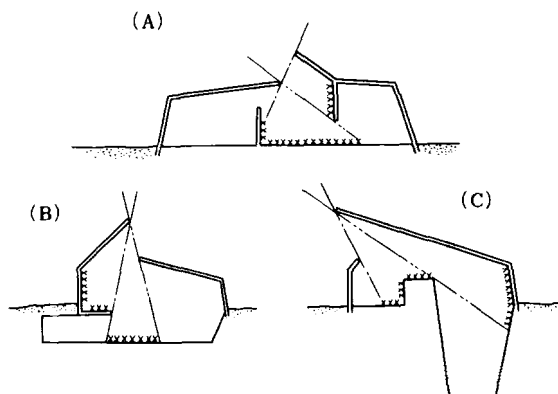
Fig. 6.8. Illustrations of areas to be provided with wave-absorbing structures.

The locations of the first arrival of intruding waves from the entrance will vary depending on the direction of the incident waves. Thus, it is best to assume that the waves can arrive from any direction and that a location from which the outer sea can be viewed through the harbor entrance may become an area of the first arrival of intruding waves. Such locations should not contain reflective structures.

Figure 6.8 gives three examples of such locations. The portions covered with diagonal crosses are to be kept as natural beaches or provided with revetments of the wave-absorbing type.

(iii) *Small-craft basins should be located in an area which cannot be viewed directly from the harbor entrances.* Small craft and many working vessels are easily set in motion by waves of small height. Thus, a basin for small craft must be given maximum protection against incoming waves. Secondary or inner breakwaters are often built at the entrances of such basins to assure tranquility there. It is important to overlap the outer and inner breakwaters against the direction of wave propagation so that no direct penetration of the incident waves will reach the small-craft basin. This is the fundamental principle in the planning of a marina. Also important are the provisions for a wave-spending beach, slipway, or wave-absorbing revetment at areas where waves diffracted by secondary breakwaters first reach. This is basically the same principle as (ii).

(iv) *A portion of the waterfront of a harbor should be reserved as an area of wave energy dissipation.* If one attempts to apply the mirror-image method to a harbor with a rectangular shape for which all the waterfront lines are made up of vertical walls, mirror images of the harbor geometry appear one after another in an endless fashion. This implies multirepetition of wave reflection. It presents the worst possible situation for harbor tranquility. The need to increase the cargo handling capacity of a port sometimes leads to the construction of a new wharf or quay at the location where a sandy beach or rocky reef existed previously. But this should be done with caution, because the removal of a wave-spending beach often results in a worsening of harbor tranquility due to the creation of reflected waves. The total cargo handling capacity of the port may well go down by the construction of an additional quay in such a strategic place.

For example, the beach between the west breakwater and Wharf G in Fig. 6.5 should not be converted into a wharf, because the beach is functioning
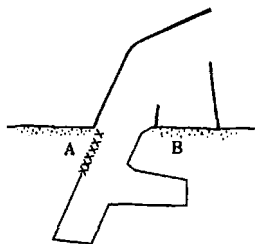
Fig. 6.9. A harbor layout.

as an important wave-spending beach. In the example shown in Fig. 6.9, the block mound revetment at A and the sandy beach at B should be kept as they are. It is not recommended to convert them into wharves of vertical walls. In fact, a port with a layout similar to that in Fig. 6.9 had problems with worsened tranquility after the area in front of the beach at B was reclaimed by construction of a vertical revetment at its waterfront.

(v) *Precautions should be taken against the reflection of waves from the back faces of vertical breakwaters.* For some harbor layouts, waves incident through the entrance or waves reflected from a wharf hit the back faces of breakwaters. If a breakwater is of the sloping mound type made of rubble stones or concrete blocks, wave reflection by the back face will be weak and the tranquility of the harbor will be less disturbed. In the case of vertical breakwaters, their back faces are formed of vertical walls and they reflect incident waves almost completely. In the example of Fig. 6.7, the back face of the south breakwater at section GH is reflecting the waves first reflected by Wharf CD, and this is causing additional disturbance at Quay AB.

Figure 6.10 is another example given by Ozaki.[8] At the time he discussed the situation, the extension of the south breakwater was insufficient for suppressing the intrusion of waves into the harbor. The intruding waves were first
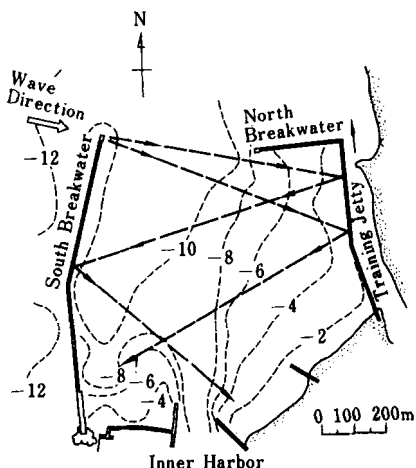
Fig. 6.10. Example of wave reflection by back face of a vertical breakwater (after Ozaki[8]).

reflected by a training jetty of the composite type. These reflected waves and re-reflected waves from the back face of the south breakwater were causing a disturbance in the water area around the entrance of the inner harbor.

Although the alignment of a breakwater is usually investigated and designed from the viewpoint of its effectiveness in diminishing the energy of waves intruding into the harbor, it is also necessary to examine the possibility of wave reflection from the back face of the breakwater. If the harbor layout is such that wave reflection is unavoidable, some measure such as the redesign of the breakwater into a non-reflective structure will become necessary.

(vi) *Comments on quaywalls of the energy-dissipating type.* In recent years, special types of quaywalls and vertical revetments capable of dissipating wave energy have been built in a number of harbors for the purpose of maintaining tranquility while providing additional facilities for port operation. They include concrete caissons with perforated or slit front walls, and several intricate forms of concrete blocks to be layed up to a required height. They all have hollow spaces which contain a mass of water connected to the outside water through many holes, slits, or irregular openings. In consonance with the undulation of the waves in front of structures, an alternating jet flow runs through there openings and wave energy is dissipated in the process by turbulence in the form of wakes and eddies.

By means of such structures, it is possible to decrease the reflection coefficient to 30% or less as indicated in Fig. 3.36 in Sec. 3.6.1, if the size of the hollow spaces and the opening ratio of the front wall are appropriately designed for the conditions of the incoming waves (mainly the wave period, or wavelength). The reflection coefficient may remain near 100% if the dimensions of the structure do not fit the wave conditions. Therefore, execution of hydraulic model tests is recommended before the adoption of structures of the energy dissipating type. Another check point is that the upper deck of such a structure should have a sufficient clearance height above the design water level so as not to hamper the free movement of the water mass in the hollow space, which is essential for the dissipation of wave energy. This aspect should be carefully examined in the case of harbors designed for small craft on a coast with a low tidal range, as users of such boats prefer the lowest possible elevation of the apron for easy landing and cargo handling.

6.5 Motions of Ships at Mooring

6.5.1 *Modes and Equations of Ship Motions*

As discussed in Sec. 6.1, tranquility of a harbor is evaluated with the safety of ships and the efficiency of cargo handling operations under constraints of construction and maintenance costs. In such evaluations, the amplitudes of ship motions at mooring provide the most important information. In contrary to fixed structures such as breakwaters and seawalls, ships floating on water have six degrees of freedom of motions and thus no straightforward formula are available for calculation of ship motions and mooring forces. If we try to give no allowance for ship motions under wave actions for example, we must employ extremely strong mooring chains, and the resultant mooring force will be great. If we provide a loose mooring just sufficient to prevent drifting of a ship on the other hand, the amplitudes of ship motions become large but the mooring forces remain small. Because ship motions at mooring are dependent on the mooring system, design of a mooring facility is often made through repetition of the analysis of ship motions by varying mooring characteristics until the ship motions are kept below an acceptable level.

To solve the problem of ship motions at mooring, we must understand the characteristics of the motions of a floating body on water, which has three degrees of freedom of reciprocating motions and three degrees of freedom of rotational motions. The six modes of motions are named individually as follows:

  (i) surge or surging : horizontal, longitudinal motion of floating body,
 (ii) sway or swaying   : horizontal, lateral motion of floating body,
(iii) heave or heaving : vertical reciprocating motion of floating body,
 (iv) pitch or pitching : rotational motion around the lateral axis of floating body,
  (v) roll or rolling   : rotational motion around the longitudinal axis of floating body,
 (vi) yaw or yawing   : rotational motion around the vertical axis through the center of gravity of floating body.

The six modes of ship motions are sketched in Fig. 6.11.

The six modes of motions do not occur independently but are excited in a coupled manner. For example, rolling of a floating body occurs simultaneously with swaying motion, and it is further coupled with a yawing motion
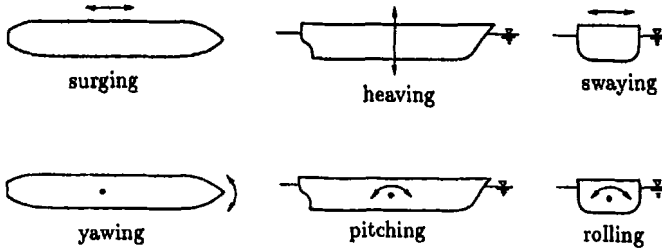
Fig. 6.11. Six modes of ship motions.

in many instances. Heaving of floating body excites a pitching motion, and it is almost impossible to restrict either one of the motions without interference with the other motion. However, surging of a long and symmetric body such as a ship can occur independently without coupling with other modes of motions.

The motions of a floating body under actions of winds and waves are analyzed by solving the equations of motions of six modes. Because the six modes of motions are coupled together, the equations of motions become the simultaneous differential equations of the second order with six unknowns. That is

$$\sum_{j=1}^{6}\{(M_{kj}+m_{kj})\ddot{x}_j + N_{kj}\dot{x}_j + C_{kj}\dot{x}_j|\dot{x}_j| + B_{kj}x_j + R_{kj}(x_j)\} = X_k(t), \quad (6.2)$$

where $k = 1 \sim 6$ corresponds to the six modes of motions respectively, j refers to the mode of motion coupled with the mode k, and x_j is the displacement or rotation of the coupled motion in the mode j. The term M_{kj} is called the inertia matrix, which represents the mass or the moment of inertia of the floating body in the direction of k when the body makes a motion in the mode j. The term m_{kj} is called the added mass, which represents the coefficient of the component of fluid resistance proportional to the acceleration in the direction of k when the floating body generates waves by moving in the mode j: for a rotational motion, the added moment of inertia is defined and the same is applied for other terms. The term N_{kj} is called the wave damping coefficient, which is the coefficient of the component of fluid resistance proportional to the velocity. The term C_{kj} represents the coefficient of nonlinear damping force such as the drag force. The term B_{kj} is the coefficient of restoration force due to buoyancy which is proportional to the displacement (rotation) of the floating body. The term R_{kj} stands for the reaction force of the mooring system, and a functional representation such as $R_{kj}(x_j)$ is employed because the reaction

force is nonlinear with the displacement x_j. The term $X_k(t)$ in the right side of Eq. (6.2) represents the external forces such as wave, wind and current loads acting in the direction k, which are evaluated as the floating body being set at the stationary state.

The motion of a floating body is determined as the result of equating the external force $X_k(t)$ with the inertia and fluid resistance generated by the motion of floating body as represented on the left side of Eq. (6.2). Because a freely floating body has a null reaction force of mooring system, its motion is governed by the external forces alone. If the motions of a floating body could be suppressed completely ($x_j = 0$), then the external forces $X_k(t)$ become the mooring force R_k. However, such a complete stop of motion is impossible, because conventional mooring arrangements do not have the capacity to withstand the external forces.

A unique component of the external forces inherent to a floating body is the wave drift force. It refers to a constant component of wave force which causes the floating body to move slowly in the direction of wave propagation. For a floating body of slender shape subject to beam seas (waves acting normal to the side), the wave drift force is estimated as[9,10]

$$F_D = \frac{1}{16}\rho g H_I^2 B \left(1 + K_R^2 - K_T^2\right) \left(1 + \frac{4\pi h/L}{\sinh 4\pi h/L}\right), \qquad (6.3)$$

where ρ is the density of sea water, g the acceleration of gravity, H_I the incident wave height, B the projected width of a floating body, K_R and K_T the coefficients of reflection and transmission of a floating body respectively, h the water depth, and L the wavelength. For a floating body subject to head seas (waves approaching from the bow) or a floating body of square or complex shape, the computation of wave drift force becomes complicated. Nevertheless, the characteristics of wave drift force being proportional to the square of wave height remain unchanged. The constant wave drift force provides the base value of mooring force for a ship at an offshore multiple-buoy berth or a floating breakwater.

In random sea waves, the mean wave drift force is evaluated with the root-mean-square height $H_{\rm rms}$. However, the wave drift force slowly fluctuates in time in response to the gradual variation of wave height in a train of waves, which is called the phenomenon of wave grouping as to be discussed in Sec. 9.2. Such slow variations of wave drift force cause the long-period oscillations of moored vessels.

6.5.2 *Ship Mooring and Natural Frequency of Ship Mooring System*

The method of mooring a ship varies depending on the place of mooring. At the anchorage in stormy conditions, a ship relies upon her anchors and the thrust of propellers to keep her position safely. At a single buoy berth, a heavy-duty hawser moors a tanker to a buoy. In the analysis of vessel movements at such a single-point mooring, the motion of buoy must be solved simultaneously with that of a vessel. At dolphin berths in the offshore and conventional wharves in a harbor, mooring lines and fenders constitute a mooring facility.

Mooring lines are made of steel wires and/or synthetic fiber lines (nylon ropes and polyester ropes), which are equipped on board a ship. The number and size of ropes are specified according to the equipment number which is calculated with the rules of ship classification societies. These ropes are intended to hold a ship alongside a berth for smooth cargo handling operations under normal weather conditions. They are not strong enough to hold a ship at stormy conditions, and they are sometimes broken at times of strong winds and/or high waves. Some harbor authorities have heavy-duty mooring lines in store to assist vessels at mooring in their harbors at stormy conditions, but their effectiveness is limited by the structural strength of bollards on board the ships.

When a ship is moored at a berth, mooring lines are given the names depending on the points of mooring as shown in Fig. 6.12. The bow (head) lines and stern lines are mainly employed to harness surging motions, while breast lines are to constrain swaying and yawing of a ship. Spring lines (aft and back) are used to fix a vessel at normal weather conditions, and are recommended to let released at stormy conditions.
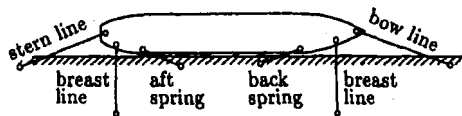
Fig. 6.12. Mooring lines for a ship at berth.

Of the two types of mooring ropes, steel wires exhibit a nearly linear relationship between the tension and elongation, and the elongation at breakage is relatively small. On the other hand, synthetic fiber ropes exhibit nonlinear

behavior of elongation with the tension, with a large elongation at breakage. In scale model tests of ship mooring, various efforts are made to simulate such a nonlinear relationship between tension and elongation of mooring lines in the model: use of a series of multiple springs with different stiffness is one of such techniques.

Fenders are primarily installed to absorb the berthing impact and to prevent damage on the vessel's hull and wharf structures. At times of mooring at stormy conditions, fenders serve as the important element to constrain swaying and yawing of a vessel. However, the load and displacement relationship of a fender is a special one: it works on the compression side only, and the load and displacement curve is highly nonlinear.

Table 6.7. Restoring forces of floating body at mooring.

Mode	Buoyancy	Mooring lines	Fender
Surging	×	○	×
Swaying	×	○	○
Heaving	○	×	×
Rolling	○	△	×
Pitching	○	×	×
Yawing	×	○	△

Note: ○ active   △ marginal   × nonexistent.

The natural frequency of a mooring system is governed by the mass (moment of inertia) of a vessel and the restoring forces. Table 6.7 lists the elements of restoring forces for the six modes of ship motions. For heaving and pitching motions, mooring lines and fenders can exercise no effect, and the restoring forces due to buoyancy of a floating body are the sole forces for restoration. Thus, the natural frequencies of heave and pitch are in the range of several seconds to less than 20 seconds. Rolling motions can be suppressed to a certain extent by the selection of mooring lines and their points of attachment. However, the natural frequency of rolling remains almost the same as of a freely floating body. For surging, swaying and yawing motions, a floating body has no restoring force due to buoyancy and it is brought back to the equilibrium position mainly through the relatively weak tension of mooring lines. The natural periods of these motions thus become long in the range

of several tens of seconds to a few minutes. As the winds and waves have the components of long-period fluctuations, moored vessel can be brought into resonance with them, resulting in a slow motion of large amplitudes. Tightening of mooring lines shortens the natural periods and is effective in suppressing resonant motions. However, the frequent tension adjustments of mooring lines must be executed with much care because tightening of mooring lines enhances the danger of line breakage.

6.5.3 *Dynamic Analysis of Ship Mooring*

The motions of a moored ship is analyzed by solving Eq. (6.2). In case of a ship navigating in the sea, no mooring force exists. The equations can be transformed into a set of linear differential equations by introducing an equivalent linearization of the term C_{kj} or by simply neglecting it. Once the terms M_{kj}, m_{kj}, N_{kj}, B_{kj}, etc. are evaluated by the strip theory or by some other numerical schemes, the simultaneous equations can be solved with relative ease. Ship motions in directional seas can be analyzed by linearly superposing the ship responses to wave spectral components. This is a frequencywise solution and is widely utilized in naval hydrodynamics.

In case of a ship moored at berth however, the nonlinear restoring forces of mooring lines and fenders are the important parameters and the wave drift force which is proportional to the square of wave height fluctuates with respect to time. Thus, the frequencywise linear superposition technique cannot be employed in the analysis. Instead, a time-domain analysis is used for the motion of a moored vessel, by giving the input of time-varying external forces $X_k(t)$ and by solving Eq. (6.2) with a time step of small increment. The time series of external forces are prepared for each mode of the six degrees of freedom of vessel motions by numerical simulation techniques based on the spectra of forces and moments exerted upon a vessel by winds and waves. The wave drift force of irregular waves is given by approximately computing the drift force of individual waves with the theory of regular waves,[11] or some other methods.

6.5.4 *Acceptable Ship Motions at Mooring for Safe Working Conditions*

A ship moored at a berth is always moved by winds, waves and currents, and so a complete suppression of ship motions is impossible. The allowable movements of a moored ships at extreme sea states are determined by the breakage strength

of mooring lines, while at normal conditions they are dictated as the amounts below which cargo handling works can be carried out safely and efficiently. The latter amounts depend on the size and type of ships, the types of cargo handling equipment and the modes of ship motions. Thus, the acceptable ship motions at mooring must be established through detailed surveys of actual cargo handling works in ports. Such surveys have been undertaken at several countries, and the results have been compiled by the Working Group No. 24 of the Permanent International Association of Navigation Congresses. Table 6.8 is an excerpt of the recommended motion criteria for safe working conditions[12]: the report of PIANC also includes recommendations for fishing vessels, ferries and ro-ro vessels, and gas tankers.

The PIANC report is based on the studies by Brunn,[13] Ueda,[14,15] Jessen *et al.*,[16] etc. As the acceptable ship motions vary considerably, depending on the type of ships and cargo handling equipment, examination of harbor tranquility needs to be made with detailed information on the port installations. With the progresses in the techniques of numerical simulation and hydraulic model tests of ships moored at berths, judgment of harbor tranquility by means of the magnitudes of ship motions is becoming a common practice in port planning.

Table 6.8. Acceptable ship motions at mooring recommended by PIANC.

Ship Type	Cargo Handling Equipment	Surge (m)	Sway (m)	Heave (m)	Yaw (°)	Pitch (°)	Roll (°)
Freighters/coasters	Ship's gear	1.0	1.2	0.6	1	1	2
	Quay cranes	1.0	1.2	0.8	2	1	3
General cargo	—	2.0	1.5	1.0	3	2	5
Container vessels	100% efficiency	1.0	0.6	0.8	1	1	3
	50% efficiency	2.0	1.2	1.2	1.5	2	6
Bulk carriers	Bucket-wheel	1.0	0.5	1.0	2	2	2
	Cranes	2.0	1.0	1.0	2	2	6
	Conveyor belt	5.0	2.5				
Oil tankers	Loading arms	3.0	3.0				

Note: 1) Motions refer to peak–peak values (except for sway: zero to peak).
2) Freighters and coasters are ships of less than 10,000 DWT.
3) The second line of container vessels refers to the container handling efficiency reduced to 50%.

6.5.5 *Some Remarks on Ship Mooring*

It is desirable to understand the characteristics of the movements of moored ships, even before a numerical simulation and/or hydraulic model test are commissioned for examination of harbor tranquility. The following are several remarks for port planners from the viewpoint of ship motions at mooring.

(i) *Waves of long periodicity cause large ship motions.* In conventional analysis of harbor tranquility, the measure of tranquility is the wave height at respective locations in a harbor as exemplified in Sec. 6.2. While the ship motions increase in proportion to the wave height, they are also affected by the wave period. Generally speaking, the ship motions become larger for long-period waves than for short-period waves, although the wave period effect varies depending on the ship size and mooring arrangement. Thus, a port which is opened to the ocean and exposed to swell should lower the threshold wave height for safe working conditions, as compared to a port which is located in an embayment sheltered from swell.

(ii) *Cautions should be taken against infragravity waves.* The term infragravity waves refers to waves with the period ranging from around 20 seconds to several minutes. They are often associated with storm waves being bounded by wave grouping, but they may enter into harbors as free waves at the time of mild to medium wave conditions. Infragravity waves with the height less than 10 cm can excite large ship movements, because the natural periods of the surge and sway of moored ships often fall in this period range. The natural periods of oscillations of moored ships could be shortened by changing mooring lines of synthetic fiber lines to steel wires with synthetic tails if applicable, and thus avoiding excitation of resonance phenomena. In port planning, studies should be made for the magnitude of infragravity waves at the site, and if their energy is not of negligible amount, the harbor layout should be so made to reduce the intrusion of infragravity waves into the harbor and to enhance their dissipation in the harbor as much as possible.

(iii) *Ships are most susceptible to beam waves and winds.* The wind and wave forces are linearly proportional to the exposed area of a ship's body, which is the largest to the direction from the side. A berth should be located at the position where a ship moored there would not be subjected to winds and waves from abeam directions. If siting of a berth at a location of beam waves is inevitable

by the constraints in port planning, the threshold wave height for safe working conditions at that berth should be lowered from that of other berths. Ueda and Shiraishi[17] recommend to include a deviation of 10° to 15° in the wave direction when carrying out numerical simulation of moored ship motions.

(iv) *Avoid a location of strong offshore seasonal winds for a berth.* Seasonal winds often have the prevailing directions at respective ports. A ship at a berth should not be exposed to strong offshore winds, because the breast lines are not strong enough to withstand the full force of offshore winds: a berth should be located at the other side of slip at which the onshore winds would act on a moored ship. If siting of a berth at a location of offshore wind is inevitable, tall sheds and other buildings are to be erected behind a quay to serve as a wind screen for reduction of wind forces.

(v) *Winds are to be specified by means of spectrum.* In design of fixed structures, the wind load is often treated as a steady force. In the analysis of the motion of a floating body moored on water, however, temporal fluctuations of wind speed need to be taken into account, because the moored body may respond to the long-period component of wind force and its movement may become large. The wind speed fluctuations are simulated with the wind spectrum such as Davenport's one.[18] In a preliminary analysis, the maximum instantaneous wind speed in consideration of the gust factor of winds may be used in estimating the mooring force. However, the time-domain numerical analysis of Eq. (6.2) must be carried out for obtaining reliable information of ship motions and mooring forces.

(vi) *The ship motions become the largest at the ballast condition.* The wind force is the largest for a ship in ballast, because of the largest area of exposure. As to the ship motions induced by waves, a ship in ballast also experiences the largest movements, contrary to a layman's expectation. It is so because the inertial force matrix and damping coefficients in the left side of Eq. (6.2) decrease much faster than the external force of waves in the right side of Eq. (6.2) does, as the ship draft decreases.

(vii) *Mooring a ship often increases the ship movements.* Currently available mooring arrangements are not strong enough to suppress the ship movements at medium to storm weather conditions. It is difficult to reduce the ship movements below those of a freely floating ship. If resonance occurs, surging and

swaying motions become quite large. The motions of a freely floating ship provide the first approximation to the motions of a moored ship and mooring forces, though more accurate information must be sought for by solving Eq. (6.2).

References

1. R. C. H. Russel, "Modern techniques for protecting the movement of ships inside harbours," *Analytical Treatment of Problems in the Berthing and Mooring of Ships* (NATO & HRS, 1973), pp. 267–275.
2. L. Barailler and P. Gaillard, "Evolution récent des modèles mathématiques d'agitation due á la houle, Calcul de la diffraction en profondeur non uniforme," *La Houille Blanche* **22** (8) (1976), pp. 861–869.
3. K. Tanimoto, K. Kobune, and K. Komatsu, "Numerical analysis of wave propagation in harbours of arbitrary shape," *Rept. Port and Harbour Res. Inst.* **14** (3) (1975), pp. 35–58 (*in Japanse*).
4. M. B. Abbott, H. M. Petersen, and O. Skovgaard, "Computation of short waves in shallow water," *Proc. 16th Int. Conf. Coastal Engrg.* (Hamburg, 1978), pp. 414–433.
5. T. Takayama and Y. Kamiyama, "Diffraction of sea waves by rigid or cushion type breakwaters," *Rept. Port and Harbour Res. Inst.* **16** (3) (1977), pp. 3–37.
6. S. Sato and Y. Goda, *Coastal and Harbour Engineering* (Shokoku-sha, Tokyo, 1972), pp. 72–77 (*in Japanse*).
7. Ed. A. T. Ippen, *Estuary and Coastline Hydrodynamics* (McGraw-Hill, 1966), pp. 319–323.
8. A. Ozaki, "Wave energy dissipating structures in harbors," *Lecture Series on Hydraulic Engineering* **65–17**, Hydraulics Committee, Japan Soc. Civil Engrs, (1965), 25p. (*in Japanse*).
9. H. Maruo, "The drift of a body floating on waves," *J. Ship Res.* **4** (3) (1960), pp. 1–10.
10. H. Newman, "The drift force and moment on ships in waves," *J. Ship Res.* **11** (1) (1967).
11. F. H. Hsu and K. A. Blenkarn, "Analysis of peak mooring force caused by slow vessel drift oscillation in random seas," *Prepr. 2nd Offshore Tech. Conf.* (1979), OTC1159.
12. Permanent Int. Association of Navigation Congresses (PIANC), "Criteria for movements of moored ships in harbours: A practical guide," *Rept. Working Group No. 24, Permanent Technical Committee II, Supplement to Bulletin No. 88* (1995), 35p.
13. P. Brunn, "Marine terminal technology, winch berthing and mooring methods, recent developments," *Proc. NATO Advanced Inst. on Advances in Berthing and Mooring of Ships and Offshore Structures* (Trondheim, 1987), pp. 31-61.

14. S. Ueda, "Motions of moored ships and their effect on wharf operations efficiency," *Rept. Port and Harbour Res. Inst.* **26** (5) (1987), pp. 319–373.
15. S. Ueda and S. Shiraishi, "Allowable ship motions for cargo handling at wharves," *Rept. Port and Harbour Res. Inst.* **27** (4) (1988), pp. 3–61.
16. O. Jensen, J. G. Viggósson, J. Thomsen, S. Bjørdal, and J. Lundgren, "Criteria for ship movements in harbours," *Proc. 23rd Int. Conf. Coastal Engrg.* (Venice, 1990), pp. 3074–3087.
17. S. Ueda and S. Shiraishi, "On the effects of wave direction and mooring lines on the motions of moored ships," *Proc. 31st Japanese Conf. Coastal Engrg.* (1984), pp. 451–455 *(in Japanese)*.
18. A. G. Davenport, "Gust loading factors," *Proc. ASCE* **98** (ST3) (1967), pp. 11–34.

Chapter 7

Hydraulic Model Tests with Irregular Waves

7.1 Similarity Laws and Model Scales

As discussed in the previous chapters, many problems in the planning and design of harbor facilities and coastal structures must be solved by means of hydraulic model tests. Although most tests over the past several decades have been performed with regular trains of waves, the advantages of hydraulic model tests with irregular waves are now well acknowledged and facilities for such tests are becoming available in laboratories around the world. Thus, the present chapter mainly discusses hydraulic model tests with irregular waves.

The fundamental condition to be satisfied in a model test is that the model must behave in a manner similar to the prototype. Similitude of the model to the prototype is required in the three general categories of geometric shape, kinematics of the various motions, and dynamic forces acting in the model and the prototype. Geometric similarity means that all lengths in the prototype are scaled down in the model by a certain ratio or ratios. Kinematic similarity requires proportionality of the velocities and accelerations of the various bodies and the fluid between the model and the prototype. Dynamic similarity demands that all dynamic forces in the prototype must be reproduced in the model with the same scale ratio. Complete dynamic similarity is seldom possible, however, because of the varied nature of the many forces acting in the prototype. Depending on the predominant forces for which dynamic similarity is to be maintained, several model laws of similitude can be derived.

In hydraulic model tests concerning sea waves, the viscosity and surface tension of water usually do not play significant roles, leaving inertia and gravitational forces as the governing forces. The scaling law for such a situation is the Froude law, which dictates that the scales for the time and velocity should be equal to the square root of the length scale. Table 7.1 gives examples of model scales obtained from the Froude law, with explanatory figures.

Table 7.1. Model scales according to the Froude law.

Item	Scale	Example	Prototype	Model
Horizontal length and wavelength	l_r	1/25	50 m	2.0 m
Water depth	$h_r = l_r$	1/25	15 m	60 cm
Wave height	$H_r = l_r$	1/25	6 m	24 cm
Wave period and time	$T_r = l_r^{1/2}$	1/5	10 s	2.0 s
Wave pressure	$P_r = l_r$	1/25	90 kPa	3.6 kPa
Force per unit length	$P_r = l_r^2$	1/625	1500 kN/m	24 N/cm
Weight per unit length*	$w_r = l_r^2$	1/625	2800 kN/m	44.8 N/cm
Weight of armor unit*	$W_r = l_r^3$	1/15,625	300 kN	19.2 N
Overtopping amount per wave per unit length	$Q_r = l_r^2$	1/625	0.6 m³/m	9.6 cm³/cm
Overtopping rate per unit length	$q_r = l_r^{3/2}$	1/125	0.06 m³/m·s	4.8 cm³/cm·s

*With the same specific weight of material.

If a model is made with the same geometric scale in the horizontal and vertical directions, it is called an undistorted model. If the geometric scales are different in the horizontal and vertical directions, the model is called a distorted model. Hydraulic model tests on tidal currents are prominent examples of distorted models, with the horizontal scale much smaller than the vertical scale, because these models usually have to cover a large water area. On the other hand, most model tests on sea waves are done with undistorted models, because the horizontal and vertical motions of water particles by wave action must be reproduced with the same scale. One possible exception may be the use of a distorted model for the analysis of tranquility of a large harbor against short wind waves, in which case only the effects of wave diffraction and reflection enter, because wave refraction is negligible.

It is desirable to make use of the largest model possible to obtain results of highest possible accuracy. The disadvantages of large models are the increased costs of construction and operation, as well as elongation of the required test

time. The model scale must be selected based on considerations of the size of the prototype structure (or harbor) and the size of the available test facility. No definite criteria can be cited on the acceptable scales of hydraulic models. Many laboratories, however, have carried out tests on harbor tranquility with scales of 1/50 to 1/150. Tests on breakwater stability and wave overtopping of seawalls are often carried out with scales of 1/10 to 1/50.

Controlling factors entering the selection of the model scale are the limiting minimum values of the period and height of the model waves. In three-dimensional tests on harbor tranquility, the period of the model waves must be longer than 0.5 s, because waves with shorter period experience excessive attenuation in height caused by the thin dusty film normally present on the water surface. It then becomes almost impossible to maintain model similarity[1] with such short period waves. For irregular waves, the limiting wave period is even greater as the spectral peak must be above the 0.5 s value. The significant period of model waves is preferably longer than 1.0 s and never shorter than 0.8 s.

The condition for the limiting minimum wave height appears when wave breaking is involved, as for breakwater stability and overtopping of a seawall. If the height of the model waves is too small, the shape and size of the breaking waves are distorted due to surface tension. As a rule of thumb, a wave height greater than 10 cm is desirable. In the case of irregular waves, the significant height is best set above 10 cm. However, if the situation is such that only standing waves are formed, a wave height of only several centimeters may be employed.

7.2 Generation of Irregular Waves and Data Analysis

7.2.1 *Irregular Wave Generator*

The working principle of an irregular wave generator is completely different from that of a conventional regular wave generator. Figure 7.1 illustrates the two kinds of wave generators. The upper figure (a) shows the typical composition of a conventional wave generator. The motor is usually of the three-phase alternating current type, which rotates at a fixed speed. The rotational speed is set to a predetermined value by a nonstep speed-variator, and then the speed is reduced by 1/10 to 1/20 with gears. The rotational speed can thus be adjusted to the required wave period.
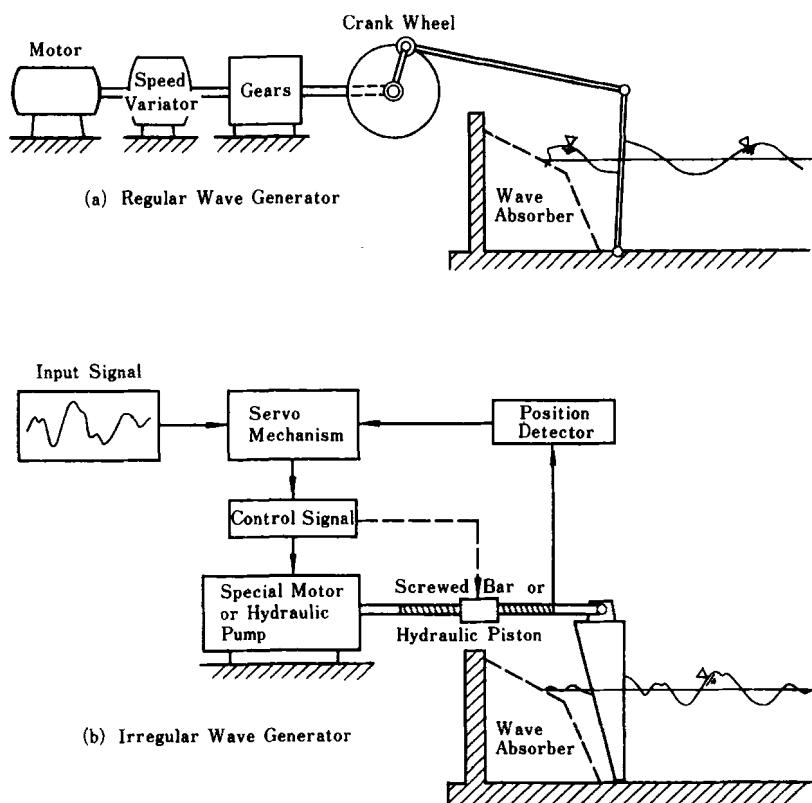
Fig. 7.1. Outline of regular and irregular wave generators.

The rotation of the output axis of the gears is transmitted to a crank wheel which rotates at a constant speed and produces a reciprocating motion of the wave paddle through a crank arm and linkage system. The figure shows the mechanism for a flap-type wave paddle with a rotational hinge at the bottom, but any type of mechanism such as piston type or a double-hinged flap type can be designed as required. The stroke of the crank arm or the amplitude of the paddle motion is usually designed to vary continuously from zero to some maximum. There are also sophisticated machines which enable changes of paddle amplitude during operation of the wave generator.

The lower figure (b) shows the basic concept of an irregular wave generator, which is characterized by a servo-mechanism system. The motor may be an

electric servo-motor, a special direct-current motor with a low rotor inertia, a hydraulic pump, or a hydraulic pulse motor. The output of the motor is onverted to reciprocating motion of the driving unit of the wave paddle through a long screw bar by means of coupling by a peripherical ball bearing or through a hydraulic piston. The position of the wave paddle is continuously monitored by a sensing device, and the information is fed back to the servo-mechanism, which compares it with the input signal and sends a control signal to the direct current motor or the control valve of the hydraulic pump. Thus, an irregular wave generator is essentially a signal-following driving machine, and it generates a train of regular waves when the input signal is a sinusoid.

Generators for irregular waves first appeared in the 1960s at ship testing basins. In the 1970s, they became popular at hydraulic facilities of civil engineering laboratories. It may be said that the production of such generators was stimulated by rapid progress in sophisticated equipment for testing of severe vibration and durability of the components of missiles and rockets, as well as by developments in numerically controlled machines and robots in industry. The level has been reached where an irregular wave generator is not a machine of special design, but is assembled with a number of standard industrial components.

Laboratory wave generators have evolved into multidirectional wave generators nowadays. Such a generator is composed of a large number of segmented wave paddles, each with the width 30 to 80 cm, which are independently controlled by servo systems. The computer-generated control signals are fed to individual wave paddles so that the water surface in front of the wave paddles will follow the temporal and spatial fluctuations of random wave profiles which are specified by a target directional spectrum. When individual wave paddles are driven with the same amplitude and frequency but with a constant phase lag between adjacent paddles, a regular train of oblique waves is generated. In the 1950s, there were mechanical wave generators called the snake-type or serpent-type generator, which were capable of generating oblique waves in laboratory basins. The multidirectional wave generators of today are the modernization of the snake-type wave generator of the past, having been given the greater capability of generating diverse profiles of random waves. Salter[2] manufactured the first wave generator of this type at Edinburgh University in the mid-1970s. Since then, many institutions throughout the world have installed the multidirectional wave generators in their hydraulic laboratories. The number

of institutions was 32 in 1992 according to a survey by Funke and Mansard,[3] and it is increasing ever since.[a]

7.2.2 *Preparation of Input Signal to the Generator*

The generator itself is manufactured in the form sketched in Fig. 7.1(b). However, the most important aspect of irregular wave generation is the preparation of the input signal to the generator for obtaining irregular waves of prescribed characteristics. This is basically done according to the flow diagram shown in Fig. 7.2.

First, the target frequency spectrum of the irregular waves is chosen. If only the significant height and period of the test waves are given, the Bretschneider–Mitsuyasu type spectrum, Eq. (2.11) in Sec. 2.3.1, provides a convenient formula for the spectrum of the model waves. If the frequency spectrum of the random waves at the site is known, it may be used as the target. Depending on the nature of the tests, many other spectra might be used, such as a narrow band spectrum of long-traveled swell, a sharply peaked spectrum of the JONSWAP type described by Eq. (2.12) in Sec. 2.3.1, which represents wind waves generated by strong winds, or a multimodal spectrum for the superposition of wind waves and swell.

The target spectrum of the water waves must be converted to the target spectrum of the wave paddle motion by means of the transfer function for wave generation. This function represents the relationship between the height of the generated waves and the amplitude of the wave paddle for waves of constant period. According to the solution of the velocity potential given by Biésel and Suquet,[5] the transfer function is

$$\text{Piston type} \; : \; F_1(f, h) = \frac{H}{2e} = \frac{4\sinh^2(2\pi h/L)}{4\pi h/L + \sinh(4\pi h/L)} , \qquad (7.1)$$

$$\text{Flap type} \; : \; F_2(f, h) = \frac{H}{2e} = \frac{4\sinh(2\pi h/L)}{2\pi h/L}$$

$$\times \frac{1 - \cosh(2\pi h/L) + (2\pi h/L)\sinh(2\pi h/L)}{4\pi h/L + \sinh(4\pi h/L)} , \qquad (7.2)$$

---

[a]A further survey by Mansard *et al.*[4] lists 42 facilities at 40 institutions, but there are many more facilities not covered by the survey.
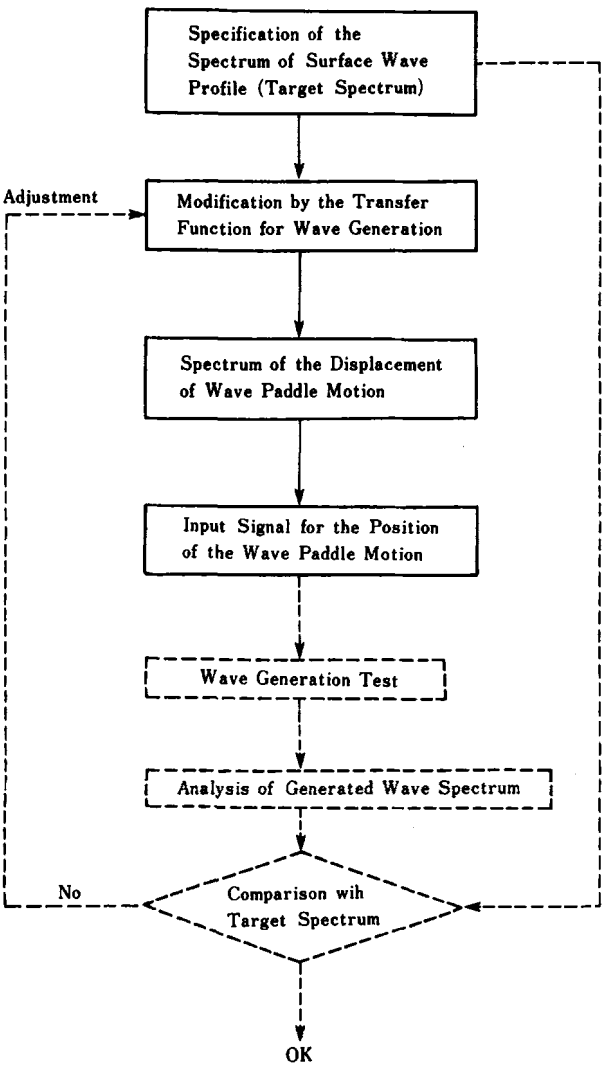
Fig. 7.2. Process of the preparation of input signal to an irregular wave generator.

where H denotes the height of the generated waves, e is the amplitude of wave paddle at the mean water level, and f stands for the wave frequency ($= 1/T$) which implicitly enters in Eqs. (7.1) or (7.2) through the wavelength L.
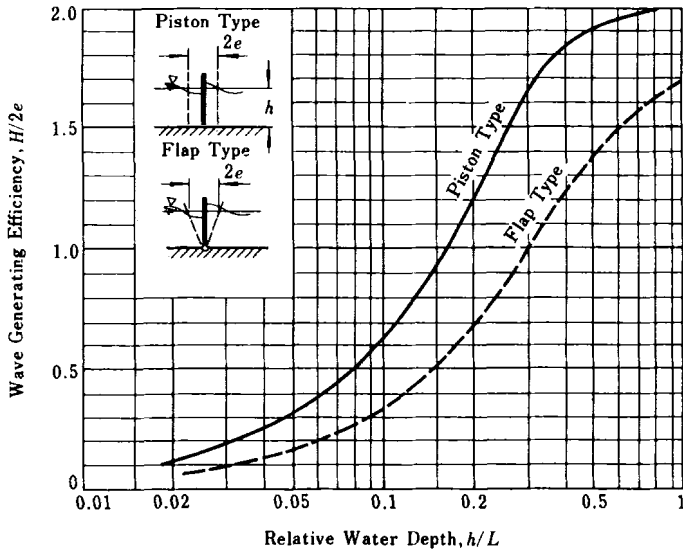
Fig. 7.3. Transfer function for wave generation by paddle motion of piston type and flap type.

The transfer functions given by Eqs. (7.1) or (7.2) are plotted in Fig. 7.3 against the relative water depth h/L. As seen in the figure, short-period waves (high frequency) have a high efficiency of wave generation, whereas long-period waves (low frequency) have low efficiency. Because the transfer function for wave generation varies with the wave frequency, the target spectrum of the wave paddle motion $S_G(f)$ is calculated for the target wave spectrum $S_w(f)$ as follows:

$$S_G(f) = S_w(f)/F_j^2(f/h) \; : \; j = 1 \text{ or } 2 \,. \tag{7.3}$$

The target paddle spectrum takes a shape enhanced at the low frequency side and damped at the high frequency side in comparison with the target wave spectrum.

The next step is a simulation of an irregular wave profile for the motion of wave paddle which satisfies the target paddle spectrum. At the early stage of irregular wave tests, the analog simulation technique was used. It employed an analog white noise generator and a set of 10 to 15 bandpass filters, which tailored the white noise signal in such a way that a desired spectral shape can be obtained by adjusting their outputs. The output signal was fed directly

into the control system of the irregular wave generator. At present, however, the digital technique is prevailing.

The digital simulation technique involves numerical generation of random signals with the aid of a personal computer. Three methods are currently employed for this purpose. One makes use of the impulse response function to digital white signals,[6] another uses the inverse fast Fourier transform algorithm, and the third method synthesizes random signals as the sum of finite number of sinusoidal waves (refer to Sec. 10.5). Each has its own advantages and disadvantages; however, the differences are not essential but operational. The digital signals thus generated are fed into a digital–analog converter and the resultant analog signals are sent to the control system of the irregular wave generator.

After the random signals for driving the wave paddle have been prepared, a test run of wave generation is carried out and the records of the generated waves are analyzed for the wave spectrum as well as for various representative wave heights and periods. If the spectrum, wave height, or period is found to have significant deviations from the expected wave characteristics, the target paddle spectrum is adjusted and the procedure is repeated until satisfactory results are obtained. In this process, attention should be paid to the statistical variability of the actual data, which is an inherent characteristic of irregular water waves (refer to Sec. 9.6). Just as in the problem of quality control in mass production in a factory, we cannot decide whether we should adjust the input signal to the generator on the basis of one set of data which shows some deviation from the target value. We need several measurements or a sufficiently long record of the wave profile before we can make a decision on the adjustment of the input signal.

It should be commented here that direct control of the profile of a generated wave train in front of a model structure is impossible. This is because the propagation of the generated waves from the generator to the model structure takes a time of ten to several tens of seconds, while servo-control of the wave generator must be made on the order of a hundredth of a second, and thus no feedback is possible from the wave record obtained in front of the model to the wave generator. The only procedure possible is compensation through the wave transformation during propagation. That is, the degree of transformation is calculated and the input signal to the generator is modified in such a way to make the compensation. For example, an ordinary irregular wave generator produces all frequency components of a spectrum simultaneously from the

beginning. The generated train of irregular waves gradually disperses, with low frequency waves propagating faster than high frequency waves. When the front of the irregular wave train reaches the site of a model structure, it contains low frequency components only. A remedy for this is phase-delayed generation of the wave spectrum; high frequency components are started early and lower frequency components are gradually added to the random signal for driving the wave paddle. The degree of phase delay must be calculated from knowledge of the propagation time of the individual component waves over the distance between the wave paddle and the model. By preparing the random input signal to the generator in this way, the test structure will receive a train of irregular waves having full spectral components from the beginning of the arrival of waves.

7.2.3 *Input Signals to a Multidirectional Wave Generator*

The principle of generating multidirectional random waves is the superposition of a large number of regular trains of oblique waves with different frequencies and directions of propagation. For a given target directional spectrum, the amplitudes and initial random phases of individual component waves are calculated for respective frequencies and directions. For each component wave, the amplitude of wave paddle motion is obtained by means of the transfer function of Eq. (7.1) or (7.2), and the phase lag of each paddle is evaluated with the frequency and direction of the component wave and the distance of the paddle from the tip of the wave generator. The phase angle of a particular wave paddle for each component wave is given by the sum of initial random phase and the phase lag of that paddle. The data of wave paddle amplitudes and phase angles of all component waves are stored for each wave paddle, and the control signal for each wave paddle motion is constructed by summing up the various sinusoidal motions prescribed for all component waves.

Surface wave profiles satisfying a target directional spectrum were initially computed by the double summation method; i.e., representation of wave profiles with the product of a series of various frequency components and that of various directional components. However, the problem of phase locking among the directional components at the same frequency was pointed out by Jefferys[7] and Miles and Funke.[8] Thus, the single summation method which assigns a single direction to each frequency component is currently employed in many laboratory basins as a standard procedure in generating multidirectional

waves. The technique for simulation of random wave profiles is discussed in Sec. 10.5.

7.2.4 *Data Recording and Analysis*

In all the tests employing irregular waves, time histories of water surface elevations at various locations are measured with wave gauges of capacitance type or resistance type. In the multidirectional wave tests, arrays of wave gauges and/or two-axis current meters are employed to monitor the directional spectrum realized in test basins. In the breakwater stability tests, wave pressure gauges, load cells, and/or strain gauges are utilized to measure the pressure intensities, wave thrusts, and/or stress incurred on structural members. These data are nowadays digitized on real time basis and recorded on floppy disks or other devices for later analysis. Several softwares installed in personal computers enable the wave height, period, spectrum and other information to be yielded immediately after the measurements. Exception for direct digital recording may be the measurement of impulsive breaking wave pressures on a vertical breakwater, which requires data sampling at the rate of several thousands per second for a number of pressure gauges. Unless a high-speed analog–digital converter is mobilized, an analog magnetic tape recorder stores the data temporarily for later digitization.

The methodology of analyzing wave data for statistical wave characteristics, frequency spectrum and directional spectrum is discussed in Chapter 10.

7.3 Experimental Techniques for Irregular Wave Tests

7.3.1 *Model Tests on Harbor Tranquility*

Although the problem of harbor tranquility was previously studied with hydraulic models employing regular waves, the use of irregular waves for harbor tranquility tests (e.g., Ref. 9) has become popular. Generally speaking, a test with irregular waves on a harbor having many reflective waterfront lines often yields a wave height distribution quite different from a test with regular waves. Figure 7.4 shows an example of test results with irregular waves on the tranquility of a small harbor;[10] the distribution of wave height is shown with contour lines as the ratio formed with the incident significant wave height. An additional test was carried out for the same harbor layout with a train of regular waves equivalent to the significant wave. The distributions of wave
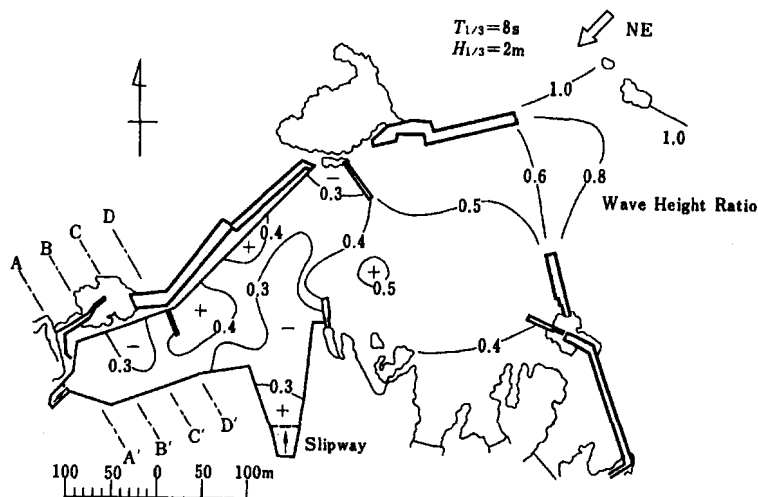
Fig. 7.4. Example of wave height distribution in a harbor by an irregular wave test.[10]
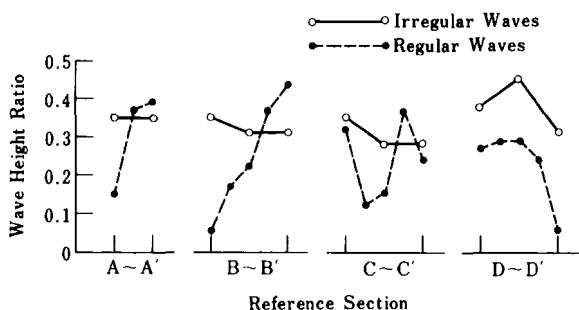
Fig. 7.5. Comparison of wave height ratios by regular and irregular wave tests.[10]

height by the irregular and regular wave tests were compared along the reference sections AA′ to DD′, and the results are shown in Fig. 7.5. The measured values of regular wave height exhibit extensive variations; a contour map of the wave height ratio would be very complicated, if it were even possible to draw. The wave height distribution also changes greatly for a slight change of wave period. In an actual field situation, the incident waves are composed of many frequency and directional components, as described by the spectra,

and different contributions of the wave components to the wave height at a particular location average out, yielding a rather smooth spatial variation of the wave height in a harbor. Model tests with an irregular train of waves are the better reproduction of the actually occurring distribution.

Model tests of harbor tranquility need to be done for multiple directions of wave approach, even if the predominant waves come from one direction only. It is due to the nature of directional spreading of random sea waves which exercises a significant effect on the wave height distribution behind breakwaters, as discussed in Sec. 3.2. The results of wave measurements for several wave directions are to be averaged using the weights representing the relative energy of respective directions. A practical formula for this process has been presented as Eq. (6.1) in Sec. 6.2.4. In addition to the hydraulic model tests, numerical simulation of wave height distributions for various harbor layouts should be carried out before the tests are undertaken. Because a harbor tranquility test requires a considerable duration of time for measurements of one harbor layout, the number of layouts which can be examined in the test is rather limited. A preliminary examination by numerical simulation can save the total cost, and yield the best solution with much credibility.

If a test basin with a conventional regular wave generator has to be mobilized for some reason, tests should be carried out for several representative component wave periods for one value of the significant wave period, as discussed in Sec. 3.1 for the analysis of random wave refraction with regular wave refraction diagrams. The values of the wave height ratio at various locations for several wave periods are to be combined to yield an energy-averaged value of the wave height ratio with the weights of the spectral areas for the respective wave periods. The tests should be repeated for several directions of wave approach, and the results are combined to yield weighted averages of the wave height ratio at various locations.

When a spectrally averaged data analysis is undertaken with a regular wave test facility, the number of measuring points should be reduced to a few tens or so. Otherwise, the test may have to be continued for a long time and the running cost may greatly increase. For this purpose, the engineer in charge of harbor planning should not ask for a general contour map of the wave height in the harbor from the hydraulic laboratory; rather, a limited number of points located at strategic locations in the harbor should be designated from the viewpoint of port operation. The test results not only should be analyzed in the form of a table of wave height ratios, or a distribution map, but they should

also be processed in the form of the exceedance probability of absolute values of the wave height at selected points in the harbor. This manner of processing the test results is important for full utilization of the information gained by a hydraulic model test of harbor tranquility.

7.3.2 *Model Tests for Breakwater Stability*

Experimental techniques for investigating breakwater stability differ depending on the type of breakwater. In the case of vertical breakwaters, there are two problems — the stability of the upright section and the stability of the armor units for the rubble mound foundation. The stability of an upright section can be studied either by measuring the wave pressure with miniature pressure gauges attached to the model breakwater, or by examining the sliding limit of the upright section, the weight of which is adjusted according to the similarity law. The measurements of was pressure, while providing detailed information on the time history and spatial variation of wave pressure, may not yield a clear answer to the question of breakwater stability, because a very high pressure recorded by a gauge does not necessarily indicate the danger of the sliding of an upright section if the duration of the high pressure is very short. The instrumentation for measurement of wave pressure on a model breakwater is rather complicated as well. Thus, the analysis of breakwater stability by means of pressure mesurement has the character of research-oriented experiments. It would appear that tests of breakwater stability with an examination of the sliding limit would be a more practical approach.

   In a sliding test of a model breakwater, the dimensions of the test section and the wave parameters should be reproduced according to the Froude law exemplified in Table 7.1. Before a test, the main features of the sea bottom topography are reproduced in a wave basin or flume, and the relationship between the wave height at the site of the breakwater and the amplitude of the wave paddle are investigated for test waves of different periods. Then a model of the upright section, the weight of which has been duly adjusted according to the Froude law, is placed on top of a model rubble mound, and the coefficient of friction is measured by means of a horizontal pulling test of the upright section. Finally, the test waves equivalent to the design wave (the highest wave in a wave group) are applied to the model breakwater, and inspection is made to determine if the test section slid under wave action. If no sliding occurred under the design wave, an effort should be made to determine

the limit of sliding either by increasing the height of the test waves or by gradually reducing the weight of the upright section.

Figure 7.6 is an example of results of sliding tests of model breakwaters reported by Tanimoto,[11] though it is rather research-oriented. He tested three models of vertical breakwaters by varying the berm width of the rubble mound foundation in front of an upright section. Using constant wave conditions, the weight of the upright section was varied, and the sliding distance per wave was measured. From such test data, the threshold weight of the upright section against sliding was estimated and the effective wave force for breakwater sliding was evaluated. In sliding tests with model breakwaters, the data of sliding distance usually show wide scatter with decrease in the mean sliding distance as the threshold condition is approached. Thus, the wave height or model weight should be varied over a broad range, so that the threshold condition of sliding can be determined with confidence.

As for the type of test waves, irregular waves are preferred. But irregular waves often suffer the problem of multireflection[b] between model breakwater
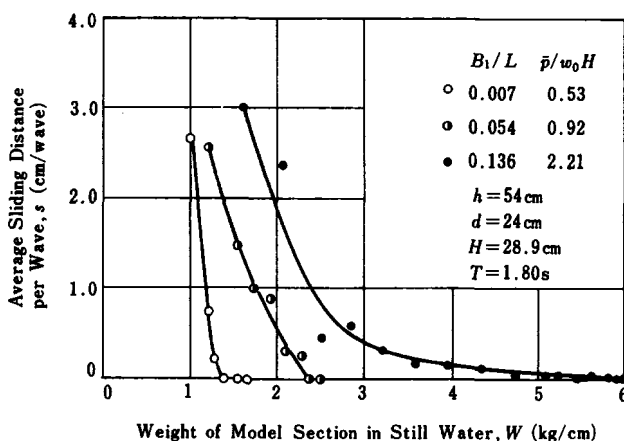
Fig. 7.6. Example of sliding test of the upright section of a vertical breakwater (after Tanimoto[11]).

---

[b]Waves are repeatedly reflected by both the model structure and the wave paddle, and travel back and forth many times between them in a wave flume. As a result, the wave conditions become quite different from the original system of a single train of incident waves. This phenomenon is called multireflection of waves in a wave flume.

and wave paddle, especially in the case of vertical breakwaters, which are highly reflective. In order to perform a test on a model structure with irregular waves for a sufficiently long duration, the effective coefficient of wave reflection between the paddle and the model should be less than about 60%.[12] One way to achieve this condition is to use a very long flume with effective wave damping by frictional energy loss. Another way is to provide a partition within the flume: the model is set in one of the partitioned flume and the other side is used to let part of the wave energy dissipate at the wave absorber at the end. With the use of the resolution technique of incident and reflected waves to be described in Sec. 10.4, a partitioned wave flume with an irregular wave generator is one of the standard facilities for tests of breakwaters and seawalls.

If the use of irregular waves is not feasible, stability testing of a vertical breakwater may be carried out with regular waves. This is possible because the stability of an upright section is mainly governed by the action of the single highest wave in a train of irregular waves. The calculation method of design wave force on a breakwater is based on the highest wave concept as described in Sec. 4.2.2.

The primary purpose of a scale model test of a breakwater is to confirm the stability of the design section against the attack of the design wave and to determine the threshold wave height or breakwater weight against sliding or other modes of failure. It is also interesting to examine the effective wave pressure acting on the design section of breakwater as related to the threshold weight of the upright section. The calculation formula is simply

$$P = \mu(W_c - U), \tag{7.4}$$

where P is the average wave pressure per unit length of breakwater, W_c the weight of the upright section per unit length in still water, μ the coefficient of friction between the model structure and rubble mound, and U the total uplift force per unit length. It is necessary to assume some kind of distribution of wave pressure along the front face and similarly for the uplift pressure along the bottom of upright section, as the wave uplift is an unknown quantity varying in proportion to the frontal wave pressure. The distribution shown in Fig. 4.4 may be employed for this purpose.

The stability of armor units of the rubble mound foundation of a vertical breakwater is studied with the same procedure as that for upright sections. That is, models of armor stones or concrete blocks are manufactured with

the scale selected and the same specific weight as that of the prototype, and their stability against the attack of the design wave is examined by visual inspection. If they are found to be stable against the design wave, the stability limit should be examined by gradually increasing the wave height. Such tests are best carried out with irregular waves. When regular waves have to be employed, there is some evidence of necessity to set the wave height above $H_{1/10}$.[13]

The stability of sloping mound breakwaters should be examined with irregular waves. Because sloping type structures in general exhibit low values of the wave reflection coefficient, the problem of multireflection between model structure and wave paddle is not serious. Test waves can be generated continuously, and an irregular train of test waves can be applied to sloping structures for a long duration. As in the case of vertical breakwaters, the first procedure is the calibration of the progressive waves at the site of the breakwater before its installation. This can be done by gradually varying the amplitude of the wave paddle at the appropriate wave periods through adjustment of the output level of the control signal to the wave generator. Various statistical parameters are analyzed from the wave records. At the same time, it is a good procedure to place a wave gauge at some distance offshore from the installation site of the test structure as a reference, especially when the breakwater is to be located within the surf zone.

After the installation of the model breakwater, it is useful to set two wave gauges separated by a short distance at a distance of more than one wavelength from the model. By employing the method of analysis described in Sec. 10.4, the two-gauge system makes possible the resolution of the incident and reflected heights of irregular waves during the test. Stability tests are carried out by gradually increasing the wave energy level (or significant wave height) and observing the stability of the armor units of the sloping mound. The wave height should be increased beyond the stability limit so as to obtain the relationship between the damage ratio of a particular breakwater section and the significant wave height.

A feature of irregular wave tests on armor unit stability is sensitivity of test results to the "wave-groupiness" of irregular wave trains employed. The wave-groupiness is a parameter proposed by Funke and Mansard[14] to describe the degree of the variation of instantaneous wave energy level. The wave-groupiness becomes large when the fluctuation of wave heights in a wave train

is large, compared to a wave train of small height fluctuation with the same mean height. According to a model test by Galland and Manoha,[15] the damage on armor stones of a sloping breakwater increased with the increase in the wave-groupiness, even though the target spectrum was the same. The profiles of irregular wave trains generated in a laboratory are dependent on the random phases assigned to individual frequency components. If twenty runs of irregular waves, say, are generated in a wave flume under the same target spectrum, the significant wave height of individual wave trains will exhibit a variation of several percent (see Sec. 9.6) and the wave-groupiness will vary to a larger extent. The damage on armor units will be different from one wave train to another. The results are better analyzed in a statistical manner to yield a distribution function of the damage ratio. Such a data will provide a vital information for establishment of the reliability-based design method for breakwaters. In any case, irregular wave tests should be repeated for several runs with different wave profiles under the same input condition so as to increase the reliability of test results.

7.3.3 *Model Tests for Wave Overtopping and Reflection of Seawalls and Other Structures*

The problems of wave run-up on coastal dikes, wave overtopping of revetments, and wave reflection by quaywalls of the energy-dissipating type are not easily solved theoretically. They are mainly investigated with hydraulic model tests. Various design diagrams of wave run-up and overtopping have been obtained through model experiments.

Model tests on wave overtopping should be made with irregular waves. A continuous train of one hundred to a few hundred waves is applied to a model seawall, and the total quantity of overtopped water mass is measured. If the seawall is highly reflective, such as in the case of vertical revetment, the technique of providing a partition in the test flume should be employed to suppress the multireflection of waves between the model seawall and the wave paddle. If the test has to be performed with a regular train of waves because no irregular wave facility is available, the wave overtopping should be measured over a range of wave height so that the calculation of the expected wave overtopping rate as discussed in Sec. 5.1.1 can be carried out.

The reflection coefficient of quaywalls and similar structures seems not to be greatly affected by wave irregularity. Thus, tests with regular waves may suffice for the purpose, though a test with irregular waves is recommended. Most energy-dissipating type quaywalls such as perforated or slit caissons and quaywalls made of specially shaped hollow concrete blocks, however, have a coefficient of wave reflection which depends on the ratio of the width of the hollow section to the wavelength. Tests with regular waves tend to exaggerate the period-dependent characteristics of the reflection coefficient. Test results of the reflection coefficient by regular waves should be interpreted by averaging over some range of wave period. Attention should be paid to the tendency of a vertical wall of the energy-dissipating type to generate reflected waves having components with harmonic frequencies of the incident waves; i.e., wave periods of one half, one third, etc. of the incident wave. In such a case, the conventional method of estimating the reflection coefficient from the maxima and minima of the wave envelope tends to yield a reflection coefficient lower than the actual value. It is recommended to employ the technique of resolving the incident and reflected wave height with a set of two wave gauges as described in Sec. 10.4.

7.4 Model Tests Using Multidirectional Wave Generators

The first multidirectional wave generator by Salter[2] was invented to study the effect of wave directionality on a special wave power extraction device of the floating type called the Salter duck. Offshore structures, especially of the floating type, have been the topics of intensive studies using multidirectional wave generators. The movements of an oil tanker berthed at a single-point mooring buoy, for example, are greatly enhanced in the multidirectional wave field in comparison with those in unidirectional irregular waves. On the other hand, an offshore platform experiences a reduction in the in-line wave load and an increase in the transverse wave load by introduction of multidirectional wave systems in model tests. Funke and Mansard[3] cite a number of cases in which the wave directionality becomes important in hydraulic model tests. Hiraishi[16] also presents several cases of model tests with multidirectional waves and discusses the directionality effects.

A constraint in the use of multidirectional waves in model tests is the relatively narrow test area in a wave basin, where the wave condition can be regarded homogeneous. Oblique waves generated from a finite width of

a generator cannot propagate into the full area of basin; they are attenuated in the zone of geometric shadow by the diffraction effect, and the wave height distribution along the wave crest becomes nonuniform. Because multidirectional random waves are made up of many oblique wave components of various directions, the effective width of the homogeneous wave area decreases as the distance from the generator increases. Some laboratories are trying to eliminate the restriction of the limited test area by providing two sets of multidirectional wave generators along the two sides of a rectangular basin and by employing sophisticated algorithms to control the two sets of wave generators in a coordinated manner; e.g., Ito *et al.*[17]

Another technical problem in a multidirectional wave basin is the absorption of reflected waves from a structure in a basin. In the case of wave flume tests, the technique for absorption of reflected waves by wave paddles has well been established and incorporated in the design of wave generators. In a multidirectional wave basin, reflected waves come back to the wave paddles with oblique angles of approach, the values of which are difficult to detect. Thus, wave absorption is usually made by assuming the normal incidence of reflected waves, though attempts are being made to realize full absorption of oblique reflected waves. A review on this wave absorption problem is found in Schäffer and Klopman.[18]

A model test of harbor tranquility in a multidirectional wave basin is feasible if the harbor entrance is single and fits within the zone of effective test area. A three-dimensional stability test of a breakwater head seems to be suited for a multidirectional wave basin, because Matsumi *et al.*[19] have observed larger damage on a breakwater head by multidirectional waves than by unidirectional irregular waves. Another subject to be tested in a multidirectional basin is the spatial variation of wave run-up and/or overtopping along a finite extension of seawall. It is known that wave heights along a barrier of finite extension vary by the effect of wave diffraction from the tips of the barrier. Because the diffraction effect is a function of wave frequency and direction, a test with multidirectional random waves is expected to yield a smaller variation of wave heights, and thus more uniform run-up and/or overtopping than a test with unidirectional irregular waves.

Use of multidirectional wave basins has become popular only recently. Many model tests of various types will be performed in these basins, and the experiences will advance the knowledge and technology of random wave tests.

References

1. Y. Goda, "Discussion of several factors for the improvement of the accuracy of wave tests in laboratory tanks," *Proc. 15th Japanese Conf. Coastal Engrg.* (1968), pp. 50–56 (*in Japanese*).
2. S. H. Salter, "Absorbing wave-makers and wide tanks," *Proc. Symp. Directional Wave Spectra Applications*, ASCE (1981), pp. 185–202.
3. E. R. Funke and E. P. D. Mansard, "On the testing of models in multidirectional seas," *Proc. 23rd Int. Conf. Coastal Engrg.* (Delft, 1992), pp. 3454–3465.
4. E. P. D. Mansard, "A survey of multidirectional wave facilities," *Proc. IAHR Seminar on Multidirectional Waves and Their Interaction with Structures*, (27th IAHR Congress, San Francisco, 1977), published by National Research Council of Canada, pp. 195–226.
5. F. Biésel and F. Suquet, "Les apparails générateurs de houle en laboratoire," *La Houille Blanche*, 6 (2, 4, et 5) (1951) (translated by St. Anthony Falls Hydr. Lab., Univ. Minnesota, Rept. No. 39).
6. D. K. Freyer, G. Gilbert, and M. J. Wilkie, "A wave spectrum synthesizer," *J. Hydraulic Res.* 11 (3) (1973), pp. 193–204.
7. E. R. Jefferys, "Directional seas should be erogodic," *Applied Ocean Res.* 9 (4) (1987), pp. 186–191.
8. M. D. Miles and E. R. Funke, "A comparison of methods for synthesis of directional seas," *Proc. 6th Int. Offshore Mech. and Arctic Engrg.* (1987), pp. 247–255.
9. T. Sorensen, "Model tests with irregular waves," *The Docks and Harbour Authority* (May 1973).
10. Y. Goda, Y. Suzuki, and K. Hachisuka, "The analysis of the calmness in a harbor with irregular waves," *Tech. Note, Port and Harbour Res. Inst.* (271) (1977), 53p. (*in Japanese*).
11. K. Tanimoto, "Wave forces on a composite type breakwater," *Proc. 1976 Annual Res. Presentation of Port and Harbour Res. Inst.* (1976), pp. 1–26 (*in Japanese*).
12. K. Tanimoto, E. Tomida, and T. Muranaga, "Influence of re-reflection from a wave paddle on irregular incident waves," *Tech. Note, Port and Harbour Res. Inst.* (467) (1983), 23p. (*in Japanese*).
13. K. Tanimoto, T. Yagyu, and Y. Goda, "Irregular wave tests for composite breakwater foundations," *Proc. 18th Int. Conf. Coastal Engrg.* (Cape Town, 1982), pp. 2144–2163.
14. E. R. Funke and E. P. D. Mansard, "On the synthesis of realistic sea state," *Proc. 17th Int. Conf. Coastal Engrg.* (Sydney, 1980), pp. 2974–2991.
15. J. C. Galland and B. Manoha, "Influence of wave grouping on the stability of rubble mound breakwaters," *Proc. 24th Int. Assoc. Hydr. Res. (IAHR) Congress* (Madrid, 1991), pp. B-43–B-49.
16. T. Hiraishi, "Effect of wave directionality to wave action on coastal structures," *Proc. IAHR Seminar on Multidirectional Waves and Their Interaction with Structures* (27th IAHR Congress, San Francisco, 1977), published by National Research Council of Canada, pp. 399–412.

17. K. Ito, H. Katsui, M. Mochizuki, and M. Isobe, "Non-reflected multidirectional wave maker theory and experiments of verification," *Proc. 25th Int. Conf. Coastal Engrg.* (Orlando, U.S.A., 1996).

18. H. A. Schäffer and G. Klopman, "Review of multidirectional active wave absorption methods," *Proc. IAHR Seminar on Multidirectional Waves and Their Interaction with Structures* (27th IAHR Congress, San Francisco, 1977), published by National Research Council of Canada, pp. 159–182.

19. Y. Matsumi, E. P. D. Mansard, and J. Rutledge, "Influence of wave directionality on stability of breakwater heads," *Proc. 24th Int. Conf. Coastal Engrg.* (Kobe, 1994), pp. 1397–1441.

Part II

Statistical Theories of Random Sea Waves

Chapter 8

Description of Random Sea Waves

8.1 Profiles of Progressive Waves and Dispersion Relationship

In Part I, we discussed engineering applications of irregular wave theories to the design of coastal and harbor structures. In Chapter 8 to 10, we are going to describe the theories of random sea waves themselves and techniques for the analysis of random wave data.

As presented in Sec. 2.3, random sea waves are assumed to be representable as a superposition of an infinite number of small amplitude waves having different frequencies and directions of propagation. The profile of an individual wave is expressed as

$$\eta = a \, \cos(kx \, \cos \theta + ky \, \sin \theta - 2\pi f t + \varepsilon) \,, \tag{8.1}$$

where η denotes the elevation of the water surface above the mean water level, a is the wave amplitude, $k = 2\pi/L$ is the wavenumber with L being the wavelength, θ is the angle between the x-axis and the direction of wave propagation, f is the wave frequency, ε is the phase angle, and x, y, and t are the space and time coordinates.

This component wave has the properties of a small amplitude wave as derived from velocity potential theory, and it is assumed to propagate freely without interacting with the other component waves. While this component wave propagates, an energy E is added to the body of water having unit surface area:

$$E = \frac{1}{2}\rho g a^2 \,. \tag{8.2}$$

This is actually the density of the wave energy. The symbol ρ denotes the density of sea water and g denotes the acceleration of gravity. There exists the following relationship between the wavenumber k and the frequency f:

$$\omega^2 = 4\pi^2 f^2 = gk \tanh kh, \tag{8.3}$$

in which $\omega = 2\pi f$ denotes the angular frequency and h is the water depth.

Equation (8.3) is called the dispersion relationship, which is obtained from the surface boundary condition at the water surface. This equation can be rewritten to give the standard relationship between the wavelength L and the wave period T:

$$L = \frac{g}{2\pi} T^2 \tanh \frac{2\pi h}{L}. \tag{8.4}$$

This is a transcendental equation, and the value of L for the given h and T can be obtained numerically to a specified accuracy by an iterative computation.[a] In any calculation related to the problems of sea waves, either Eq. (8.3) or (8.4) must be solved to obtain L. Here we shall give an iterative solution procedure.

First, Eq. (8.3) is transformed to

$$x \tanh x = D, \tag{8.5}$$

in which

$$\left. \begin{array}{l} D = \omega^2 h/g = 2\pi h/L_0, \quad L_0 = 2\pi g/\omega^2 = gT^2/2\pi, \\ x = kh = 2\pi h/L. \end{array} \right\} \tag{8.6}$$

Although Eq. (8.5) can be solved directly using Newton's method, it is a good procedure to first rewrite it as follows in order to remove the inflection point:

$$y(x) = x - D \coth x. \tag{8.7}$$

By this technique, an iterative solution can be obtained through the following equation:

$$x_2 = x_1 - \frac{y(x_1)}{y'(x_1)} = x_1 - \frac{x_1 - D \coth x_1}{1 + D(\coth^2 x_1 - 1)}. \tag{8.8}$$

The best estimate for the initial value is

$$x_1 = \begin{cases} D & : D \geq 1, \\ D^{1/2} & : D < 1. \end{cases} \tag{8.9}$$

---

[a] An explicit polynomial approximation for the wavelength is also available, due to Hunt.[1]

The error in Eq. (8.8) rapidly decreases with increase in the iteration number. In fact, the absolute error $|1 - x_2/x_1|$ is less than 0.05% by the third iteration (for x_4). Figure 8.1 provides the FORTRAN program for the computation of the wavelength by the above method. Tables A-1 to A-4 in the Appendix list values of the wavelength and wave celerity as a function of water depth and wave period as computed with this program.

```
PI2 = 2. * 3.141592654
D = PI2 * DEPTH/(9.8 * T ** 2/PI2)
WAVEL = PI2 * DEPTH/WAVE(D)

        FUNCTION WAVE(D)
        IF(D-10.0) 2 , 2 , 1
    1   XX = D
        GŌ TŌ 6
    2   IF(D-1.0) 3 , 4 , 4
    3   X = SQRT(D)
        GŌ TŌ 5
    4   X = D
    5   CŌTHX = 1./ TANH(X)
        XX = X - ( X - D * CŌTHX)/
      +     (1. + D * ( CŌTHX ** 2 - 1.))
        E = 1. - XX/X
        X = XX
        IF(ABS(E) - 0.0005) 6 , 5 , 5
    6   WAVE = XX
        RETURN
        END
```

Water Depth : DEPTH (m)
Wave Period : T (sec)
Wavelength : WAVEL (m)

Fig 8.1. FORTRAN program for the computation of wavelength.

8.2 Description of Random Sea Waves by Means of Variance Spectrum

Profiles of random sea waves can be expressed by means of various mathematical representations, including one using complex vectors. The differences among these representations are purely a matter of convenience for the particular mathematical manipulations of interest. For general purposes, the following

series expression is the most easily understood:

$$\eta = \eta(x, y, t) = \sum_{n=1}^{\infty} a_n \, \cos(k_n x \, \cos \theta_n + k_n y \, \sin \theta_n - 2\pi f_n t + \varepsilon_n). \quad (8.10)$$

This expression assigns a number to each combination of frequency and propagation direction of the infinite number of component waves and then sums up the components; it was first employed by Longuet-Higgins.[2]

The interpretation of random sea waves as a linear superposition of free progressive waves is an assumption, the correctness of which cannot be proven but, rather, must be supported through evidence of agreement between the properties of real sea waves and those derived from the mathematical model. Most properties of sea waves have been successfully explained with the model of Eq. (8.10), except for some nonlinear behavior to be discussed in Sec. 9.5. Thus, Eq. (8.10) can be considered to be a valid assumption.

The validity of Eq. (8.10) rests on four conditions. First, the frequencies f_n must be densely distributed between zero and infinity in such a manner that any infinitesimal interval df contains an infinite number of frequencies f_n. Second, the directions θ_n must be densely distributed between $-\pi$ and π with an infinite number of θ_n contained in an infinitesimal interval $d\theta$. Third, the phase angles ε_n must be randomly and uniformly distributed between 0 and 2π. Fourth, though the amplitude of each wave is infinitesimal, the summation of its square should have a finite and unique value. By denoting this value as $S(f, \theta)$, it is expressed as

$$\sum_{f}^{f+df} \sum_{\theta}^{\theta+d\theta} \frac{1}{2} a_n^2 = S(f, \theta) df \, d\theta. \quad (8.11)$$

The function $S(f, \theta)$ defined by Eq. (8.11) is called the directional wave spectrum density function, or the *directional wave spectrum*. It represents the manner in which wave energy[b] is distributed with respect to frequency f and angle θ.

The directional wave spectrum can also be expressed as a function of wavenumber k and angle θ. By considering the energy density contained in the interval from k to $k + dk$ and from θ to $\theta + d\theta$, we can obtain the following

---

[b]Although the energy of a wave is given by $\rho g a^2 / 2$ as in Eq.. (8.2), it is customary to omit the factor ρg for simplicity.

expression for the directional wave spectrum in the wavenumber domain:

$$\sum_{k}^{k+dk} \sum_{\theta}^{\theta+d\theta} \frac{1}{2}a_n^2 = S_k(k,\theta)dk\,d\theta.\tag{8.12}$$

Figure 8.2 schematically shows $S_k(k,\theta)$ in the $k-\theta$ domain; the coordinate (u,v) is the Cartesian representation of the polar coordinate (k,θ). The figure only exhibits the density function for a given wavenumber k; the general representation of $S_k(k,\theta)$ is an envelope surface in the range of $0 < k < \infty$.
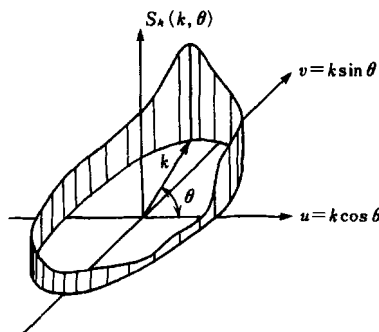
Fig. 8.2. Schematic representation of directional wave spectrum.

Often the directional wave spectrum is expressed in the form of a map of contour lines, the value on each line representing the absolute value of $S_k(k,\theta)$.

The directional wave spectrum in terms of the wave frequency, $S(f,\theta)$, and that in terms of the wavenumber, $S_k(k,\theta)$, are connected through the dispersion relationship, Eq. (8.3). The conversion between $S(f,\theta)$ and $S_k(k,\theta)$ is not a linear transformation but a one-to-one correspondence. In a detailed analysis of actual wave spectra, however, the conversion between $S_k(k,\theta)$ and $S(f,\theta)$ cannot be made in a one-to-one manner because of the existence of nonlinear wave components. In the case of wind waves, the presence of drift currents deforms the dispersion relation and the conversion becomes somewhat complex.

Equation (8.10) provides a description of random sea waves, the profiles of which are changing from place to place and from time to time. When we consider the profile of irregular waves observed at a fixed point in the sea such

as recorded by a wave gauge, the wave profile is expressed as

$$\eta = \eta(t) = \sum_{n=1}^{\infty} a_n \, \cos(2\pi f_n t + \varepsilon_n) \,. \tag{8.13}$$

The amplitudes a_n and the phase angles ε_n carry meanings slightly different from those associated with Eq. (8.10), in which a_n and ε_n represented the amplitudes and the phase angles of freely propagating independent waves. In the case of Eq. (8.13), however, the elementary amplitudes and phases are the result of mathematical manipulation of all waves propagating into different directions but having the same frequencies, such that they are added together, and the result is rewritten as a sum of sinusoidal functions. Thus, the component waves in Eq. (8.13) do not represent physical reality by themselves. Of course, we are always free to analyze an irregular time-varying function, such as shown in Fig. 2.2 in Sec. 2.1, in the form of a Fourier series without attaching any particular physical meaning.

In any case, Eq. (8.13) implies that the summation of the squares of wave amplitudes over an interval from f to $f + df$ is finite and unique. The value of the sum is denoted by $S(f)$ and is given by

$$\sum_{f}^{f+df} \frac{1}{2} a_n^2 = S(f) df \,. \tag{8.14}$$

The function of $S(f)$ is called the *variance wave spectrum density* or, simply, the *frequency spectrum.*

8.3 Stochastic Process and Variance Spectrum

The representation of random sea waves by Eqs. (8.10) and (8.13) in the foregoing section implies that the profile of sea waves η can be expressed as a stochastic process satisfying the three conditions of stationarity, ergodicity, and a Gaussian process. Here, the terminology of stochastic process refers to the ensemble of variables such that the quantity in question varies randomly with time; its value at a specific time cannot be given deterministically, but each value occurs according to a certain probabilistic law. The independent variable can also be a space coordinate instead of time.

Let us assume that we could obtain an infinite number of wave records of $\eta_1(t), \eta_2(t), \ldots$, all of different profiles, but corresponding to the same sea state

having the same significant wave height and period.[c] Then, the above wave profiles as a stochastic process are expressed as

$$\eta(t) = \{\eta_1(t), \eta_2(t), \dots, \eta_j(t), \dots\}. \tag{8.15}$$

The braces { } denote an ensemble, and Eq. (8.15) means that the sample records are considered to have come from the ensemble. Furthermore, we assume that the probability density of the wave profile η is given not for one sample $\eta_j(t)$ but for the ensemble itself at a particular time t.

The first condition, *stationarity*, refers to the property that all statistical properties as ensemble means are time-invariant. For example, the stationarity condition applied to the arithmetic mean and the autocorrelation function gives

$$E[\eta(t)] = E[\eta(0)] \equiv \bar{m} \quad -\infty < t < \infty, \tag{8.16}$$

$$E[\eta(t+\tau)\eta(t)] = E[\eta(\tau)\eta(0)] \equiv \Psi(\tau) \quad -\infty < t < \infty, \tag{8.17}$$

in which

$$E[\eta(t)] = \lim_{N \to \infty} \frac{1}{N} \sum_{j=1}^{N} \eta_j(t), \tag{8.18}$$

$$E[\eta(t+\tau)\eta(t)] = \lim_{N \to \infty} \frac{1}{N} \sum_{j=1}^{N} \eta_j(t+\tau)\eta_j(t). \tag{8.19}$$

We can define several other statistics. Nevertheless, when a process satisfies the conditions of Eqs. (8.16) and (8.17) alone and the variance $\mathrm{Var}[\eta(t)] = E[(\eta - E[\eta])^2]$ is finite, it is called a weakly stationary stochastic process.[2] If the probability density of η is expressed by a Gaussian distribution, however, Eqs. (8.16) and (8.17) become sufficient conditions to make the process a stationary stochastic process in the strict sense, and all other statistics become stationary. When the independent variable is the space coordinate and the process is spatially stationary, it is called homogeneous.

The second condition, *ergodicity*, refers to the property that the time-averaged statistics for a particular sample $\eta_j(t)$ are equal to those of the

---

[c]This cannot be achieved in the real sea. But we can approach this situation in wind–water tunnel experiments by repeating the same test condition. The starting point of the time coordinate in such experiments should be taken after the same elapsed time of a sufficiently long duration after the turning-on of the wind blower.

ensemble average, that is,

$$E[\eta(t)] = \overline{\eta_j(t)} = \lim_{t_0 \to \infty} \frac{1}{t_0} \int_0^{t_0} \eta_j(t) dt \,, \tag{8.20}$$

$$E[\eta(t+\tau)\eta(t)] = \overline{\eta_j(t+\tau)\eta_j(t)} = \lim_{t_0 \to \infty} \frac{1}{t_0} \int_0^{t_0} \eta_j(t+\tau)\eta_j(t) dt \,. \tag{8.21}$$

A stochastic process which possesses ergodicity is always a stationary process, but the reverse is not necessarily true. However, if the probability density of the wave profile is described by a Gaussian distribution and the process does not contain periodic functions with certain periods (i.e., no components of regular waves), then the stationary process possesses the property of ergodicity.[3] For such a process, any statistic of the wave profile can be obtained by taking the time average of a sample; i.e., a wave record. The standard procedures for the spectral calculation of sea wave records to be discussed in Chapter 10 are based on the assumption of ergodicity.

The third condition, a *Gaussian process*, refers to the property that the probability density of a wave profile taking a value between η and $\eta + d\eta$ at a certain time is given by a Gaussian (or normal) distribution as in the following:

$$p(\eta)d\eta = \frac{1}{(2\pi m_0)^{1/2}} \exp\left[-\frac{(\eta - E[\eta])^2}{2m_0}\right] d\eta \,, \tag{8.22}$$

in which

$$m_0 = E[(\eta - E[\eta])^2] = E[\eta^2] - E[\eta]^2 = \eta_{\text{rms}}^2 \,. \tag{8.23}$$

The quantity defined by Eq. (8.23) is the variance of the wave profile, which can be calculated from the time-average of $\eta^2(t)$ if the ergodicity condition is satisfied.

The applicability of the above three conditions for random sea waves has not been rigorously verified. First, it is impossible to collect a true ensemble of wave records for a prescribed sea state, because sea states are all different in time and space. This is easily understood when we think of the physical processes of wave generation, growth and decay. Therefore, stationarity and ergodicity can never be verified for sea waves. We may, in principle, collect an ensemble for a stochastic process by taking a wave record of long duration, but we cannot expect stationarity because the significant wave height and other statistics are known to vary with respect to time. However, we can expect constancy of a sea state for a short duration of several minutes to a few tens

of minutes, and thus we can assume stationarity for such short wave records. As for ergodicity, we usually assume that it holds for sea waves as there is no reason or evidence to believe that it does not hold. Thus, we shall employ the theory of stationary stochastic processes for the analysis of random sea waves.

The assumption of a Gaussian distribution for the wave profile is known to be inapplicable, as demonstrated by a slight departure from the Gaussian distribution, to be discussed in Sec. 9.5. The discrepancy becomes quite noticeable for waves in shallow water. However, as the assumption of a Gaussian process is essential for decomposing random sea waves into an infinite number of component waves being superposed linearly, we intentionally make this assumption so that we can employ various statistical theories for the analysis of sea waves. It should be mentioned here that the theory of stationary stochastic processes is not limited to Gaussian processes (see Ref. 4, for example).

In the analysis of stationary stochastic process possessing ergodicity, the process is assumed to have a zero mean value, $E[\eta(t)] = 0$, in most cases. This condition is easily realized by subtracting the arithmetic mean from the original process. Thus, in the following, discussion is limited to processes satisfying

$$E[\eta(t)] = \overline{\eta(t)} \equiv 0 \,. \tag{8.24}$$

For the case of a gradually varying mean water level such as encountered on wave records in waters with large tidal ranges, Eq. (8.24) can be satisfied by subtracting the time-varying mean water level from the record and by regarding the resultant wave profile as a stochastic process.

The autocorrelation function expressed by Eq. (8.17) is called the autocovariance function for a zero-mean process in the strict sense, but the terminology "autocorrelation function" is also often applied to a stochastic process with a zero mean value when the necessity to distinguish between them is slight. For a stationary stochastic process, there exists a function $S(f)$ as defined by the following equation for a given autocovariance function $\Psi(\tau)$ defined by Eq. (8.17):

$$\Psi(\tau) = \int_0^\infty S(f) \cos 2\pi f \tau \, df \,. \tag{8.25}$$

The function $S(f)$ can be expressed as follows, according to the theory of the Fourier transform, under the condition that the integral of $|\Psi(\tau)|^2$ over the full

range of τ remains finite:

$$S(f) = 4 \int_0^\infty \Psi(\tau) \cos 2\pi f \tau d\tau . \tag{8.26}$$

The set of Eqs. (8.25) and (8.26) is called the Wiener–Khintchine relations, the generalized expression of which has symmetry of the following form defined in the ranges of τ and f from $-\infty$ to ∞:

$$\left. \begin{aligned} \Psi(\tau) &= \int_{-\infty}^\infty S_0(f) e^{i2\pi f \tau} df \\ S_0(f) &= \int_{-\infty}^\infty \Psi(\tau) e^{-i2\pi f \tau} d\tau \end{aligned} \right\} . \tag{8.27}$$

The suffix '0' is attached to the frequency spectrum $S_0(f)$ in Eq. (8.27) in order to identify its definition in the range of $f = -\infty$ to ∞. By redefining Eq. (8.27) in the positive range $[0, \infty)$ for both τ and f, and by taking the Fourier cosine transform of Eq. (8.27), we can obtain Eqs. (8.25) and (8.26).

Let us examine the above relations by calculating the autocovariance function of the irregular wave profile expressed by Eq. (8.13).

$$\begin{aligned} \Psi(\tau) &= \lim_{t_0 \to \infty} \frac{1}{t_0} \int_0^{t_0} \sum_{n=1}^\infty \sum_{m=1}^\infty a_n a_m [\cos(2\pi f_n(t+\tau) + \varepsilon_n] \cos[2\pi f_m t + \varepsilon_m] dt \\ &= \lim_{t_0 \to \infty} \frac{1}{t_0} \int_0^{t_0} \sum_{n=1}^\infty \sum_{m=1}^\infty a_n a_m \\ &\quad \times [\cos(2\pi f_n t + \varepsilon_n) \cos(2\pi f_m t + \varepsilon_m) \cos 2\pi f_n \tau \\ &\quad - \sin(2\pi f_n t + \varepsilon_n) \cos(2\pi f_m t + \varepsilon_m) \sin 2\pi f_n \tau] dt \\ &= \frac{1}{2} \sum_{n=1}^\infty a_n^2 \cos 2\pi f_n \tau . \end{aligned} \tag{8.28}$$

In the above calculation, we have made use of the orthogonality property of trigonometric functions (integrals of the products of cosine functions with $n \ne m$ converge to zero as $t_0 \to \infty$ and integrals of all products of sine and cosine functions including $n = m$ converge to zero as $t_0 \to \infty$). By substituting

Eq. (8.28) into (8.26), we obtain

$$S(f) = 2 \int_0^\infty \sum_{n=1}^\infty a_n^2 \cos, 2\pi f_n \tau \ \cos 2\pi f \tau d\tau$$

$$= \sum_{n=1}^\infty a_n^2 \int_0^\infty [\cos 2\pi(f_n + f)\tau + \cos 2\pi(f_n - f)\tau]d\tau . \qquad (8.29)$$

The frequency f is regarded as a constant in the above manipulation. The integral on the right side of Eq. (8.29) gives two Dirac–delta functions, at $f_n = -f$ and $f_n = f$. Here we take only the delta function at $f_n = f$ as we are dealing with the problem in the half range of positive frequency, $0 \geq f < \infty$. Furthermore, the standard delta function is defined as an integral over the full range of $(-\infty, \infty)$, and therefore we should take one half the value of the delta function for Eq. (8.29). The result becomes

$$S(f) = \sum_{n=1}^\infty \frac{1}{2} a_n^2 \delta(f_n - f) . \qquad (8.30)$$

The delta function $\delta(f_n - f)$ is now approximated as $1/df$ for the frequency range from f to $f + df$ and zero outside the range. Thus, we have

$$S(f) = \frac{1}{df} \sum_f^{f+df} \frac{1}{2} a_n^2 . \qquad (8.31)$$

This is in agreement with Eq. (8.14) which defines the frequency spectrum for irregular waves. Thus, the function $S(f)$ defined by Eq. (8.26) in terms of the autocovariance function is shown to be the variance spectral density function. The above relation forms the basis of a calculational procedure for making spectral estimates of random processes, known as the Blackman–Tukey method,[6] by means of the autocorrelation function.

It should be added here that by definition, the autocovariance function of Eq. (8.17) for $\tau = 0$ gives the variance of the wave profile m_0, and that the following relation between m_0 and the integral of the spectrum can be derived from Eq. (8.25) as

$$m_0 = \overline{\eta^2} = \Psi(0) = \int_0^\infty S(f)df . \qquad (8.32)$$

This relation can also be derived from Eqs. (8.13) and (8.14).

References

1. J. N. Hunt, "Direct solution of wave dispersion equation," *Proc. ASCE* **105** (WW4) (1979), pp. 457–460.
2. M. S. Longuet-Higgins, "The statistical analysis of a random, moving surface," *Philos. Trans. R. Soc. London, Ser. A* (*966*) **249** (1957), pp. 321–387.
3. L. H. Koopmans, *The Spectral Analysis of Time Series* (Academic Press, 1974), p. 38.
4. Koopmans, loc. cit., p. 54.
5. Koopmans, loc. cit., p. 258.
6. R. B. Blackman and J. W. Tukey, *The Measurement of Power Spectra* (Dover Pub., Inc., 1958), 190p.

Chapter 9

Statistical Theory of Irregular Waves

9.1 Distribution of Waves Heights

9.1.1 *Envelope of Irregular Wave Profile*

In this chapter, we deal with the statistics of irregular wave trains on the basis of their mathematical expression by Eq. (8.13) in Sec. 8.1. The first item of the statistical description to be defined for an irregular wave profile is the wave amplitude, or height. The basic theory of the statistics of wave amplitudes was given by Rice.[1] Let us consider the case in which the energy of the wave spectrum is concentrated within a narrow range of frequency. Such a spectrum is said to be narrow-banded. A typical profile of waves with a narrow-band spectrum is schematically drawn in Fig. 9.1, for which it is seen that the individual waves have almost the same period but gradually varying amplitudes. In order to express such a feature of wave profiles more clearly, Eq. (8.13) is rewritten as follows:

$$\eta(t) = \sum_{n=1}^{\infty} a_n \cos(2\pi f_n t + \varepsilon_n) = Y_c(t) \cos 2\pi \bar{f} t - Y_s(t) \sin 2\pi \bar{f} t, \qquad (9.1)$$

where

$$\left.\begin{array}{l} Y_c(t) = \displaystyle\sum_{n=1}^{\infty} a_n \cos(2\pi f_n t - 2\pi \bar{f} t + \varepsilon_n)\,, \\[2mm] Y_s(t) = \displaystyle\sum_{n=1}^{\infty} a_n \sin(2\pi f_n t - 2\pi \bar{f} t + \varepsilon_n)\,. \end{array}\right\} \qquad (9.2)$$

The frequency $\bar{f}$ can be any representative frequency in the spectral range where most of the wave energy is concentrated. For example, the following
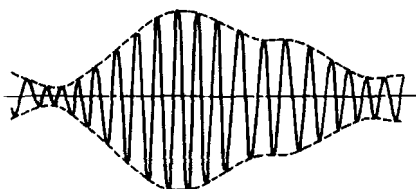
Fig. 9.1. Envelope of an irregular wave profile.

mean frequency defined with the first and zeroth spectral moments is one of the candidates:

$$\bar{f} = m_1/m_0 \,, \tag{9.3}$$

where

$$m_n = \int_0^\infty f^n S(f) df \,. \tag{9.4}$$

Furthermore, the amplitude R and phase angle ϕ are defined in terms of Y_c and Y_s in Eq. (9.2) as

$$R = R(t) = \sqrt{Y_c^2(t) + Y_s^2(t)} \,, \tag{9.5}$$

$$\phi = \phi(t) = \tan^{-1}[Y_s(t)/Y_c(t)] \,. \tag{9.6}$$

These relations can be rewritten as

$$Y_c(t) = R \cos \phi \,, \quad Y_s(t) = R \sin \phi \,. \tag{9.7}$$

Then by using the quantities R and ϕ, the wave profile $\eta(t)$ can be expressed as follows:

$$\eta = R(t) \cos \left[2\pi \bar{f} t + \phi(t) \right] \,. \tag{9.8}$$

This equation shows that the amplitude R and phase angle ϕ of the oscillations with the mean frequency $\bar{f}$ vary with elapsed time. The variation is quite gradual in the case of a narrow-band spectrum, and the amplitude $R = R(t)$ gives the amplitude of the wave envelope, which is indicated by the dashed lines in Fig. 9.1.

Next, the probability distribution of the envelope amplitude R is considered. Examination of the nature of the amplitudes Y_c and Y_s reveals that both amplitudes are stationary Gaussian stochastic processes (by virtue of the central limit theorem). Both amplitudes have the variance of

$$E[Y_c^2] = E[Y_s^2] = E[\eta^2] = m_0 \,. \tag{9.9}$$

Also, we find $E[Y_c Y_s] = 0$, and thus they are mutually independent. The probability that Y_c and Y_s simultaneously take values between $[Y_c, Y_c + dY_c]$ and $[Y_s, Y_s + dY_s]$, respectively, is given as the product of the probability density functions of two normal distributions. Thus,

$$p(Y_c, Y_s)dY_c dY_s = \frac{1}{2\pi m_0} \exp\left[-\frac{Y_c^2 + Y_s^2}{2m_0}\right] dY_c dY_s. \tag{9.10}$$

By changing variables to R and ϕ by means of Eq. (9.7) and using the relation $dY_c dY_s = R\, dR\, d\phi$, we obtain

$$p(R, \phi)dR\, d\phi = \frac{R}{2\pi m_0} \exp\left[-\frac{R^2}{2m_0}\right] dR\, d\phi. \tag{9.11}$$

However, R and ϕ are uncorrelated independent variables. Therefore, the probability density function $p(R, \phi)$ can be expressed as the product of two functions $p(R)$ and $p(\phi)$. Moreover, since Eq. (9.11) does not contain a function of ϕ, $p(\phi)$ must be constant in the range between $\phi = 0$ and 2π. That is, ϕ is distributed uniformly between 0 and 2π, with the probability density $1/2\pi$. Thus, the probability density function of R is derived as

$$p(R)dR = \frac{R}{m_0} \exp\left[-\frac{R^2}{2m_0}\right] dR. \tag{9.12}$$

9.1.2 *The Rayleigh Distribution of Wave Heights*

(A) *Theory for narrow-band spectral waves*

Equation (9.12) was derived by Rayleigh as the equation describing the distribution of the intensity of sound, which is the superposition of sound waves from an infinite number of sources. It is therefore called the Rayleigh distribution. From this theory of envelope amplitude, the probability density function of wave height is directly obtained as described below.

The assumption of a narrow-band spectrum leads to the very small probability that the maxima of the wave profile are located elsewhere other than as the wave crests, as will be described in Sec. 9.4. Therefore, the wave envelope $R = R(t)$ is regarded to represent the amplitudes of the individual waves themselves. Furthermore, the probabilities of wave crests and troughs are symmetric, because the theory presupposes linearity of the wave profile. Thus, the

wave height H can be regarded as twice the envelope amplitude R, and its probability density function is immediately obtained as

$$p(H)dH = \frac{H}{4m_0} \exp\left[-\frac{H^2}{8m_0}\right] dH\,.\tag{9.13}$$

Longuet-Higgins[2] derived the relationships between several characteristic wave heights based on this probability density function.

First, the mean height and the root-mean-square height are calculated to be

$$\overline{H} = \int_0^\infty H\,p(H)dH = (2\pi m_0)^{1/2}\,,\tag{9.14}$$

$$H_{\mathrm{rms}}^2 = \overline{H^2} = \int_0^\infty H^2 p(H)dH = 8m_0\,.\tag{9.15}$$

With these results, Eq. (9.13) can be rewritten in a generalized form as

$$p(x)dx = 2a^2 x \exp[-a^2 x^2]dx\,,\tag{9.16}$$

where
$$x = H/H_*\ :\ H_*\text{an arbitrary reference wave height}$$

$$a = \frac{H_*}{(8m_0)^{1/2}} = \begin{cases} 1/2\sqrt{2} : H_* = m_0^{1/2} = \eta_{\mathrm{rms}}\,, \\ \sqrt{\pi}/2\ \ : H_* = \overline{H}\,, \\ 1\ \ \ \ \ \ : H_* = H_{\mathrm{rms}}\,. \end{cases}\tag{9.17}$$

Equation (2.1) in Sec. 2.2.1 is the expression of Eq. (9.16) when the reference wave height is taken as $H_* = \overline{H}$.

Next, the mean of the highest $1/N$th waves is calculated. It is necessary to obtain the threshold wave height which has the probability of exceedance of $1/N$. By employing Eq. (9.16) for the purpose of a general discussion, the probability of exceedance[a] of the wave height ratio x is obtained as

$$P(x) = P[\xi > x] = \int_x^\infty p(\xi)d\xi = \exp[-a^2 x^2]\,.\tag{9.18}$$

---

[a] $P(x)$ is equal to the difference between 1 and the value of the distribution function of x.

Thus, the wave height ratio x_N, which has the exceedance probability of $P(x_N) = 1/N$, is calculated as

$$\exp[-a^2 x_N^2] = 1/N, \quad \text{or} \quad x_N = \frac{1}{a}(\ln N)^{1/2}. \tag{9.19}$$

The mean of the highest $1/N$th waves, denoted as $x_{1/N}$, is then calculated as

$$x_{1/N} = \frac{\int_{x_N}^{\infty} x p(x) dx}{\int_{x_N}^{\infty} p(x) dx} = \frac{1}{1/N} \int_{x_N}^{\infty} x p(x) dx$$

$$= N \left\{ x_N \exp[-a^2 x_N^2] + \int_{x_N}^{\infty} \exp[-a^2 x^2] dx \right\}. \tag{9.20}$$

Evaluation of the integral in the above equation yields the following result for $x_{1/N}$:

$$x_{1/N} = x_N + \frac{N}{a} \text{Erfc}[a x_N], \tag{9.21}$$

where Erfc is the complementary error function,

$$\text{Erfc}[x] = \int_{x}^{\infty} e^{-t^2} dt. \tag{9.22}$$

The relationships between several of the characteristic wave height have been numerically evaluated by Eq. (9.21), as listed in Table 9.1. From this table, we note that he constant a in the generalized formula of the Rayleigh distribution, Eq. (9.16), takes the value of 1.416 when the reference wave height is $H_* = H_{1/3}$. The ratios between wave heights given by Eq. (2.3) in Sec. 2.2.2 and the relationship between the significant wave height and the zeroth spectral moment given by Eq. (2.33) in Sec. 2.4.1 were derived from such a numerical calculation.

Table 9.1. Characteristic wave heights for the Rayleigh distribution.

N	$H_{1/N}/(m_0)^{1/2}$	$H_{1/N}/\overline{H}$	$H_{1/N}/H_{\text{rms}}$	Remarks
100	6.673	2.662	2.359	—
50	6.241	2.490	2.207	—
20	5.616	2.241	1.986	—
10	5.090	2.031	1.800	Highest 1/10th wave
5	4.501	1.796	1.591	—
3	4.004	1.597	1.416	Significant wave
2	3.553	1.417	1.256	—
1	2.507	1	0.886	Mean wave

The function Erfc[x] of Eq. (9.22) can be asymptotically expanded as follows:

$$\text{Erfc}[x] \sim \exp[-x^2] \sum_{n=0}^{\infty} (-1)^n \frac{(2n-1)!!}{2^{n+1} x^{2n+1}} \quad : \quad x \to \infty. \qquad (9.23)$$

By making use of this expansion to second order and Eq. (9.19), the following approximate expression for $x_{1/N}$ is obtained:

$$x_{1/N} \simeq x_N + \frac{1}{2a(\ln N)^{1/2}} \left\{ 1 - \frac{1}{4\ln N} \right\}. \qquad (9.24)$$

For $N = 10$, this approximation gives an error of about 0.6% in excess of the exact value.

(B) *Effect of spectral bandwidth*

The above theory of the Rayleigh distribution is intended to be applied to irregular wave profiles having narrow-band spectra. An index of the narrowness of the spectral bandwidth is given by the following parameter defined with the spectral moments of Eq. (9.4):

$$\varepsilon = [1 - m_2^2/(m_0 m_4)]^{1/2} \quad : 0 < \varepsilon < 1. \qquad (9.25)$$

This parameter was introduced by Cartwright and Longuet-Higgins[3] and is called the spectral width parameter. A spectrum is considered to be narrow-banded if the parameter ε takes a value near zero, whereas it is broad-banded if ε is near unity. For many types of irregular waves without high frequency components, such as electric noise signals after processing by a low-pass filter, the parameter ε is an effective measure of the frequency spread (bandwidth) of the spectral peak. However, random sea waves exhibit a spectral form with the high frequency range attenuating as f^{-5}, as described by the standard wave spectra of Eqs. (2.10) to (2.16). Therefore, if sea surface elevations are recorded with excellent frequency resolution and the wave spectrum is estimated to sufficiently high frequencies, then the parameter ε takes a value quite near unity regardless of the shape of its peak.[b] In this sense, random sea waves possess broad-band spectra and their height distribution is not suited for application of

---

[b]The parameter ε for the observed spectrum of sea waves primarily indicates not the spectral width but the degree of the fineness of the data sampling interval relative to the peak period (see Ref. 4).

the Rayleigh distribution theory. Nevertheless, the artifice of zero-upcrossing (or downcrossing) to define individual waves as described in Sec. 2.1.2 results in a wave height distribution quite close to the Rayleighan. It is said that the operations involved in the zero-upcrossing definition exercise the effect of making the spectrum narrow-banded, but the correctness of the above comment has not been scrutinized.

The effect of spectral bandwidth on the distribution of wave heights has theoretically been examined by Tayfun[5] and Naess,[6] among others. Their theories, though not the same, are based on the inequality of the height of wave crest and the depth of the following wave trough; that is, a wave height H is smaller than twice the envelope amplitude R on the average. The tendency of the actual wave height distribution being narrower than the Rayleighan, as exemplified by Eq. (2.34) in Sec. 2.4.1, supports such theoretical derivations. Forristall[7] has demonstrated the applicability of Tayfun's theory with the field observation data for the case when the spectral peaks are fairly narrow. However, the theories do not succeed in predicting the deviation of wave heights from the Rayleigh distribution for wind waves with broad spectra such as the Bretschneider–Mitsuyasu spectrum, according to the comparison of theoretical results with numerical simulation data listed in Table 2.3 in Sec. 2.4.1.

9.1.3 *Probability Distribution of Largest Wave Height*

The Rayleigh distribution does not have an upper bound. The probability density decreases exponentially as the independent variable x becomes large, but never becomes zero. Thus, the largest wave height $H_{\max}$ is only statistically defined in such a manner that it is the largest value among a particular sample of wave heights arbitrarily chosen[c] from the population of wave heights. It cannot be a physically meaningful largest value of the wave height in a deterministic sense. The largest wave height is a statistical variable, which varies from one sample to another. We can only estimate the probability of $H_{\max}$. Derivations of the probability density function of $H_{\max}$ have been given by Longuet-Higgins[2] and Davenport,[8] the latter presenting a slightly simplified derivation for the largest value of wind gust loading.

---

[c] As pointed out by Longuet-Higgins,[2] ordinary records of continuous waves do not constitute a sample of wave heights in the above statistical sense, because successive wave heights are mutually correlated and not independent. However, the correlation is generally weak in case of wind waves, and thus we are allowed to apply the theory of the Rayleigh distribution to a sample of wave heights from continuous wave records.

Let us take N_0 wave heights from a population of wave heights which follows the Rayleigh distribution and denote the largest value among the group of N_0 wave heights (in nondimensional form) as x_{max}. By denoting the probability density functions of x_{max} as $p^*(x_{max})$, the probability that the largest value of x takes a value in the range of $[x_{max}, x_{max} + dx_{max}]$ is given by $p^*(x_{max})dx_{max}$ by definition. This probability is also calculated as the probability that only one wave among N_0 waves takes the height x_{max} in the range from x_{max} to $x_{max} + dx_{max}$ and the remainder of the $(N_0 - 1)$ waves have heights less than x_{max}. Thus,

$$p^*(x_{max})dx_{max} = N_0[1 - P(x_{max})]^{N_0-1}p(x_{max})dx_{max}$$

$$= d[1 - P(x_{max})]^{N_0} , \qquad (9.26)$$

where $P(x)$ is the exceedance probability given by Eq. (9.18) and $p(x)$ is the probability density function given by Eq. (9.16).

When N_0 is very large, the right side of Eq. (9.26) can be approximated as follows:

$$\lim_{N_0 \to \infty} [1 - P(x_{max})]^{N_0} = \lim_{N_0 \to \infty} \left[1 - \frac{\xi}{N_0}\right]^{N_0} = e^{-\xi} , \qquad (9.27)$$

where

$$\xi = N_0 P(x_{max}) = N_0 \exp[-a^2 x_{max}^2] . \qquad (9.28)$$

By substituting Eq. (9.27) into Eq. (9.26) and carrying out some manipulations, we obtain the probability density function of x_{max} as follows:

$$p^*(x_{max})dx_{max} = -e^{-\xi}d\xi = 2a^2 x_{max} \xi e^{-\xi}dx_{max} . \qquad (9.29)$$

The theoretical curves of $H_{max}/H_{1/3}$ shown in Fig. 2.7 in Sec. 2.2.1 were calculated by means of Eq. (9.29) by employing the reference height $H_* = H_{1/3}$ and taking the value $a = 1.416..$

Once the probability density function is obtained, the mode, the mean and the variance can be calculated. First, the mode $(x_{max})_{mode}$ is derived from the condition $dp^*/dx_{max} = 0$ as

$$(x_{max})_{mode} \simeq \frac{1}{a}(\ln N_0)^{1/2} \left\{1 + \frac{1}{4(\ln N_0)^2} + \cdots\right\} . \qquad (9.30)$$

Equation (2.4) in Sec. 2.2.2 for the expression of the most probable value of H_{max} has been obtained by regarding the second term on the right side of

Eq. (9.30) as being negligible, and by using $a = 1.416$ for $H_* = H_{1/3}$. A more accurate expression for $(x_{max})_{mode}$ than that given by Eq. (9.30) was presented by Longuet-Higgins.[2]

The arithmetic mean and the root-mean-square values are calculated by

$$E[x_{max}] = \int_0^\infty x_{max}\, p^*(x_{max})dx_{max} = \int_0^{N_0} x_{max}\, e^{-\xi}d\xi, \qquad (9.31)$$

$$E[x^2_{max}] = \int_0^\infty x^2_{max}\, p^*(x_{max})dx_{max} = \int_0^{N_0} x^2_{max}\, e^{-\xi}d\xi. \qquad (9.32)$$

Next, an explicit form of x_{max} in terms of ξ is obtained by rewriting Eq. (9.28) as

$$x_{max} = \frac{1}{a}(\ln N_0 - \ln \xi)^{1/2} \simeq \frac{1}{a}(\ln N_0)^{1/2} - \frac{\ln \xi}{2a(\ln N_0)^{1/2}}$$

$$- \frac{(\ln \xi^2)}{8a(\ln N_0)^{3/2}} + \cdots. \qquad (9.33)$$

This equation is substituted into Eq. (9.31) and the integration is carried out with respect to ξ. The result is[d]

$$E[x_{max}] = (x_{max})_{mean} \simeq \frac{1}{a}(\ln N_0)^{1/2} + \frac{\gamma}{2a(\ln N_0)^{1/2}} - \frac{\pi^2 + 6\gamma^2}{48a(\ln N_0)^{3/2}} + \cdots, \qquad (9.34)$$

where

$$\gamma = -\int_0^\infty (\ln \xi)e^{-\xi}d\xi = 0.5772\ldots \quad \text{(Euler's constant)}.$$

Equation (9.32) is also integrated with respect to ξ by using Eq. (9.28). The results is

$$E[x^2_{max}] \simeq \frac{1}{a^2}\ln N_0 + \frac{1}{a^2}\gamma. \qquad (9.35)$$

Therefore, the standard deviation of x_{max} is calculated as follows:

$$\sigma(x_{max}) = \left\{E[x^2_{max}] - E[x_{max}]^2\right\}^{1/2} \simeq \frac{\pi}{2\sqrt{6}a(\ln N_0)^{1/2}}. \qquad (9.36)$$

---

[d]In this integration, the following formula by Cramer[9] is employed:

$$\int_0^\infty (\ln \xi)^2 e^{-\xi}d\xi = \frac{\pi^2}{6} + \gamma^2.$$

Furthermore, the probability μ that $x_{\max}$ exceeds a specified value is calculated as

$$\mu = 1 - \int_0^{x_{\max}} p^*(\zeta)d\zeta = 1 - [1 - P(x_{\max})]^{N_0} \simeq 1 - \exp[-N_0 P(x_{\max})] . \quad (9.37)$$

From this result, the largest wave height $(x_{\max})_\mu$, such that the probability of being exceeded is μ, is easily obtained as

$$(x_{\max})_\mu \simeq \frac{1}{a} \left\{ \ln \left[\frac{N_0}{\ln 1/(1-\mu)} \right] \right\}^{1/2} . \quad (9.38)$$

Equation (2.6) in Sec. 2.2.2 is based on the above result.

Comparison of Eqs. (9.30) and (9.34) with Eqs. (9.19) and (9.24) yields the following inequality for large values of N_0:

$$x_{N_0} \simeq (x_{\max})_{\text{mode}} < (x_{\max})_{\text{mean}} < x_{1/N_0} . \quad (9.39)$$

As approximations, we have

$$(x_{\max})_{\text{mean}} \simeq x_{1.8N_0} , \quad x_{1/N_0} \simeq x_{2.6N_0} . \quad (9.40)$$

9.2 Wave Grouping

9.2.1 *Wave Grouping and Its Quantitative Description*

Although sea waves may look random, inspection of wave records indicates that high waves fall into groups rather than appear individually. Figure 9.2 is an example of a wave profile exhibiting grouping observed at Caldera Port,
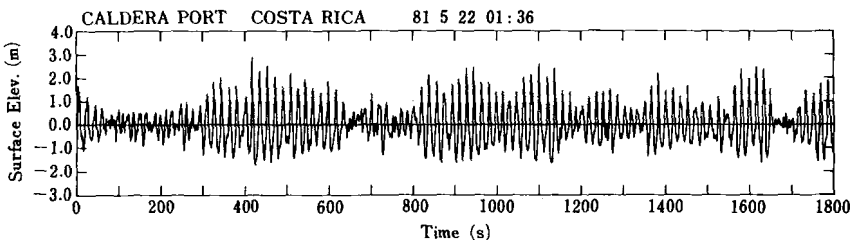

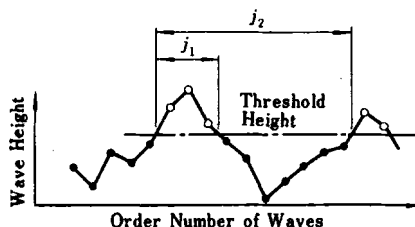Fig. 9.2. Example of a wave record with conspicuous wave grouping.[11]

Fig. 9.3. Definition sketch for the run length.

Costa Rica, in Central America.[10] The record is of the swell that traveled over a distance of some 9000 km from the generating area in the Southwest Pacific Basin.

The grouping of high waves may influence i) effective number of consecutive waves necessary to produce resonance in structures and to capsize ships, ii) stability of armor stones and blocks of sloping breakwaters, and iii) fluctuation of wave overtopping quantity of seawalls. Furthermore, a well-developed wave grouping is often associated with the presence of long-period waves, which are called surf beats or infragravity waves. A detailed analysis of these and other problems incorporating the effect of wave grouping remains for the future.

The length of wave grouping can be quantitatively described by counting the number of waves exceeding a specified value of the wave height H_c without falling below that height. A succession of such high waves is called a *run* of high wave heights, and the number of waves is termed the run length. As sketched in Fig. 9.3, the run length will be denoted by j_1. We can also define a repetition length of high waves such that a run begins at the first exceedance of wave height over the threshold value, continuing through a sequence of waves exceeding and then falling below the threshold value, and ending at the first re-exceedance of threshold were height.[11] The repetition length of high waves is analogous to the definition of the zero-upcrossing period of the wave profile. We may call such a repetition of high waves as a *total run* and denote its length by j_2. Measurements of the run length of wave heights as well as of the total run length have been made on many wave records. Table 9.2 gives some example results, based on 171 records of wind waves and young swell.[12] The threshold heights were set at $H_c = H_{1/3}$ and $H_c = H_{med}$ (median height $\simeq 0.94\,\bar{H}$). The table shows the distribution of individual length j_1 of the runs of wave height exceeding the threshold height H_c. The most frequently appearing run has the length of only one wave, and the frequency decreases

Table 9.2. Frequency distribution of observed lengths of runs of wave heights.[12]

Run length	Ordinary runs of wave heights		Conditional runs inclusive of H_{max}	
j_1	$H > H_{1/3}$	$H > H_{med}$	$H > H_{1/3}$	$H > H_{med}$
1	1,327	1,560	43	5
2	374	944	62	17
3	122	590	39	30
4	37	327	19	35
5	9	220	5	24
6	2	112	2	25
7	1	90	1	13
8		46		5
9		30		5
10		16		3
11		13		3
over 12		12		6
Total	1,872	3,960	171	171
Mean	1.42	2.54	2.36	5.12
Standard deviation	0.77	1.99	1.18	3.08

Note: Total of 20,051 waves from 171 wave records.

monotonically as the run length increases. Table 9.2 also gives the length of the run that includes the highest wave in each wave record, here called the *conditional run*. There are 171 such conditional runs from 171 wave records, and they exhibit much longer run lengths than ordinary runs of wave heights. This indicates that he highest wave rarely appears as an isolated wave, but is accompanied by several other high waves.

There is another method of describing wave grouping, through means of the wave energy envelope, which is called the smoothed instantaneous wave energy history (abbreviated as SIWEH) by Funke and Mansard.[13] They introduced the concept of wave-groupiness and introduced the groupiness factor *GF*, which is a measure of the degree of the variation of wave heights in a given wave record. The interested reader is referred to their paper for details.

9.2.2 *Probability Distribution of Run Length for Uncorrelated Waves*

If successive wave heights are uncorrelated, the probability distribution of the run length is derived by a simple calculation of probability.[11,12] Let the occurrence probability that $H > H_c$ be denoted by p_0 and its nonoccurrence probability by $q_0 = 1 - p_0$. A run of length j_1 is such a process in that the first wave height exceeds the threshold height H_c, the succeeding $(j_1 - 1)$ wave heights also exceed H_c, and the $(j_1 + 1)$th wave height falls below H_c. Thus, the probability of a run with length j_1 is expressed as

$$P(j_1) = p_0^{j_1 - 1} q_0 . \tag{9.41}$$

Since $p_0 < 1$ by the definition of probability, a run with $j_1 = 1$ has the largest probability of occurrence. The mean and the standard deviation of the run length are calculated as follows:

$$\bar{j}_1 = \sum_{j_1=1}^{\infty} j_1 P(j_1) = \frac{q_0}{p_0} \sum_{j_1=1}^{\infty} j_1 p_0^{j_1} = \frac{1}{q_0} , \tag{9.42}$$

$$\sigma(j_1) = \left[\sum_{j_1=1}^{\infty} j_1^2 P(j_1) - \bar{j}_1^2 \right]^{1/2} = \frac{\sqrt{p_0}}{q_0} . \tag{9.43}$$

The probability of a total run with the length j_2 can be derived by mathematical induction to give

$$P(j_2) = \frac{p_0 q_0}{p_0 - q_0} (p_0^{j_2 - 1} - q_0^{j_2 - 1}) . \tag{9.44}$$

The mean and the standard deviation of the total run length are calculated as

$$\bar{j}_2 = \frac{1}{p_0} + \frac{1}{q_0} , \tag{9.45}$$

$$\sigma(j_2) = \sqrt{\frac{p_0}{q_0^2} + \frac{q_0}{p_0^2}} . \tag{9.46}$$

When the threshold wave height is taken as the median height H_{med}, the probabilities of p_0 and q_0 are $p_0 = q_0 = 1/2$ by definition. In the case of $H_c = H_{1/3}$, the probabilities are calculated as $p_0 = 0.1348$ and $q_0 = 0.8652$ by

substituting the values $x = H_c/m_0^{1/2} = 4.004$ and $a = 1/\sqrt{8}$ into Eq. (9.18). Substitution of these values of probability into Eq. (9.41) results in distributions of run lengths shorter than those recorded in the sea. The difference is due to the presence of some correlation between successive wave heights. For example, Rye[14] has found a correlation coefficient of $+0.24$ for successive heights of wind waves, while records of long-traveled swells such as those shown in Fig. 9.2 have the correlation coefficient in the range of 0.5 to 0.8.[10]

9.2.3 *Correlation Coefficient between Successive Wave Heights*

The reliable theory of run length for sea waves requires incorporation of the correlation coefficient between successive wave heights. The theory was first given by Kimura,[13] and then re-presented by Battjes and van Vledder[14] and Longuet-Higgins,[15] both of whom expressed the relationship between the correlation coefficient by Kimura and the frequency spectrum in a more explicit manner. All the derivations are made on the calculation of the envelope amplitude sketched in Fig. 9.1, and they have the origin in the classical paper by Rice[1] for the statistical theory of random noise.

First, the envelope amplitudes at the time t and $t+dt$ are denoted as R_1 and R_2 for the irregular wave profile expressed by Eq. (9.8), and their relationship is examined. For this purpose, the wave profiles at the above two time steps are expressed in a manner of Eq. (9.1) as follows:

$$\left.\begin{array}{l} \eta(t) = Y_{c1} \cos 2\pi \bar{f} t - Y_{s1} \sin 2\pi \bar{f} t\,, \\ \eta(t + dt) = Y_{c2} \cos 2\pi \bar{f}(t + \tau) - Y_{s2} \sin 2\pi \bar{f}(t + \tau)\,, \end{array}\right\} \quad (9.47)$$

where

$$\left.\begin{array}{l} Y_{c1} = \displaystyle\sum_{n=1}^{\infty} a_n \cos[2\pi(f_n - \bar{f})t + \epsilon_n]\,, \\[2mm] Y_{s1} = \displaystyle\sum_{n=1}^{\infty} a_n \sin[2\pi(f_n - \bar{f})t + \epsilon_n]\,, \\[2mm] Y_{c2} = \displaystyle\sum_{n=1}^{\infty} a_n \cos[2\pi(f_n - \bar{f})(t + \tau) + \epsilon_n]\,, \\[2mm] Y_{s2} = \displaystyle\sum_{n=1}^{\infty} a_n \sin[2\pi(f_n - \bar{f})(t + \tau) + \epsilon_n]\,. \end{array}\right\} \quad (9.48)$$

The amplitudes Y_{c1}, Y_{s1}, Y_{c2} and Y_{s2} defined above are the stationary stochastic processes satisfying the Gaussian distribution. Their variances and covariances are calculated as below.

$$\left. \begin{aligned}
E[Y_{c1}^2] &= E[Y_{s1}^2] = E[Y_{c2}^2] = E[Y_{s2}^2] = m_0 \,, \\
E[Y_{c1}Y_{s1}] &= E[Y_{s1}Y_{c1}] = E[Y_{c2}Y_{s2}] = E[Y_{s2}Y_{c2}] = 0 \,, \\
E[Y_{c1}Y_{c2}] &= E[Y_{c2}Y_{c1}] = E[Y_{s1}Y_{s2}] = E[Y_{s2}Y_{s1}] \\
&= \int_0^\infty S(f) \cos 2\pi(f - \bar{f})\tau \, df = \mu_{13} \,, \\
E[Y_{c1}Y_{s2}] &= E[Y_{s2}Y_{c1}] = -E[Y_{s1}Y_{c2}] = -E[Y_{c2}Y_{s1}] \\
&= \int_0^\infty S(f) \sin 2\pi(f - \bar{f})\tau \, df = \mu_{14} \,.
\end{aligned} \right\} \tag{9.49}$$

The four stationary stochastic processes Y_{c1}, Y_{s1}, Y_{c2} and Y_{s2} are assigned the numbers 1 to 4 in this order. The covariance matrix is formed as follows:

$$M = \begin{pmatrix} m_0 & 0 & \mu_{13} & \mu_{14} \\ 0 & m_0 & -\mu_{14} & \mu_{13} \\ \mu_{13} & -\mu_{14} & m_0 & 0 \\ \mu_{14} & \mu_{13} & 0 & m_0 \end{pmatrix} \,. \tag{9.50}$$

The determinant of the above matrix is

$$|M| = (m_0^2 - \mu_{13}^2 - \mu_{14}^2)^2 = m_0^4(1 - \kappa^2)^2 \,, \tag{9.51}$$

where

$$\begin{aligned}
\kappa^2 &= \frac{1}{m_0^2}(\mu_{13}^2 + \mu_{14}^2) \\
&= \left| \frac{1}{m_0} \int_0^\infty S(f) \cos 2\pi(f - \bar{f})\tau \, df \right|^2 + \left| \frac{1}{m_0} \int_0^\infty S(f) \sin 2\pi(f - \bar{f})\tau \, df \right|^2 \\
&= \left| \frac{1}{m_0} \int_0^\infty S(f) \cos 2\pi f\tau \, df \right|^2 + \left| \frac{1}{m_0} \int_0^\infty S(f) \sin 2\pi f\tau \, df \right|^2 \,. \tag{9.52}
\end{aligned}$$

The joint probability density function of the normal variates having the covariance matrix of Eq. (9.50) can be written down by using the cofactor of

the determinant $|M|$ as follows:

$$p(Y_{c1}, Y_{s1}, Y_{c2}, Y_{s2}) = \frac{1}{4\pi^2 m_0^2 (1 - \kappa^2)} \exp\left\{- \frac{1}{2m_0^2(1 - \kappa^2)}\right.$$

$$\times \left[m_0(Y_{c1}^2 + Y_{s1}^2 + Y_{c2}^2 + Y_{s2}^2) - \mu_{13}(Y_{c1}Y_{c2} + Y_{s1}Y_{s2})\right.$$

$$\left.\left. - \mu_{14}(Y_{c1}Y_{s2} + Y_{s1}Y_{c2})\right]\right\}. \qquad (9.53)$$

Then, the following transformation of variates is introduced:

$$\left.\begin{array}{ll} Y_{c1} = R_1 \cos\phi_1\,, & Y_{s1} = R_1 \sin\phi_1\,, \\ Y_{c2} = R_2 \cos\phi_2\,, & Y_{s2} = R_2 \sin\phi_2\,. \end{array}\right\} \qquad (9.54)$$

The joint probability density function of Eq. (9.53) is now rewritten for the variates R_1, R_2, ϕ_1 and ϕ_2 as

$$p(R_1, R_2, \phi_1, \phi_2) = \frac{R_1 R_2}{4\pi^2 m_0^2 (1 - \kappa^2)} \exp\left\{- \frac{1}{2m_0^2(1 - \kappa^2)}\left[m_0(R_1^2 + R_2^2)\right.\right.$$

$$\left.\left. - 2\mu_{13}R_1 R_2 \cos(\phi_2 - \phi_1) - 2\mu_{14}R_1 R_2 \sin(\phi_2 - \phi_1)\right]\right\}. \qquad (9.55)$$

Because the phase angles ϕ_1 and ϕ_2 are independent of the envelope amplitudes R_1 and R_2, Eq. (9.55) can be integrated with respect to ϕ_1 and ϕ_2 for the range of $[0, 2\pi]$, respectively. For execution of integration, a new variable $\alpha = \phi_2 - \phi_1 - \tan^{-1}(\mu_{13}/\mu_{14})$ is introduced. By utilizing the fact that the exponential function on the right side of Eq. (9.55) is a periodic function of ϕ_2, the terms containing ϕ_1 and ϕ_2 are integrated as below.[18]

$$\frac{1}{4\pi^2} \int_0^{2\pi} d\phi_1 \int_0^{2\pi} \exp\left\{\frac{R_1 R_2}{m_0^2(1 - \kappa^2)}[\mu_{13}\cos(\phi_2 - \phi_1) + \mu_{14}\sin(\phi_2 - \phi_1)]\right\} d\phi_2$$

$$= \frac{1}{4\pi^2} \int_0^{2\pi} d\phi_1 \int_0^{2\pi} \exp\left\{\frac{R_1 R_2}{m_0^2(1 - \kappa^2)}(\mu_{13}^2 + \mu_{14}^2)^{1/2} \cos\alpha\right\} d\alpha$$

$$= I_0\left[\frac{\kappa R_1 R_2}{(1 - \kappa^2)m_0}\right]. \qquad (9.56)$$

Full integration of Eq. (9.55) yields the following joint probability density function of R_1 and R_2:

$$p(R_1, R_2) = \frac{R_1 R_2}{m_0^2(1 - \kappa^2)} \exp\left[-\frac{R_1^2 + R_2^2}{2m_0(1 - \kappa^2)}\right] I_0\left[\frac{\kappa R_1 R_2}{(1 - \kappa^2)m_0}\right], \quad (9.57)$$

where I_0 denotes the modified Bessel function of the first kind of zeroth order.

With the joint probability density function thus obtained, the correlation coefficient between R_1 and R_2 is defined by the following:

$$r(R_1, R_2) = \frac{M_{11}}{(M_{20}M_{02})^{1/2}}, \quad (9.58)$$

where

$$M_{mn} = \int_0^\infty \int_0^\infty (R_1 - \bar{R}_1)^m (R_2 - \bar{R}_2)^n p(R_1, R_2) dR_1 dR_2. \quad (9.59)$$

Evaluation of Eq. (9.58) yields the following result for the correlation coefficient between R_1 and R_2:

$$r(R_1, R_2) = \frac{E(\kappa) - (1 - \kappa^2)K(\kappa)/2 - \pi/4}{1 - \pi/4}, \quad (9.60)$$

where K and E are the complete elliptic integrals of the first and second kinds, respectively.

For the case that the frequency spectrum is relatively narrow-banded and the wave height H can be assumed to be equal to twice the envelope amplitude R, the correlation coefficient between the successive wave heights is given the same formula as Eq. (9.60). The parameter κ is evaluated from the wave spectrum by mean of Eq. (9.52), by setting the time lag τ as equal to the mean wave period $\overline{T}$. The joint probability density function of the successive wave heights H_1 and H_2 is also obtained by rewriting Eq. (9.56) as follows:

$$p(H_1, H_2) = \frac{4H_1 H_2}{(1 - \kappa^2)H_{\text{rms}}^4} \exp\left[-\frac{H_1^2 + H_2^2}{(1 - \kappa^2)H_{\text{rms}}^2}\right] I_0\left[\frac{2\kappa H_1 H_2}{(1 - \kappa^2)H_{\text{rms}}^2}\right]. \quad (9.61)$$

The correlation coefficient between successive wave heights observed on field data and numerically simulated data is compared with prediction by the envelope theory of the above, as shown in Fig. 9.4.[19] The abscissa represents the value of $\kappa(\overline{T})$, here called the envelope correlation parameter, and the ordinate

is the correlation coefficient $r(H_1, H_2)$. Field data come from two sources: one from Caldera Port in Costa Rica (marked with the filled circle) and the other from Sakata Port in Japan (marked with the filled box). The former contains 51 records of long-traveled swell, including one record shown in Fig. 9.2, while the latter contains 68 records of wind waves. The lengths of the vertical and horizontal lines from the filled circle or box represent the magnitude of the standard deviations of respective data sources. The numerical simulation of wave profiles have been made for 15 different spectral shapes so as to yield a wide range of κ value: for each spectral shape one hundred different profiles were generated and analyzed. In the calculated of κ by Eq. (9.52) for the data of Caldera Port, the spectral density in the range of the frequency below 0.5 times the peak frequency and that above 1.8 times the peak frequency were set to zero. Such a removal of spectral density was so made to eliminate a possible contamination of the frequency spectrum by nonlinear interaction terms to be discussed in Sec. 9.5. The data of Sakata Port were judged not to contain an appreciable amount of nonlinear interaction terms because of the large water depth (50 m), and thus no adjustment was made for the wave spectra.
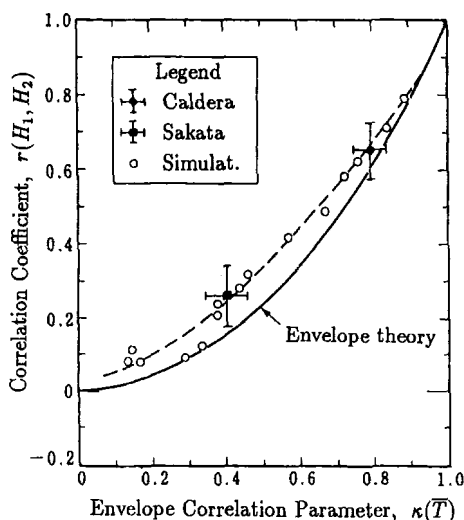

Fig. 9.4. Relationship between the correlation coefficient $r(H_1, H_2)$ and the envelope correlation parameter $\kappa(\overline{T})$.[19]

Figure 9.4 indicates that the wave height correlation coefficient measured on wave profiles is slightly larger than the theoretical prediction. The difference is owing to the assumption of the wave height being twice the envelope amplitude. As discussed in the paragraphs on the effect of spectral bandwidth on wave height distributions, the wave height is slightly smaller than twice the envelope amplitude on the average. In other words, the temporal variation of wave heights is slightly gradual in comparison with that of envelope amplitudes, and thus produces a greater value of correlation coefficient. Despite the above discussion, the degree of the difference between the observed value of correlation coefficient and the theoretical prediction is rather small. The theory of correlation between wave envelope amplitudes introduced in the above can be said to be well applicable for waves in the sea.

9.2.4 *Theory of Run Length for Mutually Correlated Wave Heights*

By employing the definition by Kimura,[15] a notation of p_{11} is given to the probability that an arbitrary wave height H_2 in a wave train does not exceed the threshold height H_c, under the condition that the preceding wave height H_1 has not exceeded H_c. Another notation of p_{22} is given to the probability that H_2 exceeds H_c under the condition that H_1 has already exceeded H_c. These probabilities are evaluated by the envelope theory as

$$\left.\begin{array}{l} p_{11} = \displaystyle\int_0^{H_c} \int_0^{H_c} p(H_1, H_2) dH_1 dH_2 \Big/ \int_0^{H_c} p(H_1) dH_1 \,, \\[4mm] p_{22} = \displaystyle\int_{H_c}^{\infty} \int_{H_c}^{\infty} p(H_1, H_2) dH_1 dH_2 \Big/ \int_{H_c}^{\infty} p(H_1) dH_1 \,, \end{array}\right\} \tag{9.62}$$

where $p(H_1)$ denotes the marginal probability density function of wave heights and is approximated with Eq. (9.13) of the Rayleigh distribution.

The probability of a run $H > H_c$ with length j_1 is then derived in a manner similar to the derivation of the run length for uncorrelated wave heights. Thus,

$$P(j_1) = p_{22}^{j_1-1}(1 - p_{22})\,. \tag{9.63}$$

The mean and the standard deviation of the run length are calculated as

$$\bar{j}_1 = \frac{1}{1 - p_{22}},\tag{9.64}$$

$$\sigma(j_1) = \frac{\sqrt{p_{22}}}{1 - p_{22}}.\tag{9.65}$$

The probability of the total run is also derived as follows:

$$P(j_2) = \frac{(1 - p_{11})(1 - p_{22})}{p_{11} - p_{22}}(p_{11}^{j_2-1} - p_{22}^{j_2-1}).\tag{9.66}$$

The mean and the standard deviation of the total run are calculated as

$$\bar{j}_2 = \frac{1}{1 - p_{11}} + \frac{1}{1 - p_{22}},\tag{9.67}$$

$$\sigma(j_2) = \left[\frac{1}{(1 - p_{11})^2} + \frac{1}{(1 - p_{11})^2} - \frac{1}{(1 - p_{11})} - \frac{1}{(1 - p_{11})}\right]^{1/2}.\tag{9.68}$$

When Kimura[15] applied his theory to the actual data, he did not calculate the envelope correlation parameter κ from the frequency spectrum. Instead, he used the wave height correlation coefficient by the temporal wave height records and estimated κ by inversely solving Eq. (9.60). The same technique was applied for the three continuous wave records at Caldera Port, each containing 734 waves, 947 waves and 2278 waves, respectively, for calculation of the probabilities of the run length with $H_c = H_{\text{med}}$ and $H_c = H_{1/3}$.[10] The observed probabilities agree well with the theory as shown in Fig. 9.5.

The variation of the mean run length with respect to the envelope correlation parameter is examined in Fig. 9.6 for the run of $H > H_{\text{med}}$. Figure 9.7 shows the mean length of the total run of $H > H_{1/3}$.19 The data sources are same as those employed in Fig. 9.4, and so is the calculation method of κ for Caldera Port. As seen in Figs. 9.6 and 9.7, the agreement between the data and theory is generally good, though there are some deviations. Thus, the envelope correlation parameter κ defined by Eq. (9.52) can be concluded as the parameter governing the phenomenon of the run of wave heights.

The author[11] previously proposed the following parameter to describe the "peakedness" of the spectral peak:

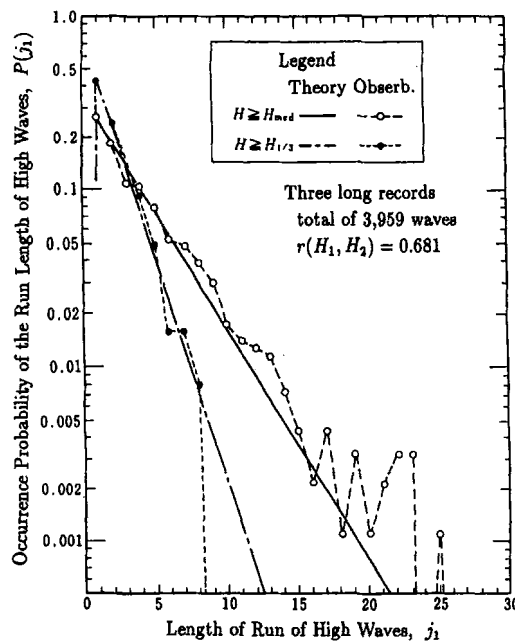$$Q_p = \frac{2}{m_0^2} \int_0^\infty f S^2(f) df.\tag{9.69}$$

Fig. 9.5. Distribution of the lengths of runs of high waves exceeding the median and significant heights.[10]
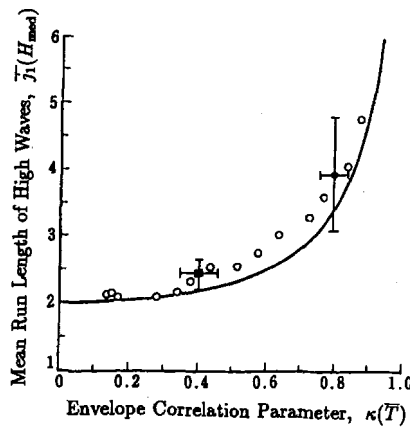

Fig. 9.6. Comparison of the theory and observations for the mean lengths of the runs of high waves of $H > H_{med}$.[19]
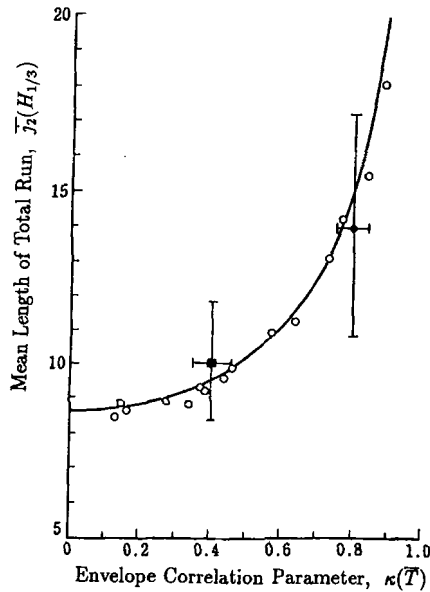
Fig. 9.7. Comparison of the theory and observations for the mean length of the total runs defined by $H_c = H_{1/3}$.[19]

The above spectral peakedness parameter also has the capability to describe the statistics of run lengths. However, the spectral peakedness parameter Q_p has a shortcoming that its value is sensitive to the resolution of spectral analysis.[10] Though the envelope correlation parameter κ is also affected by the spectral resolution,[19] its sensitivity is less as compared to Q_p. Thus, it is recommended to employ κ for the analysis of the run of wave heights based on the information of wave spectrum.

9.3 Distribution of Wave Periods

9.3.1 *Mean Period of Zero-upcrossing Waves*

The number of zero-upcrossing of irregular waves per unit time has been examined by Rice,[1] who presented a theoretical formula for the mean period of zero-upcrossing waves (Eq. (2.35) in Sec. 2.4.2). By using Eq. (8.13) for an

irregular wave profile, the time derivative of the profile is expressed as

$$\dot{\eta}(t) = -\sum_{n=1}^{\infty} 2\pi f_n a_n \sin(2\pi f_n t + \epsilon_n). \tag{9.70}$$

Let the event of zero-upcrossing be assumed of taking place in the time interval $t = t_0 \sim (t_0 + dt)$ with the time derivative in the range $\dot{\eta} \sim (\dot{\eta} + d\dot{\eta})$. For the occurrence of such an event, the surface elevation at $t = t_0$, denoted by η_0, must be less than zero, but it must not be too small to have zero-upcrossing before the time $t = t_0 + dt$. The temporal variation of surface elevation can be approximated by a straight line if the time duration dt is sufficiently short. Because the surface elevation at $t = t_0 + dt$ is approximated as $\eta = \eta_0 + \dot{\eta}dt$, which is greater than zero by the above assumption, η_0 must be greater than $-\dot{\eta}dt$. Thus, the permissible range of the surface elevation at the time t is given as $-\dot{\eta}dt < \eta_0 < 0$. The occurrence probability of the above event is then expressed as

$$\int_{-\dot{\eta}dt}^{0} [p(\eta, \dot{\eta}d\dot{\eta})]d\eta = p(0, \dot{\eta})\dot{\eta}dt\, d\dot{\eta}, \tag{9.71}$$

in which $p(\eta, \dot{\eta})$ denotes the joint probability density function of η and $\dot{\eta}$. Because $\dot{\eta}$ can take any value between 0 and ∞, the probability that the surface elevation crosses the zero line upward in the interval $t = t_0 \sim (t_0 + dt)$ is given as

$$dP = dt \int_{0}^{\infty} \dot{\eta} p(0, \dot{\eta})d\dot{\eta}. \tag{9.72}$$

The mean number of zero-upcrossings of the wave profile per unit time, denoted by N_0^*, is obtained by integrating Eq. (9.71) with respect to time. The result is

$$N_0^* = \int_{0}^{\infty} \dot{\eta} p(0, \dot{\eta})d\dot{\eta}. \tag{9.73}$$

The wave profile η and its time derivative $\dot{\eta}$ have ensemble means of zero and obey the normal distribution by virtue of the central limit theorem, as easily understood from their expressions, Eq. (9.70). Their variances are

$$E[\eta^2] = m_0, \quad E[\dot{\eta}^2] = (2\pi)^2 m_2. \tag{9.74}$$

The quantities η and $\dot{\eta}$ are mutually independent because the covariance $E[\eta\,\dot{\eta}]$ is zero. Thus, $p(\eta, \dot{\eta})$ is obtained as the product of two normal distribution

functions as

$$p(\eta, \dot{\eta}) = \frac{1}{4\pi^2 (m_0 m_2)^{1/2}} \exp\left[-\frac{1}{2}\left(\frac{\eta^2}{m_0} + \frac{\dot{\eta}^2}{4\pi^2 m_2} \right) \right] . \qquad (9.75)$$

By substituting this equation into Eq. (9.73) and performing the integration, we obtain

$$N_0^* = (m_2/m_0)^{1/2} . \qquad (9.76)$$

The mean period of the zero-upcrossing waves is the reciprocal of N_0^*. By denoting the mean period as T_{02}, we have the result

$$T_{02} = 1/N_0^* = (m_0/m_2)^{1/2} , \qquad (9.77)$$

which was presented as Eq. (2.35) in Sec. 2.4.2.

9.3.2 *Marginal Distribution of Wave Periods and Joint Distribution of Wave Heights and Periods*

(A) *Joint probability density function of envelope amplitude and phase angle*

The next problem concerns the probability distribution of individual wave periods. Rice[1] gave an approximate formula for the wave period distribution. Longuet-Higgins[20] presented a theory of the joint distribution of the heights and periods of waves with narrow-band spectra and discussed its applicability to actual sea waves.[21]

The starting point of the theory is Eq. (9.8) for the amplitude R and phase angle ϕ of the wave envelope, re-expressed in the following form:

$$\eta = R\cos\chi , \qquad \chi = 2\pi \bar{f} t + \phi = \bar{\omega} t + \phi , \qquad (9.78)$$

where $\bar{f}$ is the mean frequency defined by Eq. (9.3), and χ may be called the total phase angle.

It is necessary to derive the joint probability of R, ϕ, and their time derivatives for the analysis of wave period distributions. For this purpose, the

following four variables are introduced:

$$
\left.\begin{aligned}
\xi_1 &= R\cos\phi = \sum_{n=1}^{\infty} a_n \cos(2\pi f_n t - 2\pi \bar{f}t + \epsilon_n)\,, \\
\xi_2 &= R\sin\phi = \sum_{n=1}^{\infty} a_n \sin(2\pi f_n t - 2\pi \bar{f}t + \epsilon_n)\,, \\
\xi_3 &= \dot{\xi}_1 = -\sum_{n=1}^{\infty} 2\pi a_n (f_n - \bar{f}) \sin(2\pi f_n t - 2\pi \bar{f}t + \epsilon_n)\,, \\
\xi_4 &= \dot{\xi}_2 = \sum_{n=1}^{\infty} 2\pi a_n (f_n - \bar{f}) \cos(2\pi f_n t - 2\pi \bar{f}t + \epsilon_n)\,,
\end{aligned}\right\} \tag{9.79}
$$

in which ξ_1 and ξ_2 are the same as Y_c and Y_s in Eq. (9.2), respectively. The variables ξ_1 to ξ_4 are normally distributed with zero mean by virtue of the central limit theory. Their variances are evaluated as follows by employing Eq. (8.14):

$$
\left.\begin{aligned}
E[\xi_1^2] = E[\xi_2^2] &= \sum_{n=1}^{\infty} \frac{1}{2} a_n^2 = m_0\,, \\
E[\xi_3^2] = E[\xi_4^2] &= \sum_{n=1}^{\infty} \frac{1}{2} (2\pi a_n)^2 (f_n - \bar{f})^2 = \hat{\mu}_2\,,
\end{aligned}\right\} \tag{9.80}
$$

where

$$
\hat{\mu}_2 = (2\pi)^2 \mu_2\,, \quad \mu_2 = \int_0^{\infty} (f - \bar{f})^2 S(f)\,df = m_2 - \frac{m_1^2}{m_0}\,. \tag{9.81}
$$

The moments m_0, m_1 and m_2 have been defined in Eq. (9.4). The covariance $E[\xi_i \xi_j]$ vanishes for $i \neq j$ if the mean frequency $\bar{f}$ is defined through the moments m_0 and m_1 as in Eq. (9.3), and thus $\xi_1 \sim \xi_4$ are mutually independent. Therefore, the joint probability density function for $(\xi_1, \xi_2, \xi_3, \xi_4)$ can be expressed as the product of individual probability density function of normal distributions. Thus,

$$
p(\xi_1, \xi_2, \xi_3, \xi_4) = \frac{1}{4\pi^2 m_0 \hat{\mu}_2} \exp\left[-\frac{\xi_1^2 + \xi_2^2}{2m_0}\right] \exp\left[-\frac{\xi_3^2 + \xi_4^2}{2\hat{\mu}_2}\right]\,. \tag{9.82}
$$

The variables ξ_3 and ξ_4 in Eq. (9.79) can also be expressed as

$$
\left.\begin{aligned}
\xi_3 &= \dot{R}\cos\phi - R\dot{\phi}\sin\phi\,, \\
\xi_4 &= \dot{R}\sin\phi + R\dot{\phi}\cos\phi\,.
\end{aligned}\right\} \tag{9.83}
$$

The Jacobian between $(\xi_1, \xi_2, \xi_3, \xi_4)$ and $(R, \phi, \dot{R}, \dot{\phi})$ is calculated to be

$$|J| = \frac{\partial(\xi_1, \xi_2, \xi_3, \xi_4)}{\partial(R, \phi, \dot{R}, \dot{\phi})} = R^2 . \qquad (9.84)$$

By transforming variables, the following joint probability density function is derived from Eq. (9.82):

$$p(R, \phi, \dot{R}, \dot{\phi}) = \frac{R^2}{4\pi^2 m_0 \hat{\mu}_2} \exp\left[-\frac{R^2}{2m_0}\right] \exp\left[-\frac{\dot{R}^2 + R^2\dot{\phi}^2}{2\hat{\mu}_2}\right] . \qquad (9.85)$$

(B) *Marginal probability density function of wave period*

The wave period is related with the time derivative of the total phase angle χ as will be discussed later. The joint probability density function for ϕ and $\dot{\phi}$ is derived by integrating Eq. (9.85) with respect to R from 0 to ∞ and $\dot{R}$ from $-\infty$ to ∞. The result is

$$p(\phi, \dot{\phi}) = \frac{(m_0/\hat{\mu}_2)^{1/2}}{4\pi[1 + (m_0/\hat{\mu}_2)\dot{\phi}^2]^{3/2}} . \qquad (9.86)$$

By rewriting the above equation with the variables χ and $\dot{\chi}$ and using $\partial(\chi, \dot{\chi})/\partial(\phi, \dot{\phi}) = 1$, we obtain

$$p(\chi, \dot{\chi}) = \frac{(m_0/\hat{\mu}_2)^{1/2}}{4\pi[1 + (m_0/\hat{\mu}_2)(\dot{\chi} - \bar{\omega})^2]^{3/2}} . \qquad (9.87)$$

The variable χ does not appear on the right side of the above equation, which means that χ is uniformly distributed in the range 0 to 2π. The marginal distribution of $\dot{\chi}$ is then expressed by the following probability density function:

$$p(\dot{\chi}) = \frac{(m_0/\hat{\mu}_2)^{1/2}}{2[1 + (m_0/\hat{\mu}_2)(\dot{\chi} - \bar{\omega})^2]^{3/2}} . \qquad (9.88)$$

Theoretically speaking, $\dot{\chi}$ can take any value between $-\infty$ and ∞. The probability of $\dot{\chi}$ taking a negative value is obtained by integrating Eq. (9.88) over the negative range as

$$\int_{-\infty}^{0} p(\dot{\chi})d\dot{\chi} = \frac{1}{2}\left\{1 - \frac{(m_0/\hat{\mu}_2)^{1/2}\bar{\omega}}{[1 + (m_0/\hat{\mu}_2)\bar{\omega}^2]^{1/2}}\right\}$$

$$= \frac{1}{2}\left\{1 - \frac{1}{(1 + \nu^2)^{1/2}}\right\} \simeq \frac{1}{4}\nu^2 - \frac{3}{16}\nu^4 + \cdots . \qquad (9.89)$$

The parameter ν in the above was introduced by Longuet-Higgins[20] to represent the narrowness of the spectral bandwidth and is defined by

$$\nu = \frac{1}{\bar{\omega}} \left(\frac{\hat{\mu}_2}{m_0} \right)^{1/2} = \left[\frac{m_0 m_2}{m_1^2} - 1 \right]^{1/2} . \tag{9.90}$$

Longuet-Higgins[21] mentions that ν is nearly equal to one half the value of another spectral bandwidth parameter ϵ of Eq. (9.25) when the parameter ν takes a sufficiently small value. In such a case, the probability of $\dot{\chi}$ being negative is negligibly small as indicated by Eq. (9.90), and the total phase angle χ can be regarded as an almost-always-increasing function.

Next, attention is given to the event that the wave profile $\eta = \eta(t)$ crosses the zero line upward. The event takes place when χ becomes $(2n - 1/2)\pi$ while increasing, or when χ becomes $(2n + 1/2)\pi$ while decreasing. Thus, the probability that a zero-upcrossing event occurs in the time interval $[t, t + dt]$ is given in a manner similar to the derivation of Eq. (9.72):

$$H(\chi)dt = dt \int_0^\infty \dot{\chi}[p(\chi, \dot{\chi})]_{\chi=(2n-1/2)\pi} d\dot{\chi}$$

$$+ dt \int_{-\infty}^0 \dot{\chi}[p(\chi, \dot{\chi})]_{\chi=(2n+1/2)\pi} d\dot{\chi} . \tag{9.91}$$

The two terms on the right side of the above equation can be evaluated by using Eqs. (9.3), (9.81) and (9.87), and the result is

$$\left. \begin{array}{l} \displaystyle\int_0^\infty \dot{\chi}\, p(\chi, \dot{\chi})d\dot{\chi} = \frac{1}{2} \left(\frac{m_2}{m_0} \right)^{1/2} \left[1 + \frac{m_1}{(m_0 m_2)^{1/2}} \right] , \\[4mm] \displaystyle\int_{-\infty}^0 \dot{\chi}\, p(\chi, \dot{\chi})d\dot{\chi} = \frac{1}{2} \left(\frac{m_2}{m_0} \right)^{1/2} \left[1 - \frac{m_1}{(m_0 m_2)^{1/2}} \right] . \end{array} \right\} \tag{9.92}$$

Thus, the probability $H(\chi)dt$ is obtained as

$$H(\chi)dt = (m_2/m_0)^{1/2}dt . \tag{9.93}$$

If we integrate the above probability over the duration of unit time, we get the mean number of zero-upcrossings per unit time, which is the same as Eq. (9.76).

The expressions inside the brackets on the right sides of Eq. (9.92) can be expanded as

$$\left.\begin{aligned} 1 + \frac{m_1}{(m_0 m_2)^{1/2}} &= 1 + (1 + \nu^2)^{-1/2} \simeq 2 - \frac{1}{2}\nu^2 + \cdots, \\ 1 - \frac{m_1}{(m_0 m_2)^{1/2}} &= 1 - (1 + \nu^2)^{-1/2} \simeq \frac{1}{2}\nu^2 + \cdots. \end{aligned}\right\} \tag{9.94}$$

Therefore, it is noted that the probability that χ takes the value $(2n + 1/2)\pi$ while decreasing is very small if $\nu \ll 1$. This is another confirmation that the probability of $\dot{\chi}$ taking a negative value is very small, here demonstrated for the particular value $\chi = (2n + 1/2)\pi$.

The zero-upcrossing wave period can be defined as the difference between the time $\chi = [2(n+1)-1/2]\pi$ and the time $\chi = [2n-1/2]\pi$ under the condition that $\nu \ll 1$. By assuming that $\ddot{\chi}$ is sufficiently small[e] and by approximating the variation of χ during the above time interval with a straight line, we obtain the following expression for the zero-upcrossing wave period:

$$T \simeq \frac{2\pi}{\dot{\chi}} \simeq T_{01}\left(1 - \frac{\dot{\phi}}{\bar{\omega}}\right), \tag{9.95}$$

where T_{01} is one kind of mean wave period defined by

$$T_{01} = \frac{1}{\bar{f}} = \frac{2\pi}{\bar{\omega}} = \frac{m_0}{m_1}. \tag{9.96}$$

In order to derive the probability density function for the period T, we need to know the conditional probability density function of $\dot{\phi}$ when χ takes the value $(2n - 1/2)\pi$. This function can be derived by the same reasoning as employed in the derivation of Eq. (9.71), which describes the probability density function of *eta* under the condition that the wave envelope $\eta = \eta(t)$ crosses the level $\eta = 0$ in the time interval $[t, t + dt]$. The result is

$$p(\dot{\phi}|\chi) = p(\dot{\chi}|\chi) = \frac{p(\chi, \dot{\chi})|\dot{\chi}|}{H(\chi)}. \tag{9.97}$$

The existence of a linear transformation between $\dot{\phi}$ and $\dot{\chi}$ as dictated by Eq. (9.78) was employed in the above derivation. It is possible to approximate the term $|\dot{\chi}|$ on the right side of the above equation as

$$\dot{\chi} = \bar{\omega}[1 + 0(\nu)]. \tag{9.98}$$

---

[e]Longuet-Higgins[20] has stated that $\ddot{\chi}$ is a quantity of the order of ν^2.

By employing only the first term in the above equation, Eq. (9.97) is evaluated as follows, after using Eqs. (9.87), (9.93) and (9.95):

$$p(\dot{\phi}|\chi) \simeq \frac{T_{02}\nu^2}{4\pi[\nu^2 + (1 - T/T_{01})^2]^{3/2}} \, . \tag{9.99}$$

The probability density function for the period T is then obtained from the above result as

$$p(T) = \left|\frac{d\dot{\phi}}{dT}\right| p(\dot{\phi}|\chi) = \frac{\bar{\omega}T_{02}}{2\pi T_{01}} \frac{\nu^2}{2[\nu^2 + (1 - T/T_{01})^2]^{3/2}} \, . \tag{9.100}$$

The derivations are all based on the assumption that $\nu \ll 1$, which yields the quasi-equality $T_{02} \simeq T_{01}$. Thus, by introducing the new symbol $\overline{T} \simeq T_{02} \simeq T_{01} = 2\pi/\bar{\omega}$, the probability density function for the nondimensional wave period is finally obtained as

$$p(\tau) = \frac{\nu^2}{2[\nu^2 + (\tau - 1)^2]^{3/2}} : \tau = T/\overline{T} \, . \tag{9.101}$$

(C) *Joint probability density function of wave height and period*

The joint distribution of wave heights and periods is next examined. By integrating the joint probability density function of Eq. (9.85) for R, ϕ, $\dot{R}$ and $\dot{\phi}$ with respect to ϕ in the range 0 to 2π and $\dot{R}$ in the range $-\infty$ to ∞, we obtain the following joint probability density function of R and $\dot{\phi}$:

$$p(R, \dot{\phi}) = \frac{R^2}{m_0(2\pi\hat{\mu}_2)^{1/2}} \exp\left[-\frac{R^2}{2m_0}\left(1 + \frac{m_0}{\hat{\mu}_2}\dot{\phi}^2\right)\right] \, . \tag{9.102}$$

Now the variable $\dot{\phi}$ is replaced with τ by the following relation from Eq. (9.95)

$$\tau = T/\overline{T} \simeq 1 - \dot{\phi}/\bar{\omega} \, . \tag{9.103}$$

The envelope amplitude R is also replaced with the wave height H, regarded as $H = 2R$, and the latter is then nondimensionalized in the form $x = H/H_*$ with the introduction of the constant a in Eq. (9.17). The resultant joint probability density function for the nondimensional wave height x and period τ becomes

$$p(x, \tau) = \frac{dR}{dx}\left|\frac{d\dot{\phi}}{d\tau}\right| p(R, \dot{\phi}) = \frac{2a^3 x^2}{\sqrt{\pi}\nu} \exp\left\{-a^2 x^2\left[1 + \frac{(\tau - 1)^2}{\nu^2}\right]\right\} \, . \tag{9.104}$$

The above function is characterized by symmetry about the τ-axis at $\tau = 1$, and thus the correlation between x and τ is zero. It is easily confirmed that the marginal probability density function expressed by Eq. (9.101) for the nondimensional wave period τ is obtained by integrating Eq. (9.104) with respect to x over the range 0 to ∞, whereas the density function expressed by Eq. (9.16) for the nondimensional height x is obtained by integrating Eq. (9.104) with respect to τ in the range $-\infty$ to ∞.

Finally, the distribution of wave periods in a certain range of wave height can be derived by the formula for the conditional probability density function as

$$p(\tau|x) = \frac{p(x,\tau)}{p(x)} = \frac{ax}{\sqrt{\pi}\nu} \exp\left[-\frac{a^2 x^2}{\nu^2}(\tau - 1)^2 \right] . \qquad (9.105)$$

This probability density function is a normal distribution with a mean of unity. The standard deviation is immediately found from its functional form as

$$\sigma\left(\frac{T}{\overline{T}} \right)_x = \frac{\nu}{\sqrt{2}ax} = \left(\frac{2}{\pi} \right)^{1/2} \frac{\overline{H}}{H}\nu . \qquad (9.106)$$

This equation indicates that the range of the distribution of the wave periods classified according to the wave height is inversely porportional to the wave height; that is, waves in the class of the smallest height exhibit the widest distribution in wave periods. Equation (9.106) also indicates that the period distribution is narrow for waves having small values of ν. It should be mentioned that Eq. (9.106) is not applicable in the limit $H \to 0$ and the standard deviation of the period distribution of Eq. (9.101) as a whole cannot be evaluated because the integration for the variance diverges.

(D) *Joint distribution of heights and periods of actual sea waves*

The above theory of period distribution by Longuet-Higgins[21] has been confirmed as being applicable to waves with very narrow-band spectra, based on the data of numerically simulated wave profiles.[22] In the case of actual sea waves, their spectra are rather broad-banded with large values of the parameter ν. The standard frequency spectrum of Eq. (2.10) in Sec. 2.3.1 yields $\nu = 0.425$, whereas values of ν in observed wave spectra typically lie in the range of about 0.3 to 0.8. Apparently the theory cannot be applied to waves

with such large values of ν, as is understood from the process of its derivation. However, if the value of ν is determined from the interquartile range of the observed marginal distribution of wave periods,[21] the theory can become workable in explaining the properties of wave period distributions. Longuet-Higgins,[21] for example, has argued for the applicability of his theory to the data of a scatter diagram of H and T presented by Bretschneider[23] with the fitted value of $\nu = 0.234$.
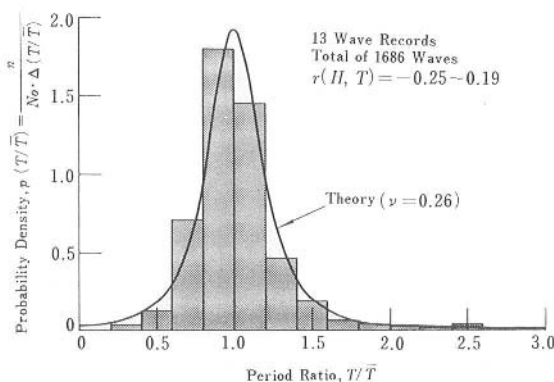

Fig. 9.8. Marginal distribution of wave periods with low correlation between individual heights and periods.[22]

Figure 9.8 shows the nondimensional period distribution for 13 records of surface waves (total number of 1686 waves), which had correlation coefficients between individual heights and periods in the range of -0.25 and 0.19.[22] The abscissa is the nondimensional wave period normalized by the mean period of the individual records, and the ordinate represents the cumulative frequencies at respective period classes expressed in the form of a probability density. Although the mean value of ν calculated from the observed wave spectra of these 13 records is 0.51, the assignment of the value of $\nu = 0.26$, based on the period distribution, produces fairly good agreement between the theoretical distribution of Eq. (9.101) and the recorded one. Figure 9.8 gives the standard deviations of wave periods at various levels of the wave height classes for the same wave data as an index of the width of distribution range. Agreement between theory and observation is also acceptable.
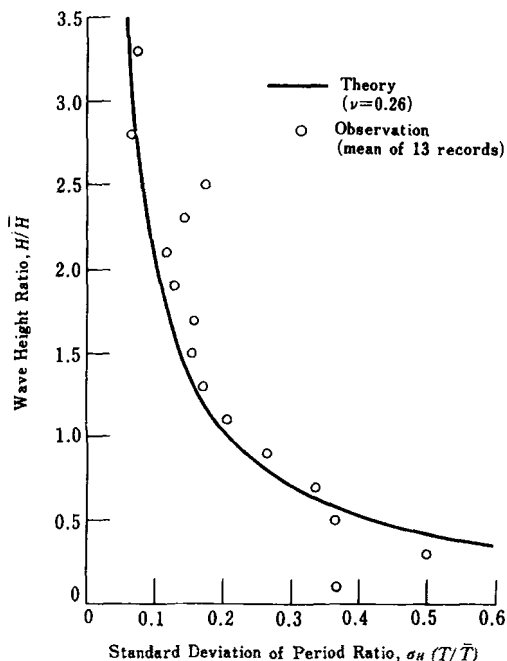
Fig. 9.9. Standard deviation of wave period with respect to the class of the height.[22]

The examples given in Figs. 9.8 and 9.9 represent the situation that the correlation between individual heights and periods is almost nil. As the correlation becomes stronger, there appears a tendency for waves of small height to have short periods and the joint distribution of wave heights and periods becomes distorted from the symmetric shape indicated by Eq. (9.104). Figure 9.10 shows a nondimensional scatter diagram of observed heights and periods of 2593 waves from 23 surface records, which had correlation coefficients $r(H,T)$ in the range 0.40 to 0.59; the class bands of nondimensional heights and periods are set as $\Delta H/\overline{H} = \Delta T/\overline{T} = 0.2$. The scatter diagram shown here exhibits a tail toward the origin in the region of nondimensional wave height lower than about 1. The shape of the tail becomes clearer as the correlation coefficient $r(H,T)$ further increases,[22] though not shown here. At the same time, the range in the periods of waves having large heights gradually shifts toward the right; that is, toward larger values of the nondimensional wave period. This tendency causes an increase in period ratios such as $T_{1/3}/\overline{T}$.
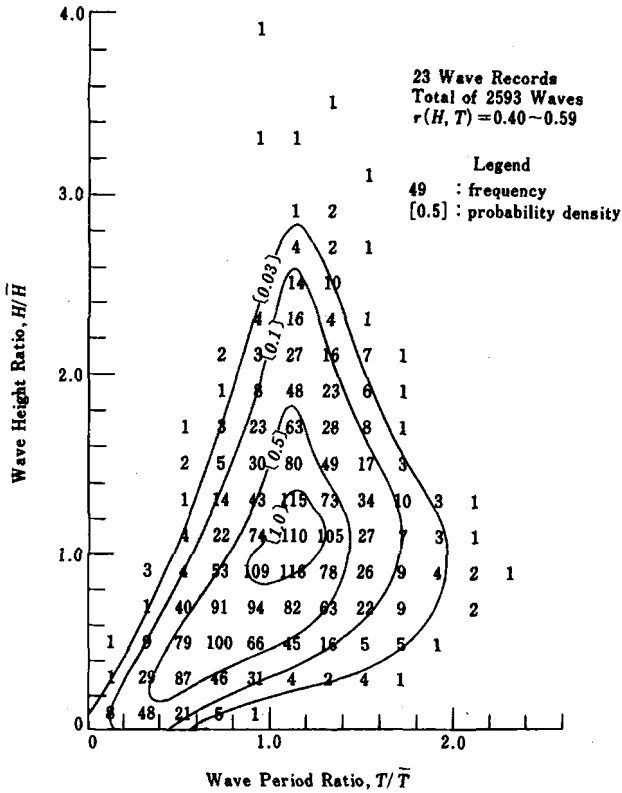
Fig. 9.10. Joint distribution of observed wave heights and periods.[22]

It is interesting to note that in scatter diagrams such as Fig. 9.10, the region of waves with large heights exhibits an almost symmetric distribution with respect to the period. Symmetry of the distribution implies that the wave heights and periods are uncorrelated in that region. For example, if the correlation coefficient is calculated for only those waves comprising the higher one-third of the record ($H/\bar{H} > 1.2$), which are used for calculating the significant wave height, the mean and the standard deviation of the correlation coefficients of the 23 records become 0.01 and 0.16, respectively. The feature of a lack of correlation among high waves does not disappear even if the overall correlation coefficient between wave height and period increases.

There is another theory of the joint distribution of the wave heights and periods, proposed by Cavanié, Arhan, and Ezraty.[24] It is a semi-empirical

extension of the theory of the maxima of the wave profile with introduction of the spectral width parameter ε. By properly choosing the value of ε, the unsymmetrical feature of the joint height and period distribution can be demonstrated. But the selection of ε is somewhat subjective and the noncorrelation among high waves cannot be maintained with increases in the overall correlation.

Longuet-Higgins[25] himself reformulated his theory of the joint distribution of wave heights and periods by expressing the zero-upcrossing wave periods as $T = T_{01}/(1 - \dot{\phi}/\overline{\omega})$, instead of the approximation by Eq. (9.95). His new theory can simulate the characteristics of observed waves such that short-period waves tend to have small heights. But the reformulated joint distribution function exhibits a slowly attenuating tail towards large wave periods. The mean wave period cannot be evaluated by the new theory, because the marginal probability density of wave periods behaves almost proportional to τ^{-2}. Numerical evaluation of the mean wave period, which is made possible by introducing an upper limit in wave period, indicates that the mean period gradually increases as the spectral width parameter ν increases. The overall correlation coefficient between wave heights and periods by theory is slightly negative, which causes the significant period to be shorter than the mean period. These features do not agree with the observed characteristics of sea waves. Thus, the new theory by Longuet-Higgins[25] cannot quantitatively describe the observed joint distribution of wave heights and periods, although it can qualitatively express the general feature of the observed joint distribution by means of a relatively simple formula.

9.4 Maxima of Irregular Wave Profiles

If the profiles of the sea waves shown in Fig. 2.2 in Sec. 2.1.2 are closely inspected, one can notice several ups and downs in the wave profiles which are not of sufficient amplitude to cross the line of the mean water level. It is an interesting problem in statistics to investigate the probability distribution of such maxima and minima of irregular wave profiles. On this topic, Rice[1] has given a theory in conjunction with the statistical properties of random noise. Later, Cartwright and Longuet-Higgins[3] demonstrated that the theory is applicable to the distribution of the maxima of random sea wave profiles, and they introduced the spectral width parameter ε defined by Eq. (9.25) in the derivation.

The maxima of an irregular wave profile expressed by $\eta = \eta(t)$ are defined as the points which satisfy the conditions $\dot{\eta} = 0$ and $\ddot{\eta} < 0$. By using Eq. (8.13) as the wave profile, the time derivatives are written as follows:

$$\left.\begin{aligned}
\eta &= \sum_{n=1}^{\infty} a_n \cos(2\pi f_n t + \varepsilon_n)\,, \\
\dot{\eta} &= -\sum_{n=1}^{\infty} 2\pi f_n a_n \sin(2\pi f_n t + \varepsilon_n)\,, \\
\ddot{\eta} &= -\sum_{n=1}^{\infty} (2\pi f_n)^2 a_n \cos(2\pi f_n t + \varepsilon_n)\,.
\end{aligned}\right\} \tag{9.107}$$

Let us consider an event in which the wave profile η exhibits a maximum in the interval $[\eta_0, \eta_0 + d\eta_0]$ and during the time interval $[t_0, t_0 + dt_0]$. The probability of such an event is readily obtained as

$$dt \int_{-\infty}^{0} [p(\eta_0, 0, \ddot{\eta}) d\eta_0 |\ddot{\eta}|] d\ddot{\eta} \tag{9.108}$$

by replacing the variables in the derivation of Eq. (9.72) according to $R \to \dot{\eta}$ and $\dot{R} \to \ddot{\eta}$. The function $p(\eta, \dot{\eta}, \ddot{\eta})$ is the joint probability density function of η, $\dot{\eta}$ and $\ddot{\eta}$. The mean number of occurrences per unit time for which a maximum of η takes a value between η_0 and $\eta_0 + d\eta_0$, which is expressed as $F(\eta_0) d\eta_0$, is given by

$$F(\eta_0) d\eta_0 = \int_{-\infty}^{0} [p(\eta_0, 0, \ddot{\eta}) |\ddot{\eta}| d\eta_0] d\ddot{\eta}\,. \tag{9.109}$$

On the other hand, the mean number of occurrences of maxima of η per unit time is given by

$$N_1^* = \int_{-\infty}^{\infty} \left\{ \int_{-\infty}^{0} [p(\eta_0, 0, \ddot{\eta}) |\ddot{\eta}| d\eta_0] d\ddot{\eta} \right\}\,. \tag{9.110}$$

Thus, the probability density function of the maxima of an irregular wave profile is described as

$$p(\eta_{\max}) d\eta_{\max} = F(\eta_{\max}) d\eta_{\max} / N_1^*\,. \tag{9.111}$$

Actual calculation of $p(\eta_{\max})$ requires evaluation of $p(\eta, \dot{\eta}, \ddot{\eta})$. We know by the definition of Eq. (9.107) that the variables η, $\dot{\eta}$ and $\ddot{\eta}$ are normally

distributed with the mean value of zero and that they have the following covariance matrix:

$$M = \begin{pmatrix} m_0 & 0 & -\hat{m}_2 \\ 0 & \hat{m}_2 & 0 \\ -\hat{m}_2 & 0 & \hat{m}_4 \end{pmatrix}, \qquad (9.112)$$

where

$$\hat{m}_n = (2\pi)^n \int_0^\infty f^n S(f) df = (2\pi)^n m_n . \qquad (9.113)$$

As a result of these properties, the function $p(\eta, \dot{\eta}, \ddot{\eta})$ can be shown to have the form[3]

$$p(\eta, \dot{\eta}, \ddot{\eta}) = \frac{1}{(2\pi)^{3/2}(\hat{m}_2 \Delta)^{1/2}}$$

$$\times \exp \left\{ -\frac{1}{2} \left[\frac{\dot{\eta}^2}{\hat{m}_2} + \frac{1}{\Delta}(\hat{m}_4 \eta^2 + 2\hat{m}_2 \eta \ddot{\eta} + m_0 \ddot{\eta}^2) \right] \right\}, \qquad (9.114)$$

where

$$\Delta = |M|/\hat{m}_2 = m_0 \hat{m}_4 - \hat{m}_2^2 . \qquad (9.115)$$

Substitution of Eq. (9.114) into Eq. (9.109) and evaluation of the integral yield the following result for $F(\eta_0)$:

$$F(\eta_0) = \frac{\Delta^{1/2}}{m_0 (2\pi)^{3/2}(\hat{m}_2)^{1/2}} \exp \left[-\frac{x_0^2}{2} \right]$$

$$\times \left\{ \exp \left[-\frac{x_0^2}{2\delta^2} \right] + \frac{x_0}{\delta} \int_{-x_0/\delta}^\infty \exp \left[-\frac{x^2}{2} \right] dx \right\}, \qquad (9.116)$$

where

$$x_0 = \eta_0/m_0^{1/2}, \quad \delta = \Delta^{1/2}/\hat{m}_2 . \qquad (9.117)$$

The number of maxima per unit time is then obtained from Eq. (9.110) as

$$N_1^* = \frac{1}{2\pi} \left(\frac{\hat{m}_4}{\hat{m}_2} \right)^{1/2} = \left(\frac{m_4}{m_2} \right)^{1/2} . \qquad (9.118)$$

The above result can also be derived simply by the replacements $\eta \to \dot{\eta}$ and $\dot{\eta} \to \ddot{\eta}$, as in the derivation of Eq. (9.76) for the mean zero-upcrossing wave period, with the corresponding replacements $m_0 \to m_2$ and $m_2 \to m_4$.

The probability density function of the maxima of an irregular wave profile is obtained by substituting Eqs. (9.116) and (9.118) into Eq. (9.111). The result, expressed in terms of the nondimensional variable $x_* = \eta_{\max}/m_0^{1/2}$, is

$$p(x_*) = \frac{1}{(2\pi)^{1/2}}\left\{ \varepsilon \exp\left[-\frac{x_*^2}{2\varepsilon^2}\right] + (1-\varepsilon^2)^{1/2} x_* \exp\left[-\frac{x_*^2}{2}\right] \right.$$

$$\left. \times \int_{-\infty}^{x_*\sqrt{1-\varepsilon^2}/\varepsilon} \exp\left[-\frac{x^2}{2}\right] dx \right\}, \qquad (9.119)$$

where

$$\varepsilon^2 = \frac{\delta^2}{1+\delta^2} = \frac{\Delta/\hat{m}_2^2}{1+\Delta/\hat{m}_2^2} = \frac{\Delta}{m_0\hat{m}_4} = \frac{m_0 m_4 - m_2^2}{m_0 m_4}. \qquad (9.120)$$

The parameter ε was introduced in Eq. (9.25).

The probability density function of the maxima of a wave profile extends into the region $x_* < 0$, unless $\varepsilon = 0$. This explains the fact that some of the maxima in a wave profile appear in wave troughs. If we take the limiting condition $\varepsilon \to 0$, Eq. (9.119) reduces to Eq. (9.12) in Sec. 9.1.1 for the probability density function of the wave envelope amplitude. This is a natural consequence, because the wave profile does not have maxima other than at the wave crest for $\varepsilon = 0$, as shown in the profile of Fig. 9.1. The other limiting condition for ε is $\varepsilon \to 1$, when $\delta \to \infty$. In this limit, Eq. (9.119) converges to the normal distribution expressed by $(1/\sqrt{2\pi})\exp[-x_*^2/2]$. A physical realization of such a situation is the case when ripples are riding on the surface of a swell of a long period. In this case, the individual ripple crests become the maxima of the overall wave profile, while the distribution of the heights of such crests is approximated by that of instantaneous swell profile, which follows the normal distribution.

The ratio of the number of negative maxima to total number of maxima of the wave profile can be found by integrating Eq. (9.119) in the range $(-\infty, 0)$. It can also be derived through simple reasoning as follows. First, the total number N_1^* of maxima of the wave profile is divided into the numbers N_1^+ for $\eta_{\max} > 0$ and N_1^- for $\eta_{\max} < 0$. Similarly, the numbers of positive and negative minima are introduced with the notation N_2^+ and N_2^-, depending on

whether $\eta_{\min} \gtrless 0$. Thus,

$$
\left.\begin{array}{l}
\text{Number of maxima}: N_1^* = N_1^+ + N_1^- , \\
\text{Number of minima}: N_2^* = N_2^+ + N_2^- .
\end{array}\right\} \tag{9.121}
$$

The profile of irregular waves under investigation is made up of linearly superposed wave components as described by Eq. (9.107), and the wave profile is statistically symmetric with respect to the zero line. Therefore, the number of minima is the same as the number of maxima given by Eq. (9.118), and the following equality exists with regard to N_2^+ and N_2^-.

$$
\left.\begin{array}{l}
N_2^+ = N_1^- = rN_1^* , \\
N_2^- = N_1^+ = (1 - r)N_1^* ,
\end{array}\right\} \tag{9.122}
$$

where r denotes the ratio of the number of negative maxima to the total number of maxima. By examining the relation between the number of zero-upcrossing points and the numbers of maxima and minima, we find that the number of maxima during the continuation of a wave crest $(\eta > 0)$ from one zero-upcrossing to the succeeding zero-downcrossing point must be equal to the number of minima in the same period plus one. This leads to the following relation:

$$
N_0^* = N_1^+ - N_2^+ = (1 - r)N_1^* - rN_1^* = (1 - 2r)N_1^* . \tag{9.123}
$$

By rewriting the above relation, we obtain

$$
r = \frac{1}{2}\left(1 - \frac{N_0^*}{N_1^*}\right) . \tag{9.124}
$$

By substituting Eqs. (9.76) and (9.118) into the above and utilizing Eq. (9.120), we can arrive at the following relationship between r and ε:

$$
r = \frac{1}{2}[1 - (1 - \varepsilon^2)^{1/2}], \quad \text{or} \quad \varepsilon = [1 - (1 - 2r)^2]^{1/2} . \tag{9.125}
$$

The above equation indicates that the spectral width parameter ε can be estimated by counting the number of negative maxima and calculating the ratio formed by it to the total number of maxima, without computing a wave spectrum. In the actual practice of wave data analysis, the following formula based

on the numbers of maxima N_1^* and zero-upcrossing points N_0^* is often employed to estimate the value of ε:

$$\varepsilon = [1 - (N_0^*/N_1^*)^2]^{1/2} \,. \tag{9.126}$$

For most sea wave records, it is found that the value of ε estimated from N_1^* and N_0^* by Eq. (9.126) is slightly than the value of ε calculated from the moments of the wave spectrum, Eq. (9.120). The cause of this difference is attributed to the increase in the observed spectral density in the high frequency range due to the effects of wave nonlinearity and to noise in the record.

The problem of determining the largest value among the maxima of a wave profile was investigated by Cartwright and Longuet-Higgins.[3] They gave the following formula for the expected value of the highest maximum when an irregular wave profile has N_1 maximum points:

$$E[(x_*)_{\max}] \simeq \left[2 \ln N_1 \sqrt{1 - \varepsilon^2}\right]^{1/2} + \gamma \left[2 \ln N_1 \sqrt{1 - \varepsilon^2}\right]^{-1/2} \,, \tag{9.127}$$

where γ is Euler's constant $(0.5772\ldots)$. The above equation can be rewritten in terms of the number of zero-upcrossing points N_0, which is related to the number of maxima N_1 as $N_0 = N_1\sqrt{1 - \varepsilon^2}$, by Eq. (9.126). The result is

$$E[(x_*)_{\max}] \simeq (2 \ln N_0)^{1/2} + \gamma (2 \ln N_0)^{-1/2} \,. \tag{9.128}$$

This expression has the same functional form as Eq. (9.34) for the largest wave height. In fact, Eq. (9.128) can be made to coincide with Eq. (9.34) by setting $H_{\max} = 2\eta_{\max}$.

9.5 Nonlinearity of Sea Waves

9.5.1 *Nonlinearity of Surface Elevation*

The statistical theories of sea waves discussed up to here are all based on the assumption that the statistical distribution of the instantaneous surface elevation can be expressed by a normal distribution. Examination of actual sea wave records, however, indicates some deviation of the surface elevations from the normal distribution. Figure 9.11 gives one such example, which was
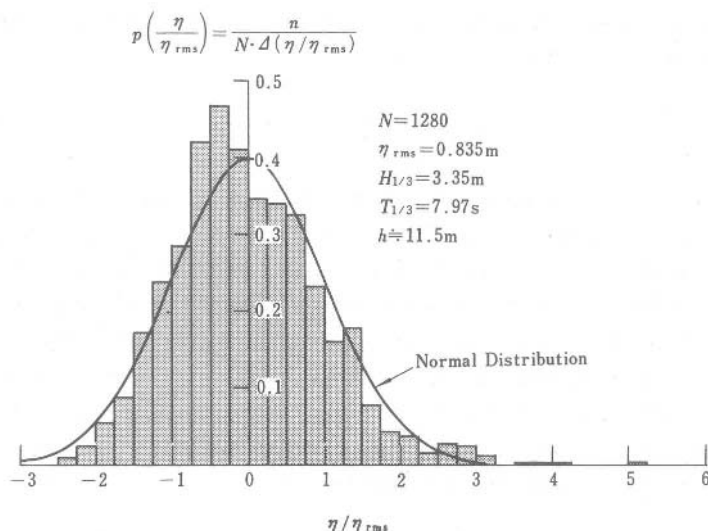
Fig. 9.11. Example of distribution of surface elevation in relatively shallow water.

recorded in relatively shallow water. The extent of the distortion of the statistical distribution from the normal is usually described by the skewness and kurtosis defined as

$$\text{Skewness}: \quad \sqrt{\beta_1} = \frac{1}{\eta_{\text{rms}}^3} \cdot \frac{1}{N} \sum_{i=1}^{N} (\eta_i - \bar{\eta})^3 , \qquad (9.129)$$

$$\text{Kurtosis}: \quad \beta_2 = \frac{1}{\eta_{\text{rms}}^4} \cdot \frac{1}{N} \sum_{i=1}^{N} (\eta_i - \bar{\eta})^4 . \qquad (9.130)$$

The normal distribution has the values $\sqrt{\beta_1} = 0$ and $\beta_2 = 3.0$, which is easily confirmed by calculation of Eqs. (9.129) and (9.130) with the probability density function of Eq. (8.22) in Sec. 8.3. The example shown in Fig. 9.11, however, has a skewness of $\sqrt{\beta_1} = 0.656$ and kurtosis of $\beta_2 = 4.09$. As seen from the definition, the skewness is zero when the distribution is symmetric with respect to the mean value. When the mode of the distribution is located lower than the mean and the distribution has a long tail in the range greater than the mean, the skewness takes a positive value. Records of sea waves mostly show positive skewness values. For wind waves in deep water, the

skewness is found to be proportional to the wave steepness. An empirical relation has been proposed by Huang and Long,[26] which is rewritten here as

$$\sqrt{\beta_1} \simeq 2\pi H/L \,. \tag{9.131}$$

In relatively shallow water, the deviation of the skewness from the value of zero of the normal distribution is enhanced.

The author[27] has proposed the following parameter as an index of the extent of wave nonlinearity:

$$\Pi = (H/L_A) \coth^3 k_A h \,, \tag{9.132}$$

where

$$\omega^2 = (2\pi/T)^2 = g k_A \tanh k_A h \quad \text{and} \quad k_A = 2\pi/L_A \,, \tag{9.133}$$

and h denotes the water depth. The subscript A denotes that a quantity with this subscript is evaluated with the small amplitude (Airy) wave theory. The skewness of actual surface waves in deep to shallow water are plotted in Fig. 9.12 as a function of the wave nonlinearity parameter Π. The solid line represents the skewness of the theoretical profiles of regular waves of finite amplitude.

The kurtosis gives an indication of the peakedness of the mode of the statistical distribution. If the peak is higher than that of corresponding normal distribution, the kurtosis becomes $\beta_2 > 3.0$, and vice versa. If $\beta_2 > 3.0$, the distribution shows long tails on both sides in compensation for the high peak. Recently Mori and Yasuda[28] demonstrated, by applying a theory of Yasuda and Mori[28] on weakly nonlinear random waves, that the kurtosis is a key parameter describing the occurrence probability of large waves in a wave record: the larger the kurtosis, the greater the probability. The theory seems to explain a strong correlation between the kurtosis and the wave height ratios such as $H_{1/10}/H_{1/3}$, $\eta_{max}/H_{1/3}$, etc. reported by Goda and Nagai.[30]

9.5.2 *Asymmetry of Wave Profiles*

The profiles of the crests and troughs of sea waves are asymmetric with respect to the mean water level (zero line). The skewness $\sqrt{\beta_1}$ of the wave profile is the parameter directly connected with the asymmetry with respect
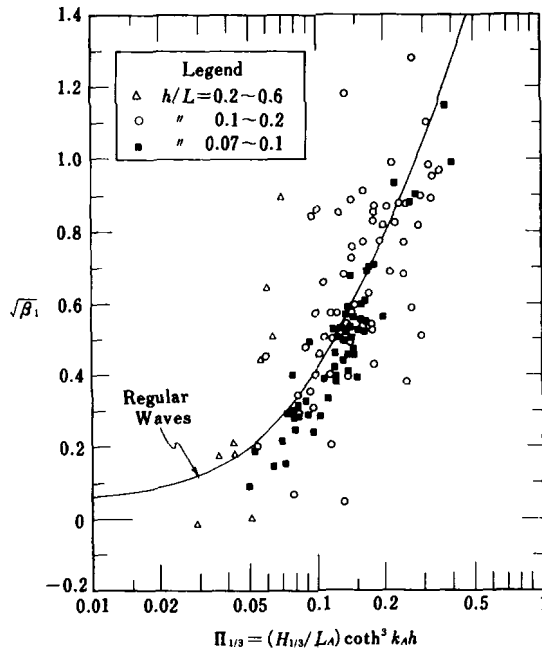
Fig. 9.12. Coastal wave data of skewness of surface elevation versus wave nonlinearity parameter defined with significant wave.[27]

to the zero line. The positive value of the skewness exhibited in Fig. 9.12 suggests that the wave crest heights are greater than the wave trough depths. The crest heights of regular waves in the laboratory typically occupy more than 50% of the wave height, sometimes up to 80%. Such features are well predicted by the theories of finite amplitude waves. Random waves in the sea also demonstrate the same feature. Figure 9.13 shows the ratio of the largest crest height to the largest wave height within the same record obtained in the field; these heights may not necessarily belong to the same wave.[27] The wave data were recorded with step-resistance gauges and ultrasonic wave sensors (inverted echo-sounder). Although the scatter of the data is large, the data generally follow the relationship given by the finite amplitude waves, which is indicates by the solid line. However, another set of wave data in deep water has indicated the mean value of $\eta_{\max}/H_{\max}$ being about 0.6,[30] which is greater than the prediction by the finite amplitude wave theory. Thus, the wave irregularity
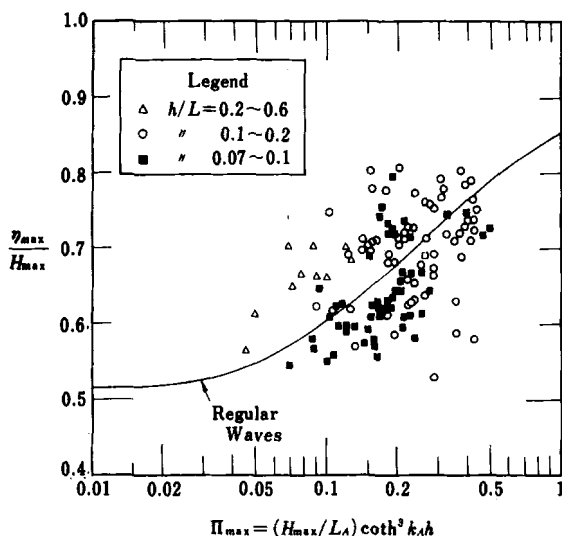
Fig. 9.13. Coastal wave data of relative crest elevation versus wave nonlinearity parameter defined with highest wave.[27]

enhances the possibility of high crest elevation, which is one of the important design parameter for offshore platforms.

Water waves also exhibit an asymmetry in the direction of wave propagation. It is common observation that the slope of a wave front becomes steep as waves approach to the surf zone and the crest point shifts toward the front from the center position; the plunging breaker is the limiting state of such an asymmetry of wave profiles. Wave forces exerted upon offshore structures are said to be affected by the degree of tilting of wave profiles. Myrhaug and Kjeldsen[31,32] have proposed an index of wave asymmetry in the direction of wave propagation by taking the ratio of the time interval between a zero-upcrossing point and the following crest point to the time interval between the crest point to the following zero-downcrossing point.

Apart from such an index for individual waves, the author[33] has proposed the following parameter called the "atiltness" to express the overall asymmetry of wave profiles of a wave record:

$$\beta_3 = \frac{1}{N-1} \sum_{i=1}^{N-1} (\dot{\eta}_i - \bar{\dot{\eta}})^3 \bigg/ \left[\frac{1}{N-1} \sum_{i=1}^{N-1} (\dot{\eta}_i - \bar{\dot{\eta}})^2 \right]^{3/2} . \qquad (9.134)$$

When the atiltness parameter takes a positive value, wave profiles show a forward tilting as a whole: when negative, a backward tilting. Wind waves which are growing by strong winds seem to indicate slightly positive values, but swell and ordinary sea waves in the offshore indicate $\beta_3 \simeq 0$ on the average without any correlation with the skewness $\sqrt{\beta_1}$. However, as waves approach to the beach, the atiltness parameter increases rapidly near the surf zone and exceeds 1.0 within the surf zone.

When the atiltness parameter has a large, positive value, the zero-upcrossing method yields slightly larger values of representative wave periods than the zero-downcrossing method (except for the mean period which remains the same).[33] The difference is due to the tendency that the waves of large heights defined by the former method have longer periods than the waves defined by the latter method. On the other hand, the representative wave heights remain statistically the same regardless of the method of wave definition. Nevertheless, for the analysis of waves in and near the surf zone, it is safe to employ the zero-downcrossing method for definition of individual waves. For waves with $\beta_3 \simeq 0$, however, the zero-upcrossing method can be utilized as well, because both methods yield statistically the same results.

9.5.3 *Effects of Wave Nonlinearity on Wave Heights and Periods*

The effect of wave nonlinearity on wave heights has theoretically been investigated by several researchers. Tayfun[34] computed the secondary interaction terms of irregular waves for examination of wave crest elevations and wave heights. He showed that the wave heights are not affected by the wave nonlinearity to the second order, while the crest elevations are heightened. The results concur with expectation by the finite amplitude theory of regular waves.

Longuet-Higgins,[35] on the other hand, clarified the relationship between the wave height and the potential energy of the third order Stokes waves in deep water. Then the computed the total potential energy of a train of irregular waves under the assumptions that individual waves can be replaced with theoretical finite amplitude waves and that the wave heights follow the Rayleigh distribution. From this potential energy, he evaluated the ratio $H_{rms}\eta_{rms}$ and showed that the ratio increases several percent as the wave steepness becomes large.

The effects of wave nonlinearity are enhanced in shallow water. Figure 9.14 shows the ratio of the significant wave height $H_{1/3}$ to the root-mean-square surface elevation η_{rms} versus the wave nonlinearity parameter defined by Eq. (9.132).[27] The solid line represents the result of calculation by adopting the method of Longuet-Higgins.[35] The third order Stokes wave theory (in relatively deep water) and the second order cnoidal wave theory (in relatively shallow water) were used to calculate the potential energy of individual waves. In the zone of $\Pi_{1/3} < 0.1$, the data of $H_{1/3}/\eta_{rms}$ are scattered around the value 3.8. Such a value smaller than the theoretical value 4.0 of the Rayleigh distribution is brought about by the spread of the spectral bandwidth of actual sea waves as discussed in Sec. 2.4.1. As the wave nonlinearity increases beyond about 0.1, however, the ratio $H_{1/3}/\eta_{rms}$ begins to increase gradually beyond the value 4.0. A large value of the ratio $H_{1/3}/\eta_{rms}$ means that the distribution of wave heights becomes broad as much as the Rayleigh distribution and possibly broader. In other words, the distribution of wave heights is narrowed by the spread of the spectral bandwidth of sea waves, but it is broadened again
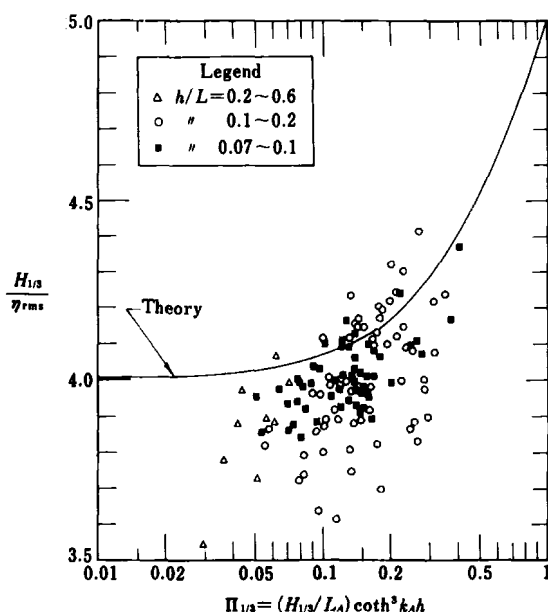

Fig. 9.14. Coastal wave data of the ratio of significant wave height to root-mean-square surface elevation versus wave nonlinearity parameter defined with significant wave.[27]

by the wave nonlinearity effect. Vinje[36] obtained a similar conclusion in support of the Rayleigh distribution for wave heights from a large number of wave records in deep water in the northern North Sea.

The effect of wave nonlinearity does not appear on the periods of individual waves. However, the mean wave period T_{02}, estimated by the spectral moments m_0 and m_2 by means of Eq. (9.77), is grossly underestimated, because the second spectral moment m_2 is overestimated owing to the presence of the nonlinear spectral components to be discussed in the next subsection. The apparent decrease in the mean wave period is enhanced as the wave nonlinearity parameter becomes large: T_{02} may become less than 70% of the mean period actually counted on a wave record when $\Pi_{1/3} > 0.3$.[27] Because of such wave nonlinearity effects, linearization of a wave spectrum by cutting the low frequency range of $f < 0.5\,f_p$ and the high frequency range of $f > (1.5 \sim 1.8)f_p$ (where f_p denotes the spectral peak frequency) is often undertaken, when statistical theories on wave heights and periods based on the frequency spectrum are tested against the field wave data.[25,37,38]

9.5.4 *Nonlinear Components of Wave Spectrum*

The deviation in the statistical distribution of surface elevation from the normal distribution indicates presence of nonlinear wave components. The theory of random sea waves is based on the linear superposition of an infinite number of infinitesimal amplitude component waves, as expressed by Eq. (8.10) or Eq. (8.13). The phase angle ε_n is assumed to be uniformly and randomly distributed. The presence of nonlinear wave components means that some of the phase angles are not independent, but hold some fixed relation among each other, and that the component waves having such mutually dependent phase angles do not satisfy the dispersion relationship, Eq. (8.3).

The analysis of nonlinear components in random sea waves is made by the calculation of the interactions among linear spectral components. As a result of interactions, wave spectra appear to have additional nonlinear components. For deepwater waves, Masuda *et al.*[39] calculated the secondary and tertiary interaction terms for directional random waves, and resolved the linear and nonlinear spectral components of the observed spectra. Mitsuyasu *et al.*[40] demonstrated that the apparent failure of the dispersion relationship for the high frequency range is due to the presence of nonlinear spectral components.

For irregular waves in relatively shallow water, a secondary interaction theory was given by Tick,[41] with a correction later made by Hamada,[42] though no directional spreading is taken into account. The secondary interaction term of the frequency spectrum, denoted by $S^{(2)}(f)$, is given by

$$S^{(2)}(f_1) = \int_{-\infty}^{\infty} K(\omega, \omega_1) S^{(1)}(f_1 - f) S^{(1)}(f) df, \qquad (9.135)$$

in which

$$K(\omega, \omega_1) = \frac{1}{4} \left\{ \frac{gkk'}{\omega(\omega_1 - \omega)} + \frac{\omega(\omega_1 - \omega)}{g} - \frac{\omega_1^2}{g} \right.$$

$$\left. + \frac{\omega_1^2 \left[\frac{g(\omega_1 - \omega)k^2 + g\omega k'^2}{\omega(\omega_1 - \omega)\omega_1} + \frac{2gkk'}{\omega(\omega_1 - \omega)} + \frac{\omega(\omega_1 - \omega)}{g} - \frac{\omega_1^2}{g} \right]}{g|k + k'| \tanh |k + k'| h - \omega_1^2} \right\}^2, \qquad (9.136)$$

$$\omega^2 = gk \tanh kh, \quad (\omega_1 - \omega)^2 = gk' \tanh k'h. \qquad (9.137)$$

The original (linear) spectrum is denoted by $S^{(1)}(f)$ in the above. The recorded spectra of the long-traveled waves at Caldera Port in Costa Rica were resolved into linear components and their secondary interaction components by using the above formula and an iteration solution method.[10] Figure 9.15 is an example of the resolution. The water depth is about 17 m. The auxiliary spectral peak at the second harmonic of the primary peak is seen to be entirely he product of secondary interactions, while the main peak itself does not contain nonlinear terms. Although the nonlinear wave interaction theory in water of finite depth is limited to the second order at present, tertiary and higher-order interactions are taking place in nature. This is exemplified in the appearance of auxiliary spectral peaks at higher harmonics of the frequency of the primary peak in some of the wave spectra recorded in relatively shallow water.

The secondary interactions among spectral components also produce the group-bounded long waves. The presence of spectral energy in the low frequency range such as shown in Fig. 9.15 reflects the result of the secondary wave interactions. Sand[43] presents other examples in which the magnitudes of the low frequency component of the observed wave spectra agree with the theoretical prediction of the secondary interaction terms. Group-bounded waves cause a lowering of the mean water level beneath a group of high waves, or the
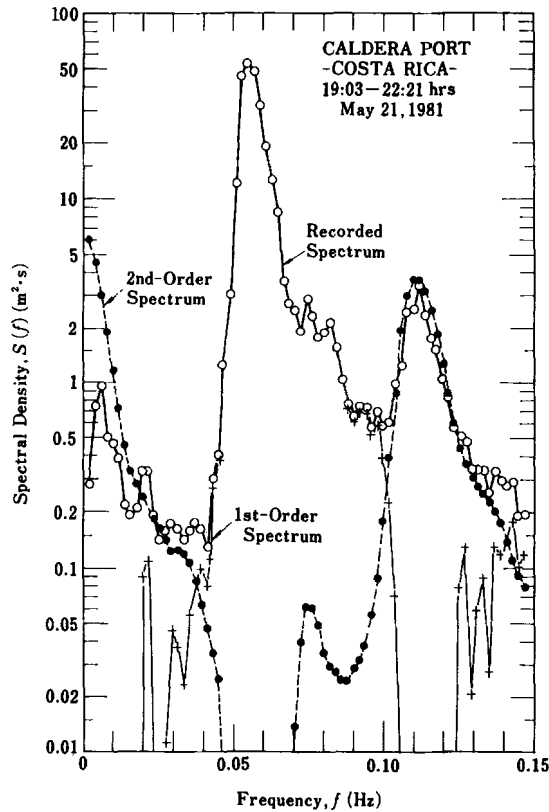
Fig. 9.15. Resolution of linear and nonlinear spectral components for a recorded spectrum.[10]

phenomenon of wave setdown which was predicted by Longuet-Higgins and Stewart[44] by using the concept of the radiation stress. Barthel *et al.*[44] discuss the problem of correctly reproducing such group-bounded long waves in laboratories.

Nonlinear interactions of spectral components in directional seas are more complicated, because the vector sum and difference of interacting wave number vectors must be calculated. Theory of the secondary interactions among directional spectral components was first given by Sand,[46] and then Kimura[47] and Okihiro *et al.*[48]: Kimura's formula have been re-presented by Sekimoto of *et al.*[49] Such theories have mainly been developed to clarify the mechanism of infragravity waves (with the period in the range of about 20 s to several

minutes), from the viewpoint that a major part of infragravity waves must be the group-bounded long waves. The nonlinear interactions among directional wave components are known to produce the amplitude of low frequency waves much smaller than that produced by unidirectional wave interactions, because a slight difference between the directions of two interacting components causes an appreciable decrease in the resultant amplitude in the low frequency range. Though it is acknowledge that the group-bounded long waves produced by nonlinear interactions constitute the major part of infragravity waves, there are several other mechanisms such as the temporal and spatial variations of radiation stresses in the surf zone, grouping of wave up-rush on the beach and its reflection as a long wave, free long waves released in the surf zone through wave breaking, etc. It will be some time before a quantitative prediction of infragravity wave activity will become possible.

9.6 Sampling Variability of Sea Waves

The irregularity of the profiles of sea waves suggests that the mean wave height, period and other statistical parameter must be treated not as deterministic quantities but as stochastic quantities. An example of the variation of a statistical quantity can be prepared by arbitrarily drawing a row of numbers from a table of random numbers as shown below and by taking the average of five consecutive numbers. The statistic of the average forms the row of a secondary random quantity as shown in the parentheses.

... 09025 07210 47765 77192 81842 62204 30413 47793 ...
... (3.2) (2.0) (5.8) (5.2) (4.6) (2.8) (2.2) (6.0) ...

Such variability in statistical quantities is inherent to any phenomenon if it is a stochastic process. A record of measured wave profiles is just a sample from the ensembel of sea wave records. Even if the sea state is homogeneous and stationary, another wave record taken at the next observation time or at a neighboring site will surely exhibit a different pattern of wave profiles. The statistical quantities calculated from he second record will not be the same as those from the first record. The reason we analyze wave records for various statistical quantities and calculate wave spectra is to gather clues to the sea conditions which existed at the time of our observation. Statistically speaking, we are trying to estimate the properties of the ensemble from the data of the samples we have obtained. The quantities derived from a sample (i.e., record

of wave profile) themselves are not our final objectives. If we are assured of stationarity of the sea state during the observation, we can take a number of successive wave records and improve the accuracy of the estimate by averaging the results of many records. But stationarity of the sea state is never realized, and we have to make our best efforts to estimate the true properties of the sea state from the wave records we have in our hands.

The statistical quantities of the ensemble which have been estimated from a sample do not represent true value but have a certain range of estimation error. For example, if the observed height of the significant wave is 6.24 m and the coefficient of variation of that observation is 6%, then what we can say is that there is a 50% probability that the true value of the significant wave height of that sea state lies in the range of 5.99 to 6.49 m and that there is a 90% probability that it lies in the range of 5.62 to 6.86 m. In order to make an evaluation of the range of estimation errors, it is necessary to know the distributions of the sample statistics. Many statistics of sea waves can be regarded to follow the normal distribution, with the exception of the statistics of η_{max}, H_{max} and T_{max}. Thus, we can evaluate the range of estimation errors once we know the standard deviations of the various wave statistics.

If the data consist of random samples, established results of statistics can be used. Let us suppose that we take n random samplings of a statistical variable x and calculate the arithmetic mean $\bar{x}$, the root-mean-square value x_{rms}, the skewness $\sqrt{\beta_1}$, and the kurtosis β_2. These statistics have the following variances [9.50]:

$$\text{Mean}: \text{Var}[\bar{x}] = \mu_2/n = \sigma^2/n\,, \tag{9.138}$$

$$\text{Standard deviation}: \text{Var}[x_{rms}] = (\mu_4 - \mu_2^2)/4\mu_2 n\,, \tag{9.139}$$

$$\text{Skewness}: \text{Var}[\sqrt{\beta_1}] = 6/n\,, \tag{9.140}$$

$$\text{Kurtosis}: \text{Var}[\beta_2] = 24/n\,, \tag{9.141}$$

where

$$\text{Var}[X] = E[(X - E[X])^2] = E[X^2] - E[X]^2\,, \tag{9.142}$$

$$\mu_n = \int_{-\infty}^{\infty} (x - \bar{x})^n p(x)dx\,. \tag{9.143}$$

The quantity $p(x)$ denotes the probability density function of x, and σ^2 is the variance of the ensemble of x.

Among the above formulas, the first two can be applied to an ensemble with any statistical distribution, whereas the formulas for the skewness and kurtosis are only applicable to an ensemble possessing the normal distribution. Thus, the mean length of a run of wave height given by Eq. (9.64), for example, has the following variance:

$$\text{Var}[\bar{j}_1] = \frac{p_{22}}{N_R(1 - p_{22})^2}, \qquad (9.144)$$

in which N_R refers to the numbers of runs of the wave heights in a record, though it is not a random sampling in the strict sense. Because N_R is on the order of ten for many wave records, relatively large variations are inevitably associated with the statistics of wave groups.

The correlation coefficient between two statistical variables has the following variance [9.51]:

$$\text{Var}[\rho] = (1 - \rho^2)^2/n, \qquad (9.145)$$

where n denotes the number of pairs of variables and ρ is the correlation coefficient between the two ensembles. Equation (9.142) indicates that the variance of the correlation coefficient decreases as the correlation becomes higher.

Equations (9.138) to (9.141) cannot be applied directly to the data from wave records, because water surface elevations read off at constant time intervals are mutually correlated and do not constitute a data of random sampling. The correlation between instantaneous surface elevations is dictated by the frequency spectrum, and thus the variability of wave statistics is governed by the functional shape of wave spectrum. The coefficient of variation of the variance of surface elevation $\eta_{\text{rms}}^2 = m_0$, for example, has theoretically been given by Tucker[52] and Cavanié.[53] The result can be rewritten in the following expression:

$$\text{C.V.}[m_0] = \frac{\sigma(m_0)}{E[m_0]} = \frac{1}{\sqrt{N_0} m_0} \left[\int_0^\infty \bar{f} S^2(f) df \right]^{1/2}, \qquad (9.146)$$

where C.V. $[x]$ denotes the coefficient of variation of an arbitrary statistic x, $\sigma(x)$ is the standard deviation, $E[x]$ refers to the expected value, N_0 stands for the number of waves in a record, and $\bar{f}$ is the mean frequency. The coefficient of variation of the root-mean-square value of surface elevation η_{rms} is evaluated as one half of that of η_{rms}^2 given by Eq. (9.146), unless the latter is not so large.

As for the coefficient of variation of the mean period T_{02}, estimated from the wave spectrum, Cavanié[53] has given a theoretical prediction, which is rewritten

using the number of waves in a record as follows:

$$\text{C.V. } [T_{02}] = \frac{1}{2\sqrt{N_0}} \left\{ \overline{f} \int_0^\infty S^2(f) \left[\frac{f^4}{m_2^2} - \frac{2f^2}{m_0 m_2} + \frac{1}{m_0^2} \right]^{1/2} df \right\} . \quad (9.147)$$

Except for the above two, no theory is available for the variability of wave statistics in general. To fill the gap of information, the author[54] has carried out a series of numerical simulations of wave profiles for various spectral shapes: these simulation data have been utilized for rewriting the JONSWAP and Wallops spectra in terms of the significant wave height and period as described in Sec. 2.3.1 and for preparing Tables 2.3 and 2.4 in Sec. 2.4. For each wave spectrum, 2000 samples of different wave profiles with 4096 data points (12 data per peak period) were generated with the inverse FFT method by means of the Monte Carlo simulation technique, and various wave statistics of surface elevation, characteristic wave heights and periods were analyzed by the zero-upcrossing method. The standard deviation and the coefficient of variation of each wave statistic were computed from this 2000 data set, respectively. Because the variability of most of the wave statistics is inversely proportional to the square root of the number of waves as expressed in Eqs. (9.146) and (9.147), the resultant standard deviation and coefficient of variation have been formulated in the following equations by introducing a proportionally coefficient α:

$$\sigma(x) = \frac{\alpha}{\sqrt{N_0}} , \quad \text{C.V. } [x] = \frac{\alpha}{\sqrt{N_0}} . \quad (9.148)$$

The proportionality coefficient α has been determined for each wave statistic as listed in Tables 9.3 and 9.4.

According to the above numerical simulations, the variations of the skewness $\sqrt{\beta_1}$ and the atiltness β_3 decrease as the spectral peak becomes sharp, while the variation of the kurtosis β_2 increases. The kurtosis indicates a slight departure from the power of $-1/2$ in its proportionality to N_0; its variability seems proportional to the power of $-1/3$ of N_0 when the exponent m of the Wallops spectrum or the peak enhancement factor γ of the JONSWAP spectrum is large.

The variability of the characteristic wave heights increases as the spectral peak becomes sharp. This tendency is expected by Tucker's theory: the coefficient of variation of η_{rms} by numerical experiments almost agrees with

Table 9.3. Proportionality coefficient α for the standard deviation of parameters of surface elevation for various wave spectra[54]

$$\sigma(\beta_i) = \alpha/\sqrt{N_0}.$$

Parameter	Wallops-type Spectrum				JONSWAP-type Spectrum		
	$m = 3$	$m = 5$	$m = 10$	$m = 20$	$\gamma = 3.3$	$\gamma = 10$	$\gamma = 20$
Skewness $\sqrt{\beta_1}$	0.93	0.72	0.32	0.08	0.62	0.47	0.38
Kurtosis β_2	2.29	2.57	3.05	3.49	2.77	3.27	3.68
Atiltness β_3	0.88	0.77	0.40	0.09	0.75	0.68	0.60

Note: The values listed in this table are based on the results of numerical simulations of wave profiles with given wave spectra in the frequency range of $f = (0.5 \sim 6.0)f_p$.

Table 9.4. Proportionality coefficient α for characteristic wave heights and periods for various wave spectra[54]

$$\text{C.V.}\,[x] = \alpha/\sqrt{N_0}.$$

Height & Period Ratio	Wallops-type Spectrum				JONSWAP-type Spectrum		
	$m = 3$	$m = 5$	$m = 10$	$m = 20$	$\gamma = 3.3$	$\gamma = 10$	$\gamma = 20$
$H_{1/10}$	0.64	0.70	0.81	0.94	0.83	1.03	1.17
$H_{1/3}$	0.57	0.60	0.69	0.80	0.72	0.91	1.04
$\bar{H}$	0.61	0.64	0.70	0.81	0.77	0.96	1.08
$\sigma(H)$	0.74	0.79	0.93	1.09	0.92	1.13	1.31
$T_{1/10}$	0.64	0.48	0.31	0.22	0.35	0.24	0.19
$T_{1/3}$	0.49	0.35	0.24	0.17	0.26	0.17	0.14
$\bar{T}$	0.51	0.40	0.28	0.22	0.40	0.37	0.32
$\sigma(T)$	0.66	0.66	0.74	0.88	0.66	0.97	1.32

Note: The values listed in this table are based on the results of numerical simulations of wave profiles with given wave spectra in the frequency range of $f = (0.5 \sim 6.0)f_p$.

the prediction by Eq. (9.146). Though the standard deviation of $H_{\max}$ is not listed in Table 9.4, it can be evaluated by Eq. (9.36) in Sec. 9.1.3. However, the coefficient of variation of $H_{\max}$ observed in numerical experiments was smaller by up to 10% than the theoretical prediction, when the spectrum had a broad peak.[54] The difference seems to be related with the narrowness of the distribution of wave heights by simulations compared with the Rayleighan. Contrary to the variation of wave heights, the coefficient of variation of characteristic wave period decreases as the spectral peak becomes sharp.

Table 9.4 also reveals that the significant wave has smaller variations in both the height and period than the mean wave. In the case of $m = 5$ representing typical wind waves and for a record length of 100 waves, the coefficient of variation of $H_{1/3}$ is 6.0% against that of 6.4% for $\overline{H}$, while the coefficient of variation of $T_{1/3}$ is 3.5% against that of 4.0% for $\overline{T}$. The inferiority of the statistical stability of the mean wave to that of the significant wave seems to be caused by inclusion of many small waves in a wave record, which are more susceptible to sampling variability, for calculation of the mean wave height and period.

Variations in the characteristic wave heights and periods mean that wave height ratios such as $H_{1/3}/\overline{H}$ and the period ratios such as $T_{1/3}/\overline{T}$ are also subject to statistical variability. The fluctuations of the height and period ratios from wave records presented in Sec. 2.2.2 are examples of sampling variability. Although the full varification of the statistical variability of sea waves by the field data is not feasible because of the lack of stationarity, the data in Sec. 2.2.2 and the data of simultaneous wave measurements at three sites off Sakata Port (Fig. 3.28 in Sec. 3.5) provide the evidence of statistical variability: these data seems to indicate a slightly greater variability than those in Table 9.4 by numerical simulations.

Attention must be paid to the sampling variability of sea waves in the planning of wave observations, in the utilization of analyzed wave data, and in hydraulic model testing with random waves. For example, if wave recorders are set at two locations separated by several hundred meters in coastal water of nearly uniform topography, the two recorders may yield significant wave heights differing by 10%. It is not possible, however, to determine from one set of such data alone whether the difference is physically meaningful or was caused by sampling variability.

In general, the variance of a statistical variable defined by linear operations on normal variates is given by the sum of the variances of the individual variables. Thus, the difference between the characteristic wave heights and periods at two stations has a standard deviation of $\sqrt{2}$ times that of a single station. A comparison of hindcasted and recorded wave data should also be made with due allowance for he range of sampling variability of the recorded data.

Sampling variability of sea waves also appear in estimations of the spectral density. This subject is discussed in Sec. 10.2.1.

References

1. S. O. Rice, "Mathematical analysis of random noise," 1944, reprinted in *Selected Papers on Noise and Stochastic Processes* (Dover Pub., 1954) pp. 132–294.
2. M. S. Longuet-Higgins, "On the statistical distributions of sea waves," *J. Marine Res.* **XI** (3) (1952), pp. 245–265.
3. D. E. Cartwright and M. S. Longuet-Higgins, "The statistical distribution of the maxima of random function," *Proc. R. Soc. London, Ser. A.* **237** (1956), pp. 212–232.
4. Y. Goda, "Estimation of wave statistics from spectral information," *Proc. Int. Symp. Ocean Wave Measurement and Analysis (WAVES'74)*, ASCE 1 (1974), pp. 320–337.
5. M. A. Tayfun, "Effects of spectrum band width on the distribution of wave heights and periods," *Ocean Engrg.* **10** (2) (1983), pp. 107-118.
6. A. Naess, "On the distribution of crest to trough wave heights," *Ocean Engrg.* **12** (3) (1985), pp. 221–234.
7. G. Z. Forristall, "The distribution of measured and simulated wave heights as a function of spectral shape," *J. Geophys. Res.* **89** (C6) (1984), pp. 10,547–10,552.
8. A. G. Davenport, "Note on the distribution of the largest value of a random function with application to gust loading," *Proc. Inst. Civil Engrg.* **28** (1964), pp. 187–224.
9. H. Cramer, *Mathematical Methods of Statistics* (Princeton Univ. Press, 1946), p. 376.
10. Y. Goda, "Analysis of wave grouping and spectra of long-travelled swell," *Rept. Port and Harbour Res. Inst.* **22** (1) (1983), pp. 3–41.
11. Y. Goda, "Numerical experiments on wave statistics with spectral simulation," *Rept. Port and Harbour Res. Inst.* **9** (3) (1970), pp. 3–57.
12. Y. Goda, "On wave groups," *Proc. BOSS' 76* 1 (Trondheim, 1976), pp. 115–128.
13. E. R. Funke and E. P. D. Mansard, "On the synthesis of realistic sea states," *Proc. 17th Int. Conf. Coastal Engrg.* (Sydney, 1980), pp. 3-57.
14. H. Rye, "Ocean wave groups," *Dept. Marine Tech., Norwegian Inst. Tech.* Rept. UR-82-18 (1982), 214p.
15. A. Kimura, "Statistical properties of random wave groups," *Proc. 17th Int. Conf. Coastal Engrg.* (Sydney, 1980), pp. 2955–2973.
16. J. A. Battjes, and G. Ph. van Vledder, "Verification of Kimura's theory for wave group statistics," *Proc. 19th Int. Conf. Coastal Engrg.* (Houston, 1984), pp. 642–648.
17. M. S. Longuet-Higgins, "Statistical properties of wave groups in a random sea state," *Phil. Trans. R. Soc. London, Ser. A* **312** (1984), pp. 219–250.
18. W. B. Davenport and W. L. Root, *Introduction to the Theory of Random Signals and Noise* (McGraw-Hill, 1958).
19. Y. Goda, "Numerical examination of several statistical parameters of sea waves," *Rept. Port and Harbour Res. Inst.* **24** (4) (1985), pp. 65–102 (*in Japanese*).

20. M. S. Longuet-Higgins, "The statistical analysis of a random, moving surface," *Phil. Trans. R. Soc. London, Ser. A (966)* **249** (1957), pp. 321–387.

21. M. S. Longuet-Higgins, "On the joint distribution of the periods and amplitudes of sea waves," *J. Geophys. Res.* **80** (18) (1975), pp. 2688–2694.

22. Y. Goda, "The observed joint distribution of periods and heights of sea waves," *Proc. 16th Int. Conf. Coastal Engrg.* (Hamburg, 1978), pp. 227–246.

23. C. L. Bretschneider, "Wave variability and wave spectra for wind-generated gravity waves," *U. S. Army Corps of Engrg, Beach Erosion Board, Tech. Memo.* (113) (1959), 192p.

24. A. Cavanié, A. Arhan, and R. Ezraty, "A statistical relationship between individual heights and periods of sea waves," *Proc. BOSS' 76* **II** (Trondheim, 1976), pp. 354–360.

25. M. S. Longuet-Higgins, "On the joint distribution of wave periods and amplitudes in a random wave field," *Proc. R. Soc. London, Ser. A.* (1983), pp. 241–258.

26. N. E. Huang and S. R. Long, "An experimental study of the surface elevation probability distribution and statistics of wind-generated waves," *J. Fluid Mech.* **101** (1980), pp. 179–200.

27. Y. Goda, "A unified nonlinearity parameter of water waves," *Rept. Port and Harbour Res. Inst.* **22** (3) (1983), pp. 3–30.

28. N. Mori and T. Yasuda, "Weakly non-Gaussian model of wave height distribution for random wave train, *Proc. 16th Int. Conf. Offshore Mech. Arctic Engrg. (OMAE)* **II** (1997), pp. 99–104.

29. T. Yasuda and N. Mori, "Weakly non-Gaussian model of wave height distribution for random waves," *Proc. 25th Int. Conf. Coastal Engrg.* (Orlando, 1996), pp. 850–863.

30. Y. Goda and K. Nagai, "Investigation of the statistical properties of sea waves with field and simulation data," *Rept. Port and Harbour Res. Inst.* **13** (1) (1974), pp. 3–38 (*in Japanese*).

31. D. Myrhaug and S. P. Kjeldsen, "Parametric modelling of joint probability density functions for steepness and asymmetry in deep water waves," *Applied Ocean Res.* **6** (4) (1984), pp. 207–220.

32. D. Myrhaug and S. P. Kjeldsen, "Steepness and asymmetry of extreme waves and the highest waves in deep water," *Ocean Engrg.* **13** (6) (1986), pp. 187–224.

33. Y. Goda, "Effect of wave tilting on zero-crossing wave heights and periods," *Coastal Engrg. in Japan* **29** (1986), pp. 79–90.

34. M. A. Tayfun, "Nonlinear effects on the distribution of crest-to-trough wave heights," *Ocean Engrg.* **10** (2) (1983), pp. 97–106.

35. M. S. Longuet-Higgins, "On the distribution of the heights of sea waves: Some effects of nonlinearity and finite band width," *J. Geophys. Res.* **85** (C3) (1980), pp. 1519–1523.

36. T. Vinje, "The statistical distribution of wave heights in a random seaway," *Applied Ocean Res.* **11** (3) (1989), pp. 143–152.

37. K. G. Nolte and F. S. Hsu, "Statistics of larger waves in a sea state," *Proc. ASCE* **105** (WW4) (1979), pp. 389–404.

38. T. Honda and H. Mitsuyasu, "On the joint distribution of the heights and periods of ocean waves," *Proc. 25th Japanese Conf. Coastal Engrg.* (1978), pp. 75-79 (*in Japanese*).

39. A. Masuda, Y. Kuo, and H. Mitsuyasu, "On the dispersion relation of random gravity waves. Part 1. Theoretical framework," *J. Fluid Mech.* **92** (1979), pp. 717–730.

40. H. Mitsuyasu, Y. Kuo, and A. Masuda, "On the dispersion relation of random gravity waves. Part 2. An experiment," *J. Fluid Mech.* **92** (1979), pp. 731–749.

41. L. J. Tick, "Nonlinear probability models of ocean waves," *Ocean Wave Spectra* (Prentice-Hall, 1963), pp. 163–169.

42. T. Hamada, "The secondary interactions of surface waves," *Rept. Port and Harbour Res. Inst.* (10) (1965), 28p.

43. S. E. Sand, "Wave grouping described by bounded long waves," *Ocean Engrg.* **9** (6) (1982), pp. 567–580.

44. M. S. Longuet-Higgins and R. W. Stewart, "Radiation stresses in water waves; A physical discussion, with applications," *Deep-Sea Res.* **11** (1964), pp. 529–562.

45. V. Barthel, E. P. D. Mansard, S. E. Sand, and F. C. vis, "Group bounded long waves in physical models," *Ocean Engrg.* **10** (4) (1983) pp. 261–294.

46. S. E. Sand, "Long waves in directional seas," *Coastal Engrg.* **6** (3) (1982), pp. 195–208.

47. A. Kimura, "Average two-dimensional low-frequency wave spectrum of wind waves," *Commun. Hydraulics, Dept. Civil Engrg., Delft Univ. Tech., Rept.* (84-3) (1984), 54p.

48. M. Okihiro, R. T. Guza, and R. J. Seymour, "Bound infragravity waves," *J. Geophys. Res.* **97** (C7) (1992), pp. 11453–11469.

49. T. Sekimoto, T. Simizu, K. Kondo, and Y. Kubo, "Field observation of surf beat outside the surf zone," *Proc. 23rd Int. Conf. Coastal Engrg.* (Venice, 1992), pp. 804–817.

50. M. G. Kendall and A. T. Stuart, *The Advanced Theory of Statistics* 1 3rd ed., (Griffin, 1969), p. 243.

51. Kendall and Stuart, *loc. cit.* p. 236.

52. M. J. Tucker, "The analysis of finite-length records of fluctuating signals," *Brit. J. Applied Phys.* **8** (Apr. 1957), pp. 137–142.

53. A. G. Cavanié, "Evaluation of the standard error in the estimation of mean and significant wave heights as well as mean period from records of finite length," *Proc. Int. Conf. Sea. Climatology* Édition Technip (Paris, 1979), pp. 73–88.

54. Y. Goda, "Statistical variability of sea state parameters as a function of a wave spectrum," *Coastal Engrg. in Japan* **31** (1) (1988), pp. 39–52.

Chapter 10

Techniques of Irregular
Wave Analysis

10.1 Statistical Quantities of Wave Data

10.1.1 *Analysis of Analog Data*

Many wave recorders at present are equipped with electronic units which convert analog signals of the surface wave profile into digital signals and record them on a real-time basis. These signals are later processed by computers to yield information of the wave heights and periods as well as the spectra. Old types of wave recorders, however, processed information of the wave profile as an analog signal and registered it on a strip-chart. These records needed to be analyzed manually. Because such conventional wave recorders are still in some use, the analysis techniques for analog data are discussed in this subsection.

The first operation to be performed on a strip-chart record is to draw the line representing the mean water level. This is done by visual judgment. If a gradual variation in the mean water level is observable owing to the effects of tidal variations or other factors, a sloping straight line or even a curve can be fitted to the data. Then individual waves are defined by the zero-upcrossing (or zero-downcrossing) method described in Sec. 2.1.2. The zero line of the mean water level which was set initially must be observed strictly, as every crossing of the zero line must be counted as one wave. Then the heights and periods of the individual waves are read off the records, and the results are written on a sheet such as that in Table 2.1. The heights and periods of the highest wave, one-tenth highest wave, significant wave, and mean wave are calculated on the basis of such a table. If information on only the sea state
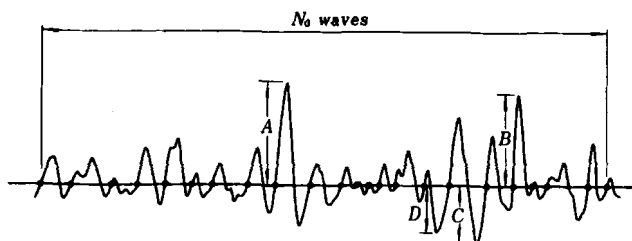
316

Fig. 10.1. Definition sketch for application of the Tucker method.

is sought, the calculation may be limited to the significant wave height and period, because these quantities are the representative parameters among the various characteristic wave heights and periods.

For a rapid analysis of a wave record, the method proposed by Tucker[1] may be employed. The method is based on the assumption of the Rayleigh distribution of the wave height, examined in Sec. 9.1.2. Procedures of the analysis are as follows. After drawing the zero line, readings are made for the largest positive amplitude A, the second largest positive amplitude B, the largest negative amplitude C, and the second largest negative amplitude D, as illustrated in Fig. 10.1. Also, the number of zero-upcrossing waves N_0 contained in the wave record is counted. Next, the heights H_1 and H_2 are defined as follows:

$$H_1 = A + C, \quad H_2 = B + D. \tag{10.1}$$

Then the root-mean-square surface elevation can be estimated as

$$\eta_{\rm rms} = \frac{1}{2}(\eta_1 + \eta_2), \tag{10.2}$$

where

$$\eta_1 = \frac{H_1}{2\sqrt{2\ln N_0}\left[1 + \frac{0.289}{\ln N_0} - \frac{0.247}{(\ln N_0)^2}\right]}, \tag{10.3}$$

$$\eta_2 = \frac{H_2}{2\sqrt{2\ln N_0}\left[1 - \frac{0.211}{\ln N_0} - \frac{0.103}{(\ln N_0)^2}\right]}. \tag{10.4}$$

Once the value of $\eta_{\rm rms} = m_0^{1/2}$ is estimated, characteristic wave heights such as $H_{1/10}$, $H_{1/3}$ and $\overline{H}$ can be estimated by means of the relations in Table 9.1.

The mean wave period is simply obtained by dividing the record length by N_0. The periods $T_{1/10}$ and $T_{1/3}$ may be estimated with Eq. (2.9) of Sec. 2.2.3. The values of H_{max} and T_{max} are directly read from the wave record.

The reliablity of the Tucker method depends on the accuracy of the fit of the Rayleigh distribution to the wave height. If the highest wave tends to appear with a height greater than predicted by the Rayleigh distribution, η_{rms} will be overestimated. On the other hand, if the upper portion of the wave height distribution tends to appear with less probability than given by the Rayleigh distribution, η_{rms} will be underestimated. Even if the estimate of η_{rms} is correct on the average, the statistical variability of these estimated wave heights is large because only four quantities are employed; the coefficient of variation is about 10% or greater.

If it is required to make a more detailed analysis of a strip-chart record, such as for the wave spectra, the analog record of the wave profiles should be digitized with the aid of a digitizing machine or by manual reading of the wave profiles at intervals of 1 s or so.

10.1.2 *Analysis of digital data*

The analysis of digital wave records by a computer is made in several steps. Figure 10.2 presents an example of the flow of the data analysis. Since the flow diagram is self-explanatory, only selected portions of the data processing techniques will be discussed.

(A) *Data length and time interval of data sampling*

The standard duration of a sea wave recording is 20 min. If the mean wave period is 10 s, a wave record with the above duration contains 120 waves. This number of waves is considered sufficient to keep the sampling variability of the characteristic wave heights and periods below an acceptable level. At the same time, changes in the sea state may become appreciable if the recording length is much longer. The duration of 20 min is employed as a compromise between the requirements of wanting low sampling variability and having a stationary sea state. Some digital recordings employ the duration of 17 min 4 s, which yields 2048 data points for a sampling rate of twice per second. This is done to economize the computation time for the spectral analysis using the fast Fourier transform algorithm. In hydraulic
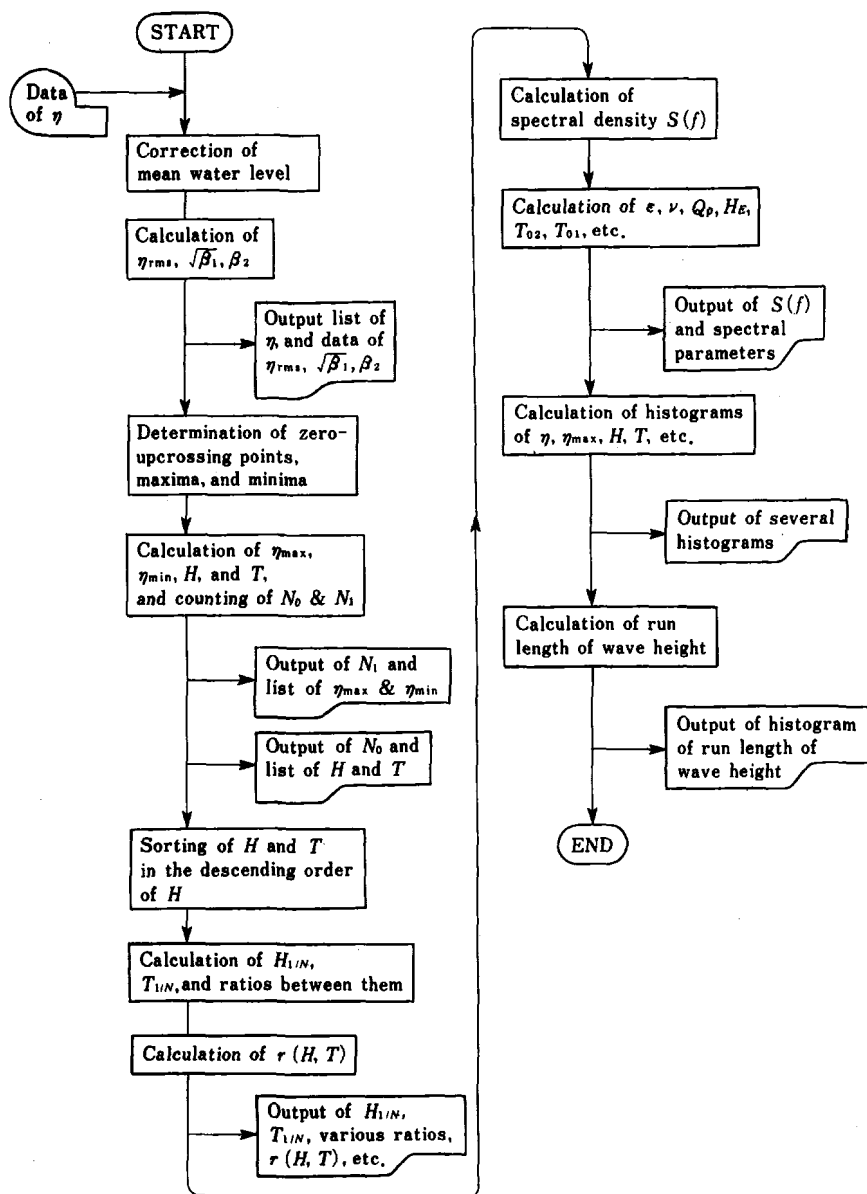
Fig. 10.2. Example of flow of wave data analysis.

model testing with irregular waves, however, wave records are best made for the duration of 200 waves or longer so as to decrease the sampling variation of the wave statistics. Even for field wave observations, the duration of 30 min or longer may be desirable if the sea state is considered rather stationary, as in the case of swell arriving from a remote source.

The sampling interval for the wave profile, on the other hand, should be set as short as practicable. The standard is less than a tenth of the significant wave period, and preferably a twentieth. A finer sampling is not considered beneficial, because the volume of the data processing increases excessively without producing a corresponding increase in the resultant information. A coarser sampling than the above standard introduces the problems of missing small waves, underestimation of the maxima and minima of the wave profiles, underestimation of wave heights, and so on.

(B) *Correction for mean water level*

A simple procedure to determine the mean water level is to use the arithmetic mean of all the data points measured from any reference level. However, as most wave records contain the influence of the tide level variation, it is better to incorporate the following linear or parabolic correction in the analysis of wave data. The formula for the correction of linear change of the mean water level as derived from the least squares method is

$$\bar{\eta} = A_0 + A_1 n \qquad : \quad n = 1, 2, \ldots, N, \tag{10.5}$$

where

$$A_0 = \frac{N_2 Y_0 - N_1 Y_1}{N_0 N_2 - N_1^2}, \quad A_1 = \frac{N_0 Y_1 - N_1 Y_0}{N_0 N_2 - N_1^2}, \tag{10.6}$$

$$N_r = \sum_{n=1}^{N} n^r, \quad Y_r = \sum_{n=1}^{N} n^r \eta_n, \tag{10.7}$$

in which N denotes the total number of data points.

The formula for the correction of the mean water level for a parabolic change by the least squares method is derived as

$$\bar{\eta} = B_0 + B_1 n + B_2 n^2 \qquad : \quad n = 1, 2, \ldots, N, \tag{10.8}$$

where

$$
\left.
\begin{aligned}
B_0 &= \frac{1}{\Delta}[Y_0(N_2N_4 - N_3^2) + Y_1(N_2N_3 - N_1N_4) + Y_2(N_1N_3 - N_2^2)]\,, \\
B_1 &= \frac{1}{\Delta}[Y_0(N_2N_3 - N_1N_4) + Y_1(N_0N_4 - N_2^2) + Y_2(N_1N_2 - N_0N_3)]\,, \\
B_2 &= \frac{1}{\Delta}[Y_0(N_1N_3 - N_2^2) + Y_1(N_1N_2 - N_0N_3) + Y_2(N_0N_2 - N_1^2)]\,, \\
\Delta &= N_0N_2N_4 + 2N_1N_2N_3 - N_2^3 - N_0N_3^2 - N_1^2N_4\,.
\end{aligned}
\right\}
$$

$$(10.9)$$

If a wave record indicates the presence of conspicuous surf beat or long-period oscillations in the mean water level, application of the numerical filter described in Sec. 10.5, is one method for their removal. In any case, correction of the mean water level is the first processing to be made on a wave record.

(C) *Analysis of zero-upcrossing points, maxima and minima*

Zero-upcrossing of the wave profile is detected through the following criteria:

$$\eta_i \cdot \eta_{i+1} < 0 \quad \text{and} \quad \eta_{i+1} > 0\,, \tag{10.10}$$

where η_i denotes the ith data point of the surface elevation after correction of the mean water level. The time of the zero-upcrossing is determined by linear interpolation between the sampling times of η_i and η_{i+1}. The time difference from this point to the next zero-upcrossing point yields the zero-upcrossing wave period. If the zero-downcrossing method is employed, the second inequality in Eq. (10.10) is changed to $\eta_{i+1} < 0$.

The conditions defining a maximum in the wave profile are

$$\eta_{i-1} < \eta_i \quad \text{and} \quad \eta_i > \eta_{i+1}\,. \tag{10.11}$$

It is suggested that the time and the elevation of the maximum point be estimated by fitting a parabolic curve to the three points η_{i-1}, η_i and η_{i+1} in order to eliminate the problem of underestimating the true maximum between two discrete sampling points. The formula for a parabolic fitting is

$$\eta_{\max} = C - B^2/4A \quad \text{and} \quad t_{\max} = t_i - \Delta t B/2A\,, \tag{10.12}$$

where Δt is the data sampling interval and

$$A = \frac{1}{2}(\eta_{i-1} - 2\eta_i + \eta_{i+1}), \quad B = \frac{1}{2}(\eta_{i+1} - \eta_{i-1}), \quad C = \eta_i. \qquad (10.13)$$

In order to determine the zero-upcrossing wave height, the highest point on the surface elevation must be searched for in the time interval between two zero-upcrossing points. Once this point is found among the sampled points, it is designated as η_i, and then η_{max} is estimated by means of Eqs. (10.12) and (10.13) by use of the neighboring data points η_{i-1} and η_{i+1}. The lowest surface elevation η_{min} is obtained by a similar process, and the wave height is calculated as the sum of the absolute values of η_{max} and η_{min}. Unless the technique of parabolic fitting is employed, the data sampling interval must be quite narrow to avoid an artificially introduced decrease in wave height derived from digitized data.

(D) *Calculation of the correlation coefficient between wave height and period*

The correlation coefficient between individual wave heights and periods, $r(H, T)$, may not have immediate practical application, but it is a useful parameter in statistical studies of sea waves. For example, the correlation coefficient is found to be related to the distribution of wave periods,[2] the ratios $T_{1/3}/\overline{T}$ and $\overline{T}/T_p$,[3] and other quantities. Examination of the correlation coefficient among the higher one-third waves may also turn out to be useful in future studies.

In the analysis of wave grouping, the correlation coefficient between successive wave heights is a governing parameter as presented in the theory of Kimura.[4] Thus, it is recommended that this correlation coefficient be incorporated in standard programs of wave data analysis.

(E) *Calculation of spectral parameters*

After the frequency spectrum of the sea waves is analyzed as through the procedure described in the next section, the spectral width parameters ε and ν, the envelope correlation parameter κ, and the spectral peakedness Q_p can be calculated by Eqs. (9.25), (9.90), (9.52) and (9.69), respectively. These parameters are utilized in the comparison of statistical theories of sea waves with data. The spectral width parameter ε can be estimated by Eq. (9.126)

with the numbers of zero-upcrossings and maxima in the wave profiles, and the resultant value can be compared with the spectrally-estimated value.

From the estimate of the frequency spectral density, the mean wave periods T_{02} and T_{01} are obtained from Eqs. (9.77) and (9.96). The various wave heights can be estimated from the relations in Table 9.1 by using the value $\eta_{\mathrm{rms}} = m_0^{1/2}$. These heights are denoted as H_E in Fig. 10.2. As discussed in Sec. 9.5.4, attention should be paid to the presence of nonlinear spectral components in the high frequency range in the calculation of these spectrum-based parameters.

(F) *Frequency distribution of surface elevations, wave heights and periods*

The values of η_i, η_{max}, H and T are conveniently tabulated in the form of frequency distribution. It is also recommended that the joint frequency distribution of H and T be prepared. Frequency distributions provide a convenient means for comparison of wave data with statistical theories, as described in Chapter 9. The distributions are displayed by using absolute values or by nondimensional forms normalized with the mean values. When a large number of wave data sets are analyzed statistically, the latter method is employed. The counting of frequencies in each class is facilitated by using the following algorithm; first, use a constant class interval ΔH, convert the result of the operation $(H_i + \Delta H)/\Delta H$ into an integer, and then add the count of 1 to the class with the same order number as the above integer.

10.2 Frequency Spectrum of Irregular Waves

10.2.1 *Theory of Spectral Analysis*

Equation (8.14) is the fundamental equation for the analysis of the frequency spectrum of the irregular wave profile recorded at a fixed station, and it defines the spectral density function. This equation, however, contains an infinite number of amplitudes a_n of the component waves, and it is not applicable to practical computations. In this section, we consider the situation of wave profiles given in the sequential form of N data points $\eta(\Delta t), \eta(2\Delta t), \ldots, \eta(N\Delta t)$ sampled at a constant interval Δt, and we try to estimate the associated spectral density function. To simplify the explanation, N is taken to be an even number.

By making a harmonic analysis of the time series of the wave profile $\eta(t)$, the profile can be expressed as the following finite Fourier series:

$$\eta(t_*) = \frac{A_0}{2} + \sum_{k=1}^{N/2-1} \left(A_k \cos \frac{2\pi k}{N} t_* + B_k \sin \frac{2\pi k}{N} t_* \right) + \frac{A_{N/2}}{2} \cos \pi t_* , \quad (10.14)$$

where

$$t_* = t/\Delta t \qquad : \quad t_* = 1, 2, \ldots, N .$$

Equation (10.14) gives the same surface elevations as the original wave profile $\eta(n\Delta t)$ at the points of $t_* = 1, 2, \ldots, N$, if the Fourier coefficients are determined as

$$A_k = \frac{2}{N} \sum_{t_*=1}^{N} \eta(t_*) \cos \frac{2\pi k}{N} t_* \qquad : \quad 0 \le k \le N/2 , \qquad (10.15)$$

$$B_k = \frac{2}{N} \sum_{t_*=1}^{N} \eta(t_*) \sin \frac{2\pi k}{N} t_* \qquad : \quad 1 \le k \le N/2 - 1 . \qquad (10.16)$$

Although a harmonic analysis provides definite values for the Fourier amplitudes of a deterministic process, it yields only a probabilistic answer for a stochastic process. Because sea waves form a random process, different values of the Fourier amplitudes A_k and B_k will be obtained whenever different sample records of the surface elevation $\eta(t)$ are analyzed. As described in Sec. 8.3, $\eta(t)$ can be regarded as a stationary stochastic process which follows the normal distribution. If the number of data points N is sufficiently large, the amplitudes A_k and B_k also follow the normal distribution with a zero mean by virtue of the central limit theorem, as seen from the form of Eqs. (10.15) and (10.16). Their variances are calculated as follows.

First, A_k^2 is calculated for the case of $k \ne 0$ or $k \ne N/2$. The result is

$$A_k^2 = \frac{4}{N^2} \left\{ \sum_{t_*=1}^{N} \eta(t_*) \cos \frac{2\pi k}{N} t_* \right\}^2 = \frac{4}{N^2} \left\{ \sum_{t_*=1}^{N} \eta^2(t_*) \left(\cos \frac{2\pi k}{N} t_* \right)^2 \right.$$

$$\left. + 2 \sum_{\tau_*=1}^{N-1} \sum_{t_*=1}^{N-\tau_*} \eta(t_*)\eta(t_* + \tau_*) \cos \frac{2\pi k}{N} t_* \cos \frac{2\pi k}{N} (t_* + \tau_*) \right\} . \quad (10.17)$$

By taking the asymptotic condition of $N \to \infty$, the expected value of A_k^2 is calculated as

$$E[A_k^2] = \lim_{N \to \infty} \frac{2}{N^2} \left\{ \sum_{t_* = 1}^{N} \eta^2(t_*) + 2 \sum_{\tau_* = 1}^{N-1} \sum_{t_* = 1}^{N - \tau_*} \eta(t_*) \eta(t_* + \tau_*) \cos \frac{2\pi k}{N} \tau_* \right\}.$$

(10.18)

To arrive at the above result, use was made of the fact that the expected value of $(\cos 2\pi k t_*/N)^2$ is $1/2$ and that of $(\cos 2\pi k t_*/N) \times (\sin 2\pi k t_*/N)$ is zero. By making use of the autocorrelation function defined by Eq. (8.17) in Sec. 8.3, Eq. (10.18) is rewritten as

$$E[A_k^2] = \lim_{N \to \infty} \frac{2}{N} \left\{ \Psi(0) + 2 \sum_{\tau_* = 1}^{N-1} \Psi(\tau_*) \cos \frac{2\pi k}{N} \tau_* \right\}.$$

(10.19)

This equation is further rewritten as follows, by utilizing the fact that $\cos \theta$ is an even function of θ:

$$E[A_k^2] = \lim_{N \to \infty} \frac{2}{N} \sum_{\tau_* = -\infty}^{\infty} \Psi(\tau_*) \cos \frac{2\pi k}{N} \tau_*$$

$$= \lim_{N \to \infty} \frac{2}{N\Delta t} \sum_{\tau = -\infty}^{\infty} \Psi(\tau)(\cos 2\pi f_k \tau) \Delta t,$$

(10.20)

where

$$f_k = k/(N\Delta t) = k/t_0, \quad \tau = \tau_* \Delta t,$$

(10.21)

in which t_0 denotes the duration of the wave record.

We recognize that the right side of Eq. (10.20) is the series representation of the right side of Eq. (8.27) for $S_0(f)$ in Sec. 8.3. Thus, the variance of A_k is related to the spectral density function as

$$E[A_k^2] = \frac{2}{N\Delta t} S_0(f_k) = \frac{1}{N\Delta t} S(f_k) \quad : \quad 1 \le k \le \frac{N}{2} - 1,$$

(10.22)

in which $S_0(f)$ is the two-sided spectral density function defined in the range $-\infty < f < \infty$ and is equal to $S(f)/2$. The variance of B_k is also calculated in the same way to give

$$E[B_k^2] = \frac{1}{N\Delta t} S(f_k) \quad : \quad 1 \le k \le \frac{N}{2} - 1.$$

(10.23)

We can also obtain the following results for A_0 and $A_{N/2}$:

$$E[A_0^2] = \frac{2}{N\Delta t} S(f_0) \,, \quad E[A_{N/2}^2] = \frac{2}{N\Delta t} S(f_{N/2}) \,. \tag{10.24}$$

We have shown that the Fourier coefficients A_k and B_k are both stochastic variables which follow the normal distribution, and have a zero mean and variance $S(f)/(N\Delta t)$.[a] The correlation between A_k and B_k is examined below through their covariance:

$$\begin{aligned} E[A_k B_k] &= \lim_{N\to\infty} \frac{4}{N^2} \left\{ \sum_{t_*=1}^{N} \eta(t_*) \cos\frac{2\pi k}{N} t_* \right\} \left\{ \sum_{t_*=1}^{N} \eta(t_*) \sin\frac{2\pi k}{N} t_* \right\} \\ &= \lim_{N\to\infty} \frac{4}{N} \sum_{\tau_*=1}^{N-1} \Psi(\tau_*) \sin\frac{2\pi k}{N}\tau_* \,. \end{aligned} \tag{10.25}$$

By recalling that $\Psi(\tau)$ can be expressed as the cosine transformation of $S(f)$ by means of Eq. (8.25), we conclude that the right side of Eq. (10.25) converges to zero. That is to say, A_k and B_k are statistically independent.

With the above preparations, we can now proceed to the estimation of the spectral density. First, we introduce the variable I_k defined by

$$I_k = \begin{cases} N(A_k^2 + B_k^2) & : \quad 1 \le k \le N/2 - 1 \,, \\ N A_0^2 & : \quad k = 0 \,, \\ N A_{N/2}^2 & : \quad k = N/2 \,. \end{cases} \tag{10.26}$$

Because I_k is the sum of the squares of two independent stochastic variables of a normal distribution, I_k is a stochastic variable which follows the chi-square distribution with two degrees of freedom. Only the I_k for $k = 0$ and $N/2$ follow the chi-square distribution with one degree of freedom. The chi-square distribution is the distribution of stochastic variable defined by

$$\chi_r^2 = \sum_{i=1}^{r} x_i^2/\sigma^2 \,, \tag{10.27}$$

where x_i is a normally distributed variable with zero mean and variance of σ^2. The probability density function of χ_r is given by

$$p(\chi_r^2) = \frac{1}{2^{r/2}\Gamma(r/2)} (\chi_r^2)^{r/2-1} e^{-\chi_r^2/2} \,, \tag{10.28}$$

---

[a]The derivation given here is not mathematically rigorous. The reader is referred to Koopmans[5] or other references on statistics for details.

in which $\Gamma(x)$ denotes the gamma function. The number of terms r is called the degree of freedom of the chi-square distribution. By using χ_r^2, the variable I_k is rewritten as

$$I_k = \begin{cases} \dfrac{1}{\Delta t} S(f_k) \chi_2^2 & : \quad 1 \le k \le N/2 - 1, \\[2mm] \dfrac{2}{\Delta t} S(0) \chi_1^2 & : \quad k = 0, \\[2mm] \dfrac{2}{\Delta t} S(f_{N/2}) \chi_1^2 & : \quad k = N/2. \end{cases} \qquad (10.29)$$

From the properties of the chi-square distribution, the expected value and variance of I_k are obtained as

$$E[I_k] = \frac{2}{\Delta t} S(f_k) \qquad : \quad 0 \le k \le N/2, \qquad (10.30)$$

$$\mathrm{Var}[I_k] = \frac{4}{(\Delta t)^2} S^2(f_k) \quad : \quad 0 \le k \le N/2. \qquad (10.31)$$

A plot of the variable I_k, defined by Eq. (10.29), against the frequency f_k is called a periodogram. The variable I_k itself is sometimes called a periodogram. Equation (10.30) indicates that the spectral density $S(f_k)$ at the frequency f_k can be estimated through the expected value of the periodogram, but at the same time Eq. (10.31) indicates that the absolute value of I_k varies greatly, with the magnitude of its standard deviation equal to its mean value. Furthermore, the variability does not decrease even if the data length N is increased. Therefore, if we calculate the periodogram from the Fourier coefficients for a sample of wave profile $\eta(t)$, the resultant periodogram fluctuates greatly from one frequency to another, and the spectral density thus estimated for each frequency f_k has low statistical reliability.

The great variability of the periodogram has been known from early times, and several techniques have been developed to suppress the fluctuation and to increase the reliability of the spectral estimate. One of the popular techniques is the autocorrelation method proposed by Blackman and Tukey[6] in 1958, which is based on Eq. (8.26) in Sec. 8.3. Another technique is a smoothing of the periodogram over a certain frequency band under the assumption that the spectral density function $S(f)$ varies only gradually with respect to the frequency. This is called the smoothed periodogram method[b] here. Smoothing

---

[b]This method is usually called the FFT method, because the calculation of the periodogram is usually done with the fast Fourier transform technique.

is done by using one of several weight functions. In the following, a discussion is given for the case of simple averaging with uniform weight.

The formula for the simple averaging method to obtain the estimate of the spectral density $\hat{S}(f_k)$ is

$$\hat{S}(f_k) = \frac{1}{n} \sum_{j=k-[(n-1)/2]}^{k+[n/2]} I_j \frac{\Delta t}{2}, \tag{10.32}$$

in which $[n/2]$ denotes the largest integer not exceeding $n/2$.

If the condition

$$S(f_i) \simeq S(f_k) \qquad : \quad k - [(n-1)/2] \leq j \leq k + [n/2] \tag{10.33}$$

holds, then $\hat{S}(f_k)$ is the sum of n chi-square variables with two degrees of freedom each, because the periodograms are mutually independent in the statistical sense. Therefore, $\hat{S}(f_k)$ follows the chi-square distribution with $2n$ degrees of freedom. That is,

$$\hat{S}(f_k) = S(f_k) \chi_{2n}^2 / 2n. \tag{10.34}$$

Because the expected value of χ_{2n}^2 is $2n$, the expected value $E[\hat{S}(f_k)]$ is the same as that of $S(f_k)$. Also, by increasing the data length N and averaging number n while keeping the condition $N \gg n$, the reliability of the spectral estimate can be increased as the variance of $\hat{S}(f_k)$ decreases inversely with increase in n. In fact, the coefficient of variation of the spectral estimate is obtained from the properties of the chi-square distribution as

$$\text{C.V.}[\hat{S}(f_k)] = \frac{\text{Var}[\hat{S}(f_k)]^{1/2}}{E[\hat{S}(f_k)]} = \frac{1}{\sqrt{n}}, \tag{10.35}$$

in which C.V. and Var refer to the coefficient of variation and the variance, respectively.

A quantitative evaluation of the reliability of the spectral estimate is usually made by means of the confidence interval based on the chi-square distribution. That is, we estimate the interval in which the value of the true spectral density lies within a certain range corresponding to a preset level of probability. For example, suppose we have obtained a spectral estimate by averaging 20

periodograms and try to estimate the true spectral density with a 95% confidence interval. The number of degrees of freedom is $2n = 40$ for this case. The upper limit of the 95% confidence interval is obtained from the value of the chi-square variable that satisfies the condition of $P(\chi^2_{40} \leq a) = 0.975$. From a probability table of the chi-square distribution, we obtain $a = 59.34$ or $a/2n = 1.48$. Similarly, the lower limit is obtained as $b/2n = 0.61$ for the condition of $P(\chi^2_{40} \leq b) = 0.025$. Therefore, the true spectral density is estimated to lie in the interval from 0.61 to 1.48 times the observed spectral density. If a spectral estimate is obtained by averaging 40 periodograms, the lower and upper limits of the 95% confidence interval become 0.71 and 1.33 times the estimated values, respectively.

Owing to such variability in the estimated spectral density, the true spectrum of sea waves plotted against the frequency may take any shape within a confidence interval above and below the wave spectrum estimated from one sample of wave records. Figure 10.3 shows an example of the sampling variability of estimated spectra.[7] A continuous record of swell for the duration of 2 hr 30 min was divided into five segments of 30 min length, and the wave spectrum was estimated for the five segments with an effective number of degrees of freedom of 20.9 (the parabolic smoothing function, Eq. (10.48) in the next section, was employed). The five spectral estimates are seen to be scattered around the mean, though the mean does not represent the true spectrum. The mean spectrum has a narrower band of reliability than individual estimates because of the increase in the number of degrees of freedom. A similar analysis of the sampling variability of spectral estimates of field and laboratory wind waves has been reported by Donelan and Pierson,[8] who demonstrated the accuracy of the spectral variability theory described above.

The reliability of the spectral estimate can be improved by increasing the number of periodograms to be averaged together and by increasing the number of degrees of freedom in the spectral estimate. However, this causes a decrease in spectral resolution. The term "spectral resolution" refers to the capability to distinguish two neighboring spectral peaks, and its measure is the minimum frequency distance between two independent spectral estimates. This distance is called the bandwidth. In the case of smoothing by simple averaging as in Eq. (10.32), the bandwidth is given by

$$f_B = f_{k+n} - f_k = \frac{n}{N\Delta t} = \frac{n}{t_0}. \tag{10.36}$$
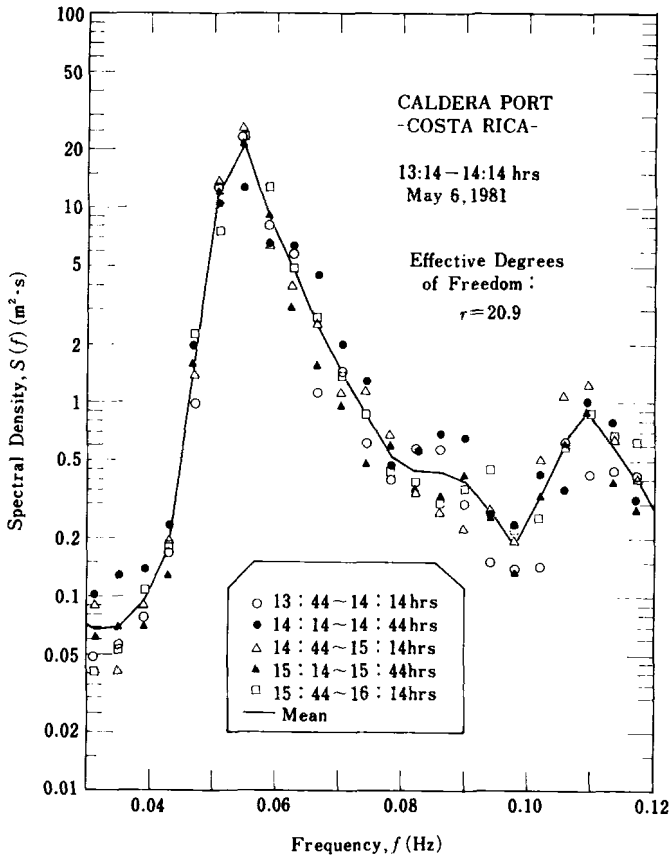
Fig. 10.3. Variations of independent spectral estimates.[7]

The spectral resolution is high when the bandwidth f_B is narrow. The denominator t_0 on the right side of Eq. (10.36) is the duration of the wave record. When t_0 is fixed, f_B is linearly proportional to n, and therefore the resolution is inversely proportional to n. On the other hand, the reliability increases with n. Therefore, a simultaneous improvement in the reliability and resolution of the spectral estimate cannot be made for a wave record of fixed length. This situation is called the Grenander uncertainty principle (see Ref. 9). It should be mentioned here that the minimum possible bandwidth is $(f_B)_{min} = 1/t_0$, which represents a component wave with period equal to the record length.

10.2.2 *Spectral Estimate with Smoothed Periodograms*

As discussed in the previous section, the autocorrelation method and the smoothed periodogram method are both employed for the estimation of the spectral density from a given record of a wave profile. But their theoretical basis is common, and their spectral resolutions and reliabilities are essentially the same. Although differences exist in their computation procedures, Rikiishi[10] has shown that the differences are essentially those of smoothing functions. Since the fast Fourier transform algorithm is available on almost all computers these days, a description and comments will be given on the practical procedures of making spectral estimates with the smoothed periodogram method.

(A) *Record length and data sampling interval*

A wave record should be as long as possible, because the spectral resolution is governed by the record length as given by Eq. (10.36). The data sampling interval of $1/10$ to $1/20$ of the significant wave period is generally recommended for a wave analysis, as discussed in Sec. 10.1. Once the sampling interval Δt is chosen, the highest frequency to which the spectrum can be estimated is automatically determined by

$$f_c = 1/2\Delta t. \tag{10.37}$$

This frequency is called the folding frequency or the Nyquist frequency, and the symbol f_N is sometimes employed. The wave component with this frequency is sampled at the rate of two data points per wave. The word "folding" is used, because any wave energy contained in the frequency range $f > f_c$ is added to the wave energy in the range $0 < f < f_c$ in such a manner that the wave spectrum is folded with the axis at the frequency f_c. This phenomenon is called *aliasing*. In the case of sea waves, the spectral density attenuates in the high frequency range in proportion to f^{-5}, and thus aliasing does not present a serious problem in a spectral analysis if the data sampling interval is selected as discussed in Sec. 10.1.2. In the neighborhood of $f = f_c$, however, the spectral estimate may be increased slightly by the effect of aliasing.

(B) *Correction for mean water level*

This is important in a spectral analysis, too. If the mean value of the surface elevation is not properly adjusted, or a possible gradual trend in the change

of mean water level is not corrected, the spectral estimate near $f = 0$ appears large; this effect extends to other frequency ranges, too.

(C) *Data window*

A wave profile data after making the correction for the mean water level is usually subjected to an operation of data modification before the harmonic analysis. The operation is expressed as

$$\eta(t_*) \to b(t_*)\eta(t_*) \qquad : \quad t_* = 1, 2, \ldots, N. \qquad (10.38)$$

The set of coefficients $b(t_*)$ is generally called the data window. In spectral analysis, a data window is usually designed to attenuate the front and rear portions of the wave record, and such a window is called a taper. Koopmans[11] cites the following two important tapers:

a) Trapezoidal taper

$$b_1(t_*) = \begin{cases} t_*/l & : \quad 0 \leq t_* < l, \\ 1 & : \quad l \leq t_* \leq N - l, \\ N - t_*/l & : \quad N - l < t \leq N. \end{cases} \qquad (10.39)$$

b) Cosine taper

$$b_2(t_*) = \begin{cases} \frac{1}{2}[1 - \cos \pi t_*]/l & : \quad 0 < t_* < l, \\ 1 & : \quad l \leq t_* \leq N - 1, \\ \frac{1}{2}[1 - \cos \pi(N - t_*)/l] & : \quad N - l < t \leq N. \end{cases} \qquad (10.40)$$

The data window has the function of suppressing the amount of leakage of the sharply peaked spectral energy to the spectral estimates at neighboring frequencies. A window functions most effectively when the wave record contains single-frequency components of regular waves with appreciable energies. Kuwajima and Nagai[12] recommend the cosine taper with $l = 0.1N$ on the bais of numerical studies. A demerit of the data window is the decrease in the number of degrees of freedom, the rate of which is estimated by the following formula[11]:

$$\frac{1}{\kappa_b} = \frac{\left[\displaystyle\int_0^N b^2(t_*)dt_*\right]^2}{\displaystyle\int_0^N b^4(t_*)dt_*}. \qquad (10.41)$$

The rate of decrease is about the same for the trapezoidal and cosine tapers; for $l = 0.1N, 1/\kappa_b$ becomes about 0.9. In consideration of such a decrease in the number of degrees of freedom, Rikiishi and Mitsuyasu[13] discourage the use of a data window for records of sea waves with continuous spectra.

When a data window is applied to a wave record, the total energy level is decreased and all the values of the spectral estimate appear at a level lower than the true values. Therefore, the calculated values of periodograms must be corrected by multiplying them by the ratio $N/\Sigma b^2(t_*)$.

(D) *Computation of Fourier coefficients*

This is done with the fast Fourier transform (FFT) technique, which is one of the service software routines provided for modern computers. A limitation of the standard FFT algorithm is that the data length must be a power of 2, that is, $N = 2^m$. Thus, the recording of wave data is done to obtain this condition, or the data length is later adjusted by cutting the end of the record or adding a certain number of zero data. Addition of zero data is made to the tail of the record after the application of the data window, if it is to be applied. The addition of zero data decreases the total energy level as well as the number of degrees of freedom. The correction for the latter decrease is made by treating the addition of zero data as equivalent to the application of a data window of $b(t_*) = 0$ beyond the original data length in Eq. (10.43) below.

Kuwajima and Nagai[12] have proposed an extended algorithm for the FFT technique for a record of length $N = 2^m \times M$, with M being an odd integer.

(E) *Calculation of periodogram*

After the Fourier coefficients A_k and B_k have been obtained, I_k is calculated via Eq. (10.26), and corrections are made to the total energy level for the effects of the data window and adjustment of the number of data. That is,

$$I_k = \alpha(A_k^2 + B_k^2),\qquad(10.42)$$

in which

$$\alpha = N_2/NU, \quad U = \left\{\sum_{t_*=1}^{N_2} b^2(t_*)\right\}\bigg/N_2,\qquad(10.43)$$

and N_2 denotes the number of data employed in the computation of the fast Fourier transform including zero data if they were added to the original wave record. In the calculation of Eq. (10.42), the coefficient B_k is set to 0 for $k = 0$ and $N_2/2$.

(F) *Smoothing of periodograms*

Equation (10.32) represents the simple averaging method for the smoothing of periodograms. Koopmans[14] gives a general formula for the smoothing of periodograms for the estimation of spectral density as

$$\hat{S}(f_k) = \frac{\Delta t}{2} \sum_{j=k-[(n-1)/2]}^{k+[n/2]} K(f_k - f_j)\, I_j \,, \tag{10.44}$$

in which

$$\sum_{j=k-[(n-1)/2]}^{k+[n/2]} K(f_k - f_j) = 1 \,. \tag{10.45}$$

The smoothing function $K(f)$ is also called the weight function, or simply the filter. The function $K(f)$ is equivalent to the spectral window employed in the autocorrelation method of spectral analysis.

Commonly used filters are as follows:

a) Rectangular filter

$$K_1(f_j) = \frac{1}{n} \qquad : \quad -[(n-1)/2] \le j \le [n/2] \,, \tag{10.46}$$

b) Triangular filter

$$K_2(f_j) = \frac{1}{K_2} \left\{ 1 - \frac{|j|}{[(n-1)/2]} \right\} \qquad : \quad -[(n-1)/2] \le j \le [n/2] \,, \tag{10.47}$$

c) Parabolic filter

$$K_3(f_j) = \frac{1}{K_3} \left\{ 1 - \left(\frac{j}{[(n-1)/2]} \right)^2 \right\} \qquad : \quad -[(n-1)/2] \le j \le [n/2] \,, \tag{10.48}$$

in which $\overline{K}_2$ and $\overline{K}_3$ are the normalization constants to satisfy the condition of Eq. (10.45).

In practice, the number of periodograms to be used in the smoothing is taken as an even integer for the rectangular filter, and an odd integer for the triangular and parabolic filters. The central frequency of the smoothing is usually shifted by n for the rectangular filter and by $(n + 1)/2$ for the other filters with a half overlapping of periodograms in the spectral estimate.

The rectangular filter has $2n$ degrees of freedom, as described previously, and the bandwidth of the spectral resolution is given by Eq. (10.36). For other filters, the effective number of degrees of freedom is calculated with the following formula, according to Koopmans[14]:

$$r = \frac{2}{\displaystyle\sum_{j=-[(n-1)/2]}^{[n/2]} K^2(f_j)} \, . \tag{10.49}$$

For large n, the following approximations are available:

$$r \simeq 1.5n \qquad : \quad \text{triangular filter}, \tag{10.50}$$

$$r \simeq \frac{5}{3}n \qquad : \quad \text{parabolic filter}. \tag{10.51}$$

When the data window described in subsection (C) is employed, the effective number of degrees of freedom is evaluated by multiplying the value given in the above with $1/\kappa_b$ of Eq. (10.41). The bandwidth of the spectral resolution is evaluated similarly, and its equivalent value is given by

$$f_B \simeq \frac{3n}{4N\Delta t} \qquad : \quad \text{triangular filter}, \tag{10.52}$$

$$f_B \simeq \frac{5n}{6N\Delta t} \qquad : \quad \text{parabolic filter}. \tag{10.53}$$

The triangular and parabolic filters yield spectral estimates at a frequency interval of one half that of the rectangular filter, but it should be remembered that the adjacent two spectral estimates are not statistically independent for triangular and parabolic filters.

The number of periodograms to be smoothed is selected by consideration of the effective number of degrees of freedom and the bandwidth of the spectral resolution. Although one may think that the number of degrees of freedom can

be increased by narrowing the sampling interval Δt together with an increase of N and n, the narrowing only extends the range of the spectral analysis to higher frequencies and the resolution around the spectral peak is rather worsened by an increase in n. The spectral resolution is improved only through the use of a long wave record as exhibited in Eq. (10.36). Although the minimum number of degrees of freedom to be maintained in a spectral analysis cannot be stated definitely, most studies have been done with the effective number greater than about 20. In the evaluation of the spectral peakedness parameter Q_p defined by Eq. (9.69), Rye[15] recommend that the number of degrees of freedom be equal to about 16, because the evaluation of Q_p requires quite fine resolution of the spectral peak.

The number of the periodograms to be smoothed is not necessarily a fixed value, and it can be varied over the range of frequency. Examination of low frequency spectral components is sometimes made with a small value of n and a narrow bandwidth of the spectral resolution, but it should be remembered that low reliability of the spectral estimate will result in such an analysis.

(G) *Final adjustment of energy level*

The adjustment of the total energy level for the effect of the data window may not be perfect when Eq. (10.43) alone is applied, because of some particular feature in the wave record, some residues arising from the treatment of overlapping of the periodograms in smoothing, especially for the lowest and highest frequencies, differences originating from the use of an uneven bandwidth for the spectral resolution, and other reasons. Thus, the zeroth moment of the estimated spectrum m_0 may be slightly different from the variance of the surface elevation η_{rms}^2, which was obtained in the initial step of the data analysis. A difference between m_0 and η_{rms}^2 is undesirable from consideration of the definition of the wave spectrum as described by Eq. (8.31). Therefore, the spectral estimates should be adjusted by multiplying all estimates by the ratio $\eta_{\mathrm{rms}}^2/m_0$.

10.3 Directional Spectra of Random Sea Waves

As discussed in Chapter 3, wave transformations such as diffraction, refraction, and reflection are greatly influenced by the directional spectral characteristics

of sea waves. Thus, we need to enrich our knowledge of directional wave spectra through the accumulation of a large amount of directional spectral data. However, measurements of directional wave spectra necessitate an effort several times greater than those of frequency spectra. While the latter can be obtained from a wave record at a single point, the former requires simultaneous recording of several wave components. With reference to the classification by Panicker,[16] the measuring techniques of directional wave spectra which have been tried so far are listed below.

1) Direct measurement method

$$\begin{cases} \text{Wave gauge array} \\ \text{Directional buoy} \\ \text{Two-axis current meter} \end{cases}$$

2) Remote sensing method

$$\begin{cases} \text{Optical technique} \begin{cases} \text{Stereophotogrametry} \\ \text{Holography} \end{cases} \\ \text{Microwave technique} \end{cases}$$

Among the above, the direct measurement methods and stereophotogrametry are based on the same principle of analysis, namely digital analysis of the cross-spectra between various pairs of wave records. The hologram method[17] is an analog-type analysis of an aerial photograph by means of the diffraction pattern which is produced by exposing a negative film to a laser beam. Microwave techniques are more recent, and several approaches are being made. A synthetic aperture radar, mounted on a satellite or an airplane, is one promising method. King and Shemdin[18] reported a measurement of the distribution of waves in a hurricane, taken by means of air-borne synthetic aperture radar. A shore-based HF doppler radar has a also been employed for the measurement of directional waves, as reported by Vesecky *et al.*[19] Rapid progress is expected in the field of microwave techniques for directional wave measurements.

In the present section, however, the basic theories of direct measurement methods are described, following the chronological order of theoretical developments.

10.3.1 *Relation Between Direction Spectrum and Covariance Function*

The basic quantity used to estimate the directional spectrum is the covariance function[c] of wave profiles in the spatial and time domains. By generalizing the definition Eq. (8.17) in Sec. 8.3 for the one-dimensional wave profile, we introduce the following covariance function:

$$\Psi(X,Y,\tau) = \lim_{x_0,y_0,\tau_0 \to \infty} \frac{1}{x_0 y_0 t_0} \int_{-\frac{x_0}{2}}^{\frac{x_0}{2}} \int_{-\frac{y_0}{2}}^{\frac{y_0}{2}} \int_{-\frac{t_0}{2}}^{\frac{t_0}{2}} \eta(x,y,t)$$

$$\times \, \eta(x+X, y+Y, t+\tau) \, dx \, dy \, dt \, . \qquad (10.54)$$

By substituting Eq. (8.10), which describes the two-dimensional wave profile, into the above, and by introducing the notation $\alpha = (kx \cos\theta + ky \sin\theta - \omega t + \varepsilon)$ with $\omega = 2\pi f$ for abbreviation, we have

$$\Psi(X,Y,\tau) = \lim_{x_0,y_0,\tau_0 \to \infty} \frac{1}{x_0 y_0 t_0} \int \int \int \sum_{n=1}^{\infty} \sum_{m=1}^{\infty} a_n a_m \cos\alpha_n$$

$$\times \cos(\alpha_m + k_m X \cos\theta_m + k_m Y \sin\theta_m - \omega_m \tau) \, dx \, dy \, dt \, .$$
$$(10.55)$$

Because the expected value of $\cos\alpha_n \cos\alpha_m$ is 0 for $n \neq m$, the above equation can be shown to become

$$\Psi(X,Y,\tau) = \sum_{n=1}^{\infty} \frac{1}{2} a_n^2 \cos(k_n X \cos\theta_n + k_n Y \sin\theta_n - \omega_n \tau) \, . \qquad (10.56)$$

Combination of Eq. (10.56) with the definition of the directional spectral function, Eq. (8.12), yields the following relation between the covariance function and directional spectrum:

$$\Psi(X,Y,\tau) = \int_0^{\infty} \int_0^{2\pi} S_k(k,\theta) \cos(kX \cos\theta + kY \sin\theta - \omega\tau) \, d\theta \, dk \, . \quad (10.57)$$

The inverse transform of the above can be obtained by utilizing the theorems of the Fourier transform and its inverse transform (e.g., Ref. 20). For this

---

[c]As explained in Sec. 8.3, an autocorrelation function with zero mean is called the autocovariance function.

purpose, the polar coordinates (k, θ) are transformed to the Cartesian coordinates (u, v), and ω is treated as an independent variable; that is, the dispersion relation, Eq. (8.3), is not used at this stage. After some manipulation, we obtain the following relations:

$$\Psi_0(X, Y, \tau) = \int_{-\infty}^{\infty} \int_{-\infty}^{\infty} \int_{-\infty}^{\infty} S_{k_0}(u, v, \omega) e^{i(uX+vY-\omega\tau)} du\, dv\, d\sigma, \qquad (10.58)$$

$$S_{k_0}(u, v, \omega) = \frac{1}{(2\pi)^3} \int_{-\infty}^{\infty} \int_{-\infty}^{\infty} \int_{-\infty}^{\infty} \Psi_0(X, Y, \tau) e^{-i(uX+vY-\omega\tau)} dX\, dY\, d\tau, \qquad (10.59)$$

where

$$u = k\cos\theta, \quad v = k\sin\theta. \qquad (10.60)$$

In Eqs. (10.58) and (10.59), the angular frequency ω is treated as varying independently of the wavenumber $k = |u^2 + v^2|^{1/2}$, and thus the directional spectral density is defined in the three-dimensional space of (u, v, ω). The subscript "0" on Ψ_0 and S_{k_0} is added to indicate that the functions attached are defined in the ranges $-\infty < \tau < \infty$ and $-\infty < \omega < \infty$; these functions have values of one half of the functions defined in the range $[0, \infty)$.

If the covariance function of the two-dimensional wave profile with respect to X, Y and τ is known with sufficient density in the whole domain, the directional wave spectrum can be estimated with Eq. (10.59). Information on $\Psi_0(X, Y, \tau)$ with sufficient density requires that the wave profile data be obtained uniformly in the whole area, $x = -x_0/2 \sim x_0/2$, $y = -y_0/2 \sim y_0/2$ and throughout the time span $t = -t_0/2 \sim t_0/2$. Specifically speaking, it requires several hundred consecutive stereophotographs of the sea surface taken over the same area. This is not impossible, but it is unfeasible in practice because of the excessive cost of operation and analysis. When the U.S. Navy carried out the Stereo Wave Observation Project (SWOP) in 1954, stationarity of the wave field was assumed and the directional spectrum $S_{k_0}(u, v)$ was estimated from the information of $\Psi_0(X, Y, 0)$, which was calculated from a contour map of the surface elevation (see Ref. 21, for example). A shortcoming of this technique is the incapability of distinguishing values of $S_{k_0}(u, v)$ and $S_{k_0}(-u, -v)$, that is, two wave components propagating in the directions differing by 180°. Therefore, for the purpose of the analysis of the SWOP data, it was assumed that the directional wave spectrum existed only in the azimuth within $\pm 90°$ from the mean wave direction. The situation is the same for

the hologram method. In the use of wave gauge arrays (except for the linear array) and wave buoys, such a problem does not exist and the directional wave spectrum can be estimated in the full directional range ($\theta = 0° \sim 360°$).

10.3.2 *Estimate of Directional Spectra with a Wave Gauge Array*

(A) *Direct Fourier transform method*

Stereophotogrametry for obtaining the directional wave spectrum requires a large volume of data analysis, and thus it is not suited for routine wave observation. On the other hand, the measurement of the directional wave spectrum with a wave gauge array requires only the simultaneous recording of wave profiles, and the data analysis is not as voluminous as compared to that for the stereophotogrametric method. Thus, wave gauge arrays are sometimes employed in the measurement of directional wave spectra of sea waves, though they are more popular in seismology.

In the definition of the covariance function, Eq. (10.54), the spatial lags X and Y will be regarded as fixed for the time being. By denoting the covariance function under this condition as Ψ', it is expressed as

$$\Psi'(\tau|X,Y) = \lim_{t_0 \to \infty} \frac{1}{t_0} \int_{-t_0/2}^{t_0/2} \eta(t|x,y)\ \eta(t+\tau|x+X,y+Y)\,dt\,. \qquad (10.61)$$

This function can be obtained from the simultaneous records of wave profiles at any two stations, whose locations are denoted by (x,y) and $(x+X,\ y+Y)$. We consider the function $\Phi_0(f|X,Y)$, which is the Fourier transform of Ψ', similar as in Eq. (8.27) in Sec. 8.3:

$$\Phi_0(f|X,Y) = \int_{-\infty}^{\infty} \Psi'(\tau|X,Y)\,e^{-i2\pi/\tau}d\tau\,, \qquad (10.62)$$

$$\Psi'(\tau|X,Y) = \int_{-\infty}^{\infty} \Phi_0(f|X,Y)\,e^{i2\pi/\tau}df\,, \qquad (10.63)$$

in which Φ_0 is defined in the range $-\infty < f < \infty$.

The function $\Phi_0(f|X,Y)$ is called the cross-spectrum, and it is often expressed in terms of its real and imaginary parts as

$$\Phi_0(f|X,Y) = C_0(f|X,Y) - iQ_0(f|X,Y) \qquad : \quad -\infty < f < \infty\,, \qquad (10.64)$$

where

$$C_0(f|X,Y) = \int_{-\infty}^{\infty} \Psi'(\tau|X,Y) \cos 2\pi f\tau \, d\tau \,, \qquad (10.65)$$

$$Q_0(f|X,Y) = \int_{-\infty}^{\infty} \Psi'(\tau|X,Y) \sin 2\pi f\tau \, d\tau \,. \qquad (10.66)$$

The real part is generally called the co-spectrum, and the imaginary part is called the quadrature-spectrum.

From the definition given in Eq. (10.61), the following property of Ψ' is derived:

$$\Psi'(\tau|X,Y) = \Psi'(-\tau|-X,-Y) \,. \qquad (10.67)$$

In general, $\Psi'(\tau|X,Y)$ is not equal to $\Psi'(-\tau|X,Y)$. For the cross-spectrum, there exist the following relations:

$$C_0(f|X,Y) = C_0(f|-X,-Y) = C_0(-f|-X,-Y) = C_0(-f|X,Y) \,, \qquad (10.68)$$

$$Q_0(f|X,Y) = -Q_0(f|-X,-Y) = Q_0(-f|-X,-Y) = -Q_0(-f|X,Y) \,. \qquad (10.69)$$

We can prove from these relations that the covariance function Ψ' is a real function, even though the cross-spectrum Φ_0 is a complex function.

The covariance function Ψ' corresponds to Ψ_0 on the right side of Eq. (10.59) if the triple integration of the inverse Fourier transform is first performed with respect to τ. This correspondence is based on the definitions in Eqs. (10.54) and (10.61). Thus, by performing the integration first with respect to τ in Eq. (10.59) by utilizing Eq. (10.62), we have the result

$$S_{k_0}(u,v|f_0) = \frac{1}{(2\pi)^2} \int_{-\infty}^{\infty} \int_{-\infty}^{\infty} \Phi_0^*(X,Y|f_0) \, e^{-i(uX+vY)} dX \, dY \,, \qquad (10.70)$$

where Φ_0^* is the conjugate function of the cross-spectrum Φ_0; i.e., $\Phi_0^* = C_0 + iQ_0$. Note that the frequency f_0 is fixed in this integration.

Equation (10.70) indicates that the directional wave spectrum $S_{k_0}(u,v,f)$ can be estimated if wave profiles are simultaneously recorded at a large number of points in an area with sufficient density. From such records, all possible pairs of wave gauges are formed. The distances are denoted as $(0,0)$, (X_1,Y_1),

$(X_2, Y_2), \ldots$ The cross-spectra between these pairs are calculated, and directional spectrum is estimated by replacing the integrations in Eq. (10.70) with summations. In practice, however, the number of wave gauges is rather limited and the integrations cannot be evaluated accurately.

For this situation, Barber[22] proposed that the integral in Eq. (10.70) be replaced by the following summation as a way of estimating the directional spectrum. He assigned the value of zero to the cross-spectrum at any pair of arbitrary distances X and Y other than those realized among the actual pairs of wave gauges. That is,

$$\hat{S}_{k_0}(u, v | f_0) = \frac{1}{(2\pi)^2} \sum_{n=-M}^{M} \Phi_0^*(X_n, Y_n | f_0) \, e^{-i(uX_n + vY_n)}, \qquad (10.71)$$

where M denotes the number of pairs of wave gauges and is given by $M = N(N-1)/2$ for an array of N wave gauges. The above equation can be written in terms of real variables alone by utilizing Eqs. (10.68) and (10.69):

$$\hat{S}_{k_0}(u, v | f_0) = \frac{1}{(2\pi)^2} \Bigg\{ C_0(0, 0 | f_0) + 2 \sum_{n=1}^{M} [C_0(X_n, Y_n | f_0) \cos(uX_n + vY_n)$$

$$+ Q_0(X_n, Y_n | f_0) \sin(uX_n + vY_n)] \Bigg\}. \qquad (10.72)$$

The above equation enables estimation of the directional spectral function in the wavenumber domain (u, v) in the frequency range $-\infty < f_0 < \infty$. The directional wave spectrum $S(f, \theta)$ in the frequency and direction domain such as defined by Eq. (8.11) in Sec. 8.2 can be estimated by the following procedure. First, the dispersion relationship, Eq. (8.3), is assumed to hold between f_0 and $k = |u^2 + v^2|^{1/2}$. Thus, we have

$$S(f_0, \theta) = \alpha \, S_{k_0}(u, v | f_0), \qquad (10.73)$$

where α is a proportionality constant, the value of which varies with f_0 according to the dispersion relationship. The directional spectrum $S(f, \theta)$ is assumed to be given by the product of the frequency spectrum $S(f)$ and the directional spreading function $G(f; \theta)$, as in Eq. (2.19) in Sec. 2.3.2. That is,

$$S(f_0, \theta) = S(f_0) \, G(\theta | f_0). \qquad (10.74)$$

The co-spectrum $C_0(0,0|f_0)$ appearing on the right side of Eq. (10.72) satisfies the relation $C_0(0,0|f_0) = S(f_0)/2$, as proved by comparison of Eqs. (10.65) and (8.26). Thus, the estimate of $S(f_0)$, denoted with a caret, is obtained as

$$\hat{S}(f_0) = 2C_0(0,0|f_0).\qquad(10.75)$$

The estimate of the directional spreading function $G(\theta|f_0)$ is then given by

$$\hat{G}_1(\theta|f_0) = \alpha'\{1 + 2\sum_{n=1}^{M}[C_*(X_n,Y_n|f_0)\cos(k_0 X_n\cos\theta + k_0 Y_n\sin\theta)$$

$$+ Q_*(X_n,Y_n|f_0)\sin(k_0 X_n\cos\theta + k_0 Y_n\sin\theta)]\},\qquad(10.76)$$

where

$$\left.\begin{array}{l}C_*(X_n,Y_n|f_0) = C_0(X_n,Y_n|f_0)/C_0(0,0|f_0)\,, \\ Q_*(X_n,Y_n|f_0) = C_0(X_n,Y_n|f_0)/C_0(0,0|f_0)\,.\end{array}\right\}\qquad(10.77)$$

The coefficient of proportionality α' in Eq. (10.76) is determined by the normalization condition that the integral of $\hat{G}$ in the range of $\theta = -\pi \sim \pi$ should be 1. In the normalization of the cross-spectrum by Eq. (10.77), it is recommended that the co-spectrum $C_0(0,0|f_0)$ be taken as the geometric mean of the data of the various pairs of wave gauges.

The above method of estimating the directional wave spectrum has been named as the direct Fourier transform method by Kinsman,[21] as it is based on the direct Fourier transform of the cross-spectrum between the pairs of wave gauges.

(B) *Maximum likelihood method*

Although the direct Fourier transform method is straightforward in the logic of its derivation, its performance in the estimate of the directional spectrum is not good, particularly if the number of wave gauges is small. The directional resolution is rather dull and Eq. (10.76) yields negative values of the estimated spreading function in some ranges of direction. This problem of negative spectral density is remedied by rewriting Eq. (10.76) in the following form:

$$\hat{G}_2(\theta|f_0) = \alpha' \Bigg\{ N + 2 \sum_{n=1}^{M} [C_*(X_n, Y_n|f_0) \cos(k_0 X_n \cos\theta + k_0 Y_n \sin\theta)$$

$$+ Q_*(X_n, Y_n|f_0) \sin(k_0 X_n \cos\theta + k_0 Y_n \sin\theta)] \Bigg\}, \qquad (10.78)$$

although the directional resolution is degraded.

There are other methods of estimating the directional spectrum from data of the cross-spectra. A fairly common technique is the so-called maximum likelihood method developed by Capon[23] for the analysis of seismic waves with a sensor array. It is designed to minimize the variance of the difference between the estimate and the true spectrum under the constraint that the amplitude of unidirectional plane waves with no contamination by noise is passed without bias, as described by Pawka.[24] The formula for the estimation of the directional spectral density by maximum likelihood method is

$$\hat{G}_3(\theta|f_0) = \frac{\alpha'}{\hat{S}(f_0)} \Bigg\{ \sum_{i=1}^{N} \sum_{j=1}^{N} \Phi_{ij}^{-1}(f_0)$$

$$\times \exp[-i(kX_{ij}\cos\theta + kY_{ij}\sin\theta)] \Bigg\}^{-1}, \qquad (10.79)$$

where Φ_{ij}^{-1} denotes the (i,j) component of the inverse matrix of the complex matrix composed of the conjugate cross-spectrum $\Phi_{ij}^* = C_{ij} + iQ_{ij}$, defined in the range $0 < f < \infty$, and $\hat{S}(f_0)$ is the mean of the frequency spectral density estimated from the records of N gauges.

The maximum likelihood method has a directional resolution much higher than the direct Fourier transform method. Figure 10.4 is an example of the comparison of directional resolution by both methods for unidirectional irregular waves, as determined by four wave gauges arranged in the form of star array.[25] It shows the directional spreading function at the frequency corresponding to the relative gauge spacing $D/L = 0.47$ (D = gauge spacing, L = wavelength). Even though numerical noise with a root-mean-square ratio of 20% to the signal was added to the simulated irregular wave records, the maximum likelihood method result shown with the open circles yielded quite accurate estimates of the input spectrum. The direct Fourier transform method, on the other hand, gave poor spectral estimates, as shown with the crosses.

When the actual directional spectrum is known to have very sharp directional peaks owing to the effect of shadowing by islands in the offshore, for
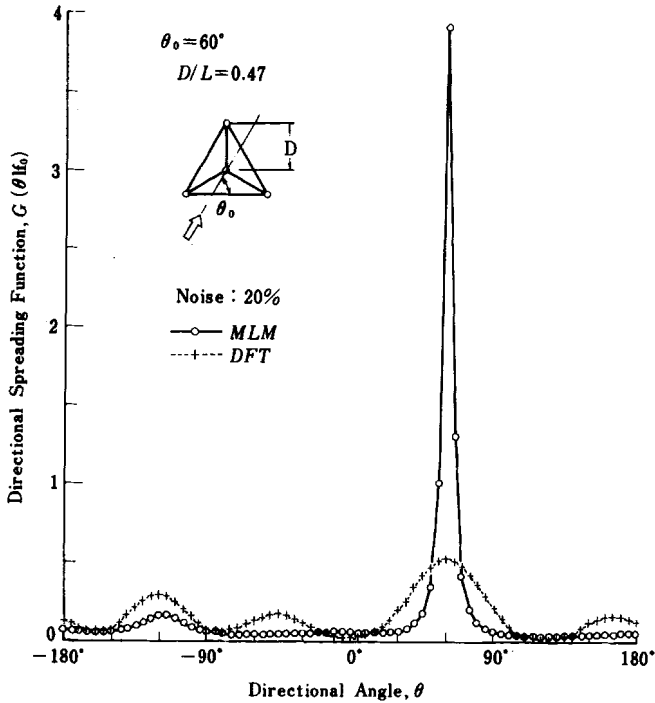
Fig. 10.4. Example of directional resolution of star array to unidirectional irregular waves by the maximum likelihood method and by the direct Fourier transform method.[25]

example, a technique for enhancing the directional resolution by the maximum likelihood method is available through an interative procedure, as presented by Pawka.[24]

A problem associated with the maximum likelihood method is the possibility of splitting of the peak in the directional spreading function, due to the property of high directional resolution of the method. Splitting has occasionally appeared when the method was tested in numerical simulations of random wave profiles for directional spectra with relatively broad peaks, as reported by Yamaguchi and Tsuchiya,[26] for example.

(C) *Layout of wave gauge arrays*

In the measurement procedure for the directional spectrum, the layout of the wave gauge array should be optimized to yield the best estimate of the

directional spectrum with the least number of wave gauges. The problem of the optimum array layout has been investigated in the fields of radio wave detection and seismology. Guidelines for the optimum gauge array may be summarized as follows:

1) No pair of wave gauges should have the same vector distance between gauges.
2) The vector distance should be distributed uniformly in as wide a range as possible.
3) The minimum separation distance between a pair of wave gauges should be less than one half of the smallest length of the component waves for which the directional analysis is to be made.

The star array shown in the inset of Fig. 10.4 satisfies the first requirement. If four gauges are arranged at the corners of a square, the two pairs of gauges at the horizontal sides of the square have the same vector distance, and so do the two pairs at the vertical sides. Thus, the number of independent pairs of wave gauges decreases to only four from six possible combinations, and the directional resolution is decreased accordingly. As discussed earlier, the estimate of the directional spectrum from information of the cross-spectra between pairs of wave gauges is based on the approximation of the integral in Eq. (10.70) by the summation of cross-spectra at a finite number of vector distances between wave gauges, as given by Eq. (10.71). The accuracy of the approximation is improved as the number of wave gauges increases and as they are arranged with a higher density. Therefore, duplication of vector distance should be avoided.

The second requirement is related to the directional resolution. When the frequency spectrum is estimated by the autocorrelation method of Blackman and Tukey,[6] the maximum value of the time lag τ governs the frequency resolution of the spectrum. Similarly, the directional resolution of the directional wave spectrum increases as the maximum distance between wave gauges increases. A uniform distribution of vector distance, on the other hand, is a requirement for homogeneity in the spectral estimate with respect to direction. A wave gauge array set along a straight line, called a line array, has sharp resolution in the direction normal to the line, but the resolution decreases as the direction of the wave incidence departs from the normal.

The third requirement is easily understood by considering the situation that a plane wave is incident to a pair of wave gauges having a separation distance

of one half the wavelength along the direction of the axis connecting the two gauges. The wave records from the two gauges will show the same profile, but with a phase difference of 180°. The cross-spectrum becomes $|C_*| = 1$ and $Q_* = 0$. For any pair of wave gauges with a separation distance of a multiple of $L/2$, the cross-spectrum becomes $|C_*| = 1$ and $Q_* = 0$. Such a gauge pair cannot detect the side from which the waves are coming. There also appear false peaks in the spectral density, called side lobes, at directions different from the true direction of wave incidence.

(a) Delta Array   (b) Star Array

(c) Haubrich's Array

(d) Barber's Line Array
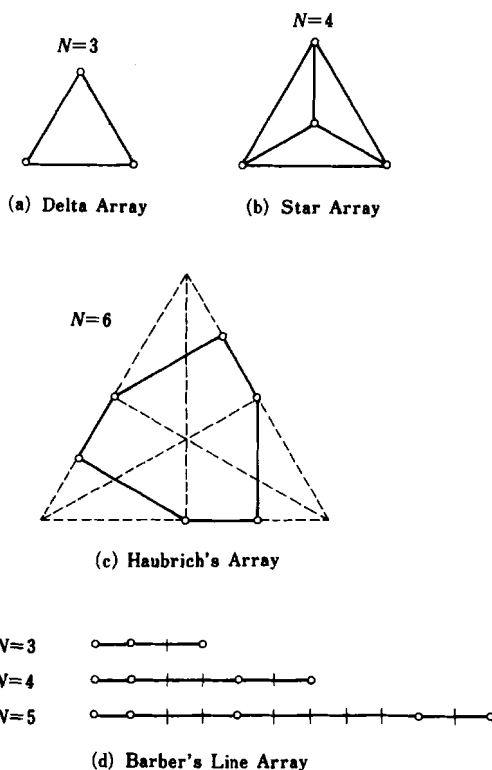
Fig. 10.5. Example of optimum gauge arrays.

In summary, measurement procedures for the directional spectrum with a wave gauge array have various limitations, and accurate and reliable measurements are difficult if the number of gauges is small. Figure 10.5 illustrates several gauge layouts which have been employed in directional measurements.

A layout for six gauges was proposed by Haubrich.[27] The line arrays are based on Barber's proposal.[22] Although line arrays cannot distinguish waves approaching from opposite sides of the line, they may be usefully employed in measurements of nearshore waves, since most of wave energy is incident from the offshore side.

10.3.3 *Estimate of Directional Wave Spectra with a Directional Buoy and with a Two-Axis Current Meter*

Many directional wave measurements have been made by means of directional wave buoys and two-axis current meters. The number of such directional measurements reported in technical papers surpasses that of wave gauge arrays. An early-developed directional buoy is the pitch and roll buoy, reported by Longuet-Higgins *et al.*,[28] which measures the angles of pitch and roll and the heaving acceleration of the buoy. Mitsuyasu *et al.*[29] employed a cloverleaf buoy, which has the capability of measuring the curvature of the water surface in addition to the pitch, roll and heave. On the basis of their detailed measurements of directional wave spectra, and other published data, Mitsuyau *et al.* proposed a standard form for the directional spreading function, as discussed in Sec. 2.3.2. Turning to current meters, Nagata[30] measured the water particle velocity components in two Cartesian coordinates by means of a two-axis electromagnetic current meter, and he estimated the directional wave spectrum from these measurements. Recent directional wave measurements with two-axis current meters are accompanied by simultaneous measurement of the surface elevation or pressure fluctuation, so as to able to distinguish from which side of the half plane the waves are arriving.

The principle of directional wave measurements by means of a buoy was given by Longuet-Higgins *et al.*[28] The quantities measurable by a pitch and roll buoy are

$$
\left.
\begin{aligned}
\xi_1 &= \eta = \sum_{n=1}^{\infty} a_n \cos(k_n x \cos\theta_n + k_n y \sin\theta_n - \omega_n t + \varepsilon_n)\,, \\
\xi_2 &= \frac{\partial \eta}{\partial x} = -\sum_{n=1}^{\infty} k_n a_n \cos\theta_n \sin(k_n x \cos\theta_n + k_n y \sin\theta_n - \omega_n t + \varepsilon_n)\,, \\
\xi_3 &= \frac{\partial \eta}{\partial y} = -\sum_{n=1}^{\infty} k_n a_n \sin\theta_n \sin(k_n x \cos\theta_n + k_n y \sin\theta_n - \omega_n t + \varepsilon_n)\,.
\end{aligned}
\right\}
$$

$$(10.80)$$

The heave displacement is obtained by twice integrating the have acceleration with respect to time. The covariance functions between these three quantities are calculated as

$$
\left.
\begin{aligned}
\Psi_{12}(\tau) &= \overline{\xi_1(t)\xi_2(t+\tau)} = \sum_{n=1}^{\infty} \frac{1}{2} k_n a_n^2 \cos\theta_n \sin\omega_n\tau \,, \\[2mm]
\Psi_{13}(\tau) &= \overline{\xi_1(t)\xi_3(t+\tau)} = \sum_{n=1}^{\infty} \frac{1}{2} k_n a_n^2 \sin\theta_n \sin\omega_n\tau \,, \\[2mm]
\Psi_{23}(\tau) &= \overline{\xi_2(t)\xi_3(t+\tau)} = \sum_{n=1}^{\infty} \frac{1}{2} k_n^2 a_n^2 \cos\theta_n \sin\theta_n \cos\omega_n\tau \,.
\end{aligned}
\right\}
\tag{10.81}
$$

Cross-spectra are calculated from these covariance functions by Eqs. (10.65) and (10.66), and they can be related to the directional wave spectrum as in the following:

$$
\left.
\begin{aligned}
C_{23}(f) &= \int_{-\infty}^{\infty} \Psi_{23}(\tau) \cos 2\pi f\tau\, d\tau = \frac{1}{2} \int_0^{2\pi} S(f,\theta) k^2 \cos\theta \sin\theta\, d\theta \,, \\[2mm]
Q_{12}(f) &= \int_{-\infty}^{\infty} \Psi_{12}(\tau) \sin 2\pi f\tau\, d\tau = \frac{1}{2} \int_0^{2\pi} S(f,\theta) k \cos\theta\, d\theta \,, \\[2mm]
Q_{13}(f) &= \int_{-\infty}^{\infty} \Psi_{13}(\tau) \sin 2\pi f\tau\, d\tau = \frac{1}{2} \int_0^{2\pi} S(f,\theta) k \sin\theta\, d\theta \,,
\end{aligned}
\right\}
\tag{10.82}
$$

$$
C_{12}(f) = C_{13}(f) = Q_{23}(f) = 0 \,. \tag{10.83}
$$

Furthermore, the autocorrelation functions yield the following co-spectra, which are related to the directional spectrum:

$$
\left.
\begin{aligned}
C_{11}(f) &= \int_{-\infty}^{\infty} \Psi_{11}(\tau) \cos 2\pi f\tau\, d\tau = \frac{1}{2} \int_0^{2\pi} S(f,\theta)\, d\theta \,, \\[2mm]
C_{22}(f) &= \int_{-\infty}^{\infty} \Psi_{22}(\tau) \cos 2\pi f\tau\, d\tau = \frac{1}{2} \int_0^{2\pi} S(f,\theta) k^2 \cos^2\theta\, d\theta \,, \\[2mm]
C_{33}(f) &= \int_{-\infty}^{\infty} \Psi_{33}(\tau) \cos 2\pi f\tau\, d\tau = \frac{1}{2} \int_0^{2\pi} S(f,\theta) k^2 \sin^2\theta\, d\theta \,,
\end{aligned}
\right\}
\tag{10.84}
$$

$$
Q_{11}(f) = Q_{22}(f) = Q_{33}(f) = 0 \,. \tag{10.85}
$$

Thus, we can obtain six quantities from the three cross-spectra and three autocorrelation functions, which are related to the integrals of the directional spectrum with respect to direction as given by Eqs. (10.82) and (10.84). To derive an estimate of the directional spectrum, we assume the $S(f, \theta)$ can be expanded in a Fourier series as follows:

$$S(f, \theta) = \frac{1}{2}A_0(f) + \sum_{n=1}^{\infty}[A_n(f)\cos n\theta + B_n(f)\sin n\theta].$$ (10.86)

By substituting Eq. (10.86) into Eqs. (10.82) and (10.84), and by carrying out the integrations, Fourier coefficients for $n = 0$, 1 and 2 can be determined as

$$\left.\begin{array}{ll} A_0(f) = \dfrac{2}{\pi}C_{11}(f), & A_1(f) = \dfrac{2}{\pi k}Q_{12}(f), \quad A_2(f) = \dfrac{2}{\pi k^2}[C_{22}(f) - C_{33}(f)], \\[2ex] & B_1(f) = \dfrac{2}{\pi k}Q_{13}(f), \quad B_2(f) = \dfrac{4}{\pi k^2}C_{23}(f). \end{array}\right\}$$ (10.87)

The resultant estimate of the directional spectrum represents the infinite Fourier series of Eq. (10.86) up to the second-order terms only, and thus, it is a biased estimate of the true spectrum. The estimate with the coefficients of Eq. (10.87), denoted as $\hat{S}_1(f, \theta)$, bears the following relationship to the true spectrum:

$$\hat{S}_1(f, \theta) = \frac{1}{2\pi}\int S(f, \theta)W_1(\phi - \theta)\,d\phi,$$ (10.88)

where

$$W_1(\phi) = \sin\frac{5}{2}\phi \Big/ \sin\frac{1}{2}\phi = 1 + 2\cos\phi + 2\cos 2\phi.$$ (10.89)

In order to reduce the extent of the bias caused by the use of the window function $W_1(\phi)$, Longuet-Higgins *et al.*[28] proposed use of the following formula for the estimation of the directional spectrum:

$$\hat{S}_2(f, \theta) = \frac{1}{2}A_0 + \frac{2}{3}(A_1\cos\theta + B_1\sin\theta) + \frac{1}{6}(A_2\cos 2\theta + B_2\sin 2\theta).$$ (10.90)

This is equivalent to application of the window function

$$W_2(\phi) = \frac{8}{3}\cos^4\frac{1}{2}\phi = 1 + \frac{4}{3}\cos\phi + \frac{1}{3}\cos 2\phi.$$ (10.91)

The above method of making the spectral estimation is characterized by th initial assumption of the spectral form and the subsequent determination

of the coefficients from the observation data. In this sense, it can be called a parametric method. A similar method is applicable to directional wave measurements with wave gauge arrays. Borgman,[31] and Panicker and Borgman[32] have proposed a parametric method for wave gauge arrays.

In the present section, the cross-spectra have been assumed to take the ensemble mean values. In practice, any value of the cross-spectra calculated form wave records is subject to sampling variability. The author [10.33] has carried out a numerical simulation study on the sampling variability of directional estimates, and has found the following empirical relationship for the co-spectra between the vertical velocity and the x and y components of the slope of the water surface:

$$\frac{\sigma[C_{ij}(f)]}{[C_{ii}(f)C_{jj}(f)]^{1/2}} = \sqrt{\frac{2}{r}}, \tag{10.92}$$

where σ denotes the standard deviation, C_{ij} is the co-spectrum between the ith and jth wave components, and r is the number of degrees of freedom. Because of variability in the cross spectral estimates, the directional spectral density estimated from wave records is accompanied by some statistical variability. In fact, Kuik and van Vledder[34] demonstrate by means of the Monte Carlo simulations that the estimate of the mean wave direction from a pitch and roll buoy data is accompanied by sampling variations and that the magnitude of the root-mean-square error is in agreement with the theoretical prediction by Borgman *et al.*[35]

10.3.4 *Advanced Theories of Directional Spectrum Estimates*

(A) *Transfer function for wave kinematics*

The estimation methods of the directional spectrum discussed above were developed for either a wave gauge array, a directional buoy, or a two-axis current meter, and they were incapable of dealing with a mixed array consisting of multiple wave gauges and current meters. Furthermore, these methods could not take into account the presence of noises in records and statistical variability of the cross-spectrum. A breakthrough was made by Isobe *et al.*[34] in 1984, who proposed the extended maximum likelihood method for an array of any combination of wave sensors. While Isobe's approach was deterministic without any consideration for noises and sampling variability, Hashimoto[37–40] developed the maximum entropy principle method and a method using the

Bayesian approach for directional spectrum estimates, based on the probabilistic concept: Hashimoto's methods are summarized in the reference.[41] A survey of the presently available methods of directional wave spectrum estimate has been made by Benoit *et al.*[42]

Hashimoto's approach is to treat the problem of directional spectrum estimation as a procedure to find the solution $S_k(k, \theta)$ of the integral Eq. (10.57) from the information of a given set of covariances Ψ. Since the covariances are estimated at discrete values of the frequency, the problem is to find the solution of the directional spreading function $G(\theta|f)$ at respective frequencies. Thus, Eq. (10.57) is rewritten as

$$\phi_m(f) = \int_0^{2\pi} H_m(f, \theta) G(\theta|f) \, d\theta \qquad : \quad m = 1, 2, \ldots, M \,, \qquad (10.93)$$

where M denotes the number of cross-spectra formed from N wave sensors of any type $(M = N(N+1)/2)$. The function $\phi_m(f)$ is a normalized form of cross-spectrum defined by

$$\phi_m(f) = \Phi_{ij}(f)/S(f) \,, \qquad (10.94)$$

and H_m is the kernel function defined by

$$H_m(f) = H_i(f, \theta) H_j^*(f, \theta)[\cos(kx_{ij}\cos\theta + ky_{ij}\sin\theta)$$
$$-i\sin(kx_{ij}\cos\theta + ky_{ij}\sin\theta)] \,, \qquad (10.95)$$

where x_{ij} and y_{ij} denote the distances in the x and y directions between the ith and jth wave sensors, respectively.

The function $H_i(f, \theta)$ is the transfer function from the water surface elevation to the wave property recorded by the ith sensor, and $H_j^*(f, \theta)$ is the conjugate complex of the transfer function for the jth sensor. The transfer function is hereby defined as

$$H(f, \theta) = K(k, f) \cos^\alpha \theta \sin^\beta \theta \,. \qquad (10.96)$$

According to Isobe *et al.*,[36] the transfer function is derived by the small amplitude wave theory as listed in Table 10.1.

Table 10.1. Transfer function for directional spectral measurements.

Wave Motion		$K(k, f)$	α	β
Surface elevation	η	1	0	0
Vertical acceleration	η_{tt}	$-4\pi^2 f^2$	0	0
Surface slope (x)	η_x	ik	1	0
Surface slope (y)	η_y	ik	0	1
Orbital velocity (x)	u	$2\pi f \dfrac{\cosh k(h+z)}{\sinh kh}$	1	0
Orbital velocity (y)	v	$2\pi f \dfrac{\sinh k(h+z)}{\sinh kh}$	0	1
Pressure variation	p	$\rho g \dfrac{\cosh k(h+z)}{\cosh kh}$	0	0

Note: z is the elevation measured upward from the mean water level, h the water depth, ρ the density of water, and g the acceleration of gravity.

(B) *Extended maximum likelihood method (EMLM)*

By introducing the transfer function of Eq. (10.96), Isobe *et al.*[36] made it possible to apply the maximum likelihood method to a mixed array of wave sensors. Equation (10.79) is modified for a mixed array as in the following:

$$\hat{G}(\theta|f) = G_0 \left\{ \sum_{i=1}^{N} \sum_{j=1}^{N} \psi_{ij}^{-1} \exp[-i(kx_{ij}\cos\theta + ky_{ij}\sin\theta)] \cos^{\alpha_i + \alpha_j}\theta \sin^{\beta_i + \beta_j}\theta \right\}^{-1},$$
(10.97)

where ψ_{ij}^{-1} is the element of the inverse matrix of a complex matrix composed of the normalized cross-spectra ψ_{ij} of the following:

$$\psi_{ij} = \frac{\Phi_{ij}^*(f)}{K_i(k, f)K_j^*(k, f)\hat{S}(f)}.$$
(10.98)

The term G_0 on the right side of Eq. (10.97) is a constant to satisfy the normalization condition of Eq. (2.22) of Sec. 2.3.2.

The EMLM has a sharp directional resolution, and it is simple to use because of a straightforward algorithm for programming: it has been widely utilized in directional wave measurements with a combination of a two-axis current meter and a pressure sensor. However, the method sometimes yields a split at the peak of spreading function, and it is inferior to the MEP and BDM methods to be described in the following paragraphs in resolving multiple directional peaks.

(C) *Maximum entropy principle method (MEP) and extended maximum entropy method (EMEP)*

Hashimoto and Kobune[37] introduced the concept of entropy for the directional spreading function as defined below,

$$H = -\int_0^{2\pi} G(\theta|f) \ln G(\theta|f)\, d\theta, \qquad (10.99)$$

and proposed to find the solution of $G(\theta|f)$ which will maximize the above entropy under the constraint of Eq. (10.93). The original proposal, called the maximum entropy principle method (MEP),[37] was for a three-element measurement system such as a pitch and roll buoy, but later Hashimoto *et al.*[40] extended it to a combination of any number of wave sensors and called it the extended maximum entropy principle method (EMEP).

To solve the problem, the directional spreading function is assumed to have the following expression:

$$G(\theta|f) = G_0 \exp\left\{\sum_{n=1}^{N^*} [a_n(f)\cos n\theta + b_n(f)\sin n\theta]\right\}, \qquad (10.100)$$

where $a_n(f)$ and $b_n(f)$ are unknown parameters and N^* is the order of the model. Equation (10.100) is substituted into Eq. (10.93) to find the solutions for these parameters. However, by considering the existence of errors by noises and sampling variability, it is modified to the following form:

$$\epsilon_m = G_0 \int_0^{2\pi} [\phi_m - H_m(f,\theta)] \exp\left\{\sum_n^{N^*} [a_n(f)\cos n\theta \right.$$
$$\left. + b_n(f)\sin n\theta]\right\} d\theta \qquad : \quad m = 1, 2, \ldots, M^*, \qquad (10.101)$$

where ϵ_m stands for the amount of error associated with the mth cross-spectrum; M^* is the number of independent equations after the elimination of meaningless equations such as those involving zero co-spectra and quadrature-spectra.

The solutions for $a_n(f)$ and $b_n(f)$ are sought for by minimizing the total amount of errors; i.e., $\sum \epsilon_m^2$. It is carried out through a numerical technique of local linearization and iteration. The order of the model N^* is chosen as

the optimal one using the minimum Akaike's Information Criterion. For the procedure of numerical computations, refer to Ref. 41. In the MEP for a three-element measurement system, the model order N^* is preset at 2, and the solutions for the unknown parameters are obtained through a numerical computation technique.

The EMEP has the capability to estimate the directional spectrum very close to the true one from a limited number of wave motion records, much better than the EMLM. Its performance is nearly as good as the Bayesian approach, which is the best method of directional spectrum estimation but requires quite a lot of computational works.

(D) *Bayesian directional spectrum estimation method (BDM)*

The Bayesian approach is a probabilistic procedure to estimate the cause of a phenomenon from the result. To find the directional spreading function $G(\theta|f)$ from a set of the observed cross-spectra $\phi_m(f)$, as stated by Eq. (10.93), is a typical subject of the Bayesian approach, which was undertaken by Hashimoto.[38,39] In this approach, the directional spreading function is not pre-assigned any specific form, but it is assumed to be of a step function having constant (positive) values over small directional intervals as expressed by

$$G(\theta|f) \approx \sum_{k=1}^{K} \exp[z_k(f)] I_k(\theta) \,, \tag{10.102}$$

in which $z_k(f)$ is the unknown constant to be solved by the Bayesian approach, K is the number of division of the directional range $0 \leq \theta \leq 2\pi$, and I_k is defined as

$$I_k(\theta) = \begin{cases} 1 & : \quad (k-1)\Delta\theta \leq k\Delta\theta \,, \\ 0 & : \quad \text{otherwise}; \quad k = 1, 2, \ldots, K \,. \end{cases} \tag{10.103}$$

By substituting Eq. (10.102) into Eq. (10.93), we have the following approximate equation, provided the number of division K is sufficiently large:

$$\phi_m(f) \approx \sum_{k=1}^{K} \alpha_{m,k} \exp[z_k(f)] + \epsilon_m \qquad : \quad m = 1, 2, \ldots, M \,, \tag{10.104}$$

where

$$\alpha_{m,k} = \int_0^{2\pi} H_m(f, \theta) I_k(\theta) d\theta \approx H_m(f, \theta)\Delta\theta \,, \tag{10.105}$$

and ϵ_m represents the error term inherent in any measurement data and is assumed to follow the normal distribution with the mean 0 and the variance σ^2 of unknown magnitude. The solutions for the unknown constant z_k can be obtained by maximizing the likelihood of z_k and σ^2 for a given set of ϕ_m. The constraint on z_k is such that its value should vary gradually over consecutive sections, because the directional spreading function is expected to vary smoothly over the directional range.

The above is the basic concept of the BDM by Hashimoto.[38] More details of the method including computational techniques are described in Ref. 41. Because the BDM does not make any assumption for the functional shape of the directional spreading function, it has a large flexibility to fit well to any shape of spreading function. Through a number of simulation tests,[38,39] the BDM has been shown to perform the best among the existing methods of directional spectrum estimation, when the number of wave sensors is equal to or greater than four. For a three-element measurement system, the evaluation of the error terms contained in the cross-spectra becomes difficult and the BDM does not perform satisfactory: the MEP is recommended instead.

10.4 Resolution of Incident and Reflected Waves of Irregular Profiles

10.4.1 *Measurement of the Reflection Coefficient in a Wave Flume*

In hydraulic model tests of maritime structures in a wave flume, the first item of measurement is the characteristics of the incident waves, and the second item is the coefficient of reflection of the model structure. Although these measurements are not difficult for a regular train of waves, the same technique cannot be employed for an irregular train of waves, because irregular waves must be generated for a sufficiently long duration to exhibit their full statistical characteristics, and thus re-reflected waves by the wave paddle inevitably contaminate the incident wave train. Concerning this problem, Kajima[43] proposed a method for resolving the incident and reflected wave spectra by using the autocorrelation function. Thornton and Calhoun[44] estimated the coefficients of reflection and transmission of a rubble mound breakwater in the field, using a method slightly different from that by Kajima. Then, Goda and Suzuki[45] developed another method using the fast Fourier transform technique,

which has become one of the standard techniques of flume wave tests in the world. This method will be described below.

In a wave flume, with the installation of a model structure to be tested, waves reflected by the model travel back to the wave paddle and are re-reflected there. They propagate toward the structure and are reflected again, and the process is repeated many times. Thus, a multi-reflection system of wave trains is formed in the wave flume. The waves propagating toward the structure therefore consist of the superposition of the original incident waves, the first waves re-reflected by the paddle, the second re-reflected waves, and so on. Although they appear complicated, the components of these multi-reflection waves having the same frequency can be synthesized into a single train of waves, because the components all have the same frequency and the phase differences are fixed. A similar expression is possible for waves traveling toward the wave paddle. The synthesized profiles of incident and reflected waves for a specific frequency can be expressed as

$$
\left.\begin{aligned}
\eta_I &= a_I \cos(kx - \omega t + \varepsilon_I), \\
\eta_R &= a_R \cos(kx + \omega t + \varepsilon_R).
\end{aligned}\right\} \tag{10.106}
$$

The suffixes "I" and "R" denote the incident and reflected waves, respectively. The horizontal coordinate x is taken as positive in the direction from the wave paddle to the model structure.

Suppose wave profiles are recorded at two locations, $x = x_1$ and $x = x_2 = x_1 + \Delta l$, with the separation distance Δl. The wave profiles are expressed as

$$
\left.\begin{aligned}
\eta_1 &= (\eta_I + \eta_R)_{x=x_1} = A_1 \cos \omega t + B_1 \sin \omega t, \\
\eta_2 &= (\eta_I + \eta_R)_{x=x_2} = A_2 \cos \omega t + B_2 \sin \omega t,
\end{aligned}\right\} \tag{10.107}
$$

where

$$
\left.\begin{aligned}
A_1 &= a_I \cos \phi_I + a_R \cos \phi_R, \\
B_1 &= a_I \sin \phi_I - a_R \sin \phi_R, \\
A_2 &= a_I \cos(k\Delta l + \phi_I) + a_R \cos(k\Delta l + \phi_R), \\
B_2 &= a_I \sin(k\Delta l + \phi_I) - a_R \sin(k\Delta l + \phi_R),
\end{aligned}\right\} \tag{10.108}
$$

$$
\phi_I = kx_1 + \varepsilon_I, \quad \phi_R = x_1 + \varepsilon_R. \tag{10.109}
$$

In the above, Eq. (10.108) represents a system of four equations containing the four unknown quantities a_I, a_R, ϕ_I and ϕ_R. By eliminating a_R and ϕ_R from the expressions for A_2 and B_2, we have

$$\left. \begin{array}{l} A_2 = (A_1 \cos k\Delta l + B_1 \sin k\Delta l) - 2a_I \sin k\Delta l \sin \phi_I \,, \\[2mm] B_2 = (-A_1 \sin k\Delta l + B_1 \cos k\Delta l) + 2a_I \sin k\Delta l \cos \phi_I \,. \end{array} \right\} \quad (10.110)$$

The quantity a_I can be obtained by eliminating the terms containing ϕ_I from the above, and similarly for a_R. The result is

$$\left. \begin{array}{l} a_I = \dfrac{1}{2|\sin k\Delta l|} [(A_2 - A_1 \cos k\Delta l - B_1 \sin k\Delta t)^2 \\[3mm] \qquad + (B_2 + A_1 \sin k\Delta l - B_1 \cos k\Delta l)^2]^{1/2} \,, \\[4mm] a_R = \dfrac{1}{2|\sin k\Delta l|} [(A_2 - A_1 \cos k\Delta l + B_1 \sin k\Delta l)^2 \\[3mm] \qquad + (B_2 - A_1 \sin k\Delta l - B_1 \cos k\Delta l)^2]^{1/2} \,. \end{array} \right\} \quad (10.111)$$

Thus, the amplitudes a_I and a_R of the incident and reflected waves can be calculated from the four amplitudes A_1, B_1, A_2 and B_2, and the phase lag $k\Delta l$. Furthermore, the phase angle ϕ_I can be obtained by eliminating the terms containing a_I in Eq. (10.110), and similarly for ϕ_R, as demonstrated by Fan.[46] The result is

$$\left. \begin{array}{l} \phi_I = \tan^{-1} \left[\dfrac{-A_2 + A_1 \cos k\Delta l + B_1 \sin k\Delta l}{B_2 + A_1 \sin k\Delta l - B_1 \cos k\Delta l} \right] \,, \\[5mm] \phi_R = \tan^{-1} \left[\dfrac{-A_2 + A_1 \cos k\Delta l - B_1 \sin k\Delta l}{-B_2 + A_1 \sin k\Delta l + B_1 \cos k\Delta l} \right] \,. \end{array} \right\} \quad (10.112)$$

The above method of resolution is applied to each Fourier component of the irregular wave profiles recorded at two locations separated by an appropriate distance, after the records have been decomposed into the Fourier series by using the fast Fourier transform technique. An assumption in this analysis is that the dispersion relationship, Eq. (8.3), is satisfied between the wavenumber k and the frequency f in the range of analysis. The amplitudes a_I and a_R, thus estimated for each Fourier component, represent the root-mean-square amplitude $|A_k^2 + B_k^2|^{1/2}$ for the wave profile expressed by Eq. (10.14). The frequency spectra of the incident and reflected waves are then estimated by the procedure described in Sec. 10.2.
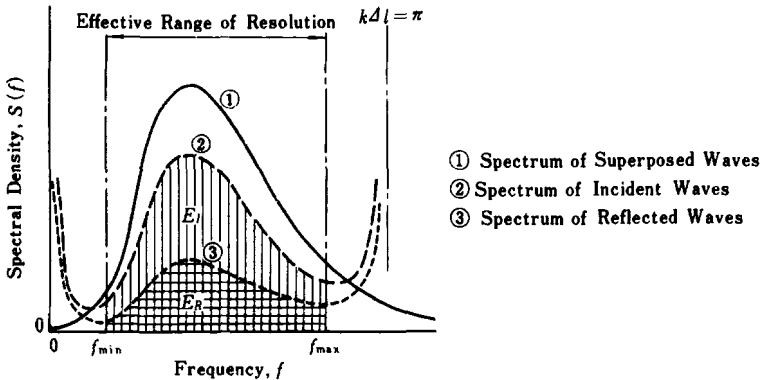
Fig. 10.6. Illustration of the spectral resolution of the incident and reflected waves.

The result of a spectral resolution by this method is schematically shown in Fig. 10.6. It is seen that the spectral estimates diverge in the neighborhood of frequencies satisfying the condition $k\Delta l = n\pi$ for $n = 0, 1, 2, \ldots$, because the factor $|\sin k\Delta l|$ in the denominator on the right side of Eq. (10.111) becomes very small, and errors due to noise are greatly amplified. The spectral estimates are effective in the frequency range outside of the neighborhood of such diverging points. The effective frequency range of resolution can be judged with the following guideline:

$$\left.\begin{array}{llll} \text{Upper limit } (f_{\max}) & : & \Delta l/L_{\min} \simeq 0.45\,, \\ \text{Lower limit } (f_{\min}) & : & \Delta l/L_{\max} \simeq 0.05\,. \end{array}\right\} \qquad (10.113)$$

The symbols $L_{\min}$ and $L_{\max}$ denote the wavelengths corresponding to the upper $(f_{\max})$ and lower $(f_{\min})$ limits of the effective frequency range, respectively. When the distance between the two wave gauges has been fixed, the effective frequency range of the resolution of the incident and reflected waves can be determined from Eq. (10.113). Working the other way, when the plan of a hydraulic model test is being prepared, the distance Δl should be selected such that the major part of the wave energy of the spectrum of the test wave is contained in the effective frequency range $f_{\min}$ to $f_{\max}$.

For the estimation of the reflection coefficient, the energies of the incident and reflected waves, E_I and E_R, within the range $f_{\min}$ to $f_{\max}$ need to be calculated. This is accomplished as

$$
\left.
\begin{aligned}
E_I &= \int_{f_{\min}}^{f_{\max}} S_I(f)df = \frac{\Delta t}{2t_0} \sum_{f_{\min}}^{f_{\max}} I_I , \\
E_R &= \int_{f_{\min}}^{f_{\max}} S_R(f)df = \frac{\Delta t}{2t_0} \sum_{f_{\min}}^{f_{\max}} I_R ,
\end{aligned}
\right\} \tag{10.114}
$$

where I_I and I_R are the periodograms of the incident and reflected waves as equal to Na_I^2 and Na_R^2, respectively. The calculation is best made with the periodograms in order to eliminate the effect of leakage of wave energy into neighboring frequency bands, which is introduced through the use of a filter in smoothing of the periodograms. Since the energies of the incident and reflected waves must be proportional to the squares of the respective wave heights, the reflection coefficient defined as the ratio of heights can be estimated from

$$
K_R = \sqrt{E_R/E_I} . \tag{10.115}
$$

This reflection coefficient represents that of the wave group as a whole. The incident wave height H_I and the reflected wave height H_R can be estimated with the above coefficient of reflection K_R and the mean value of wave heights at the two locations, which is denoted by H_S, as

$$
H_I = \frac{1}{(1 + K_R^2)^{1/2}} H_S \quad \text{and} \quad H_R = \frac{K_R}{(1 + K_R^2)^{1/2}} H_S . \tag{10.116}
$$

The wave heights H_I, H_R and H_S can refer to any definition such as the significant height, the mean height, or other heights, as long as the same definition is employed in the calculation Eq. (10.116). This calculation is based on the assumption that the observed height in the flume is equal to the square root of the sum of the squares of the incident and reflected wave heights, as expressed by Eq. (3.28) in Sec. 3.6.3. As shown in Fig. 3.40, however, Eq. (3.28) does not hold in the vicinity of a reflective boundary because of strong phase interference. Therefore, it is recommended that the wave gauges be set at a distance of more than one wavelength of the significant wave from both model structure and the wave paddle.

The above technique of resolving incident and reflected waves can be directly applied to regular wave trains. The amplitudes a_I and a_R become those of the incident and reflected waves, and the reflection coefficient is directly obtained as the ratio a_R/a_I. Furthermore, use of the phase angles ϕ_I and ϕ_R, resolved by Eq. (10.112), together with a_I and a_R makes it possible to retrieve the profiles of the incident and reflected wave trains. By applying

this technique for the whole Fourier components of irregular waves (within the effective frequency range of resolution), the profiles of irregular and reflected irregular wave trains can be reconstructed.

In several hydraulic laboratories around the world, the technique has been extended to a linear array of three wave gauges (e.g., see Refs. 47–49). The motivation behind this is to circumvent the divergence problem at $k\Delta l = n\pi$. With three gauges, one pair may fail to yield the proper solution at a particular frequency owing to the divergence problem, but the other two pairs can yield nondiverging estimates. By taking the average of the results of the pairs of wave gauges not troubled by the divergence problem at the respective frequencies, a three-gauge array can extend the effective range of wave resolution considerably.

10.4.2 *Measurement of the Reflection Coefficient of Prototype Structures*

Measurement of waves reflected from a vertical breakwater or a seawall in the field is rather difficult. We can sometimes recognize the presence of reflected waves visually at the site, on aerial photographs, or on the screens of imaging radars employed for directional wave measurements. But the heights of such reflected waves cannot be measured by these means.

The measurement of reflected waves in the field is fundamentally the same as the measurement of the directional wave spectrum. The directional resolution must be good enough to separate the directional peaks of the incident and reflected waves. A serious problem with the directional wave measurement of a wave reflection system is a phase-locked relation between the incident and reflected wave components. In the analysis of the directional wave spectrum, it is assumed that all the component waves are independent, with random and uniformly distributed phase angles. However, each pair of incident and reflected wave components maintain a fixed phase relation, which depends on the relative distance and the angle of incidence to the reflective boundary. The violation of the condition of random phase angles cause a false estimation of the directional spectral density. This has been confirmed in a numerical simulation study.[25]

For the correct estimation of directional spectra in the presence of phase-locked incident and reflected waves, Isobe and Kondo[49] proposed a modification of the maximum likelihood method under the assumption that the waves

are reflected at the reflective boundary without a phase delay and with the angle of reflection the same as the incident angle. In the modified maximum likelihood method (MMLM), the reflection coefficient which is assumed to be the function of frequency and direction is calculated by

$$
r(f,\theta) = -\left[\sum_{i=1}^{N}\sum_{j=1}^{N}\Phi_{ij}^{-1}(f)\{\exp[-ik(R_{ij}\cos\theta + Y_{ij}\sin\theta)]\right.
$$

$$
\left. + \exp[ik(R_{ij}\cos\theta - Y_{ij}\sin\theta)]\}\right] \bigg/ 2\sum_{i=1}^{N}\sum_{j=1}^{N}\Phi_{ij}^{-1}(f)
$$

$$
\times \{\exp[ik(X_{ij}\cos\theta + Y_{ij}\sin\theta)]\}\,, \tag{10.117}
$$

in which the y axis $(x = 0)$ is taken at the reflective boundary, X_{ij} and Y_{ij} are the distances in the x and y directions between the ith and jth wave sensors, respectively, $R_{ij} = X_i + X_j$ is the sum of the distances from the boundary, and $\Phi_{ij}^{-1}(f)$ denotes the (i, j) component of the inverse matrix of the complex matrix composed of the conjugate cross-spectra.

The directional spreading function of the incident waves is estimated by

$$
\hat{G}(\theta|f) = A\left[\sum_{i=1}^{N}\sum_{j=1}^{N}\Phi_{ij}^{-1}(f)\{\exp[ik(X_i\cos\theta + Y_i\sin\theta)]\right.
$$

$$
+ r(f,\theta)\exp[-ik(X_i\cos\theta - Y_i\sin\theta)]\}
$$

$$
\times \{\exp[-ik(X_j\cos\theta + Y_j\sin\theta)]\}
$$

$$
\left. + r(f,\theta)\exp[ik(X_j\cos\theta - Y_j\sin\theta)]\}\right]^{-1}\,, \tag{10.118}
$$

where A is the constant for normalization of the directional spreading function by the condition of Eq. (2.22) but has the inverse units of spectral density.

The frequency spectral density in front of a reflective structure fluctuates from place to place because of the presence of a partial standing wave system formed by the superposition of incident and reflected random waves. The observed spectral density $\hat{S}_{ii}$ by the ith wave gauge should be modified for the estimation of incident wave spectrum by the following formula:

$$\hat{S}_{ii}(f) = \frac{S_{ii}(f)}{\displaystyle\int_{-\pi/2}^{\pi/2} \hat{G}(f,\theta)[1 + 2r(f,\theta)\cos(2kX_i\cos\theta) + r^2(f,\theta)]d\theta}. \quad (10.119)$$

The modified frequency spectra of N wave sensors thus obtained are averaged to yield the estimate of the incident wave spectrum. The estimate of incident directional spectrum is obtained by the product of the above frequency spectrum and the directional spreading function by Eq. (10.118).

The MMLM has been utilized for the estimation of reflection coefficient of actual harbor and coastal structures (e.g., see Refs. 50 and 51, etc.). It is relatively simple to use, but it may not yield a good result when the incident waves have multidirectional peaks. Hashimoto et al.[52] have proposed the modified, extended maximum entropy method (MEMEP) as a more powerful method of directional spectrum estimation for the incident and reflected wave field.

An approximate value of the reflection coefficient of prototype structures may also be estimated by simultaneously measuring the wave height H_S in front of a structure (at a distance of more than one wavelength from the structure) and the incident wave height H_I at a location free from the effect of reflected waves. Then, Eq. (3.28) in Sec. 3.6.3 can be utilized to resolve the heights of the reflected and incident waves. Accurate estimation of the reflection coefficient by this method is difficult, however. Even if the reflected wave height is 50% of the incident height, the resultant height of the superposed waves is only 12% greater than the incident height. Sampling variability of random sea waves adds further difficulty to the estimation of wave reflection. A large amount of data for similar wave conditions should be collected and the mean ratio H_S/H_I should be calculated in order to reduce the effect of sampling variability on the estimate of H_R/H_I.

10.5 Numerical Simulation of Random Sea Waves and Numerical Filters

10.5.1 *Principles of Numerical Simulation*

The necessity of numerical simulation of random sea waves occurs in many aspects of the ocean and coastal engineering studies. The fundamental equation often employed for wave simulation is the following:

$$\eta(x,y,t) = \sum_{m=1}^{M}\sum_{n=1}^{N} a_{m,n}\cos(k_m x\cos\theta_n + k_m y\sin\theta_n - 2\pi f_m t + \epsilon_{m,n}), \quad (10.120)$$

which is a rewritten form of Eq. (8.10) of Sec. 8.2. The ranges of frequency and wave angle are divided into M and N segments, respectively, $a_{m,n}$ denotes the amplitude of the component wave in the mth frequency and nth directional segment, and $\epsilon_{m,n}$ is a random phase equally distributed in $[0, 2\pi]$. The amplitude $a_{m,n}$ is determined from a given function of the directional spectrum $S(f, \theta)$ by

$$a_{m,n}^2 = 2S(f_m, \theta_n)\Delta f_m \Delta \theta_n \,, \tag{10.121}$$

where Δf_m and $\Delta \theta_n$ denote the bandwidth of the mth frequency and that of the nth wave angle, respectively.

Equation (10.116) is the so-called *double summation method*. Exception for the use of this method is the preparation of the control signal for multidirectional wave generator, for which the *single summation method* is employed. The concept of representing the infinite series of Eq. (8.10) with the finite double series is also employed in the evaluation of the refraction and diffraction of directional random waves, which have been discussed in Secs. 3.1 and 3.2.

For simulation of wave kinematics ζ_i such as orbital velocities, wave pressure, and others, the fundamental equation is

$$\zeta_i(x, y, t) = \sum_{m=1}^{M} \sum_{n=1}^{N} K_i(f_m, \theta_n)\, a_{m,n}$$

$$\times \cos(k_m x \cos \theta_n + k_m y \sin \theta_n - 2\pi f_m t + \epsilon_{m,n} + \psi_i)\,, \tag{10.122}$$

where $K_i(f, \theta)$ and ψ_i are the transfer function from η to ζ_i and the phase lag, respectively. They are given using the relation listed in Table 10.1 as below.

$$\left.\begin{aligned} K_i(f, \theta) &= |H_i(k, f)| \cos^\alpha \theta \sin^\beta \theta \,, \\ \psi_i &= \arg[H_i(k, f)]\,. \end{aligned}\right\} \tag{10.123}$$

For making the control signal of a random wave generator, the transfer function is set as $K(f, \theta) = 1/F(f, h)$ using the wave generating function of $F_1(f, h)$ by Eq. (7.1) for piston type or $F_2(f, h)$ by Eq. (7.2) for flap type.

10.5.2 *Selection of Frequency and Wave Angle Components*

The frequency components are selected by two methods, depending on the technique of the superposition of component waves. If the inverse fast Fourier transform (FFT) method is employed for computation of wave profiles, the

frequency components are set as equally spaced with the increment of $1/t_0$, where t_0 is the duration of wave record to be simulated. The number $M = 2^J$ determines the maximum frequency for simulation as $f_{\max} = 2^J/t_0$ and the number of data points to be simulated is 2^{J+1}. If the sampling time Δt and the number of data point $2M = 2^{J+1}$ are set first, then $t_0 = 2M^{J+1}\Delta t$ and $f_{\max} = 1/2\Delta t$.

If the inverse FFT method is not used for computation of wave profiles, the number of frequency components is limited to several hundreds. In that case, it is better to select the frequency components in such a way that the individual amplitudes would be as nearly equal as possible; by so selecting, every wave component can contribute to the simulation result with equal weight. A convenient formula for selecting the frequency components with nearly equal component amplitudes is given by Goda[53] as

$$f_m = \frac{1.007}{T_{1/3}} \left[\ln \left(\frac{2M}{2m-1} \right) \right]^{1/4} . \tag{10.124}$$

This formula is derived by dividing the zeroth moment of the Bretschneider–Mitsuyasu spectrum (Eq. (2.10)) into the $2M$ segments of equal amount and by taking the odd number of frequencies at the boundaries of $2M$ segments. For other standard frequency spectra, the condition of equal component amplitude is not satisfied and the computation by means of Eq. (10.121) must be carried out.

The division of wave angle is usually made with an equal spacing for the sake of simplicity. The numbers of the frequency and wave angle components M and N should be taken as large as possible within the capacity of the computer at hand. A minimum of $M = 50$ and $N = 30$ is recommended for spatial simulation of wave field. For the examination of statistical variability, a much larger number of components need to be employed.

10.5.3 *Pseudorandom Number Generating Algorithm*

Selection of the random phase angle $\epsilon_{m,n}$ in Eq. (10.120) is the important step in correct simulation of random waves. It is made by means of the random number R equally distributed between 0 and 1. The author has been using the following algorithm to generate pseudorandom numbers by computer. First, select an arbitrary odd integer X_1, which is called the seed number. The second

integer X_2 is generated by

$$X_2 = \mathrm{mod}(Y, b), \quad Y = aX_1, \tag{10.125}$$

where $\mathrm{mod}(Y, b)$ denotes a remainder after Y is divided by b. Then, the process is repeated by replacing X_1 with X_2 for any number of cycles, yielding a series of integers X_i. The random number assigned between 0 and 1 is obtained by

$$R_i = X_i/q \quad : \quad i = 1, 2, \ldots. \tag{10.126}$$

The constants are given the following specific values:

$$a = 7909, \quad b = 2^{36}, \quad q = 2^{35} - 1. \tag{10.127}$$

The random integer X_i may exceed 2^{35} during the generating process. In that case, X_i is replaced by the integer $(2^{36} - X_i)$ and the process is continued. The above algorithm has been tested for the nonrepeatability and the uniformity of randomness in two-dimensions, and it has passed the test for a series of up to 2×10^7 random numbers.[54]

10.5.4 *Simulation of Time Series Data*

When a time history of the wave kinematics at a fixed location is simulated, the double summation in Eq. (10.120) or Eq. (10.122) is transformed into the following single summation[53]:

$$\eta(t|x, y) = \sum_{m=1}^{M} A_m \cos(2\pi f_m t - \psi_m), \tag{10.128}$$

where

$$\left. \begin{aligned}
A_m &= \sqrt{C_m^2 + S_m^2}, \\
\psi_m &= \tan^{-1}(S_m/C_m), \\
C_m &= \sum_{n=1}^{N} a_{m,n} \cos(k_m x \cos\theta_n + k_m y \sin\theta_n + \epsilon_{m,n}), \\
S_m &= \sum_{n=1}^{N} a_{m,n} \sin(k_m x \cos\theta_n + k_m y \sin\theta_n + \epsilon_{m,n}).
\end{aligned} \right\} \tag{10.129}$$

By computing the coefficients C_m and S_m beforehand, the computation time for the simulation is greatly reduced.

When the inverse FFT method is employed to compute Eq. (10.128), the coefficients C_m and S_m are directly used instead of the amplitude A_m. When the unequal frequency spacing is used to reduce the number of frequency components and the simulation is made at a constant time interval; i.e., $t_k = k\Delta t$, the use of either set of the following regression relations leads to a considerable saving in the computation time:

$$\left.\begin{array}{l} \cos(k+1)\Delta t = \cos k\Delta t \cos \Delta t - \sin k\Delta t \sin \Delta t\,, \\ \sin(k+1)\Delta t = \sin k\Delta t \cos \Delta t + \cos k\Delta t \sin \Delta t\,, \end{array}\right\} \qquad (10.130)$$

or

$$\left.\begin{array}{l} \cos(k+1)\Delta t = 2\cos k\Delta t \cos \Delta t - \cos(k-1)\Delta t\,, \\ \sin(k+1)\Delta t = 2\sin k\Delta t \cos \Delta t - \sin(k-1)\Delta t\,. \end{array}\right\} \qquad (10.131)$$

The former set has been used in several simulation studies by the author,[53,54] while the latter set is due to Medina *et al.*[55]

The simulation of a one-dimensional irregular wave profile for a given frequency spectrum can be done by the same principle as above. The basic equation is

$$\eta(t) = \sum_{m=1}^{M} a_m \cos(2\pi f_m t + \epsilon_m)\,. \qquad (10.132)$$

In the case of Eq. (10.129), the coefficients C_m and S_m are normally distributed with the mean 0 and the variance $S(f_m)\Delta f_m$. Thus, the amplitude a_m in Eq. (10.132) should be computed with due consideration of statistical variability as follows:

$$a_m = \sqrt{S(f_m)(z_1^2 + z_2^2)\Delta f_m}\,, \qquad (10.133)$$

where z_1 and z_2 are independent variates of the standard normal distribution with the mean of 0 and the variance of 1; they can be simulated with one of standard computer programs. If the statistical variability is to be neglected for some reason, then the expected value of $E[z_1^2 + z_2^2] = 2$ is substituted in Eq. (10.133).

10.5.5 *Preparation of Control Signals for Multidirectional Wave Generator*

As discussed in Sec. 7.2, the control signals for multidirectional wave generators are prepared by the single summation method, because the use of the double summation method introduces the problem of phase locking among wave components and violates the condition of homogeneity. According to Takayama and Hiraishi,[56] the motion of a the rth segment of a wave paddle is formulated as

$$\eta_r(t) = \sum_{m=1}^{M} \frac{a_m}{F(f_m, h)} \sin(2\pi f_m t - k_m rb \cos\theta_m + \epsilon_m) \sin\theta_m, \qquad (10.134)$$

where b denotes the width of a wave paddle so that $x = rb$ indicates the distance of the rth paddle from the origin of the coordinate. The frequency f_m and the wave amplitude a_m are determined by the methods described in the preceding paragraphs.

What makes Eq. (10.130) different from Eq. (10.116) is the designation of a single wave angle to one frequency each. The wave angle θ_m is selected by a random number R_m being uniformly distributed between 0 and 1 through the cumulative distribution of the directional distribution function; i.e.,

$$\theta_m = F^{-1}(R_m) \quad : \quad F(\theta|f_m) = \int_0^\theta G(\theta|f_m)d\theta. \qquad (10.135)$$

The inverse solution of the cumulative distribution $F(\theta|f_m)$ cannot be solved analytically, but must be sought for by a numerical procedure. Initially the random number R_m is assigned to each frequency. The spreading function $G(\theta|f_m)$ is first integrated for the full range of wave angle so as to evaluate the normalization constant G_0. The integration of the second equation of Eq. (10.135) is made step by step until the value $F(\theta|f_m)$ equals R_m, which is assigned to the frequency f_m. The angle at this condition gives the result for θ_m. The number of frequency components must be large enough: in some laboratory, one thousand component frequencies determined by means of Eq. (10.124) is employed.

The control signals for wave generators must be fed with a short time interval for smooth operation of the servo system. When Eq. (10.130) or Eq. (10.131) is used for computation of wave profiles, Δt can be set as required from the servo system. When the inverse FFT method is employed, the

computation is made with a coarse time interval and the resultant output is interpolated to yield the signals in a fine time interval.

10.5.6 *Numerical Filtering of Wave Record*

The concept of numerical simulation of irregular wave profiles is applicable to the problem of numerical filtering. For example, a record of nearshore waves is often contaminated by the fluctuation of the mean water level due to surf beat. In such a case, the data is decomposed into a finite Fourier series with the aid of the fast Fourier transform algorithm. Then all the Fourier amplitudes outside the frequency range of interest are set to zero, and the operation of the inverse FFT is performed by retaining only the amplitudes within the frequency range of interest.
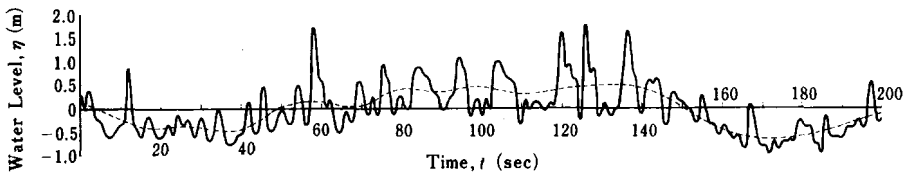
Fig. 10.7. Example of the profile of surf beat extracted by means of a numerical filter.[57]

Figure 10.7 shows an example of such a computation.[57] A wave record consisting of 1800 data points sampled at the rate of $\Delta t = 1$ s was analyzed, and the profiles of surf beat in the frequency range of $f \leq 0.05$ Hz were reconstructed with about 90 pairs of Fourier coefficients as shown with the dashed line; in this computation, the regression formula of Eq. (10.126) was used instead of the inverse FFT method. This example presents a case of extracting the profile of long period components, but the method can also be utilized for correction of the fluctuating mean water level in a wave record, by setting the Fourier coefficients of the surf beat frequency to zero and retaining those in the normal frequency range as they are.

References

1. M. J. Tucker, "Analysis of records of sea waves," *Proc. Inst. Civil Engrg.* **26** (10) (1963), pp. 305–316.
2. Y. Goda, "The observed joint distribution of periods and heights of sea waves," *Proc. 16th Int. Conf. Coastal Engrg.* (Hamburg, 1978) pp. 227–246.

3. Y. Goda, "Estimation of wave statistics from spectral information," *Proc. Int. Symp. Ocean Wave Measurement and Analysis* (*WAVES '74*) ASCE 1 (1974), pp. 320–337.

4. A. Kimura, "Statistical properties of random wave groups," *Proc. 17th Int. Conf. Coastal Engrg.* (Sydney, 1980), pp. 2955–2973.

5. L. H. Koopmans, *The Spectral Analysis of Time Series* (Academic Press, 1974) pp. 258–265.

6. R .B. Blackman and J. W. Tukey, *The Measurement of Power Spectra from the Point of View of Communications Engineering* (Dover Pub., 1958) 190p.

7. Y. Goda, "Analysis of wave grouping and spectra of long-travelled swell," *Rept. Port and Harbour Res. Inst.* **22** (1) (1983), pp. 3–41.

8. M. Donelan and W. J. Pierson, Jr., "The sampling variability of estimates of spectra of wind-generated gravity waves," *J. Geophys. Res.* **88** (C7) (1983), pp. 4381–4392.

9. Koopmans, *loc. cit.*, p. 305.

10. K. Rikiishi, "Methods of computing the power spectrum for equally-spaced time serise of finite length," *J. Applied Meteorology* **15** (10) (1976), pp. 1102–1110.

11. Koopmans, *loc. cit.*, pp. 300–302.

12. S. Kuwajima and K. Nagai, "The fast Fourier transform for the sample of arbitrary length and its application to spectral analyses," *Tech. Note of Port and Harbour Res. Inst.* **155** (1973), 33p (*in Japanese*).

13. K. Rikiishi and H. Mitsuyasu, "On the use of windows for the computation of power spectra," *Rept. Res. Inst. Applied Mech., Kyushu Univ.* **XXI** (68) (1973), pp. 53–71.

14. Koopmans, *loc. cit.*, p. 273.

15. H. Rye, "Ocean wave groups," *Dept. Marine Tech. Norwegian Inst. Tech., Rept.* **UR 82–8** (1982), 214p.

16. N. N. Panicker, "Review of techniques for directional wave spectrum," *Proc. Int. Symp. Ocean Wave Measurement and Analysis* (*WAVES '74*) ASCE 1 (1974), pp. 669–688.

17. D. Stilwell, "Directional energy spectra of the sea from photographs," *J. Geophys. Res.* **74** (8) (1969), pp. 1974–1986.

18. D. B. King and O. H. Shemdin, "Radar observations of hurricane wave directions," *Proc. 16th Int. Conf. Coastal Engrg.* (Hamburg, 1978), pp. 209–226.

19. J. F. Vesecky *et al.*, "Radar observations of wave transformations in the vicinity of island," *J. Geophys. Res.* **85** (C9) (1980), pp. 4977–4986.

20. I. A. Sneddon, *Fourier Transform* (McGraw-Hill, 1951), p. 44.

21. B. Kinsman, *Wind Waves* (Prentice-Hall, 1965), pp. 460–471.

22. N. P. Barber, "The directional resolving power of an array of wave detectors," *Ocean Wave Spectra* (Prentice-Hall, 1963), pp. 137–150.

23. J. Capon, R. J. Greenfield, and R. J. Kolker, "Multidimensional maximum-likelihood processing of a large aperture seismic array," *Proc. IEEE* **55** (1967), pp. 192–211.

24. S. S. Pawka, "Island shadows in wave directional spectra," *J. Geophys. Res.* **88** (C4) (1983), pp. 2579–2591.

25. Y. Goda, "Simulation in examination of directional resolution," *Proc. Conf. on Directional Wave Spectra Applications* (Berkeley, 1981), pp. 387–407.

26. M. Yamaguchi and Y. Tsuchiya, "Directional spectra of wind-waves in growing state," *Proc. 27th Japanese Conf. Coastal Engrg.* (1980), pp. 99–103 (*in Japanese*).

27. R. A. Haubrich, "Array design," *Bull. Seismological Soc. America* **58** (3) (1968), pp. 979–991.

28. M. S. Longuet-Higgins, D. E. Cartwright, and N. D. Smith, "Observations of the directional spectrum of sea waves using the motions of a floating buoy," *Ocean Wave Spectra* (Prentice-Hall, 1963), pp. 111–136.

29. H. Mitsuyasu *et al.*, "Observation of the directional spectrum of ocean waves using a cloverleaf buoy," *Physical Oceanography* **5** (4) (1975), pp. 750–760.

30. Y. Nagata, "The statistical properties of orbital wave motions and their application for the measurement of directional wave spectra," *Oceanogr. Soc. Japan.* **19** (4) (1964), pp. 169–191.

31. L. E. Borgman, "Directional spectral model for design use for surface waves," *Hyd. Engrg. Lab., Univ. Calif., Rept.* HEL 1–12 (1969), 56p.

32. N. N. Panicker and L. E. Borgman, "Enhancement of directional wave spectrum estimates," *Proc. 14th Int. Conf. Coastal Engrg.* (Copenhagen, 1974), pp. 258–279.

33. Y. Goda, "Numerical examination of the measuring technique of wave direction with the 'covariance method'," *Rept. Port and Harbour Res. Inst.* **20** (3) (1981), pp. 53–92 (*in Japanese*).

34. A. J. Kuik and G. Ph. van Vledder, "Proposed method for the routine analysis of pitch-roll buoy data," *Proc. Symp. Description and Modelling of Directional Seas*, Paper No. A-5, Tech. Univ. Denmark (June, 1984), 13p.

35. L. E. Borgman, R. L. Hagan, and A. J. Kuik, "Statistical precision of directional spectrum estimation with data from a tilt-and-roll buoy," *Topics in Ocean Physics*, ed. A. R. Osborne and P. Malanotte Rizzoli (Noord-Holland, Amsterdam, 1982), pp. 418–438.

36. M. Isobe, K. Kondo, and K. Horikawa, "Extension of MLM for estimating directional wave spectrum," *Proc. Symp. Description and Modelling of Directional Seas*, Tech. Univ. Denmark, Paper No. A-6, (1984), 15p.

37. N. Hashimoto and K. Kobune, "Estimation of directional spectra from the maximum entropy principle," *Rept. Port and Harbour Res. Inst.* **24** (3) (1985), pp. 123–145 (*in Japanese*).

38. N. Hashimoto, K. Kobune, and Y. Kameyama, "Estimation of directional spectrum using the Bayesian approach, and its application to field data analysis," *Rept. Port and Harbour Res. Inst.* **26** (5) (1987), pp. 57–100.

39. N. Hashimoto and K. Kobune, "Directional spectrum estimation from a Bayesian approach," *Proc. 21st Int. Conf. Coastal Engrg.* (Malaga, Spain, 1988), pp. 62–76.

40. N. Hashimoto, T. Nagai, and T. Asai, "Extension of the maximum entropy principle method for directional wave spectrum estimation," *Proc. 24th Int. Conf. Coastal Engrg.* (Kobe, 1994), pp. 232–246.

41. N. Hashimoto, "Analysis of the directional wave spectrum from field data," *Advances in Coastal and Ocean Engineering*, ed. P. L.-F. Liu **3** (1997), pp. 103–143.

42. M. Benoit, P. Frogaard, and H. A. Schäffer, "Analysing multidirectional wave spectra: A tentative classification of available methods," *Proc. IAHR Seminar on Multidirectional Waves and Their Interaction with Structures* 27th IAHR Congress (San Francisco, 1997), Published by the National Research Council of Canada, pp. 159–182.

43. R. Kajima, "Estimation of incident wave spectrum in the sea area influenced by reflection," *Coastal Engineering in Japan* **12** pp. 9–16.

44. E. B. Thornton and R. J. Calhoun, "Spectral resolution of breakwater reflected waves," *Proc. ASCE* **98** (WW4) (1972), pp. 443–460.

45. Y. Goda and Y. Suzuki, "Estimation of incident and reflected waves in random wave experiments," *Proc. 15th Int. Conf. Coastal Engrg.* (Hawaii, 1976), pp. 828–845.

46. Qijin Fan, "Separation of time series on incident and reflected waves in model test with irregular waves," *China Ocean Engrg.* **2** (4) (1988), pp. 45–60.

47. W. N. Seelig, "Effect of breakwaters on waves: Laboratory tests of wave transmission by overtopping," *Coastal Structures '79* ASCE (1979), pp. 941–961.

48. E. P. D. Mansard and E. R. Funke, "The measurement of incident and reflected wave spectra using a least squares method," *Proc. 17th Int. Conf. Coastal Engrg.* (Sydney, 1980), pp. 154–172.

49. P. Gaillard, H. Gauthier, and F. Holly, "Method of analysis of random wave experiments with reflecting coastal structures," *Proc. 17th Int. Conf. Coastal Engrg.* (Sydney, 1980), pp. 204–220.

50. M. Isobe and K. Kondo, "Method for estimation of directional wave spectrum in incident and reflected wave field," *Proc. 19th Int. Conf. Coastal Engrg.* (Houston, 1984), pp. 467–483.

51. D. A. Huntley, D. J. Simmonds, and M. A. Davidson, "Estimation of frequency-dependent reflection coefficients using current and elevation sensors," *Proc. Coastal Dynamics '95,* ASCE (Gdańsk, Poland, 1995), pp. 57–68.

52. N. Hashimoto, T. Nagai, and T. Asai, "Modification of extended maximum entropy principle method for estimating directional spectrum in incident and reflected wave field," *Rept. Port and Harbour Res. Inst.* **32** (4) (1993), pp. 25–47 (*in Japanese*) (see also *Proc. 16th OMAE '97*, **II** pp. 1–7.)

53. Y. Goda, "Numerical experiments on statistical variability of ocean waves," *Rept. Port and Harbour Res. Inst.* **16** (2) (1977), pp. 3–26.
54. Y. Goda, "Numerical examination of several statistical parameters of sea waves," *Rept. Port and Harbour Res. Inst.* **24** (4) (1985), pp. 65–102 (*in Japanese*).
55. J. R. Medina, J. Aguilar, and J. J. Diez, "Distortions associated with random sea simulators," *Proc. ASCE* **111** (WW4) (1985), pp. 603–628.
56. T. Takayama and T. Hiraishi, "Reproducibility of directional random waves in laboratory wave simulation," *Rept. Port and Harbour Res. Inst.* **28** (4) (1989), pp. 3–24.
57. Y. Goda, "Irregular wave deformation in surf zone," *Coastal Engineering in Japan* **18** (1975), pp. 13–26.

Part III

Statistical Analysis of
Extreme Waves

Chapter 11

Statistical Analysis of Extreme Waves

11.1 Introduction

11.1.1 *Data for Extreme Wave Analysis*

(A) *Preparation of sample*

The first step in designing a maritime structure is the selection of design waves. In most cases, storm wave heights which would be exceeded once in a given period of years, say 100 years, are chosen on the basis of statistical analysis of extreme events. Needs for the analysis of extremes arise in many branches of sciences and engineering. Flood discharges for floodplain protection, hurricane winds for suspension bridge designs, and storm surge heights for coastal defense works are well-known examples in civil engineering. In this chapter, statistical techniques frequently used in extreme wave analysis are introduced and discussed.

Depending on the method of selecting a set of wave data (which is called a *sample* in statistics), there are three different approaches. One method tries to utilize the whole data of wave heights observed visually or instrumentally during a number of years. The data are analyzed in a form of cumulative distribution to be fitted to some distribution function. Once a best-fitting distribution function is found, the design wave height is estimated by extrapolating the distribution function to the level of probability which corresponds to a given period of years being considered in design process. This method is called the *total sample method*. Some people call it the *initial distribution method* or the *cumulative distribution function method*.

The other two methods use only the maxima of wave heights in time series data. The *annual maxima method* picks up the largest significant wave height in each year, whereas the *peaks-over-threshold method* takes the peak heights of storm waves over a certain threshold value.

The three methods have their own proponents. The choice to make among these methods is somewhat subjective. One important requisite for a statistical sample is *independency*. It means that individual data in a sample must be statistically independent of each other; in other words, the correlation coefficient between successive data should nearly be zero. Another important requisite is *homogeneity*. Individual data in a sample must have a common parent distribution, all belonging to a single group of data, which is called the *population*. Storm waves during the monsoon season and waves during the off-monsoon season would exhibit some difference in their cumulative distributions, and thus they would belong to different populations. A population of waves generated by tropical cyclones would probably be different from that by extratropical cyclones.

The total sample method is not recommended according to the above requisites. Ocean waves have a tendency of being persistent for many hours. The correlation coefficient between wave heights, 24 hours apart, has been found to have a high value of 0.3 to 0.5;[1] thus independency is not satisfied for data sets of the total sample method. Furthermore, the group of small wave heights is likely to constitute a population different from that of the group of large heights. Van Vledder *et al.*[2] reports a case that the total sample method predicts a 100-year wave height 10% larger than that estimated by the peaks-over-threshold method, probably owing to the influence of low wave height data. Thus, no further discussion will be given to the total sample method.

The annual maxima method and peaks-over-threshold method both satisfy the requisite of independency. The annual maxima method is widely used in the analysis of extreme flood discharges and other data of environmental loads. However, existing data bases of storm waves in various countries rarely cover a period of more than 20 years. Such a short record length of extreme wave data brings forth a problem of low reliability in statistical sense; a small sample size induces a wide range of confidence interval. The peaks-over-threshold method (henceforth abbreviated as POT) can have a relatively large number of data in a sample, and thus have a smaller range of confidence interval. Therefore, the discussion hereinafter is mainly focused on POT. Nevertheless, the techniques of extreme data analysis for the annual maxima method are identical with

those of POT, and the following descriptions are also applicable for the use of the annual maxima method.

(B) *Parameters of sample of extreme data*

Two parameters are important in describing the nature of a sample of extreme data. One is the *mean rate* of the extreme events. The mean rate denoted by λ is defined with the number of events N_T during the period of K years as

$$\lambda = \frac{N_T}{K} \,. \tag{11.1}$$

In the annual maxima method, one data is taken from each year so that $\lambda = 1$. In POT, the mean rate may vary from a few to several dozens depending on the threshold value which defines the extreme events. The number of years K need not be an integer but can have a decimal.

Another parameter is related with the process of censoring. When a wave hindcasting project is undertaken for the purpose of collecting samples of extreme wave heights, there is a possibility that medium to minor storms have not been detected on weather maps and waves generated by these storms are dropped from the list of data. Thus, it is often recommended to employ the data of large storm waves only, by omitting the data of low wave heights. This is an example of censoring process. Another example is the treatment of downtime of wave measurement system. If the maximum wave during the downtime is known to be below a certain moderate value by information from some other sources, the period of downtime can be included in the effective duration of measurement period K, provided that other measured data below that value be omitted from the extreme wave analysis. In these examples, the existence of minor data should be taken into account in extreme analysis so as not to distort the shape of distribution function. For this purpose, the following parameter called the *censoring parameter* denoted by ν is introduced:

$$\nu = \frac{N}{N_T} \,, \tag{11.2}$$

where N refers to the number of data taken in the analysis and N_T the total number of storm events which would have occurred during the period of extreme wave analysis; N_T need not be accurate, but its approximate estimate suffices.

11.1.2 *Distribution Functions for Extreme Waves*

In the extreme data analysis, many theoretical distribution functions are employed for fitting to samples. In theoretical statistics, a data of extremes refers to the maximum or minimum among a sample of independent data. When extreme analysis is applied for a sample of such extreme data, it is known that three types of theoretical functions should fit such samples, depending on the population distribution of initial data.[3] However, the data of extreme wave heights collected by POT are different from the extreme data of theoretical statistics. POT data carry no meaning of maxima of samples, but they are initial data defined as the peak heights of storm waves. Therefore, there is no theoretical ground to recommend any distribution function *a priori* to samples collected by POT.

Current consensus among people practicing extreme wave analysis is such as to apply various distribution functions to a sample and to select a best-fitting one as the most probable distribution of the population. The candidate functions often employed in extreme wave analysis are listed in the following, but there are several other distribution functions favored by statisticians. The cumulative distribution is denoted by $F(x)$ and the probability density function by $f(x)$, where x stands for the extreme variate (i.e., wave height).

1) Fisher–Tippett type I (abbreviated as FT-I) or Gumbel distribution:

$$F(x) = \exp\left[-\exp\left(-\frac{x-B}{A}\right)\right] \qquad : \quad -\infty < x < \infty. \qquad (11.3)$$

2) Fisher–Tippett type II (abbreviated as FT-II) or Frechét distribution:

$$F(x) = \exp\left[-\left(1 + \frac{x-B}{kA}\right)^{-k}\right] \qquad : \quad B - kA \le x < \infty. \qquad (11.4)$$

3) Weibull distribution:

$$F(x) = 1 - \exp\left[-\left(\frac{x-B}{A}\right)^{k}\right] \qquad : \quad B \le x < \infty. \qquad (11.5)$$

4) Lognormal distribution:

$$f(x) = \frac{1}{\sqrt{2\pi}Ax}\exp\left[-\frac{(\ln x - B)^2}{2A^2}\right] \qquad : \quad 0 < x < \infty. \qquad (11.6)$$

These functions have two or three parameters. The parameter A is called the *scale parameter* because it governs the linear scale of x. The parameter B is called the *location parameter* because it fixes the location of the axis of x. The parameter k is called the *shape parameter* because it determines the functional shape of distribution. The parameter k has no dimension, but the parameters A and B have the same units with x except for the lognormal distribution. The notations for these parameters are not universal; the readers are advised to check the notations when they refer to various literatures.

The expression for the FT-II distribution has been so chosen that it does converge to the FT-I function at the limit of $k \to \infty$. Figure 11.1 exhibits the probability density of the FT-II distribution with the shape parameter $k = 2.5$, 3.3, 5 and 10 together with that of the FT-I distribution, which is designated with $k = \infty$. The abscissa of Fig. 11.1 is a dimensionless variate of $y = (x - B)/A$, which is called the *reduced variate*. As the value of the shape
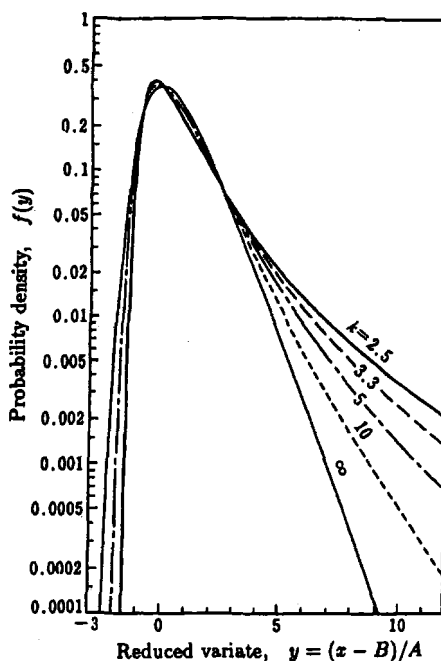
Fig. 11.1. Probability densities of FT-I ($k = \infty$) and FT-II ($k = 2.5$ to 10) distributions.[10]

parameter k decreases, the distribution of FT-II becomes broader with longer tails. A broad distribution predicts a very large 100-year wave height, when compared with a narrow distribution.

Figure 11.2 shows the probability density of the Weibull distribution with the shape parameter $k = 0.75$, 1.0, 1.4 and 2.0. The case with $k = 1$ is the exponential distribution, which is included in the Weibull distribution. With the decrease in the k value, the distribution becomes broader. The lognormal distribution demonstrates behaviors similar to the Weibull distribution with $k = 2$; the two distributions are often fitted to a sample of extreme wave heights with almost the same degree of goodness of fit.[4] Thus, a fitting of lognormal distribution can be replaced to that of the Weibull distribution with $k = 2$, and explanations on the applications of the lognormal distribution for extreme waves data are deleted hereinafter.
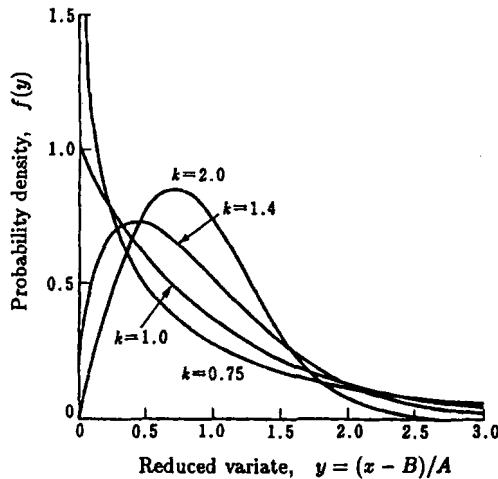
Fig. 11.2. Probability density of Weibull distribution ($k = 0.75$ to 2.0).[4]

The characteristics of the above four distributions are listed in Table 11.1 for their modes, means and standard deviations. When the shape parameter k of the FT-II distribution is less than 2, the distribution becomes too broad and its standard deviation cannot be defined. When the shape parameter k of the Weibull distribution is less than 1, the probability densities diverge as the variate x approaches B and the mode cannot be defined.

Table 11.1. Characteristics of distribution functions for extreme analysis.

Distribution	Mode	Mean	Standard Deviation
FT-II	$B + kA\left[\left(\frac{k}{1+k}\right)^{1/k} - 1\right]$	$B + kA\left[\Gamma\left(1 - \frac{1}{k}\right) - 1\right]$	$kA\left[\Gamma\left(1 - \frac{2}{k}\right) - \Gamma^2\left(1 - \frac{1}{k}\right)\right]^{1/2}$
FT-I	B	$B + A\gamma$	$\frac{\pi}{\sqrt{6}}A$
Weibull	$B + A\left(1 - \frac{1}{k}\right)^{1/k}$	$B + A\Gamma\left(1 + \frac{1}{k}\right)$	$A\left[\Gamma\left(1 + \frac{2}{k}\right) - \Gamma^2\left(1 + \frac{1}{k}\right)\right]^{1/k}$
Lognormal	$\exp(B - A^2)$	$\exp\left(B + \frac{A^2}{2}\right)$	$\exp\left(B + \frac{A^2}{2}\right)(\exp A^2 - 1)^{1/2}$

Note: $\Gamma(\ )$ is the gamma function and γ is Euler's constant $(= 0.5772\ldots)$.

11.1.3 *Return Period and Return Value*

Extreme statistics have the objective of estimating an expected value of extreme event which would occur once in a long period of time. For this purpose, the concepts of *return period* and *return value* are introduced. The return period is defined as the average duration of time during which extreme events exceeding a certain threshold value would occur once. The return value is the threshold value which defines a given return period. A 100-year wave height is a return value which would be exceeded once in every 100 years on the average.

The return period denoted by R is derived from the distribution function as follows. For the sake of simplicity, the case of annual maxima method is discussed first. The distribution function $F(x)$ is assumed to be known. The probability that the extreme variate x does not exceed a given value x_u in one year is $F(x_u)$ by definition. Suppose that the event of $x \geq x_u$ occurred in one year, the variate x did not exceed x_u during the other $n - 1$ years, and it did exceed x_u in the nth year. Because the probability of nonexceedance for $n - 1$ years is given by $F^{n-1}(x_u)$ and that of exceedance in one year is $1 - F(x_u)$, the probability of the above event is expressed as

$$P_n = F^{n-1}(x_u)[1 - F(x_u)]. \qquad (11.7)$$

The above event may occur in the first year of $n = 1$ but may not occur until $n = \infty$. The expected value of n is the return period by definition, and it is calculated as below.

$$R = E[n] = \sum_{n=1}^{\infty} nP_n = [1 - F(x_u)]\sum_{n=1}^{\infty} nF^{n-1}(x_u) = \frac{1}{1 - F(x_u)}. \qquad (11.8)$$

The return value corresponding to the return period R is denoted by x_R. It is obtained with the inverse function of the cumulative distribution as

$$x_R = F^{-1}\left(1 - \frac{1}{R}\right) .$$ (11.9)

In the case of POT with the mean rate λ, each year is divided into time segments of $1/\lambda$ year by assuming that each time segment has the same probability of extreme events (seasonal variation of events is neglected). Then, the return period and the return value can be given by the following formulas:

$$R = \frac{1}{\lambda[1 - F(x_u)]} ,$$ (11.10)

$$x_R = F^{-1}\left(1 - \frac{1}{\lambda R}\right) .$$ (11.11)

11.2 Estimation of Best-Fitting Distribution Function

11.2.1 *Selection of Fitting Method*

There are several methods of fitting a theoretical distribution function to a sample of extreme data and estimating the parameter values. They are

   (i) graphical fitting method,
  (ii) least squares method,
 (iii) method of moments,
 (iv) maximum likelihood method,
  (v) others.

The graphical fitting method and the least squares method require a rearrangement of data in a given sample in the descending order by placing the largest data at the position of number one. The rearranged data are given the probability of nonexceedance according to their order number m and the sample size N (number of data in a sample). In the graphical fitting method, a special probability paper is devised in such a way that a particular distribution would be represented as a straight line on that paper. The extreme data are plotted on the probability paper of chosen distribution, and a straight line which best fits to the data is drawn by visual judgment. The least squares method eliminates the process of visual judgment and can make objective comparison of the goodness of fit. The assignment of respective probabilities

of nonexceedance to individual data is made with the so-called *plotting position formula* to be discussed later.

The method of moments calculates the mean and standard deviation of the sample and equates the results to the characteristics of distribution listed in Table 11.1. The parameters A and B of the FT-I and lognormal distributions can be estimated through this process. The FT-II and Weibull distributions require the information of the skewness of sample so as to estimate the shape parameter k and two other parameters. The method of moments and the graphical fitting method were the favorite ones in old days as described in the classical book by Gumbel[3]; in those days, computing capacity of analysts was quite limited and the least squares method could not be carried out for a large sample. The method of moments has a demerit of having a negative bias in the estimate of scale parameter A, unless a proper adjustment of sample size is made. It is because the standard deviation gradually decreases from the value listed in Table 11.1 as the sample size decreases; this will be discussed in Sec. 11.3.1. The method of moments also does not have a theoretical or empirical formula for estimating confidence interval of return value except for the FT-I distribution (see Sec. 11.3.3(C)); a numerical simulation by using the parameters obtained is required for estimation of confidence interval.

The maximum likelihood method is an iterative numerical scheme to find the parameter values which maximize the likelihood function defined as

$$L(x_1, \ldots, x_N; A, B, k) = \prod_{m=1}^{N} f(x_m; A, B, k), \qquad (11.12)$$

where $x_1, \ldots, x_N$ represent the data values and f is the probability density function. The maximum likelihood method is favored by statisticians in recent years, because its characteristics can be examined mathematically. However the theory is not easy to understand and the algorithm of numerical scheme is rather complicated.

A sample of extreme variates always has a statistical variability as will be discussed in Sec. 11.3.1. This sample variability causes a certain amount of deviation of the return value estimated on a sample from the population value. In consideration of such deviations, two criteria are employed in selection of the fitting method in the statistics of extremes. One is *unbiasedness* and the other is *efficiency*. The former refers to the condition that the return value should have no bias from the corresponding value of the population. Bias is evaluated

not for individual samples but for the ensemble of samples. The amount of bias is calculated by means of the Monte Carlo simulation technique when no theoretical evaluation is possible. Efficiency refers to the degree of deviation of estimated return values from the population. The smaller the deviation is, the larger the efficiency of a fitting method is.

According to the above two criteria, the method of moments cannot satisfy the unbiasedness. Its efficiency is said to be inferior to the maximum likelihood method and the least squares method. The maximum likelihood method tends to have a small amount of negative bias, but its efficiency seems to be the largest as exemplified in a comparative study with numerically simulated extreme data.[5] In this chapter, however, the least squares method for extreme analysis is discussed in detail because of its simplicity in algorithm and applications. The least squares method has often been accused of yielding a positive bias in the return value. However, it was caused by the use of inappropriate plotting position formula. With the use of plotting position formulas presented in the following, it has been verified that the least squares method satisfies the condition of unbiasedness.[4,6]

11.2.2 *Plotting Position Formulas*

A sample of data arranged in the ascending or descending order belongs to the category of *ordered statistics*. As the present chapter is concerned with the statistics of extremely large wave heights, the descending order is taken and the order number is expressed with m. The variate and its nonexceedance probability of the mth order are denoted with the subscript (m). The formula which assigns the probability to the ordered variate is the plotting position formula.

The best-known plotting position formula is the Weibull formula of the following:

$$\hat{F}_{(m)} = 1 - \frac{m}{N+1}. \tag{11.13}$$

Equation (11.13) is derived as the expected probability of the mth ordered variate in the population; i.e., $E[F(x_{(m)})]$. Gumbel (Ref. 11.3, Sec 1.2.7) advocated the use of this formula based on somewhat intuitive arguments. But the Weibull plotting position formula always produces a positive bias in the return value, amounting to several percent when the sample size is less than a few dozens.[4,6]

The unbiased plotting position formula varies depending on the distribution function applied. According to a numerical simulation study, the Gringorten formula[7] yields almost no bias when applied to the FT-I distribution. For the normal distribution, the Blom formula[8] brings forth little bias. For the Weibull distribution, Petruaskas and Aagaard[9] derived a formula in such a way that it gives the probability corresponding to the expected value of the mth ordered variate; i.e., $F\{E[x_{(m)}]\}$. When examined in a numerical simulation study, however, their formula has produced a small amount of negative bias. Then Goda[4,6] proposed a modified version of the Petruaskas and Aagaard formula. For the FT-II distribution, Goda and Onozawa[10] proposed an empirical formula based on another numerical simulation study. The latter two proposals are both based on the Monte Carlo simulations for the sample size ranging from 10 to 200, each size with 10,000 samples.

The unbiased plotting position formula can be expressed in the following general form:

$$\hat{F}_{(m)} = 1 - \frac{m - \alpha}{N_T + \beta}, \quad m = 1, 2, \ldots, N. \tag{11.14}$$

The values of constants α and β are given in Table 11.2. The above formula uses the total number N_T instead of the sample size N so that the formula can be applied for both censored and uncensored samples.

Table 11.2. Constants of unbiased plotting position formula.

Distribution	α	β	Authors
FT-II	$0.44 + 0.52/k$	$0.12 - 0.11/k$	Goda and Onozawa[10]
FT-I	0.44	0.12	Gringorten[7]
Weibull	$0.20 + 0.27/\sqrt{k}$	$0.20 + 0.23/\sqrt{k}$	Goda[4,6]
Normal	0.375	0.25	Blom[8]
Lognormal	0.375	0.25	Blom[8]

11.2.3 *Parameter Estimation by the Least Squares Method*

The first step in the parameter estimation is the selection of candidate distribution functions. As discussed in Sec. 11.1.2, the FT-I, FT-II and Weibull distributions are considered in this chapter as the candidates of the distribution of a population of extreme waves; the population distribution is called

the *parent distribution*. The scale, location, and shape parameters of these candidate functions are estimated for a given sample, and the goodness of fit to each function is compared for selection of the best-fitting distribution.

The least squares method can yield the best estimate of two parameters in a single operation. As the FT-I distribution has two parameters of A and B, it can be analyzed by the least squares method directly. The FT-II and Weibull distributions have three parameters however, and thus they have to be modified into a form of two parameter functions. In this chapter, the shape parameter k is fixed at one of the following values for these distributions:

$$\left.\begin{array}{l} \text{FT-II distribution} \quad : k = 2.5,\ 3.33,\ 5.0 \text{ and } 10.0, \\[4pt] \text{Weibull distribution} : k = 0.75,\ 1.0,\ 1.4 \text{ and } 2.0. \end{array}\right\} \qquad (11.15)$$

Once the shape parameter is fixed, each distribution becomes an independent candidate function and is competed with other functions for best fitting. Thus, a proposal is hereby made to employ nine cumulative distributions (one FT-I, four FT-II's, and four Weibull's) as the candidate distributions.

The main reason for fixing the shape parameter is the difficulty in predicting the true parent distribution from a sample of small size, say a few dozen to one hundred. Goda[4,6] has demonstrated this difficulty by a Monte Carlo simulation study. The statistical variability of these distributions and confidence intervals of parameter estimates and return values have also been analyzed for the above nine distributions, and the results are presented in a form of tables and empirical formulas.

The second step in the parameter estimation is the preparation of the order statistics $x_{(m)}$ of extreme data in the descending order and the assignment of the nonexceedance probability $\hat{F}_{(m)}$ by Eq. (11.14). Then the reduced variate $y_{(m)}$ for the mth ordered data is calculated by the following equation:

$$\left.\begin{array}{l} \text{FT-I distribution} \quad : y_{(m)} = -\ln[-\ln \hat{F}_{(m)}]\,, \\[6pt] \text{FT-II distribution} \quad : y_{(m)} = k[(-\ln \hat{F}_{(m)})^{-1/k} - 1]\,, \\[6pt] \text{Weibull distribution} : y_{(m)} = [-\ln(1 - \hat{F}_{(m)})]^{1/k}\,. \end{array}\right\} \qquad (11.16)$$

The third step is the application of the least squares method for the parameters $\hat{A}$ and $\hat{B}$ in the following equation:

$$x_{(m)} = \hat{B} + \hat{A} y_{(m)}\,. \qquad (11.17)$$

The correlation coefficient r between $x_{(m)}$ and $y_{(m)}$ must be estimated together with $\hat{A}$ and $\hat{B}$. Any numerical algorithm for the least squares method suffices for solving Eq. (11.17). However, attention is called for the expression of Eq. (11.17) which is different from the conventional form of $y = a + bx$.

As an explanatory example, the Kodiak data of hindcasted storm waves[2] is analyzed below. Wave hindcasting was carried out by the Coastal Engineering Research Center of the US Army[11] for the North-Eastern Pacific Ocean. The data was retrieved from a grid point off Alaska, located at 57°50'N and 148°78'W. The data set consists of all peak storm waves with the significant height exceeding 6 m, which were generated by 78 storms during a period of 20 years. Table 11.3 lists the Kodiak data set in chronological sequences. As the exact number of storm events in this period was not scrutinized, the data set is treated here as an uncensored sample. The Kodiak data is one of the two extreme wave data sets which were jointly analyzed by a working group on extreme statistics of the Section of Maritime Hydraulics of the International Association of Hydraulic Research (IAHR), as reported by van Vledder *et al.*[2]

Table 11.3. Peak significant wave heights of Kodiak data set
($K = 20$ years, $N = N_T = 78$, $\lambda = 3.9$, $\nu = 1$).

Year	H_s (m)	Year	H_s (m)
1956	6.2	1966	7.3, 8.6, 7.4
1957	–	1967	7.1, 6.0, 6.3, 6.0, 6.7
1958	8.8, 6.6, 6.9, 7.8, 6.3	1968	6.6, 6.5, 6.9, 7.7, 8.2, 6.7, 7.4
1959	11.7, 7.2, 7.4	1969	6.4, 6.1, 7.1, 6.5, 8.5, 8.8, 9.1
1960	9.9, 8.9, 7.5, 7.0, 6.7	1970	8.0, 6.3, 9.1
1961	9.2, 6.2, 6.3	1971	6.6
1962	8.1, 6.3, 7.2, 6.3, 6.0	1972	6.7, 7.2, 10.2, 7.0, 10.1
1963	8.4, 6.8, 9.3, 6.7, 6.5, 7.2, 8.5	1973	7.8, 6.1, 6.3, 8.6, 7.1, 10.0
1964	6.9. 6.6, 9.4, 8.2	1974	8.0, 6.1, 8.4
1965	6.3, 7.6	1975	7.4, 8.2, 8.1

The Kodiak data set is rearranged in the descending order according to the magnitude of significant wave height, the nonexceeding probability is assigned, and the reduced variate is calculated for several candidate distributions. Then the least squares method is applied. Table 11.4 lists a part of the results of calculation. Graphical representation of the Kodiak data will be given in Sec. 11.3.3.

Table 11.4. Results of Kodiak data analysis by the least squares method
(sample size: $N = 78$, mean: $\bar{x} = 7.501$ m, standard deviation: $\sigma_x = 1.214$ m).

m	$x_{(m)}$	FT-II ($k = 10$)		FT-I		Weibull ($k = 1.4$)		Weibull ($k = 2.0$)	
		$\hat{F}_{(m)}$	$y_{(m)}$	$\hat{F}_{(m)}$	$y_{(m)}$	$\hat{F}_{(m)}$	$y_{(m)}$	$\hat{F}_{(m)}$	$y_{(m)}$
1	11.7	0.9935	6.540	0.9928	4.934	0.9927	3.121	0.9922	2.204
2	10.2	0.9807	4.825	0.9800	3.903	0.9800	2.648	0.9795	1.971
3	10.1	0.9679	4.081	0.9672	3.402	0.9672	2.405	0.9667	1.845
4	10.0	0.9551	3.607	0.9544	3.065	0.9544	2.238	0.9539	1.754
5	9.9	0.9423	3.261	0.9416	2.811	0.9417	2.109	0.9412	1.683
6	9.4	0.9295	2.990	0.9288	2.606	0.9289	2.003	0.9284	1.624
⋮	⋮	⋮	⋮	⋮	⋮	⋮	⋮	⋮	⋮
⋮	⋮	⋮	⋮	⋮	⋮	⋮	⋮	⋮	⋮
74	6.1	0.0589	−0.989	0.0584	−1.044	0.0615	0.140	0.007	0.250
75	6.1	0.0461	−1.063	0.0456	−1.128	0.0488	0.118	0.0479	0.222
76	6.0	0.0333	−1.152	0.0328	−1.229	0.0360	0.094	0.0351	0.189
77	6.0	0.0205	−1.270	0.0200	−1.364	0.0233	0.069	0.0224	0.150
78	6.0	0.0077	−1.464	0.0072	−1.597	0.0105	0.039	0.0096	0.098
Parameters		$\hat{A} = 0.8292$ m		$\hat{A} = 0.9567$ m		$\hat{A} = 1.8621$ m		$\hat{A} = 2.6228$ m	
		$\hat{B} = 6.937$ m		$\hat{B} = 6.955$ m		$\hat{B} = 5.805$ m		$\hat{B} = 5.178$ m	
Correlation		$r = 0.98738$		$r = 0.99191$		$r = 0.99629$		$r = 0.98906$	

11.2.4 *Selection of Most Probable Parent Distribution*

(A) *Goodness of fit tests*

As mentioned earlier, the candidate distribution which best fits to the sample is selected as the most probable parent distribution. Nevertheless this does not exclude use of a single candidate distribution based on one's postulation about the parent distribution of storm wave heights. As the data base of extreme waves by observations and hindcasting is expanded, there will be many cases of reliable extreme wave analyses. Then it could be possible in the future to establish some parent distribution of extreme wave heights, which would vary from coast to coast.

Goodness of fit is measured by several tests. The Kolmogorov–Smirnov test, the Anderson–Darling test and the chi-square test are often used for this

purpose. When the parameter estimate is done by the least squares method, however, the degree of goodness of fit is simply represented with the value of correlation coefficient between the ordered data $x_{(m)}$ and its reduced variate $y_{(m)}$; the nearer the coefficient is toward 1, the better the fitting is. The Kodiak data set has been fitted to nine distributions including the four distributions listed in Table 11.4. Among the candidate functions, the Weibull distribution with $k = 1.4$ yields the correlation coefficient closest to 1, and is judged as the best-fitting one.

The degree of correlation coefficient being near to 1 depends on a candidate distribution. Samples from a distribution with a narrow range of spreading such as the Weibull with $k = 2$ tend to yield the correlation coefficient much closer to 1 compared with samples from a distribution with a broad spreading. To examine the statistical characteristics of correlation coefficient, its residue from 1 is defined here as $\Delta r = 1 - r$. The residue is a statistical variate, the value of which varies from sample to sample. Goda and Kobune[6] reported the results of another Monte Carlo simulation study on extreme statistics. Figure 11.3 shows the mean value of the residue of correlation coefficient of samples for several distributions. Simulation was done with 10,000 samples for each sample size ranging from 10 to 400 for respective distributions. As seen in Fig. 11.3, Δr_{mean} of the Weibull distribution with $k = 0.75$ is larger than
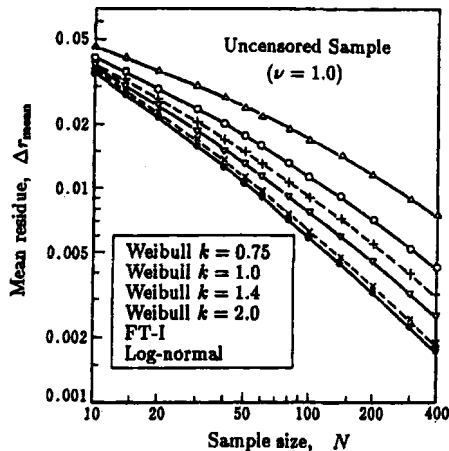
Fig. 11.3. Mean residue Δr_{mean} of various distributions.[6]
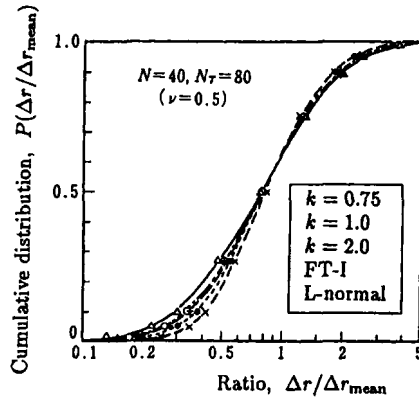
Fig. 11.4. Examples of cumulative distributions of the ratio $\Delta r/\Delta r_{\text{mean}}$.[6]

that with $k = 2$ at any sample size. Thus, a test of goodness of fit by means of the absolute value of correlation coefficient tends to yield unfavorable results against a broad distribution.

A remedy for the above bias is to use the ratio of the residue of a sample to the mean residue of a fitted distribution. Figure 11.4 shows examples of the cumulative distributions of the ratio $\Delta r/\Delta r_{\text{mean}}$; the sample size is $N = 40$ and the data are censored ones with the censoring parameter $\nu = 0.5$. When the residue of correlation coefficient is normalized with its mean value, differences between various distributions are greatly reduced and a fair comparison of goodness of fit becomes possible. Goda and Kobune[6] proposed to use the MIR (MInimum Ratio of residual correlation coefficient) criterion for judgment of best fitting; a distribution with the smallest ratio is a best fitting one. They derived an empirical formula for estimating the mean residue Δr_{mean} for a given distribution, sample size and censoring parameter from the data of simulation study. The formula is given as

$$\Delta r_{\text{mean}} = \exp[a + b \ln N + c (\ln N)^2].   \tag{11.18}$$

The coefficients a, b and c are formulated for various distributions as listed in Table 11.5. Relative error of Eq. (11.18) in predicting the mean residue value is less than $\pm 3\%$.

Table 11.5. Empirical coefficients for Δr_{mean} in the MIR criterion.

Distribution	a	b	c
FT-II $(k = 2.5)$	$-2.470 + 0.015\nu^{3/2}$	$-0.1530 - 0.0052\nu^{5/2}$	0
FT-II $(k = 3.33)$	$-2.462 - 0.009\nu^2$	$-0.1933 - 0.0037\nu^{5/2}$	-0.007
FT-II $(k = 5.0)$	-2.463	$-0.2110 - 0.0131\nu^{5/2}$	-0.019
FT-II $(k = 10.0)$	$-2.437 + 0.028\nu^{5/2}$	$-0.2280 - 0.0300\nu^{5/2}$	-0.033
FT-I	$-2.364 + 0.54\nu^{5/2}$	$-0.2665 - 0.0457\nu^{5/2}$	-0.044
Weibull $(k = 0.75)$	$-2.435 - 0.168\nu^{1/2}$	$-0.2083 + 0.1074\nu^{1/2}$	-0.047
Weibull $(k = 1.0)$	-2.355	-0.2612	-0.043
Weibull $(k = 1.4)$	$-2.277 + 0.056\nu^{1/2}$	$-0.3169 - 0.0499\nu$	-0.044
Weibull $(k = 2.0)$	$-2.160 + 0.113\nu$	$-0.3788 - 0.0979\nu$	-0.041
Log-normal	$-2.153 + 0.059\nu^2$	$-0.2627 - 0.1716\nu^{1/4}$	-0.045

For the case of the Kodiak data set with $N = 78$ and $\nu = 1$, Δr_{mean} and $\Delta r / \Delta r_{mean}$ are calculated for the four distributions of Table 11.4 as follows:

FT-II $(k = 10)$: $\Delta r_{mean} = 0.01562$, $\Delta r / \Delta r_{mean} = 0.808$,

FT-I : $\Delta r_{mean} = 0.01105$, $\Delta r / \Delta r_{mean} = 0.732$,

Weibull $(k = 1.4)$: $\Delta r_{mean} = 0.00952$, $\Delta r / \Delta r_{mean} = 0.390$,

Weibull $(k = 2.0)$: $\Delta r_{mean} = 0.00743$, $\Delta r / \Delta r_{mean} = 1.472$.

Thus, the Weibull distribution with $k = 1.4$ also satisfies the MIR criterion for best fitting.

The criteria of the largest correlation coefficient and the MIR both give the same judgment of best fitting for the Kodiak data set. However, use of the MIR criterion for the situation where the true parent distribution is unknown requires some caution. In a joint study by several hydraulic institutions on extreme wave statistics,[5] 500 samples of numerically simulated data from the population of the Weibull distribution with $k = 1.4$ were analyzed by various methods. With the least squares method, use of a simple criterion of the largest correlation coefficient produced slightly better results in predicting return values than that of the MIR criterion; further examination by numerical simulation is needed.

(B) *Outlier detection by the DOL criterion*

A sample of extreme data sometimes contains a data which exhibits the value much larger than the rest of data. When the sample is tried to fit to a candidate distribution, the particular data would be plotted at a position far above the line of a fitted distribution curve. Such a data is called an *outlier*. In other cases, the largest data $x_{(1)}$ might be only slightly greater than the second largest data $x_{(2)}$. The data $x_{(1)}$ would then be plotted far below the fitted distribution curve. It is also an outlier.

Detection of an outlier can be made with the DOL (Deviation of OutLier) criterion proposed by Goda and Kobune[6] and/or a statistical test by Barnett and Lewis (Ref. 12, pp. 144–150). The DOL criterion uses the following dimensionless deviation ξ:

$$\xi = \frac{x_{(1)} - \bar{x}}{s}, \qquad (11.19)$$

where $\bar{x}$ is the mean of a sample and s is the standard deviation of a sample defined as $s^2 = \sum_{i=1}^{N}(x_i - \bar{x})^2/N$. For the Kodiak data set, $x_{(1)} = 11.7$ m, $\bar{x} = 7.501$ m, $s = 1.206$ m, and thus $\xi =$ is 3.48.

In the statistical test of the normality of a sample, Thompson's test is used by comparing its mean value with the overall mean of a large number of samples. This test can be modified to yield the theoretical value of ξ having the nonexceedance probability P as below.

$$\xi_P = \left[\frac{(N-1)\,F(1, N-2:\alpha)}{N-2+F(1, N-2:\alpha)}\right]^{1/2}, \qquad (11.20)$$

where N is the sample size and $F(1, N-2 : \alpha)$ denotes the F distribution with the $(1, N-2)$ degrees of freedom at the exceedance probability α. For the largest data $x_{(1)}$, the probability α is given as $2(1 - P^{1/N})$.

The cumulative distribution of ξ has been calculated by Eq. (11.20) and compared with the simulation data sampled from a population of the normal distribution.[6] As shown in Fig. 11.5, the ξ value by simulation agrees with the theory except for the range of low probability. The agreement supports the validity of ξ as a statistical variate. Then the ξ value can be used to judge whether the largest data $x_{(1)}$ of a sample is an outlier or not.

For example, if the ξ value of a sample exceeds the population value $\xi_{95\%}$ corresponding to the exceedance probability of 0.95, the largest data $x_{(1)}$ is judged as an outlier at the level of significance of 0.05. If the ξ value of a sample
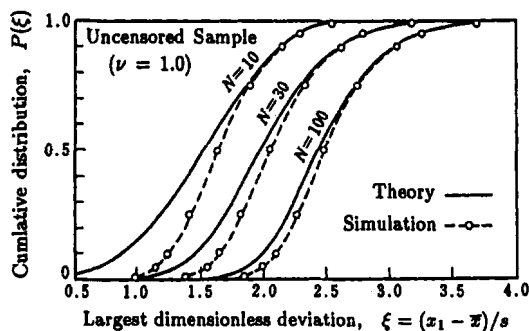
Fig. 11.5. Cumulative distribution of dimensionless deviation of the largest data ξ for samples from the normal distribution.[6]

is below the population value $\xi_{5\%}$ corresponding to the exceedance probability of 0.05, $x_{(1)}$ is also judged as an outlier at the level of significance of 0.05. The threshold value $\xi_{95\%}$ of the population is called the upper DOL, and the threshold value $\xi_{5\%}$ is called the lower DOL. The upper and lower DOLs of various distributions have been estimated with the simulation data of 10,000 samples for respective conditions, by reading the cumulative distribution curves of simulation data such as those shown in Fig. 11.5 as the function of the sample size N and the censoring parameter ν. The measured ξ values have been approximated by the following empirical formula:

$$\xi_{95\%} \text{ and } \xi_{5\%} = a + b \ln N + c \, (\ln N)^2 \, . \tag{11.21}$$

The empirical coefficients a, b and c have been formulated as listed in Tables 11.6 and 11.7. Relative error of Eq. (11.21) in predicting $\xi_{95\%}$ and $\xi_{5\%}$ is less than $\pm 2\%$.

The DOL criterion for outlier detection is applicable for any sample, and it is independent of distribution fitting methods being employed. It simply determines whether the largest data of a sample is an outlier of a distribution function fitted to a sample or not. In the case of the Kodiak data set, the largest data of 11.7 m is not an outlier for nine distributions discussed in this chapter. When the largest data of a sample is judged as an outlier, a quality check of the data should be made first. If no error is found in the data acquisition process, then the data should not be removed from a sample but the distribution fitted to the sample should be eliminated from the candidate distributions instead.

Table 11.6. Empirical coefficients for the upper DOL criterion $\zeta_{95\%}$.

Distribution	a	b	c
FT-II ($k = 2.5$)	$4.653 - 1.076\nu^{1/2}$	$-2.047 + 0.307\nu^{1/2}$	0.635
FT-II ($k = 3.33$)	$3.217 - 1.216\nu^{1/4}$	$-0.903 + 0.294\nu^{1/4}$	0.427
FT-II ($k = 5.0$)	$0.599 - 0.038\nu^2$	$0.518 - 0.045\nu^2$	0.210
FT-II ($k = 10.0$)	$-0.371 + 0.171\nu^2$	$1.283 - 0.133\nu^2$	0.045
FT-I	$-0.579 + 0.468\nu$	$1.496 - 0.227\nu^2$	-0.038
Weibull ($k = 0.75$)	$-0.256 - 0.632\nu^2$	$1.269 + 0.254\nu^2$	0.037
Weibull ($k = 1.0$)	-0.682	1.600	-0.045
Weibull ($k = 1.4$)	$-0.548 + 0.452\nu^{1/2}$	$1.521 - 0.184\nu$	-0.065
Weibull ($k = 2.0$)	$-0.322 + 0.641\nu^{1/2}$	$1.414 - 0.326\nu$	-0.069
Log-normal	$0.178 + 0.740\nu$	$1.148 - 0.480\nu^{3/2}$	-0.035

Table 11.7. Empirical coefficients for the lower DOL criterion $\xi_{5\%}$.

Distribution	a	b	c
FT-II ($k = 2.5$)	$1.481 - 0.126\nu^{1/4}$	$-0.331 - 0.031\nu^2$	0.192
FT-II ($k = 3.33$)	1.025	$-0.077 - 0.050\nu^2$	0.143
FT-II ($k = 5.0$)	$0.700 + 0.060\nu^2$	$0.139 - 0.076\nu^2$	0.100
FT-II ($k = 10.0$)	$0.424 + 0.088\nu^2$	$0.329 - 0.094\nu^2$	0.061
FT-I	$0.257 + 0.133\nu^2$	$0.452 - 0.118\nu^2$	0.032
Weibull ($k = 0.75$)	$0.534 - 0.162\nu$	$0.277 + 0.095\nu$	0.065
Weibull ($k = 1.0$)	0.308	0.423	0.037
Weibull ($k = 1.4$)	$0.192 + 0.126\nu^{3/2}$	$0.501 - 0.081\nu^{3/2}$	0.018
Weibull ($k = 2.0$)	$0.050 + 0.182\nu^{3/2}$	$0.592 - 0.139\nu^{3/2}$	0
Log-normal	$0.042 + 0.270\nu$	$0.581 - 0.217\nu^{3/2}$	0

(C) *Rejection of candidate distribution by the REC criterion*

Presence of an outlier suggests that a particular distribution is better eliminated from the candidates of parent distributions. When the distribution fitting is made with the least squares method, the value of the correlation coefficient r between the ordered variate $x_{(m)}$ and the reduced variate $y_{(m)}$ can provide another test for rejection of candidate distributions. For this purpose, the residue of correlation coefficient from 1; i.e., $\Delta r = 1 - r$, is employed.
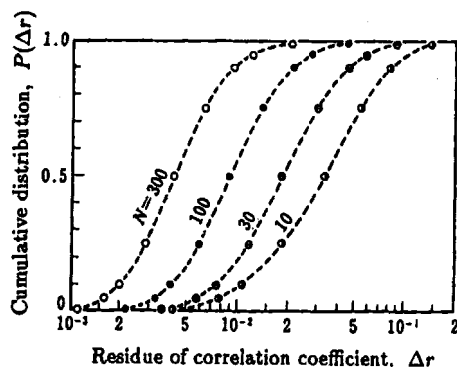
Fig. 11.6. Cumulative distribution of the residue of correlation coefficient Δr for uncensored samples from the Weibull distributions with $k = 1.0$.[6]

Figure 11.6 shows the cumulative distribution curves of Δr for the Weibull distribution with $k = 1$ for the sample size of 10 to 300, which were prepared from simulation data of 10,000 samples for respective conditions.[6] By assuming these cumulative distributions of simulated data being almost the same as those of the population, a criterion for the rejection of candidate function which is called the REC (REsidue of Correlation coefficient) has been prepared. The exceedance probability of 0.95 was set for establishing the threshold value of Δr at the level of significance of 0.05. The threshold value $\Delta r_{95\%}$ has been obtained from the simulation data and formulated in the following empirical expression of Eq. (11.22) with the coefficients listed in Table 11.8.[6] Relative error in predicting the threshold value $\Delta r_{95\%}$ is mostly less than $\pm 3\%$.

$$\Delta r_{95\%} = \exp[a + b \ln N + c (\ln N)^2]. \tag{11.22}$$

In the case of the Kodiak data, all the nine candidate distribution functions yield the residual correlation coefficient Δr below the threshold value $\Delta r_{95\%}$, and thus they are not rejected from the candidates of the parent distribution.

11.3 Estimation of Return Value and Its Confidence Interval

11.3.1 *Statistical Variability of Samples of Extreme Distributions*

In the ocean environment, we sometimes encounter the event of extremely large storm waves having the return period far exceeding the design condition. It could have been generated by a truly abnormal meteorological condition, but

Table 11.8. Empirical Coefficients for $\Delta r_{95\%}$ in the REC criterion.

Distribution	a	b	c
FT-II ($k = 2.5$)	$-1.122 - 0.037\nu$	$-0.3298 + 0.0105\nu^{1/4}$	0.016
FT-II ($k = 3.33$)	$-1.306 - 0.105\nu^{3/2}$	$-0.3001 + 0.0404\nu^{1/2}$	0
FT-II ($k = 5.0$)	$-1.463 - 0.107\nu^{3/2}$	$-0.2716 + 0.0517\nu^{1/4}$	-0.018
FT-II ($k = 10.0$)	$-1.490 - 0.073\nu$	$-0.2299 - 0.0099\nu^{5/2}$	-0.034
FT-I	-1.444	$-0.2733 - 0.0414\nu^{5/2}$	-0.045
Weibull ($k = 0.75$)	$-1.473 - 0.049\nu^2$	$-0.2181 + 0.0505\nu$	-0.041
Weibull ($k = 1.0$)	-1.433	-0.2679	-0.044
Weibull ($k = 1.4$)	-1.312	$-0.3356 - 0.0449\nu$	-0.045
Weibull ($k = 2.0$)	$-1.188 + 0.073\nu^{1/2}$	$-0.4401 - 0.0846\nu^{3/2}$	-0.039
Log-normal	$-1.362 + 0.360\nu^{1/2}$	$-0.3439 - 0.2185\nu^{1/2}$	-0.035

it often results from the situation such that the extreme distribution of storm waves estimated from the previous data set was inappropriate because the sample size was not large enough. This is the problem of statistical variability of samples of extreme statistics.

Figure 11.7 provides an example of variation of samples drawn from an extreme distribution.[5] One hundred samples with the size 100 are numerically simulated from the population of the Weibull distribution with $k = 1.4$, which has the 1-year wave height of 8 m and the 100-year wave height of 13 m at the mean rate $\lambda = 5$; the sample size 100 is equivalent to the period of $K = 20$ years
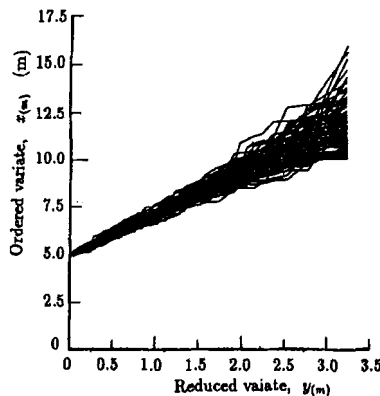
Fig. 11.7. Plot of 100 samples of simulated storm wave height data.[5]
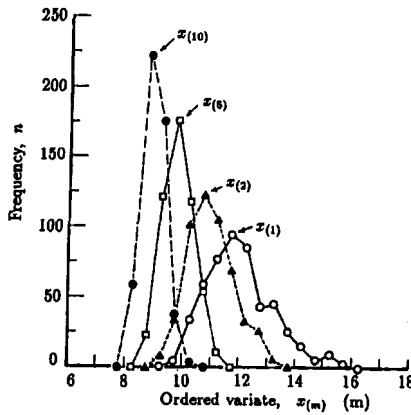
Fig. 11.8. Histograms of the first, second, fifth and tenth largest data of 500 samples.[5]

in duration. As each line in Fig. 11.7 represents the plot of $x_{(m)}$ versus $y_{(m)}$ of one sample, the spread of lines indicate the extent of sample variability. Figure 11.8 shows the histograms of the first, second, fifth and tenth largest wave heights of 500 samples drawn from the same distribution. The largest wave height in 20 years varies from 9 to 16 m, even though the 100-year wave height of the population is 13 m. The data set was another subject of joint examination by the working group of the Section of Maritime Hydraulics of IAHR.

The extent of sample variability can be examined through the analysis of the standard deviation of a sample. Although the unbiased variance of a sample defined as $\sigma_x^2 = \sum_{i=1}^{N}(x_i - \bar{x})^2/(N-1)$ has the expected value equal to the population variance, the expected value of σ_x itself is smaller than the population standard deviation as listed in Table 11.9. The difference increases as the sample size decreases. Thus, the terminology of *unbiased standard deviation* should be used with some caution.

Analysis of the statistical characteristics of sample (unbiased) standard deviation has been made for various extreme distribution functions by the author (Ref. 4 and an unpublished source) through a Monte Carlo simulation technique. Table 11.9 lists the mean and the coefficient of variation of the unbiased standard deviation of a sample of extreme distributions. The data is based on the analysis of 20,000 simulated samples for each case, and the results have been slightly modified so that a smooth variation with respect to the sample size N would be realized.

Table 11.9. Mean and coefficient of variation of the sample standard deviation.

Size	FT-II				FT-I
N	$k = 2.5$	$k = 3.33$	$k = 5.0$	$k = 10.0$	
10	0.632 (1.25)	0.798 (0.79)	0.882 (0.55)	0.928 (0.41)	0.951 (0.32)
14	0.665 (1.12)	0.829 (0.71)	0.906 (0.49)	0.946 (0.36)	0.965 (0.27)
20	0.690 (0.99)	0.851 (0.63)	0.923 (0.42)	0.958 (0.31)	0.975 (0.23)
30	0.714 (0.87)	0.873 (0.54)	0.940 (0.36)	0.969 (0.25)	0.984 (0.19)
40	0.732 (0.80)	0.886 (0.49)	0.949 (0.32)	0.975 (0.22)	0.988 (0.16)
60	0.763 (0.74)	0.905 (0.44)	0.963 (0.28)	0.983 (0.18)	0.992 (0.13)
100	0.793 (0.66)	0.929 (0.38)	0.974 (0.23)	0.989 (0.15)	0.995 (0.10)
140	0.810 (0.61)	0.941 (0.35)	0.981 (0.20)	0.992 (0.13)	0.996 (0.09)
200	0.827 (0.56)	0.951 (0.32)	0.987 (0.18)	0.994 (0.11)	0.998 (0.07)

Size	Weibull				Normal
N	$k = 0.75$	$k = 1.00$	$k = 1.4$	$k = 2.0$	
10	0.870 (0.56)	0.925 (0.42)	0.954 (0.31)	0.971 (0.25)	0.975 (0.24)
14	0.898 (0.49)	0.941 (0.36)	0.967 (0.26)	0.980 (0.20)	0.982 (0.20)
20	0.923 (0.42)	0.958 (0.30)	0.977 (0.22)	0.986 (0.17)	0.987 (0.17)
30	0.944 (0.35)	0.971 (0.25)	0.985 (0.18)	0.991 (0.14)	0.992 (0.14)
40	0.957 (0.31)	0.978 (0.22)	0.989 (0.15)	0.993 (0.12)	0.994 (0.12)
60	0.970 (0.25)	0.984 (0.18)	0.992 (0.13)	0.995 (0.10)	0.996 (0.09)
100	0.980 (0.20)	0.990 (0.14)	0.995 (0.10)	0.997 (0.08)	0.998 (0.07)
140	0.985 (0.18)	0.993 (0.12)	0.996 (0.08)	0.998 (0.06)	0.998 (0.06)
200	0.989 (0.15)	0.995 (0.10)	0.997 (0.07)	0.999 (0.06)	0.999 (0.05)

Note: The figures outside the parentheses denote the ratio of the mean of the sample standard deviation to the population value, and the figures inside the parentheses are the coefficient of variation.

Decrease of the sample standard deviation from the population value causes a consistent underestimation of the scale parameter A when the method of moments is employed. Gumbel (Ref. 3, Sec. 6.2.3) lists a table of the sample standard deviation for various sample sizes for the FT-I distribution, but the table gives the values smaller than those listed in Table 11.9. As the data source of Gumbel's table is unknown, it is safe to refer to Table 11.9 when necessary.

11.3.2 *Confidence Interval of Parameter Estimates*

Scatter of samples around the population such as those shown in Fig. 11.7 suggests a certain scatter of the parameter values fitted to each sample. Thus, the estimates of the parameters of extreme distributions constitute statistical variates having their own distributions. It is important to examine the confidence intervals of the parameter estimates. The magnitude of confidence intervals depends on the method of data fitting to a theoretical distribution. When the method of moments is employed, the variability of scale parameter is the same as that of sample standard deviation. For the case of maximum likelihood method, a few theoretical analyses on the parameter estimates are available. Lawless[13] has given a solution for the estimates of parameters of the FT-I distribution, and Challenor[14] has prepared tables of the confidence intervals of the parameter estimates.

For the case of the least squares method, no theory is available on the parameter estimates. Thus, the author (Ref. 4 and an unpublished source) has analyzed the data of the Monte Carlo simulation studies to estimate the confidence intervals of the scale and location parameters of various distributions. The results are listed in Table 11.10, which is based on the data of 20,000 samples for each case. It is found that the confidence intervals of the parameter estimates by the least squares method for the FT-I distribution are about 20% greater than those by the maximum likelihood method, according to the comparison with Challenor's tables.

Example 11.1

Estimates of $\hat{A} = 1.20$ and $\hat{B} = 4.77$ have been obtained from a sample of the FT-I distribution with the size $N = 20$. What are the 95% confidence intervals of these parameters?

Solution

By reading the row of $N = 20$ of the FT-I distribution of Table 11.10, we have the following dimensionless values at 2.5% and 97.5% levels:

$$[A/\hat{A}]_{2.5\%} = 0.67\,, \quad [A/\hat{A}]_{97.5\%} = 1.61\,,$$

$$[(\hat{B} - B)/\hat{A}]_{2.5\%} = -0.49\,, \quad [(\hat{B} - B)/\hat{A}]_{97.5\%} = 0.53\,.$$

Thus, the confidence intervals of the population parameters are calculated as follows:

$$A = (0.67 \sim 1.61) \times 1.20 = 0.80 \sim 1.93\,,$$

$$B = 4.77 + (-0.49 \sim 0.53) \times 1.20 = 4.18 \sim 5.41\,.$$

Table 11.10. Confidence intervals of parameter estimates by the least squares method.

Distribution	N	Scale parameter $A/\hat{A}$					Location parameter $(\hat{B} - B)/\hat{A}$				
		2.5%	25%	75%	97.5%	σ	2.5%	25%	75%	97.5%	σ
FT-II	10	0.30	0.89	2.04	4.05	0.98	−1.27	−0.31	0.39	1.42	0.66
($k = 2.5$)	14	0.31	0.89	1.90	3.45	0.82	−0.92	−0.25	0.37	1.21	0.53
	20	0.35	0.89	1.78	3.05	0.70	−0.66	−0.20	0.35	1.05	0.44
	30	0.37	0.89	1.65	2.65	0.59	−0.51	−0.15	0.33	0.92	0.37
	40	0.39	0.89	1.59	2.48	0.53	−0.47	−0.13	0.32	0.85	0.34
	60	0.42	0.89	1.51	2.25	0.47	−0.44	−0.10	0.30	0.75	0.30
	100	0.45	0.90	1.43	2.01	0.40	−0.43	−0.08	0.28	0.65	0.28
	140	0.48	0.90	1.39	1.90	0.36	−0.43	−0.08	0.27	0.60	0.26
	200	0.49	0.90	1.35	1.80	0.33	−0.43	−0.07	0.27	0.56	0.25
FT-II	10	0.36	0.85	1.73	3.19	0.74	−1.09	−0.28	0.30	1.11	0.54
($k = 3.33$)	14	0.38	0.86	1.62	2.73	0.61	−0.82	−0.23	0.27	0.91	0.43
	20	0.42	0.86	1.53	2.43	0.51	−0.62	−0.19	0.24	0.76	0.35
	30	0.46	0.87	1.43	2.14	0.43	−0.47	−0.15	0.21	0.65	0.28
	40	0.49	0.88	1.38	2.00	0.38	−0.40	−0.13	0.20	0.57	0.25
	60	0.52	0.88	1.32	1.83	0.33	−0.34	−0.10	0.17	0.48	0.21
	100	0.56	0.89	1.26	1.65	0.28	−0.30	−0.09	0.15	0.39	0.18
	140	0.59	0.90	1.23	1.56	0.24	−0.28	−0.08	0.14	0.34	0.16
	200	0.62	0.91	1.20	1.49	0.22	−0.26	−0.07	0.12	0.30	0.14
FT-II	10	0.43	0.84	1.53	2.63	0.57	−0.96	−0.26	0.26	0.95	0.47
($k = 5.0$)	14	0.46	0.85	1.44	2.29	0.47	−0.74	−0.21	0.22	0.76	0.37
	20	0.50	0.86	1.36	2.03	0.39	−0.57	−0.18	0.19	0.62	0.30
	30	0.55	0.87	1.29	1.81	0.32	−0.44	−0.14	0.16	0.51	0.24
	40	0.59	0.88	1.25	1.70	0.28	−0.37	−0.12	0.15	0.44	0.21
	60	0.62	0.89	1.21	1.57	0.24	−0.30	−0.10	0.12	0.36	0.17
	100	0.67	0.91	1.16	1.44	0.19	−0.24	−0.08	0.09	0.28	0.13
	140	0.71	0.91	1.14	1.37	0.17	−0.21	−0.07	0.08	0.24	0.11
	200	0.74	0.92	1.12	1.32	0.15	−0.18	−0.06	0.07	0.20	0.10
FT-II	10	0.51	0.84	1.39	2.26	0.46	−0.85	−0.24	0.25	0.86	0.42
($k = 10.0$)	14	0.54	0.86	1.32	1.98	0.37	−0.68	−0.19	0.21	0.69	0.34
	20	0.59	0.87	1.26	1.77	0.30	−0.53	−0.16	0.18	0.55	0.27
	30	0.64	0.88	1.20	1.60	0.24	−0.42	−0.13	0.15	0.44	0.22
	40	0.67	0.90	1.18	1.51	0.21	−0.36	−0.11	0.13	0.38	0.19
	60	0.71	0.91	1.14	1.41	0.18	−0.28	−0.09	0.10	0.31	0.15
	100	0.76	0.92	1.11	1.31	0.14	−0.22	−0.07	0.08	0.23	0.12
	140	0.79	0.93	1.09	1.26	0.12	−0.19	−0.06	0.07	0.20	0.10
	200	0.82	0.94	1.08	1.22	0.10	−0.16	−0.05	0.06	0.16	0.08

Note: σ stands for the standard deviation of respective parameter estimates in dimension-
less forms.

Table 11.10. (*Continued*)

Distribution	N	Scale parameter $A/\hat{A}$					Location parameter $(\hat{B} - B)/\hat{A}$				
		2.5%	25%	75%	97.5%	σ	2.5%	25%	75%	97.5%	σ
FT-I	10	0.58	0.86	1.30	2.03	0.37	−0.77	−0.21	0.25	0.83	0.40
	14	0.62	0.87	1.24	1.78	0.30	−0.61	−0.18	0.21	0.66	0.32
	20	0.67	0.88	1.19	1.61	0.24	−0.49	−0.15	0.18	0.53	0.26
	30	0.71	0.90	1.14	1.47	0.19	−0.39	−0.12	0.14	0.42	0.20
	40	0.74	0.91	1.13	1.39	0.17	−0.34	−0.11	0.12	0.36	0.18
	60	0.78	0.92	1.10	1.30	0.13	−0.27	−0.09	0.10	0.29	0.14
	100	0.82	0.94	1.08	1.23	0.10	−0.21	−0.07	0.07	0.22	0.11
	140	0.85	0.95	1.06	1.19	0.09	−0.18	−0.06	0.06	0.19	0.09
	200	0.87	0.95	1.05	1.16	0.07	−0.15	−0.05	0.05	0.18	0.08
Weibull	10	0.42	0.82	1.70	3.58	0.86	−0.41	−0.12	0.36	1.14	0.40
($k = 0.75$)	14	0.47	0.83	1.55	2.88	0.65	−0.39	−0.11	0.31	0.93	0.34
	20	0.50	0.84	1.43	2.45	0.50	−0.36	−0.11	0.26	0.75	0.29
	30	0.56	0.85	1.34	2.09	0.40	−0.33	−0.10	0.22	0.61	0.24
	40	0.59	0.87	1.28	1.89	0.33	−0.31	−0.09	0.19	0.53	0.21
	60	0.64	0.88	1.22	1.67	0.27	−0.28	−0.08	0.16	0.42	0.18
	100	0.70	0.90	1.17	1.50	0.20	−0.24	−0.07	0.12	0.33	0.15
	140	0.73	0.91	1.15	1.41	0.18	−0.22	−0.06	0.11	0.28	0.13
	200	0.77	0.92	1.12	1.34	0.15	−0.19	−0.06	0.09	0.24	0.11
Weibull	10	0.51	0.83	1.44	2.58	0.55	−0.34	−0.12	0.24	0.83	0.30
($k = 1.0$)	14	0.55	0.84	1.36	2.22	0.43	−0.31	−0.11	0.21	0.66	0.25
	20	0.60	0.86	1.28	1.92	0.34	−0.28	−0.09	0.17	0.52	0.21
	30	0.65	0.88	1.22	1.70	0.26	−0.25	−0.08	0.13	0.41	0.16
	40	0.69	0.89	1.18	1.58	0.23	−0.22	−0.08	0.12	0.35	0.15
	60	0.72	0.90	1.15	1.44	0.18	−0.20	−0.07	0.10	0.28	0.12
	100	0.78	0.92	1.11	1.33	0.14	−0.16	−0.05	0.07	0.21	0.09
	140	0.80	0.93	1.09	1.27	0.12	−0.14	−0.05	0.06	0.18	0.08
	200	0.83	0.94	1.08	1.22	0.10	−0.12	−0.04	0.05	0.15	0.07
Weibull	10	0.60	0.86	1.30	2.05	0.38	−0.30	−0.12	0.17	0.66	0.24
($k = 1.4$)	14	0.64	0.87	1.24	1.79	0.30	−0.27	−0.10	0.15	0.52	0.20
	20	0.69	0.88	1.19	1.61	0.24	−0.24	−0.09	0.11	0.38	0.15
	30	0.73	0.90	1.14	1.47	0.19	−0.20	−0.07	0.10	0.31	0.13
	40	0.75	0.91	1.12	1.39	0.16	−0.18	−0.07	0.08	0.26	0.11
	60	0.79	0.92	1.10	1.29	0.13	−0.15	−0.06	0.07	0.21	0.09
	100	0.83	0.94	1.07	1.22	0.10	−0.12	−0.05	0.05	0.16	0.07
	140	0.86	0.95	1.06	1.18	0.08	−0.11	−0.04	0.04	0.13	0.06
	200	0.88	0.96	1.05	1.15	0.07	−0.09	−0.03	0.04	0.11	0.05

Note: σ stands for the standard deviation of respective parameter estimates in dimension-less forms.

Table 11.10. (*Continued*)

Distribution	N	Scale parameter $A/\hat{A}$					Location parameter $(\hat{B} - B)/\hat{A}$				
		2.5%	25%	75%	97.5%	σ	2.5%	25%	75%	97.5%	σ
Weibull	10	0.66	0.87	1.22	1.80	0.29	−0.30	−0.12	0.17	0.66	0.24
($k = 2.0$)	14	0.70	0.88	1.17	1.60	0.23	−0.26	−0.10	0.13	0.49	0.19
	20	0.74	0.90	1.14	1.46	0.19	−0.22	−0.09	0.11	0.38	0.15
	30	0.78	0.92	1.11	1.36	0.15	−0.19	−0.07	0.08	0.29	0.12
	40	0.80	0.92	1.09	1.29	0.13	−0.17	−0.06	0.07	0.24	0.10
	60	0.83	0.94	1.07	1.23	0.10	−0.14	−0.05	0.06	0.19	0.08
	100	0.87	0.95	1.05	1.17	0.08	−0.11	−0.04	0.04	0.14	0.06
	140	0.89	0.96	1.05	1.14	0.06	−0.10	−0.04	0.04	0.12	0.05
	200	0.90	0.97	1.04	1.11	0.05	−0.08	−0.03	0.03	0.09	0.04
Normal	10	0.66	0.87	1.21	1.78	0.29	−0.68	−0.22	0.22	0.71	0.35
	14	0.70	0.89	1.16	1.58	0.22	−0.57	−0.18	0.18	0.57	0.29
	20	0.75	0.90	1.13	1.44	0.18	−0.46	−0.15	0.15	0.47	0.23
	30	0.79	0.92	1.10	1.33	0.14	−0.37	−0.12	0.12	0.37	0.19
	40	0.81	0.93	1.08	1.28	0.12	−0.32	−0.11	0.11	0.32	0.16
	60	0.84	0.94	1.07	1.21	0.09	−0.26	−0.09	0.09	0.26	0.13
	100	0.87	0.95	1.05	1.16	0.07	−0.20	−0.07	0.07	0.20	0.10
	140	0.89	0.96	1.04	1.13	0.06	−0.17	−0.06	0.06	0.17	0.09
	200	0.91	0.97	1.03	1.10	0.05	−0.14	−0.05	0.05	0.14	0.07

Note: σ stands for the standard deviation of respective parameter estimates in dimension-
less forms.

11.3.3 *Return Value and Its Confidence Interval*

(A) *Estimation of return value*

Once the most probable parent distribution is obtained as the distribution best
fitting to the sample under analysis, the return value for a given return period
is estimated with the following equation:

$$\hat{x}_R = \hat{B} + \hat{A} y_R, \qquad (11.23)$$

where the reduced variate y_R is calculated as a function of the return period R and the mean rate λ as follows:

$$
\left.
\begin{aligned}
\text{FT-I distribution} \quad &: y_R = -\ln\left\{-\ln\left[1 - \tfrac{1}{\lambda R}\right]\right\}, \\
\text{FT-II distribution} \quad &: y_R = k\left\{\left[-\ln\left(1 - \tfrac{1}{\lambda R}\right)\right]^{-1/k} - 1\right\}, \\
\text{Weibull distribution} &: y_R = [\ln(\lambda R)]^{1/k}.
\end{aligned}
\right\}
\tag{11.24}
$$

In the case of the Kodiak data, the Weibull distribution with $k = 1.4$ has been concluded as the best-fitting distribution in Sec. 11.2.3. The scale and location parameters have been estimated as $\hat{A} = 1.8621$ m and $\hat{B} = 5.805$ m. The 100-year wave height is estimated as follows:

$$
y_{100} = [\ln(3.9 \times 100)]^{1/1.4} = 3.5815,
$$

$$
x_{100} = 5.805 + 1.8621 \times 3.5815 = 12.47\,\text{m}.
$$

Figure 11.9 shows the fitting of the Kodiak data to the Weibull distribution with $k = 1.4$. The solid line represents the best-fitting line, while the dashed line indicates the 90% confidence interval to be discussed below. The scale in the upper axis indicates the return period in years.

(B) *Statistical variability of return value*

A sample of extreme wave data exhibits quite a large magnitude of variability as demonstrated in Figs. 11.7 and 11.8. The return values estimated with the best-fitting distribution function vary considerably around the true values of population. Figure 11.10 shows examples of statistical variability of return values estimated from individual samples. The FT-I distribution is employed as the population, and uncensored samples ($\nu = 1$) are simulated by a Monte Carlo technique. Two cases of the sample size $N = 20$ and $N = 100$ are analyzed. By assuming the mean rate $\lambda = 1$, the sample sizes correspond to the annual maxima data of 20 and 100 years, respectively. For each sample, the scale and location parameters are estimated with the least squares method by assuming the parent distribution being the FT-I. Then the return value corresponding to the period $R = 100$ (years) is calculated for each sample. The estimates of return value are shown in Fig. 11.10 in a form of probability
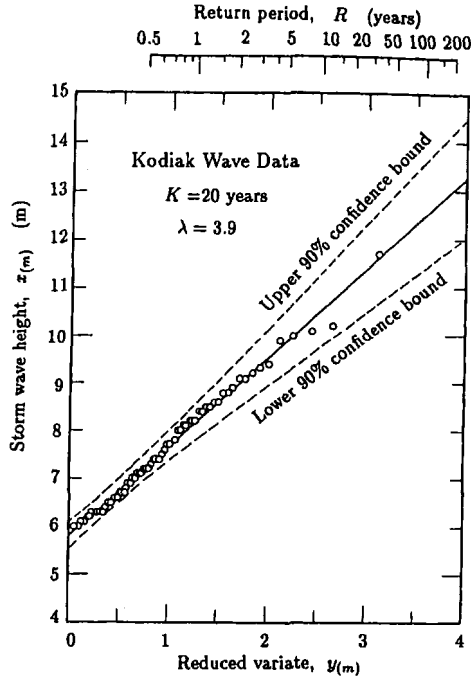
Fig. 11.9. Fitting of the Kodiak storm wave data to the Weibull distribution with $k = 1.4$.
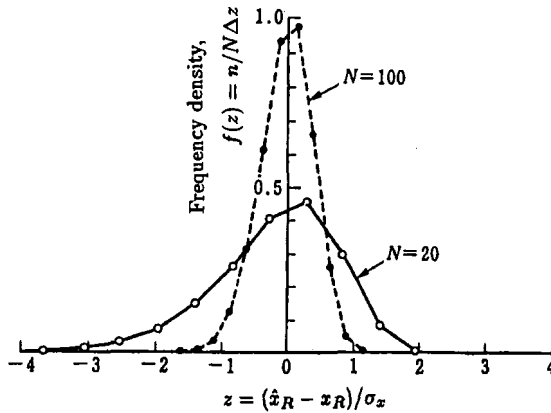
Fig. 11.10. Examples of spread of the return value estimated from uncensored samples of the FT-I distribution: sample sizes $N = 20$ and $N = 100$ for the return period $R = 100$.[17]

density function. The following reduced variate is introduced to make the results independent of parametric values:

$$z = \frac{\hat{x}_R - x_R}{\sigma_x}, \qquad (11.25)$$

where x_R is the true return value of the population and σ_x is the unbiased standard deviation of the sample.

As seen in Fig. 11.10, the 100-year wave height estimated from a sample of annual maximum height of 20 years may have a deviation of more than σ_x from the true value. In the real situation, we have only one set of extreme wave heights with no information on the parent distribution. The true return value may be on the larger side or the smaller side of the estimate, but we have no information to judge which side is the correct one. The only procedure we can take is to estimate the confidence interval of the estimated return value within which the true value would be located.

(C) *Standard deviation of return value when the parent distribution is known*

Estimate of the confidence interval of any statistics requires the information on its cumulative distribution. The data shown in Fig. 11.10 provides such an information. When a sample of extreme data is analyzed, the confidence interval can be estimated by means of a Monte Carlo simulation technique as suggested by Mathiessen *et al.*[15] The distribution fitted to the original sample is assumed to be the parent distribution; a large number of artificial samples (say 2000 samples) are simulated, return values are estimated for these samples, and a cumulative distribution of the estimated return values is established. For practical purposes, however, the normal distribution of the return value is assumed (almost true of the case of $N = 100$ but not for the case of $N = 20$ in Fig. 11.10), and the confidence interval is estimated by means of the standard deviation of the return value. The 90% confidence interval is set at the range of ± 1.645 times the standard deviation around the estimate of the return value.

For the FT-I distribution, Gumbel (Ref. 3, Sec. 6.2.3) has given the following formula as to when the method of moment is employed:

$$\sigma(\hat{x}_R) = [1 + 0.8885(y_R - \gamma) + 0.6687(y_R - \gamma)^2]^{1/2}\sigma/\sqrt{N}, \qquad (11.26)$$

where σ is the standard deviation of the population (which is unknown), y_R stands for the reduced variate for the return period R, and γ is Euler's constant.

For the case of the least squares method, the author,[4,10,16] has derived the empirical formula for the estimate of the standard deviation of the return value as in the following:

$$\sigma(\hat{x}_R) = \sigma_z \cdot \sigma_x, \tag{11.27}$$

where σ_z is the standard deviation of the reduced variate defined by Eq. (11.25) and is given by

$$\sigma_z = [1.0 + a(y_R - c + \alpha \ln \nu)^2]^{1/2}/\sqrt{N}, \tag{11.28}$$

in which the constant a is to be calculated by the following formula:

$$a = \begin{cases} a_1 \exp[a_2 N^{-1.3} + \kappa(-\ln \nu)^2] & \text{for FT-I and Weibull distributions}, \\ a_1 \exp\{a_2[\ln(N\nu^{0.5}/N_0)]^2 - \kappa[\ln(\nu/\nu_0)]\} & \text{for FT-II distribution}. \end{cases} \tag{11.29}$$

The constants appearing in Eqs. (11.28) and (11.29) have been set as listed in Tables 11.11 and 11.12 based on the data of Monte Carlo simulation studies, which have been utilized for the derivation of the DOL, REC and MIR criteria.

Table 11.11. Constants for the standard deviation of return value for FT-I and Weibull distribution.

Distribution	a_1	a_2	κ	c	α
FT-I	0.64	9.0	0.93	0	1.33
Weibull ($k = 0.75$)	1.65	11.4	-0.63	0	1.15
Weibull ($k = 1.0$)	1.92	11.4	0	0.3	0.90
Weibull ($k = 1.4$)	2.05	11.4	0.69	0.4	0.72
Weibull ($k = 2.0$)	2.24	11.4	1.34	0.5	0.54

Table 11.12. Constants for the standard deviation of return value for FT-II distribution.

Shape parameter	a_1	a_2	N_0	κ	ν_0	c	α
$k = 2.5$	1.27	0.12	23	0.24	1.34	0.3	2.3
$k = 3.33$	1.23	0.09	25	0.36	0.66	0.2	1.9
$k = 5.0$	1.34	0.07	35	0.41	0.45	0.1	1.6
$k = 10.0$	1.48	0.06	60	0.47	0.34	0	1.4

Example 11.2

Estimate the confidence interval of the 100-year wave height of the Kodiak data.

Solution

The 100-year wave height of the Kodiak data has been estimated as $x_{100} = 12.47$ m in Sec. 11.3.3(A). The corresponding reduced variate is $y_{100} = 3.5815$, and the sample standard deviation is $\sigma_x = 1.214$ m. The standard deviation of the 100-year wave height is calculated by using Eqs. (11.27) to (11.29) as follows:

$$a = 2.05 \exp[11.4 \times 78^{-1.3} + 0.69 \times (-\ln 1.0)^2] = 2.133\,,$$

$$\sigma_z = [1.0 + 2.133 \times (3.5815 - 0.4 + 0.72 \times \ln 1.0)^2]^{1/2}/\sqrt{78} = 0.538\,,$$

$$\sigma(\hat{x}_{100}) = 0.538 \times 1.214 = 0.653\,\mathrm{m}\,.$$

Thus, the confidence interval of the 100-year wave height is estimated as follows:

$$x_{100} = 12.47 \pm 1.645 \times 0.653 = 12.47 \pm 1.07 = 11.4 \sim 13.5\,\mathrm{m}\,.$$

The two dashed lines above and below the straight line in Fig. 11.9 have been drawn by calculation such as shown in the above. Thus, the confidence interval can easily be calculated for any sample of extreme wave data. However, introduction of the concept of confidence interval of design wave height into design practice is still in its infancy stage. Practitioners are not accustomed with the concept of confidence interval, and they are reluctant in dealing with it. Nevertheless, engineers in charge of designing maritime structures should keep in mind the uncertainty of design wave height and should provide a sufficient margin of safety against the attack of storm waves much severer than the design condition.

(D) *Standard deviation of return value when the parent distribution is unknown*

The question inherent in extreme wave analysis is such: what is the true parent distribution of extreme storm waves? As explained in Sec. 11.1.2, no answer exists to this question at present and the distribution best fitting to a sample among several candidates is selected as the most probable parent distribution.

However, there is a possibility to establish the parent distribution of extreme storm waves in the future. If storm wave data are collected at a number of stations in one ocean region where the nature of storm waves can be regarded homogeneous, they will constitute multiple samples drawn from the same population. By applying the DOL and REC criteria for these samples, the least rejectable distribution for the particular ocean region will emerge by such analysis. In fact, Goda and Kobune[6] made such an analysis and reported that several coastal regions around Japan seem to have particular types of extreme distribution functions. Their results were incomplete because the data base employed covered a relatively short span of time duration. With expansion of the storm wave data base, more detailed analyses similar with Goda and Kobune would indicate the parent distribution of extreme waves along respective ocean regions.

In the present situation in which no parent distribution is established yet, we are always faced with the problem of misfitting a sample to a distribution different from the true parent distribution, because of sample variability such as shown in Fig. 11.7. In a joint simulation study reported by Goda *et al.*,[5] samples drawn from the Weibull distribution with $k = 1.4$ were fitted to a wide range of distributions including the FT-I and the Weibull with k being less than 1 to greater than 2. The empirical formulas of Eqs. (11.27) to (11.29) for the standard deviation of return values are based on the condition that the samples are fitted to the parent distribution. When a sample is fitted to a distribution different from the parent, the confidence interval of return value would be wider than that estimated with the empirical formulas of Eqs. (11.27) to (11.29). However, there is no way to know the difference in amount. The only thing we can endeavor is to increase the sample size N by extending the duration of data base K and by increasing the mean rate λ. By increasing the sample size, we can diminish the possibility of misfitting and decrease the range of confidence interval.

(E) *Effect of sample size on confidence interval*

As indicated in Eqs. (11.26) and (11.28), the standard deviation of return value is inversely proportional to the square root of sample size N. A trial calculation has been made to demonstrate the effect of sample size on the magnitude of the standard deviation of return value.[17] The FT-I distribution is taken as a model, and the ratio of $\sigma(x_{\hat{1}00})$ to σ_x is calculated with Eqs. (11.28) and (11.29) for the case of no censoring ($\nu = 1$). The result is shown in Figs. 11.11.
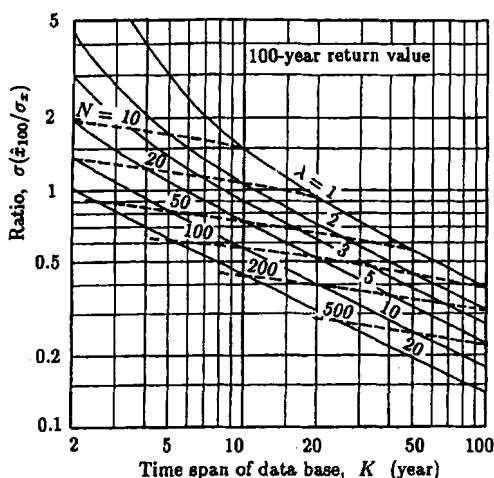
Fig. 11.11. Standard deviation of a 100-year return value of FT-I distribution $\sigma(\hat{x}_{100})$ relative to the sample standard deviation σ_x for uncensored samples.[17]

The abscissa is the duration of extreme wave data set K and the mean rate λ is taken as the main parameter, while the sample size N is shown as the secondary parameter. For a given value of λ, the ratio $\sigma(\hat{x}_{100})/\sigma_x$ gradually decreases as the duration K becomes long. In practice, the duration K for a particular site is fixed by the availability of wave data source. Adoption of as many of the storm waves as possible by the peaks-over-threshold (POT) method enables the increase of the mean rate and sample size, thus reducing the magnitude of the standard deviation of return value.

11.3.4 *Treatment of Mixed Populations*

(A) *Cumulative distribution of extreme variate for mixed populations*

As discussed in the beginning of this chapter, homogeneity is one of the important requisites in extreme statistics. Ideally speaking, each storm wave height is to be classified according to the types of meteorological disturbances, and each group of storm wave heights should be analyzed separately. In practice, the examination of individual storm waves is a tedious work, and extreme wave analysis is often carried out without due regard to the homogeneity condition. However, storm wave data can be classified by seasons with little difficulty if

not by the type of wave generation source. Extremal analysis of such classified storm wave data should be encouraged.

When multiple groups of extreme wave data are analyzed, different distribution functions will be fitted to respective groups. Then it becomes necessary to combine these distributions into a single cumulative distribution. Carter and Challenor[18] made estimates of return values of wave heights and wind speeds around U.K., by using the monthly maximum values. They derived the cumulative distribution of annual maxima as the product of 12 monthly cumulative distributions; i.e.,

$$F(x) = \text{Prob.}(X \le x) = \prod_{j=1}^{12} F_j(x), \tag{11.30}$$

where $F(x)$ refers to the cumulative distribution of annual maxim and $F_j(x)$ that of monthly maxima.

For POT data, its cumulative distribution is first converted to that of annual maxima by assuming that the number of storm events per year follows the Poisson distribution expressed as

$$P_r = \frac{1}{r!} e^{-\lambda} \lambda^r, \quad r = 0, 1, 2, \ldots, \tag{11.31}$$

where r denotes the storm number per year. Examination of the Kodiak data in Table 11.3 indicates the assumption of Poisson distribution acceptable. When r peak wave heights occur in one year, the annual maximum is the largest of r data and its nonexceedance probability is given as $F_*^r(x)$, where $F_*(x)$ denotes the nonexceedance probability (i.e., distribution function) of individual storm events. Because the number of storm events r is a statistical variate, the cumulative distribution of annual maxima $F(x)$ is derived as the expected value of the probability from $r = 0$ to ∞. Thus,

$$F(x) = \sum_{r=0}^{\infty} P_r F_*^r(x) = \exp\{-\lambda[1 - F_*(x)]\}. \tag{11.32}$$

When there are n groups of extreme storm waves, the cumulative distribution for the annual maxima can be derived by applying the technique of Eq. (11.30) as follows:

$$F(x) = \prod_{j=1}^{n} \exp\{-\lambda_j[1 - F_j(x)]\} = \exp\left\{-\sum_{j=1}^{n} \lambda_j[1 - F_j(x)]\right\}, \tag{11.33}$$

where $F_j(x)$ denotes the distribution function of the jth group of POT data.

(B) *Return value and confidence interval*

As Eq. (11.33) defines the cumulative distribution of the annual maxima, the return value for the return period R is derived as $F^{-1}(1 - 1/R)$ by Eq. (3.9). Except for the case that all the distribution function of POT data belong to the FT-I distribution, $F(x)$ is obtained in a tabular form only and the return value must be obtained by interpolation.

In statistics, the variance of a sample containing multiple subsamples is expressed as a sum of variances of individual subsamples. This concept can be applied for the estimation of confidence interval. Thus, it is proposed to estimate the variance of return value for multiple groups as follows:

$$\sigma^2(\hat{x}_R) = \frac{\displaystyle\sum_{j=1}^{n} N_j[1 - F_j(\hat{x}_R)]\sigma_j^2(\hat{x}_R)}{\displaystyle\sum_{j=1}^{n} N_j[1 - F_j(\hat{x}_R)]}, \tag{11.34}$$

where N_j and $\sigma_j^2(\hat{x}_R)$ denotes the sample size and variance of the jth group, respectively. The weight $[1 - F_j(\hat{x}_R)]$ is applied to minimize influence of groups of minor storm events. The standard deviation and the confidence interval can easily be derived from the above variance.

11.4 Design Waves and Related Problems

11.4.1 *Encounter Probability and L-year Maximum Height*

(A) *Encounter probability*

Estimation of a return value for a given return period is one thing in extreme wave statistics, and specification of the return period is another thing. Borgman[19] has presented the concept of encounter probability for selection of the return period. Let the service lifetime of a structure be L and the design return period of the structure be R. The cumulative distribution of the annual maxima of storm wave heights is assumed to have been established as $F(x)$. The probability that an annual maximum wave height in one year exceeds the design value x_R is $1 - F(x_R)$ by definition, and it is equal to $1/R$ by Eq. (11.8). The probability that the structure will not experience storm waves greater than the design condition in one year is given by $F(x_R) = 1 - 1/R$. The encounter

probability that the structure will experience storm waves greater than the design condition during L years is then obtained as

$$P_L = 1 - \left(1 - \frac{1}{R}\right)^L . \tag{11.35}$$

If the design condition is set with the return period $R = 100$ years for a structure which is planned to serve for $L = 30$ years, there will be a probability of 0.26 that the structure will encounter storm waves exceeding the design condition. Borgman prepared a table of encounter probability for various combinations of the service lifetime and return period. However, the following approximation to Eq. (11.35) is available when both L and R are sufficiently large:

$$P_L = 1 - \exp\left(-\frac{L}{R}\right) . \tag{11.36}$$

The above equation indicates that if R is set equal to L, the encounter probability will be as high as 0.63. If the encounter probability is to be kept below 0.3, the return period should be longer than 2.8 times the service lifetime.

(B) *L-year maximum wave height*

Another approach to the selection of design wave height is to use the expected value of the largest wave height during the service lifetime of a structure, which is hereby called the L-year maximum height. Use of the L-year maximum load is a common practice in reliability-based designs (e.g., see Refs. 20 and 21).

First, the largest wave height within L years is denoted with x_L and its cumulative distribution with $\Phi(x_L)$. The meaning of $\Phi(x_L)$ is explained as follows. A very long stationary time series of annual maximum wave heights is supposed to exist. The time series is segmented into a large number of samples with the duration of L years each. The value of x_L varies from sample to sample, and a histogram of x_L can be prepared. By summing up the histogram from the lowest to the largest x_L, a cumulative distribution of x_L will be constructed. This is an empirical form of $\Phi(x_L)$. In statistical sense, $\Phi(x_L)$ is defined with the cumulative distribution of annual maximum wave height $F(x)$ as in the following:

$$\Phi(x_L) = \text{Prob.}(X \leq x_L) = F^L(x_L) . \tag{11.37}$$

The probability density function of x_L denoted with $\phi(x_L)$ is derived by taking the derivative of Eq. (11.37) as follows:

$$\phi(x_L) = L\, F^{L-1}(x_L)\, f(x_L)\,. \tag{11.38}$$

The L-year maximum wave height is the mean of x_L of many samples; i.e., $\overline{x}_L = E[x_L]$, which is calculated using Eq. (11.38). The magnitude of variation of x_L of individual samples is represented with its standard deviation, and it is derived from the variance $E[(x_L - \overline{x}_L)^2]$. Computation of the mean and standard deviation of x_L generally requires numerical integration for the first and second moments of Eq. (11.38). When the annual maximum wave heights are fitted by the FT-I or FT-II distribution, however, the analytical expression for $\Phi(x_L)$ can be readily derived, and the mean and standard deviation are obtained by referring to Table 11.1. The results are as follows:

FT-I distribution:

$$\text{Distribution}: \Phi(x_L) = \exp\left\{ -\exp\left[-\frac{x - (B + A\ln L)}{A} \right] \right\}, \tag{11.39}$$

$$\text{Mean}: \overline{x}_L = B + A(\ln L + \gamma)\,, \tag{11.40}$$

$$\text{Standard deviation}: \delta(x_L) = \frac{\pi}{\sqrt{6}}A\,. \tag{11.41}$$

FT-II distribution:

$$\text{Distribution}: \Phi(x_L) = \exp\left\{ -\left[1 + \frac{x - (B + kAL^{1/k} - kA)}{kAL^{1/k}} \right]^{-k} \right\}, \tag{11.42}$$

$$\text{Mean}: \overline{x}_L = B + kA\left[L^{1/k}\Gamma\left(1 - \frac{1}{k}\right) - 1 \right]\,, \tag{11.43}$$

$$\text{Standard deviation}: \delta(x_L) = kAL^{1/k}\left[\Gamma\left(1 - \frac{2}{k}\right) - \Gamma^2\left(1 - \frac{1}{k}\right) \right]^{1/2}\,. \tag{11.44}$$

In the case of the FT-I distribution, the return period corresponding to the L-year maximum wave height $\bar{x}_L$ is calculated by substituting Eq. (11.40) into Eq. (11.3) and by using Eq. (11.8) as follows:

$$R(\bar{x}_L) = \frac{1}{1 - \exp[-\exp(-\ln L - \gamma)]} \simeq 1.78L + \frac{1}{2}. \tag{11.45}$$

Thus, the return period of $\bar{x}_L$ is approximately equal to $1.8L$. In the case of the FT-II distribution, $R(\bar{x}_L)$ increases with the decrease in the shape parameter k up to about $2.7L$. In the case of the Weibull distribution, $R(\bar{x}_L)$ is longer than $1.8L$ for $k = 0.75$, equal to $1.8L$ for $k = 1.0$, and shorter than $1.8L$ for $k = 1.4$ and 2.0.

Discussions with Eqs. (11.39) to (11.45) apply to the distribution function of annual maximum wave heights. For the data of peaks-over-threshold storm wave heights, the distribution fitted to a sample must be converted to that of annual maximum heights by means of Eq. (11.32). Therefore, even if the POT data is fitted to the FT-I distribution, Eqs. (11.39) to (11.41) cannot be applied directly and numerical integration involving $\phi(x_L)$ must be carried out. A compromise is possible, however, by replacing the service lifetime L with λL. As the reliability-based design of maritime structures is at its early stage of development, further examinations of the characteristics of L-year maximum wave height will be necessary.

(C) *Confidence interval of L-year maximum wave height*

The reliability-based design examines the probability of failure during the lifetime of a structure. Examination is made through the analysis of statistical distributions of the magnitudes of the loads to be exerted on structures and the capacity of structures in resisting the loads. The concepts of load and resistance factors are thus introduced. The coefficients of variation of these factors constitute the important elements in the reliability-based design. The standard deviation $\delta(x_L)$ in Eqs. (11.41) and (11.44) is a measure of dispersion of x_L of individual samples with the duration of L years each. It is evaluated on the assumption that the functions $F(x_L)$ and $f(x_L)$ being employed in Eq. (11.38) represent the true parent distribution. In practice, however, the extreme distribution function has to be estimated from one sample of storm wave data, and there remains the uncertainty in the estimate of return value due to sample variability as discussed in the preceding sections. This uncertainty should

be added in the evaluation of the coefficient of variation of L-year maximum wave height. It can be done by taking a sum of the variance of x_L due to the nature of parent distribution itself and that due to statistical variability of a sample of storm wave data. Thus,

$$\text{C.V.}[\bar{x}_L] = \frac{[\delta^2(x_L) + \sigma^2(\hat{x}_L)]^{1/2}}{\bar{x}_L} \,, \qquad (11.46)$$

where $\sigma(\hat{x}_L)$ denotes the standard deviation of $\bar{x}_L$ due to sample variability which can be estimated with Eqs. (11.27) to (11.29), when the distribution fitting is made by means of the least squares method.

Example 11.3

A service lifetime of a structure is set at $L = 50$ years. Suppose the extreme wave statistics of the site is almost the same as that of the Kodiak data. Estimate the L-year maximum wave height and its coefficient of variation.

Solution

As the most probable parent distribution of the Kodiak data is the Weibull with $k = 1.4$, the exact calculation of $\bar{x}_L$ requires numerical integration of the probability density function defined by Eq. (11.38). However, the behavior of the Weibull distribution with $k = 1.4$ is not much different from that of FT-I, and for the Kodiak data the FT-I is the second best-fitting distribution. Thus, the L-year maximum wave height is estimated as the return value corresponding $R = 1.8L = 90$ years as follows:

$$y_{90} = [\ln(3.9 \times 90)]^{1/1.4} = 3.536 \,,$$

$$\bar{x}_{50} \simeq \hat{x}_{90} = 5.805 + 1.8621 \times 3.536 = 12.39 \,\text{m} \,.$$

The uncertainty of $\bar{x}_{50}$ due to sample variability is estimated in a similar manner as Example 11.2, and the result becomes

$$\sigma_z = 0.531 \,, \quad \sigma(\hat{x}_{90}) = 0.645 \,\text{m} \,.$$

The standard deviation of $\bar{x}_{50}$ itself is approximated with the formula Eq. (11.40) for the FT-I distribution with $A = 0.9567$ which is listed in Table 11.3. Thus,

$$\delta(x_{50}) = \frac{\pi}{\sqrt{6}} \times 0.9657 = 1.227 \,\text{m} \,,$$

$$\text{C.V.}[\bar{x}_{50}] = \frac{\sqrt{1.227^2 + 0.645^2}}{12.39} = 0.112 \,.$$

The uncertainty due to sample variability is thus taking into account in the reliability-based design of maritime structures as shown in the above example.

11.4.2 *Some Remarks for Extreme Wave Data Analysis*

(A) *Database of extreme waves*

Several sources of wave data are used in the extreme wave analysis. They are

(i) long record of instrumentally measured data of wave heights and periods,

(ii) long record of visually observed data of wave heights and periods,

(iii) wave hindcasting project for storm waves over a long time span,

(iv) data bank of routine wave forecasting over oceans.

Among them, instrumentally measured data are the best source, provided that they cover a sufficiently long time span and the downtime is kept minimum. Hindcasted data of storm waves are the second best source, provided that the wave hindcasting method has been well calibrated with several storm wave records in the area of interest. Routine wave forecasting has been carried out in recent years by meteorological agencies of many countries, and the data bank accumulated through these works has the potential to provide a good source of extreme wave data in near future. However, the accuracy of wave height information would be inferior to instrumental records and hindcasted wave data, because wave forecasting is made on uncertain weather conditions forecasted in advance.

Visually observed wave data are classified into two types. One is the observations made at a fixed station at regular interval. Not many data sets of this type exist, and they usually fail to report very large storm waves. The other type of visual wave data is a compilation of ship report data, which are presented in a form of a joint distribution (or a scatter diagram) of wave heights and periods, (e.g., see Refs. 22 and 23). Visual observation data should be used as the last recourse, because the accuracy of individual wave data is low. Furthermore, ocean-going ships try to avoid the area of high waves as much as possible, and thus wave data compiled from ship reports tend to have a negative bias in high wave ranges.

When a set of wave data is analyzed for extreme statistics, three requirements must be met as the database of extreme waves. The first requirement is that all the data are free of any error. Malfunctioning of a wave recorder at the peaks of storm waves is a typical error in instrumental measurements; if it did occur, the erroneous data should be replaced with some estimate based on wave hindcasting or information from neighboring stations.

The second requirement is the duration of record. Duration should be as long as possible, preferably more than 30 years and a minimum of several years. A short time span of wave data yields only a small number of storm wave data, and thus increases the magnitude of uncertainty due to sample variability. From this point of view, hindcasted wave data would be preferred to instrumental wave data at present, because the duration of the latter rarely exceeds 20 years.

The third requirement is that all major storms during the period of concern be included in the database. In the case of instrumental wave data, a check should be made on the depth of water at the measurement site, in order to guarantee that no data is affected by a depth-limited wave breaking process; if affected, the distribution of wave heights exhibits a tendency of saturation on the upper tail. Also, if a wave recorder failed to register a peak height of big storm waves in one year for some reason, and if it was unable to fill the gap by any means, then the particular season or year should be deleted from the effective duration of wave data. In case an extremely large storm event occurred and the peak wave height is undoubtedly the largest in the past, but without any reliable height estimate, the least squares method can deal with such a situation. Just leave the position of the largest data $x_{(1)}$ vacant but include the event in counting the sample size; the largest among the existing wave data is assigned the order number 2, the rest are given the order number 3 onward, and the least squares method is carried out normally.

When a wave hindcasting project is undertaken, a detailed search should be made at the beginning for meteorological disturbances capable of generating medium to large storm waves. Even so, we cannot eliminate a possibility that some undetected meteorological disturbances might have generated storm waves of appreciable heights. Thus, it is recommended to drop the lower one third to one quarter of peak wave heights from the set of wave data so as to guarantee all major storms are included in the data set. In such a situation, the total number N_T is better set to a slightly larger than the number of hindcasted cases, and the data is treated as a censored one. The censoring

parameter ν is calculated as the ratio of the number of adopted storm events to the probable number of total events N_T.

There has been raised a concern that wave measurements taken at three to six hour intervals might miss the peak of storm waves, and thus return values estimated on the basis of such data might have a negative bias.[15] A recent study by Forristall *et al.*[24] clarified this problem. The significant wave height derived from a record of limited length, say 20 min, has a statistical variability with the coefficient of variation of the order of several percent, as discussed in Sec. 9.6. As the peak wave height of storm waves is defined as the largest among the measured data, a negative bias due to a failure to measure the storm peak at regular recording times is mostly canceled by a positive bias due to the statistical variability by a limited record length, although the amount of error depends on the recording interval relative to the storm duration.

(B) *Preparation of a sample of extreme wave data*

As stated in the beginning of this chapter, the total sample method is not recommended for extreme wave analysis. However, when a visually observed wave data is the only available data source, the total sample method is an inevitable choice. In such a case, a search should be made for the average duration τ of storm waves in the area under study. It provides the unit time of storm event in extreme analysis. During a given return period R, there will be R/τ units of storm events, and the cumulative distribution for the return wave height x_R is given by $F(x_R) = 1 - \tau/R$ (units of time must be the same for τ and R). The same principle is applied for the total sample method using the instrumentally recorded wave data.

In the peaks-over-threshold (POT) method, setting of the threshold is a delicate problem. If it is set too high, the number of peak wave heights becomes too small. If it is set too low, a sequence of several storms might be judged as one storm and the number will be decreased. Even if the threshold is set at a moderate level, a storm wave activity may be slackened midway and one storm event is judged to consist of two events. To prevent such an artificial division, a limitation of minimum time interval between successive peaks should be imposed, for example, Mathiessen *et al.*[15] recommend two to four days. Probably the threshold would be better set to maximize the number of storm events in a year or season; by increasing the sample size, a possibility of misfitting is reduced and the range of confidence interval is narrowed.

There is a criticism against the POT method such that the estimate of return value is lowered as the threshold level is raised because the sample standard deviation decreases. The criticism is correct if the distribution parameters are estimated by the method of moments, but incorrect when the parameters are estimated by the least squares method with due consideration for the rate of data censoring.

Another problem associated with the POT method is how to maintain homogeneity of wave data. Examination of each wave source on weather maps is not practical, even though it is a desirable procedure. When the working group of the Maritime Hydraulics Section of IAHR analyzed the Halkenbanken data off Norway for nine years together with the Kodiak data, the group noted that the estimate of 100-year wave height gradually decreased as the threshold was raised.[2] It was considered that peak wave heights at lower levels might have belonged to a population different from that at higher levels. A possible way to separate different populations of storm waves would be to divide wave records by season and to make individual analyses for respective sets of wave data. The results of analyses need to be combined as of mixed populations as discussed in Sec. 11.3.4.

11.4.3 *Selection of Design Wave Height and Period*

(A) *Selection of design wave height*

The foregoing discussion in this chapter concerns with the estimation of a return wave height for a given value of a return period. The return wave height provides the basic information for selection of the design wave height, but the selection is not a straightforward procedure, because several factors await the decision of the engineer in charge of designing a structure.

First, distinction must be made between the two approaches of deterministic and probabilistic designs. In the former approach, the design wave height is selected as a fixed value, and detailed analysis of structural stability and strength is carried out to insure a sufficient margin of safety against the design condition. In the latter approach, the reliability of structure or the probability of failure during the service lifetime of a structure is examined under a certain set of conditions; the probability of safety is required to be kept below a certain level.

In the deterministic approach, the return period of a design wave height needs to be assigned *a priori*. The encounter probability provides some

guidelines for setting a return period, but there is no recommendable rule to set the encounter probability. In many designs of maritime structures, a return period of 50 to 100 years is often employed for evaluation of a design wave height. However, it remains as a conventional practice without a theoretical background. The confidence interval of a return wave height is only utilized for a safety check against the attack of design load greater than the design condition.

The reliability-based design or the probabilistic approach has a theoretical superiority over the deterministic approach, because it takes into account the uncertainties of various factors involved in structural designs. However, the service lifetime of a structure may not be easily defined for the case of breakwaters and seawalls; they should maintain their functions as long as possible. Another problem is such that it will take some time before a consensus is formed for the allowable level of failure probability.

A possible way out of such problems would be the cost-benefit analysis, which calculates the cost of construction at a given level of design loads and the expected amount of damage in the event of structure failure. For breakwaters and seawalls, the damage are usually taken as the initial construction cost of structures, because the amount of benefit being protected by the structure is hard to assess. The sum of the cost and expected amount of damage is to be computed at various levels of design loads, and the design loads which would minimize the sum of cost and damage is adopted in the final design of structure. Computation of failure probability in the reliability-based design provides a rational estimate. At present, this procedure remains as an ideal procedure, and no example of actual designs exists yet.

One of the important problems in the extreme wave statistics is the long-term climatic changes in the ocean environment. Tropical cyclones, for example, are known to be under the influence of the El Niño–Southern Oscillations, which have a time scale of several years (e.g., Refs. 25 and 26). In the evaluation of extreme storm surge levels, historical events in the past several hundred years can shed light to the previous abnormal storm surge levels. In the case of storm wave heights, however, measured data exist only after the 1960s and they often cover a relatively short time span at each site. Meteorological information on storms before World War II is not detailed enough to make wave hindcasting reliable. We do not know what wave climatic changes took place in the past and neither do we know what will occur in the future. Selection of design wave heights on the basis of extreme wave statistics is simply made

on the wishful postulation that the future wave climate during the lifetime of structure will remain the same as that in the past.

(B) *Wave period associated with design wave height*

Wave loads on structures are mainly determined by the wave height, but it is also dependent on the wave period. Once the design wave height is selected, then the range of wave period for the design condition needs to be fixed. A scatter diagram of wave heights and periods usually provides a guide to make a selection.

Except for the location where the long-traveled swell dominates the wave climate, wind waves are the major component of extreme waves. The steepness of wind waves defined as $H_{1/3}/(gT_{1/3}^2/2\pi)$ gradually decreases from 0.04 to 0.03 as wind waves grow in the ocean. For the metric units, this steepness gives the following relation between the storm wave height and period:

$$T_{1/3} = (4.0 \sim 4.6)\sqrt{H_{1/3}}, \qquad (11.47)$$

in which the constant 4.0 is for large wave heights and 4.6 for extremely large heights. Examination of a scatter diagram of wave heights and periods at the site of interest would establish a relation such as $T_{1/3} = \alpha H_{1/3}^{\beta}$ in which β will take a value slightly greater than 0.5. If the spectral peak wave period T_p is employed instead of the significant wave period $T_{1/3}$, the former is about 10% larger than the latter as indicated in Chapter 2.

References

1. Y. Goda, "A review on statistical interpretation of wave data," *Rept. Port and Harbour Res. Inst.* **18** (1) (1979), pp. 5–32.
2. G. van Vledder, Y. Goda, P. Hawkes, E. Mansard, M. H. Martin, M. Mathiesen, E. Peltier, and E. Thompson, "Case studies of extreme wave analysis: a comparative analysis," *Proc. 2nd Int. Symp. Ocean Wave Measurement and Analysis*, ASCE (1993), pp. 978–992.
3. E. J. Gumbel, *Statistics of Extremes* (Columbia Univ. Press, New York, 1953).
4. Y. Goda, "Numerical investigations on plotting formulas and confidence intervals of return values in extreme statistics," *Rept. Port and Harbour Res. Inst.* **27** (1) (1988), pp. 31–92 (*in Japanese*), also Y. Goda, "On the methodology of selecting design wave height," *Proc. 21st Int. Conf. Coastal Engrg.* (Malaga, 1988), pp. 899–913.

5. Y. Goda, P. Hawkes, E. Mansard, M. H. Martin, M. Mathiesen, E. Peltier, E. Thompson, and G. van Vledder, "Intercomparison of extremal wave analysis method using numerically simulated wave data," *Proc. 2nd Int. Symp. Ocean Wave Measurement and Analysis*, ASCE (1993), pp. 963–977.

6. Y. Goda and K. Kobune, "Distribution function fitting for storm wave data," *Proc. 22nd Int. Conf. Coastal Engrg.* (Delft, 1990), pp. 18–31.

7. I. I. Gringorten, "A plotting rule for extreme probability paper," *J. Geophys. Res.* **68** (3) (1963), pp. 813–814.

8. G. Blom, *Statistical Estimates and Transformed Beta-Variates* (John Wiley & Sons, New York, 1958), Chapter 12.

9. C. Petruaskas and P. M. Aagaard, "Extrapolation of historical storm data for estimating design wave heights," *J. Soc. Petroleum Engrg.* **11** (1971), pp. 23–37 (also, Prepr. 2nd OTC, 1970, Paper No. 1190).

10. Y. Goda and M. Onozawa, "Characteristics of the Fisher-Tippett type II distribution and their confidence intervals," *Proc. Japan Soc. Civil Engrg.* (417/II-13) (1990), pp. 289–292 (*in Japanese*).

11. M. Andrew, O. P. Smith, and J. M. Mckee, "Extremal analysis of hindcast wind and wave data at Kodiak, Alaska," *Tech. Rept., CERC-85-4*, U.S. Army Corps of Engrg., Waterways Experiment Station (Vicksburg, Miss., 1985).

12. V. Barnett and T. Lewis, *Outliers in Statistical Data (2nd ed.)* (John Wiley & Sons., 1984), 463p.

13. J. F. Lawless, *Statistical Models and Methods for Lifetime Data* (John Wiley & Sons, New York, 1982), 580p.

14. P. G. Challenor, "Confidence limits for extreme value statistics," *Inst. Oceanographic Sciences, Rept.* **82** (1979), 27p.

15. M. Mathiesen, Y. Goda, P. Hawkes, E. Mansard, M. H. Martin, E. Peltier, E. Thompson, and G. van Vledder, "Recommended practice for extreme wave analysis," *J. Hydraulic Res.*, IAHR **32** (6) (1994), pp. 803–814.

16. Y. Goda, "Uncertainty of design parameters from viewpoint of extreme statistics," *Trans. Amer. Soc. Mech. Engrg.* **114** (1992), pp. 76–82.

17. Y. Goda, "On the uncertainties of wave heights as the design load for maritime structures," *Proc. Int. Workshop on Wave Barriers in Deep Waters*, Port and Harbour Res. Inst. (Yokosuka, Japan, 1994).

18. D. J. T. Carter and P. G. Challenor, "Estimating return values of environmental parameters," *Quart. Jour. Roy. Meteorol. Soc.* **107** (1981), pp. 259–266.

19. R. E. Borgman, "Risk criteria," *J. Wtrwy. & Harb. Div., Proc. ASCE* **89** (WW3) (1963), pp. 1–35.

20. M. K. C. Ravindra, C. A. Cornell, and T. V. Galambos, "Wind and snow load factors for use in LRFD," *J. Structural Engrg., Proc. ASCE* **104** (ST9) (1978), pp. 1443–1457.

21. H. F. Burcharth, "Reliability-based design of coastal structures," *Advances in Coastal and Ocean Engineering* **3** ed. P. L.-F. Liu (World Scientific, Singapore, 1997), pp. 145–214.

22. N. Hogben, and F. E. Lumb, *Ocean Wave Statistics* H.M.S.O. (London, 1967).
23. British Maritime Technology, *Global Wave Statistics* (Unwin Brothers Ltd., 1986).
24. G. Z. Forristall, J. C. Heideman, I. A. Legget, B. Roskam, and L. Vanderschuren, "Effect of sampling variability on hindcast and measured wave heights," *J. Wtrwy., Port, Coast., and Ocn. Engrg.*, ASCE **122** (5) (1996), pp. 216–225.
25. R. J. Seymour, R. R. Strange III, D. R. Cayan, and R. A. Nathan, "Influence of El Niños on California's wave climate," *Proc. Int. Conf. Coastal Engrg.* (Houston, 1984), pp. 577-592.
26. R. J. Seymour, "Wave climate variability in Southern California," *J. Wtrwy., Port, Coast. and Ocn. Engrg.* **122** (4) (1996), pp. 182-186.
27. P. A. Hastings, "Southern oscillation influences on tropical activity in the Australian/south-west Pacific region," *Int. J. Climatology* **10** (1990), pp. 291–298.
28. D. L. Proh, and M. R. Gourlay, "Interannual climate variations and tropical cyclones in the eastern Australian region," *Proc. 13th Australasian Coastal and Ocean Engrg. Conf. and 6th Australasian Port and Harbour Conf.* (Christchurch, 1997), pp. 681–686.

List of Wavelength and Celerity for a Given Wave Period and Water Depth

Table A-1. List of wavelength and celerity for a given wave period and water depth ($g =$ 9.8 m/s^2).

Wave period (s) Water depth (m)	2.0		2.5		3.0		4.0		5.0	
	Wave-length (m)	Cel-erity (m/s)	Wave-length (m)	Cel-erity (m/s)	Wave-length (m)	Cel-erity (m/s)	Wave-length (m)	Cel-erity (m/s)	Wave-length (m)	Cel-erity (m/s)
0.1	1.97	0.97	2.45	0.98	2.95	0.98	3.94	0.99	4.94	0.99
0.2	2.71	1.35	3.42	1.37	4.14	1.38	5.55	1.39	6.96	1.39
0.3	3.26	1.63	4.15	1.66	5.03	1.68	6.77	1.69	8.50	1.70
0.4	3.69	1.85	4.74	1.89	5.76	1.92	7.79	1.95	9.79	1.96
0.5	4.05	2.03	5.24	2.09	6.39	2.13	8.67	2.17	10.92	2.18
0.6	4.36	2.18	5.67	2.27	6.95	2.32	9.45	2.36	11.93	2.39
0.7	4.62	2.31	6.05	2.42	7.45	2.48	10.17	2.54	12.85	2.57
0.8	4.85	2.42	6.40	2.56	7.90	2.63	10.82	2.71	13.70	2.74
0.9	5.04	2.52	6.70	2.68	8.31	2.77	11.43	2.86	14.49	2.90
1.0	5.21	2.61	6.98	2.79	8.69	2.90	11.99	3.00	15.23	3.05
1.1	5.36	2.68	7.23	2.89	9.04	3.01	12.52	3.13	15.93	3.19
1.2	5.49	2.74	7.46	2.99	9.36	3.12	13.02	3.26	16.59	3.32
1.3	5.60	2.80	7.67	3.07	9.66	3.22	13.50	3.37	17.22	3.44
1.4	5.70	2.85	7.87	3.15	9.95	3.32	13.94	3.49	17.82	3.56
1.5	5.78	2.89	8.04	3.22	10.21	3.40	14.37	3.59	18.40	3.68
1.6	5.85	2.93	8.20	3.28	10.46	3.49	14.77	3.69	18.95	3.79
1.8	5.96	2.98	8.48	3.39	10.90	3.63	15.53	3.88	19.98	4.00
2.0	6.05	3.02	8.72	3.49	11.30	3.77	16.22	4.05	20.94	4.19
2.2	6.11	3.05	8.91	3.56	11.65	3.88	16.85	4.21	21.84	4.37
2.5	6.16	3.08	9.14	3.66	12.09	4.03	17.71	4.43	23.08	4.62
3.0	6.21	3.11	9.40	3.76	12.67	4.22	18.95	4.74	24.92	4.98
3.5	6.23	3.11	9.55	3.82	13.09	4.36	19.98	5.00	26.52	5.30
4.0	6.23	3.12	9.64	3.86	13.39	4.46	20.85	5.21	27.93	5.59
4.5	6.24	3.12	9.69	3.88	13.60	4.53	21.57	5.39	29.18	5.84
5.0	6.24	3.12	9.72	3.89	13.75	4.58	22.18	5.55	30.29	6.06
6.0	6.24	3.12	9.74	3.90	13.91	4.64	23.11	5.78	32.17	6.43
7.0	6.24	3.12	9.75	3.90	13.99	4.66	23.75	5.94	33.67	6.73
8.0	6.24	3.12	9.75	3.90	14.02	4.67	24.19	6.05	34.86	6.97
9.0	6.24	3.12	9.75	3.90	14.03	4.68	24.47	6.12	35.81	7.16
10.0	6.24	3.12	9.75	3.90	14.03	4.68	24.65	6.16	36.56	7.31
11.0	6.24	3.12	9.75	3.90	14.04	4.68	24.77	6.19	37.15	7.43
12.0	6.24	3.12	9.75	3.90	14.04	4.68	24.84	6.21	37.60	7.52
13.0	6.24	3.12	9.75	3.90	14.04	4.68	24.89	6.22	37.95	7.59
14.0	6.24	3.12	9.75	3.90	14.04	4.68	24.91	6.23	38.22	7.64
15.0	6.24	3.12	9.75	3.90	14.04	4.68	24.93	6.23	38.42	7.68
16.0	6.24	3.12	9.75	3.90	14.04	4.68	24.94	6.23	38.57	7.71
17.0	6.24	3.12	9.75	3.90	14.04	4.68	24.95	6.24	38.68	7.74
18.0	6.24	3.12	9.75	3.90	14.04	4.68	24.95	6.24	38.77	7.75
19.0	6.24	3.12	9.75	3.90	14.04	4.68	24.95	6.24	38.83	7.77
20.0	6.24	3.12	9.75	3.90	14.04	4.68	24.95	6.24	38.87	7.77
Deepwater waves	6.24	3.12	9.75	3.90	14.04	4.68	24.96	6.24	38.99	7.80

Table A-2. List of wavelength and celerity for a given wave period and water depth ($g = 9.8 \text{ m/s}^2$).

Wave period (s) Water depth (m)	6.0 Wave-length (m)	6.0 Cel-erity (m/s)	7.0 Wave-length (m)	7.0 Cel-erity (m/s)	8.0 Wave-length (m)	8.0 Cel-erity (m/s)	9.0 Wave-length (m)	9.0 Cel-erity (m/s)	10.0 Wave-length (m)	10.0 Cel-erity (m/s)
0.5	13.16	2.19	15.39	2.20	17.62	2.20	19.84	2.20	22.06	2.21
1.0	18.43	3.07	21.61	3.09	24.78	3.10	27.94	3.10	31.09	3.11
1.5	22.36	3.73	26.29	3.76	30.19	3.77	34.08	3.79	37.95	3.80
2.0	25.57	4.26	30.14	4.31	34.67	4.33	39.18	4.35	43.68	4.37
2.5	28.31	4.72	33.46	4.78	38.56	4.82	43.62	4.85	48.67	4.87
3.0	30.71	5.12	36.39	5.20	42.01	5.25	47.58	5.29	53.13	5.31
3.5	32.84	5.47	39.02	5.57	45.13	5.64	51.18	5.69	57.19	5.72
4.0	34.75	5.79	41.42	5.92	47.98	6.00	54.48	6.05	60.92	6.09
4.5	36.49	6.08	43.61	6.23	50.61	6.33	57.53	6.39	64.40	6.44
5.0	38.07	6.34	45.63	6.52	53.05	6.63	60.38	6.71	67.64	6.75
6.0	40.84	6.81	49.24	7.03	57.47	7.18	65.57	7.29	73.58	7.36
7.0	43.19	7.20	52.39	7.48	61.37	7.67	70.20	7.80	78.92	7.89
8.0	45.19	7.53	55.16	7.88	64.86	8.11	74.38	8.26	83.77	8.38
9.0	46.91	7.82	57.61	8.23	68.01	8.50	78.19	8.69	88.22	8.82
10.0	48.37	8.06	59.78	8.54	70.85	8.86	81.68	9.08	92.32	9.23
11.0	49.62	8.27	61.72	8.82	73.44	9.18	84.89	9.43	96.12	9.61
12.0	50.69	8.45	63.44	9.06	75.80	9.48	87.85	9.76	99.67	9.97
13.0	51.60	8.60	64.98	9.28	77.96	9.74	90.59	10.07	102.98	10.30
14.0	52.38	8.73	66.35	9.48	79.93	9.99	93.14	10.35	106.07	10.61
15.0	53.03	8.84	67.58	9.65	81.73	10.22	95.51	10.61	108.98	10.90
16.0	53.58	8.93	68.66	9.81	83.39	10.42	97.71	10.86	111.71	11.17
17.0	54.04	9.01	69.63	9.95	84.90	10.61	99.77	11.09	114.29	11.43
18.0	54.42	9.07	70.49	10.07	86.29	10.79	101.68	11.30	116.71	11.67
19.0	54.74	9.12	71.25	10.18	87.56	10.95	103.47	11.50	119.00	11.90
20.0	55.00	9.17	71.92	10.27	88.72	11.09	105.14	11.68	121.16	12.21
22.0	55.39	9.23	73.03	10.43	90.76	11.35	108.14	12.02	125.12	12.51
24.0	55.65	9.28	73.89	10.56	92.46	11.56	110.76	12.31	128.66	12.87
26.0	55.83	9.30	74.54	10.65	93.86	11.73	113.04	12.56	131.83	13.18
28.0	55.94	9.32	75.03	10.72	95.02	11.88	115.01	12.78	134.66	13.47
30.0	56.02	9.34	75.40	10.77	95.97	12.00	116.72	12.97	137.19	13.72
35.0	56.11	9.35	75.96	10.85	97.64	12.20	120.03	13.34	142.38	14.24
40.0	56.14	9.36	76.22	10.89	98.61	12.33	122.26	13.58	146.25	14.63
45.0	56.15	9.36	76.33	10.90	99.16	12.39	123.75	13.75	149.10	14.91
50.0	56.15	9.36	76.39	10.91	99.46	12.43	124.71	13.86	151.16	15.12
55.0	56.15	9.36	76.41	10.92	99.63	12.45	125.32	13.92	152.64	15.26
60.0	56.15	9.36	76.42	10.92	99.72	12.46	125.71	13.97	153.68	15.37
65.0	56.15	9.36	76.42	10.92	99.77	12.47	125.95	13.99	154.41	15.44
70.0	56.15	9.36	76.42	10.92	99.97	12.47	126.10	14.01	154.91	15.49
75.0	56.15	9.36	76.43	10.92	99.81	12.48	126.19	14.02	155.25	15.53
80.0	56.15	9.36	76.43	10.92	99.81	12.48	126.25	14.03	155.49	15.55
Deepwater waves	56.15	9.36	76.43	10.92	99.82	12.48	126.34	14.04	155.97	15.60

Table A-3. List of wavelength and celerity for a given wave period and water depth ($g = 9.8$ m/s^2).

Wave period (s) Water depth (m)	11.0 Wave-length (m)	11.0 Cel-erity (m/s)	12.0 Wave-length (m)	12.0 Cel-erity (m/s)	13.0 Wave-length (m)	13.0 Cel-erity (m/s)	14.0 Wave-length (m)	14.0 Cel-erity (m/s)	15.0 Wave-length (m)	15.0 Cel-erity (m/s)
1.0	34.2	3.11	37.4	3.12	40.5	3.12	43.7	3.12	46.8	3.12
2.0	48.2	4.38	52.6	4.39	57.1	4.39	61.6	4.40	66.0	4.40
3.0	58.6	5.33	64.2	5.35	69.6	5.36	75.1	5.37	80.6	5.37
4.0	67.3	6.12	73.7	6.14	80.1	6.16	86.5	6.18	92.8	6.19
5.0	74.9	6.81	82.0	6.84	89.2	6.86	96.3	6.88	103.4	6.90
6.0	81.5	7.41	89.4	7.45	97.3	7.48	105.1	7.51	113.0	7.53
7.0	87.6	7.96	96.1	8.01	104.7	8.05	113.2	8.08	121.6	8.11
8.0	93.1	8.46	102.3	8.52	111.4	8.57	120.6	8.61	129.6	8.64
9.0	98.1	8.92	108.0	9.00	117.7	9.05	127.4	9.10	137.1	9.14
10.0	102.8	9.35	113.2	9.44	123.6	9.50	133.8	9.56	144.1	9.60
11.0	107.2	9.75	118.2	9.85	129.1	9.93	139.9	9.99	150.6	10.04
12.0	111.3	10.12	122.8	10.24	134.2	10.33	145.6	10.40	156.8	10.45
13.0	115.2	10.47	127.2	10.60	139.1	10.70	151.0	10.78	162.7	10.85
14.0	118.8	10.80	131.3	10.95	143.8	11.06	156.1	11.15	168.3	11.22
15.0	122.2	11.11	135.3	11.27	148.2	11.40	161.0	11.50	173.7	11.58
16.0	125.5	11.41	139.0	11.58	152.4	11.72	165.7	11.83	178.8	11.92
17.0	128.5	11.68	142.6	11.88	156.4	12.03	170.1	12.15	183.8	12.25
18.0	131.4	11.95	145.9	12.16	160.3	12.33	174.4	12.46	188.5	12.57
19.0	134.2	12.20	149.2	12.43	163.9	12.61	178.6	12.75	193.0	12.87
20.0	136.8	12.44	152.3	12.69	167.5	12.88	182.5	13.04	197.4	13.16
22.0	141.7	12.89	158.1	13.17	174.1	13.39	190.0	13.57	205.7	13.72
24.0	146.2	13.29	163.4	13.61	180.3	13.87	197.0	14.07	213.5	14.23
26.0	150.2	13.66	168.3	14.02	186.0	14.31	203.5	14.53	220.8	14.72
28.0	153.9	13.99	172.8	14.40	191.3	14.72	209.6	14.97	227.6	15.17
30.0	157.3	14.30	176.9	14.74	196.2	15.10	215.3	15.38	234.1	15.60
35.0	164.4	14.95	186.0	15.50	207.2	15.94	228.1	16.29	248.7	16.58
40.0	170.1	15.46	193.5	16.12	216.5	16.65	239.1	17.08	261.4	17.43
45.0	174.5	15.86	199.6	16.64	224.4	17.26	248.7	17.76	272.6	18.17
50.0	178.0	16.18	204.7	17.06	231.0	17.77	256.9	18.35	282.5	18.83
55.0	180.7	16.42	208.8	17.40	236.6	18.20	264.1	18.86	291.1	19.41
60.0	182.7	16.61	212.1	17.68	241.4	18.57	270.3	19.31	298.8	19.92
70.0	185.5	16.86	216.9	18.08	248.7	19.13	280.3	20.02	311.6	20.77
80.0	187.0	17.00	220.0	18.33	253.7	19.52	287.7	20.55	321.5	21.43
90.0	187.8	17.07	221.9	18.49	257.2	19.78	293.1	20.93	329.1	21.94
100.0	188.3	17.11	233.0	18.58	259.5	19.96	297.0	21.21	334.9	22.32
120.0	188.6	17.15	224.1	18.67	261.9	20.15	301.6	21.54	342.5	22.83
140.0	188.7	17.15	244.4	18.70	262.9	20.23	303.8	21.70	346.6	23.11
160.0	188.7	17.16	224.5	18.71	263.3	20.26	304.9	21.78	348.7	23.25
180.0	188.7	17.16	224.6	18.72	263.5	20.27	305.3	21.81	349.8	23.32
200.0	188.7	17.16	224.6	18.72	263.6	20.27	305.5	21.82	350.4	23.36
Deepwater waves	188.7	17.16	224.6	18.72	263.6	20.28	305.7	21.84	350.9	23.40

Table A-4. List of wavelength and celerity for a given wave period and water depth ($g = 9.8$ m/s^2).

Wave period (s) Water depth (m)	16.0 Wavelength (m)	Celerity (m/s)	17.0 Wavelength (m)	Celerity (m/s)	18.0 Wavelength (m)	Celerity (m/s)	19.0 Wavelength (m)	Celerity (m/s)	20.0 Wavelength (m)	Celerity (m/s)
1.0	50.0	3.12	53.1	3.12	56.2	3.12	59.4	3.12	62.5	3.13
2.0	70.5	4.40	74.9	4.41	79.4	4.41	83.8	4.41	88.2	4.41
3.0	86.1	5.38	91.5	5.38	97.0	5.39	102.4	5.39	107.9	5.39
4.0	99.1	6.20	105.4	6.20	111.8	6.21	118.1	6.21	124.4	6.22
5.0	110.5	6.91	117.6	6.92	124.7	6.93	131.8	6.93	138.8	6.94
6.0	120.8	7.55	128.5	7.56	136.3	7.57	144.1	7.58	151.8	7.59
7.0	130.1	8.13	138.5	8.15	146.9	8.16	155.3	8.17	163.7	8.19
8.0	138.7	8.67	147.7	8.69	156.7	8.71	165.7	8.72	174.7	8.74
9.0	146.7	9.17	156.3	9.19	165.9	9.22	175.4	9.23	185.0	9.25
10.0	154.2	9.64	164.4	9.67	174.6	9.69	184.6	9.72	194.7	9.73
11.0	161.3	10.08	172.0	10.12	182.6	10.15	193.2	10.17	203.8	10.19
12.0	168.0	10.50	179.2	10.54	190.3	10.57	201.4	10.60	212.5	10.63
13.0	174.4	10.90	186.1	10.95	197.7	10.98	209.3	11.01	220.8	11.04
14.0	180.5	11.28	192.6	11.33	204.7	11.37	216.7	11.41	228.7	11.44
15.0	186.3	11.65	198.9	11.70	211.4	11.75	223.9	11.79	236.4	11.82
16.0	191.9	11.99	204.9	12.06	217.9	12.11	230.8	12.15	243.7	12.18
17.0	197.3	12.33	210.7	12.40	224.1	12.45	237.5	12.50	250.8	12.54
18.0	202.4	12.65	216.3	12.72	230.1	12.78	243.9	12.84	257.6	12.88
19.0	207.4	12.96	221.7	13.04	235.9	13.11	250.1	13.16	264.2	13.21
20.0	212.2	13.26	226.9	13.35	241.5	13.42	256.1	13.48	270.6	13.53
22.0	221.3	13.83	236.8	13.93	252.2	14.01	267.5	14.08	282.8	14.14
24.0	229.9	14.37	246.1	14.48	262.3	14.57	278.3	14.65	294.3	14.72
26.0	237.9	14.87	254.9	14.99	271.8	15.10	288.6	15.19	305.3	15.26
28.0	245.5	15.34	263.2	15.48	280.8	15.60	298.3	15.70	315.7	15.78
30.0	252.7	15.79	271.1	15.95	289.4	16.08	307.5	16.19	325.6	16.28
35.0	269.0	16.81	289.1	17.01	309.1	17.17	328.9	17.31	348.6	17.43
40.0	283.4	17.71	305.2	17.95	326.7	18.15	348.1	18.32	369.3	18.46
45.0	296.2	18.51	319.5	18.80	342.6	19.03	365.5	19.23	388.1	19.41
50.0	307.6	19.23	332.4	19.56	357.0	19.83	381.3	20.07	405.4	20.27
55.0	317.8	19.86	344.1	20.24	370.1	20.56	395.8	20.83	421.3	21.06
60.0	326.9	20.43	354.7	20.86	382.0	21.22	409.1	21.53	435.9	21.80
70.0	342.4	21.40	372.9	21.94	403.0	22.39	432.7	22.77	462.1	23.10
80.0	354.9	22.18	387.9	22.82	420.5	23.36	452.8	23.83	484.6	24.23
90.0	364.9	22.80	400.3	23.55	435.3	24.19	470.0	24.73	504.2	25.21
100.0	372.8	23.30	410.4	24.14	447.8	24.88	484.7	25.51	521.2	26.06
120.0	383.9	23.99	425.4	25.03	466.9	25.94	508.0	16.74	548.8	27.44
140.0	390.6	24.41	435.2	25.60	480.1	26.67	524.9	27.63	569.6	28.48
160.0	394.4	24.65	441.4	25.96	489.1	27.17	537.0	28.26	585.0	26.25
180.0	396.6	24.79	445.2	26.19	495.0	27.50	545.5	28.71	596.4	29.82
200.0	397.8	24.87	447.5	26.32	498.8	27.71	551.4	29.02	604.6	30.23
Deepwater waves	399.3	24.96	450.8	26.52	505.3	28.07	563.1	29.63	623.9	31.19

Index